Synthesis, Characterization, and Development of Boron-based *Pyrazole*s that can serve as Potential Therapeutic Redox Regulators in Amyotrophic Lateral Sclerosis (ALS): Introducing Borsantrazole™

by

Nitesh Sanghai

A Thesis submitted to the Faculty of Graduate and Postdoctoral Studies

of the University of Manitoba

in partial fulfillment of the requirements of the degree of

Doctor of Philosophy

College of Pharmacy, Rady Faculty of Health Sciences

University of Manitoba

Winnipeg, Manitoba, Canada

Dedication

Dedicated to the memory of my late father

Jay Praksh Sanghai

And

To the memory of my late mother-in-law

Bhushan Rani

Acknowledgements

I sincerely want to thank my wife, Bhavna Sanghai, who has been a tremendous support to me from the start of my PhD. Without her encouragement to leave my well-paying job and come to Canada to pursue my PhD under Dr. Geoffrey K. Tranmer, this wouldn't have been possible. Additionally, she stayed resilient while supporting my daughters in India for a year without my support. During my project, she became involved by contributing her weekends, staying with me in the department along with my daughters (Parin Sanghai and Gauri Sanghai) while I was conducting animal experiments. I also want to thank my eldest daughter, Parin Sanghai, who has been very patient throughout my PhD journey. She always told me, “Papa, I can play by myself.” She encouraged me to focus on my research and studies, reminding me, “You are a scientist, and you need to work towards finding a cure for ALS patients.” Furthermore, Parin has volunteered for the ALS Society of Manitoba since 2020, which motivated me to do my best in the project.

I would first like to acknowledge and thank my advisor, mentor, and guru, Dr. Geoffrey K. Tranmer, for providing me with mentoring, support throughout my project, and advice during my time in the PhD program. Without his guidance, this work would not be possible, and I am grateful for his time and dedication. I am fortunate to have Dr. Geoffrey K. Tranmer as my mentor. I treat Dr. Tranmer as my “Guru,” the highest honor we give to teachers back in India who have illuminated my path at every step of my research journey. He empowered me with his knowledge and inculcated a positive mindset from the beginning of my project. Whenever I felt discouraged by the results, he encouraged me by saying, “Don’t worry, we will get it; just try to do your best.” Further, he taught me the principles of staying mentally relaxed, which is essential to success. Only a healthy mind

could bring impactful science from bench to bedside. Besides guiding the academic journey, he is always open to listening and resolving daily work-life issues. In addition, he is an incredible leader with a growing mindset. He always listens to me very patiently and appreciates my hard work, which makes me feel more positive about solving a problem. Furthermore, Dr. Tranmer has always motivated and inspired me to collaborate and discuss the lab's research with people around the globe. This has improved my vision of creating “Hope” and working with the multidisciplinary team. In addition, he always allows me to initiate an idea with enthusiasm. Additionally, he boosted my confidence by involving me as a collaborator in grants such as CIHR and Research Manitoba. He also gave me chances to lead several manuscripts as the corresponding author and part of communications in all the important subject matter. These experiences taught me the importance of empowering others and helped me develop my scholarly potential.

Also, he appreciated my intentions of giving back to the community through community services, which helped me learn to connect with the ALS community and align my drug discovery goals with the resilience of ALS patients.

I genuinely believe he is an incredible person; without him, I could not have imagined my path to success. I wish him all the best from the bottom of my heart.

I also want to thank Dr. Jiming Kong for his expert guidance on the project; his generosity inspired me during my PhD work. His support, including providing humanized SOD1 ALS mouse models and NSC-34 cells, was instrumental in helping us to complete *in vitro* and preclinical studies. Attending his lab meetings expanded my understanding of neuroscience. I still remember his words, **“Nitesh, you are smart and hardworking,"** which inspired me to strive for excellence in my project. Furthermore, he gave me the

opportunity to contribute to different manuscripts, which helped me to develop my scholarly potential.

I want to thank Dr. Frank Burczynski for his valuable insights in the project. Dr. Frank has always inspired and motivated me by offering suggestions and recommendations to improve my project. His valuable words, **“Hard work does pay off in the long run. Keep asking yourself, what new information did I learn today,”** encourage me to learn more about my project and beyond.

I want to acknowledge the central animal care services of the University of Manitoba for providing me with animal training and continuous support and guidance throughout my project. I want to thank Rhonda Kelly, Rachelle Mariash, Denise Borowski, and Mikaela Mcgee for being collegial, supportive, and enriching my knowledge during my animal studies.

I would also like to acknowledge and thank contributors to the project, Dr. Rene Zahedi, Director, Manitoba Centre for Proteomics and Systems Biology, for collaborating on our biomarker studies. Despite his busy schedule, he supported and guided me, clearing my doubts. We wouldn’t have achieved our biomarker studies without the support of Dr. Rene. Also, Ying Lao, from the Manitoba Centre for Proteomics and Systems Biology, has supported me with a proteomics and phosphoproteomics study.

Also, I would like to acknowledge Dr. Jun Feng Wang, Department of Pharmacology, for providing me with training and assisting me with primary cortical neuronal cells to run in vitro experiments.

I would like to sincerely thank the Electron Microscopy Core & Histology Services, Department of Human Anatomy and Cell Science, Rady Faculty of Health Sciences, for providing me with training and supporting the histological and microscopic work.

Thank you to all former and current members of the Tranmer lab for their support and guidance during the project. Above all, maintain a collegial and positive environment in the lab. Dr. Billy Vyong, Dr. Teng Guan, Dr. Yuhua Fang, Paul Szymanski, Ahmet Burak Berk, and Shaharyar Afridi. Thank you to both current and former graduate and summer students at the College of Pharmacy for their support and thank you to all the faculty and staff at the College of Pharmacy for their support.

I also want to thank **Research Manitoba** for honoring me by selecting me for the esteemed PhD Research Studentship Award in 2024. Additionally, I am grateful to Mitacs for their funding support through the **Lab2Market** entrepreneurship program. Furthermore, I would like to acknowledge and thank **CIHR**, **NSERC Discovery Grant**, and **Research Manitoba** for providing funding for the project. I would like to thank ALS Canada for honouring me with travel grants to attend the ALS/MND international symposium in Montreal, Canada, in 2024 and the Gordon Research Conferences in Maine, USA, in 2025. Finally, I want to thank **CAS, a division of the American Chemical Society**, for recognizing my scholarly potential and leadership qualities and for honoring me with the **2025 CAS Future Leaders Top 100**, an international recognition. This global program emphasizes the importance of learning, engaging, and connecting, and it celebrates academic excellence and mentorship qualities.

Motivation

Education is a privilege in my family. I vividly recall my father often telling me, ***"Do something new,"*** as it was the key to strengthening our family's standing in the community. He emphasized that, since we lacked money, becoming successful was the only way to earn both income and respect, all of which was a dream for us. My father was hardworking, perseverant, and compassionate toward everyone. Every day, he would tell me, “Akhil (my nickname), you can do it." He urged me to work hard and not give up, even in the face of our challenging family circumstances, encouraging me to face the truth and persevere in the face of adversity. His unwavering trust inspired me to keep telling myself, ***"Nitesh, you have to do it."*** It wasn’t easy; it was challenging for six years after my grade 12th, and I faced and tested many failures. It was challenging to get admission to medical school. Yet, my father never failed to support me; his continuous support kept pushing me to work hard, reminding me, ***“Don’t worry, you’ll succeed, believe in yourself. I am here for you."*** With his encouragement, I ended up in pharmacy school, which was my second choice after medical school. This did not bring me internal satisfaction; my goal was to achieve excellence and transform my family's future by doing something new. Then I worked hard and aimed to join the Centre of Excellence at the National Institute of Pharmaceutical Education and Research (NIPER), a dream institution for many aspiring Indian pharmacists. I passed three national-level exams (GATE/GPAT/NIPER). Getting into NIPER marked a turning point for my family and earned my father respect in the community. One day, he called me, happy and proud, saying, ***"Akhil, you did it,"*** and reminded me again to always do something new. His words have always motivated me to strive for innovation. Sadly, I lost him very early in my life in 2014. My father has since

passed away, but my curiosity, passion, and dedication to do something new remain strong.

To achieve something new, I came to Canada for graduate studies, a path that was almost impossible for me and my family. I feel blessed to have Dr. Geoffrey K. Tranmer, who has motivated me to give my best. Dr. Tranmer is like a **“Guru”** for me. I never imagined that one day I would become an inventor of an innovative and novel molecule, **Borsantrazole**. Although the project was challenging, I reminded myself daily of my father’s words: to do something new. I motivated myself to excel, caring for mice as if they were patients with ALS. I tried to maintain a safe, positive, and inclusive environment around me. Dr. Tranmer has been phenomenal in inspiring and guiding me throughout my graduate journey. Moreover, Lee-Ann Tranmer, Dr. Tranmer’s wife, supported us like family here in Canada, providing encouragement that inspired me to give my best. Additionally, my father-in-law, Rajesh Dhawan, motivates me daily with his positivity and advice to ***"be grateful in every circumstance and do your best,"*** creating a positive environment around me. My wife, Bhavna Sanghai, and my two daughters, Parin and Gauri Sanghai, have supported and motivated me to do my best throughout my PhD journey.

I know my father would be happy to hear the story of **Borsantrazole**. I honestly feel he's still with me, watching over everything I do. His blessings motivate me every day to do my best. I firmly believe that without motivation to do something new every second, progress is impossible. Furthermore, your positive thoughts determine your energy, and your thoughts become your reality. Life will challenge you. Believe in God; He is always there, as a third eye watching your hard work, commitment, passion, and dedication. One day, you will achieve success. Now, with this innovative and highly motivated PhD project,

my main goal is to create ***"Hope"*** in the lives of people suffering from Amyotrophic Lateral Sclerosis, an incurable and fatal disease.

Extended Abstract

Amyotrophic lateral sclerosis (ALS), also known as Lou Gehrig's disease, is a highly complex, devastating condition with a high unmet medical need that necessitates the immediate development of disease-modifying drugs. ALS is considered a heterogeneous fatal disease that affects multiple pathophysiological pathways; however, one of the most studied pathways, which is well demonstrated in both preclinical ALS mouse models and human clinical ALS cases, is oxidative stress. Further, hydrogen peroxide (H_2O_2) is one of the most studied free radicals in the etiopathogenesis of ALS. The pathological concentration of H_2O_2 causes aberrant oxidative modification and, hence, misfolding of both human wildtype and mutant SOD1, the ubiquitous antioxidant SOD1 protein, a known cause of both sporadic and familial ALS. Despite significant efforts, the scientific community has had limited success in developing effective treatments for ALS. Since the discovery of ALS in 1869 by Charcot, only two FDA-approved drugs, Edaravone (EDR), an antioxidant, and Riluzole, an antiglutamatergic, have been widely used clinically, albeit with modest effects on the clinical course of ALS disease progression. Additionally, preclinical studies of both these drugs in SOD1 ALS mouse models have not shown any significant survival benefit; however, some amelioration in disease progression has been observed and has been translated from preclinical animal studies to clinical human studies with these two molecules. Nevertheless, the potential of small molecule therapeutics, such as EDR, which seeks to reduce the global oxidative stress implicated in the pathophysiology of ALS, cannot be overlooked.

Therefore, our overall goal, as part of a longitudinal early-phase drug discovery project, is to develop novel oxidative stress-targeting boron-based pyrazoles (B-Pyr) that could

improve the neurological phenotypes, as well as modify other motor clinical disease phenotypes, in the highly aggressive and early onset humanized SOD1-G37R line (42) mice model of ALS. Herein, we report our investigations into the development of a trifunctional boron-based pyrazole, NS-1-2 (Borsantrazole™), that can serve as a prodrug of EDR, which has shown a satisfactory safety profile and statistically significant preclinical, proof-of-concept efficacy in a humanized SOD1 mouse model of ALS. Overall, these results validate the therapeutic potential of our B-Pyr scaffold for extending survival and modifying the motor clinical disease phenotypes of ALS, in terms of delaying the onset of disease, symptom onset, and reducing ALS-induced weight loss (cachexia). Finally, comprehensive, global, quantitative, unbiased, and untargeted profiling of the proteome and phosphoproteome in treated SOD1-G37R mice reveals changes and differential regulation of known pathological proteins in ALS, as well as previously unreported proteins and phosphoproteins associated with ALS. Additionally, the previously unknown proteomic results show a pathological link to other neurodegenerative diseases. Therefore, tailoring the privileged scaffold of antioxidant EDR with the added advantage of boron (*vide infra*) has the potential to increase upon the marginal therapeutic benefits provided by current therapies. Overall, the translation of the statistically significant survival benefit and slowing of disease progression reported herein, via the selective targeting of oxidative stress by NS-1-2 (**Borsantrazole™**), a trifunctional boron-based pyrazole, offers an opportunity to develop a best-in-class ALS therapeutic. In addition, the reported changes in the global proteome and phosphoproteome may represent novel druggable targets in ALS. Furthermore, as a part of an early-phase drug development project, the EDR prodrug NS-1-2 was trademarked

as Borsantrazole™ following a strong international search report (ISR) from the World Intellectual Property Organization (WIPO) for its novelty, inventive step, industrial applicability, and utility. In the present work, we report that Borsantrazole has demonstrated superior efficacy compared to currently approved therapies in ALS mouse models and holds the potential to become a ‘best-in-class’ treatment for ALS with further clinical development. Borsantrazole introduces a novel approach to small organic molecule targeting global oxidative stress, which may reduce neuronal deterioration and serve as a potential therapeutic option for other neurodegenerative diseases characterized by oxidative stress.

Key Words: Amyotrophic lateral sclerosis, hydrogen peroxide, SOD1, oxidative stress, edaravone, Borsantrazole™, SOD1-G37R ALS mouse model.

Short Abstract

Amyotrophic lateral sclerosis (ALS) is a heterogeneous and fatal motor neurodegenerative disease. Since ALS was discovered in 1869, only two FDA-approved drugs, Edaravone (EDR) and Riluzole, have had clinically validated impacts on disease progression. However, preclinical studies of these approved drugs in SOD1 ALS mouse models haven't shown any survival benefits. Here, we report the discovery and development of a boron-based improved version of FDA-approved EDR, which could modify motor disease phenotypes in SOD1 ALS mice models, demonstrating target engagement. Using a novel green chemistry approach, we synthesized four boron-based EDR analogues and EDR prodrugs (B5-EDR). All six compounds showed excellent safety and efficacy in vitro. Single and daily doses of NS-1-2 (10mg/kg) (Borsantrazole™) caused no tissue toxicity in wild-type mice; furthermore, presymptomatic NS-1-2 treatment in G37R (42) mice effectively modified clinical motor disease phenotypes. Moreover, the untargeted biomarker analysis showed differential protein expression in the brain and spinal cord of SOD1 ALS mice, supporting the therapeutic potential of NS-1-2. Furthermore, the lead compound NS-1-2 is registered as a trademark under the name **Borsantrazole™ (BSZ)** and is protected by a patent. It is supported by a comprehensive international search report from the World Intellectual Property Organization, ***PCT/CA2023/051352 (WO/2024/103151)***, which affirms its novelty, inventive step, industrial utility, and industrial applicability.

Key Words: Amyotrophic lateral sclerosis, hydrogen peroxide, SOD1, oxidative stress, edaravone, Borsantrazole™, SOD1-G37R ALS mouse model.

Graphical Abstract

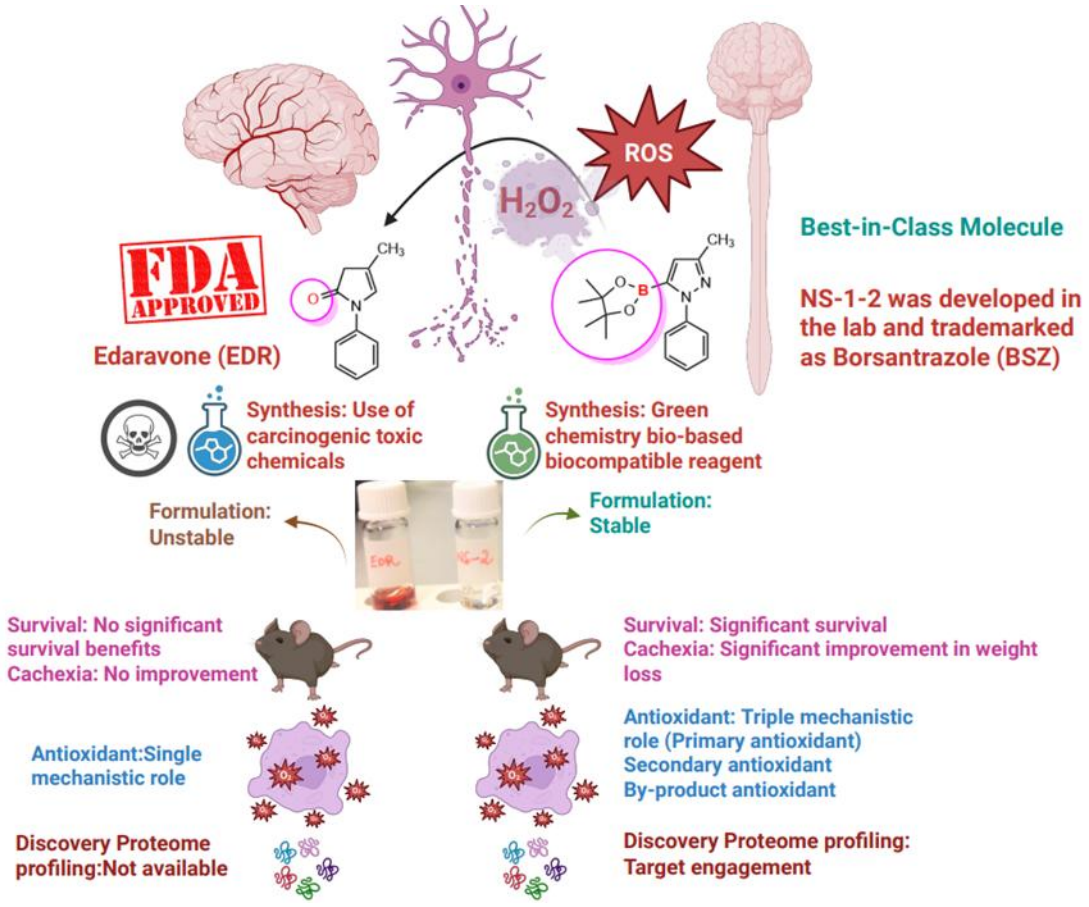

Artificial Intelligence Training Statement:

"Except as otherwise permitted by any open licensing applied to this work, the author expressly reserves all rights to use of this work for Generative Artificial Intelligence training, the development of machine learning language models, and similar technologies. Where open licensing applies to this work, the author expresses their preference to opt out of the preceding uses." This addresses modern copyright concerns.

Table of Contents

1 Introduction 36

1.1 Neurodegeneration 36

1.2 Amyotrophic lateral sclerosis 37

1.2.1 Epidemiology: Incidence and prevalence of amyotrophic lateral sclerosis 39

1.2.2 Contributing risk factors for amyotrophic lateral sclerosis 40

1.2.3 Physical exertion 40

1.2.4 Smoking 41

1.2.5 Excitotoxicity 41

1.2.6 Oxidative stress and metal ions 45

1.3 Hydrogen peroxide as a double-edged sword in the living cells 48

1.4 Antioxidant superoxide dismutase enzyme 51

1.5 Role of neurotoxic hydrogen peroxide (H_2O_2) in misfolding of SOD1 53

1.6 Current treatment options available to treat amyotrophic lateral sclerosis and their drawbacks 64

1.6.1 Patient compliance 66

1.6.2 Pharmacokinetics 66

1.6.3 Stability 67

1.6.4 Synthetic route 68

1.7 Structure-Activity Relationship (SAR) of EDR (3-methyl-1-phenyl-2-pyrazolin-5-one) 70

1.8 Boron in drug discovery 72

1.8.1 Boron: A potential element 72

1.8.2 Boric Acid containing boron with a low toxicological profile 77

1.8.3 Potential of boron-containing compounds in neurodegenerative diseases 80

1.8.4 Evidence showing effects of boron-containing compounds in neurons as neuroprotective Agents 80

1.8.5 Neuroprotective role of boric acid, a by-product of boron-containing compounds 83

1.8.6 Kinetics of boron-containing compounds with different free radicals 86

1.8.7 Added advantages of boron scaffold: pharmacokinetics, chemo selectivity, blood-brain barrier permeability, and non-toxic by-products 87

1.8.8 Cross-talk between boron and the most prevalent free radical, hydrogen peroxide (H_2O_2): Role in ALS disease progression 96

2 Overall summary of research approaches....99

2.1 Rationale/Research Questions/Hypothesis/Objectives and AIMS 99

2.2 Overall research aim....103

2.3 Overall research hypothesis 103

2.4 Rationale for proposed hypothesis....105

3 Research approaches: Hypothesis/Aims/Objectives 109

3.1 **Objective 1:** The synthesis of a series of B5-EDR prodrugs and B5-EDR analogues. 109

3.1.1 **Specific Aim 1 for Objective 1:** To synthesize and characterize boron-based edaravone prodrugs (B5-EDR)....109

3.1.2 **Specific Aim 2 for Objective 1:** To synthesize and characterize additional boron-based edaravone analogues (B5-EDR)....109

3.2 **Objective 2:** The *in vitro* transformation of B5-EDR prodrugs into EDR to establish a 'proof-of-concept' that our compounds can serve as prodrugs of EDR. 110

3.2.1 **Specific Aim 1 for Objective 2:** To demonstrate the Proof-of-concept *in vitro* transformation applying a novel synthetic procedure for synthesizing EDR from Boron-based prodrugs (B5-EDR). 110

3.2.2 **Specific Aim 2 for Objective 2:** To demonstrate the Proof-of-concept *in vitro* transformation applying a novel NMR kinetic experiment for conversion of EDR from Boron-based prodrugs (B5-EDR)....110

3.3 **Objective 3:** To study the *in vitro* properties and antioxidant abilities of our drug candidates and examine their capabilities to serve as ROS/RNS scavengers. 111

3.3.1 **Specific Aim 1 for Objective 3:** To evaluate the neurotoxicity and cell viability of B5-EDR prodrugs and analogues on neuroblastoma-spinal cord hybrid cells (NSC-34) and primary cortical neuronal cells by WST-8 analysis, in comparison to EDR. 111

3.3.2 **Specific Aim 2 for Objective 3:** To evaluate the neuroprotective effects of B5-EDR prodrugs and analogues against hydrogen peroxide-induced oxidative stress on NSC-34 cells by WST-8 analysis, in comparison to EDR. 111

3.3.3 **Specific Aim 3 for Objective 3:** To evaluate the change in mitochondrial membrane potential by B5-EDR prodrug (NS-1-2) using staurosporine as a positive control for apoptosis in comparison to EDR. 111

3.3.4 **Specific Aim 4 for Objective 3:** To evaluate the hydrogen peroxide (H_2O_2) scavenging ability of B5-EDR prodrugs (NS-1-2) using an Amplex red assay in comparison to EDR. 111

3.4 **Objective 4:** To study the effect of NS-1-2 on fibrillization of SOD1 monomers. 111

3.4.1 **Specific Aim 1 for Objective 4:** To evaluate the biochemical activity of our drug candidates in reducing the fibrillization of SOD1 monomers. 111

3.5 **Objective 5:** To study the acute and chronic safety profile with longitudinal monitoring of NS-1-2 in the wild-type mice. 112

3.5.1 **Specific Aim 1 for Objective 5:** To evaluate the acute toxicity profile (single dose), with longitudinal monitoring of NS-1-2 in a wild-type mouse *in vivo*. 112

3.5.2 **Specific Aim 2 for Objective 5:** To evaluate the chronic toxicity profile (120 doses), with longitudinal monitoring of NS-1-2 in a wild-type mouse *in vivo*. 112

3.6 **Objective 6:** To study the therapeutic effects of NS-1-2 in modifying disease phenotypes in the humanized SOD1-G37R (line 42) mouse model of amyotrophic lateral sclerosis. 113

3.6.1 **Specific Aim 1 for Objective 6:** To evaluate the efficacy of NS-1-2, in terms of delaying the onset of disease in SOD1-G37R (line 42) mouse model of amyotrophic lateral sclerosis: Time to peak body weight (days). 113

3.6.2 **Specific Aim 2 for Objective 6:** To evaluate the efficacy of NS-1-2, in terms of delaying the symptom onset of disease in SOD1-G37R (line 42) mouse model of amyotrophic lateral sclerosis: Loss of 10% body weight based on the highest recorded weight (days) with muscle weakness. 113

3.6.3 **Specific Aim 3 for Objective 6:** To evaluate the efficacy of NS-1-2, in terms of extending the survival age/life span of SOD1-G37R (line 42) mouse model of amyotrophic lateral sclerosis: Principal primary endpoint of preclinical studies. 113

3.6.4 **Specific Aim 4 for Objective 6:** To evaluate the efficacy of NS-1-2, in terms of preventing weight loss (ALS-induced cachexia) in SOD1-G37R (line 42) mouse model of amyotrophic lateral sclerosis: Prognostic marker for ALS. 113

3.6.5 **Specific Aim 4 for Objective 6:** To evaluate the efficacy of NS-1-2, in terms of improving clinical motor phenotypes with longitudinal monitoring in SOD1-G37R (line 42) mouse model of amyotrophic lateral sclerosis: Marker of motor neurodegeneration. 113

3.7 **Objective 7:** To apply global mass-spectrometry-based proteomic and phosphoproteomic approaches to discover and identify biomarkers within treated SOD1-G37R mice, B5-EDR prodrug NS-1-2 versus sham controls. 114

3.7.1 **Specific Aim 1 for Objective 7:** To investigate the mechanism of a novel (NS-1-2), utilizing a discovery-based untargeted/unbiased LC-MS based global proteomics approach for the investigation/and discovery of known/and novel biomarkers correlating with the efficacy of NS-1-2 in the spinal cord of mutant human G37R SOD1 mice. 114

3.7.2 **Specific Aim 1 for Objective 7:** To investigate the mechanism of a novel (NS-1-2), utilizing a discovery-based untargeted/unbiased LC-MS based global proteomics approach for the investigation/and discovery of known/and novel biomarkers correlating with the efficacy of NS-1-2 in the brain of mutant human G37R SOD1 mice. 114

3.7.3 **Specific Aim 2 for Objective 7:** To investigate the mechanism of a novel (NS-1-2), utilizing a discovery-based untargeted/unbiased discovery LC-MS-based global phosphoproteome approach for the investigation/and discovery of known/and novel biomarkers correlating with the efficacy of NS-1-2 in the spinal cord of mutant human G37R SOD1 mice. 114

3.7.4 **Specific Aim 2 for Objective 7:** To investigate the mechanism of a novel (NS-1-2), utilizing a discovery-based untargeted/unbiased discovery LC-MS-based global phosphoproteome approach for the investigation/and discovery of known/and novel biomarkers correlating with the efficacy of NS-1-2 in the brain of mutant human G37R SOD1 mice. 114

3.8 **Objective 8:** To apply global mass spectrometry-based proteomic approaches to discover and identify biomarkers from samples collected at symptom onset, clinical end of study, and humane endpoint within treated SOD1-G37R mice, B5-EDR prodrug NS-1-2 versus sham controls. 115

4 Results 115

4.1 Scheme I for the synthesis of the first prodrug of Edaravone 115

4.2 Scheme II for the synthesis of the second prodrug of Edaravone 116

4.3 Scheme III for the synthesis of boron-based Edaravone analogues (B5-EDR) from *N*-arylated substituted pyrazole boronic acid pinacol ester 118

4.4 Scheme IV Synthesis of 4-fluoro-*N*-arylated pyrazole boronic acid pinacol ester from 4-fluoro-*N*-arylated substituted pyrazole starting material via a two-step synthetic procedure *in situ* 118

4.5 Scheme III (a) for the synthesis of Edaravone from boron-based prodrugs (B^5-EDR) 120

4.5.1 First approach for biotransformation: Using both lactic acid and hydrogen peroxide. 120

4.6 Scheme III (b) for the synthesis of Edaravone from boron-based prodrugs (B^5-EDR) 121

4.6.1 Second approach for biotransformation: Using only hydrogen peroxide. 121

4.7 Green, bio-inspired, catalyst-free method for the synthesis of Edaravone from its boron-based prodrug (NS-1-2). *In vitro* proof of concept of H_2O_2-induced oxidative transformation of B5-EDR to Edaravone 122

4.8 Putative mechanism for biotransformation of boron-based Edaravone prodrug NS-1-2 into Edaravone (EDR) 124

4.9 The advantages of an optimized and efficient microwave synthesis of Edaravone .. 125

4.10 NMR kinetics experiments to validate the proof of concept for the conversion of Edaravone from its prodrug NS-1-2 126

4.11 Neurotoxicity and cell viability analysis 132

4.11.1 NSC-34 cell line as a suitable model to study ALS 132

4.11.2 Primary cortical neuronal cell cultures (PCNC) 132

4.11.3 WST-8 Assay (WST-8 Metabolism End point) 133

4.11.4 Effect of Edaravone prodrug (NS-1-2, NS-1-21) and Edaravone analogues (NS-1-12, NS-1-13, and NS-1-19) on neurotoxicity/cell viability of NSC-34 cells and PCNC 134

4.11.5 Neurotoxicity effect of hydrogen peroxide (H_2O_2) on NSC-34 cells 138

4.11.6 Neuroprotective effect of Edaravone prodrug (NS-1-2, NS-1-21) and Edaravone analogues (NS-1-12, NS-1-13, and NS-1-19) on NSC-34 cells 139

4.12 Effects of Edaravone and Edaravone prodrug NS-1-2 on the mitochondrial membrane potential (ΔΨM) of NSC-34 cells, using staurosporin as a positive control for apoptosis 149

4.12.1 Principle for JC-10 Assay 149

4.12.2 Staurosporine as an Apoptotic Agent 150

4.13 Hydrogen peroxide (H_2O_2) scavenging ability of EDR prodrug NS-1-2.....152

4.14 Anti-SOD1 monomer fibrillization activity of EDR prodrug NS-1-2 thioflavin T fluorescence (ThT) 155

4.14.1 Strength of the Study 157

4.14.2 Important observations 157

4.15 A single dose (acute toxicity assessment) of Edaravone prodrug NS-1-2 and 120 daily doses (chronic toxicity assessment) of NS-1-2 for 120 days, with longitudinal monitoring, demonstrate a satisfactory safety profile.....163

4.15.1 Morphological alteration:.....163

4.15.2 Assessment of body weight 166

4.15.3 Histopathological findings 169

4.16 Longitudinal preclinical study with Edaravone prodrug NS-1-2 delayed disease onset in SOD1-G37R mouse model of ALS.....176

4.17 Edaravone prodrug NS-1-2 delayed the progression of symptom onset, defined as age to reach 10% weight loss, with muscle weakness, in the SOD1-G37R mouse model of ALS 179

4.18 Edaravone prodrug NS-1-2 prolongs the life span and increases survival in the SOD1-G37R mouse model of ALS 182

4.19 Edaravone prodrug NS-1-2 prevents ALS-induced weight loss or cachexia in the SOD1-linked model of ALS.....185

4.20 Edaravone prodrug NS-1-2, with longitudinal monitoring, improves several motor clinical phenotypes in the SOD1-G37R mouse model of ALS.....188

4.21 Proteomic and phosphoproteomic analyses reveal differentially regulated proteins in lumbar spinal cord samples from the SOD1-G37R mouse model of ALS, correlating with the efficacy of Edaravone prodrug NS-1-2 192

4.22 Proteomic and phosphoproteomic analyses reveal differentially regulated proteins in the brain samples from the SOD1-G37R mouse model of ALS, correlating with the efficacy of Edaravone prodrug NS-1-2 200

4.23 Edaravone prodrug NS-1-2 ameliorated symptom onset (symptom onset, defined as age to reach 10% weight loss, with muscle weakness) in SOD1-G37R mouse model of ALS 207

4.24 Longitudinal symptom onset biomarker study: Proteomic analyses reveal differentially regulated proteins in lumbar spinal cord samples from the SOD1-G37R mouse model of ALS, correlating with the efficacy of Edaravone prodrug NS-1-2 211

5 Discussions 215

6 Significance of the study 257

7 Limitations of the study 264

8 Future directions of the study 267

9 Conclusions 277

10 Total number of compounds synthesized 282

11 Materials, methods, and characterization of organic molecules 282

11.1 Experimental 282

11.2 Representative experimental procedure for synthesis of *N*-arylated pyrazole boronic acid pinacol ester was carried out according to the below reported procedure with slight modifications, as shown in the Scheme I 283

11.2.1 Characterization 284

11.3 Representative procedure for synthesis of *N*-arylated pyrazole potassium trifluoroborates from *N*-arylated substituted pyrazole boronic acid pinacol ester was carried out according to the below-reported procedure with slight modifications 285

11.3.1 Characterization 286

11.4 Microwave synthesis of Edaravone from its prodrug (NS-1-2) 3-methyl-5-(4,4,5,5-tetramethyl-1,3,2-dioxaborolan-2-yl)-1-phenyl1H-pyrazole. Utilizing scheme III (a) 287

11.4.1 Characterization....288

11.5 Scheme IV for the synthesis of Boron-based Edaravone analogue (*N*-arylated pyrazole boronic acid pinacol ester) via a two-step synthetic procedure in situ....289

11.5.1 Characterization....289

11.6 Representative experimental procedure for synthesis of 3-trifluoro-methyl-5-(4,4,5,5-tetramethyl-1,3,2-dioxaborolan-2-yl)-4-Fluoro-1-phenyl1H-pyrazole was carried out according to the below-reported procedure with slight modifications....291

11.6.1 Characterization....292

11.7 Representative experimental procedure for NMR kinetics....293

11.8 Methodology for neurotoxicity/cell viability analysis of EDR prodrug NS-1-2 in primary cortical neuronal cells (PCNC)....293

11.9 Methodology for neurotoxicity/cell viability analysis of EDR prodrug NS-1-2 in neuroblastoma-spinal cord hybrid (NSC-34) cells....294

11.10 Methodology for neuroprotective effect/cell viability analysis of EDR prodrug NS-1-2 in neuroblastoma-spinal cord hybrid (NSC-34) cells....295

11.11 Methodology for assessment of mitochondrial membrane potential (ΔΨM) as an indicator of neurotoxicity in NSC-34 cells using JC-10 probe....296

11.12 Methodology for amplex red assay to determine the hydrogen peroxide (H_2O_2)-scavenging ability of EDR and NS-1-2....296

11.13 Methodology for SOD1 monomer fibrillization assay using thioflavin T fluorescence297

11.14 Animal models....298

11.15 Mice and tissue preparation....300

11.16 DNA isolation and genotyping....300

11.17 Group assignment, drug formulation, storage, and administration of compound group assignment for determination of acute toxicity in wild-type SOD1mice....301

11.18 Group assignment, drug formulation, storage, and administration of compound for determination of chronic toxicity in wild-type SOD1 mice....302

11.19 Drug formulation, storage, and route of administration determination for the acute and chronic toxicity evaluation in the wild-type SOD1 mice....303

11.20 Hematoxylin and eosin (H&E) staining and microscopy 303
11.21 Group assignment for evaluation of therapeutic efficacy in terms of delaying the disease onset, symptom onset, extending survival, and decreasing weight loss (cachexia) of EDR prodrug BSZ, in direct comparison to the control/sham group in the human SOD1-G37R mouse model of ALS 305
11.22 Definitions and criteria for determining disease onset and symptom onset 305
11.22.1 Criteria for disease onset 306
11.22.2 Criteria for symptom onset 306
11.23 Injection sites and determination of sample size for efficacy studies of BSZ 306
11.24 The rationale for the presymptomatic treatment start date 307
11.25 Discovery-based untargeted and unbiased proteomics on human mutant G37R mouse lumbar spinal cord and brain tissue samples 309
11.25.1 Tissue sample preparation 309
11.25.2 Proteolytic digestion 309
11.25.3 Phosphopeptide enrichment 310
11.25.4 LC-MS/MS analysis of the spinal cord proteome 310
11.25.5 LC-MS/MS analysis of the spinal cord phosphoproteome 311
11.25.6 Data analysis of the spinal cord proteome 311
11.25.7 Data analysis of the spinal cord phosphoproteome 313
11.25.8 LC-MS/MS analysis of the brain proteome 314
11.25.9 Data analysis of the brain proteome 315
11.26 Discovery-based untargeted and unbiased LC-MS/MS analysis of symptom onset biomarker proteome of human mutant G37R ALS mice model 315
11.26.1 Data analysis symptom onset proteome 316
11.27 Statistical analysis 317
12 References 318
13 Appendices 347
13.1 Appendix Figure 1: Chromatogram of NS-1-2 (BSZ) 347

13.2 Appendix Figure 2: ^{1}HNMR of NS-1-2 (BSZ) 348
13.3 Appendix Figure 3: ^{13}CNMR of NS-1-2 (BSZ) 349
13.4 Appendix Figure 4: ^{11}BNMR of NS-1-2 (BSZ)....350
13.5 Appendix Figure 5: HRMS of NS-1-2 (BSZ)....351
13.6 Appendix Figure 6: ESI of NS-1-2 (BSZ)....352
13.7 Appendix Figure 7: ^{1}HNMR of NS-1-21....353
13.8 Appendix Figure 8: ^{13}CNMR of NS-1-21 354
13.9 Appendix Figure 9: HRMS of NS-1-21 355
13.10 Appendix Figure 10: Chromatogram of NS-1-10(EDR) 356
13.11 Appendix Figure 11: ^{1}HNMR of NS-1-10 (EDR) 357
13.12 Appendix Figure 12: ^{13}CNMR of NS-1-10 (EDR)....358
13.13 Appendix Figure 13: HRMS of NS-1-2 (EDR) 359
13.14 Appendix Figure 14: ^{1}HNMR of NS-1-12....360
13.15 Appendix Figure 15: ^{13}CNMR of NS-1-12 361
13.16 Appendix Figure 16: HRMS of NS-1-12 362
13.17 Appendix Figure 17: ^{1}HNMR of NS-1-19....363
13.18 Appendix Figure 18: ^{13}CNMR of NS-1-19 364
13.19 Appendix Figure 19: HRMS of NS-1-19 365
13.20 Appendix Figure 20: ^{1}HNMR of NS-1-23....366
13.21 Appendix Figure 21: ^{13}CNMR of NS-1-23 367
13.22 Appendix Figure 22: ^{19}FNMR of NS-1-23....368
13.23 Appendix Figure 23: HRMS of NS-1-23 369

List of Figures

Figure 1. Schematic presentation of various biochemical cross-talks, involving calcium ion (Ca^{+2}), ferrous ion (Fe^{+2}), and Zinc ion (Zn^{+2}) implicated in the progression of neurodegenerative diseases like Alzheimer's disease (AD), Parkinson's disease (PD), and amyotrophic lateral sclerosis (ALS). 43

Figure 2. Schematic presentation of various biochemical cross-talks and their detrimental manifestations (**A**–**I**) in the brain provoked by oxidative stress and their implications in the progression of neurodegenerative diseases like Alzheimer's disease (AD), Parkinson's disease (PD), and amyotrophic lateral sclerosis (ALS). 46

Figure 3. Role of H_2O_2 in controlling the oxidative redox balance of the cell at different concentrations 50

Figure 4. Structure of superoxide dismutase1 (SOD1) dimer (pdb code:1SPD). 53

Figure 5. The X-ray crystallographic structure of wild-type SOD1 (wSOD1). 59

Figure 6. A hypothetical model implicating how pathological concentrations of hydrogen peroxide (H_2O_2) trigger the toxic gain-of-function of superoxide dismutase (SOD1). 62

Figure 7. Structure of the primary phase II metabolite of EDR excreted in urine. 67

Figure 8. Mechanism for the release of Edaravone (EDR). 68

Figure 9. Knorr pyrazole synthesis of EDR. 70

Figure 10. Structure-Activity Relationship (SAR) of Edaravone (EDR). 72

Figure 11. Diagram showing the potential of Boron (B). 75

Figure 12. Boron (B) in drug discovery. FDA-approved (B) containing compounds. 76

Figure 13. Self-association of boric acid to boroxines. 77

Figure 14. Boron-containing compounds are used as neuroprotective agents. 83

Figure 15. Free radicals directed oxidation product of coumarin-based boronic acid to highly fluorescent hydroxycoumarin, using a user-friendly probe. 87

Figure 16. A. Schematic representation of the chemo-selective reactive oxygen species (ROS)-triggered prodrug concept. 90

Figure 17. Boron-containing compounds serve as chemoselective prodrugs in various disease pathologies. 93

Figure 18. Boron-containing compounds are used as A. chemoselective fluorescent sensors and B. chemoselective prodrug of methotrexate. 96

Figure 19. Boron-containing compounds as chemo-selective prodrugs used in neurodegenerative disease. 96
Figure 20. Various emerging roles of boron (B) heterocycles in the drug discovery of CNS therapeutics. 98
Figure 21. Hypothetical representation of the proposed research. 104
Figure 22. Mechanism to show how (B^5-EDR) analogues act as redox regulators (in vivo reaction with H_2O_2) and prodrugs/generation for EDR. 105
Figure 23. Overall rationale for the proposed hypothesis and research work. 108
Figure 24. Scheme I for synthesizing N-arylated pyrazole boronic acid pinacol ester NS-1-2 from the commercially available N-arylated substituted pyrazole. 116
Figure 25. Scheme II for synthesizing N-arylated pyrazole potassium trifluoroborates (NS-1-21) from the commercially available N-arylated substituted pyrazole. 117
Figure 26. Synthesis of 4-flouro-N-arylated pyrazole boronic acid pinacol ester from 4-fluoro-N-arylated substituted pyrazole starting material. 119
Figure 27. Scheme III (a) synthesis of EDR from its prodrug (B5-EDR). 120
Figure 28. Scheme III (b) synthesis of EDR from its prodrug (B5-EDR). 121
Figure 29. Schematic illustration of a hydrogen peroxide (H_2O_2) triggered boron-based prodrug approach. 123
Figure 30. Schematic proposed mechanism to show how NS-1-2 could act as a redox regulator prodrug under an oxidative cellular environment (in vivo biotransformation with H_2O_2) for the generation of EDR. 124
Figure 31. The TLC observation demonstrated that, in the presence of H_2O_2, NS-1-2 containing boronate was oxidized to generate Edaravone (EDR) with keto-enol. 128
Figure 32. 1H NMR spectra illustrating the chemical shift values (ppm) of control samples before hydrolysis. 129
Figure 33. 1H NMR spectra illustrate the chemical shift (ppm) values, demonstrating the time-course conversion of NS-1-2 to edaravone (EDR). 130
Figure 34. 1H NMR spectra illustrate the chemical shift (ppm) values, demonstrating the time-course conversion of NS-1-2 to edaravone (EDR). 131
Figure 35. WST-8 conversion to colored formazan. 134
Figure 36 (a,b,c). Evaluation of neurotoxicity/cell viability profile of Edaravone (EDR), EDR prodrug (NS-1-2, NS-1-21), and EDR analogues (NS-1-12, NS-1-13, NS-1-19) on

neuroblastoma-spinal cord hybrid NSC-34 cells using WST-8 analysis (a marker of neurotoxicity) in vitro. 135
Figure 37 (a). Diagram illustrating the schematic of the neurotoxicity and cell viability experiment on primary cortical neuronal cells (PCNC), (b, c,d). 137
Figure 38. Evaluation of neurotoxicity/cell viability profile of hydrogen peroxide (H_2O_2) on neuroblastoma-spinal cord hybrid NSC-34 cells using WST-8 analysis (a marker of neurotoxicity) in vitro. 138
Figure 39 (a,b,c,d,e). Evaluation of neuroprotective profile of Edaravone (EDR), EDR prodrug (NS-1-2, NS-1-21), and EDR analogues (NS-1-12, NS-1-13, NS-1-19) against hydrogen peroxide (H_2O_2) induced oxidative stress on neuroblastoma-spinal cord hybrid cells by WST-8 analysis in vitro. 141
Figure 40. A demonstration of the stability of Edaravone (EDR), its prodrugs (NS-1-2, NS-1-21), and EDR analogues (NS-1-12, NS-1-13, and NS-1-19) in cold aerobic environments..... 143
Figure 41. Evaluation of neuroprotective profile of boric acid (H_3BO_3), against hydrogen peroxide (H_2O_2) induced oxidative stress on neuroblastoma-spinal cord hybrid cells by WST-8 analysis in vitro. 147
Figure 42. Schematic putative mechanism to show the effects of boric acid (BA), when given in combination with edaravone (EDR) in neuroblastoma-spinal cord hybrid cells in vitro..... 149
Figure 43. (a) Schematic diagram showing the brief experimental plan for the determination of mitochondrial membrane potential (ΔΨM) in NSC-34 cells..... 151
Figure 44. Schematic diagram showing the brief experimental plan for the determination of hydrogen peroxide (H_2O_2) scavenging ability of B5-EDR prodrugs (NS-1-2) using an Amplex red assay in comparison to EDR. 153
Figure 45 (a). Schematic diagram showing the brief experimental plan for the determination of hydrogen peroxide (H_2O_2) scavenging ability of B5-EDR prodrugs (NS-1-2) using an Amplex red assay in comparison to EDR. 154
Figure 46. Schematic diagram showing the brief rationale for the determination of the anti-SOD1 monomer fibrillization ability of B5-EDR prodrug (NS-1-2) using Thioflavin T (ThT) Assay. 158
Figure 47. Anti-SOD1 monomer fibrillization activity. 159
Figure 48. Anti-SOD1 monomer fibrillization activity. 161
Figure 49. Structural activity relationship of 3-Methyl-1-Phenyl Pyrazole and the effects of substituents at its C-5 position on anti-SOD1 monomer fibrillization activity. 162

Figure 50. Schematic diagram showing acute toxicity evaluation and treatment plan, with corresponding longitudinal monitoring (14 days) and n=6 for each group (3 male and 3 female). 163
Figure 51. Schematic diagram showing chronic toxicity evaluation and treatment plan, with corresponding longitudinal monitoring (120 days) and n=6 for each group (3 male and 3 female). 164
Figure 52. Chronic NS-1-2 treatment showed no NS-1-2-associated clinical signs of toxicity in both sexes. 165
Figure 53. a) Diagram depicting a single-dose acute toxicity treatment study plan. **b)** Diagram depicting 120 doses of chronic toxicity treatment study plan for 120 days. 166
Figure 54. Results of acute and chronic toxicity assessments on mean body weight over 14 days (acute) and 120 days (chronic) starting at 60 and 90 days of age, respectively. 168
Figure 55. Photomicrographs of Hematoxylin and Eosin (H&E) stained sections of wildtype (WT) SOD1, male mice from acute toxicity evaluation. 170
Figure 56. Photomicrographs of Hematoxylin and Eosin (H&E) stained sections of wildtype (WT) SOD1, female mice from acute toxicity evaluation. 171
Figure 57. Photomicrographs of Hematoxylin and Eosin (H&E) stained sections of wildtype (WT) SOD1, male and female mice from chronic toxicity evaluation. 173
Figure 58. Photomicrographs of Hematoxylin and Eosin (H&E) stained sections of wildtype (WT) SOD1, male and female mice from chronic toxicity evaluation. 174
Figure 59. Schematic illustration of the experimental plan with different clinical stages of progression of disease in G37R(42) mice. 177
Figure 60. Schematic illustration of the experimental plan for the preclinical study in Humanized mutSOD1G37R(42) mice. 178
Figure 61. Edaravone prodrug NS-1-2 delays the disease onset (based on age to peak body weight before weight begins to decline). 178
Figure 62. Edaravone prodrug NS-1-2 delays the symptom onset or early symptom progression (age to reach 10% weight loss, with muscle weakness). 181
Figure 63. Edaravone prodrug NS-1-2 extends the lifespan in SOD1-G37R ALS mice. 184
Figure 64. Edaravone prodrug NS-1-2 rescued weight loss in SOD1-G37R ALS mice. 187
Figure 65. Representative pictures showing the longitudinal assessment of various gross motor clinical phenotypes and the effects of treatment BSZ in modifying the motor disease clinical phenotypes in G37R ALS mice. 191

Figure 66 (a,b,c). Differential analysis of global proteome changes in hmutSOD1-G37R ALS mice. 195
Figure 67. Overview of the sample processing workflow for LC/MS-based global proteomics and phosphoproteomics from the brain samples of G37R male mice. 203
Figure 68. Differential analysis of global proteome changes in hmutSOD1-G37R ALS mice. 204
Figure 69. Differential analysis of global proteome changes in hmutSOD1-G37R ALS mice. 204
Figure 70. Diagram outlining the experimental plan for symptom onset biomarker study with end-of-study clinical humane endpoint in SOD1-G37R ALS mouse model of ALS. 209
Figure 71. Edaravone prodrug NS-1-2 rescued ALS-induced weight loss at clinical symptom onset. 210
Figure 72. Overview of the sample processing workflow for LC/MS-based global proteomics and phosphoproteomics from the lumbar spinal cord samples of G37R female mice. 214
Figure 73. Differential analysis of symptom onset global proteome changes in hmutSOD1-G37R ALS mice. 214
Figure 74. Schematic illustration of the targeted delivery of a triple-role boron-based pyrazole BSZ as an ALS therapeutic. 220
Figure 75. Schematic picture illustrating several advantages of proteomics, demonstrating proof of principle and translational value from ALS mouse models to human ALS cases. 240
Figure 76. Schematic illustration of the putative mechanism of NS-1-2 based on the differential expression of proteins in an unbiased, untargeted discovery-based global proteomics approach. 246
Figure 77. Prodrug of Edaravone (NS-1-2). 285
Figure 78. Prodrug of Edaravone (NS-1-21). 286
Figure 79. Edaravone (NS-1-10). 289
Figure 80. Scheme IV synthesis of EDR analogues. 289
Figure 81. Boron Edaravone (B5-EDR) analogue (NS-1-12). 290
Figure 82. Boron Edaravone (B5-EDR) analogue (NS-1-12). 290
Figure 83. Boron Edaravone (B5-EDR) analogue (NS-1-23). 293
Figure 84. Diagram outlining the definition of pathological stages of the SOD1-G37R ALS mice mouse model of ALS. 306

List of Tables

Table 1. Synthesis of the first boron-based EDR **(B5-EDR)** prodrug NS-1-2. 116
Table 2. Synthesis of second boron-based EDR **(B5-EDR)** prodrug. 117
Table 3. Synthesis of boron-based EDR **(B5-EDR)** analogues. 119
Table 4. Synthesis of EDR from (B5-EDR) prodrugs**.** 121
Table 5. Total number of age and sex-matched SOD1-G37R (42) mouse model used to evaluate the efficacy of the Edaravone prodrug NS-1-2 (BSZ). 191
Table 6. Selected known and novel proteins with significantly differential abundance (adj p<0.05; n=4) in the lumbar spinal cord of human mutantSOD1 G37R male mice treated with NS-1-2 and sham (vehicle) based on quantitative proteomics. 194
Table 7. List of 51 proteins with significantly differential abundance (adj p<0.05; n=4) in the lumbar spinal cord of human mutantSOD1 G37R male mice treated with BSZ, and sham (vehicle), discovery-based, unbiased global quantitative proteomics. 196
Table 8. List of 29 phosphoproteins with significantly differential abundance (adj p<0.05; n=4) in the lumbar spinal cord of human mutantSOD1 G37R male mice treated with BSZ, and sham (vehicle), discovery-based, unbiased global quantitative phosphoproteomics. 198
Table 9. Summary of known and novel proteins with significantly differential phosphorylation (adj. p<0.05; n=4) in the lumbar spinal cord of mutant SOD1 G37R male mice treated with BSZ and sham (vehicle), based on quantitative phosphoproteomics. For a full summary of the phosphoproteomics data for NS-1-2 and Sham (vehicle) samples, see **Table 8**. 199
Table 10. List of 44 proteins with significantly differential abundance (adj p<0.05; n=4) in the brain of human mutantSOD1 G37R male mice treated with BSZ, and sham (vehicle), discovery-based, unbiased global quantitative proteomics. 201
Table 11. Selected known and novel proteins with significantly differential abundance (adj p<0.05; n=4) in the brain of human mutantSOD1 G37R male mice treated with NS-1-2 and sham (vehicle) discovery-based, unbiased global quantitative proteomics. 202
Table 12. Summary of known and novel proteins with significantly differential phosphorylation (adj. p<0.05; n=4) in the lumbar spinal cord and brain of mutant SOD1 G37R male mice treated with NS-1-2 and sham (vehicle), based on quantitative phosphoproteomics and their pathological association and role with various neurological diseases. 205
Table 13. List of 7 proteins with significantly differential abundance (adj p<0.05; n=3) in the lumbar spinal cord of human mutantSOD1 G37R male mice treated with BSZ, and sham (vehicle), discovery-based, unbiased global quantitative proteomics. 212

Table 14. Selected known and novel proteins with significantly differential abundance (adj p<0.05; n=3) in the lumbar spinal cord of human mutantSOD1 G37R male mice treated with BSZ, and sham (vehicle) based on quantitative proteomics. 213

Abbreviations

Amyotrophic lateral sclerosis (ALS); upper motor neurons (UMN); lower motor neurons (LMN); Edaravone (EDR); Riluzole (RLZ); Borsantrazole™ (BSZ); familial ALS (fALS); sporadic ALS (sALS); hydrogen peroxide (H_2O_2); primary cortical neuronal cell cultures (PCNC); neuroblastoma-spinal cord hybrid NSC-34 (NSC-34); K-nearest neighbor (KNN); Complexin 2 (Cplx2), Low-density lipoprotein receptor-related protein 4 (Lrp4); sequestosome 1 (Sqstm1/p62); Gigaxonin(Gan/KLHL16); sorting nexin-13 (Snx13); Neurofilament light chain (Nefl); and Neurofilament Heavy Chain (Nefh); Phosphoglycerate kinase 1 (Pgk1) ;2-oxo-3-(phenylhydrazono)butanoic acid (OPB) ; superoxide dismutase 1 (SOD1); hydroxyl radical (HO•); reactive oxygen species (ROS); N-butyl lithium (n-BuLi); directed Ortho metalation (DOM); isopropoxy 4,4,5,5-tetramethyl-1,3,2-dioxaborolane (PINBOP); diethyl ether (DEE); neuroblastoma-spinal cord (NSC); Dulbecco's modified eagle medium (DMEM); Central Animal Care Services (CACS); Polymerase Chain Reaction (PCR); dithiothreitol (DTT) ; acetonitrile (ACN) ; trifluoracetic acid (TFA); data-dependent acquisition mode (DDA) ;K-nearest neighbor (KNN) ; World Health Organization (WHO); RDH: Redox dyshomeostasis; MND: Motor neurodegenerative disease ;Cu/Zn SOD, SOD1: Copper/zinc superoxide dismutase; mSOD1: Mutant SOD1;ROS: Reactive oxygen species ;sALS: Sporadic ALS ;fALS: Familial ALS; SOD1: Superoxide dismutase 1; H_2O_2: Hydrogen peroxide ;TDP-43: TAR-DNA binding protein 43 ;NCI: Neuronal cytoplasmic inclusions; AD: Alzheimer's disease; PD; Parkinson's disease; HD; Huntington's disease; (O_2): Molecular oxygen; Fe: Iron; Cu: Copper; Complex IV: Cytochrome c oxidase; ($O_2^{\bullet-}$): Superoxide radical anion ; ($HO^{\bullet}$): Hydroxyl radical; Met: Methionine; Cys: Cysteine; (-SOH): Sulphenic acid; (SH): Sulhydryl

or thiol group; (-S-S-): Disulphide bond; (-SO_2H): Sulfinic acid (-SO_3H): Sulfonic acid; ($NO^{\bullet}$): Nitric oxide radical ;($ONOO^{-}$): Peroxynitrite; RNS: Reactive nitrogen species; 3-NT 3-nitrotyrosine; PTMs: Post translational modifications; HOCl: Pypochlorous acid; (-OOH): Hydroperoxide nucleophile;(O−O): Peroxide; ($-S^{-}$): Thiolate;(SN2); Bimolecular nucleophilic substitution;(QM-MM): Quantum-classical molecular dynamics simulations; (Ca^{+2}): calcium ion; NOXs: NAD(P)H oxidases; OP: oxidative potential; 4-HNE: 4-Hydroxy-2-Nonenal; Fe^{+2}: Ferrous ion; Fe^{+3}: Ferric ion; C9ORF72: Chromosome 9 open reading frame 72;FUS : RNA-binding protein fused in Sarcoma; Tg: Transgenic; Zn: Zinc; hSOD1: HumanSOD1; Km: Michaelis constant; Kcat: turnover number of the *enzyme*;(Cu, E SOD): Zn deficient SOD; MalPEG: Maleimide-polyethylene glycol; ThT: Thioflavin T; SH-SY5Y: Neuroblastoma *cell line*; CSF: Cerebro spinal fluid. NS-shuttle: Nucleocytoplasmic shuttle. NDDs: Neurodegenerative diseases; AD: Alzeimer's disease; PD: Parkinson's disease; ATP: Adenosine triphosphate; Cu/Zn SOD, SOD1: Copper/zinc superoxide dismutase; OS: Oxidative stress; RATM: Redox active transition metals; Fe^{+2}: Ferrous ion; Cu^{+}: Cuprous ion; (O): Oxygen; (N): Nitrogen; CCS: Chaperone for SOD1; CcO: Cytochrome c oxidase; (-S-S-): Disulphide bond; Zn: Zinc; TBARS: Thiobarbituric acid reactive substances; HNE: 4-Hydroxynonenal; 8-OHG: 8-hydroxyguanosine; 8-OHdG: 8-hydroxy-2′-deoxyguanosine; DNA/RNA: Deoxyribonucleic acid/Ribonucleic acid; NOXs: NAD(P)H oxidases; (ONOO−): Peroxynitrite; 3-NO2Tyr: 3-nitrotyrosine; (-OOH): Hydroperoxide; (ROO.): Lipid peroxides; (NO•): Nitric oxide radical (Zn^{+2}): Zinc ion; (Ca^{+2}): Calcium ions; EAAT: Excitatory amino acid transporters;EAAT2: Excitatory amino acid transporter 2; AMPA: Alpha-amino-3-hydroxy-5-methylisoxazole-4-propionic acid; ER: Endoplasmic reticulum;(NMDAR): N-methyl-D-aspartic acid

receptors; ΔpH: Proton gradient; PLA2: Phospholipase A2; PGE2: Prostaglandin E2; SOD1: Superoxide dismutase; sHSPs: Small heat shock proteins; mTOR: Mammalian target of rapamycin; CNS: Central nervous system; PINK1: PTEN-induced kinase 1; (Nf): Neurofilaments; pNf: Phosphorylated neurofilament; CSF: Cerebrospinal fluid; NfL: Neurofilament light chain; pNFH: Phosphorylated neurofilament heavy chain; MQC: Mitochondrial quality control.

1 Introduction

1.1 Neurodegeneration

Neurodegeneration refers to the pathological condition where there is a progressive death and loss of function of neurons in the brain and spinal cord. Neurons are the basic unit of the central nervous system (CNS), and they are incapable of self-repair and regeneration. Neurodegenerative diseases (NDDs) are devastating and incurable, causing problems with movement (ataxias) or resulting in neurological conditions called dementias[1].

To date, there is no well-defined cause of neurodegenerative diseases. However, aging is regarded as the most important contributor to the development of NDDs such as Alzheimer's disease (AD), Parkinson's disease (PD), Huntington's disease (HD), and amyotrophic lateral sclerosis (ALS) or Lou Gehrig's disease. Thus, it is anticipated that the incidence of neurodegenerative disease will increase due to the increasing average age of the global population. Due to the unknown cause(s) of NDDs, there is no definitive treatment available. However, substantial research has shown that the misfolding or aggregation of specific proteins that are induced by reactive oxygen species (ROS) and reactive nitrogen species (RNS) serves as a hallmark of NDDs[2]. Over 57 million people worldwide are affected by NDDs, a number projected to double every two decades. Despite this increasing prevalence, no cures currently exist, and treatment options are limited. Challenges include clinical disease heterogeneity, lengthy preclinical and prodromal stages, a poor understanding of underlying mechanisms, and difficulties in diagnosis[3].

1.2 Amyotrophic lateral sclerosis

The excerpt below has been adapted from the published manuscript with some modifications for the thesis. Please see the full published paper in the appendix.

Sanghai, N.; Tranmer, G.K. Hydrogen Peroxide and Amyotrophic Lateral Sclerosis: From Biochemistry to Pathophysiology. *Antioxidants* 2022, *11*, 52. https://doi.org/10.3390/antiox11010052

ALS is a motor neurodegenerative disease (MND) that is due to the gradual deterioration of voluntary muscle function due to progressive loss of the lower and upper motor neurons. It is a progressive paralytic disorder that causes degeneration of motor neurons in the brain and spinal cord[4]. The disease was first described in 1869 by French neurologist Jean-Martin Charcot. Therefore, ALS is also known as Charcot's disease in honour of the first person who described it[4]. The disease became well known in the United States (US) when famous baseball player Lou Gehrig was diagnosed with the disease and died at the age of 37 years[5]. Early symptoms of ALS generally include muscle weakness. Slowly, all voluntary muscles are wasted throughout the body, and eventually, the brain loses its ability to control voluntary body movements. Individuals suffering from ALS lose their strength, ability to speak, eat, move, and even breathe, although their intellect is largely unaffected[5]. Eventually, people with ALS die due to respiratory failure, usually within 3-5 years after first diagnosis[4, 6]. ALS is the most common MND, and it accounts for 80-90% of all MND cases[7]. There is an increasing number of patients diagnosed with ALS globally. Recent reports have shown that the incidence of ALS is between 0.6 and 3.8 per 100,000 persons-years[8-11]. Recent studies have reported that the prevalence of ALS is between 4.1 and 8.4 per 100,000 persons[11-

15], showing the increase in the burden of ALS globally[15]. ALS is characterized by two forms, sporadic (sALS) and familial (fALS). The most common form of this disease is sALS (90-95%), the aetiology of which is still unknown, and there is no apparent genetic component associated. The remaining (5-10%) of the cases are fALS, which is due to the association of a dominant genetic inheritance factor[5].

ALS is a highly complex, incurable, idiopathic illness and a life-threatening disease. It is thought to be a multifactorial disease, with no single cause being well established to date[16]. In 1993, mutations in the superoxide dismutase (SOD1) gene encoding Cu,ZnSOD1 protein were reported as the first genetic link to fALS[17]. Presently, more than 185 mutations are reported in the SOD1 gene[18, 19]. Recent updates show the presence of more than 200 SOD1 variants, primarily due to missense variants[20].

The most common cause of ALS is a mutation of the SOD1 gene encoding the ubiquitous antioxidant enzyme SOD1[21]. Due to the high incidence of SOD1 mutations, which account for 20-25% of fALS cases, representing 1-2% of all ALS cases, SOD1 is regarded as the most comprehensively studied gene. It is one of the prime targets to find therapeutic options for the treatment of ALS[22]. fALS, which includes mutant SOD1 (mSOD1), among other mutations, is almost identical to the late-onset, classical form of ALS called sALS. Both of these forms of ALS are clinically indistinguishable and both share common clinical features, such as the presence of inclusion bodies, motor neuron death and dysfunction, and glial reactivity[23]. The only difference between SOD1-fALS and classic sALS is that individuals with sALS have an average age of onset of 56 years, compared with 46 years for fALS with SOD1 mutations[24]. The variability in the clinical course of disease presentation among fALS patients is observed due to the presence of

various genetic mutations in the SOD1 gene, which is similar in the case of sALS[25]. Research has shown that fALS cases are mainly due to the mutations of four genes: The chromosome 9 open reading frame 72 (C9ORF72)[26], SOD1[17], RNA-binding protein fused in Sarcoma (FUS)[27] and TAR DNA binding protein 43 (TDP-43)[28].

A large body of evidence suggested that SOD1 plays a critical role in the pathogenicity of both forms of ALS, i.e., fALS and sALS, and is a common protein, which is pathologically associated with both forms. In the case of fALS, a mutation in the SOD1 gene called mSOD1 causes the misfolding of the SOD1 protein. On the other hand, in the case of sALS, non-genetic post-translational modifications (PTMs), such as loss of metal, disruption of quaternary structure, and oxidation of human wild-type SOD1 protein by free radicals, could cause misfolding of the SOD1 protein[25, 29]. These aberrant conformations cause wtSOD1, in the case of sALS, to acquire the same toxic function that is observed for fALS-associated mSOD1variants[21, 22, 25, 30, 31]. Moreover, previous studies have established that the misfolding of the SOD1 protein is the major culprit in causing the loss of around 70% of spinal cord motor neurons[32-37]. In addition, a breakthrough in ALS animal models was the discovery of SOD1 transgenic mutant mice like ($SOD1^{G93A}$Tg), ($SOD1^{G37R}$Tg) or ($SOD1^{G85R}$Tg). These mSOD1mice developed a motor neuron disease with many pathological changes reminiscent of human ALS[38] and further increased our understanding towards the association of the SOD1 gene in ALS[39].

1.2.1 Epidemiology: Incidence and prevalence of amyotrophic lateral sclerosis

Approximately 80% of people diagnosed with ALS worldwide die within 2 to 5 years[40]. ALS currently affects 2.16 in 1,000,000 people per year in Europe. Also, the incidence of

this disease is higher in men (3.0 in 100,000 per year) than in women (2.4 in 100,000 per year). The peak age range for onset of the disease is 58-63 years for sporadic cases (i.e., without family history) and 47-52 years for familial cases[41]. There is a report of 1 or 2 new cases of ALS every year per 100,000 people in Europe and the United States. The prevalence of ALS in the USA is 5 in every 100,000 people. About 10% of cases are familial, and the remaining 90% are sporadic. The first symptoms of ALS can manifest as early as 12 months prior to diagnosis[42]**.** Approximately more than 200,000 people worldwide are living with ALS; of these, more than 3,000 Canadians are suffering from ALS[43]. Furthermore, 1000 Canadians are diagnosed annually, while a similar number die from the disease in the same year[43]. Recently, it has been proposed that there will be a huge surge in ALS cases from 222,801 in 2015 to 376,674 in 2040, representing an epidemiologic increase of 69%[44].

1.2.2 Contributing risk factors for amyotrophic lateral sclerosis

The pathogenesis of ALS is still unknown. Extensive research is being conducted to understand the etiology of this life-threatening and heterogeneous disease. Recent knowledge states that ALS etiology is multifactorial, having complex genetic mechanisms and molecular pathways[45]**.** Below are some risk factors of this incurable disease.

1.2.3 Physical exertion

Intense sports and physical activity during one's lifetime can increase the risk of ALS**.** Retrospective studies from the Italian Football League showed that the probability was higher for the development of ALS in football/soccer players[46]**.** Recent studies conducted by Chapman and his colleagues[47] investigated strenuous, anaerobic physical activity as a risk factor for ALS. Additionally, a study by Julian and his team[48]

employed the Mendelian randomisation approach and, interestingly, found a positive causal relationship between ALS and physical exercise. Exercise is likely to cause motor neuron injury only in patients with a specific genetic risk. However, further research is warranted to establish a link between exercise and ALS.

1.2.4 Smoking

A study by the European Prospective Investigation Cohort showed that cigarette smoking is one of the most significant contributing factors for developing ALS in a dose-dependent manner[49]**.** Furthermore, research from large longitudinal studies supports the hypothesis that cigarette smoking raises the risk of ALS. The significance of the age at which smoking begins and the absence of a clear dose-response relationship warrant further research[50].

1.2.5 Excitotoxicity

The excerpt and the schematic diagram below have been adapted from the published manuscript with some modifications for the thesis. Please see the full published paper in the appendix.

Sanghai, N.; Tranmer, G.K. Biochemical and Molecular Pathways in Neurodegenerative Diseases: An Integrated View. *Cells* 2023, *12*, 2318.

https://doi.org/10.3390/cells12182318

Glutamate-induced excitotoxicity is one of the risk factors for the pathogenesis of ALS. Excessive excitation of *N*-methyl-D-aspartic acid receptors (NMDAR) and α-amino-3-hydroxy-5-methyl-4-isoxazolepropionic acid (AMPA) receptors by glutamate in the postsynaptic membranes of motor neurons triggers neuronal death through the activation

of calcium influx (Ca^{+2}) into the cytosol and mitochondria. This excitotoxicity results in oxidative stress through the release of pathogenic free radicals and is thereby implicated in the progression of motor neurodegeneration[51, 52]**.**

The biochemical mechanism that triggers excitotoxicity involves alterations of glutamate receptors, mainly NMDAR, which are highly permeable to (Ca^{+2}) and sodium ions (Na^{+})[53]. The prolonged or excessive activation of glutamate receptors initiates a cascade of molecular pathways, including cation influx, mitochondrial dysfunction, oxidative stress, and overproduction of ROS[54]. Mounting evidence shows that calcium ions ($Ca^{2+)}$ play a crucial role in the biochemical pathways of ALS[55, 56] and other neurodegenerative diseases, including AD[57] and PD[58]. This involves excitotoxic neurotransmitter glutamate, Zn^{+2}, and Fe^{+2}, along with the cascade known as the neurotoxic excitotoxicity cascade[59-62]**(Figure 1).**

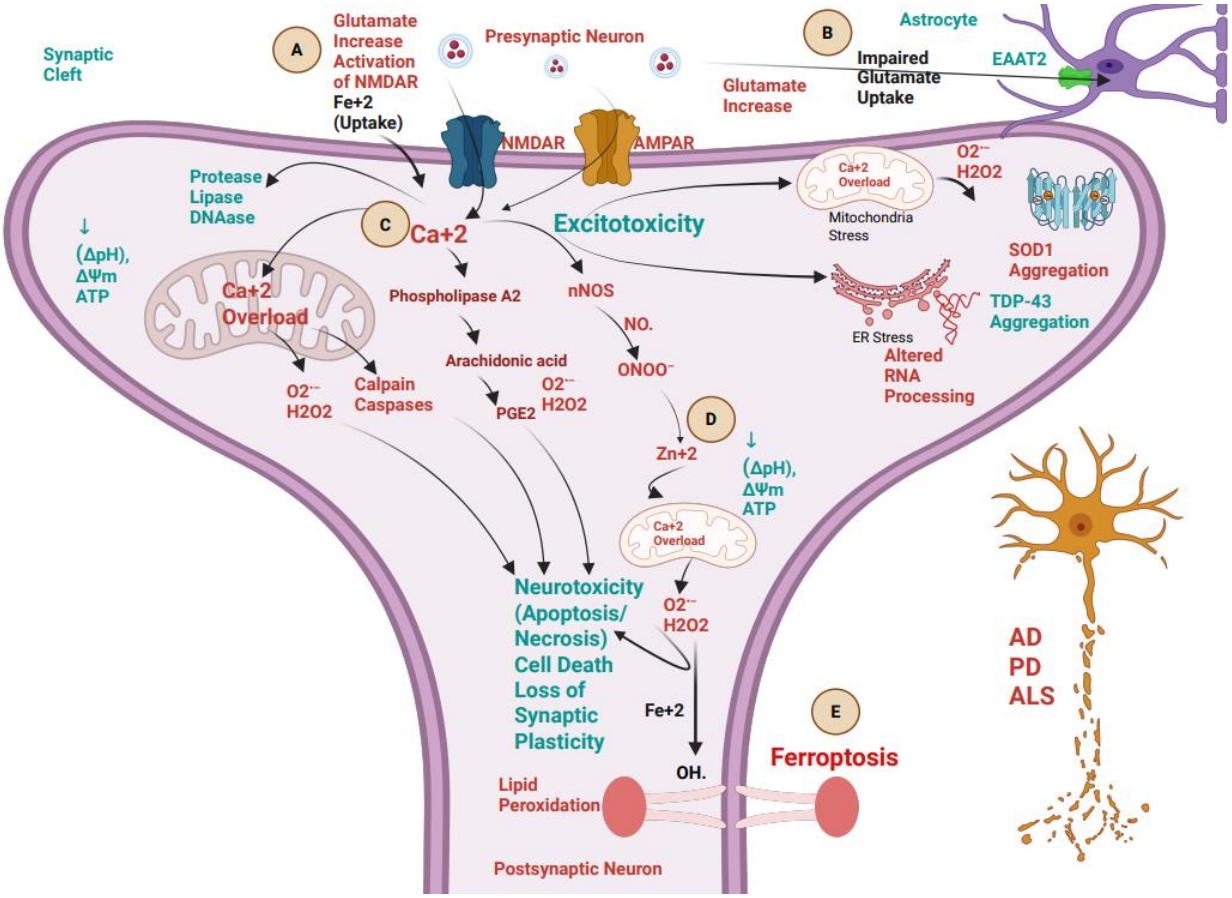

Figure 1. Schematic presentation of various biochemical cross-talks, involving calcium ion (Ca^{+2}), ferrous ion (Fe^{+2}), and Zinc ion (Zn^{+2}) implicated in the progression of neurodegenerative diseases like Alzheimer's disease (AD), Parkinson's disease (PD), and amyotrophic lateral sclerosis (ALS).

(A). Excitotoxicity (neuronal death) is triggered by the excessive release of the excitatory neurotransmitter glutamate (neurotoxic) from the presynaptic neuron and leads to activation of various biochemical cascades, leading to neurotoxicity and hence, neuronal death. This process is initiated by the activation of *N*-methyl-D-aspartic acid receptors (NMDARs) by excessive glutamate at postsynaptic neurons, thereby releasing and accumulating toxic intraneuronal Ca^{2+}. (B). Glutamate-mediated excitotoxicity is

increased because of the astrocyte-mediated downregulation of excitatory amino acid transporters 2 (EAAT2), which slows down the uptake of glutamate from the synaptic cleft and incites the excitotoxicity cascade. (C). Ca2+ overload initiates most of the deleterious downstream mechanisms of the cascade, through increasing Ca2+ overload in mitochondria, induction of proteases (calpains and caspases), decreasing the proton gradient (ΔpH), mitochondrial membrane potential (ΔΨm) and adenosine triphosphate (ATP), activation of phospholipase A2 (PLA2) pathway initiating downstream activation of arachidonic acid and prostaglandin E2 (PGE2), aggravation of mitochondrial and endoplasmic reticulum stress leading to superoxide dismutase (SOD1) and TAR DNA-binding protein (TDP-43) aggregation. (D). Surge of reactive oxygen species (ROS) like hydrogen peroxide (H_2O_2) and hydroxyl radical (HO•), and reactive nitrogen species (RNS) like nitric oxide (NO•) radical, formation of peroxynitrite anion (ONOO−) increases the intraneuronal Zn^{2+} mobilization, which targets mitochondria and further exacerbates Ca^{2+} dysregulation and ROS production. (E). Ca^{+2} and Fe^{+2} dysregulation participates in the ferroptosis death of neurons. Iron dysregulation leads to Ca^{2+} dysregulation and vice versa. Excessive glutamate increases Fe^{+2} intake inside neurons, thereby leading to excitotoxicity and lipid peroxidation via Fenton's reaction, a process known as ferroptosis.

1.2.6 Oxidative stress and metal ions

The excerpt and the schematic diagram below have been adapted from the published manuscript with some modifications for the thesis. Please see the full published paper in the appendix.

Sanghai, N.; Tranmer, G.K. Biochemical and Molecular Pathways in Neurodegenerative Diseases: An Integrated View. *Cells* 2023, *12*, 2318.

https://doi.org/10.3390/cells12182318

The human brain weighs merely ~1400 g; however, it consumes ~20% of the total basal oxygen (O_2) budget to power its ~86 billion neurons and their highly complex synapses, fueled by adenosine triphosphate (ATP) formed in mitochondria. The O_2 we breathe is a mutagenic gas, due to its diradical and triplet spin state, and is implicated in the formation of the precursors of all free radicals via superoxide anion radical ($O_2^{\bullet-}$)[63]. The ($O_2^{\bullet-}$) undergoes a chemical redox reaction to produce reactive oxygen species (ROS) or reactive nitrogen species (RNS) including non-radicals, free radicals, and anions, such as hydrogen peroxide (H_2O_2), hydroxyl radical ($HO^{\bullet}$), and peroxynitrite ($ONOO^-$), causing an imbalance in cellular homeostasis called oxidative stress (OS) **(Figure 2)**.

OS is primarily implicated in the biochemical pathophysiology of ALS and NDDs like AD and PD[64]. Emerging evidence from various scientific studies over the years has demonstrated the critical importance of redox balance in the CNS. Furthermore, numerous metal ions like ferrous ion (Fe^{2+}) and cuprous ion (Cu^{+}), Zinc ion (Zn^{+2}), and bio-reactive free radicals act as common factors in altering redox signaling, thereby initiating pathological processes in neuronal degeneration in the case of ALS[65-68] and

other NDDs like AD[69] and PD[68]. Additionally, these metals and OS biomarkers serve as universal hallmarks of neurodegeneration across all NDDs[62] **(Figure 2).**

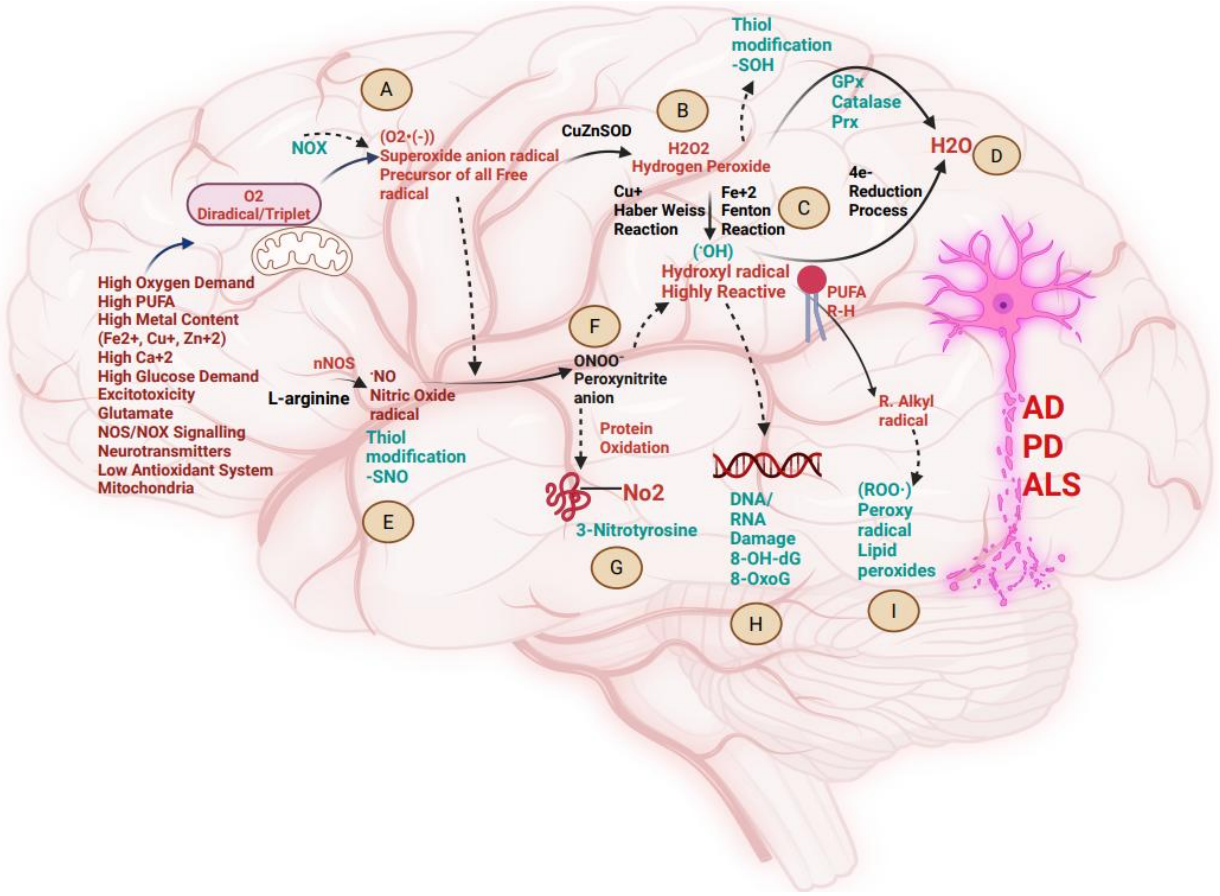

Figure 2. Schematic presentation of various biochemical cross-talks and their detrimental manifestations (**A**–**I**) in the brain provoked by oxidative stress and their implications in the progression of neurodegenerative diseases like Alzheimer's disease (AD), Parkinson's disease (PD), and amyotrophic lateral sclerosis (ALS).

Brain is highly vulnerable to oxidative stress due to low regenerative capacity, enrichment of polyunsaturated fatty acids, high dependency on mitochondria for adenosine triphosphate (ATP) generation, elevated glucose demand, high concentration of metals like ferrous ion (Fe^{+2}), cuprous ion (Cu^{+}), zinc ion (Zn^{+2}) and calcium ion (Ca^{+2}),

glutamate-induced excitotoxicity, high oxygen (O_2) consumption, and relatively low antioxidant system. These multiple factors initiate various reaction pathways to create redox imbalance called oxidative and nitrosative stress in the brain, implicated in multiple NDDs. (**A**)**.** The triplet unstable O_2 undergoes reduction to produce the precursor of all radicals called superoxide anion radical ($O_2^{\bullet -}$) via NAD(P)H oxidases (NOXs) pathway, i.e., one-electron trans-membrane transfer to (O_2) [95]. (**B**)**.** Antioxidant superoxide dismutase (SOD1) undergoes dismutation to scavenge ($O_2^{\bullet -}$) to produce hydrogen peroxide (H_2O_2). (**C**)**.** The weakly liganded (Fe^{+2}) and (Cu^{+}) undergo reduction to produce nature's most vulnerable oxidant hydroxyl radical ($HO^{\bullet}$) through Fenton's reaction and Haber-Weiss reaction. (**D**)**.** The final 4th electron reduction of H_2O_2 in the presence of antioxidants, like glutathione peroxidase (Gpx), catalase (cat), and peroxiredoxin system (Prx), forms water (H_2O). (**E**)**.** Overactivation of neuronal nitric oxide synthase (nNOS) produces nitric oxide ($NO^{\bullet}$) radicals from L-arginine, which create nitrosative stress by modification of thiol group (SH) containing proteins. (**F**)**.** Excessive superoxide anion radicals lead to inactivation of nitric oxide production and switch the biology to production of highly potent oxidant peroxynitrite anion ($ONOO^{-}$), which leads to the nitrosative stress by (SH) modification of free tyrosine (Tyr) residues to form 3-nitrotyrosine (3-NO2Tyr) (**G**), which acts as a versatile biomarker of nitrosative stress and NDDs. (**H**)**.** Highly reactive and mutagenic oxidant ($HO^{\bullet}$) damages the nucleic acid deoxyribonucleic acid/ribonucleic acid (DNA/RNA) to form oxidative products 8-hydroxy-2′-deoxyguanosine(8-OHdG) and (8-OxoG), and acts as a universal biomarker for oxidative stress and NDDs (important to note that guanine is the most oxidation prone nucleobase because of low reduction potential [96]). Furthermore, the HO•radical causes lipid peroxidation in lipid-rich neuronal

membranes, leading to neuronal cell death. Lipid peroxides (ROO·) act as a biomarker of oxidative stress and NDDs. Created with BioRender.com.

1.3 Hydrogen peroxide as a double-edged sword in the living cells

The excerpt and the schematic diagram below have been adapted from the published manuscript with some modifications for the thesis. Please see the full published paper in the appendix.

Sanghai, N.; Tranmer, G.K. Hydrogen Peroxide and Amyotrophic Lateral Sclerosis: From Biochemistry to Pathophysiology. *Antioxidants* 2022, *11*, 52. https://doi.org/10.3390/antiox11010052

Hydrogen peroxide (H_2O_2) acts both as a redox signaling molecule and an oxidative stress molecule. As a signal transduction molecule, H_2O_2 has a role in controlling various key cellular processes like cell shape changes, initiating proliferation, recruitment of immune cells, calcium ion (Ca^{+2}) signaling in the lumen of endoplasmic reticulum, and mitochondria-associated membranes[70, 71]. It acts as a secondary messenger in insulin signalling and in several growth factor-induced signaling cascades[70]. Also, H_2O_2 is involved in the chemical modifications of specific Cys amino acids, which are expressed in some cellular proteins[72]. H_2O_2 generated during physiological oxidative stress conditions in the concentration of around (1–10 nM) acts as a redox signalling molecule in various cellular processes, creating oxidative eustress, although, higher or pathological concentration of H_2O_2 of around (> 100 nM) is known to cause deleterious effects to cellular biomolecules; this effect is called oxidative distress **(figure 3)**[73]. According to

many reports, the higher pathological concentration of H_2O_2 in oxidative stress conditions can go up to 150μM[30, 74, 75].

Various studies have been conducted to examine the concentration at which the H_2O_2 acts as a cytotoxic and neurotoxic agent. Further, multiple studies have investigated the mode of cell death caused by H_2O_2, mainly due to apoptosis or necrosis[76-78]. It was found that the effects of H_2O_2 are largely dependent upon the mode of cell death induced (apoptosis or necrosis) depending on the cell type used, its physiological state, length of exposure to H_2O_2, the H_2O_2 concentration used, and the cell culture media employed[76, 79]. Yoshiro and colleagues (2006)[80], investigated that 50μM of H_2O_2 exhibited caspase-9 and caspase-3 activation, finally leading to apoptotic cell death in human T-lymphoma Jurkat cells, whereas a higher concentration of 500 μM caused necrotic death. Teramoto and the group (1999)[81], demonstrated that a lower concentration of 10-100 μM predominantly caused apoptosis, however, a higher concentration of 1-10mM induced necrosis in human lung fibroblasts cells. Troyano and associates (2003)[82], demonstrated caspase-9 and caspase-3 activation and death by apoptosis in U-937 human promonocytic cells, when treated with 200 μM H_2O_2. Although, treatment with 2 mM H_2O_2 caused necrosis. Gulden and the group (2010)[74], investigated in detail how exposure time and cell concentration affect the cytotoxic potency of H_2O_2 *in vitro*. They found that the median cytotoxic concentrations decreased from 500 to 30 μM as the incubation time increased from 1 to 24 hours. The cytotoxic effects of H_2O_2 were also evaluated in neuroblastoma × spinal cord motor neuron cell line (NSC34). A short (30 min) exposure to H_2O_2 caused delayed cell death with the median effective concentration (EC_{50}) of ~1 mM[83]. Also, treatment of 500 μM H_2O_2 for 24h in a hippocampal neuronal

cell line (HT-22) induces around 50% of cell death[84]. Further investigation of exposure to 1 mM H_2O_2 for 2 hours on human embryonic kidney 293 cells (HEK293) *in vitro*, cells displayed the extent of programmed cell death, characterized by condensed chromatin and apoptotic nuclei[85]. The above-reported studies and various other studies[86-90] elucidated the H_2O_2 concentration-dependent change in cell signalling and death. A very low concentration of H_2O_2 causes cell signalling and hence, cell growth, a mid-higher concentration of around (120 µM to 150 µM) induces a temporary growth arrest, the intermediate concentration of (250 µM -400 µM) causes permanent growth arrest, and a higher concentration of (≥1mM) causes cell damage by necrosis and hence death[91].

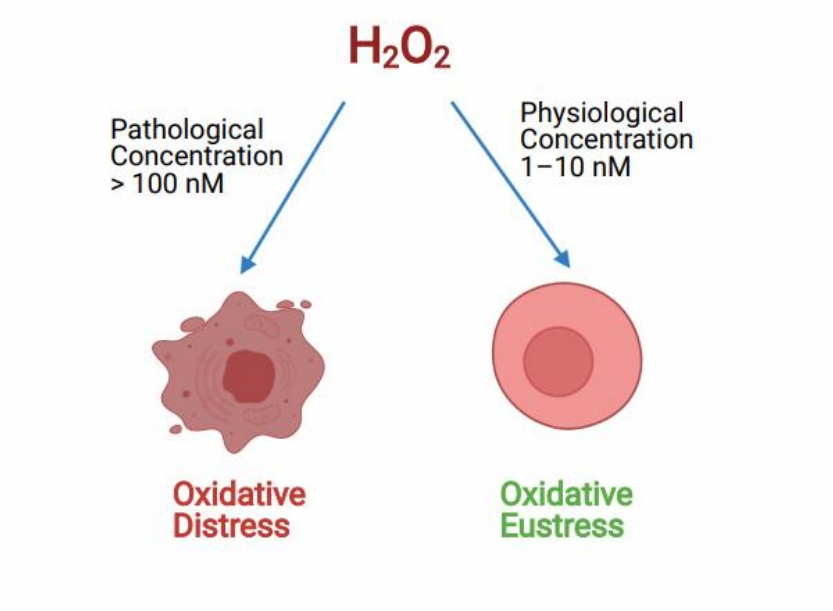

Figure 3. Role of H_2O_2 in controlling the oxidative redox balance of the cell at different concentrations.

Hydrogen peroxide (H_2O_2) regulates the cell signaling process at physiological concentrations, known as oxidative Eustress. Whereas, at pathological concentrations, H_2O_2 causes cell death due to oxidative stress.

1.4 Antioxidant superoxide dismutase enzyme

The excerpt and the schematic diagram below have been adapted from the published manuscript with some modifications for the thesis. Please see the full published paper in the appendix.

Sanghai, N.; Tranmer, G.K. Hydrogen Peroxide and Amyotrophic Lateral Sclerosis: From Biochemistry to Pathophysiology. *Antioxidants* 2022, *11*, 52. https://doi.org/10.3390/antiox11010052

SOD1 is a highly conserved member of the human superoxide dismutase (SOD) family of proteins, which also includes SOD2 and SOD3. All three proteins are distinct from each other and act as antioxidants by scavenging $O_2^{\bullet-}$ to H_2O_2[92]. SOD1 is mainly found in the cytosol and the inner membrane of the mitochondria[93] and comprises ~1% of the total protein in the cell[94]. SOD2 is found mainly in the mitochondrial matrix. Contrary to SOD1 and SOD2, SOD3 is mostly located outside the cell in the extracellular matrix. Another major difference is that SOD1 is a homodimer while SOD2 and SOD3 are homotetrameric proteins; SOD1 and SOD3 catalyse the dismutation of $O2^{\bullet-}$ through dismutation of Cu^{+2}, whereas SOD2 utilizes manganese (Mn) as a redox-active transition metal for dismutation. The SOD1 isoform of the protein is mainly involved in the pathology of ALS[25].

The Eukaryotic SOD1 is a stable homodimer[95]. The dimer is held together principally by hydrophobic interactions. Each SOD1 monomer contains two transition metal ions, one Cu and one Zinc (Zn), both of which play an essential catalytic and structural role in the enzyme[95]. SOD 1 is a 32 kDa homodimeric SOD1 protein and adopts an eight-stranded Greek key beta-barrel structural motif. Homodimerization of the SOD1 protein

reduces the solvent accessible area, making it more stable. The fully metalated form of SOD1 protein melts at 85-95°C[96]. Two functional loops are present in SOD1: the electrostatic loop that guides superoxide into the redox active site, where (Cu^{+2}) and the Zn-binding loop are located[29, 95]. The catalytic Cu is coordinated to SOD1 by four histidine(46,48,63, and 120) residues in oxidised form Cu^{+2} and three histidine residues (46,48, and 120) in its reduced form(Cu^{+1})[97, 98]. The structurally vital Zn ion acts as a monodentate ligand and is thought to play an important role in maintaining the structure of SOD1 and acts as a positive charge ion sink. The Zn ion is coordinated by three histidines (63,71 and 80) and one aspartate (83). Coordination of Cu to SOD1 is required for its catalytic dismutation activity to scavenge $O_2^{\bullet-}$ [93] through a ping pong mechanism **(Figure 4)**[29]. Other PTMs like coordination of Zn^{2+}, modulating the folding free energy of SOD1[99], and oxidation of a (-S-S-), are important to form the mature, structurally stable SOD1 protein. A distinctive functional feature of SOD1 is the presence of an intra-subunit (-S-S-) between Cys^{57} and Cys^{146} (C^{57}–C^{146}), which is atypical for proteins that reside in the highly reducing environment of the cytosol[91, 95].

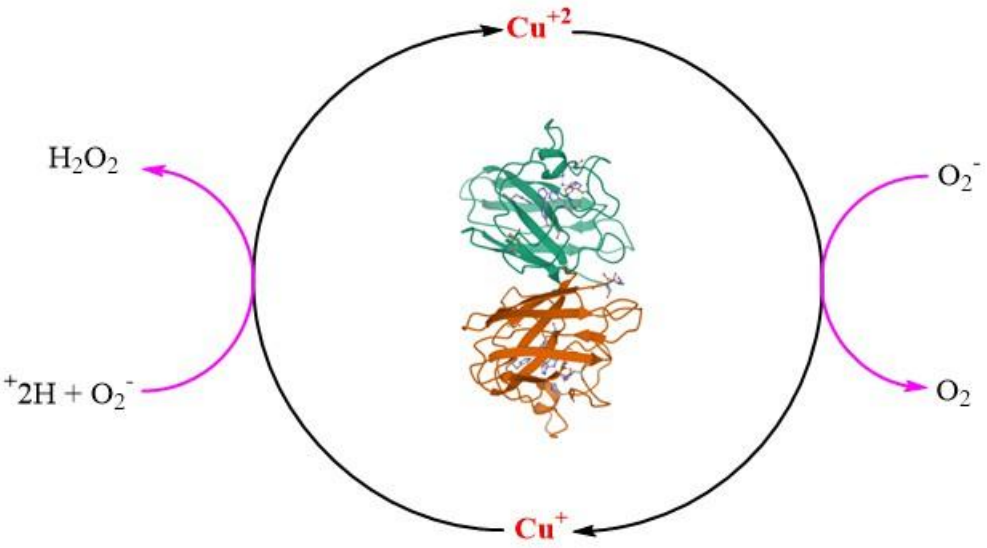

Figure 4. Structure of superoxide dismutase1 (SOD1) dimer (pdb code:1SPD). The catalytic role of copper (Cu) in the dismutation reaction of superoxide radical anion ($O_2^{\bullet -}$).

1.5 Role of neurotoxic hydrogen peroxide (H_2O_2) in misfolding of SOD1

The excerpt and the schematic diagram below have been adapted from the published manuscript with some modifications for the thesis. Please see the full published paper in the appendix.

Sanghai, N.; Tranmer, G.K. Hydrogen Peroxide and Amyotrophic Lateral Sclerosis: From Biochemistry to Pathophysiology. *Antioxidants* 2022, *11*, 52. https://doi.org/10.3390/antiox11010052

As evidenced by the above literature findings, it can be said that ALS is a highly complex disease, and its molecular mechanism and etiology remain unknown and unresolved. However, a large body of evidence has shown that SOD1 is the major protein that serves as a hallmark in the ALS disease progression. Current research and findings have primarily identified two leading hypotheses, which are believed to play a crucial role in ALS disease. Firstly, increased oxidative stress causes SOD1 toxicity, and secondly, toxicity caused by aberrant misfolding of the SOD1 protein structure. These two factors are interrelated to each other[100]. Before going into the hypothesis of SOD1 misfolding herein, we should discuss what is misfolding of a protein. A protein is said to be folded if it is present in its regular conformation or structure, including the elements of secondary structure[29]. The native state of a protein is often folded and forms the operative structure

of a protein. A protein is said to be unfolded if it does not possess a regular structure and is highly soluble[101].

SOD1 maturation or SOD1 folding requires four post-translational maturation steps in addition to *N*-terminal acetylation. Firstly, Cu insertion, secondly, Zn insertion, thirdly, dimerization of monomer units, and lastly, (-S-S-) formation between monomer units. These post-translational modifications (PTMs) contribute to the structure, function, and stability of SOD1. Therefore, any alteration in these PTMs causes the accumulation of immature SOD1, causing improper folding or unfolding of SOD1[29]. It is evident that maturation of SOD1 to its functional form itself is a universal process that requires oxidation; however, the misfolding of SOD1 that acquires toxic function is due to the result of an oxidative environment of the motor neuron. Several reports have shown that misfolding and toxicity are caused by oxidative free radicals[21, 100, 102, 103]. Therefore, according to our current understanding, from the literature of the past three decades, we aim to contemplate that the most important free radical responsible for the misfolding and toxicity of SOD1 is H_2O_2, thereby playing a critical role in the pathophysiology of ALS.

Initial evidence to support our conjecture was given by Liu and co-workers (2020)[104], they have for the first time, using unique micro dialysis and microcannula sampling techniques in transgenic mutant mice, demonstrated that the levels of H_2O_2 and $HO^{\bullet}$ are significantly higher, than the level of $O_2^{\bullet-}$ in ALS transgenic mutant mice compared to control. Showing the *in vivo* evidence that the “mSOD1 catalyzes” the formation of $HO^{\bullet}$ radical. In addition, these studies suggested that H_2O_2 formed by overexpression of human SOD1 (hSOD1) is effectively degraded, while the additional H_2O_2 generated by mSOD1 leaks into the tissue, potentially causing damaging $HO^{\bullet}$, thereby causing the

oxidation of protein, DNA, and membrane phospholipids, causing motor degeneration in ALS. Moreover, this study also supports the theory that mSOD1 acquires a toxic gain of function, thus allowing more $HO^{\bullet}$ formation from H_2O_2[104]. Furthermore, it indicates that the SOD1 mutation hinders the usual H_2O_2 detoxification pathway.

The gain-of-function theory for mSOD1 in ALS pathogenesis was supported by Yim and co-workers (1990)[105]. They demonstrated the enhancement of free radical formation due to a decrease in the Michaelis constant (Km) for H_2O_2 as measured by the spin trapping method in the $SOD1^{G93A}$ ALS model. According to their studies, the free radical-generating function of the mutant G93A is enhanced compared to the wild-type enzyme, particularly at lower concentrations of H_2O_2. This was found to be due to the decrease in the value of Km for H_2O_2 for G93A, with the same turnover number of the enzyme (Kcat) value for both mSOD1 and wSOD1; thus, the ALS symptom observed in the G93A ALS model is due to the gain-of-function, i.e., an increase in the function to generate free radicals[105]. Thus, this study supported the fact that H_2O_2 acts as a substrate to produce an elevated amount of toxic free radicals $HO^{\bullet}$, which is due to the low Km value of H_2O_2 for mSOD1 compared to wSOD1. This enhancement of the free radical generating function is thought to inactivate the enzyme, through disturbance in the PTMs process to form mature SOD1. Jewett and his team observed that the oxidation of mature SOD1 with H_2O_2 causes a sequence of events, the first being the formation of 2-oxo-histidine, Cu loss, and thus causing inactivation of the catalytic property of SOD1[106]. This study again suggested the role of H_2O_2 as a substrate in the inactivation of SOD1.

Further, Sampson and co-workers (2001)[107], studied the effects of H_2O_2 on Zn-deficient SOD (Cu, E SOD) and Cu,Zn SOD using bovine SOD *in vitro*. They demonstrated firstly

that H_2O_2 exposure to Cu, E SOD inactivated zinc binding activity six times faster than dismutase activity. Although the rate of loss of dismutase activity is the same for both the SOD. Secondly, they detected through UV circular dichroism that H_2O_2 instigates elusive changes in the tertiary structure of Cu, E SOD, but not the secondary structure. Finally, they showed that H_2O_2 in a lower concentration of 1mM amplifies the toxicity of Zn-deficient Cu, E SOD to motor neurons in ALS, manifesting the Zn loss from SOD[107]. The aberrant misfolding of mSOD1 adversely affects the binding of Zn in the Zn binding sites of mSOD1, thereby decreasing the affinity of Zn in mSOD1[108-110]. The gain of toxic function of SOD1 is due to the loss of Zn metal. Two primary factors are involved in the loss of Zn from SOD1 in the case of ALS pathology. The first being the presence of high levels of neurofilaments (NFs), and the second being the presence of a pathological concentration of H_2O_2. NFs are intermediate filaments that comprise the neuronal cytoskeleton and are abundant in the axons. Recent evidence has shown the presence of elevated NFs light chain and phosphorylated NFs heavy chain levels in the CSF and serum of ALS patients, suggesting the extensive damage of motor neurons and axons[111-113]. Similar to SOD1, NFs are found abundantly in motor neurons and are known to bind to metals[114]. In cases of elevated levels of NFs in ALS, NFs could act as a sink for Zn and could remove Zn from both wSOD1 and mSOD1, making SOD1 deficient of Zn, thereby enhancing the catalysis of tyrosine nitration by $ONOO^-$. Because zinc shares a common histidine ligand with Cu, Zn deficiency may also alter the redox properties of copper[115, 116]. Whereas the second factor is the neurotoxic levels of H_2O_2 that modify the (SH) status of both wSOD1 and mSOD1 to acquire the toxic gain of function and thus, causing elimination of Zn. In the case of increased ROS in motor

neurons, the pathological concentration of H_2O_2 makes the process of Zn recovery irreversible and thus causing structural defects in SOD1 structure even in the presence of small antioxidants inducing misfolding and thus toxicity to motor neurons[107]. The above findings supported the fact that, the pool of Zn in SOD1 is an important factor in the neuropathology of ALS.

The above findings were additionally supported by Rakhit and co-workers (2002)[100], with the help of dynamic light scattering and analytical ultracentrifugation, they found that the most aggregation prone species is Zn-deficient SOD1 and is amenable to form toxic aggregates. As mSOD1 is less stable than wtSOD1, oxidative stress through the generation of H_2O_2 as substrate causes the formation of an irreversible Zn-deficient and consequently a monomeric intermediate state of the protein. These two intermediate acts as a transition state intermediate before aggregation[100]. Thus, this study demonstrated that oxidative stress-induced Zn-deficient SOD1 is vulnerable to aggregation and misfolding.

Further, studies have identified that the disruption of Cu homeostasis due to oxidative stress is responsible for toxic SOD1 aggregate formation[117, 118]. Also, Cu deficiency was found in the spinal cord of transgenic mutant mice having poor locomotor function, supporting the role of Cu in maintaining the integrity and folding of SOD1 structure[119, 120]. Evidence from literature have shown that pathological H_2O_2 attack the Cu binding histidine[121, 122], eventually leads to Cu loss and hence, SOD1 deactivation[106].

The functional role of metals in maintaining the dynamics of SOD1 is well established by the fact that SOD1 monomers, which are metal-deficient apoSOD1 species, are vulnerable to changes in dynamics leading to misfolding and hence act as a precursor for

aggregation. [29, 100, 123-125]. Therefore, both metals are vital in maintaining the homeostasis and redox properties of the SOD1 protein, and the loss of metals, called demetallation, due to oxidative stress caused by pathological H_2O_2 from holoSOD1, leads to misfolding and, consequently, disease progression in ALS**.**

The peroxidase hypothesis describes that mSOD1 could act as a peroxidase and has the ability to generate $HO^{\bullet}$ radical from H_2O_2, thus creating an oxidative environment in motor neurons, creating toxic aggregates[126]. Other studies showed that the biologically ubiquitous bicarbonate buffer-dependent reaction initiated by H_2O_2 generated by peroxidase activity of hSOD1 causes the formation of oxidation products of the hSOD1-Trp32 residue, particularly the covalent dimer, in triggering the non-amyloid aggregation of hSOD1[127]. This study was well supported by other reports, which suggested that the overexpression of hSOD1WT in mice causes ALS[128], and the presence of over-oxidized/carbonylated hSOD1WT in sporadic ALS patients[129].

Moreover, the importance of thiol (SH) status in the central nervous system (CNS) also determines the cytotoxic level of H_2O_2. During the cellular process, (SH) oxidation mainly of Cys and glutathione acts as a hot spot in the CNS, to produce neurotoxic H_2O_2, thereby making neurons vulnerable to $HO^{\bullet}$ radicals[130]. A large body of evidence has shown that the redox modification of a Cys amino acid, primarily Cys^{111} in SOD1, by H_2O_2 is primarily implicated in the pathology of ALS[131-134]. Cys^{111} is a primary target for oxidative modification and plays a crucial role in oxidative damage to hSOD1, including mSOD1[131] **(Figure 5).** Bosco and colleagues (2010) [135], employed Fourier-transform mass spectrometry (FT-MS) to confirm the oxidation of wtSOD1 with the exposure to H_2O_2. They found that there was an increase of 48 Da for the predominant species in the

spectrum of oxidised wSOD1, compared to unmodified wSOD1. Furthermore, they confirmed, with the help of the electron capture dissociation (ECD) technique, that the (SH) group in Cys^{111}, encoded in exon 4, is the most vulnerable amino acid, which is found to be irreversibly oxidized to a sulphonic acid through the addition of three atoms of oxygen. Therefore, Cys^{111} acts as a hotspot for oxidative modification by H_2O_2[135]. Supporting the role of H_2O_2 in altering the spectroscopic and biophysical properties of Cys^{111} in SOD1[91, 132].

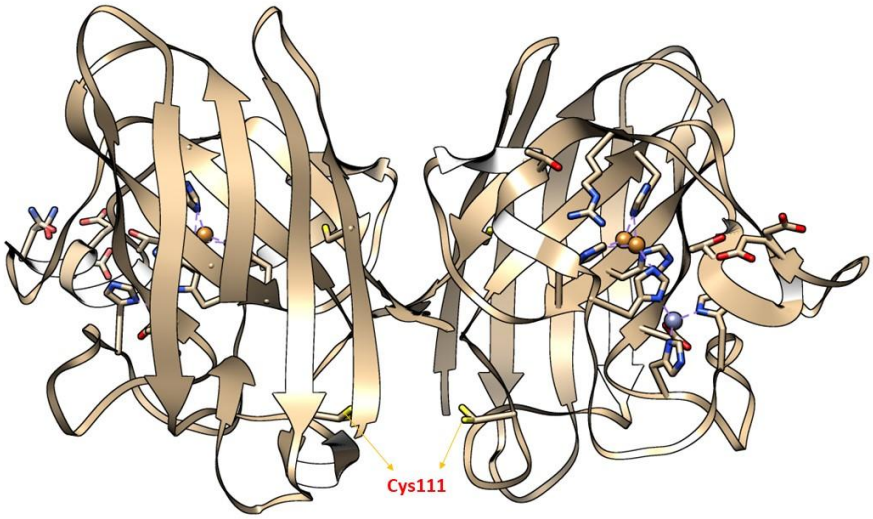

Figure 5. The X-ray crystallographic structure of wild-type SOD1 (wSOD1).

(Pdb#2C9V)[136] is shown, modelled in Chimera. Cysteine 111(Cys^{111}), highlighted in yellow, acts as a “HOT SPOT” for oxidative modification by hydrogen peroxide (H_2O_2) and is labelled red in the cartoon. The Zinc (Zn) and Copper (Cu) atoms are shown in cyan and orange, respectively[135].

Kong and group (2012)[133], examined the redox state of SOD1 Cys residues in the G37R transgenic animal model under oxidative stress induced by H_2O_2. The data suggested that with the progression of disease, there is an increase in oxidation of (SH) groups of Cys residues due to an oxidative burden inside the spinal cord motor neurons. This was further confirmed by an upper shift band in reducing SDS-PAGE, which was identified as a Cys^{111}-peroxidized SOD1 species using MalPEG. MalPEG is an alkylating agent linked with 5 kDa PEG, readily reacts with sulfhydryl groups of Cys residues, and causes a 5 kDa increase in molecular weight per one modification on SDS-PAGE. They demonstrated that oxidation by H_2O_2 decreased the MalPEG modification and increased Cys^{111}-peroxidation in G37R spinal cord extract. In addition, they also found formation of different aggregates and multimers during the disease progression, which is thought to be due to the formation of abnormal conformational change of SOD1 due to Cys^{111} modification[133]. Thus, the more reactive thiolate of Cys^{111} is critically involved in the aggregation of the SOD1 process rather than a (-S-S-) causing (-S-S-) independent SOD1 aggregation. Thus, this data supported the role of H_2O_2 in the aggregation of SOD1 via the formation of ($-S^-$) in the Cys amino acid residue.

Like SOD1, TDP-43 is also implicated in the etiology of ALS, and this is well supported by numerous studies[137-141]. Cohen (2012)[137] provided evidence that oxidative stress inhibits TDP-43-mediated RNA regulatory functions. Further, they found that redox imbalance caused by stressors like pathological concentration of H_2O_2 (1-10mM), causes unusual TDP-43 cross-linking via Cys oxidation and (-S-S-) formation leading to decreased TDP-43 solubility and hence, TDP-43 formation of toxic aggregates, implicated in the pathology of ALS. Moreover, the pathological modification is due to the

mislocalization of TDP-43 from the nucleus to the cytoplasm. Further, TDP-43 proteinopathies induced by pathological concentration of H_2O_2 were well demonstrated by Chang (2013)[142]. Lin and group (2020)[143] demonstrated the phenomenon of aberrant oxidative modification of sulphur-containing amino acid Met. The studies mentioned above have shown the role of pathological H_2O_2 induced TDP-43 proteinopathy in the pathogenesis of ALS[144].

Cheng Xu and colleagues (2018)[141], explained how the pathological concentration of H_2O_2 regulates the redox biology of Cys^{111} and regulates the misfolding and toxicity of SOD1 and TDP-43 associated with ALS and suggested that sulfenic acid modification of wSOD1 plays a crucial role in the pathogenesis of sporadic ALS. They demonstrated firstly that the increasing concentration of H_2O_2 from 20 to 200 μM increased the concentration of apo-SOD1 filaments by incredibly increasing maximum thioflavin T (ThT) fluorescence intensity. Secondly, they presented that a pathological concentration of 100 μM H_2O_2 activates the fibrillization of wild-type human SOD1 in the neuroblastoma cell line (SH-SY5Y). Finally, they detected the sulfenic acid modification of SOD1 via the sulfenation of Cys^{111} by pathological concentrations of (0–200 μM) H_2O_2. Based on the intriguing *in vitro* experimental data, they continued the experiments to see whether these PTMs could also be observed in the cerebrospinal fluid (CSF) of sALS patients. Interestingly, they observed the increased level of sulfenic acid-modified wild-type SOD1 level in cerebrospinal fluid (CSF) of 15 sALS patients compared with 6 age-matched non-ALS control patients. Finally, they hypothesized that pathological concentration of H_2O_2 triggers SOD1 fibrillization, by overoxidizing the (SH) of Cys-111. These (-SOH) modified SOD1 proteins are expected to cause cytoplasmic mislocalization of human TDP-43 (from

the nucleus to the cytosol), resulting in the formation of cytoplasmic TDP-43 oligomers[141]. Thus, a change in the abnormal (SH) status of Cys^{111} in SOD1 has been implicated in the toxicity of SOD1 and TDP-43 in motor neurons and is illustrated below **(Figure 6)**. These studies once again proved the role of pathological H_2O_2 in the pathogenesis of ALS. Furthermore, it also supported the notion that SOD1 aggregates could increase the propensity for TDP-43 aggregation[91].

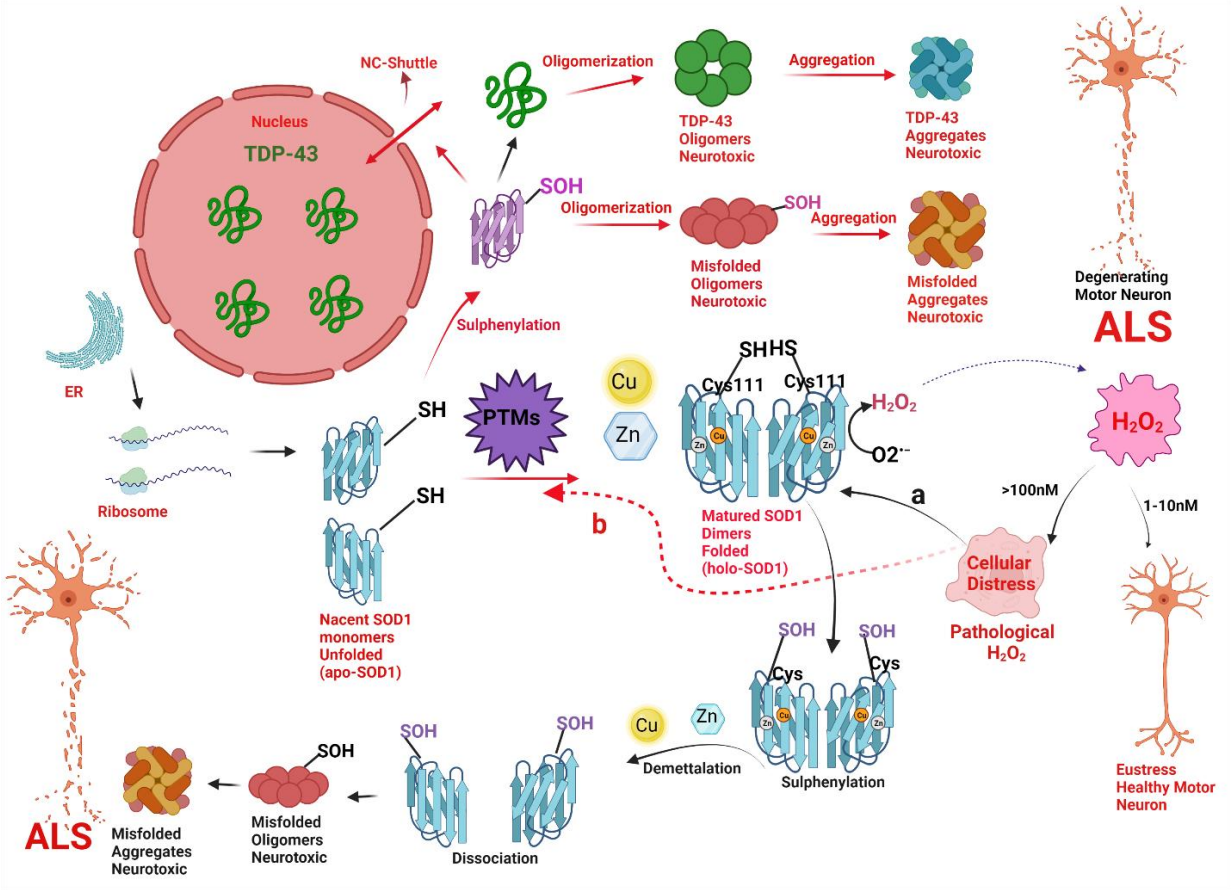

Figure 6. A hypothetical model implicating how pathological concentrations of hydrogen peroxide (H_2O_2) trigger the toxic gain-of-function of superoxide dismutase (SOD1).

Pathological concentrations of H_2O_2 induce a change in the conformation and biophysical properties of SOD1, primarily through alterations in the thiol (SH) status

of Cys^{111}, thereby triggering SOD1 and TAR DNA-binding protein (TDP-43) toxicity in motor neuronal cells, ultimately leading to the degeneration of motor neurons in amyotrophic lateral sclerosis (ALS). Nascent SOD1 (unfolded, apoSOD1) released from the ribosomes, undergoes post-translational modifications (PTMs) to form homodimerized mature SOD1 (folded, holoSOD1) through the addition of Copper (Cu) and Zinc (Zn) to the correct binding sites of apoSOD1 and formation of a disulfide bond (-S-S-). Mature SOD1 catalyzes the dismutation of superoxide radical anion ($O_2^{\bullet-}$) to H_2O_2. H_2O_2 acts as a double-edged sword molecule, and in low concentrations, i.e., the physiological concentrations of (1-10nM), act as a signal molecule to create eustress in the cell. However, at higher concentrations, i.e., pathological concentrations (> 100 nM), it acts to create an oxidative environment, causing cellular distress. The pathological concentration of H_2O_2 acts as a reactive oxygen species (ROS) and could cause misfolding of SOD1 via two molecular pathways **(Path a and Path b). Path a (black arrow):** The pathological concentration of H_2O_2 will cause an abnormal change in the thiol status of Cys^{111} (from SOD1-SH to SOD1-SOH) from holoSOD1, called sulphenylation, and cause the release of metal-bound ligands like Cu and Zn from the active site of holoSOD1, called demetallation. Sulphenylation with demetallation **(path a)** leads to dissociation of homodimerized holoSOD1 to its monomeric metal-deficient SOD1, hence, encourages the oligomerization and aggregation of SOD1 to neurotoxic misfolded oligomers and aggregates of SOD1, respectively. Both the oligomers and aggregates of SOD1 are neurotoxic to motor neurons and are implicated in the pathogenesis of ALS.

Path b (Red arrow): The pathological concentration of H_2O_2 will cause disruptive post-translational modifications (PTMs) via a change in the thiol status of Cys^{111} (from SOD1-SH to SOD1-SOH) called sulphenylation of apoSOD1. Sulphenylation thus provokes the oligomerization and aggregation of SOD1 to neurotoxic misfolded oligomers and aggregates of SOD1, respectively. Sulfenic acid-modified SOD1 oligomers could also disrupt the nucleocytoplasmic shuttle (NS-shuttle) between nucleus and cytoplasm, which is responsible for correct translocation of TDP-43 from cytoplasm to nucleus, thus inciting the mislocalization of TDP-43 from nucleus to cytoplasm and therefore, provoking the oligomerization and aggregation of TDP-43 to neurotoxic misfolded oligomers and aggregates of TDP-43, respectively. Both the oligomers and aggregates of SOD1 and TDP-43 are neurotoxic to motor neurons and are implicated in the pathogenesis of ALS.

1.6 Current treatment options available to treat amyotrophic lateral sclerosis and their drawbacks

Dysregulation of redox homeostasis inside living cells produces abnormal oxidative stress by creating ROS/RNS. These bioreactive, unstable species eventually participate in a cascade of pathways that abnormally modify biomolecules in living cells, affecting the central dogma of life. A large number of experiments and clinical trials are done to combat these clinically proven fatal diseases, such as Ischemic stroke, AD, and ALS. However, before 2017, a glutamatergic neurotransmission inhibitor known as Riluzole was the only drug approved by the US Food and Drug Administration (USFDA) for ALS treatment and provided only modest improvements in survival. Riluzole is a glutamate antagonist. It blocks the abnormal increase of glutamate in motor neurons. Excessive glutamate causes an influx of calcium ions into the glia and motor neurons, which in turn leads to the

damage of nucleic acids, peroxidation of lipid membranes, and disruption of mitochondria. Riluzole inhibits the excitotoxicity caused by the excessive release of glutamate and therefore, prevents the calcium overload**.** On average, Riluzole extends survival time by only 2-3 months, but this can extend up to approximately 9 months[145]**.** Riluzole remained the only ALS treatment for 22 years, until EDR was approved for ALS in 2017.

More recently, an antioxidant drug, Edaravone (EDR), was developed by Mitsubishi Tanabe Pharma (MTP) and was found to be effective in alleviating ALS progression during the early stages[146]**.** EDR (3-methyl-1-phenyl-2-pyrazolin-5-one, MCI 186) is an amphiphilic, low molecular weight redox regulator in cellular processes that acts by reducing both ROS/RNS free radicals (i.e., superoxide anions, hydroxyl radicals, singlet oxygen, peroxy radicals, hydrogen peroxide, peroxy nitrite) to their stable configuration state. Since EDR is an amphoteric molecule, it can reduce both aqueous and lipid-soluble free radicals by donating one electron to complete their octet and making them electronically stable. This mechanism is called a single-electron transfer process (SET)[147]**.** EDR diffuses into most organs to regulate the oxidation-reduction cycle, including highly metabolic organs such as the brain and heart[148, 149]**.**

Due to its diverse and versatile pharmacological importance as an anti-apoptotic, anti-necrotic, and anti-cytokine agent, only parenteral solutions are available on the market. Radicut® is the first parental dosage form developed, marketed, and approved by Mitsubishi Tanabe Pharma (MTP) in 2001. It was also the first neuroprotective drug produced in Japan for the treatment of cerebral ischemic stroke[149]**.** In 2005, it was approved for the treatment of ALS in Japan. In 2017, it was approved by the USFDA for the treatment of ALS[150]. A breakthrough occurred on October 4th, 2018, when Health

Canada also approved Radicava® (EDR) for ALS treatment[151]**.** However, EDR has several limitations, as listed below.

1.6.1 Patient compliance

The current intravenous (i.v.) formulation for treating ischemic stroke is available as a single ampoule (30 mg EDR), diluted with physiological saline, and administered twice daily over 14 days intravenously[152]**.** Whereas the recommended dose for Radicava® for ALS is 60mg administered over a 60-minute period for 14 days, followed by a 14-day drug-free period[153]**.** As NDDs are mostly prevalent in geriatric patients, daily IV. Administration for 14 days is problematic. For these patients, the oral route is highly preferable due to its ease of administration, flexibility in dose, reduced hospitalization periods, cost-effectiveness, and improved quality of life[154]**.**

1.6.2 Pharmacokinetics

EDR has a molecular weight of 174.2g/mol is defined as a class IV amphiphilic molecule by the Biopharmaceutics Classification System (BCS) due to its poor aqueous solubility (1.85mg/ml), permeability ($P_{eff} = 3.18 \pm 0.0706 * 10^{-7}$ cm/s), short half-life of 0.15-5.16 hours, and pKa value of 7[150, 155]**.** Additionally, EDR is a substrate for P-glycoprotein (P-gp) efflux pumps and is metabolized pre-systemically by CYP3A4 enzymes. It also undergoes extensive phase II metabolism, primarily through glucuronidation (68-83%) by uridine 5-diphospho-glucurononosyl-transferase (UGT) enzymes and sulphation (5-13%) by sulphotransferases, forming pharmacologically inactive glucuronide and sulphate conjugates. This leads to high passive permeability and low therapeutic concentrations at the target site[150, 156] **(figure 7).**

Note: pKa is the negative logarithm of the acid dissociation constant (Ka) and indicates acid strength; lower pKa values correspond to stronger acids.

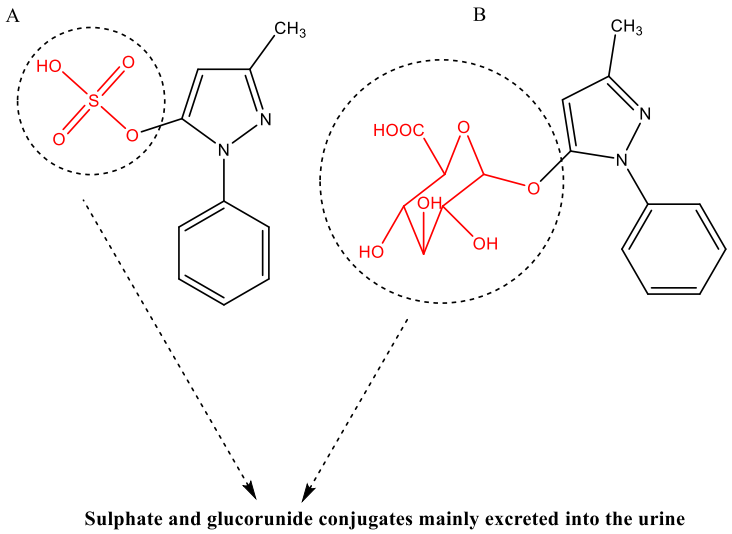

Figure 7. Structure of the primary phase II metabolite of EDR excreted in urine.

1.6.3 Stability

EDR exists as a solid in keto tautomer form. However, its tautomeric enol form exists as a highly unstable anion in aqueous solution. The pKa of EDR is 7.0, and its solubility in aqueous solution depends upon the pH. As the pH of the solution increases beyond 8, EDR acts as an acid and furnishes hydronium ions to form its conjugate base, EDR anion. At physiological (pH 7.4), 71.5% of EDR exists as an anion, while the remaining 28.5% exists in neutral form[147]**.** The anion is capable of reducing radicals or even molecular oxygen through a single electron transfer process, forming stable EDR radicals that are stabilized by three resonance structures (enol, keto, and amine forms). These radicals subsequently form inactive EDR trimers in the absence of oxygen, which appear as a yellow precipitate[157]**.** Molecular oxygen is prone to accepting single electrons and forming highly reactive $O_2^{\bullet-}$ radicals, which disproportionate to form H_2O_2. Decomposition of EDR takes place to form oxidative, stable products like OPB, 4-Oxo EDR, EDR peroxy

radical, BPOH, and the highly carcinogenic PHZ[158, 159] **(figure 8)**. The poor oral bioavailability of EDR is attributed to its low aqueous solubility, low permeability, poor stability, and extensive pre-systemic metabolism[160].

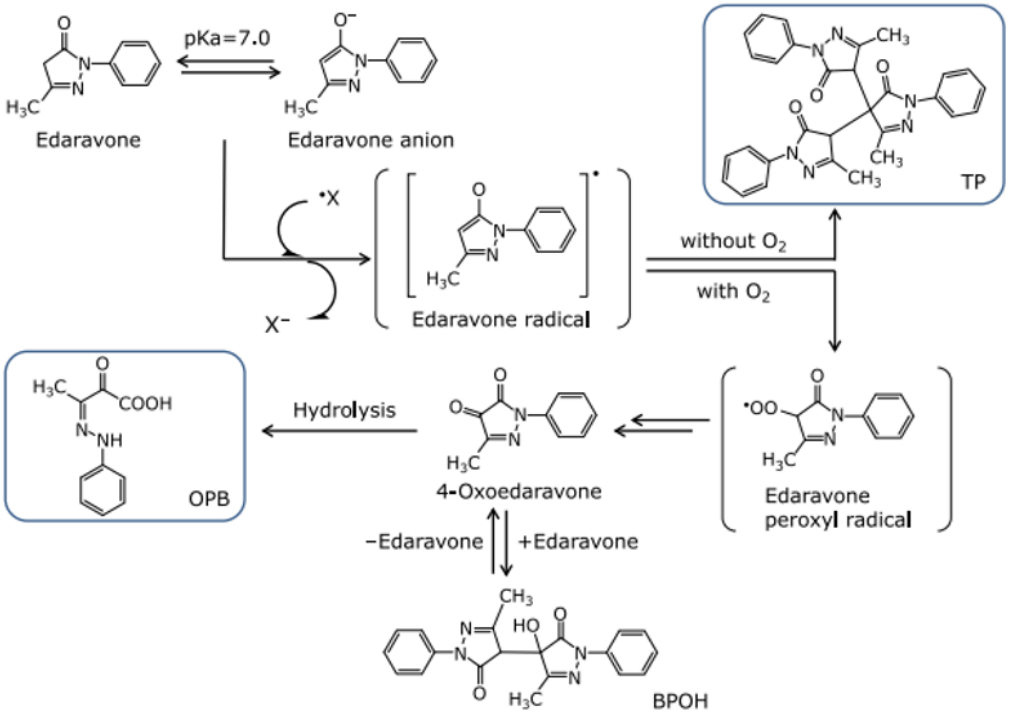

Figure 8. Mechanism for the release of Edaravone (EDR). The figure is adapted from Watanabe T, Tahara M, Todo S. The novel antioxidant edaravone: from bench to bedside. Cardiovasc Ther. 2008;26(2):101-14.

Mechanism of action (MOA) of EDR radical by electron transfer from EDR anion to peroxy radical and the formation of oxidation products[161].

1.6.4 Synthetic route

Below are the shortcomings present in the current synthetic route of EDR.

- Compared to the new synthetic method developed herein, the conventional method requires more time for the synthesis of EDR[162].
- Low purity of the isolated product EDR is due to the presence of impurities, including phenyl hydrazine, and other oxygen-consuming catalysts like sodium dithionate. In accordance with the specifications for EDR injection, the colour purity of the EDR solution is required. In the present synthetic route, utilizing phenyl hydrazine at temperatures higher than 30°C deepened the colour of EDR.
- Presence of the starting material, phenyl hydrazine, which is a colourless to yellow oily liquid or crystals that can be oxidized to a brown-red colour in the presence of light and air. Phenylhydrazine (PHZ) causes hematotoxicity, leading to hemolytic anemia. It also inhibits erythropoietin binding to its corresponding receptor. Moreover, it also acts as a genotoxic agent, causing breakage of single-stranded DNA[163, 164].
- Presence of oxidizing chemicals in the reaction mixture oxidizes EDR to EDR radical, thereby forming inactive EDR decomposition products.
- High costs of starting materials, such as ketone amide.
- Maintaining a pH of 6-6.5 is imperative during the reaction because EDR is highly unstable and at high pH, it transforms into its conjugate base (EDR anion). EDR anion reacts with molecular oxygen in the air to form EDR radical. This radical acts as a precursor for the formation of insoluble EDR trimer, having a yellow precipitate with no therapeutic value[158].

Present synthetic routes for the synthesis of EDR

The first synthetic route invented for the synthesis of EDR was the Knorr pyrazole synthesis, which utilizes PHZ and ethylacetoacetate as starting materials[162] **(figure 9).** Afterwards, other routes were developed using this synthetic method as a foundation for the synthesis of EDR. None of the reported synthetic methodology schemes for the synthesis of EDR or EDR analogues is without the use of PHZ, a carcinogenic starting material[165-170].

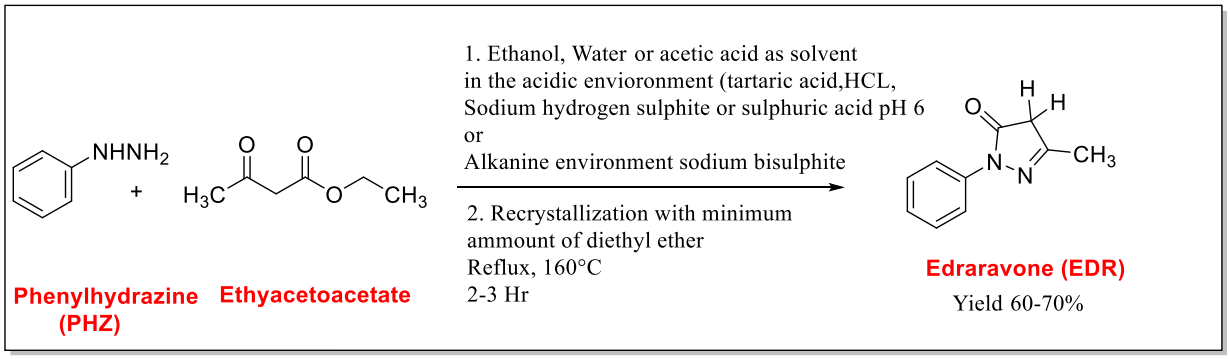

Figure 9. Knorr pyrazole synthesis of EDR.

1.7 Structure-Activity Relationship (SAR) of EDR (3-methyl-1-phenyl-2-pyrazolin-5-one)

First, the influence of the substituent at the 1-position was evaluated. While small steric substituents like hydrogen and methyl did not exhibit activity, carbocyclic groups such as cyclohexyl, naphthyl, and benzyl either maintained or enhanced the *in vitro* lipid peroxidation-inhibitory activity. The low activity of a 2-hydroxyethyl compound was attributed to the expectation that lipophilic substituents tend to be more effective. This activity was further increased by lipophilic groups like alkyl and halogen, with longer alkyl and alkoxy chains showing greater activity. Disubstituted halogen derivatives demonstrated higher activity compared to monosubstituted halogen analogs, although a disubstituted alkyl variant had different results. Regarding the 3-position substituents,

lipophilic groups also improved activity, with longer alkyl chains enhancing effectiveness, while nitrogen-containing heterocycles only showed moderate activity. Furthermore, position-4 substituents by lipophilic group increase the activity, whereas the hydrophilic group decreases the activity. In addition, 4, 4-disubstitution blocks the keto-enol tautomerism, hence, no activity. The 5-position demonstrates keto-enol tautomerism, which explains EDR's antioxidant activity. EDR has a PKa of 7, functioning as a weak acid. At alkaline pH levels of 8-10, it forms an unstable EDR anion. This anion can scavenge radicals by donating an electron to free radicals, including molecular oxygen, producing the EDR radical. To reduce the instability of EDR anion in solutions, lowering the pH, deoxygenating the solution, and stabilizing the EDR anion are effective strategies. [157, 158, 171] **(figure 10).**

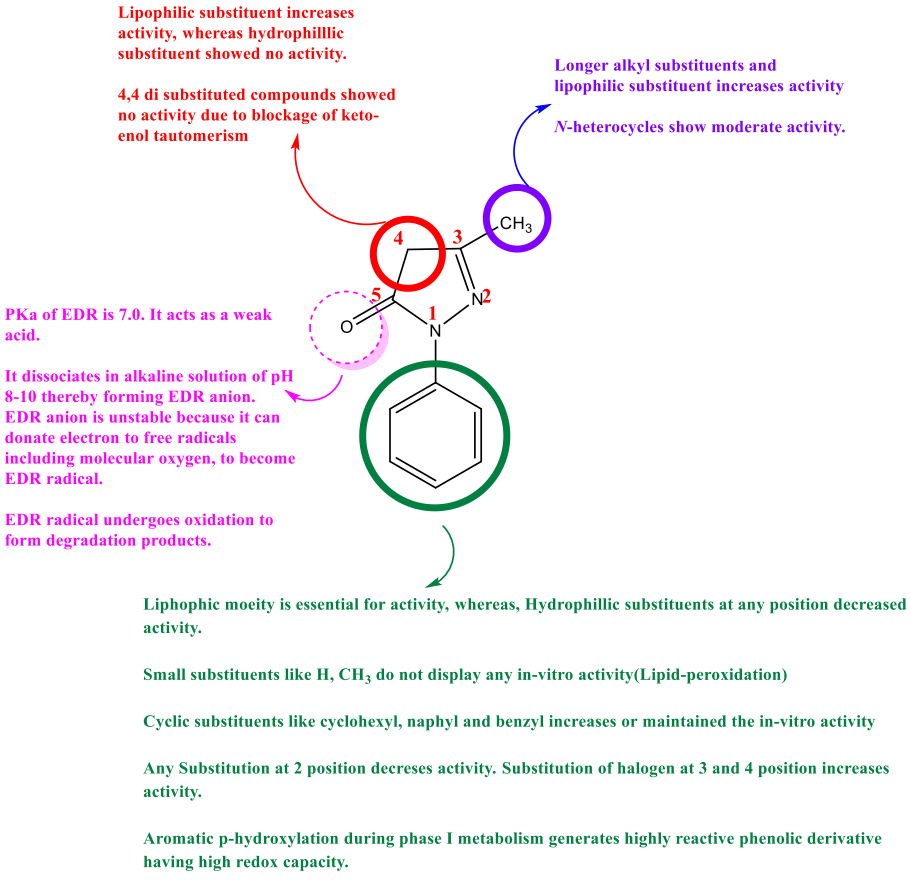

Figure 10. Structure-Activity Relationship (SAR) of Edaravone (EDR).

1.8 Boron in drug discovery

1.8.1 Boron: A potential element

Boron (B) is a group 13 metalloid element. It is distinct from other group 13 elements, having similar chemical properties to those of carbon (C) and silicon (Si). However, boron is more electrophilic than both C and Si. Elemental boron was first isolated in 1808 by British chemist Sir Humphry Davy and French chemists Joseph Louis Gay-Lussac and Louis-Jacques Thénard[172]. The ground-state electronic configuration of boron (B) is $1s^2 2s^2 2p^1$. B atom typically forms a trigonal geometry with Sp2 hybridization, having six valence electrons in the outermost shell. It possesses the feature of electrophilicity because of the presence of a vacant p-orbital. Due to six valence electrons, B is isoelectronic to carbocations. Also, the isoelectronic nature of C=C and B-N has surged the use of B in organic synthesis[173, 174]. The Lewis acid character of B has been immensely exploited in medicinal chemistry. Furthermore, B can also form a negatively charged tetravalent compound having Sp3 hybridization, with tetrahedral geometry[175]. With a history spanning over 160 years, B has attracted the attention of medicinal chemists due to its wide range of applications, extending from chemistry to biochemistry. Because of the stability and easy to synthesize, B has been utilized in various organic chemistry reactions for the formation of various chemical bonds like hydroboration reaction (C-H, C-OH bonds), Suzuki-Miyaura coupling (C-C bonds) and the Chan-Lam coupling (C-N and C-O bonds). Among all the Suzuki-Miyaura coupling reactions brought a revolution in the field of medicinal chemistry, due to several advantages, include the use of mild reaction conditions, easy commercial and cost-effective availability of boronic acid as reactants, and further its tolerance in wide reaction conditions, high conversion

rates to products and mild conditions[176]. In 2014, after amide bond formation, the Suzuki coupling reaction was used as the most resourceful reaction by the pharmaceutical industry for forming carbon–carbon bonds with aromatic or heterocyclic compounds groups[177].

Similar to the utility in the organic synthesis, the biochemistry of B organic boron molecules arises from the ability of B to convert its trigonal planar geometry to tetrahedral geometry by accepting a lone pair of electrons from a biological nucleophile, generally an amino acid side chains in the protein biomolecule or from sugars of nucleic acids. Thus, organoborane compounds are one of the versatile organic molecules that play a crucial role in biological systems due to their ability to form reversible covalent bonds with biomolecules containing hydroxyl or amine groups. The result of the reversible tetrahedral complex is called borates, which is involved in covalent enzyme inhibition. This property of protein target engagement confers the chameleonic ability to the organoboron compound due to the change of uncharged (Sp^2) hybridization to an anionic (Sp^3) hybridization, essential for target engagement and inactivation of the enzyme[178]. Recently, the electrophilic B compounds have been designated as covalent warheads because of their ability to act as a reversible covalent ligation with the active site of nucleophiles in biomolecules for their inhibition[179]. Organoboranes like boronic acid also form reversible covalent complexes with sugars diols[180], amino alcohols[181], alkoxides[182], and hydroxamic acids[183].

The boronic acid-sugar (BA-S) covalent complex could be used as a biomarker in certain disease conditions like cancers where, carbohydrate-related antigens are found[184, 185]. Numerous reports in recent times have exploited the use of boronic acids to

recognize and sensing carbohydrates using fluorescence as an endpoint for detection[186, 187]. This is because of the use of boronic acid, which shows a change in fluorescence intensities upon binding with different sugar polyols[188-190]. Further, the boronic acids give an additional advantage of increased pharmacophore binding with amino acid residues, due to the presence of two hydroxyl groups rendering four lone pair electrons and two hydrogen bond donors, thus offering six favourable opportunities for hydrogen bonding with different biomolecules (**figure 11**). Furthermore, the enhanced binding with the target even in the presence of drug-resistant gene abnormalities[191, 192]. In addition, boron has a unique property of emitting alfa particles under neutron spray bombardment, this forms a basis for using B in Boron Neutron Capture Therapy (BNCT) for the treatment of cancers, overcoming the challenges of clinical oncology[193].

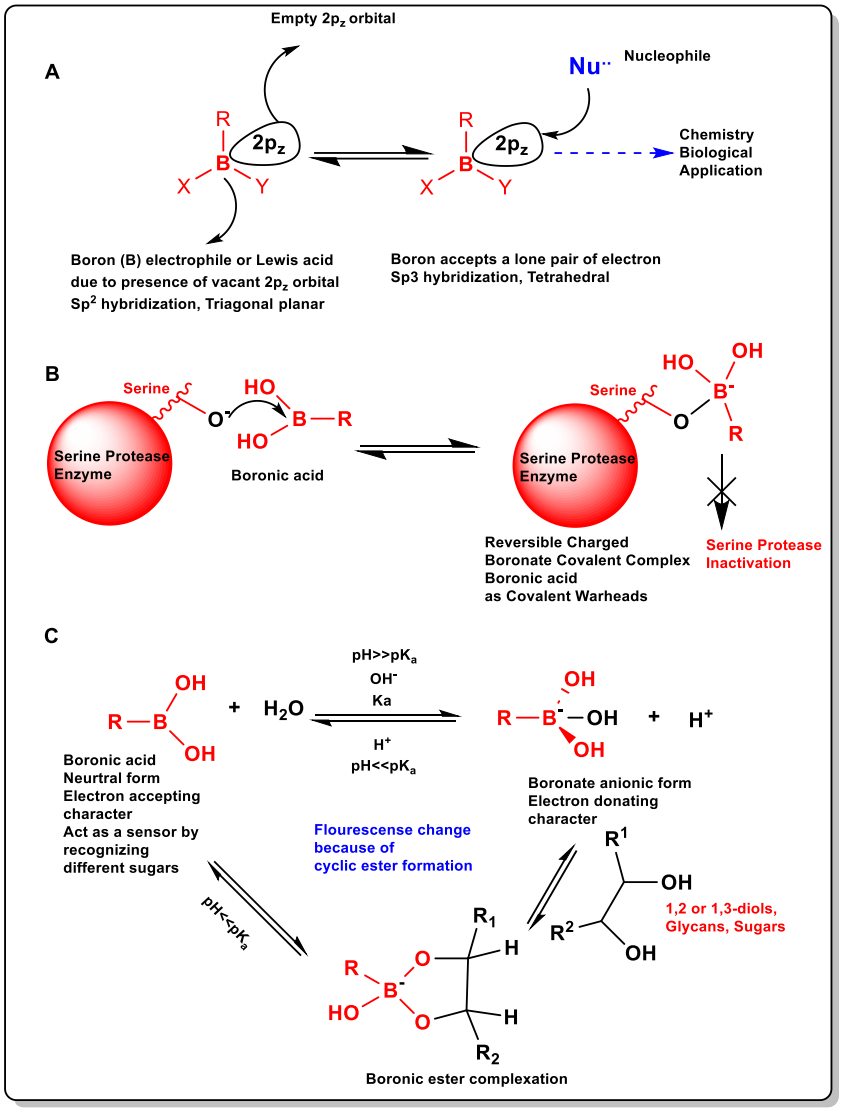

Figure 11. Diagram showing the potential of Boron (B).

A. Boron acting as a Lewis acid with vacant 2pz orbital **B.** Boron compounds act as covalent warheads interacting with different biomolecules **C.** Boron interacts covalently with carbohydrates under different pH of the solutions to act as sensors.

The potential of B as a therapeutic agent was realized with the discovery of bortezomib (Velcade®), in 2003, a first-in-class anticancer drug, approved by the Food and Drug Administration (FDA) as a proteasome inhibitor for the treatment of relapsed multiple

myeloma and mantle cell lymphoma[194]. Since then, several other B-containing compounds have been approved by the FDA, which include tavaborole(onychomycosis)[195], Ixazomib (multiple myeloma)[196], crisaborole (atopic dermatitis)[197] and vaborbactam (bacterial infections)[198] **(figure 12)**. Further, several other B compounds are in clinical stages of development. It is noteworthy to mention the role of B as a heterogeneous green catalyst in driving many chemical reactions, eliminating the hazards of using metal catalysts [199]. The last few decades have witnessed tremendous development in the potential of B in pharmaceuticals by exploring the chemical properties of B, hence making it a special element. Further research is warranted to uncover its future potential.

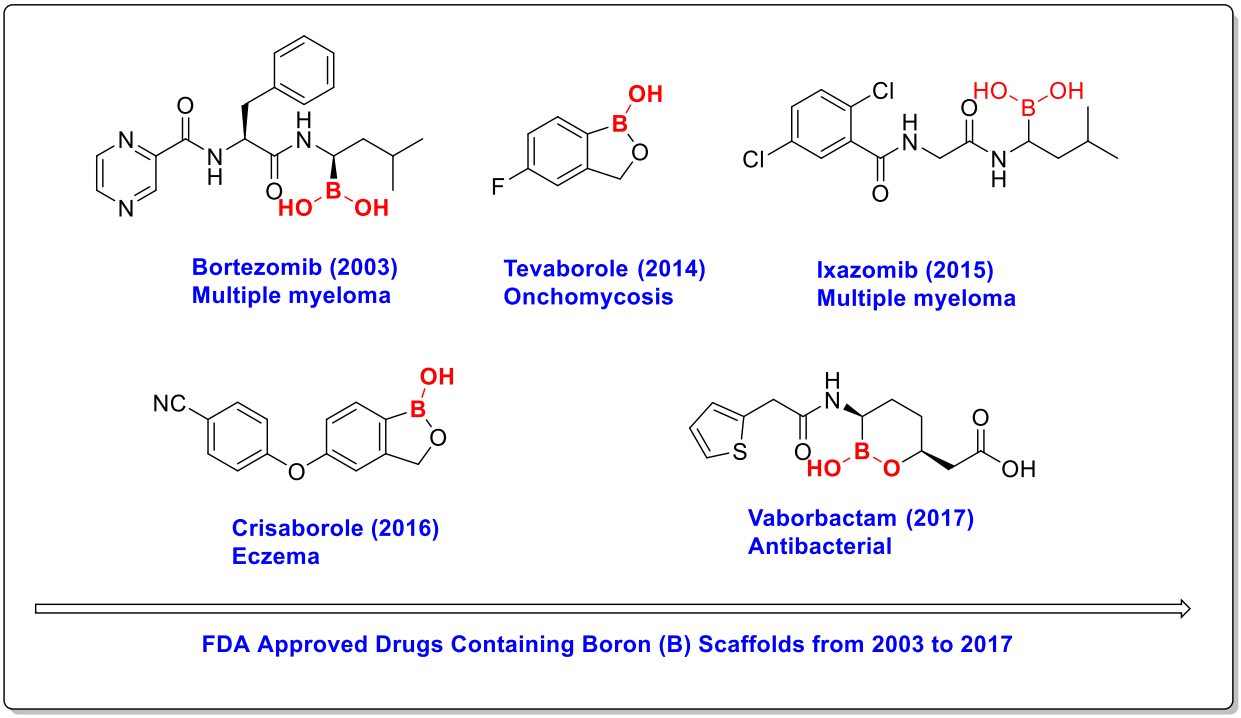

Figure 12. Boron (B) in drug discovery. FDA-approved (B) containing compounds.

1.8.2 Boric Acid containing boron with a low toxicological profile

Boric acid (BA) is a weak Lewis acid or weak monobasic acid with a pKa of 8.92-9.24, which is sensitive to changes in temperature, ionic strength, and concentration. BA has a general formula of $B(OH)_3$ and has a trigonal planar sp^2 hybridization with a vacant $2p_Z$-orbital. BA, being an electrophile, accepts electrons from coordinating/nucleophilic bases/ligands as H_2O to yield the tetrahedral borate anion $B(OH)_4^-$. The pKa of the BA changes with the concentration because it shows the property of polymerization above 0.02M and thus forms polynuclear complexes at higher concentrations [200]. Similar to the reaction of H_2O with the vacant p-orbital of BA, second and third or more molecules of BA can react with each other to form reversible dimeric, trimeric, or cyclic polynuclear complexes. Ingri et al. Showed that in concentration above 0.02M, there is the formation of a trimeric cyclic anhydride, $B_3O_3(OH)_3$, and its anion, $B_3O_3(OH)_4$. These cyclo tricyclic dehydration products are tricyclic anhydrides and are called boroxines 3 R– $B(OH)_2 \rightarrow R_3B_3O_3 + 3\ H_2O$. There is a diverse use of boronic acid anhydrides; it is used for building polymers, and covalent organic frameworks, in optics[201] **(figure 13)**.

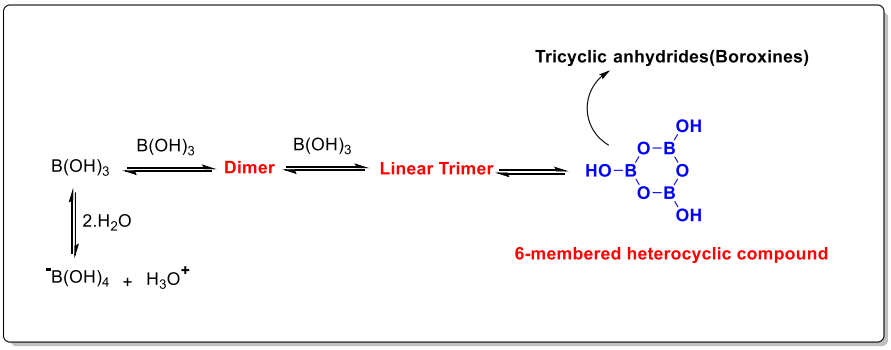

Figure 13. Self-association of boric acid to boroxines.

Scheme showing the self-association of boric acid to tricyclic anhydride product called boroxines with increasing aqueous solution concentration of greater than 0.02 M.

BA forms complexes with sugars; therefore, it acts as a carrier for the transport of carbohydrates and nucleotides. As a Lewis acid, it forms covalent reversible complexes with hydroxyl groups of different amino acids, carboxylic acids, sugars, nucleotides, and vitamins via esterification reactions. Monoesters are formed via partial esterification, while bicyclic esters are formed via complete esterification of BA. These reactions are pH dependent and ester formation with Di-ol sugars takes place in basic media, whereas acidic media favours esterification with hydroxy-carboxylic acids. These esters are readily hydrolyzed in aqueous media[202]. The binding of BA to sugars depends on both the solution's pH and the pKa of the BA. Binding is more likely when the pH exceeds the BA's pKa, encouraging the formation of the negatively charged, tetrahedral boronate species that binds more effectively to the sugars' diol structure. Research indicates that the BA binding affinity is often related to its pKa, although the strongest binding does not always occur near or above this value. In addition, several studies suggest that the optimal interaction between BA and sugars happens at a pH level between the BA's pKa and the pKa of the sugar's diol[203].

Cells regulate the concentration of B via a specialized transport system. Neutral B complex could transport via passive diffusion; on the other hand, the charged borate anions are transported with the help of aquaporins (AQP9)[204], or transporters like ubiquitous Na^+-coupled borate ($B(OH)_4^-$) transporter (NABC1) in human beings[205]. Sugar transporters help in the transport of Sugar boron complex (mostly the non-charged borate complex). However, the charged borate complex is transported via the process of

translocation[206]. Presumably, fructose transporter (Glut5) and glucose-6-phosphate translocase are involved in the transport of the boron sugar complex. Because of the differential expression of different sugar transporters in cancer cells, cancer cells are more exposed to the boron sugar complex than normal cells in physiological conditions[207].

BA is well absorbed in all species, including humans. The average half-life of BA is 1 day and is and is excreted unchanged in the urine (>95%)[208-210]. Further, BA is not metabolized and exists mainly in the form of BA in the blood of both humans and animals[211, 212]. Greater than 90% of BA is excreted unchanged in the urine of animals and humans, independent of the route of administration[200, 213]. The BA is not metabolized by the living system because of the high bond dissociation energy of the boron-oxygen bond (523 kJ/mol)[200]. Renal clearance is three times faster in rats compared to humans. BA majorly accumulates in the bone however, it is well detected in the brain, liver, and fatty tissues[212, 214]. The LD50 reported for BA in mice is 3450 mg/kg[212], whereas the LD50 of BA in rats is 2660-5140 mg boric acid/kg body weight[212, 215]. A Single-dose acute oral LD_{50} for sodium tetraborate decahydrate (borax) in rats ranges from 3,493 to 6,080 mg borax/kg body weight[216]. The World Health Organization (WHO) estimates that an acceptable safe range of boron intake for human adults is 1–13 mg/day[217]. Importantly, the mean daily intakes of B from food and drinks in male and female adults are 1.28 and 1.00 mg respectively[218]. It is now evident that B compounds have the advantage of being a pharmaceutical product; however, there is always a concern about the metabolite or the by-product of B medicinal products. It is noteworthy to mention here that, B is an essential trace element that we

eat on a daily basis and the main by-product of organoboron medicines mentioned above is mainly BA, which has an LD_{50} comparable to table salt, hence, the metabolites of B drugs, doesn't have any toxicity to the human cells, further, this also adds to the greener approach of drug development from synthesis to Pharmacokinetics (PK) in living cells[178, 218-221]. Notably, BA is a very common green agent in the environment, as well as present in our daily diet[216].

1.8.3 Potential of boron-containing compounds in neurodegenerative diseases

Recent lines of evidence have shown that B-containing compounds (BCCs) exert therapeutic benefits in rescuing neurons from several etiopathological factors, including oxidative stress, heavy metal toxicity, inflammation, and abnormal electrical firing. Additionally, BCC, being an attractive element in multiple disease conditions described above, has recently shown its potential as a neuroprotective and neuromodulatory agent on neurons, mainly due to its neurotrophic, antioxidant, metal chelating, and anti-inflammatory actions. Accumulating evidence has shown the positive effects of BCC in AD and PD. However, several hypotheses could be generated by looking at the overlapping and common pathways in neurodegeneration, such as AD, PD, and ALS. Further, we will present scientific evidence of cross-talks between B and the etiology of fatal and incurable ALS for our hypothesis that BCC could slow down the disease progression and improve the QOL in ALS patients.

1.8.4 Evidence showing effects of boron-containing compounds in neurons as neuroprotective Agents

Jun Lu et al[222]. discovered that BCC has multifunctional effects in rescuing neurodegeneration in the case of AD. The novel compounds exhibit significant

therapeutic efficacy as inhibitors of toxic amyloid-beta (Aβ) protein, ROS scavengers, and biometal chelators. The newly synthesized compound 17h demonstrated significant chelation activity towards Cu (II) and Fe (II). Further, studies by Ozansoy et al[223] investigated the role of two BCC sodium borate decahydrate and BA in reducing the Aβ toxicity, and hence increasing the survival of SH-SY5Y (a cell model for neurodegenerative disorders). Furthermore, the neuroprotective effects of these two compounds are attributed to an increase in the expression of GSK-3α/β (cellular pro-survival pathways) and Sirt1 (a NAD+-dependent histone deacetylase), which protects against cellular oxidative insult. A current study by Ciofani and group[224] proposed the innovative use of the piezoelectric effect of nanoparticles containing boron nitride nanotubes, a structural analog of carbon nanotubes, to electrically stimulate the neuronal-like PC12 cells. Electric stimulation of these neuronal cells using boron nitride nanotubes resulted in neuronal extension and outgrowth compared to the control after 9 days of long-term treatment. This technology could be further utilized for neuronal regeneration.

An important work was done by Cacciatore[225] and his team to synthesize new B-based novel compounds as neuroprotective agents. The newly synthesized B-based hybrid compounds showed increased cell viability due to inhibition of the cell death induced by incubation of Aβ1-42 (neurotoxic amyloid β protein) in SH-SY5Y neuronal cell culture. Moreover, the inhibition is shown to be due to the capacity to reduce oxidative stress in pathological conditions. Moreover, the new molecules inhibit acetylcholinesterase (AChE), which is found to be increased during the progression of AD. The latest study by Maiti and his team[226] demonstrated that BCC like trans-beta-styryl-boronic-acid (TBSA) improved neuropathological defects *in vitro* (N2a neuronal cells) and invivo

(5xFAD mouse model). These novel compounds containing B reduced neurotoxicity by alleviating Aβ plaques and necrosis in the cortical and hippocampal regions of the brain, thereby ameliorating cognitive function in 5xFAD AD mouse models.

Likewise, Routray and Ali[227]It illustrated the indispensable role of element B in inhibiting hyperapoptosis via stabilizing the changes in mitochondrial membrane potential. Increased apoptosis is seen during the pathophysiology of several disease conditions, including the NDDs, which is due to the disturbance in the homeostasis of mitochondrial membrane potential[228]. Moreover, abnormal mitochondrial potential triggers apoptosis by regulating matrix configuration and release of cytochrome c (proapoptotic protein), an apoptosis-triggering protein, due to further activation of cysteine proteases called caspases-3. The protective effects of B were due to the significant recovery of mitochondrial potential, thus inhibiting the release of apoptotic mediators.

Besides this, Baldwin et al[229]. discovered a new oxazaborine ring containing B compounds (NBC6) as inhibitors of the NOD-like receptor (NLR) family, pyrin domain-containing protein 3 (NLRP3) inflammasome, without having any off-target effects on Ca^{+2} modulation. NLRP3 is associated with cytokine burst and is related to the etiology of several diseases [230] including AD[231]Furthermore, the newly developed oxazoline molecules were found to be potent and selective inhibitors of NLRP3, which could lead to the development of new inhibitors in BCC as anti-inflammatory agents in several diseases **(figure 14)**.

Penland[232] with his eight years of work, he conducted five independent studies, both in animals and humans, and found a meaningful connection between the physiological intake of B and brain and psychological function. His pioneering work demonstrated that

a lack of a physiological amount of B results in poor cognitive and psychomotor function in both higher animals and humans **(figure 14)**.

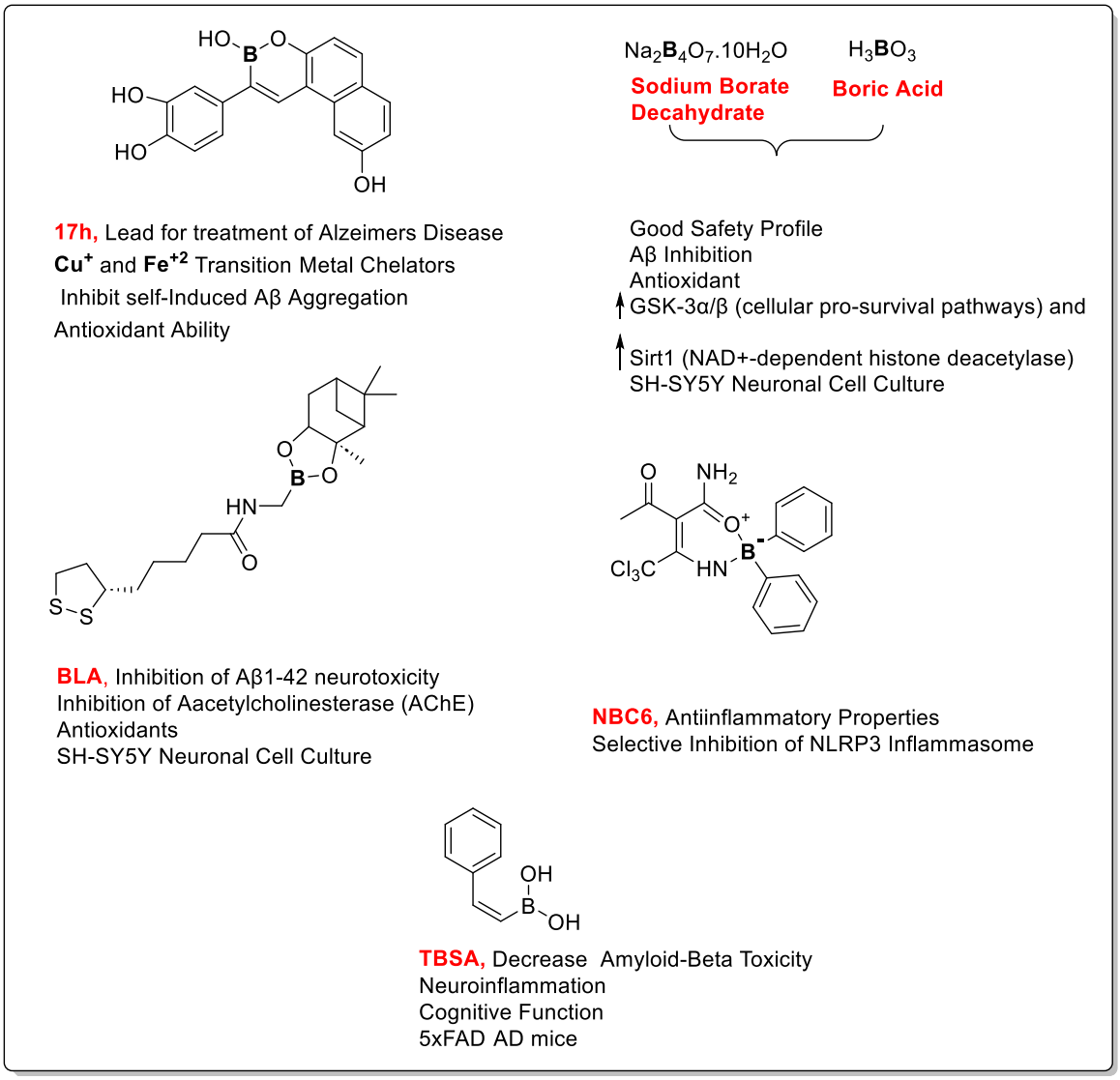

Figure 14. Boron-containing compounds are used as neuroprotective agents.

1.8.5 Neuroprotective role of boric acid, a by-product of boron-containing compounds

Surmounting evidence has shown the detrimental role of ROS in NDDs like AD, PD, and ALS due to redox dyshomeostasis[62]. Also, the dysregulation of redox homeostasis is due to various factors, one being that most studies are due to toxic concentrations of

metal ions like Fe^{+2}, Zn^{+2}, Cu^{+2}, Ca^{+2}, and Al^{+3} (Aluminium)[233-236]. Evidence from the literature has shown that BA mitigates oxidative stress in neuronal cells. Below we will explore some seminal work from various groups, who have demonstrated the role of BA in combating oxidative stress and metal toxicity.

Recent studies from Özdemir and group[237] have shown the beneficial role of BA treatment in combating the streptozotocin (STZ) induced AD pathology in AD rat models. In this study, BA significantly reduced oxidative stress based on the evaluation of markers such as TAS, TOS, OSI, and PON-1 in rat brains. In addition, hippocampus integrity was maintained after BA application, thereby positively affecting cognitive functions in the case of AD. This study was well supported by evidence published by the important work from Penland[238], where, he reviewed the beneficial role of B in the brain, improving psychomotor and cognitive function. Likewise, Ince and the team recognized the potential of BA and BCC, borax. They studied the supplementation of BA and borax in the rat diet and showed a significant increase in the antioxidant defence mechanism and vitamins. This therapeutic effect is supported by a decrease in lipid peroxides (MDA) levels, DNA damage, and protein carbonylation levels in the blood. Additionally, it increases the water-soluble vitamin C concentration in plasma and the GSH level in blood, which is concomitant with a decrease in lipid peroxidation.

Similarly, Yildirim et al[239], investigated the potential of BA in ameliorating cisplatin-induced peripheral neuropathy in rats. They observed a reduced level of lipid peroxidation (MDA) level in the BA treatment group, which was elevated due to cisplatin. Also, there was a significant increase in ubiquitous antioxidant SOD, which was decreased by cisplatin. Moreover, the tissue histopathology exhibited a decrease in neuronal

degeneration and vacuolization due to cisplatin. This study might be consistent with the antioxidant effects of BA. The neuroprotective effects of BA in decreasing the neurotoxicity induced by aluminum chloride ($AlCl_3$) in male Sprague-Dawley rats were further explored by Colak et al. Furthermore, the study demonstrated that the low dose of BA prevents the brain from the lethal effects of $AlCl_3$. Moreover, the tissue histology of the cerebral cortex revealed that BA is a proteasome inhibitor, thereby exerting its beneficial effects on AlCl3-induced neurotoxicity. An important work by Ataizi et al. examined the role of BA as a neuroprotective agent. This study showed that pre-treatment of BA ameliorated traumatic brain injury (TBI) in rats. Furthermore, evidence of neuroprotection was evident in the significant decrease in lipid peroxidation and the increased catalase activity in the TBI group compared with the TBI+BA group. Also, brain damage due to edema and death of neurons was visible in the TBI group. This study further supports the results showing BA as an antioxidant, as reported in other literature.

Landmark studies by Kızılay et al[240], investigated the preventive effect of BA on axonal and myelin damage. They studied the impact of BA on the Yasargil aneurysm clip-induced model of sciatic nerve injury in rats. Furthermore, they demonstrated a significant increase in nerve conduction velocity and the number of axons compared to the control group with no BA. Moreover, the damage to myelin and immunoreactivity, as indicated by the neuroinflammation marker NFKβ, is weak and reduced in the treatment group. These benefits might be supported by the antioxidant effects of BA. Recently, the potential of BA has been uncovered in AD. Hacioglu et al[241], investigated the role of co-treatment of BA+curcumin in synaptosomes obtained from the rat cerebral cortex (an ex vivo model of neurodegeneration). Co-treatment of BA+curcumin on Aβ1-42-exposed synaptosomes

alleviates the DNA fragmentation values, MDA levels, and AChE activities. This study strengthens the role of BA as an antioxidant.

1.8.6 Kinetics of boron-containing compounds with different free radicals

Boron, being electrophilic, reacts with strong free radical nucleophiles generated under pathological concentrations in order of descending order of their nucleophilicity like peroxynitrite ($ONOO^-$)>hypohalous acid (HOCl)>^-OOH under physiological conditions at pH 7.4. Kuivila[242], in his exemplary work in 1954, reported the electrophilic displacement reaction between H_2O_2 and phenylboronic acid. Further, he demonstrated that the kinetics of BCC with H_2O_2 is slow compared to other free radicals[242]. The second order reaction rate with H_2O_2 is ($k \sim 1-2\ M^{-1}\ s^{-1}$)[243]. However, the reaction rates for $ONOO^-$ and HOCl, at pH 7.4 of 106 $M^{-1}s^{-1}$ and 104 $M^{-1}s^{-1}$ respectively. The reaction rates depend upon the stoichiometry of reactions; therefore, the BCC reacts stoichiometrically (1:1) with $ONOO^-$ millions of times faster than H_2O_2 to phenol[244, 245], whereas the hypochlorite anion (OCl^-) reacts 1000 times faster than H_2O_2 to yield phenolic oxidative product[244]. Because of the weak nucleophilicity and stability of the H_2O_2, in a buffered aqueous solution of (pH 7.4), the stoichiometry or the concentration of H_2O_2 is high, thus oxidizing the BCC quantitatively. On the other hand, the physiological concentration of H_2O_2 is low because it's being diffused and scavenged as a signal molecule in different tissues; therefore, the stoichiometry or the concentration of BCC should be high to scavenge the small concentration of H_2O_2. Cumulatively, the BCC could be used as an imaging fluorescent probe for different pathological conditions to track the pathophysiology of neurodegeneration due to oxidative stress[246]. To compare the reaction times of BCC at an equal concentration of 0.1mM of phenyl boronates, the

reaction time scales are seconds for ($ONOO^-$), seconds for (HOCl), and hours for (H_2O_2)[244]. The potential of BCC as a scavenger of both reactive nitrogen species (RNS) and ROS has given additional merit to the use of BCC as a detoxifying agent and imaging probe in different pathological conditions instigated by both ROS/RNS NDDs. It is important to note that BCC having conjugated ring scaffolds are generally used as a fluorophore system **(figure 15)**[244].

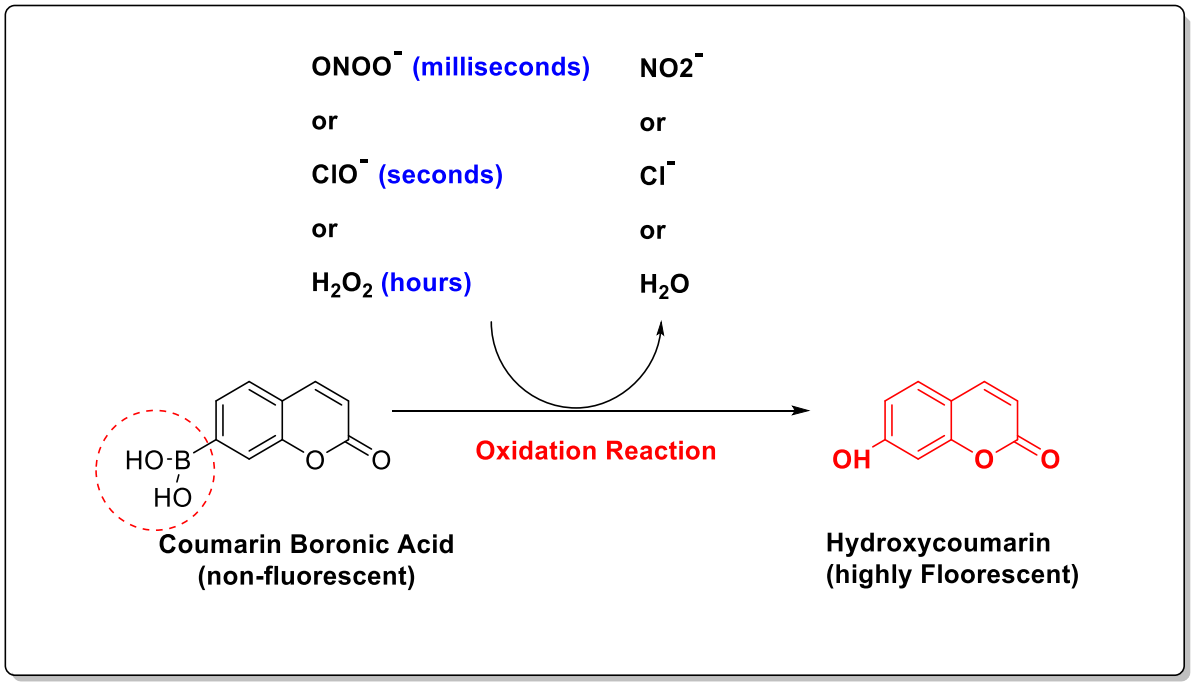

Figure 15. Free radicals directed oxidation product of coumarin-based boronic acid to highly fluorescent hydroxycoumarin, using a user-friendly probe.

1.8.7 Added advantages of boron scaffold: pharmacokinetics, chemo selectivity, blood-brain barrier permeability, and non-toxic by-products

As mentioned above, B is an indispensable element having a diverse and versatile role in the evolution of living beings. It has vast potential in modulating biological activities; therefore, several drugs have been approved by regulatory bodies in the past decades.

One of the most important characteristics of including B scaffolds in the organic molecules is their ability to positively modulate the pharmacokinetic activities of the organic molecules, hence, affecting the absorption, distribution, metabolism, and excretion of medicinal agents. High doses of medicinal agents are administered due to the poor bioavailability and low solubility of drugs[247, 248]. Although this also increases the risk of side effects and causes adverse drug reactions[249, 250]. Neurodegenerative diseases are more prevalent in aged populations. further, the organ functions get poor in the aging population; therefore, the pharmacokinetics of drugs is an important challenge in the elderly population[251]. B compounds have been shown to overcome the challenge of poor pharmacokinetics. A large number of studies have shown the role of ROS in the pathogenesis of NDDS. Furthermore, H_2O_2 and metals like Fe and Cu are involved in the formation of highly harmful bio-reactive species called hydroxyl radical (OH) via Fenton and Haber-Weiss reaction in a living system. To mitigate the neurotoxicity of OH, the 'boron advantage' has been utilized by medicinal chemists, which gives an edge of having chemo-selective H_2O_2-mediated deprotection or scavenging of H_2O_2 rather than nonspecific oxidation with enhanced cell membrane permeability. The introduction of masked chemo-selective boronate in drug discovery to scavenge ROS, like H_2O_2, gives an edge in the field of neurodegenerative diseases and aging[252] **(figure 16)**. Studies have shown the distribution and accumulation of B across the brain, crossing the lipoidal BBB, thereby taking advantage of B to target tumors.

The discovery of BNCT, to kill brain tumors, and glioma, was successful because the B compounds were able to cross the BBB and concentrate on the tumors. mercaptoundecahydrododecaborate (B12H11SH, BSH), was the first compound to lead

to the discovery of BNCT to treat malignant glioma[253]. Treatment of glioma using BSH gave profound evidence that BSH crosses the BBB and concentrates in tumors. This was well supported by retrospective pharmacokinetic studies done by Kagegi et al[253] to evaluate the tumor/blood (T/B) ratio of BSH after intravenous infusion in patients suffering from brain gliomas. This seminal study further investigated that the high accumulation of BSH in tumors clinically, which is due to the uptake of BSH across the BBB. Further, studies by Mishima and colleagues[254] investigated the role of l-para-boronophenylalanine (l-BPA), a boronated amino acid drug, in treating malignant glioma[255]. This was due to the transport of l-BPA through the amino acid transport[256]. It has been well demonstrated three decades ago by Penland that B improves cognitive function, thus B can cross the BBB[232, 238]. The evidence that B can cross the BBB is supported by the evidence provided by Rabia Koc et al[257]. They demonstrated the potential of B-containing compound borax in improving the neurological function and reducing oxidative stress after ischemia/reperfusion (IR) injury of the rat spinal cord. Thus, it acts as a neuroprotectant.

Surmounting evidence suggests that the accumulation of B in the brain alleviates the neuronal injury. Experiments on dogs with BA have shown that the accumulation of BA is highest in the gray matter of the brain[258] additional studies have shown evidence of B being a neuroprotectant because of its antioxidant ability[259] and anti-inflammatory properties[260]. Additionally, research has been demonstrated that boron-containing nanoparticles can distribute preferentially in the brain and heart[261]. However, not all the BCC crosses the BBB, because of the preferential transport system across the BBB. The BBB allows BA to cross the BBB, but limits the distribution of bortezomib[262]. The BCC

has shown potential in treating brain tumors in humans; however, the supporting evidence of B being preferentially cross BBB could be utilized to target various NDDs, including AD, PD, and ALS.

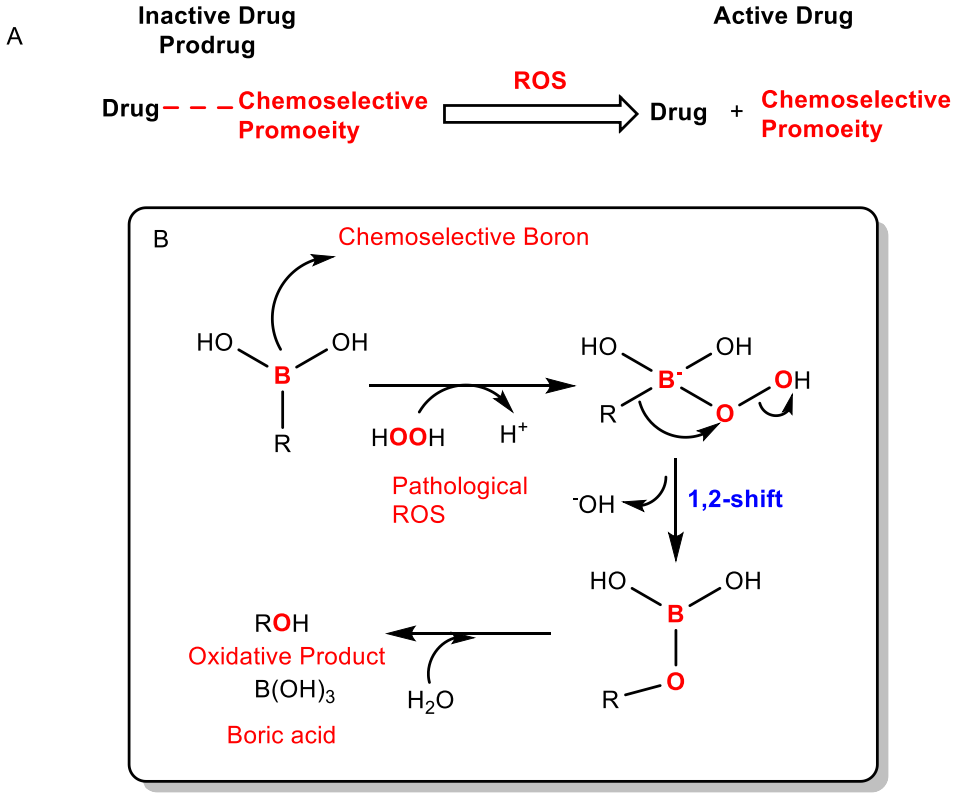

Figure 16. A. Schematic representation of the chemo-selective reactive oxygen species (ROS)-triggered prodrug concept.

The inactive drug becomes active in the presence of pathological ROS inside cells under pathological conditions in neurodegeneration. The by-product, boric acid, is non-toxic and excreted in urine. **B.** Putative mechanism of chemoselective and oxidative deboronation reaction with pathological hydrogen peroxide (H_2O_2) in neurodegenerative diseases (NDDs).

Zhong et al[263]. synthesized a new boronic acid prodrug of tamoxifen called ZB497, which readily converted to 4-OHT (active medicinal agent) in mice; also, the bioavailability of 4-OHT increased 30 times when given at the same dose of either 4-OHT or tamoxifen. The synthesis of a boronic acid prodrug of tamoxifen enhanced its bioavailability for several reasons. Firstly, it bypasses the first-pass metabolism due to the microsomal CYP2D6 enzyme, which is required for the activation of tamoxifen to 4-OHT. Secondly, it bypasses the metabolic clearance by O-glucuronidation. Thirdly, the biotransformation of ZB497 to 4-OHT (the active drug) is catalyzed by CYP450 enzymes through oxidative deprotonation, utilizing a greener approach *in situ*, in the presence of a high concentration of ROS in the tumor microenvironment. Lastly, the byproducts boric acid and pinacol are non-toxic metabolites released; the LD_{50} of BA is comparable to table salt, whereas the LD_{50} of pinacol is 3,380 mg/kg oral dose. These improved properties could lead to the administration of lower dosages in clinics for elderly patients, improving compliance and reducing the side effects of thrombosis and hot flashes.

Park and colleagues [264], recently synthesized hydrogen peroxide (H_2O_2) activated estrogen receptor beta ligands to modulate inflammation in neurodegenerative disorders. They used boronate esters (6c) to mask the phenolic group, to increase the selectivity of the pro-estrogen towards H_2O_2-rich pathological conditions, and further, release the ERβ-selective estrogen in neurodegeneration.

Charkoudian and coworkers[265], synthesized a boronate-based pro-chelator (BSIH), which is selectively bio-transformed in situ in the presence of ROS like hydrogen peroxide. Nature's most vulnerable free radical oxidant is the hydroxyl radical, which is highly neurotoxic and formed via the Fenton reaction, prompted by ferrous (Fe^{+2}) ions.

However, it is important to note that ascorbic acid acts as a pro-oxidant and recycles the ferric ion (Fe^{+3}) to ferrous (Fe^{+2}), thereby instigating the generation of ROS through the Fenton's reaction [91]cycles. The discovery of a new pro-chelator[266] is advantageous over Iron chelates due to specificity because chelating agents compete with iron-containing enzymes and with physiological metals like zinc and Cu that are important for cellular function. Furthermore, they are associated with systemic toxicities[267] **(figure. 17)**.

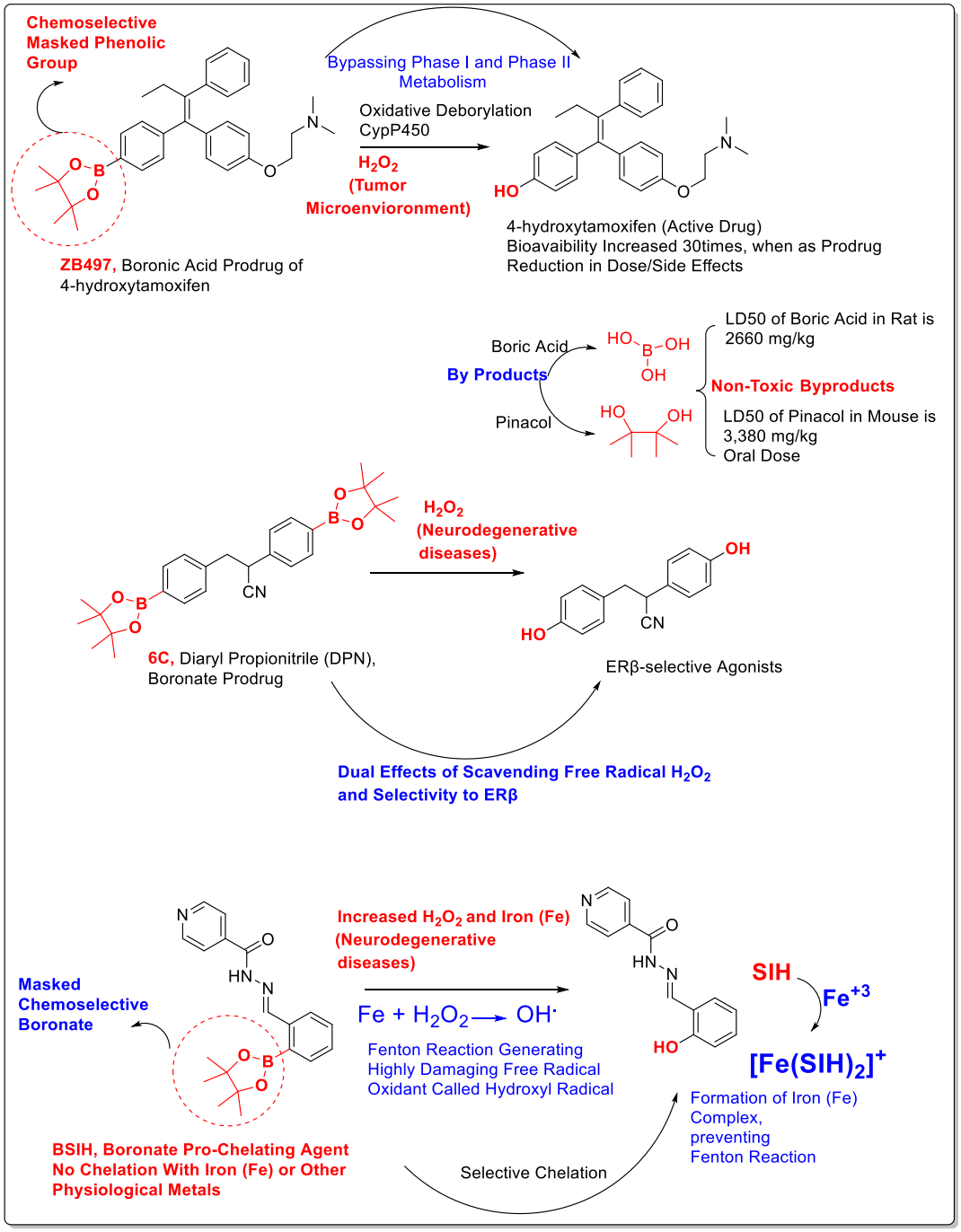

Figure 17. Boron-containing compounds serve as chemoselective prodrugs in various disease pathologies.

Miller and group[268], synthesized a new class of chemo-selective peroxy sensors with enhanced cell permeability, and a new class of fluorescent sensors to probe H_2O_2 in a

micromolar range in physiological conditions, including hippocampal neuronal cells. These compounds provide a merit of boronate deprotection, scavenging the micromolar concentration of H_2O_2, in cells and neurons insulted by free radicals, hence protecting them from the harmful effects of radicals. Moreover, these fluorescent boronate probes, have improved permeability and, thereby, are used to measure the pathological concentration of H_2O_2 inside cells (<50μM causes apoptosis, whereas higher than >50 μM causes necrosis)[269] and neurons.

Cadahia and team[270], synthesized new H_2O_2-sensitive prodrugs of methotrexate and aminopterin for the treatment of rheumatoid arthritis. The new boronic acid prodrugs showed improved pharmacokinetics, with increased solubility, and high chemical and enzymatic stability, thereby bypassing the first-pass metabolism, and hence increasing plasma concentration and therapeutic efficacy compared to parent drugs. This approach with boronic acid properties could be exploited to increase the PK and mitigate the ROS in NDDs. Also, this strategy of designing drugs gives high patient compliance **(figure. 18)**.

Hoang and his colleagues[271] recognized the potential of B in rare, fatal, and complex motor neurodegenerative diseases called ALS. Further, they synthesized a new ROS-responsive semisynthetic mask phenyl boronic acid conjugate of human ANG (angiogenin, a human ribonuclease, implicated in ALS progression[272, 273]). The novel boronic acid compound impedes the nuclear activity of ANG. The active ANG, required for neuroprotection through its intracellular ribonucleolytic activity, was released by the cleavage of boronic acids in the presence of the most prevalent ROS (H_2O_2). Thus, the masked ANG prevents astrocytes from the risk of oxidative stress, involved in the pathophysiology of ALS[274]. Moreover, the by-products (BA and 4-hydroxybenzyl

alcohol) of the unmasking boronic acid ANG conjugates, didn't result in any physiological toxicity in human astrocytes **(figure 19)**.

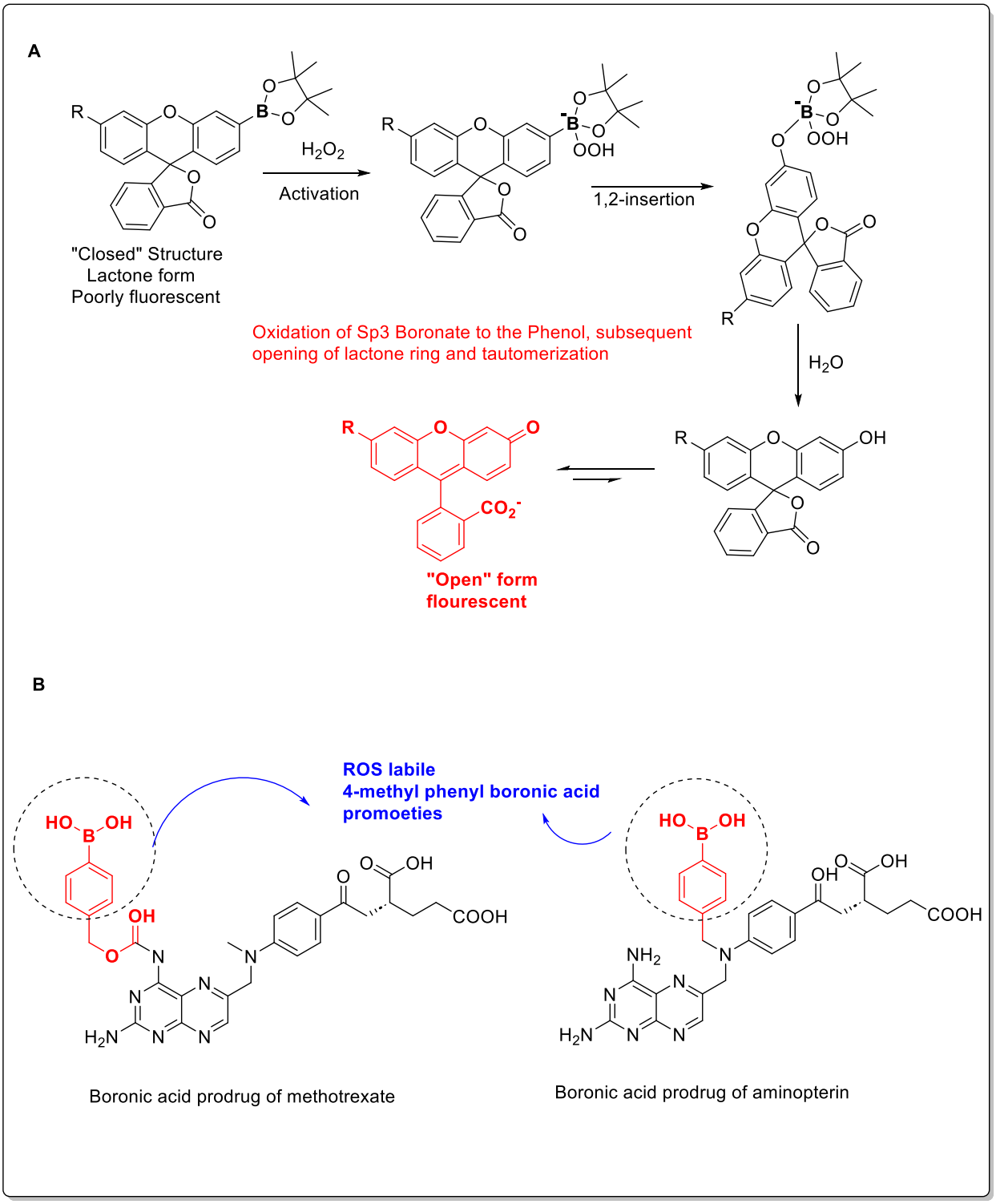

Figure 18. Boron-containing compounds are used as A. chemoselective fluorescent sensors and B. chemoselective prodrug of methotrexate.

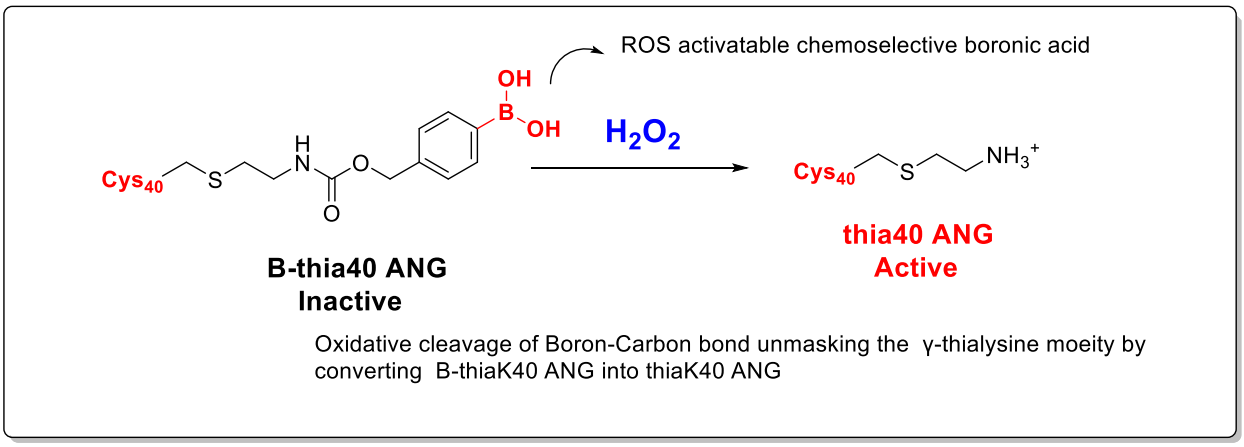

Figure 19. Boron-containing compounds as chemo-selective prodrugs used in neurodegenerative disease.

1.8.8 Cross-talk between boron and the most prevalent free radical, hydrogen peroxide (H_2O_2): Role in ALS disease progression

Substantial evidence suggests that oxidative stress is one of the major etiological factors in the pathogenesis of both forms of ALS, sporadic (sALS) and familial (fALS). Damaging free radicals due to oxidative stress causes degeneration of motor neurons both in the spinal cord and motor cortex in ALS[275-278]. Further, various oxidative stress biomarkers are reported in the postmortem tissue of both forms of ALS, suggesting the pathological role of oxidative stress in motor neuron neurodegenerative disease[279-284]. These results are consistent with the increase in oxidative stress biomarkers due to the damaging effects of free radicals on proteins, lipids, and nucleic acids in mutant SOD1 (mSOD1) ALS mice mimicking the clinical phenotypes of ALS[284-286]. Moreover, studies have revealed that the toxicity of both mSOD1 and wildtype(wSOD1) is due to

toxic gain of function, leading to ALS pathogenesis in both forms of ALS. Mutations in the SOD1 gene lead to a toxic gain-of-function of SOD1 proteins. These misfolded toxic SOD1 proteins cause dysregulated biochemical and molecular pathways in the brain and spinal cord, leading to the degeneration and death of motor neurons. Overexpression or toxic gain of function of SOD1 leads to the generation of a pathological amount of H_2O_2, which is a weak oxidizing agent and is a non-ionized, poorly reactive free radical. Nevertheless, it produces highly reactive, unstable, and toxic free radical species called hydroxyl radical (HO•), via Fenton's reaction in the presence of ferrous ion (Fe^{+2}) or Haber-Weiss reaction in the presence of ($O2^{\cdot -}$) and (Fe^{+3}). The (HO•) being a strong oxidant of all the ROS reported leads to oxidative stress-induced lipid peroxidation, mitochondrial dysfunction, excitotoxicity, and eventually results in redox dysregulation within the cell, leading to neuronal death in the case of ALS[287-290]. Thus, the reported evidence suggests that increased concentration of the most relevant ROS, H_2O_2, and Fe load leads to the pathogenesis of Neuronal death due to the generation of HO• radicals.

Therefore, if we could find an approach to scavenge the excessive concentrations of pathological H_2O_2 or Fe, this could alleviate oxidative stress in cells, thereby protecting neurons. One novel approach is the utilization of BCC as H_2O_2 scavengers and prochelators. The compounds containing B scaffolds selectively remove an excess of pathological H_2O_2 and Fe^{+2}. Moreover, the chemoselectivity of these BCCs has an added feature of targeted bioimaging of the vulnerable areas of neurodegeneration.

B has several advantages, firstly, H_2O_2 scavengers in several oxidative stress-induced neurotoxicity, secondly, pro chelators (H_2O_2, activated metal chelators) of Fe^{+2} and Cu, thirdly, bioimaging of H_2O_2, fourthly, targeted drug delivery, fifthly, as theragnostic agents

(site specific detection or measurement of double edge sword molecule H_2O_2), sixthly, minimizing the unwanted off-target effects of physiological metal-chelation and physiological H_2O_2 (acting as a signal molecule in cellular processes), and lastly, generation of non-toxic metabolites like BA, thus increasing the selectivity and improving the therapeutic potential of drug[291-297].

Evidence from the reported literature to date supports our hypothesis that BCC is an attractive scaffold for slowing the progression of fatal and incurable ALS by alleviating the oxidative stress caused by the damaging and most prevalent free radicals, H_2O_2 **(figure 20)**.

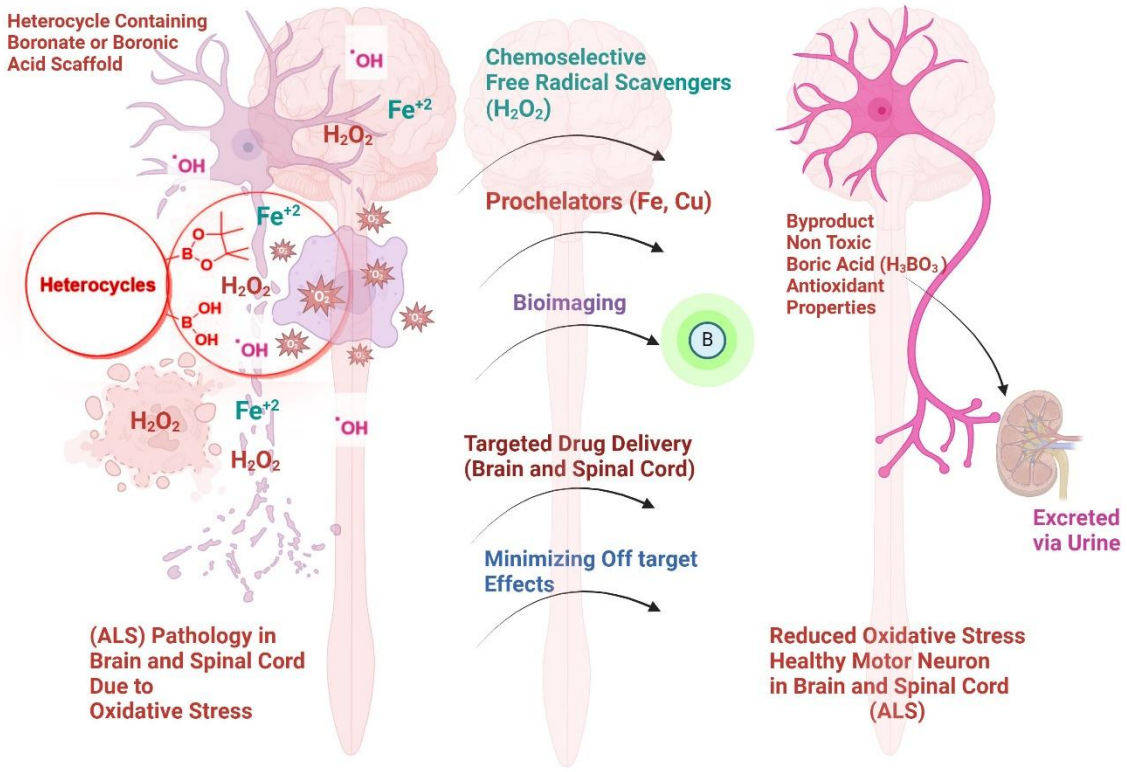

Figure 20. Various emerging roles of boron (B) heterocycles in the drug discovery of CNS therapeutics.

The B scaffolds, such as boronic acids and boronates, act as a chemoselective moiety to sequester the free radicals implicated in the pathophysiology of amyotrophic lateral sclerosis (ALS). B scaffold containing heterocycles also acts as pro-chelators of transition metals, such as copper (Cu) and Iron (Fe), implicated in oxidative stress (OS) and global aging. Further, B molecules act as a fluorescent sensor to detect the delivery of B across the central nervous system. The by-products of B organic molecules, such as boric acid (BA), are nontoxic and exert their neuroprotective effects through their antioxidant properties. They are highly water-soluble and pharmacokinetically excreted via urine.

2 Overall summary of research approaches

2.1 Rationale/Research Questions/Hypothesis/Objectives and AIMS

Amyotrophic lateral sclerosis (ALS) is a relentlessly progressive motor neurodegenerative disease that results from the death of both upper motor neurons (UMN) and lower motor neurons (LMN) in the brain and spinal cord. ALS is not a single disease, as it is a highly complex, clinically heterogeneous, pathologically multifactorial neurodegenerative disease. ALS is a rare neurodegenerative disease with an ultimately fatal clinical endpoint. It is proposed that there will be a massive surge in ALS cases from 222,801 in 2015 to 376,674 in 2040, representing an epidemiologic increase of 69%[44]. Since the discovery of ALS in 1869 by Jean-Martin Charcot and the landmark identification of the SOD1 mutation by Rosen et al. in 1993 as a causal factor for the progression of human familial ALS (fALS), only two FDA-approved drugs, Edaravone (EDR), an antioxidant, and Riluzole (RLZ), an antiglutamatergic, have been widely accessible and used clinically, though with limited impact on the disease course. Both drugs have been used in clinical settings with modest effects on ALS progression. However, preclinical studies in SOD1

ALS mouse models have not demonstrated any significant survival benefits[298-306]. However, some delay in disease progression has been observed, and this finding has been translated to human studies. Despite this, the potential of small molecule therapeutics, such as EDR, which aim to reduce the global oxidative stress involved in ALS pathophysiology, remains significant. This is supported by the presence of oxidative stress biomarkers during ALS progression in both transgenic ALS murine models of [307-312] and patients with sporadic and familial ALS[307, 313-319], further confirming the role of free radical-mediated oxidative damage in the disease's etiopathogenesis. Additionally, it is important to note that the ALS scientific community has been making great efforts to develop drugs that modify disease phenotypes in ALS patients, considering that they do not have much time after diagnosis to wait for long-term treatment. However, recent efforts have not yielded any benefits, and all the major clinical trials have recently failed[320]. Recently, the FDA granted accelerated approval to tofersen based on its ability to reduce neurofilament light chain (NfL), a pharmacodynamic biomarker. However, NfL remains a nonspecific biomarker for neurodegenerative disease diagnosis and complicates differentiation between ALS and other conditions[321]. Additionally, the potential of the neurofilament heavy chain (NfH) is underestimated due to issues with assay sensitivity[322]. Further, emerging evidence suggests that Tofersen use in patients is non-compliant and causes serious neurological adverse events and warrants further investigation of its benefit-to-risk ratio[323].

Emerging evidence from the last three decades after the discovery of SOD1 ALS mouse models suggests that oxidative stress caused by pathological H_2O_2 is a key hallmark in ALS pathology, making it a primary target for therapeutic intervention in ALS[324-331].

Moreover, Cysteine 111 (Cys^{111}) of the SOD1 protein serves as a hotspot for oxidative modification under elevated concentrations of the neurotoxic H_2O_2[131, 133, 141, 332-336]. The acquired toxicity of both mutant and wild-type human SOD1 triggers numerous abnormal oxidative redox pathways in neurons and non-neuronal cells, leading to progressive, fatal paralysis caused by motor neuron degeneration neurons[337]. In our current early-phase drug discovery efforts, we have recognized the diverse and versatile potential of small organic molecule EDR and have aimed to overcome its limitations ranging from synthesis to formulation while enhancing safety and efficacy in humanized SOD1 ALS mouse models. To achieve this, we employed a novel strategy that uniquely incorporated a boron scaffold into the FDA-approved EDR molecule. Boron's low toxicity profile and its role as a chemoselective warhead targeting free radicals involved in motor neuron degeneration in ALS could have significant advantages. However, several reports have demonstrated the effective role of boron compounds as anti-cancer agents. In addition, emerging reports have shown the potential of boron compounds in maintaining neuronal health; none have been utilized to slow the progression of ALS.

Using this boron-based approach, we aim, for the first time, to modify several motor disease phenotypes and extend survival in SOD1 ALS mice.

Based on investigations from emerging literature over the past three decades, we asked a few key questions to develop our research hypothesis for the *proof-of-concept (POC)* studies.

1. **Is oxidative stress a key global etiological factor in both sALS and fALS?**
2. **Do the currently FDA-approved EDR and Riluzole effectively extend the lifespans of ALS mouse models/and human ALS patients?**

3. **Do ALS mouse models provide strong support for transitioning from preclinical to clinical studies?**
4. **Can the new boron-containing EDR analogues be safe and effective in *in vitro* studies compared to EDR?**
5. **Is the new boron-containing EDR analogue safe and capable of prolonging lifespan and improving clinical motor phenotypes in humanized SOD1 ALS mice?**
6. **Can the novel boron-containing EDR analogue demonstrate target engagement and modulate the pathways implicated in neurodegeneration?**
7. **Can discovery-based, unbiased, untargeted proteomic and phosphoproteome profiling offer compelling evidence that correlates the efficacy of the new boron-containing EDR analogue with its therapeutic potential?**

To answer these research questions, we formulated our hypothesis. It is anticipated that the new analogs will improve pharmacokinetics, overcoming the present limitations of EDR. The cost of edaravone is $1,424 per patient per day or $185,182 per patient annually ($190,880 in the first year of treatment). Making it a costly drug. However, the question of how long patients should take EDR remains unresolved. Moreover, the FDA has not defined the limit for treatment duration. This creates a perplexing situation for patients suffering from ALS. Additionally, intravenous administration creates further apprehension in patients. It is anticipated that the new analogs of EDR would be able to solve this issue. Additionally, the new synthetic route is expected to be more cost-effective and less prone to synthetic hurdles compared to EDR[151].

Therefore, our overall hypothesis is that tailored boron-based pyrazoles, which could serve as EDR boron analogues and EDR prodrugs, could act as a novel, chemoselective, H_2O_2-activatable warheads to mitigate the global pathological concentrations of free radicals, such as H_2O_2, implicated in the pathophysiology of ALS. Furthermore, we hypothesize that boron-containing EDR molecules can modulate oxidative stress propagation both in the spinal cord and brain, thereby influencing clinical motor phenotypes, delaying disease and symptom onset, extending survival, and mitigating weight loss or ALS-induced cachexia in the humanized SOD1-G37R ALS preclinical mouse model. Additionally, the new molecules containing boron could modulate the expression of various known and unknown discovery-based global proteins and phosphoproteins in the spinal cord and brain of preclinical SOD1 G37R ALS mice model. We believe this work will represent the first discovery of best-in-class boron-containing EDR analogues or prodrugs that could potentially slow the progression of ALS. This advance signifies a promising step toward developing more effective treatments for this high-need, fatal orphan disease.

2.2 Overall research aim

Synthesis, characterization, and development of boron-based EDR analogues **(B^5-EDR)** that can serve as potential redox regulators in combating the progression of ALS.

2.3 Overall research hypothesis

i) We are proposing that **B^5-EDR** analogues could serve as prodrugs of EDR via an *in vitro* and *in vivo* metabolic transformation.

ii) We are also proposing that **B^5-EDR** analogues can serve as independent redox regulators, and as stand-alone compounds via the therapeutic effects of boron.

iii) As an added benefit, we propose that our **B[5]-EDR** analogues can also serve as a triple-role therapeutic agent, via the benefits of the newly attached Boron scaffold.

Below is the diagrammatic representation of the proposed research proposal **(figure 21).**

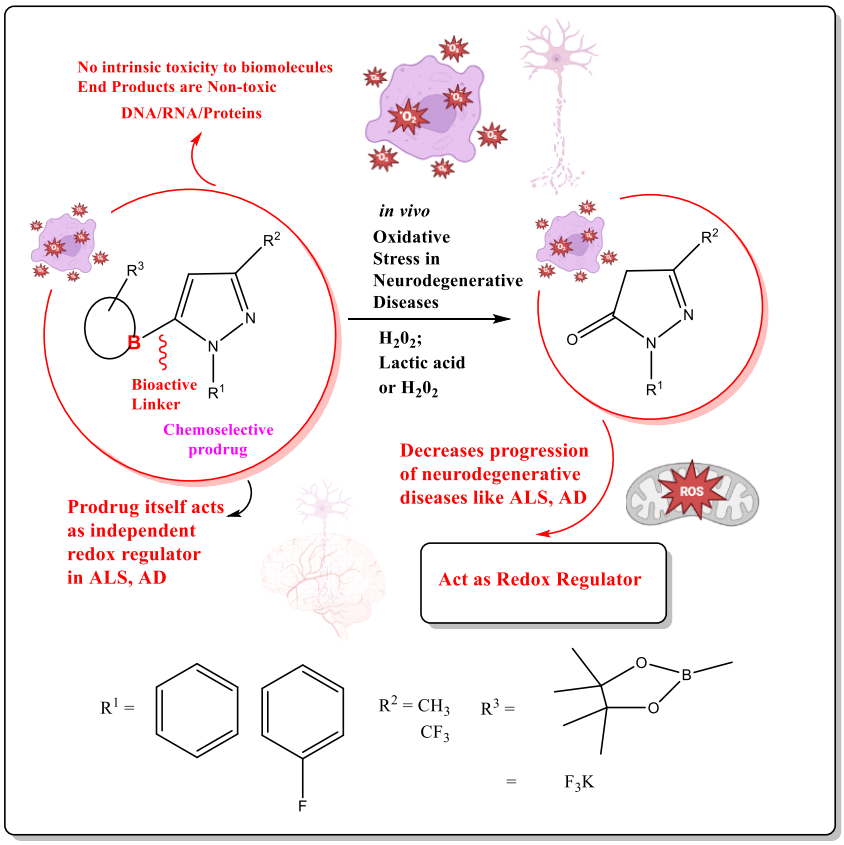

Figure 21. Hypothetical representation of the proposed research.

Below is the proposed mechanism **(figure 22).**

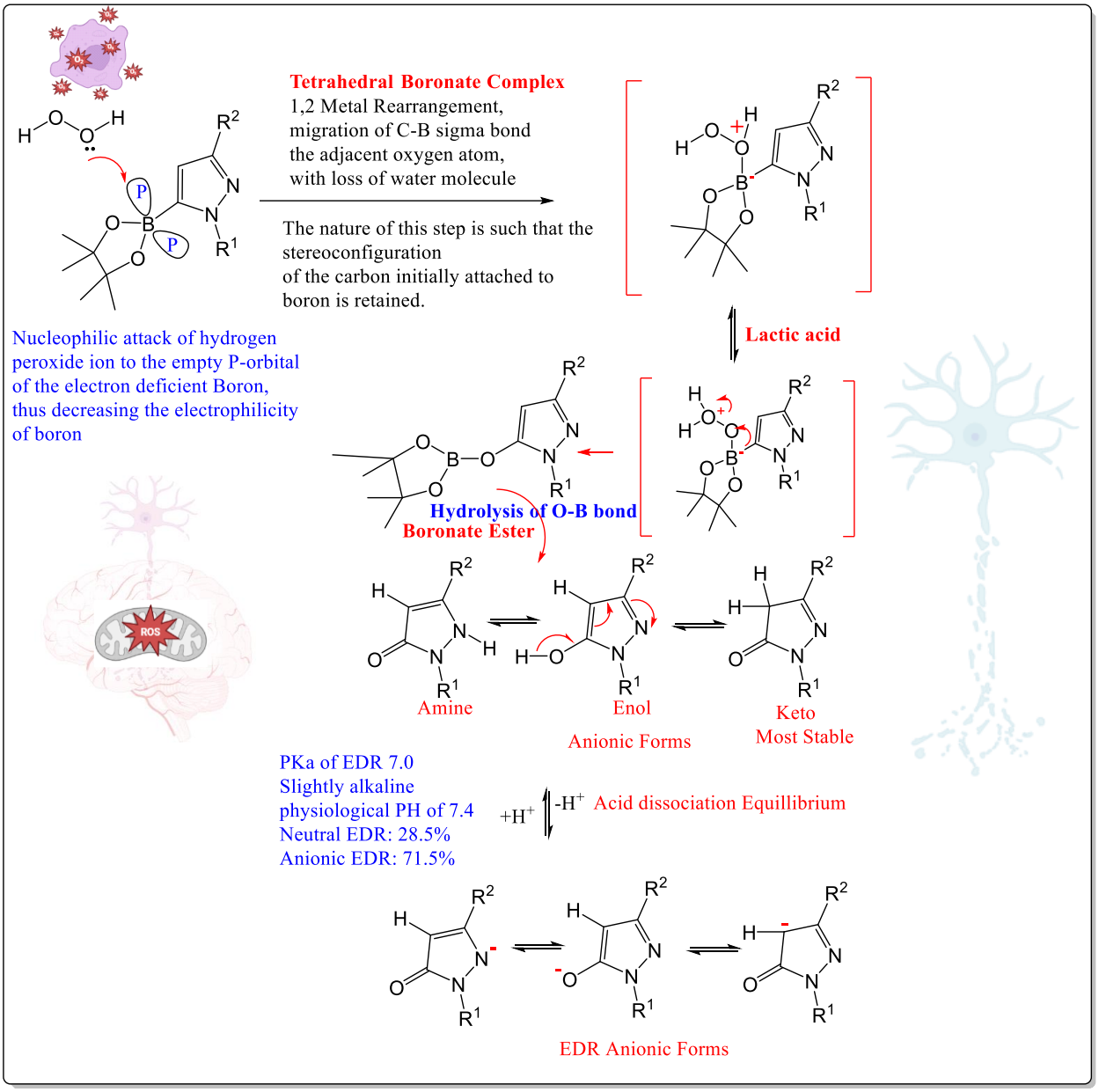

Figure 22. Mechanism to show how (B^5-EDR) analogues act as redox regulators (in vivo reaction with H_2O_2) and prodrugs/generation for EDR.

2.4 Rationale for proposed hypothesis

We proposed different modifications in the EDR structure to tailor its pharmacokinetic (PK) and pharmacodynamic (PD) properties.

- **Modification in *N*-1-phenyl position of EDR:** Blocking the *para-hydroxylation* by introduction of *a* fluorine moiety is expected to decrease toxicity and increase lipophilicity[338]**.**
- **Modification in C-3 position of EDR:** Bioisosteric replacement of a hydrogen atom with fluorine mimics a methyl group. It is anticipated that fluorine substitution would modulate potency, metabolism, and membrane permeability, decrease Pgp recognition across the BBB, hence, increasing bioavailability across neurons in the CNS, undergoing stress due to pathological concentrations of free radicals like H_2O_2. Thus, expected to alleviate the oxidative stress implicated in the pathophysiology of ALS[339]**.**
- **Modification in C-4 position of EDR:** EDR efficiently neutralizes free radicals through single electron transfer in physiological conditions. The anionic form of EDA is predicted to react 8.6 times faster than its neutral counterpart. The main reaction mechanism varies with the form of EDA; for the anionic form, single-electron transfer (SET) plays a dominant role in reactivity. To accurately evaluate edaravone's antioxidant activity, the ionic form must be taken into consideration. SET can occur quickly, either before or alongside proton transfer from the C-4 methine proton, known as Sequential Electron-Proton Transfer (SEPT) and Proton-Coupled Electron Transfer (PCET), respectively. Therefore, any modification at the C-4 position will compromising EDR's antioxidant capability[340, 341].
- **Modification in C-5 position of EDR with a boron atom:** C-5 of EDR contains a keto-enol tautomeric functional group, which is an essential functional group for

antioxidant activity. Derivatization of this group by a non-toxic, chemoselective, biocompatible boron pro-group is believed to be activated by ROS (e.g., H2O2) to release a redox regulator (EDR or EDR analogues) that scavenge ROS/RNS. Boron, being a metal chelator and antioxidant warhead, may alleviate the genotoxic effects instigated by low doses of heavy metals in NDDs. However, we can also modulate the electrophilicity and stability of the boron protecting group by changing the different substituents in the progroup[342, 343]**.**

Below is the diagrammatic representation of the rationale for the proposed hypothesis for tailoring pharmacokinetic (PK) and pharmacodynamic (PD) properties **(figure. 23).**

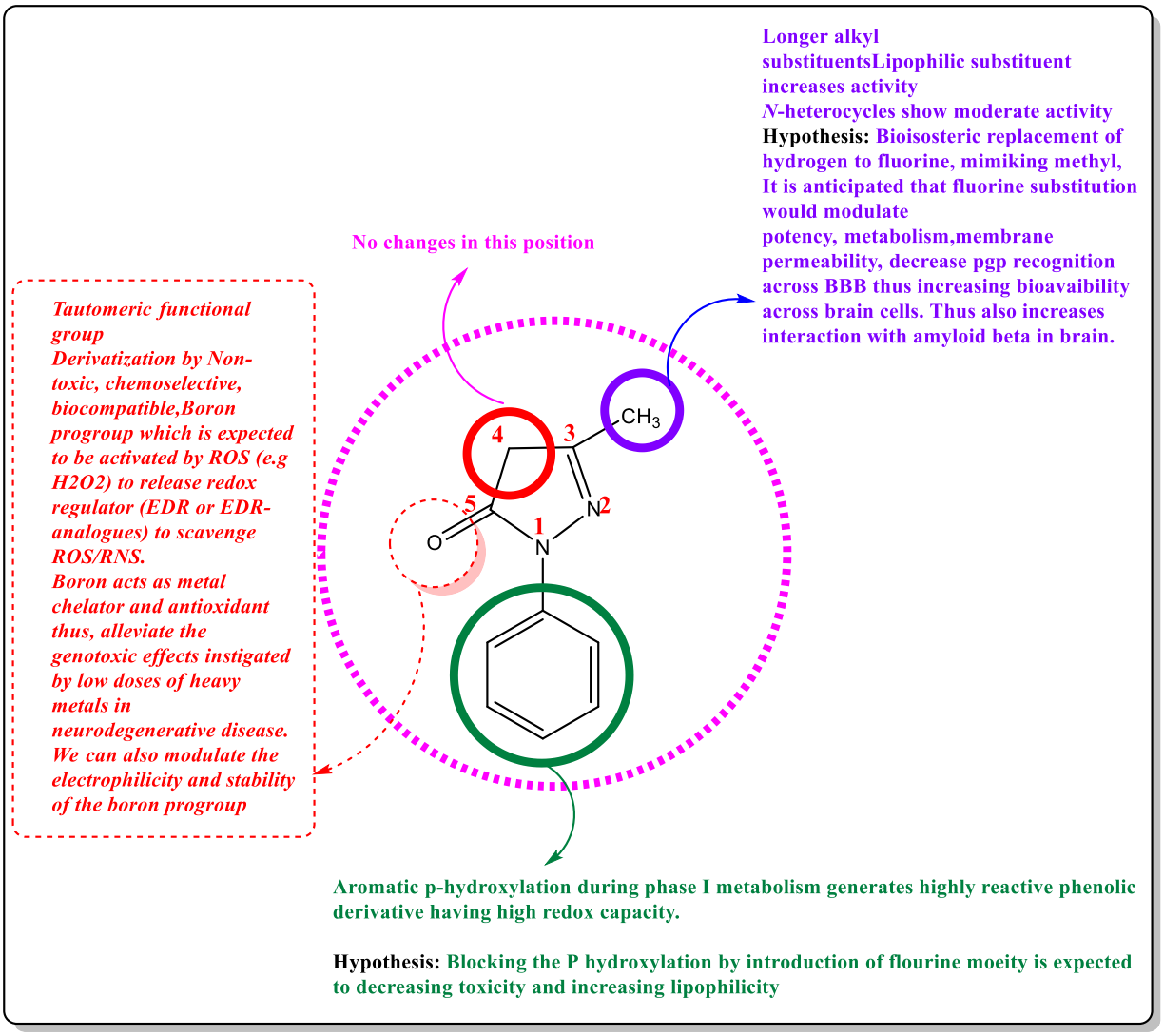

Figure 23. Overall rationale for the proposed hypothesis and research work.

The following objectives and specific aims will test the above hypothesis:

3 Research approaches: Hypothesis/Aims/Objectives

1) We propose to synthesize boron-based **B5-EDR** prodrugs and analogues utilizing the principles of green chemistry, overcoming the synthetic limitations of current EDR synthetic procedures, that will serve as prodrugs of EDR via oxidative metabolic transformations.

3.1 **Objective 1:** The synthesis of a series of B5-EDR prodrugs and B5-EDR analogues.

3.1.1 **Specific Aim 1 for Objective 1:** To synthesize and characterize boron-based edaravone prodrugs (B5-EDR).

3.1.2 **Specific Aim 2 for Objective 1:** To synthesize and characterize additional boron-based edaravone analogues (B5-EDR).

2) We hypothesize that the synthesized B5-EDR prodrugs will demonstrate *in vitro* proof of concept by converting into edaravone in the oxidative environment created by free radicals such as hydrogen peroxide (H_2O_2).

3.2 **Objective 2:** The *in vitro* transformation of B5-EDR prodrugs into EDR to establish a 'proof-of-concept' that our compounds can serve as prodrugs of EDR.

3.2.1 **Specific Aim 1 for Objective 2:** To demonstrate the Proof-of-concept *in vitro* transformation applying a novel synthetic procedure for synthesizing EDR from Boron-based prodrugs (B5-EDR).

3.2.2 **Specific Aim 2 for Objective 2:** To demonstrate the Proof-of-concept *in vitro* transformation applying a novel NMR kinetic experiment for conversion of EDR from Boron-based prodrugs (B5-EDR).

3) We hypothesize that our B5-EDR prodrugs and analogues can serve as independent redox regulators via the antioxidant effects of boron and serve as neurocytoprotective agents, in a similar manner to EDR, including a similar neurotoxicity/cell viability profile to EDR.

3.3 **Objective 3:** To study the *in vitro* properties and antioxidant abilities of our drug candidates and examine their capabilities to serve as ROS/RNS scavengers.

3.3.1 **Specific Aim 1 for Objective 3:** To evaluate the neurotoxicity and cell viability of B5-EDR prodrugs and analogues on neuroblastoma-spinal cord hybrid cells (NSC-34) and primary cortical neuronal cells by WST-8 analysis, in comparison to EDR.

3.3.2 **Specific Aim 2 for Objective 3:** To evaluate the neuroprotective effects of B5-EDR prodrugs and analogues against hydrogen peroxide-induced oxidative stress on NSC-34 cells by WST-8 analysis, in comparison to EDR.

3.3.3 **Specific Aim 3 for Objective 3:** To evaluate the change in mitochondrial membrane potential by B5-EDR prodrug (NS-1-2) using staurosporine as a positive control for apoptosis in comparison to EDR.

3.3.4 **Specific Aim 4 for Objective 3:** To evaluate the hydrogen peroxide (H_2O_2) scavenging ability of B5-EDR prodrugs (NS-1-2) using an Amplex red assay in comparison to EDR.

4) We hypothesize that our B5-EDR prodrugs NS-1-2 can reduce the fibrillization of SOD1 monomers due to their antioxidant effects and redox regulatory function.

3.4 **Objective 4:** To study the effect of NS-1-2 on fibrillization of SOD1 monomers.

3.4.1 **Specific Aim 1 for Objective 4:** To evaluate the biochemical activity of our drug candidates in reducing the fibrillization of SOD1 monomers.

5) We propose that our B5-EDR prodrug NS-1-2, containing a non-toxic boron scaffold, will be safe in wild-type mice.

3.5 **Objective 5:** To study the acute and chronic safety profile with longitudinal monitoring of NS-1-2 in the wild-type mice.

3.5.1 **Specific Aim 1 for Objective 5:** To evaluate the acute toxicity profile (single dose), with longitudinal monitoring of NS-1-2 in a wild-type mouse *in vivo*.

3.5.2 **Specific Aim 2 for Objective 5:** To evaluate the chronic toxicity profile (120 doses), with longitudinal monitoring of NS-1-2 in a wild-type mouse *in vivo*.

6) We propose that our B5-EDR prodrug NS-1-2 can also serve as triple-role therapeutic agents, via the benefits of the boron functionality and by serving as a prodrug for EDR, and lead to a similar or improved therapeutic index to EDR and improved pharmacokinetic properties.

3.6 **Objective 6:** To study the therapeutic effects of NS-1-2 in modifying disease phenotypes in the humanized SOD1-G37R (line 42) mouse model of amyotrophic lateral sclerosis.

3.6.1 **Specific Aim 1 for Objective 6:** To evaluate the efficacy of NS-1-2, in terms of delaying the onset of disease in SOD1-G37R (line 42) mouse model of amyotrophic lateral sclerosis: Time to peak body weight (days).

3.6.2 **Specific Aim 2 for Objective 6:** To evaluate the efficacy of NS-1-2, in terms of delaying the symptom onset of disease in SOD1-G37R (line 42) mouse model of amyotrophic lateral sclerosis: Loss of 10% body weight based on the highest recorded weight (days) with muscle weakness.

3.6.3 **Specific Aim 3 for Objective 6:** To evaluate the efficacy of NS-1-2, in terms of extending the survival age/life span of SOD1-G37R (line 42) mouse model of amyotrophic lateral sclerosis: Principal primary endpoint of preclinical studies.

3.6.4 **Specific Aim 4 for Objective 6:** To evaluate the efficacy of NS-1-2, in terms of preventing weight loss (ALS-induced cachexia) in SOD1-G37R (line 42) mouse model of amyotrophic lateral sclerosis: Prognostic marker for ALS.

3.6.5 **Specific Aim 4 for Objective 6:** To evaluate the efficacy of NS-1-2, in terms of improving clinical motor phenotypes with longitudinal monitoring in SOD1-G37R (line 42) mouse model of amyotrophic lateral sclerosis: Marker of motor neurodegeneration.

7) We propose that our B5-EDR prodrug NS-1-2 can show target engagement by changing the expression of cellular proteins and phosphoproteins associated with motor neurodegeneration.

3.7 **Objective 7:** To apply global mass-spectrometry-based proteomic and phosphoproteomic approaches to discover and identify biomarkers within treated SOD1-G37R mice, B5-EDR prodrug NS-1-2 versus sham controls.

3.7.1 **Specific Aim 1 for Objective 7:** To investigate the mechanism of a novel (NS-1-2), utilizing a discovery-based untargeted/unbiased LC-MS based global proteomics approach for the investigation/and discovery of known/and novel biomarkers correlating with the efficacy of NS-1-2 in the spinal cord of mutant human G37R SOD1 mice.

3.7.2 **Specific Aim 1 for Objective 7:** To investigate the mechanism of a novel (NS-1-2), utilizing a discovery-based untargeted/unbiased LC-MS based global proteomics approach for the investigation/and discovery of known/and novel biomarkers correlating with the efficacy of NS-1-2 in the brain of mutant human G37R SOD1 mice.

3.7.3 **Specific Aim 2 for Objective 7:** To investigate the mechanism of a novel (NS-1-2), utilizing a discovery-based untargeted/unbiased discovery LC-MS-based global phosphoproteome approach for the investigation/and discovery of known/and novel biomarkers correlating with the efficacy of NS-1-2 in the spinal cord of mutant human G37R SOD1 mice.

3.7.4 **Specific Aim 2 for Objective 7:** To investigate the mechanism of a novel (NS-1-2), utilizing a discovery-based untargeted/unbiased discovery LC-MS-based global phosphoproteome approach for the investigation/and discovery of known/and novel biomarkers correlating with the efficacy of NS-1-2 in the brain of mutant human G37R SOD1 mice.

8) We suggest that our B5-EDR prodrug NS-1-2 can improve the onset of symptoms in G37R mice by preventing the 10% weight loss observed at the study endpoint, demonstrating target engagement through alterations in the expression of cellular proteins linked to motor neurodegeneration.

3.8 **Objective 8:** To apply global mass spectrometry-based proteomic approaches to discover and identify biomarkers from samples collected at symptom onset, clinical end of study, and humane endpoint within treated SOD1-G37R mice, B5-EDR prodrug NS-1-2 versus sham controls.

4 Results

Objective 1: The synthesis of a series of B5-EDR prodrugs and B5-EDR analogues.

Specific Aim 1 for Objective 1: To synthesize and characterize boron-based edaravone prodrugs (**B5-EDR**).

4.1 Scheme I for the synthesis of the first prodrug of Edaravone

Scheme I for the synthesis of Edaravone prodrug NS-1-2 (*N*-arylated pyrazole boronic acid pinacol ester) via a two-step synthetic procedure *in situ*.

The synthetic route for the synthesis of NS-1-2 involves the synthesis of *N*-arylated pyrazole boronic acid pinacol ester from the commercially available *N*-arylated substituted pyrazole starting material via a two-step synthetic procedure. The first step **A)** involves lithiation at the C-5 position of *N*-arylated substituted pyrazole with *N*-butyl lithium (n-BuLi), by a directed Ortho metalation (DOM) mechanism. The second step **B)** involves the electrophilic substitution of Lithium at the C-5 position with isopropoxy 4,4,5,5-tetramethyl-1,3,2-dioxaborolane (PINBOP). This is followed by an acidic workup, which yielded *N*-arylated substituted pyrazole boronic acid pinacol ester as our first proposed boron-based EDR prodrug, NS-1-2 (**figure 24)**, with an experimental yield of **90- 95%**. **Table 1.**

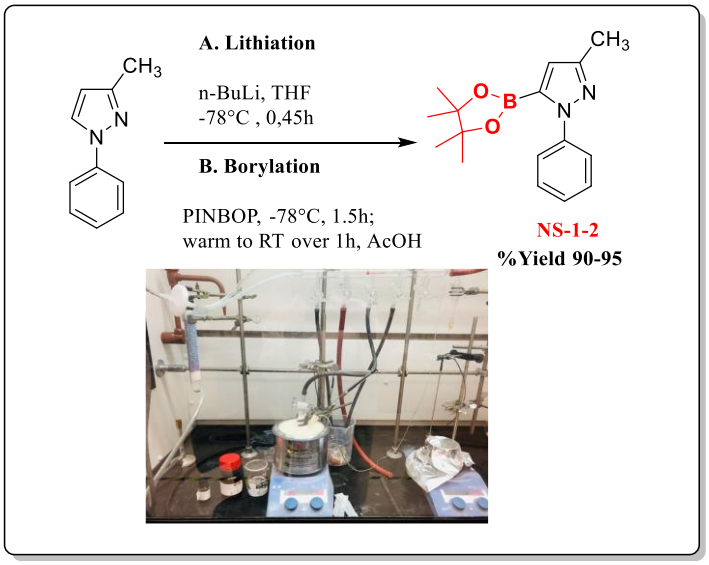

Figure 24. Scheme I for synthesizing N-arylated pyrazole boronic acid pinacol ester NS-1-2 from the commercially available N-arylated substituted pyrazole.

Table 1. Synthesis of the first boron-based EDR **(B5-EDR)** prodrug NS-1-2.

Entries	Compound	%Yield
NS-1-2	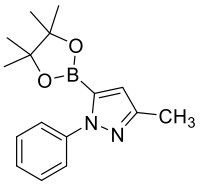	90-95

4.2 Scheme II for the synthesis of the second prodrug of Edaravone

Scheme II for the synthesis of *N*-arylated pyrazole potassium trifluoroborates from *N*-arylated substituted pyrazole boronic acid pinacol ester.

The synthetic route involves the synthesis of *N*-arylated pyrazole potassium trifluoroborates from commercially available *N*-arylated substituted pyrazole starting material. It is a two-step synthesis which involves lithiation in the first step, borylation in

the second step to get *N*-arylated pyrazole boronic acid pinacol ester, followed by conversion of the pinacolyl boronate to the corresponding trifluoro borate with aqueous potassium hydrogen fluoride in the third step[344] as our second proposed boron-based EDR prodrug, NS-1-21 **(figure 25)**, with an experimental yield of **90-95%**. **Table 2.**

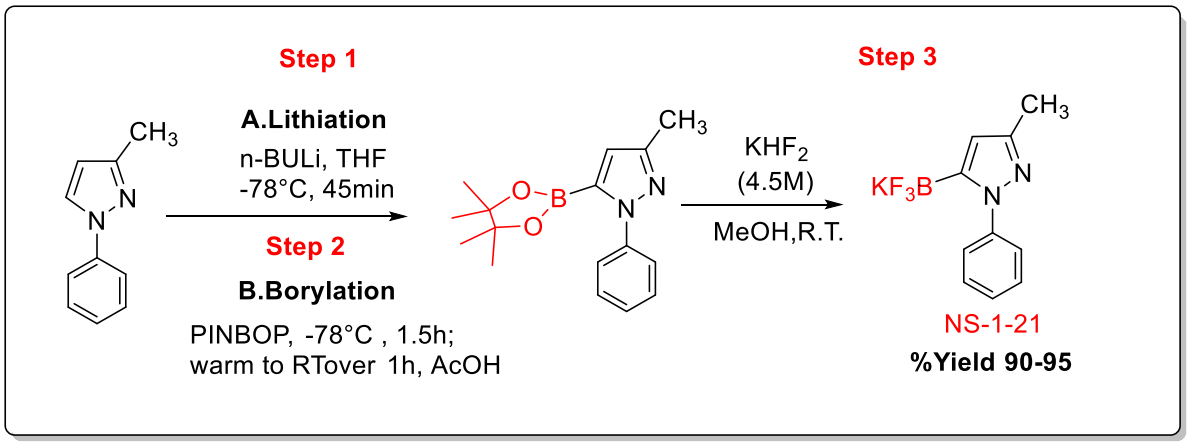

Figure 25. Scheme II for synthesizing N-arylated pyrazole potassium trifluoroborates (NS-1-21) from the commercially available N-arylated substituted pyrazole.

Table 2. Synthesis of second boron-based EDR **(B5-EDR)** prodrug.

Entries	Compound	%Yield
NS-1-2	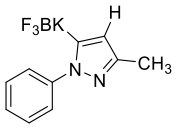	90-95

Specific Aim 2 for Objective 1: To synthesize and characterize boron-based edaravone analogues (B5-EDR).

4.3 Scheme III for the synthesis of boron-based Edaravone analogues (B5-EDR) from *N*-arylated substituted pyrazole boronic acid pinacol ester

The synthetic route for the synthesis of NS-1-12 and NS-1-19 involves scheme I and scheme II, respectively. The only change is the starting material with substituted trifluoromethyl in the C-3 position of *N*-arylated substituted pyrazole instead of C-3 methyl. Following scheme I and scheme II, NS-1-12 and NS-1-19 were synthesized (**figures 1 and 2)**, with an experimental yield of **90- 95%**. **Table 3.**

4.4 Scheme IV Synthesis of 4-fluoro-*N*-arylated pyrazole boronic acid pinacol ester from 4-fluoro-*N*-arylated substituted pyrazole starting material via a two-step synthetic procedure *in situ*

The synthetic route involves the synthesis of 4-fluoro-*N*-arylated pyrazole boronic acid pinacol ester from 4-fluoro-*N*-arylated substituted pyrazole starting material via a two-step synthetic procedure *in situ*. The first step involves Chan-Lam coupling with *N*-arylation of pyrazoles with aryl boronic acids using heterogeneous Copper (I) oxide in methanol at room temperature under base-free conditions. The second step involves lithiation at the C-5 position of *N*-arylated substituted pyrazole with *N*-butyl lithium (n-BuLi), by directed ortho metalation (DOM) mechanism, followed by the third step that involves electrophilic substitution of Lithium at the C-5 position with isopropoxy 4,4,5,5-tetramethyl-1,3,2-dioxaborolane (PINBOP). This is followed by an acidic workup, which yielded 4-fluoro-*N*-arylated pyrazole boronic acid pinacol ester. Following scheme IV, NS-1-23 was synthesized (**figure 26**), with an experimental yield of 90- 95%. **table 3**.[345].

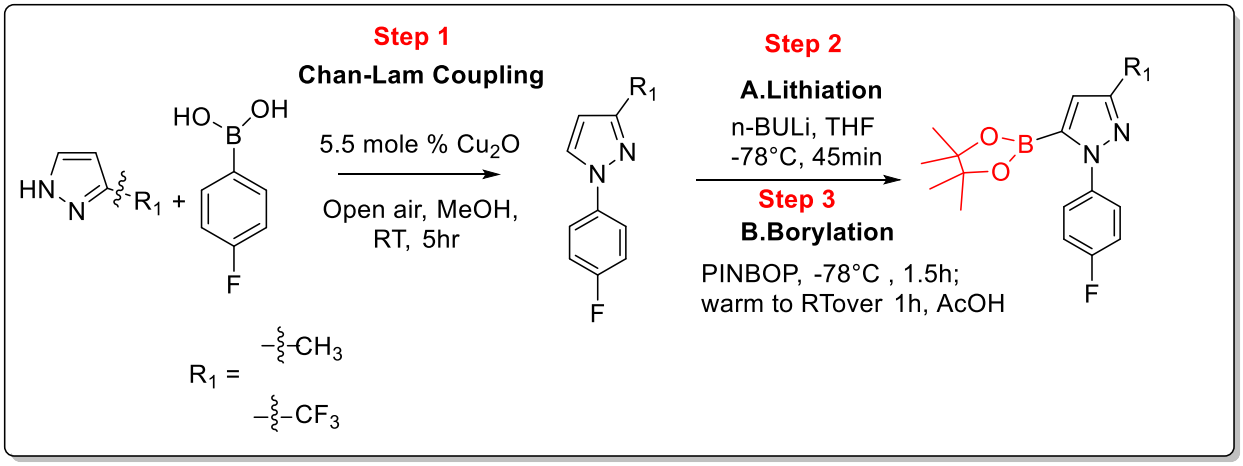

Figure 26. Synthesis of 4-flouro-N-arylated pyrazole boronic acid pinacol ester from 4-fluoro-N-arylated substituted pyrazole starting material.

Table 3. Synthesis of boron-based EDR **(B5-EDR)** analogues.

Entries	Compound	%Yield
NS-1-12	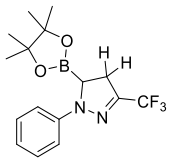	90-95
NS-1-19	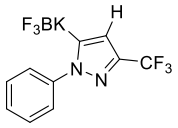	90-95
NS-1-23	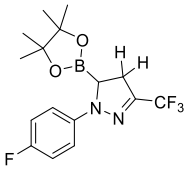	90-95

Objective 2: The *in vitro* transformation of B5-EDR prodrugs into EDR to establish a 'proof-of-concept' that our compounds can serve as prodrugs of EDR.

Specific Aim 1 for Objective 2: To demonstrate the Proof-of-concept *in vitro* transformation applying a novel synthetic procedure for synthesizing EDR from Boron-based prodrugs (B5-EDR).

4.5 Scheme III (a) for the synthesis of Edaravone from boron-based prodrugs (B^5-EDR)

4.5.1 First approach for biotransformation: Using both lactic acid and hydrogen peroxide.

Synthesis of EDR involves chemoselective *ipso* hydroxylation of boron-based prodrugs under microwave conditions. Bio-based green reagents, which are biocompatible and non-toxic, like boronic acid ester, trifloroborates, lactic acid, and hydrogen peroxide, were utilized for the synthesis of EDR (**figure 27), with an experimental yield of 90- 95%. Table 4.**

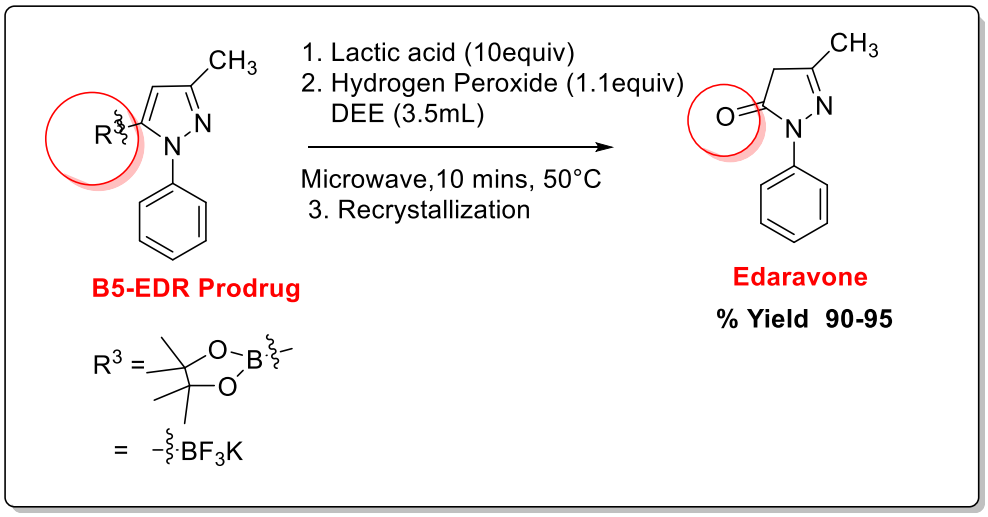

Figure 27. Scheme III (a) synthesis of EDR from its prodrug (B5-EDR).

4.6 Scheme III (b) for the synthesis of Edaravone from boron-based prodrugs (B^5-EDR)

4.6.1 Second approach for biotransformation: Using only hydrogen peroxide.

Synthesis of EDR involves chemoselective *ipso* hydroxylation of boron-based prodrugs under microwave conditions. Bio-based green reagents, which are biocompatible and non-toxic, like boronic acid ester, trifluoro borates, and hydrogen peroxide, were utilized for the synthesis of EDR (**figure 28), with an experimental yield of 85- 90%. Table 5.**

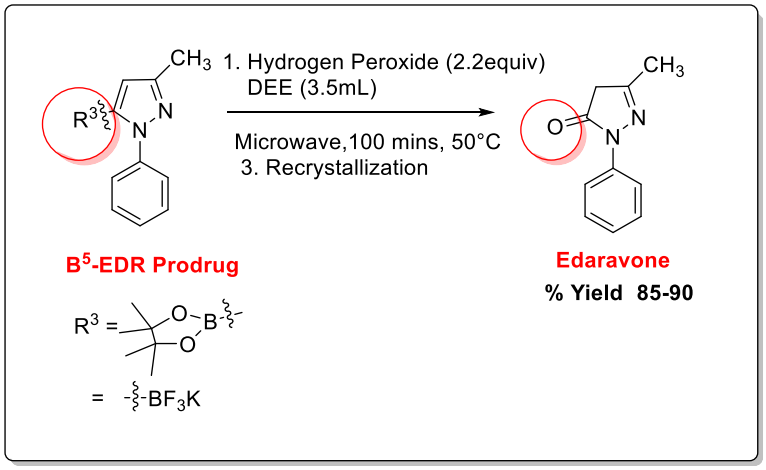

Figure 28. Scheme III (b) synthesis of EDR from its prodrug (B5-EDR).

Table 4. Synthesis of EDR from (B5-EDR) prodrugs**.**

Entries	Compound	%Yield
NS-1-10	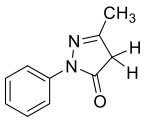	90-95
NS-1-26	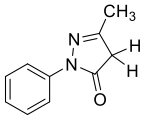	85-90

*First approach; ** Second approach

4.7 Green, bio-inspired, catalyst-free method for the synthesis of Edaravone from its boron-based prodrug (NS-1-2). *In vitro* proof of concept of H_2O_2-induced oxidative transformation of B5-EDR to Edaravone

Our current synthesis of EDR from its prodrug NS-1-2 is based on a green, bio-inspired, catalyst-free transformation of NS-1-2 into EDR. Synthesis of EDR involves chemoselective *ipso*-hydroxylation of boron-based prodrug NS-1-2 under microwave conditions. Bio-based green reagents that are biocompatible and non-toxic, such as boronic acid ester, lactic acid, and hydrogen peroxide (H_2O_2), were utilized for the synthesis of EDR. To the best of our knowledge to date, no literature reports have detailed this green chemistry approach for the synthesis of EDR. Further, we propose that our chemical process mimics a chemoselective H_2O_2-induced oxidative transformation of boron-based prodrugs within a cellular environment undergoing oxidative stress during neurodegeneration. This concept could be further referred to as selective targeting of neurodegenerative disease within regions of high oxidative stress, as a target-based approach to mitigating the progression of motor neurodegeneration in ALS, **(figure 29)**.

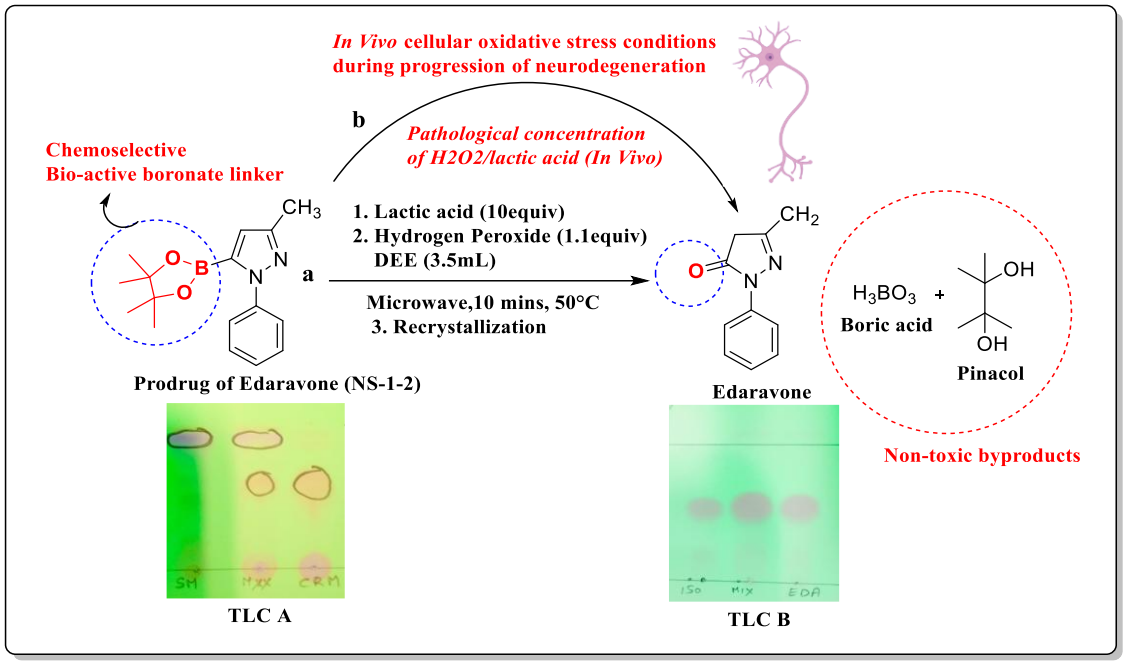

Figure 29. Schematic illustration of a hydrogen peroxide (H_2O_2) triggered boron-based prodrug approach.

NS-1-2, (a boron-based prodrug of edaravone (EDR)) synthesized according to the scheme I (see Methods and Materials), is masked with a H_2O_2-sensitive, pinacol boronate prodrug moiety, **a.** The NS-1-2 prodrug is oxidatively transformed/deprotected in the presence of H_2O_2 and lactic acid under microwave conditions *in situ* to form EDR, **b.** NS-1-2 prodrug **a** is proposed to be biotransformed into EDR (**b**), *in vivo* on exposure to pathological concentration of H_2O_2, with or without lactate, as associated with the oxidative stress pathology of ALS. **1A-B** shows examples of a chemical reaction between B5-EDR analogue (**a)** and H_2O_2 to produce EDR (**b**) and corresponding TLC plots. TLC A: SM = starting material; Mix = mixture of SM and CRM; CRM = Crude Reaction Mixture; TLC B: ISO = isolated product; Mix = mixture of isolated product and EDR; and EDR = Edaravone.

4.8 Putative mechanism for biotransformation of boron-based Edaravone prodrug NS-1-2 into Edaravone (EDR)

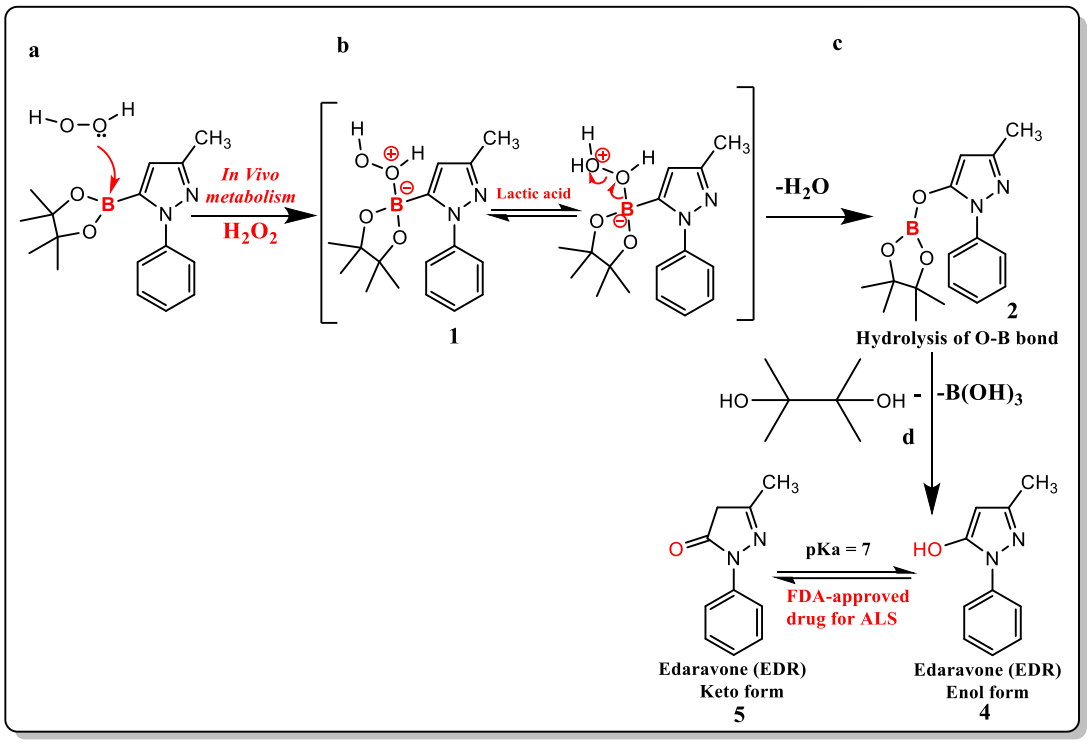

Figure 30. Schematic proposed mechanism to show how NS-1-2 could act as a redox regulator prodrug under an oxidative cellular environment (*in vivo* biotransformation with H_2O_2) for the generation of EDR.

The mechanism involves **a)** Nucleophilic attack from the increased concentration of pathological hydrogen peroxide (H_2O_2) inside the cells during oxidative stress to the empty *p*-orbital of the electron-deficient boron (B) atom to form a tetrahedral boronate complex (**1**). **b)** The boronate complex **1** undergoes a rearrangement/migration of the C-B sigma bond onto the adjacent oxygen atom facilitating the loss of a water molecule. Lactic acid in step **b** can create an acidic environment facilitating the reaction in the forward direction to form **2**. **c)** Finally, hydrolysis O–B bond to afford deprotected *ipso*-hydroxylation product to yield deprotected alcohol **3** and the by-product of pinacol and

boric acid. **d)** The pKa of EDR is 7.0, and it exists as a solid in keto tautomer form **4**. However, its tautomeric enol form **5** exists as a highly unstable anion in aqueous solution.

4.9 The advantages of an optimized and efficient microwave synthesis of Edaravone

The innovative synthetic methodology used for synthesizing FDA-approved EDR has successfully resolved previous synthetic limitations. This new approach presents multiple advantages. High-purity EDR was synthesized and characterized using cost-effective starting materials. The toxicity associated with the starting material, phenylhydrazine, was effectively mitigated through this facile synthetic route, which employed bio-based, green reagents. These reagents such as boronic acid, lactic acid, and H_2O_2 demonstrate biocompatibility and were utilized in the EDR synthesis. Furthermore, the catalyst-free synthesis of EDR was marked by a simple work-up process, making purification and extraction relatively simple. Additionally, the pH of the crude reaction mixture was maintained by avoiding stronger oxidizing acids; instead, mild oxidizing acids were used, keeping the reaction pH within the 6 to 6.5 range. The use of mild oxidizing agents supported EDR's stability and prevented decomposition during the reaction, leading to a higher yield (90-91%) compared to the conventional process (60-70%). The recrystallized product demonstrates stability in aerobic conditions when stored at 4°C, with no discoloration, likely due to the greater stability of the product resulting from the different starting materials and reaction conditions. Energy minimization occurred as the reaction was conducted for 10 minutes at 50°C in a microwave reactor, unlike conventional methods that involve prolonged heating at higher temperatures of 160°C for 2 to 4 hours, which can result in EDR degradation. The use of lactic acid, a bio-based green solvent,

allows for catalyst-free oxidation of boronic esters and facilitates selective ipso hydroxylation, producing phenolic compounds with high efficiency. In summary, with the new synthetic procedure, we have achieved clean synthesis of FDA-approved EDR with high purity by applying sustainable chemistry principles. Our new synthetic methodology for the synthesis of EDR from its prodrug, utilizing principles of sustainable green chemistry, is a unique approach with novelty, industrial utility, and applicability.

Specific Aim 2 for Objective 2: To demonstrate the Proof-of-concept *in vitro* transformation applying a novel NMR kinetic experiment for conversion of EDR from Boron-based prodrugs (B5-EDR).

4.10 NMR kinetics experiments to validate the proof of concept for the conversion of Edaravone from its prodrug NS-1-2

The prodrug Edaravone NS-1-2 was well characterized using NMR and ESI-HRMS techniques. Furthermore, the proof of concept for the transformation of NS-1-2 in the oxidative environment of H_2O_2 was optimized and validated through the following scheme, and the formation of EDR was well characterized using NMR (H1 and C13) and ESI-HRMS techniques. However, we aimed to investigate the sensitivity of NS-1-2 to H_2O_2 with the H1 NMR technique. For the first time, we developed and optimized the H1 NMR technique to monitor the reaction's progress over time, converting the FDA-approved EDR from its prodrug, NS-1-2. For the NMR kinetic experiment, we first optimized the molar concentration of NS-1-2 to be dissolved with H_2O_2 for the conversion of NS-1-2 to EDR. The TLC observation of the NMR sample prepared showed that in the presence of H_2O_2, NS-1-2 was oxidized to generate EDR. As observed in the TLC, after 20 minutes (TLC not shown), the NS-1-2 (SM) began to convert to EDR, and after 20 hours, 100% of

the SM had converted into EDR. Nearly all of the boronic ester groups (40 mM) were cleaved by a 10-fold excess of H_2O_2 (400 mM) in 20h. We could conclude that the designed boron prodrugs undergo H_2O_2-triggered hydrolysis in a time-dependent manner **Figure 8**. Furthermore, in the presence of H_2O_2, NS-1-2 was oxidized to generate EDR in a time-dependent manner. This was confirmed by the appearance of new aromatic proton peaks: evolution of 5.36 ppm (from 6.6 ppm) and 2.1 ppm (from 2.2 ppm), which matches with the 1H NMR spectra of control samples of both NS-1-2 and EDR before hydrolysis (**figure 31)**.

We aimed to investigate the reason for the change in chemical shift when EDR undergoes H_2O_2-triggered oxidative hydrolysis of NS-1-2 to EDR. DMSO is an aprotic polar solvent that utilizes its lone pair on oxygen to donate to the protons of other molecules, functioning as an H-bond acceptor. This stabilizes the acidic hydrogen of the methine at the C-4 position in EDR, thereby shielding and decreasing the chemical shift of the methine proton. Evolution of two new proton (H1) peaks at position C-4 and C-3 with the hydrolysis of NS-1-2 to EDR with a time course is illustrated in **(figures 33 and 34), respectively, which matches with the control proton peaks (H1) in (figure 32)**.

As shown in **figure 33**, the evolution of EDR over time is clearly demonstrated by the change in chemical shift of the methine proton at the C-4 position. The chemical shift of the methine proton at the C-4 position in NS-1-2 is 6.6 ppm, while it is 5.3 ppm for EDR. Over time, the 6.6 ppm chemical shift decreases as a 5.3 ppm chemical shift develops. In the first 0-2 minutes, the 5.3 ppm peak corresponding to EDR begins to form, increasing in height with time; by 21 hours, the height of the 5.3 ppm peak is nearly three times that

of the 6.6 ppm peak, rising to four times by 24 hours, indicating approximately 90% conversion of the NS-1-2 prodrug to EDR **(figure 33)**.

Moreover, as illustrated in **figure 34**, the evolution of EDR over time is clearly demonstrated by the change in chemical shift of the methyl proton at the C-3 position. The chemical shift of the methyl proton at the C-3 position in NS-1-2 is 2.2 ppm, while it is 2.1 ppm for EDR. Over time, the 2.2 ppm chemical shift vanishes as a 2.1 ppm chemical shift develops. In the first 0-2 minutes, the 2.1 ppm peak corresponding to EDR begins to form, increasing in height with time; by 21 hours, the height of the 2.1 ppm peak is nearly three times that of the 2.2 ppm peak, rising to four times by 24 hours, indicating approximately 90% conversion of the NS-1-2 prodrug to EDR **(figure 34)**.

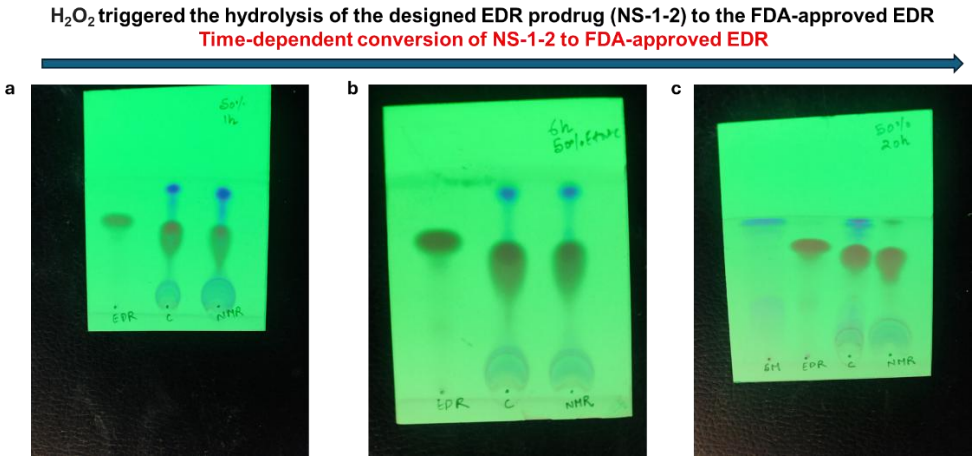

Figure 31. The TLC observation demonstrated that, in the presence of H_2O_2, NS-1-2 containing boronate was oxidized to generate Edaravone (EDR) with keto-enol.

Panels a, b, and c display the progress of NS-1-2 boronate oxidation by H_2O_2, leading to the generation of an equivalent amount of EDR. Almost all boronic ester

groups (40 mM) were cleaved and consumed by a 10-fold excess of H_2O_2 (400 mM) over 20 hours, demonstrating that the designed boron prodrugs undergo H_2O_2-triggered hydrolysis in a time-dependent manner. Edaravone **(EDR)** spots, Co-spot **(C)**, starting material **(SM)**, and nuclear magnetic resonance **(NMR)** stocks were prepared in a 1.5 ml tube by dissolving NS-1-2 (DMSO)+ H_2O_2 in dH_2O at room temperature.

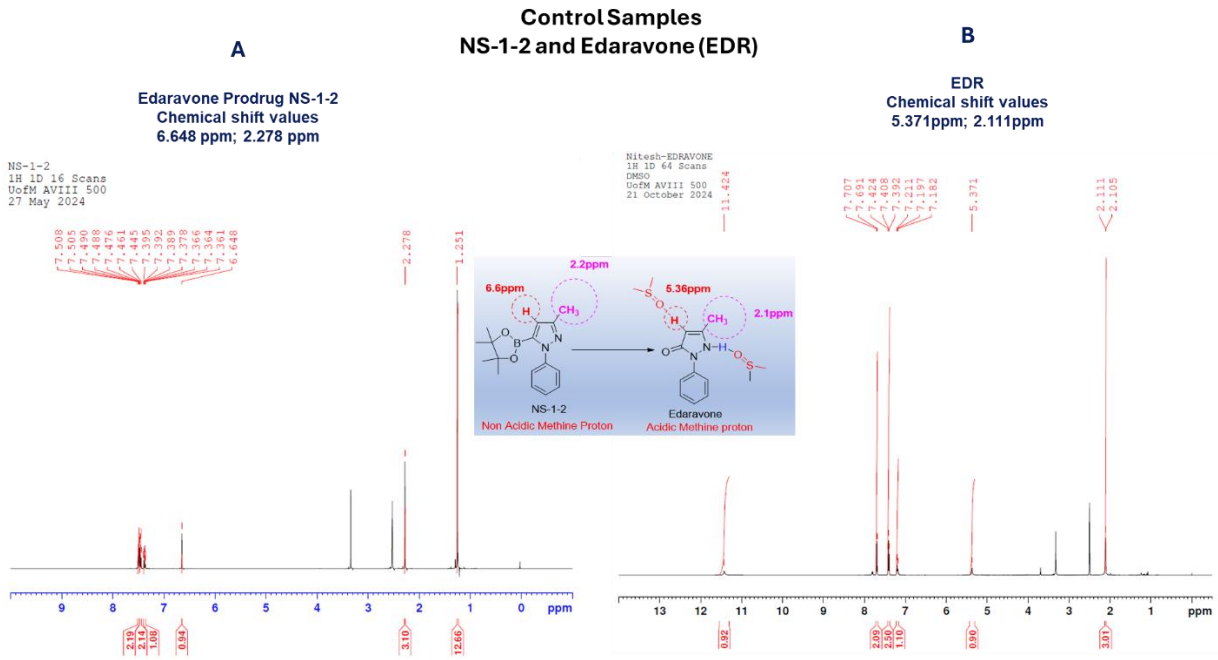

Figure 32. 1H NMR spectra illustrating the chemical shift values (ppm) of control samples before hydrolysis.

A. Edaravone prodrug NS-1-2 before hydrolysis. The methine proton peak, which is not acidic, shows a chemical shift of 6.6 ppm, while the methyl peak indicates a chemical shift of 2.2 ppm. **B.** Edaravone (EDR) before hydrolysis. The methine proton peak is acidic, exhibiting a chemical shift of 5.36 ppm due to the stabilization provided by the DMSO

solvent, which acts as a hydrogen-bond acceptor. In contrast, the methyl peak exhibits a chemical shift of 2.1 ppm due to the shielding effects of DMSO on the methine proton.

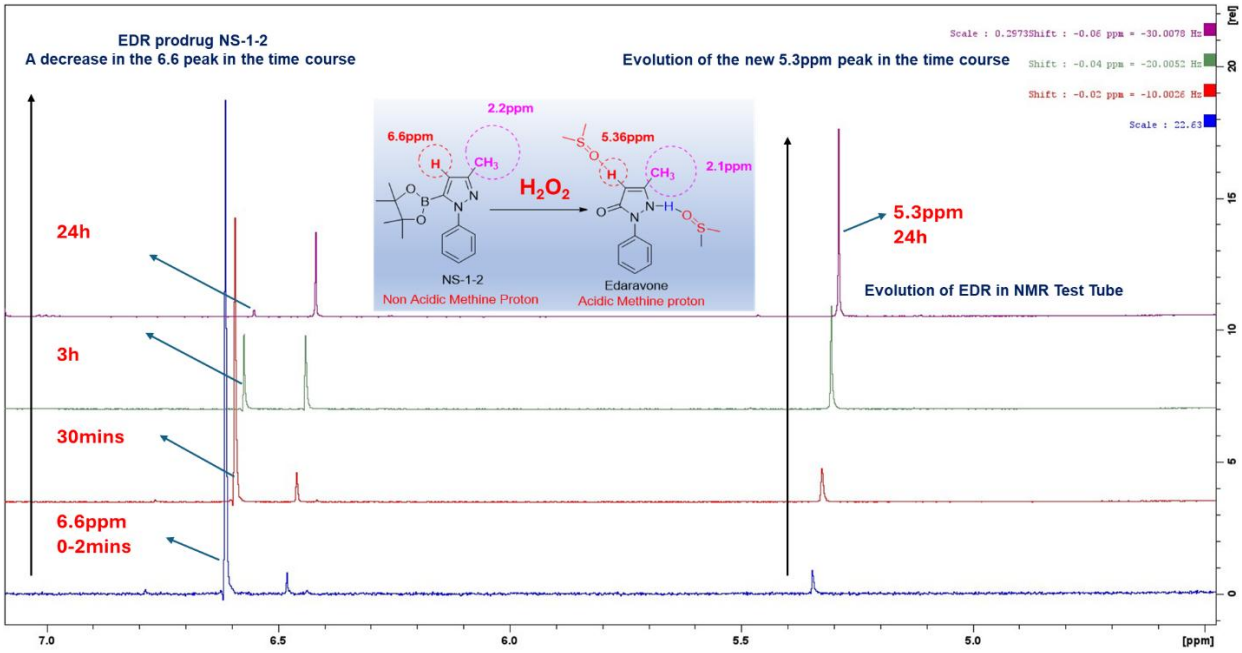

Figure 33. 1H NMR spectra illustrate the chemical shift (ppm) values, demonstrating the time-course conversion of NS-1-2 to edaravone (EDR).

1H NMR spectra illustrate the chemical shifts (ppm) of the EDR prodrug NS-1-2 after H_2O_2-mediated oxidative hydrolysis, depicting the time-course conversion of NS-1-2 to EDR at 0, 2 minutes, 30 minutes, 3 hours, and 24 hours. The emergence of a new signal at 5.36 ppm (from 6.6 ppm in the NS-1-2 control samples) for the methine proton at position C-4 corresponds to that of the control EDR samples.

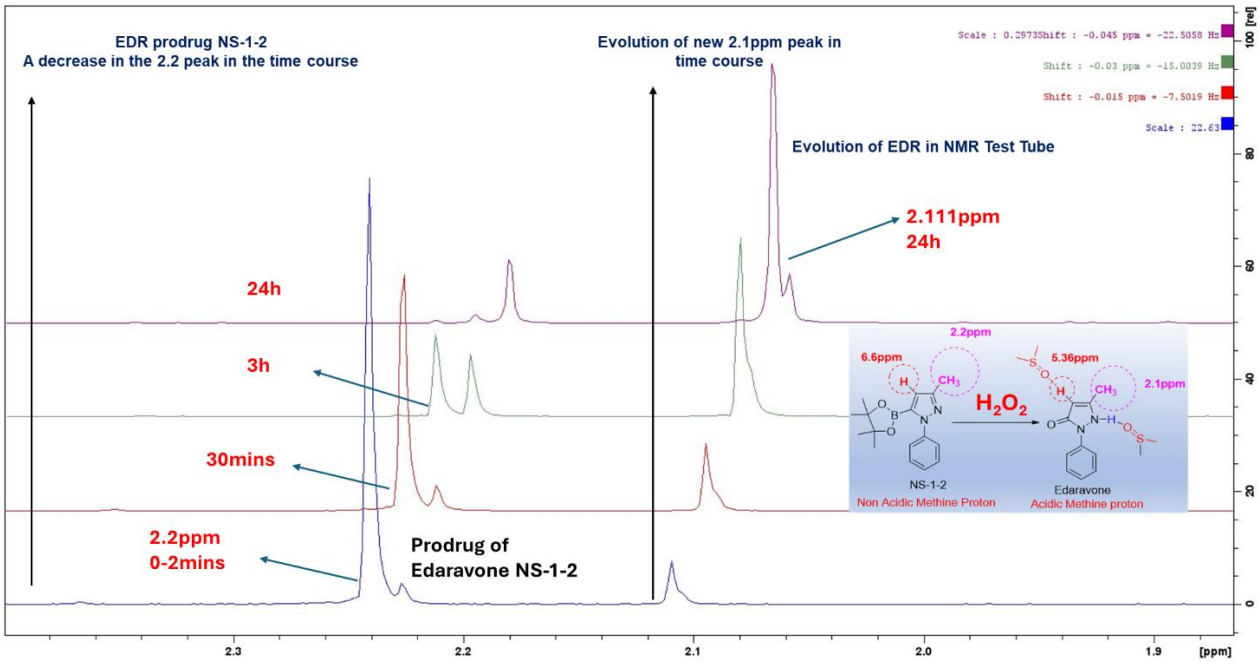

Figure 34. 1H NMR spectra illustrate the chemical shift (ppm) values, demonstrating the time-course conversion of NS-1-2 to edaravone (EDR).

1H NMR spectra illustrate the chemical shifts (ppm) of the Edaravone prodrug NS-1-2 after H_2O_2-mediated oxidative hydrolysis, depicting the time-course conversion of NS-1-2 to EDR at 0, 2 minutes, 30 minutes, 3 hours, and 24 hours. The emergence of a new signal at 2.11 ppm (from 2.22 ppm in the NS-1-2 control samples) for the methyl proton at position C-3 corresponds to that of the control EDR samples.

Specific Aim 1 for Objective 3: To evaluate the neurotoxicity and cell viability of B5-EDR prodrugs and analogues on neuroblastoma-spinal cord hybrid cells (NSC-34) and primary cortical neuronal cells by WST-8 analysis, in comparison to EDR.

4.11 Neurotoxicity and cell viability analysis

4.11.1 NSC-34 cell line as a suitable model to study ALS

The NSC-34 cell line, also called the neuroblastoma-spinal cord (NSC) hybrid cell line, was first developed by Cashman *et al*. by fusing the aminopterin-sensitive neuroblastoma N18TG2 with motor neuron-enriched embryonic day 12-14 spinal cord cells. These mouse-mouse neural hybrid cell line hybrids possess characteristics of adherent multipolar cells with long neurites that resemble motor neurons and display additional key features of motor neurons, such as the generation of action potentials, expression of neurofilament triplet proteins, and acetylcholine synthesis, storage, and release. These immortalized, clonally uniform cell lines were developed as a tool for studying motor neurons without the need for isolation from animals.

As primary motor neurons have low proliferative capacity, yield low quantities, and are short-lived in culture, NSC-34 cells allow for extended passage (as a neuroblastoma) and produce high quantities of motor neuron-like cells following differentiation. Functionally, NSC-34 cells are similar to motor neurons, as demonstrated by their ability to form transient synapses with myotubes, that is, neuromuscular junctions *in vitro* with muscle cells. Several studies have extensively utilized NSC34 mouse motor neuron cells in drug screening for ALS and in investigating biochemical pathways during neurodegeneration. Therefore, these NSC34 mouse motor neuron cells serve as a suitable model to study motor neuronal pathophysiology in neurodegenerative diseases like ALS[346-348].

4.11.2 Primary cortical neuronal cell cultures (PCNC)

Primary neurons exhibit various unique features that cell lines cannot adequately mimic. Primary cortical neurons were collected from fetuses of CD1 mice at gestational day 17-

18. The most crucial feature of primary embryonic rodent cultures is that they are generally prepared from embryonic day 17-18 (E17-E18) brains, equivalent to the third trimester of human pregnancy. Therefore, these rodent brains contain many more post-mitotic neurons than the human fetal neuron cultures. PNCC provides several advantages over neuronal cell culture lines. Firstly, PNCC maintains the same phenotype, including morphological, neurochemical, and electrophysiological features similar to *in vivo* models or situ neurons. Secondly, they can develop mature neurites under proper culture conditions, comparable to human neurons. Lastly, the neurites from PNCC differentiate into dendrites and axons with synapses, which are not present in typical cell lines in culture[349].

4.11.3 WST-8 Assay (WST-8 Metabolism End point)

Principle: Dojindo developed highly water-soluble tetrazolium salts known as WSTs. The WST-8 reagent serves as a surrogate for mitochondrial function, helping to determine cell metabolism, which is regulated by mitochondrial reducing enzymes like NAD(P)H dehydrogenase[350]**.** These enzymes belong to the class of oxidoreductases that catalyze both oxidation and reduction reactions, also known as NADPH:acceptor oxidoreductase. They play an important role in maintaining cellular homeostasis, cellular metabolism, mitochondrial redox functions, signal transduction, aging, and cell death**.** Thus, NADP-dehydrogenase systems should be regarded as a second line of defense to maintain the effective functioning of the central antioxidative systems[351]**.** Cytotoxicity/cell viability assays in response to different treatments were evaluated using the WST-8 assay. This assay is based on the reduction of the tetrazolium dye (WST-8) to an orange-colored soluble formazan dye by mitochondrial dehydrogenases (reducing

enzymes). An increase in the number of living cells leads to an increase in the activity of mitochondrial dehydrogenases, which in turn results in a higher production of formazan dye. This can be quantified by measuring the absorbance of the dye at OD=450 nm, **(figure 35)**.

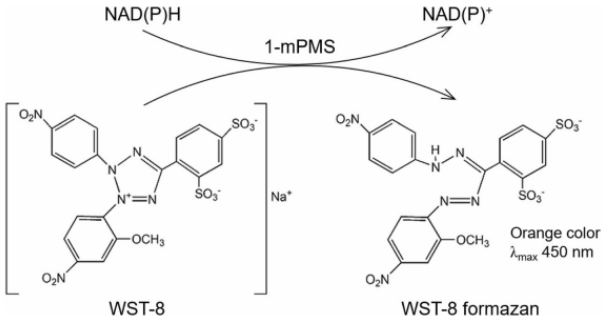

Figure 35. WST-8 conversion to colored formazan.

There are many advantages to using the WST reagent compared to the MTT assay. Firstly, the toxicity of the organic solvent required to solubilize the needle-shaped formazan crystals before measuring absorbance leads to cytotoxicity, causing the cells to float and resulting in reading errors. In contrast, with WST-8, the formation of soluble formazan eliminates the need for additional steps such as washing, harvesting, or cell solubilization. Secondly, the CCK-8 assay involves most of the dehydrogenases in a cell, while the MTT assay only involves mitochondrial dehydrogenase. Therefore, the MTT assay is dependent on mitochondrial activity, rather than the cell itself[352].

4.11.4 Effect of Edaravone prodrug (NS-1-2, NS-1-21) and Edaravone analogues (NS-1-12, NS-1-13, and NS-1-19) on neurotoxicity/cell viability of NSC-34 cells and PCNC

As demonstrated in **(figure 36a)**, EDR and EDR prodrug (NS-1-2, NS-1-21), showed increased cell viability with no cytotoxicity and neurotoxicity compared to control groups.

In addition, EDR and its prodrug demonstrated cell viability of approximately 85-100% at nearly every concentration (1 to 100 µM). However, NS-1-2 at a higher concentration of 100µM showed slight neurotoxicity and cytotoxicity with a cell viability of 85.51% (P value of 0.0468) towards NSC-34 motor neuronal cells. Further, as demonstrated in **(figure 36bc)**, EDR and EDR analogues (NS-1-12, NS-1-13, and NS-1-19) showed increased cell viability with no cytotoxicity and neurotoxicity compared to control groups. In addition, EDR and its analogues demonstrated cell viability of approximately 85-100% across nearly every concentration range (1 to 100 µM). However, EDR analogue NS-1-12 showed increased viability of approximately 118% compared to the control DMSO at a concentration of 1 µM.

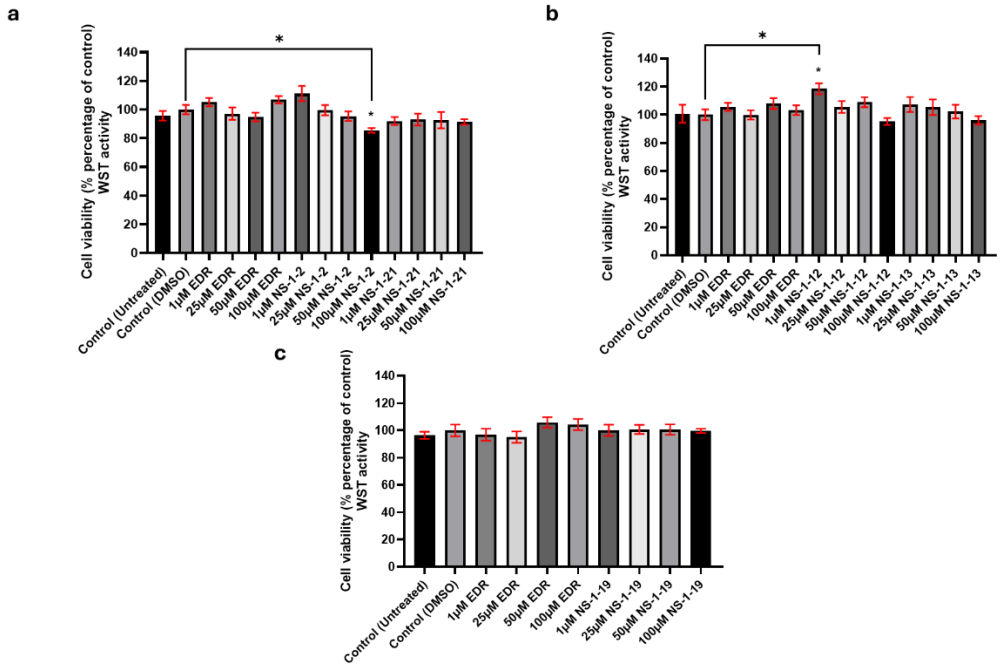

Figure 36 (a,b,c). Evaluation of neurotoxicity/cell viability profile of Edaravone (EDR), EDR prodrug (NS-1-2, NS-1-21), and EDR analogues (NS-1-12, NS-1-13, NS-1-19) on

neuroblastoma-spinal cord hybrid NSC-34 cells using WST-8 analysis (a marker of neurotoxicity) in vitro.

20kcells/100µl/well were seeded in 96 well plates for 20h in triplicates. After 20 hours at confluency of 70%, the cells were treated with different concentrations of EDR (1, 25, 50, and 100 µM), EDR prodrug (NS-1-2, NS-1-21), and EDR analogues (NS-1-12, NS-1-13, NS-1-19) (1, 25, 50, and 100 µM) for 20 hours. After 20 hours of treatment, 10 µL of WST reagent was added, and the readings were recorded after 2.5 hours at 450 nm. The data represent the percentage viability relative to control (DMSO). The data were analyzed using one-way analysis of variance (ANOVA) followed by Dunnett's multiple comparison tests, with a significance level set at ***P < 0.05***. Data are presented as a mean value ± standard error of mean (error bars), where n=9 data points or sample size. ****P<0.05*** versus control (DMSO). Data are representative of three independent experiments, with each concentration tested in triplicate. All the statistical analyses were carried out by using GraphPad Prism 8 software (GraphPad Software, La Jolla, CA).

As demonstrated in **(figure 37b,c,d)**, EDR, EDR prodrug (NS-1-2, NS-1-21), and EDR analogues (NS-1-12, NS-1-19, and NS-1-13) showed increased cell viability with no cytotoxicity and neurotoxicity compared to control groups. The lower dose of 1 and 10µM demonstrates an excellent safety profile of around 90-100%. Whereas the higher doses showed satisfactory cell viability of around 70-80%.

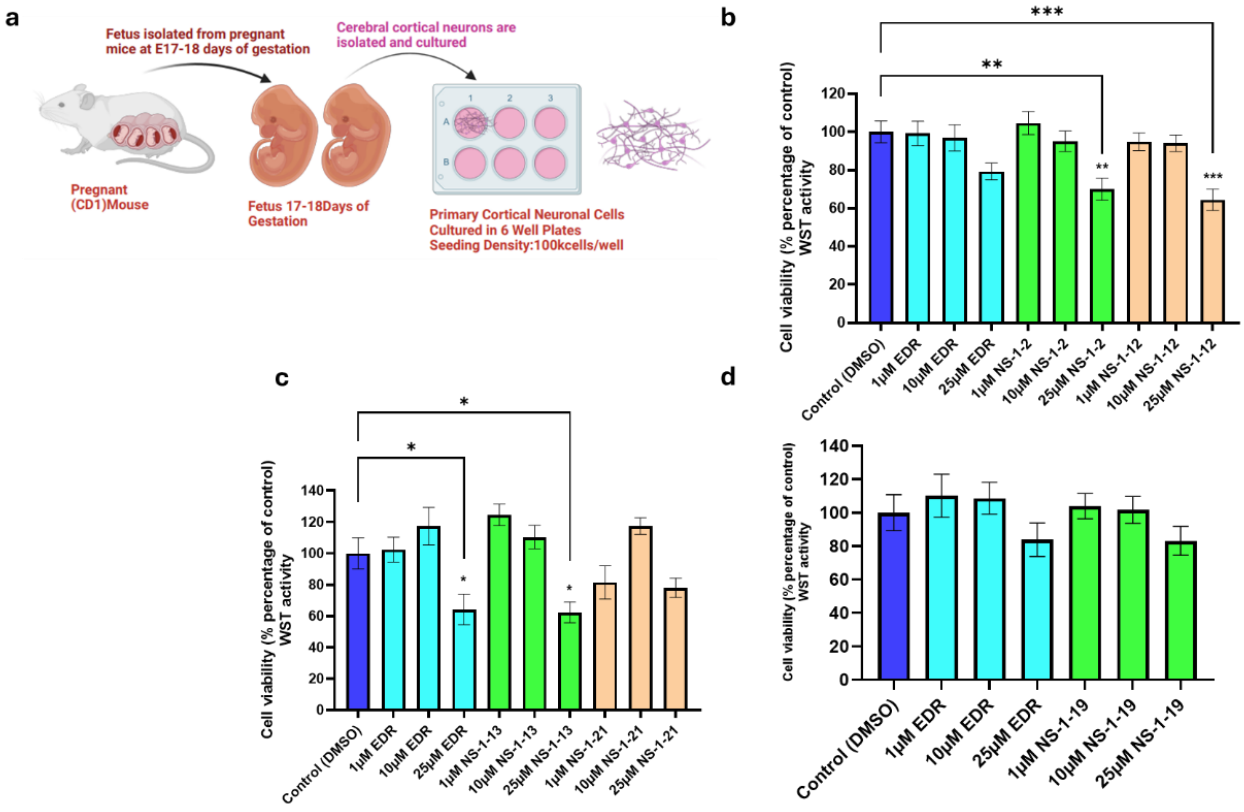

Figure 37 (a). Diagram illustrating the schematic of the neurotoxicity and cell viability experiment on primary cortical neuronal cells (PCNC), (b, c,d).

Evaluation of neurotoxicity/cell viability profile of Edaravone (EDR), EDR prodrug (NS-1-2, NS-1-21), and EDR analogues (NS-1-12, NS-1-13, NS-1-19) on primary cortical neuronal cells (PCNC) using WST-8 analysis (a marker of neurotoxicity) *in vitro*. Data 100kcells/100μl/well were seeded in 96-well plates for 2Div. At 2Div, the neurons were treated with different concentrations of EDR (1, 10, and 25 μM), EDR prodrug (NS-1-2, NS-1-21), and EDR analogues (NS-1-12, NS-1-13, NS-1-19) incubated until 8Div. On the 8th Div of neurons, 10μl of WST reagent was added, and the readings were recorded after 2h at 450nm. The data were analyzed using one-way analysis of variance (ANOVA) followed by Dunnett's multiple comparison tests, with a significance

level set at ***P < 0.05***. Data are presented as a mean value ± standard error of mean (error bars); where n=12 data points. ***P<0.05 **P<0.005, ***P<0.0005** versus control (DMSO). Data are representative of two independent experiments, with each concentration was tested in (n=6). All the statistical analyses were carried out by using GraphPad Prism 8 software (GraphPad Software, La Jolla, CA).

4.11.5 Neurotoxicity effect of hydrogen peroxide (H_2O_2) on NSC-34 cells

To determine the optimal dose of H_2O_2 for evaluating the neuroprotective effects of EDR, EDR prodrugs, and EDR analogues under H_2O_2 oxidative stress, we first assessed the neurotoxicity profile of H_2O_2 at different concentrations in a dose-dependent manner (125, 250, 500, and 1000 µM). We found that at 250 µM of H_2O_2, approximately 50 ± 5% of cells remain viable; therefore, we selected 250 µM as the optimal dose for subsequent neuroprotection analysis **(figure 38)**.

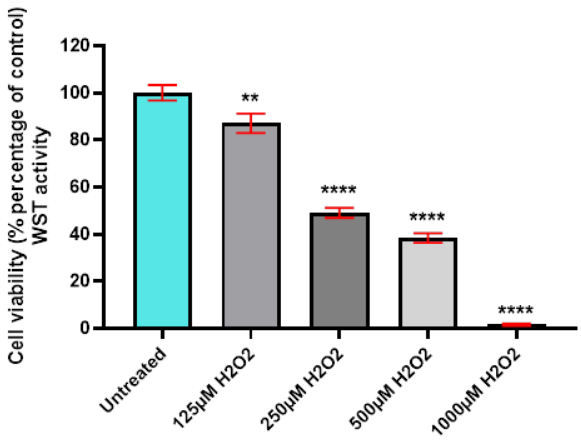

Figure 38. Evaluation of neurotoxicity/cell viability profile of hydrogen peroxide (H_2O_2) on neuroblastoma-spinal cord hybrid NSC-34 cells using WST-8 analysis (a marker of neurotoxicity) in vitro.

20kcells/100µl/well were seeded in 96-well plates for 20h in triplicates. After 20 hours at confluency of 70%, the cells were treated with different concentrations of H_2O_2 (125, 250, 500, and 1000) µM for 20 hours. After 20 hours of treatment, 10 µL of WST reagent was added, and the readings were recorded after 2.5 hours at 450 nm. The data represent the percentage viability relative to control (untreated cells). The data were analyzed using one-way analysis of variance (ANOVA) followed by Dunnett's multiple comparison tests, with a significance level set at ***P < 0.05***. Data are presented as a mean value ± standard error of mean (error bars), where n=9 data points or sample size. ****P<0.05, ****P<0.0001*** versus control (untreated cells). Data are representative of three independent experiments, with each concentration tested in triplicate. All the statistical analyses were carried out by using GraphPad Prism 8 software (GraphPad Software, La Jolla, CA).

4.11.6 Neuroprotective effect of Edaravone prodrug (NS-1-2, NS-1-21) and Edaravone analogues (NS-1-12, NS-1-13, and NS-1-19) on NSC-34 cells

As demonstrated in (**figure 39 a, b, c, d, e**), prophylactic treatment of EDR, EDR prodrugs, and analogues protected NSC-34 cells from loss of cell viability induced by 250 µM H_2O_2 neurotoxin. They demonstrated favorable neuroprotective activity against H_2O_2-induced oxidative stress.

The following observations derive from the results obtained **(figure 39 a, b, c, d, e).**

- The 0.2% of DMSO has no significant effect on the cell viability of NSC-34 cells, as shown by no significant difference between the cell viability of "control untreated cells" and "control DMSO-treated cells".

- It was also observed that 0.2% of DMSO has no hydrogen peroxide scavenging activity. This can be shown by no significant difference between the cell viability of "250 μM H_2O_2 treated group" and "250 μM H_2O_2; DMSO group".
- We found that "250 μM H_2O_2; DMSO group" reduces the cell viability to approximately (**59±1.8%; $^{\#\#\#\#}P$<0.0001**) compared to "control DMSO treated cells"
- EDR prodrugs (NS-1-2, NS-1-21) and EDR analogues (NS-1-13, NS-1-19, NS-1-12) demonstrated highly significant results with nearly equal viability at a 50 μM dose compared to EDR.
- All five B5-EDR compounds, including prodrugs (NS-1-2, NS-1-21) and EDR analogues (NS-1-13, NS-1-19, NS-1-12), demonstrated better neuroprotection by scavenging the neurotoxic effects of H_2O_2 compared to EDR at lower doses (25 μM). This indicates that EDR prodrugs and analogues are more potent than EDR in scavenging H_2O_2 at lower concentrations.
- EDR prodrugs (NS-1-2 and NS-1-21) and EDR analogues (NS-1-13 and NS-1-19) demonstrated greater neuroprotection in scavenging the neurotoxic effects of H_2O_2 compared to EDR at lower doses of 1μM. This indicates that EDR analogues are more potent than EDR at lower doses in mitigating the neurotoxic effects of H_2O_2.
- With increased neuroprotection seen at lower doses of 1μM and 25μM, and equal neuroprotection at 50μM, we found that higher doses of EDR prodrugs and analogues, specifically 100 μM, exhibited 10-15% less viability compared to EDR.

Based on our findings, we can conclude that EDR analogues exhibit better neuroprotection against neurotoxic H_2O_2 at lower doses, yielding highly significant values compared to EDR. This indicates that the B5-EDR molecules are more potent than EDR.

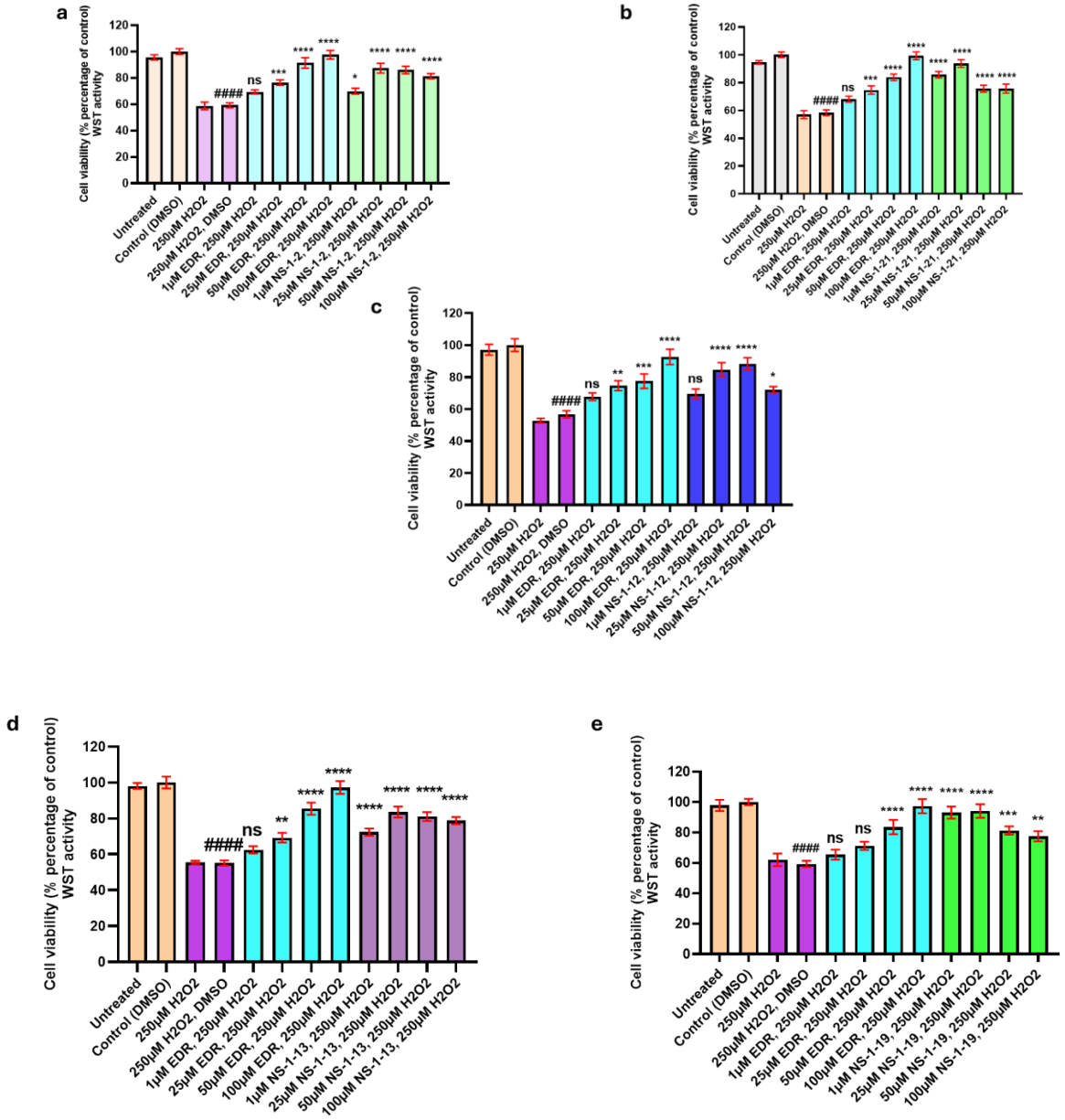

Figure 39 (a,b,c,d,e). Evaluation of neuroprotective profile of Edaravone (EDR), EDR prodrug (NS-1-2, NS-1-21), and EDR analogues (NS-1-12, NS-1-13, NS-1-19) against

hydrogen peroxide (H_2O_2) induced oxidative stress on neuroblastoma-spinal cord hybrid cells by WST-8 analysis in vitro.

20kcells/100µl/well were seeded in 96 well plates for 20h in triplicates. After 20h at confluency 70%, the cells were, pre-treated with different concentration of EDR (1, 25, 50 and 100 µM) and a) B^5-EDR analogue NS-1-2 (1, 25, 50 and 100 µM) and b) B^5-EDR analogue NS-1-12 (1, 25, 50 and 100 µM) for 1h at 37°C and 5% CO_2 and then exposed to 250µM of H_2O_2 for 2h at 37°C and 5% CO_2. After a total time period of 3h, 10µl of WST reagent was added and the readings were recorded after 2.5h at 450nm. The data represent the percentage viability relative to control (DMSO). The data were analysed using one-way analysis of variance (ANOVA) followed by Dunnett's multiple comparison tests with the significance level set at ***P<0.05***. Data are presented as a mean value ± standard error of mean (error bars); where n=9 data points or sample size. ***####P<0.0001*** control (DMSO), ****P<0.05,*** ******P<0.0005,*** *******P<0.0001*** versus H_2O_2, DMSO. Data are representative of three independent experiments, with each concentration tested in triplicate. All the statistical analyses were carried out by using GraphPad Prism 8 software (GraphPad Software, La Jolla, CA).

Further, we also aimed to investigate why the neuroprotective effects of B5-EDR prodrugs and analogues are enhanced at lower doses, specifically 1 µM and 25 µM, compared to EDR. This enhancement can be attributed to the physical and chemical stability of the B5-EDR prodrugs and analogues at room temperature and under aerobic conditions.

As demonstrated in **(figure 40)**, EDR at room temperature or even when kept at 4ºC under aerobic conditions, is degraded into yellow, brown-colored inactive products. This was observed when we kept the solutions of EDR and EDR analogues at a lower

temperature of 4 ºC for 8 weeks, and we found that EDR is unstable. The newly synthesized analogues were found to be highly stable under these conditions, **(figure 40)**. So, we can conclude that due to instability, the lower dose of EDR shows less significant effects in alleviating the effects of hydrogen peroxide compared to EDR analogues (NS-1-2); (NS-1-13); (NS-1-21); (NS-1-12). The higher potency could also be explained by the higher lipophilicity of the compound, which increases the penetrability into the target site to protect the target neurons from the adverse effects of neurotoxic H_2O_2.

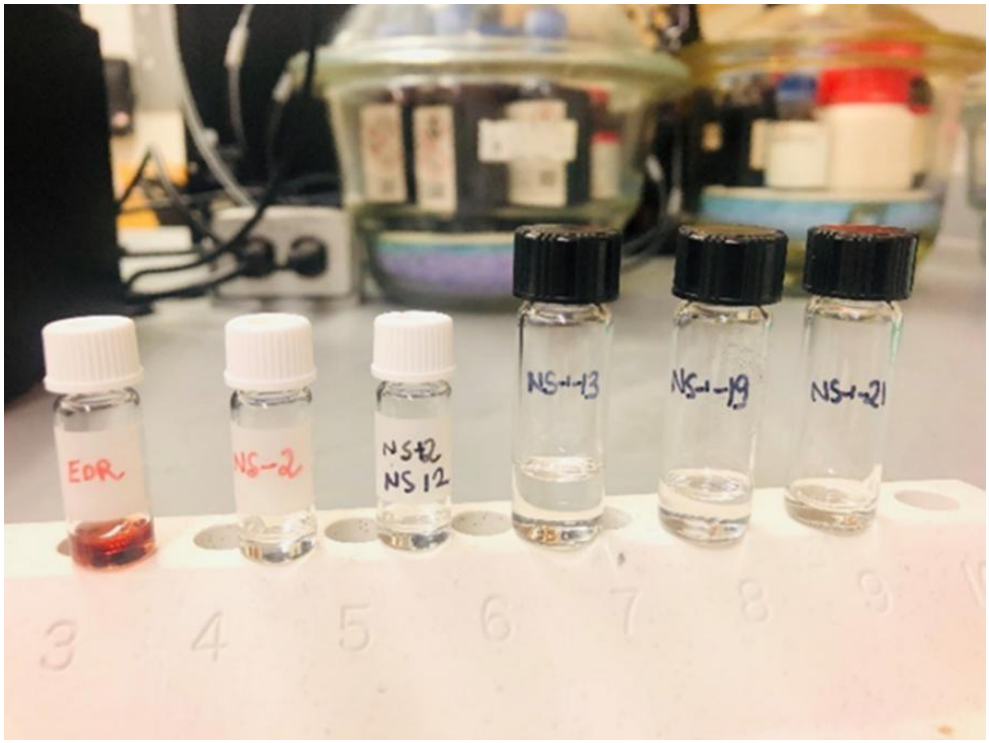

Figure 40. A demonstration of the stability of Edaravone (EDR), its prodrugs (NS-1-2, NS-1-21), and EDR analogues (NS-1-12, NS-1-13, and NS-1-19) in cold aerobic environments.

Pale yellow precipitate formed during the storage of 50 mM EDR solution in DMSO at 4°C for 8 weeks under aerobic conditions. In contrast, 50 mM solutions of NS-1-2, NS-1-12, NS-1-13 in DMSO, as well as NS-1-19 and NS-1-21 in PBS, were found to be highly stable with no discoloration at 4°C for 8 weeks under aerobic conditions.

Additionally, we aimed to understand why a higher dose of 100 μM of B5-EDR compounds, including prodrugs (NS-1-2, NS-1-21) and EDR analogues (NS-1-13, NS-1-19, NS-1-12), resulted in 10-15% lower cell viability/neuroprotection, yet still significantly protected against H_2O_2 toxicity when compared to the EDR 100 μM group. This can be explained by the following points.

Reductive Stress: According to our hypothesis, the synthesized compounds are expected to be depots of phenols and could show a dual mechanism of cell protection. Firstly, the pro-moiety will show chemoselective biorthogonal reaction, with pathological amount of H_2O_2, secondly, the released EDR after the biotransformation would be able to scavenge hydroxyl radical induced by pathological H_2O_2, through Fenton's reaction. In this process (NS-1-2), having a pinacol boronate pro-moiety is expected to show a combination of secondary and primary antioxidative action. The secondary antioxidant action is due to its ability to show exquisite chemoselective reversible coordination profile with a variety of nucleophiles and radicals at physiological pH and bio-transformed to release primary antioxidant EDR, which is a known cytoprotective molecule. The byproducts of this biotransformation are pinacol and boric acid, which have no cytotoxicity[353, 354]. In addition, boric acid has an LD_{50} that is comparable to table salt. Interestingly, boric acid is a known antioxidant and is known to increase antioxidant enzyme activity inside the cells. According to this discussion, it is anticipated that a low

dose is sufficient to protect the cells; however, a high dose paradoxically leads to oxidative stress, which is termed as reductive stress. It can be due to excessive scavenging of physiological H_2O_2; biological nucleophiles also decrease mitochondrial performance and activity of their dehydrogenases to reduce the WST reagent.

Stoichiometric Equivalents: A second plausible explanation could be due to the stoichiometric equivalents required for boronate oxidation. It is expected that 100 µM of EDR analogues are not entirely converted into EDR, or 2.5 times H_2O_2 is not sufficient for boronate oxidation. However, 5- to 10-times of H_2O_2 is better scavenged by the boronate group for all the synthesized analogues. In addition, (NS-1-19) and (NS-1-13) are found to be highly effective in scavenging a 250-fold excess of neurotoxic H_2O_2 compared to EDR.

Toxicity of Boric Acid: The third plausible explanation could be the toxicity caused by 100µM boric acid at higher concentrations. We assumed that 100 µM of (NS-1-2) after complete biochemical transformation would yield 100 µM of boric acid (H_3BO_3) and 100 µM of EDR. H_3BO_3 at this concentration could be toxic, decreasing the viability to 10-15%.

To test this hypothesis, we repeated neuroprotective assays with the prophylactic addition of boric acid at doses of 100 µM to 1 µM in the presence of 250 µM H_2O_2. Interestingly, as shown in **(figure 41a)**, H_3BO_3 showed no effects on cell viability against H_2O_2. These results, shown in **(figure 41a)**, lead us to think whether the H_3BO_3 formed during the conversion of EDR prodrug NS-1-2 at higher concentration is interfering chemically with EDR, forming adducts or borates as shown in **(figure 42a,b)**, respectively, thereby decreasing the cell viability of EDR and/or the ability of EDR to participate in mitigation of

H_2O_2 challenge. Assuming that H_3BO_3 could interfere chemically, we repeated the neuroprotective assay by incubating EDR+H_3BO_3 at a concentration of 50-100μM. Intriguingly, we discovered that the presence of 100 μM boric acid in combination with 100 μM Edaravone (EDR+BA) resulted in a 10-15% decrease in viability.

Formation of Adduct of Borates: As proposed in (figure 42a,b). A fourth plausible explanation could be the formation of an adduct between boric acid and the EDR anion. EDR shows keto enol tautomerism. It exists in a solid, stable keto form. Its pKa is 7.0, and at pH 7, it exists as a 50:50 mixture of keto and enol forms in aqueous solution. However, at physiological pH 7.4, it exists more in an anion form; at physiological pH 7.4, 71.5% of EDR exists as an anion, while the remaining 28.5% exists in neutral form. The anion can reduce radicals or even molecular oxygen through a single electron transfer process, forming stable EDR radicals that are stabilized by three resonance structures (enol, keto, and amine forms).

The boric acid, being a Lewis acid, could form an adduct with the EDR enolate anion (Where oxygen and carbon can both act as nucleophiles). In an alkaline physiological pH, the formation of oxygen nucleophiles is favored compared to carbon nucleophiles. This decreases the ROS scavenging activity of EDR by 10-15% at higher concentrations, or the boric acid could form higher borates with the enol form of EDR.

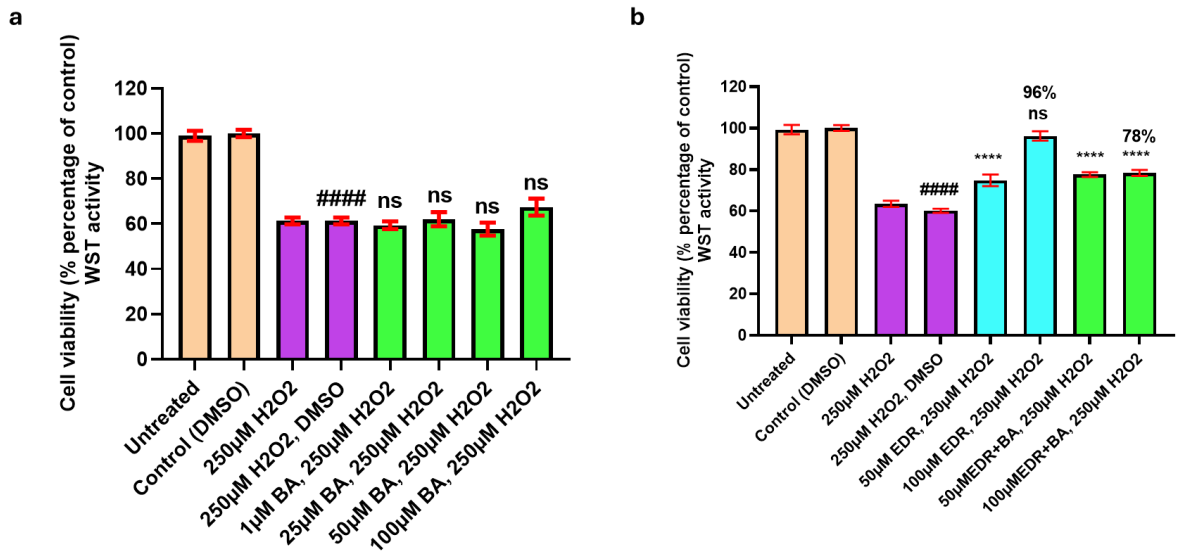

Figure 41. Evaluation of neuroprotective profile of boric acid (H_3BO_3), against hydrogen peroxide (H_2O_2) induced oxidative stress on neuroblastoma-spinal cord hybrid cells by WST-8 analysis in vitro.

20kcells/100µl/well were seeded in 96-well plates for 20h in triplicates. After 20h at confluency 70%, the cells were pre-treated with different concentrations of H_3BO_3 (1, 25, 50, and 100 µM) for 1h at 37°C and 5% CO2 and then exposed to 250µM of H_2O_2 for 2h at 37°C and 5% CO2. After a total time period of 3h, 10µl of WST reagent was added and the readings were recorded after 2.5h at 450nm. **(a). Evaluation of neuroprotective profile of boric acid (H3BO3), against hydrogen peroxide (H_2O_2) induced oxidative stress on neuroblastoma-spinal cord hybrid cells by WST-8 analysis *in vitro*.**

(b). Evaluation of neuroprotective profile of Edaravone (EDR), in the presence of boric acid (H_3BO_3), against hydrogen peroxide (H_2O_2) induced oxidative stress on neuroblastoma-spinal cord hybrid cells by WST-8 analysis *in vitro*. 20kcells/100µl/well were seeded in 96-well plates for 20h in triplicates. After 20h at

confluency 70%, the cells were, pre-treated with different concentration of EDR and H_3BO_3 (1, 25, 50 and 100 µM) for 1h at 37°C and 5% CO2 and then exposed to 250µM of H_2O_2 for 2h at 37°C and 5% CO2. After a total time period of 3h, 10µl of WST reagent was added, and the readings were recorded after 2.5h at 450nm. The data represent the percentage viability relative to control (DMSO). The data were analyzed using one-way analysis of variance (ANOVA) followed by Dunnett's multiple comparison tests with the significance level set at ***P<0.05***. Data are presented as a mean value ± standard error of mean (error bars); where n=9 data points or sample size. ***####P<0.0001*** control (DMSO), ****P<0.05, ***P<0.0005, ****P<0.0001*** and **ns**= nonsignificant versus H_2O_2, DMSO. Data are representative of three independent experiments, with each concentration tested in triplicate. All the statistical analyses were carried out by using GraphPad Prism 8 software (GraphPad Software, La Jolla, CA).

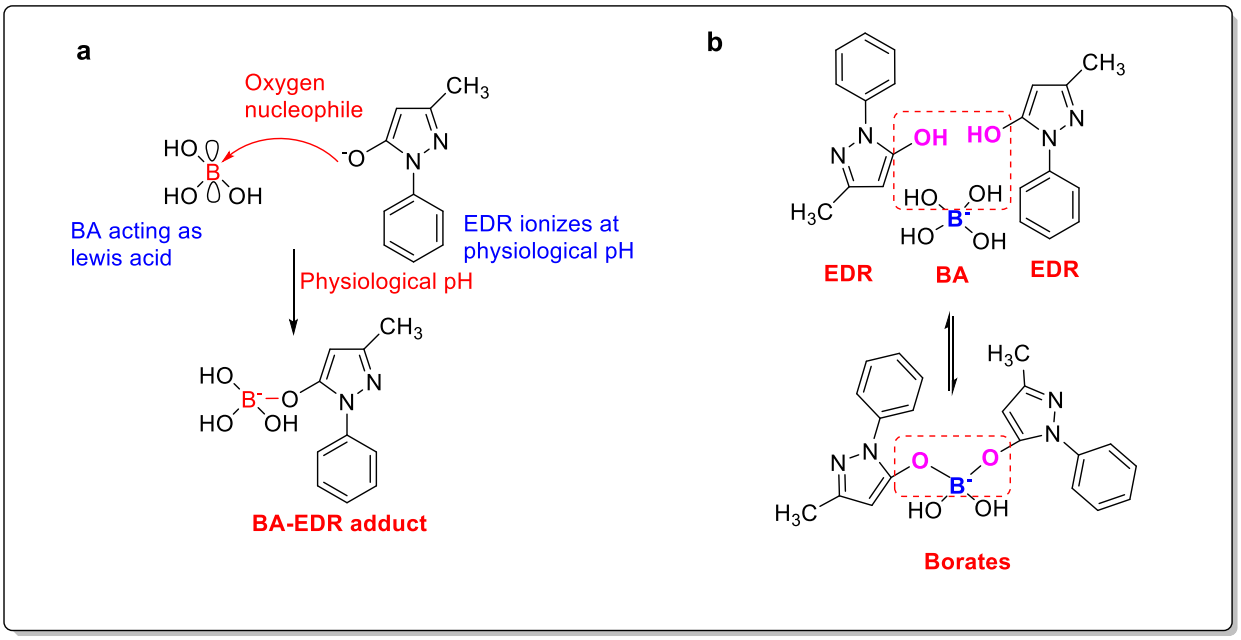

Figure 42. Schematic putative mechanism to show the effects of boric acid (BA), when given in combination with edaravone (EDR) in neuroblastoma-spinal cord hybrid cells *in vitro*.

The mechanism involves **a)** The nucleophilic attack of oxygen nucleophile to the empty *p*-orbital of the electron-deficient boron (B) atom of BA to form a tetrahedral boronate complex, an adduct with EDR. **b)** The esterification of BA with EDR involves an initial esterification step wherein two molecules of EDR are esterified with BA to generate BA-EDR ester intermediate products.

Specific Aim 3 for Objective 3: To evaluate the change in mitochondrial membrane potential (ΔΨm) by B5-EDR prodrug (NS-1-2) using staurosporine as a positive control for apoptosis in comparison to EDR.

4.12 Effects of Edaravone and Edaravone prodrug NS-1-2 on the mitochondrial membrane potential (ΔΨM) of NSC-34 cells, using staurosporin as a positive control for apoptosis

4.12.1 Principle for JC-10 Assay

The measurement of the mitochondrial membrane potential (ΔΨM) is a key aspect in determining cellular toxicity due to mitotoxicity caused by different toxic chemicals. The electron transport chain activities generate a mitochondrial membrane potential through various enzymes in the mitochondrial membranes. The healthy cell is maintained by a high mitochondrial membrane potential and is said to be in a polarized state. However, in case of cell toxicity, like in case of apoptosis, there is a collapse of the mitochondrial membrane potential due to the opening of mitochondrial permeability transition pores,

leading to the efflux or leaking of cytochrome enzymes into the cytosol and leading to a decrease in depolarization of the mitochondrial membrane[355, 356].

The JC-10 probe **(Catalog #MAK159)**, Sigma, USA) is a cationic, water-soluble fluorescent dye used to detect mitochondrial membrane potential disturbance. The principle of the dye is that in healthy cells, JC-10 forms red fluorescent aggregates as it concentrates in the mitochondrial matrix upon membrane polarization. When cells undergo apoptosis due to toxic effects, the mitochondrial membrane becomes depolarized, and the dye switches to its monomeric form, emitting green fluorescence as it diffuses out of the mitochondria that are unable to retain the dye inside mitochondria. When excited at 490nm, the colour of the JC-10 changes reversibly from green to greenish orange as the mitochondrial membrane potential becomes more polarized. It is worth noting that the JC-1 probe is widely used in the detection of ($\Delta\Psi M$). However, it has poor solubility in water, which makes JC-10 a superior alternative, as it has significantly better water solubility.

4.12.2 Staurosporine as an Apoptotic Agent

Staurosporine is a microbial alkaloid isolated from Streptomyces sp. cultures. Staurosporine has demonstrated antiproliferative activity in several human cancer cell lines and, therefore, is an effective anti-cancer agent. The predominant effect of staurosporine on cancer cells is to induce G2/M cell cycle arrest and to modulate G1 arrest of the cell cycle. Stauroporine is a non-selective inhibitor of protein kinase C (PKC) and cyclin-dependent kinase (CDKs)[357]. Staurosporine is a potent inducer of apoptosis and has been shown to activate endonucleases through a caspase-dependent mechanism[358].

As demonstrated in **(figure 43b)**, EDR and its prodrug, NS-1-2, do not cause depolarization of the mitochondrial membrane potential and, therefore, are not neurotoxic in NSC-34 cells. However, 1 µM of NS-1-2 is found to induce mitochondrial polarization compared to the control. NS-1-2 also showed better polarization of mitochondria compared to EDR. Therefore, it is expected that NS-1-2 will confer better protection of the mitochondria from oxidative damage caused by free radicals.

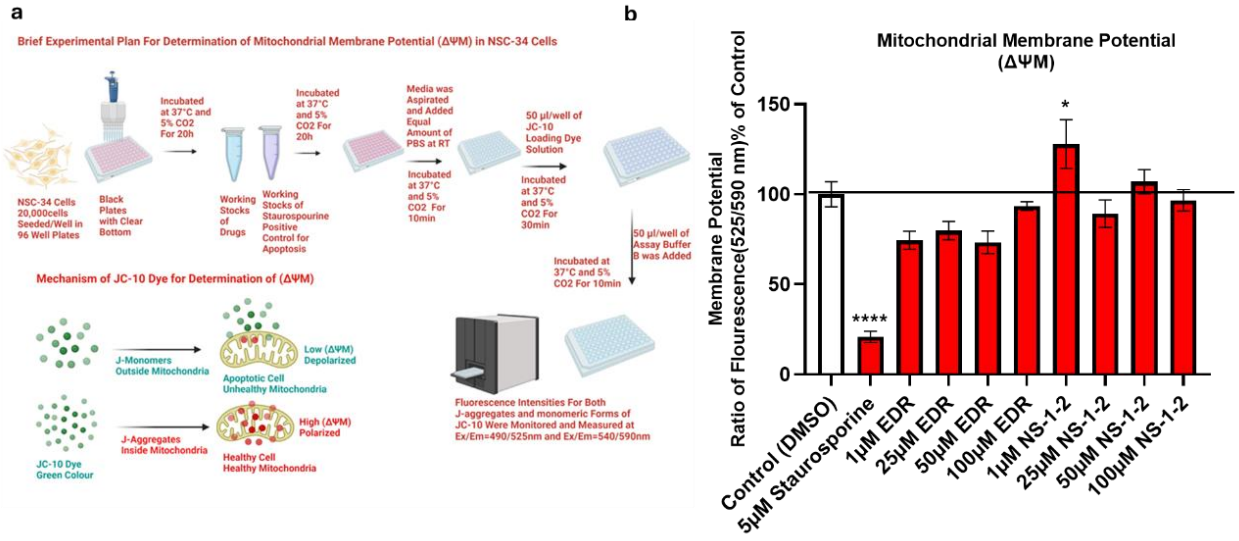

Figure 43. (a) Schematic diagram showing the brief experimental plan for the determination of mitochondrial membrane potential (ΔΨM) in NSC-34 cells.

(b). Assessment of mitochondrial membrane potential (ΔΨM) as an indicator of neurotoxicity in mouse spinal cord neuroblastoma hybrid (NSC-34) cells using different concentration of Edaravone (1-100 µM) Edaravone prodrug (NS-1-2) (1-100 µM) and Staurospourine (5µM) as (Positive control for apoptosis) by using JC-10 probe. The fluorescence intensities for both J-aggregates and monomeric forms of JC-10 were monitored and measured at Ex/Em=490/525nm and Ex/Em=540/590nm with

BioTek, Gen5 Microplate Reader (bottom read mode). The change in mitochondrial membrane potential was measured as the ratio between aggregate (EM=525nm) and monomeric forms (EM=590nm) of JC-10. Increasing ratios % of control indicate mitochondrial membrane depolarization. The data were analyzed using one-way analysis of variance (ANOVA) followed by Dunnett's multiple comparison tests, with a significance level set at ***P < 0.05***. Data are presented as a mean value ± standard error of mean (error bars); where (n=9) data points or sample size. ****P<0.0001,*P<0.05*** versus control (DMSO). Data are representative of three independent experiments, with each concentration tested in triplicate. All the statistical analyses were carried out by using GraphPad Prism 8 software (GraphPad Software, La Jolla, CA).

Specific Aim 4 for Objective 3: To evaluate the hydrogen peroxide (H_2O_2) scavenging ability of B5-EDR prodrugs (NS-1-2) using an Amplex red assay in comparison to EDR.

4.13 Hydrogen peroxide (H_2O_2) scavenging ability of EDR prodrug NS-1-2

It was hypothesized that EDR prodrug NS-1-2 could scavenge H_2O_2 during its H_2O_2-mediated chemo-selective biorthogonal boronate oxidation. We therefore investigated the ability of NS-1-2 to scavenge H_2O_2 using designed Amplex Red assay for EDR prodrug containing pro group boronate at the C-5 position, **Figure 44**. The addition of NS-1-2 at the concentrations of (500-50 μM) resulted in a markedly significant reduction in the concentration of H_2O_2. Around 176 times the concentration of H_2O_2 is scavenged by 500 μM of both EDR and NS-1-2. Further, 352 times and 704 times of H_2O_2 were scavenged by both EDR and NS-1-2 at the concentration of 250 μM and 125 μM simultaneously. In contrast, EDR and NS-1-2 at the concentration of (50μM) marginally reduced the

concentration of H_2O_2. However, the H_2O_2 scavenging activity at 50 µM of both EDR and NS-1-2 is found to be significant, with a greater mean difference of 24.56 and 13.90, respectively, against the positive H_2O_2 control. These observations demonstrate that NS-1-2 readily reacts following chemo-selective biorthogonal chemistry with H_2O_2, exhibiting efficient sequestration of H_2O_2 **(figure 45a, b, c).**

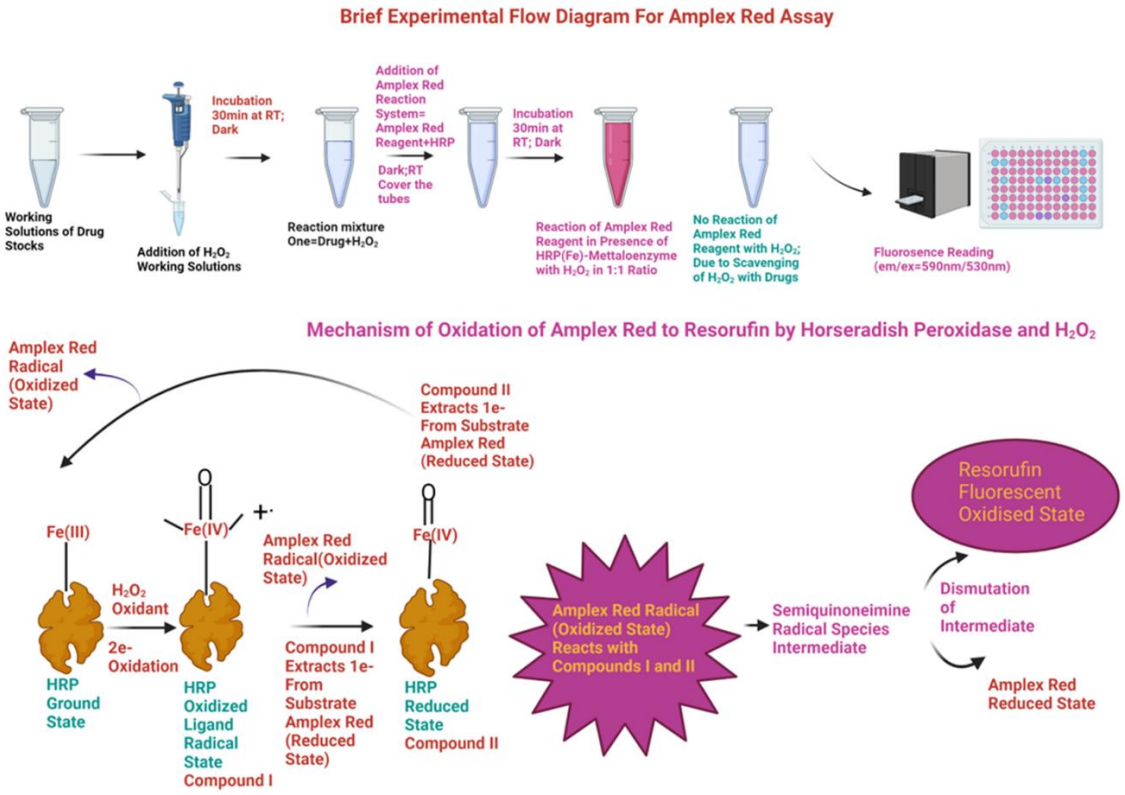

Figure 44. Schematic diagram showing the brief experimental plan for the determination of hydrogen peroxide (H_2O_2) scavenging ability of B5-EDR prodrugs (NS-1-2) using an Amplex red assay in comparison to EDR.

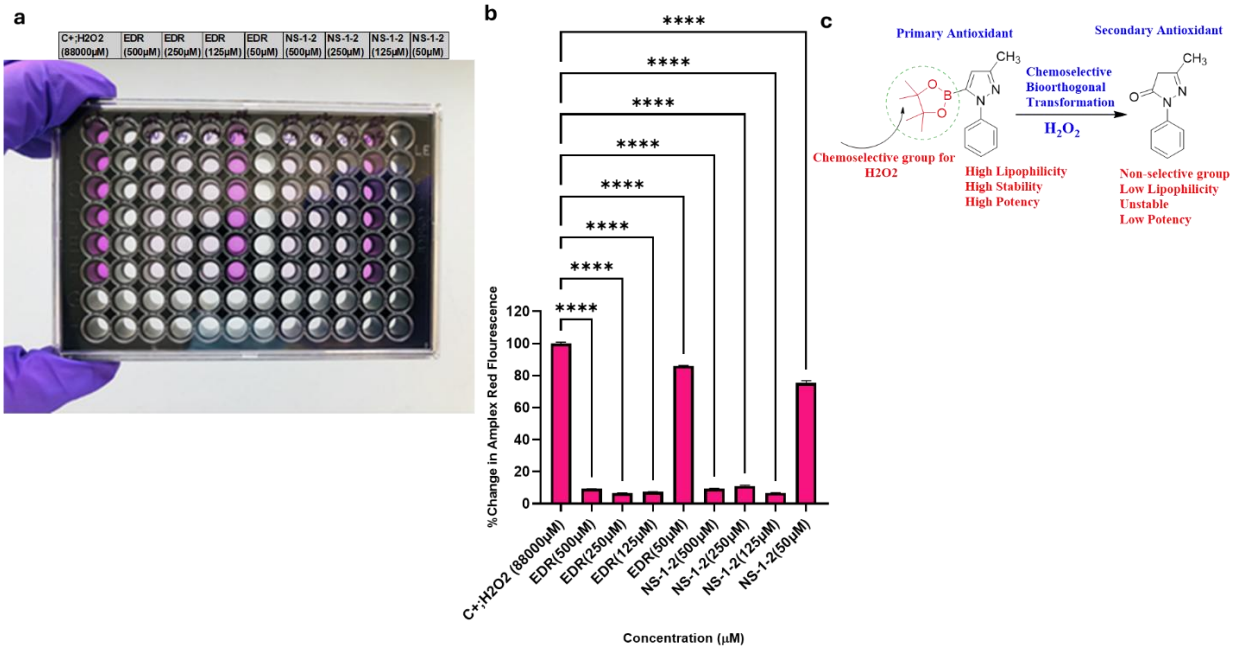

Figure 45 (a). Schematic diagram showing the brief experimental plan for the determination of hydrogen peroxide (H_2O_2) scavenging ability of B5-EDR prodrugs (NS-1-2) using an Amplex red assay in comparison to EDR.

(b). H_2O_2-scavenging ability of Edaravone and NS-1-2. H_2O_2 solution (88 mM) was mixed with Edaravone and NS-1-2 for 30 min, and the level of H_2O_2 was measured by Amplex Red assay. The data represent the percentage viability relative to control (DMSO). The data were analyzed using one-way analysis of variance (ANOVA) followed by Dunnett's multiple comparison tests, with a significance level set at ***P < 0.05***. Data are representative of three independent experiments, with each measurement tested six times. Data are presented as a mean value ± standard error of the mean (error bars); where n = 18 data points or sample size. ****P<0.0001** positive control (H_2O_2) versus EDR (500), EDR(250), EDR(125), EDR(50) and NS-1-2(500), NS-1-2(250), NS-1-2(125), NS-1-2(50).

(c). Schematic putative mechanism to show how NS-1-2 could act as a redox regulator prodrug under an oxidative cellular environment (*in vivo* biotransformation with H_2O_2) for the generation of EDR. The boronate ester at the C-5 position of pyrazole acts as a chemoselective group due to the Lewis acidity of the boron element. Boronates at the C-5 position of NS-1-2, in the presence of hydrogen peroxide, undergo oxidative deboronation to form a keto-enol group, resulting in EDR.

Specific Aim 1 for Objective 4: To evaluate the biochemical activity of Edaravone prodrug NS-1-2 in reducing the fibrillization of SOD1 monomers using Thioflavin T (ThT) Assay.

Figure 46 illustrates the rationale for the determination of the anti-SOD1 monomer fibrillization ability of B5-EDR prodrug (NS-1-2) using the Thioflavin T (ThT) Assay.

4.14 Anti-SOD1 monomer fibrillization activity of EDR prodrug NS-1-2 thioflavin T fluorescence (ThT)

A significant increase in fluorescence was detected due to SOD1 monomer fibrilization in the presence of pre-formed SOD1 fibrils **(figure 47a, b, c and figure 48a, b, c).** Further, **(figure 47a),** regardless of the exact mechanism behind the decrease in ThT fluorescence (ThT+SOD1 monomer+SOD1 preformed fibril) in the presence of Congo Red (CR), CR is quenching or interfering with the ThT control fluorescence. This could be due to altering the structure of ThT by CR, which prevents it from binding to the SOD1 fibrils. Consequently, further investigation into this phenomenon is essential. Moreover, as shown in **figure 47b**, methylene blue (MB) reduces ThT control fluorescence and the SOD1 fibrilization. In addition, as illustrated in **figure 47c**, riluzole (RLZ) significantly inhibits the fibrillization of SOD1, while the control ThT fluorescence remains unaffected.

Furthermore, as shown in **(figure 47d and figure 48a, b, c)**, there was no decrease in ThT fluorescence with the addition of EDR, NS-1-2, and MPP, indicating that EDR, NS-1-2, and MPP do not interfere with control ThT fluorescence. The increase in ThT fluorescence from the fibrillization of SOD1 monomers was significantly enhanced by the addition of MMP **(figure 48b)**, likely due to its role in promoting the fibrilization of SOD1. Conversely, the increase in ThT fluorescence associated with SOD1 monomers' fibrillization was reduced by the introduction of EDR and NS-1-2, likely due to their mechanism of action in decreasing the fibrilization of SOD1 monomers. As illustrated in **(figure 48c)**, there was a significant difference between EDR and NS-1-2 in reducing SOD1 fibrillization, which led to revisiting the data for an additional analysis comparing ThT and SOD1 preformed fibrils. Interestingly, we observed a significant increase in ThT fluorescence in the ThT preformed fibril group compared to the ThT alone group, suggesting that SOD1 preformed fibrils, which possess a β-sheet structure, are responsible for this increase in ThT fluorescence.

Then we considered comparing the ThT-preformed fibril group with both the EDR and NS-1-2 groups **(figure 48c)**. We found that the difference is significant in the EDR group. However, it is not significant with the NS-1-2 group. This suggests that both EDR and its prodrug NS-1-2 treatment prevent additional fibrillation. Nevertheless, NS-1-2 demonstrates a more pronounced effect with a larger effect size compared to EDR.

Next, we asked why EDR and NS-1-2 substantially diminish SOD1 monomer fibrillization. To explore this, we employed 3-methyl-1-phenylpyrazole (MMP) **(figure 48d)**. Additionally, we sought to investigate the structure-activity relationship (SAR) of these chemical groups at the C-5 position. As illustrated in **(figure 49)**, in contrast to EDR and

NS-1-2, MMP significantly enhanced the fibrillization of SOD1, as evidenced by an increase in ThT fluorescence. This finding suggests that the C-5 position in EDR, which contains a keto-enol moiety and a boronate in NS-1-2 **(figure 49)**, is crucial for attenuating SOD1 fibrillization. Consequently, further investigation into this phenomenon is warranted.

4.14.1 Strength of the Study

A robust, rapid, reliable, and reproducible assay was developed for the first time to evaluate the inhibitory effects of boron-containing EDR prodrug (B5-EDR) NS-1-2 on the modulation of SOD1 monomer fibrillization. Diverse controls were employed to investigate the previously unknown mechanisms underlying the modulation of SOD1 monomer fibrillization. CR, a negative control, was used to assess the potential interference of test molecules with the fluorescence dye ThT. The positive control, methylene blue (MB), was applied to evaluate the ability of NS-1-2 to inhibit SOD1 fibrillization. MPP was used to investigate the structure-activity relationship of the compounds NS-1-2 and EDR.

4.14.2 Important observations

The increase in ThT fluorescence indicates the formation of fibrils, as it binds specifically to amyloid-like structures. During fibrillation of SOD1 at 37 °C with plate shaking, a significant increase in ThT fluorescence was observed. This assay offered important insights (data not shown here). In contrast, without plate shaking, ThT fluorescence remained constant for at least two hours. Furthermore, experiments conducted at temperatures ranging from 20 to 25 °C did not show any rise in ThT fluorescence. These results underscore the essential roles of agitation and temperature in the SOD1 fibrillization assay.

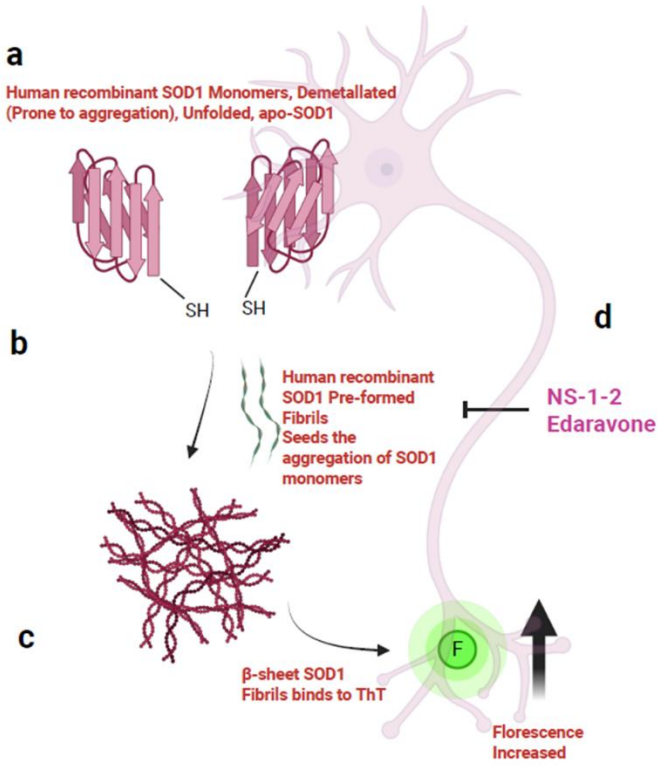

Figure 46. Schematic diagram showing the brief rationale for the determination of the anti-SOD1 monomer fibrillization ability of B5-EDR prodrug (NS-1-2) using Thioflavin T (ThT) Assay.

(a). Human recombinant SOD1 monomer, also called an unfolded form of SOD1 or apo-SOD1, is a demetallated form with free thiol groups. **(b).** The addition of human recombinant SOD1 preformed fibrils initiates or seeds the fibrilization of human recombinant SOD1 monomer. **(c).** leading to the formation of abundant β-sheet-containing misfolded human SOD1 protein fibrils. **(d).** The misfolded human SOD1 protein fibrils containing β-sheets bind to the β-sheet pocket of thioflavin T (ThT), leading to an increase in ThT fluorescence and thus facilitating the detection of ThT fluorescence.

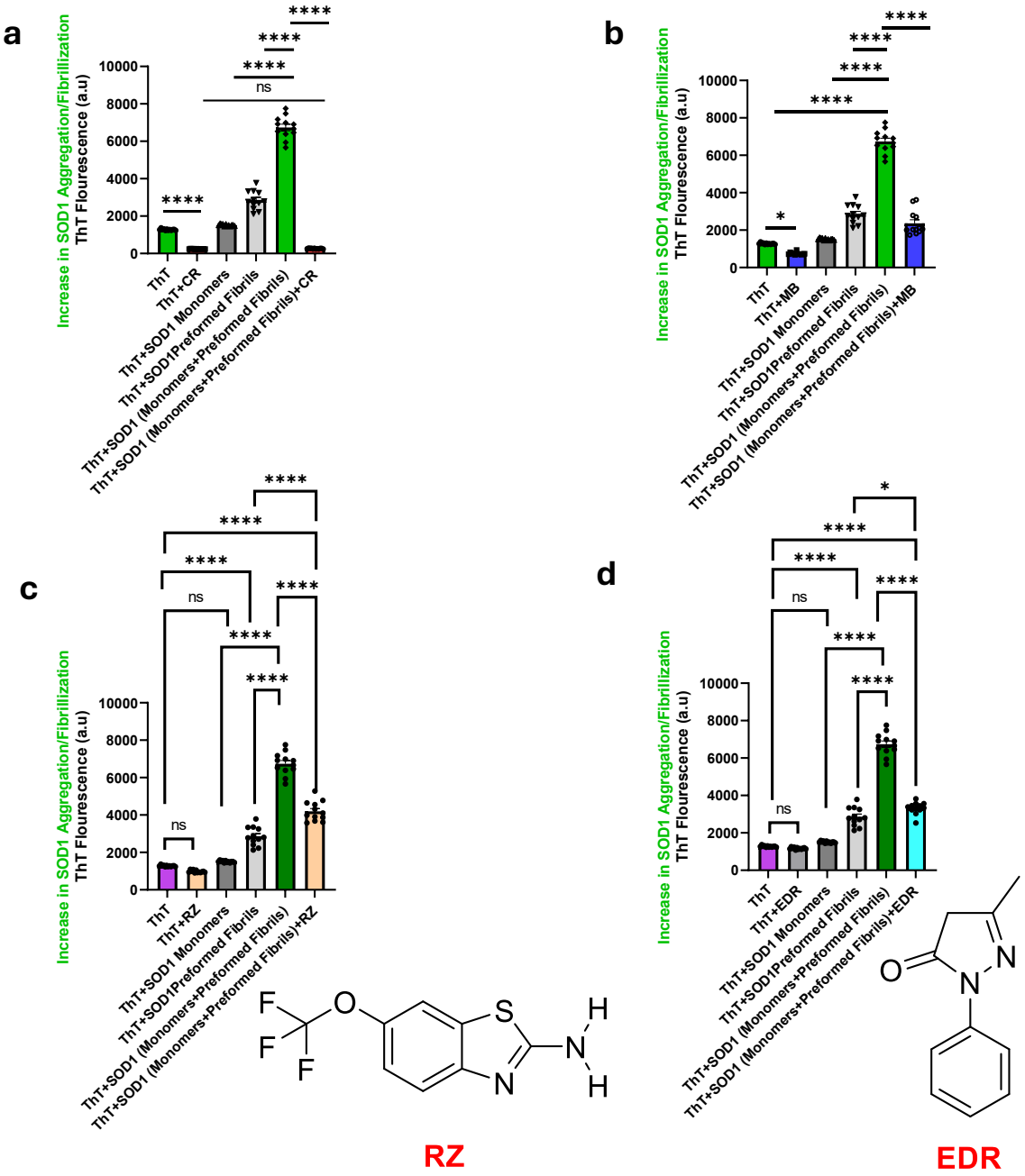

Figure 47. Anti-SOD1 monomer fibrillization activity.

a) congo red (CR), b) methylene blue (MB), c) riluzole (RZ), and d) edaravone (EDR) using thioflavin T fluorescence. Conditions: SOD1 monomers SOD1 Monomers

(10µg), SOD1 Preformed Fibrils (1µg), ThT (25µM), 250 RPM, 30mins, 37°C, 88 mM). The data represent the fluorescence value (a.u) measured at excitation and emission maxima around 450 nm and 485 nm. The data were analyzed using one-way analysis of variance (ANOVA) followed by Tukey's (1-way ANOVA) Comparison between the mean of each column and the mean of every other column, with a significance level set at ***P < 0.05***. Data are representative of three independent experiments, with each measurement tested four times. Data are presented as a mean value ± standard error of the mean (error bars), where n = 12 data points or sample size. Here ****p<0.001, ***p<0.001, *p<0.05* and ns= non-significant. All the statistical analyses were carried out by using GraphPad Prism 8 software (GraphPad Software, La Jolla, CA).

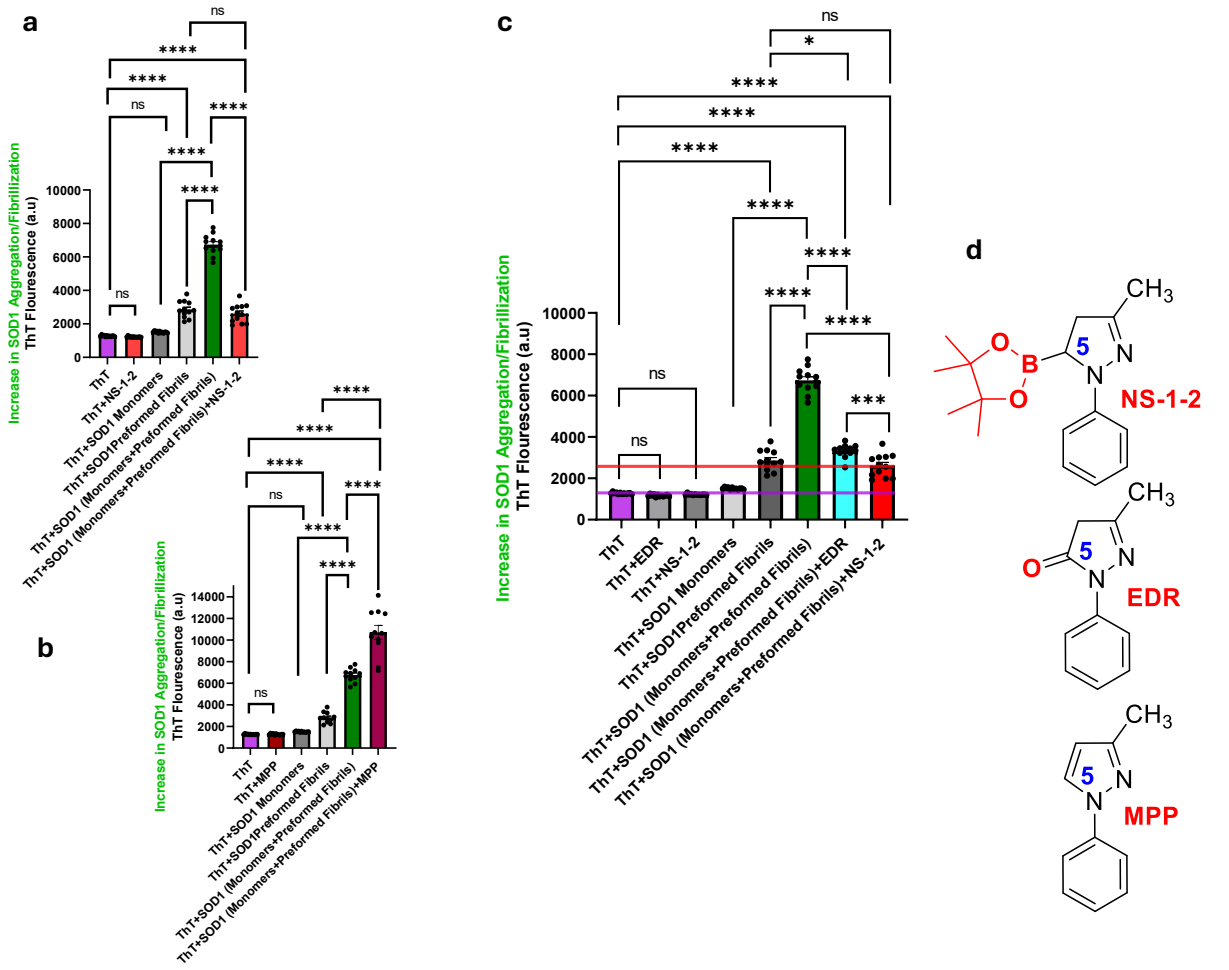

Figure 48. Anti-SOD1 monomer fibrillization activity.

a) NS-1-2, b) MPP c) EDR, and NS-1-2 using thioflavin T fluorescence, **d) Structure of NS-1-2, EDR and MPP with C-5 position functional group**. **Conditions: SOD1 monomers SOD1 Monomers (10µg), SOD1 Preformed Fibrils (1µg), ThT (25µM), 250 RPM, 30mins, 37°C88 mM). The data represent the fluorescence value (a.u) measured at excitation and emission maxima around 450 nm and 485 nm.** The data were analyzed using one-way analysis of variance (ANOVA) followed by Tukey's (1-way ANOVA) Comparison between the mean of each column and the mean of every other column, with a significance level set at ***P < 0.05***. Data are representative of three

independent experiments, with each measurement tested four times. Data are presented as a mean value ± standard error of the mean (error bars), where n = 12 data points or sample size. Here ****p<0.001, ***p<0.001, *p<0.05* and ns= non-significant. All the statistical analyses were carried out by using GraphPad Prism 8 software (GraphPad Software, La Jolla, CA).

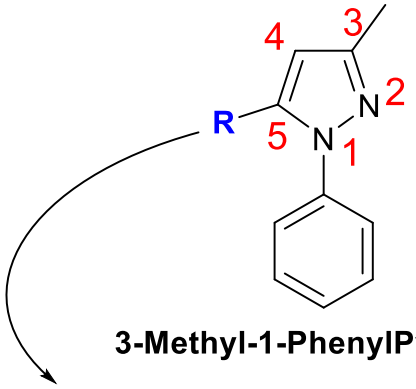

3-Methyl-1-PhenylPyrazole

C-5 Position R	SOD1 Fibrillization activity (ThT fluorescence)
No Functional group MPP	Increased
Keto-Enol Edaravone	Decreased
Boronate NS-1-2	Decreased

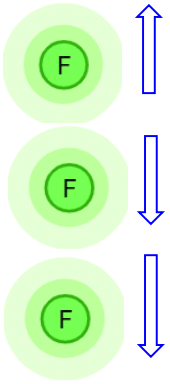

Figure 49. Structural activity relationship of 3-Methyl-1-Phenyl Pyrazole and the effects of substituents at its C-5 position on anti-SOD1 monomer fibrillization activity.

Objective 5: To study the acute and chronic safety profile with longitudinal monitoring of NS-1-2 in the wild-type mice.

Specific Aim 1 for Objective 5: To evaluate the acute toxicity profile (single dose), with longitudinal monitoring of NS-1-2 in a wild-type mouse *in vivo*.

4.15 A single dose (acute toxicity assessment) of Edaravone prodrug NS-1-2 and 120 daily doses (chronic toxicity assessment) of NS-1-2 for 120 days, with longitudinal monitoring, demonstrate a satisfactory safety profile

4.15.1 Morphological alteration:

As shown in the schematic representation **(figures 50 and 51)**, which outlines the experimental plan for evaluating the acute and chronic toxicity of the novel edaravone prodrug NS-1-2 in non-transgenic wild-type mice.

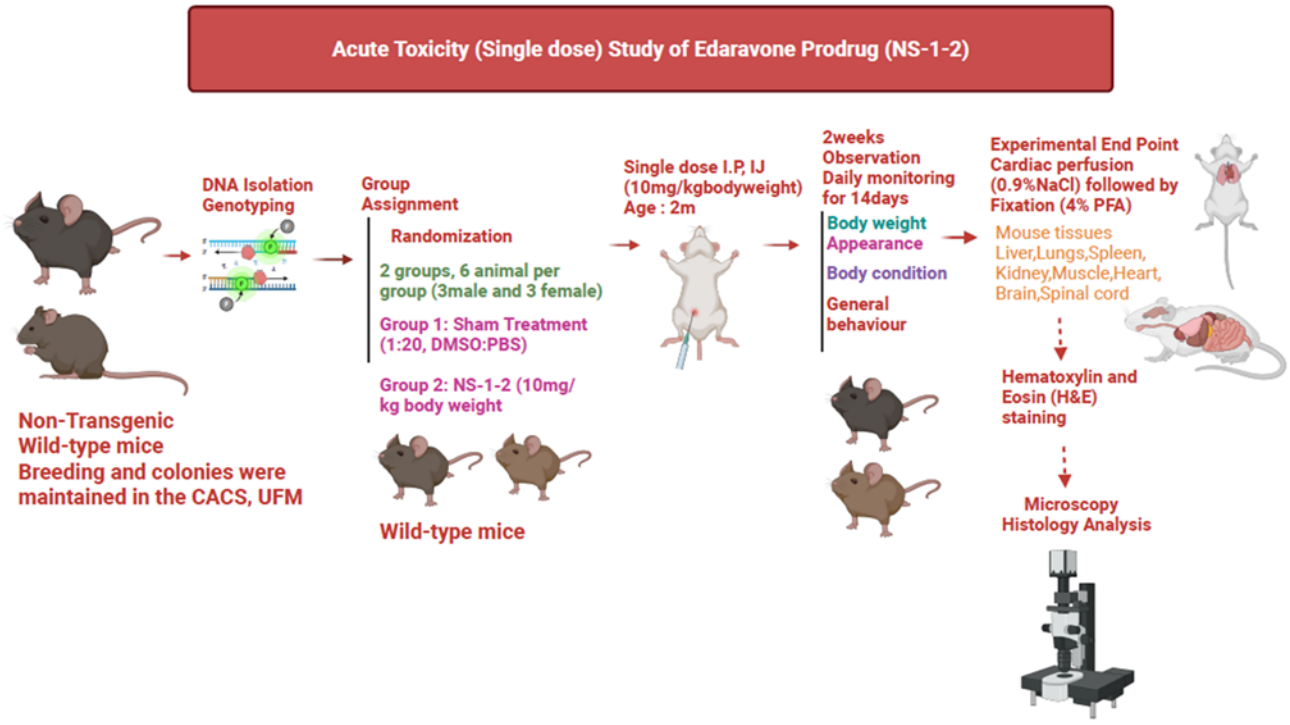

Figure 50. Schematic diagram showing acute toxicity evaluation and treatment plan, with corresponding longitudinal monitoring (14 days) and n=6 for each group (3 male and 3 female).

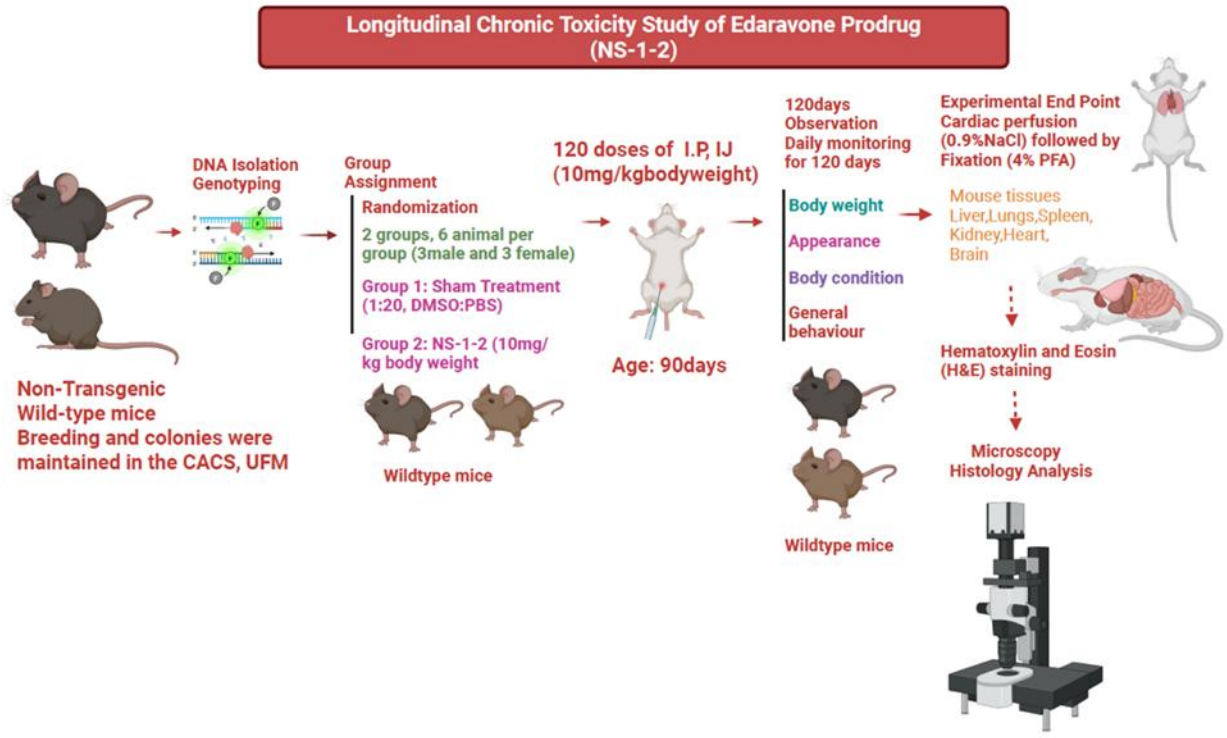

Figure 51. Schematic diagram showing chronic toxicity evaluation and treatment plan, with corresponding longitudinal monitoring (120 days) and n=6 for each group (3 male and 3 female).

First, we investigated the safety profile of the newly synthesized prodrug of EDR, NS-1-2 *in vivo*. As shown in **(figure 52)**, a single dose and 120 doses for 120 days daily with 10 mg/kg body weight of BSZ with longitudinal monitoring for 14 and 120 days, respectively, showed no treatment-associated deaths or adverse events. Daily general observations showed normal appearance and normal general behavior with well-conditioned body condition. Furthermore, both the acute and chronic treatment of NS-1-2 did not cause changes to the skin, fur color, eyes, mucous membrane, nor the occurrence of secretions and excretions, and motor activities. IP administration of NS-1-2 (10mg/kg/day) daily for

120 days, with (a total of 120 IP IJ, and 1200mg of total dose over 120 days), was seemingly well tolerated by wildtype SOD1 mice. Moreover, NS-1-2 treated mice developed no clinical signs of toxicity including a decrease in mean weight, hunched posture, orbital tightening, piloerection, nor low activity compared to vehicle-treated (1:20, DMSO: PBS) mice.

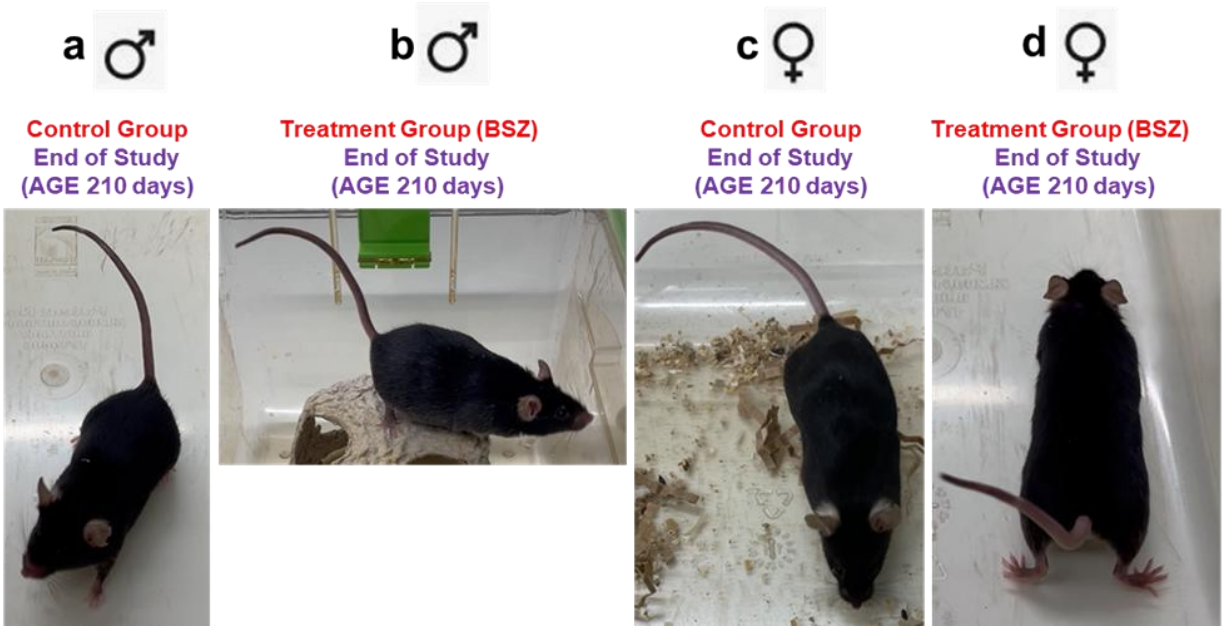

Figure 52. Chronic NS-1-2 treatment showed no NS-1-2-associated clinical signs of toxicity in both sexes.

NS-1-2 was administered intraperitoneally to age- and sex-matched wild-type SOD1 mice (120 doses, 10 mg/kg/day body weight) for 120 days with daily longitudinal monitoring until the age of 210 days, end of study. The subset of control-treated (1:20, DMSO: PBS) male mice (a) and female mice (c) showed no clinical signs of toxicity in terms of hunched posture, orbital tightening, piloerection, low activity/respiration, and weight loss compared to the NS-1-2 treated male (b) and female mice (c). Both groups exhibited normal posture and activity at the end of the study.

4.15.2 Assessment of body weight

Figures 53a and b highlight our acute and chronic toxicity evaluation plan, with corresponding longitudinal monitoring (14 days and 120 days) and n=6 for each group (3 male and 3 female).

As shown in **(figure 54),** a single dose and 120 daily doses for 120 days with 10 mg/kg bodyweight of BSZ with longitudinal monitoring for 14 and 120 days, respectively, did not induce any abnormal changes in the body weight of the mice. Moreover, there was no significant difference in the changes in body weight between the control group and the treatment groups after 120 daily doses, which further supports the absence of toxicity.

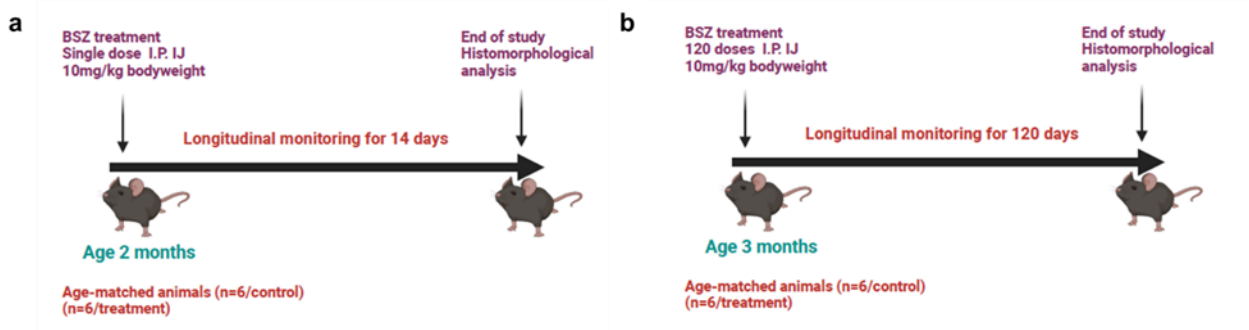

Figure 53. a) Diagram depicting a single-dose acute toxicity treatment study plan. **b)** Diagram depicting 120 doses of chronic toxicity treatment study plan for 120 days.

In the acute toxicity monitoring **(figure 54a,b),** the average initial body weight of the control group (n = 6) was 23.31 g, while the treatment group (n = 6) averaged 23.61 g. Additionally, in the chronic toxicity monitoring **(figure 54c,d)**, the average initial body weight for the control group (n = 5) was 23.74 g, compared to 25.75 g for the treatment group (n = 6). This indicates that the mice in the acute cohorts had very similar average weights at the beginning; however, a notable initial weight difference was observed in the chronic toxicity study, with the treatment group (n = 6) being 8.4% heavier than the control

group (n = 5). It is also noteworthy that after 14 days of monitoring in the acute toxicity cohorts (following a single dose), the mean percentage change in body weight from baseline (initial weight) was 3.7% in the treatment group (n = 6). In contrast, the control group (n = 6) experienced a decrease of -0.88%. These results account for less than a 5% difference between the two groups, and although statistically significant (p=0.04, figure 7b), the larger variation in the weight gain of the treated mice (two mice >5%, but <10%) could account for this statistical difference between the control and treated groups. However, based on our 120-day chronic safety study, histological data, and literature reports detailing that weight changes greater than 10% are typically biologically relevant, we believe that the acute safety study was successful. Furthermore, after 120 days of treatment in the chronic toxicity cohorts, the mean percentage change in body weight from baseline (initial weight) was found to be nearly the same (28%) with no significant difference found between the two groups. Our findings from both the acute and chronic toxicity studies show that a lack of biologically relevant percentage mean weight changes from baseline demonstrates that the BSZ group, both in acute and chronic toxicity, did not experience a large reduction in body weight compared to the controls. These results suggest that there is no weight-based indication of toxicity from NS-1-2 in any group **(Figure 54 a-d).**

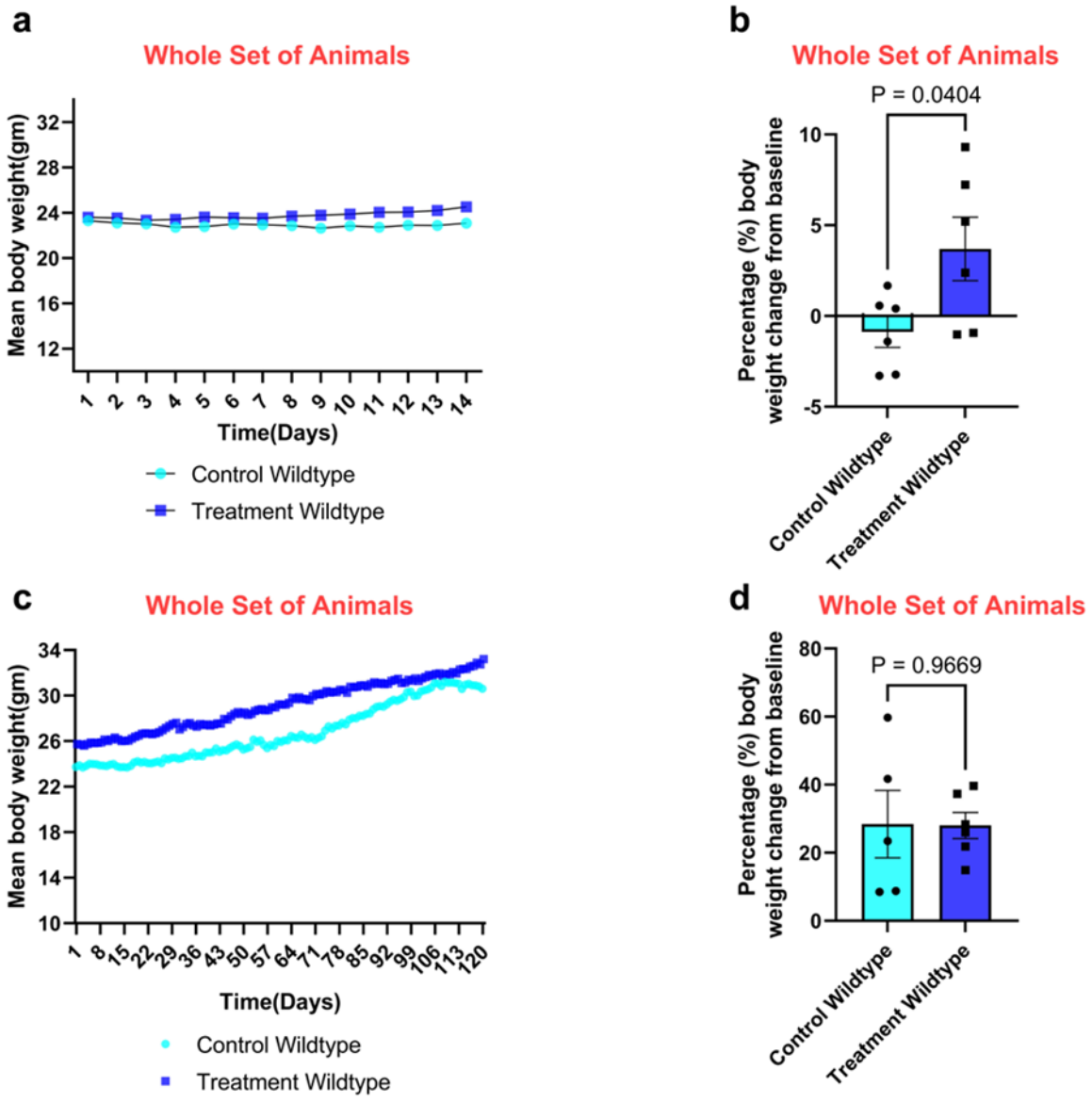

Figure 54. Results of acute and chronic toxicity assessments on mean body weight over 14 days (acute) and 120 days (chronic) starting at 60 and 90 days of age, respectively.

a) Mean body weight for control and treated groups over a 14-day period following a single dose. b) Two-tailed (unpaired t-test) of the percentage mean body weight change from baseline (initial weight) showing that NS-1-2 increases the percentage mean body weight from -0.88% for wildtype (WT) SOD1 age-matched whole set of animals

(control/n=6 mice), including (n=3 males and n=3 females) to 3.7% (NS-1-2/n=6 mice), including (n=3 males and n=3 females).**c) Mean body weight for control and treated groups over 120 days with 120 daily doses. d)** Two-tailed (unpaired t-test) of the percentage mean body weight change from baseline (initial weight) showing that NS-1-2 does not increase the percentage mean body weight 28% for wildtype (WT) SOD1 age-matched whole set of animals (control/n=5 mice), including (n=2 males and n=3 females) to 28.4% (NS-1-2/n=6 mice), including (n=3 males and n=3 females). Data are presented as percentage body weight mean difference from baseline (n=12)/acute toxicity and (n=11)/chronic toxicity for the whole set of animals. Where, n= number of animals of the designated genotype. Data were analyzed using a two-tailed (unpaired t-test), with a significance set at $p<0.05$. Here, $p=0.0404$, $p=0.9669$ with $*p<0.05$ and ns respectively versus control wildtype (WT) SOD1 animals.

4.15.3 Histopathological findings

A single dose determining acute toxicity **(figures 55 and 56)** and 120 daily doses for 120 days determining chronic toxicity **(figures 57 and 58)** with 10 mg/kg body weight of NS-1-2 with longitudinal monitoring for 14 and 120 days, respectively, exhibited no signs of treatment-associated hematological toxicity in tissues (Liver, kidney, spleen, lungs heart, and brain) tissues from both the sexes (males/females). H&E staining images of all the six major organs, as mentioned, showed no significant abnormal differences between the histology of the control and treated (BSZ) group, with no signs of overt degeneration, inflammation, and necrosis in any of the examined tissues.

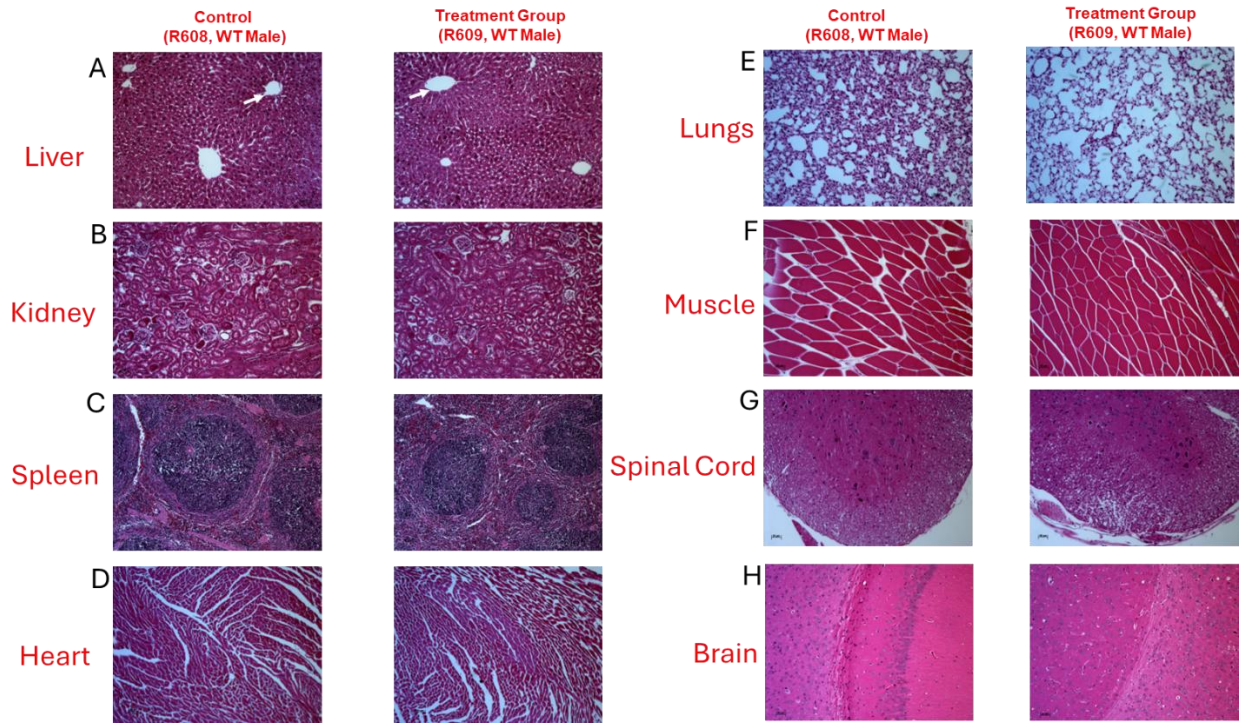

Figure 55. Photomicrographs of Hematoxylin and Eosin (H&E) stained sections of wildtype (WT) SOD1, male mice from acute toxicity evaluation.

Beginning at 60 days of age, WT female mice received a single intraperitoneal (IP) injection of NS-1-2 at a dose of 10 mg/kgbodyweight. The mice were longitudinally observed and monitored for 14 days. At the experimental endpoint, animals were euthanized, and tissues, including brain, heart, kidney, liver, lung, and spleen, were collected for analysis. In the H&E staining images, the nucleus is blue, and the cytoplasm is red. Collagen fibers show a varying red colour. There were six mice (Three male and Three female) in each group, with original magnification 10× (Scale bar represents 20μm). All the images were taken with a Microscope: Axioskop 2 mot plus microscope using AxioVision software version 4.8 (Carl Zeiss, Inc., Thornwood, NY).

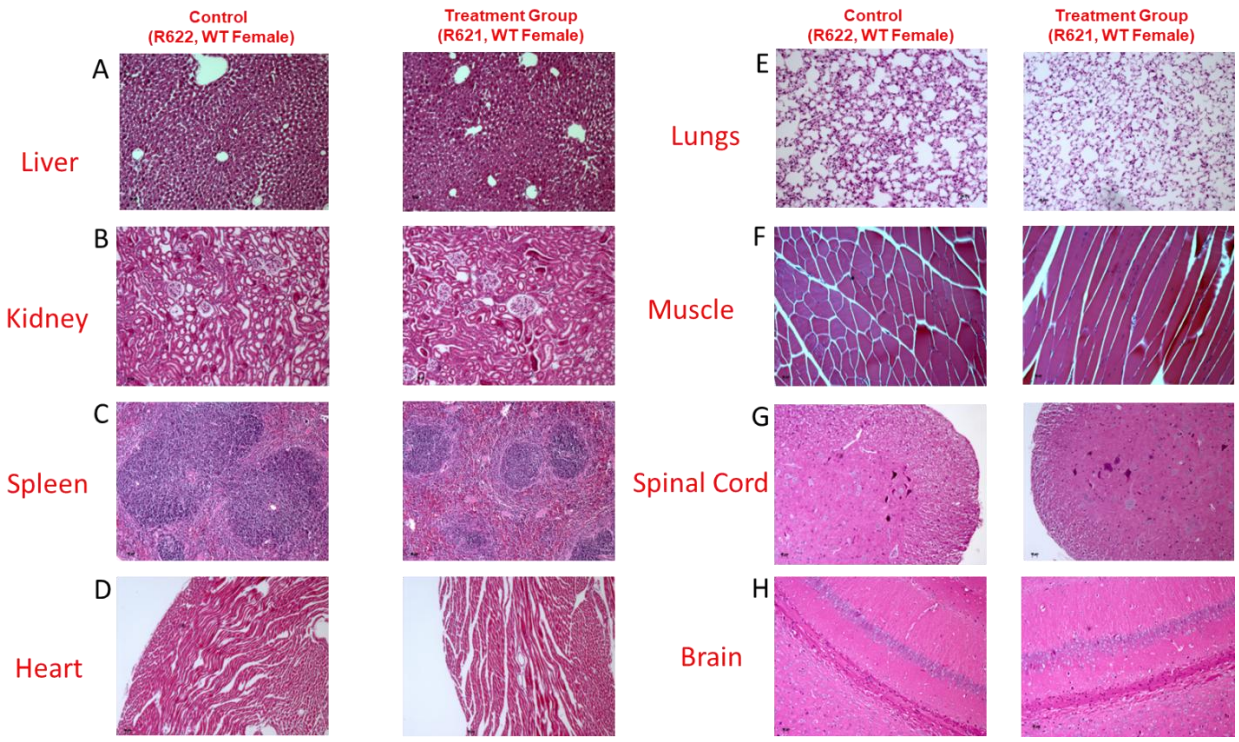

Figure 56. Photomicrographs of Hematoxylin and Eosin (H&E) stained sections of wildtype (WT) SOD1, female mice from acute toxicity evaluation.

Beginning at 60 days of age, WT female mice received a single intraperitoneal (IP) injection of NS-1-2 at a dose of 10 mg/kgbodyweight. The mice were longitudinally observed and monitored for 14 days. At the experimental endpoint, animals were euthanized and tissues, including brain, heart, kidney, liver, lung, and spleen, were collected for analysis. In the H&E staining images, the nucleus is blue, and the cytoplasm is red. Collagen fibers show a varying red colour. There were six mice (three male and three female) in each group, with original magnification 10× (Scale bar represents 20μm). All the images were taken with a Microscope: Axioskop 2 mot plus microscope using AxioVision software version 4.8 (Carl Zeiss, Inc., Thornwood, NY).

A. **Liver:** control male and treated (NS-1-2) male mice both illustrated normal lobular architecture with central veins and radiating hepatic cords. Hepatocytes were observed to be normal and there were no signs of inflammatory response in both the control and NS-1-2 treated liver tissues.
B. **Kidney:** control male and treated (NS-1-2) male mice both illustrating normal glomerular structure of the kidney and no pathological changes were observed between both the groups
C. **Spleen:** control male and treated (NS-1-2) male mice both illustrating normal micro-architecture of the white and red pulp with no morphological alteration.
D. **Heart:** control male and treated (NS-1-2) male mice both had normal myocardium morphology.
E. **Lungs:** control male and treated (NS-1-2) male mice both displayed normal lung architecture with no sign of alteration in alveolar architecture.
F. **Muscle:** control male and treated (NS-1-2) male mice, both illustrating normal homogeneous distribution of polygonal-shaped muscle fibers with peripheral nuclei. There is no degeneration of fibres, and both the group had normal morphology.
G. **Spinal cord:** control male and treated (NS-1-2) male mice, both illustrating normal morphology with central canal, neurons, and glial cells.
H. **Brain:** control male and treated (NS-1-2) male mice, both illustrating normal morphology of the hippocampus, demonstrated the regular architecture of the CA3 region, where the pyramidal cell layer neurons (P) were uniform in size and evenly arranged.

H&E staining images of these organs revealed no difference in histology between the control and treated (NS-1-2) groups, with no signs of overt degeneration, inflammation, or necrosis in any of the examined tissues.

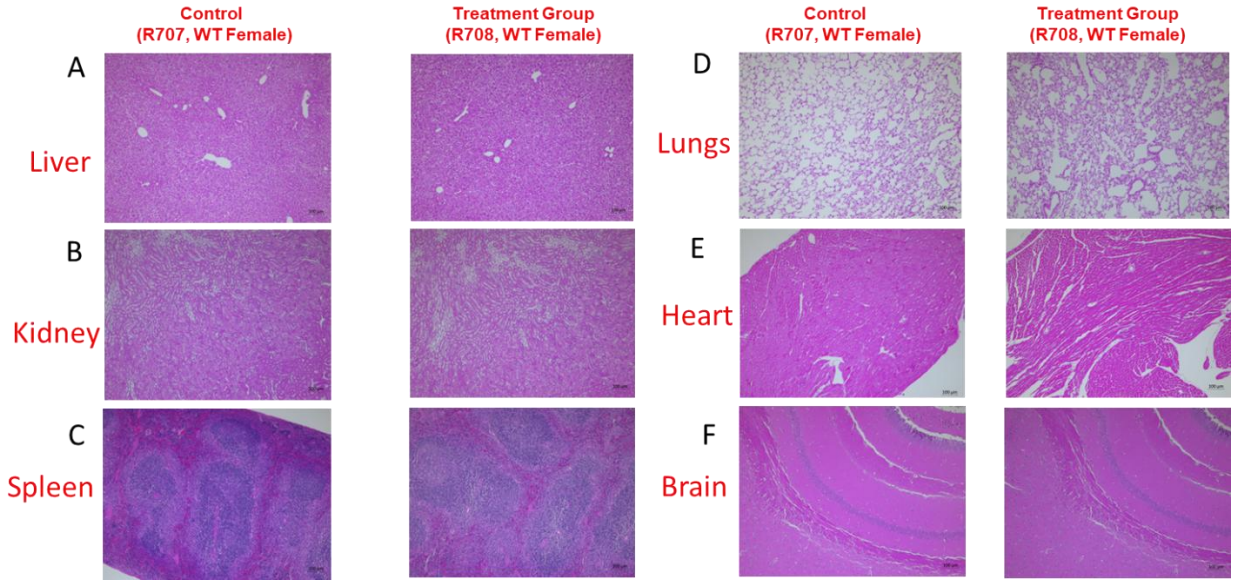

Figure 57. Photomicrographs of Hematoxylin and Eosin (H&E) stained sections of wildtype (WT) SOD1, male and female mice from chronic toxicity evaluation.

At 3 months of age, WT, male, and female mice received 10 mg/bodyweight of NS-1-2 daily for 120 days (a total of 120 doses**)**. The mice were longitudinally observed and monitored for 120 days. At the experimental endpoint, animals were euthanized, and tissues, including brain, heart, kidney, liver, lung, and spleen, were collected for analysis. In the H&E staining images, the nucleus is blue, and the cytoplasm is red. Collagen fibers show a varying red colour. There were six mice (three male and three female) in each group, with original magnification 10× (Scale bar represents 100μm). H&E staining images of such organs showed no difference between the histology of the control and treated (NS-1-2) group, with no signs of overt degeneration, inflammation, and necrosis

in any of the above-examined tissues. All the images were taken with a Zeiss Imager M2 microscope using ZEN 3 Pro software with a camera AxioCam HRc – colour.

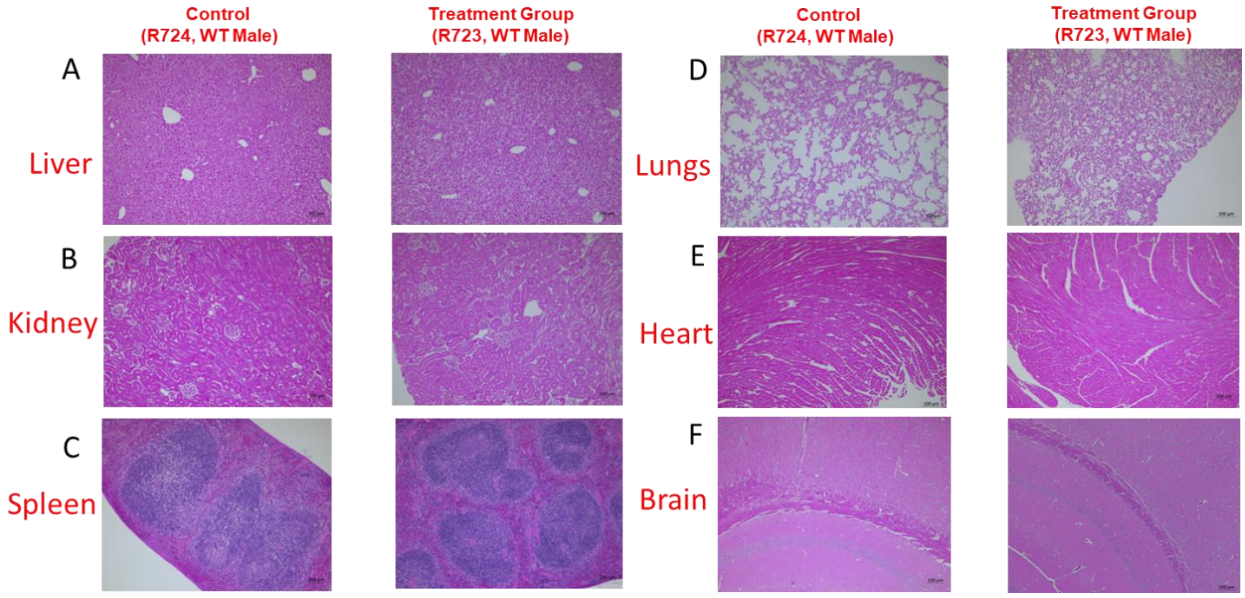

Figure 58. Photomicrographs of Hematoxylin and Eosin (H&E) stained sections of wildtype (WT) SOD1, male and female mice from chronic toxicity evaluation.

At 3 months of age, WT, male, and female mice received 10 mg/bodyweight of NS-1-2 daily for 120 days (a total of 120 doses**)**. The mice were longitudinally observed and monitored for 120 days. At the experimental endpoint, animals were euthanized and tissues, including brain, heart, kidney, liver, lung, and spleen, were collected for analysis. In the H&E staining images, the nucleus is blue, and the cytoplasm is red. Collagen fibers show a varying red colour. There were six mice (Three male and Three female) in each group, with original magnification 10× (Scale bar represents 100μm). H&E staining images of such organs showed no difference between the histology of the control and treated (NS-1-2) group, with no signs of overt degeneration, inflammation, and necrosis

in any of the above-examined tissues. All the images were taken with Microscope: Zeiss Imager M2 microscope using ZEN 3 Pro software with camera AxioCam HRc – colour.

a) **Liver:** control male and treated (NS-1-2) male mice both illustrated normal lobular architecture with central veins and radiating hepatic cords. Hepatocytes were observed to be normal and there were no signs of inflammatory response in both the control and NS-1-2 treated liver tissues.
b) **Kidney:** control male and treated (NS-1-2) male mice both illustrating normal glomerular structure of the kidney and no pathological changes were observed between both the groups
c) **Spleen:** control male and treated (NS-1-2) male mice both illustrating normal micro-architecture of the white and red pulp with no morphological alteration.
d) **Heart:** control male and treated (NS-1-2) male mice both had normal myocardium morphology.
e) **Lungs:** control male and treated (NS-1-2) male mice both displayed normal lung architecture with no sign of alteration in alveolar architecture.
f) **Brain:** control male and treated (NS-1-2) male mice both illustrating normal morphology of the hippocampus, demonstrating the regular architecture of the CA3 region where the pyramidal cell layer neurons (P) were uniform in size and evenly arranged.

4.16 Longitudinal preclinical study with Edaravone prodrug NS-1-2 delayed disease onset in SOD1-G37R mouse model of ALS

Figure 59 illustrates the experimental plan with different clinical stages of progression of disease in G37R(line 42) mice. **Figure 60** shows the experimental plan for the preclinical study. Also, shows different ALS clinical phenotypes or pathologies that mimic the clinical features of human ALS. In addition, it includes various defined humane endpoints for preclinical research.

Disease onset was retrospectively defined as the age at which the mice reached peak body weight before weight began to decline. As shown in **(figure 61)**, daily intraperitoneal injection (IP, IJ) with NS-1-2 starting pre-symptomatically from the age of 90 days until the humane endpoint (end-stage) delayed the disease onset in the age-matched whole set of animals and both sexes (male/female) of SOD1-G37R ALS mice demonstrating to a statistically significant degree, $p<0.05$. For the whole set of animals, n=12/group including (6 male and 6 female) both in the vehicle-treated (control) and NS-1-2 treated group, the mean disease onset age differed significantly between the vehicle-treated (129.7 days) and NS-1-2 treated group (155.2 days). Further, the disease onset was significantly delayed by around 25.5 days in the BSZ treatment group compared to the control group. On sexual segregation, we found that NS-1-2 treated males (n=6), and females (n=6) displayed a delay of onset (21.1 days) and (29.9 days) compared to the control group respectively, with a larger effect size in males ($p=0.0008$) compared to females ($p=0.0151$). Sex segregation demonstrated a pronounced therapeutic effect of BSZ in males compared to females, suggesting a stronger sex-specific efficacy of BSZ in delaying the progression of early symptoms in ALS mice. Alternately, there is a greater

sex-specific variability in the female control animals, compared to make control animals, or both. The disease onset data is also in tabulated form **(Table 6)** below.

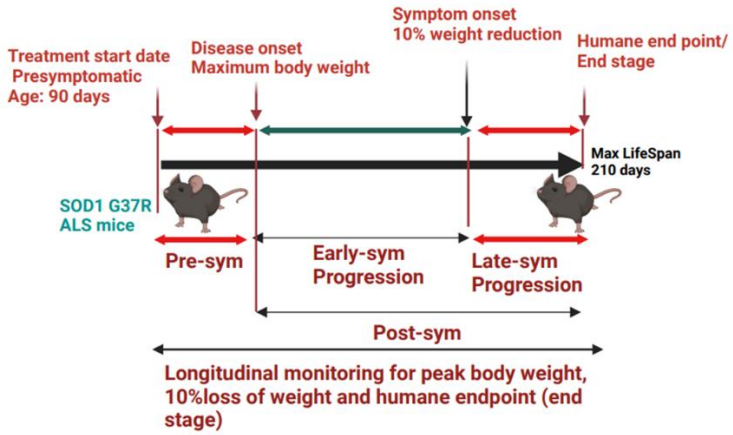

Figure 59. Schematic illustration of the experimental plan with different clinical stages of progression of disease in G37R(42) mice.

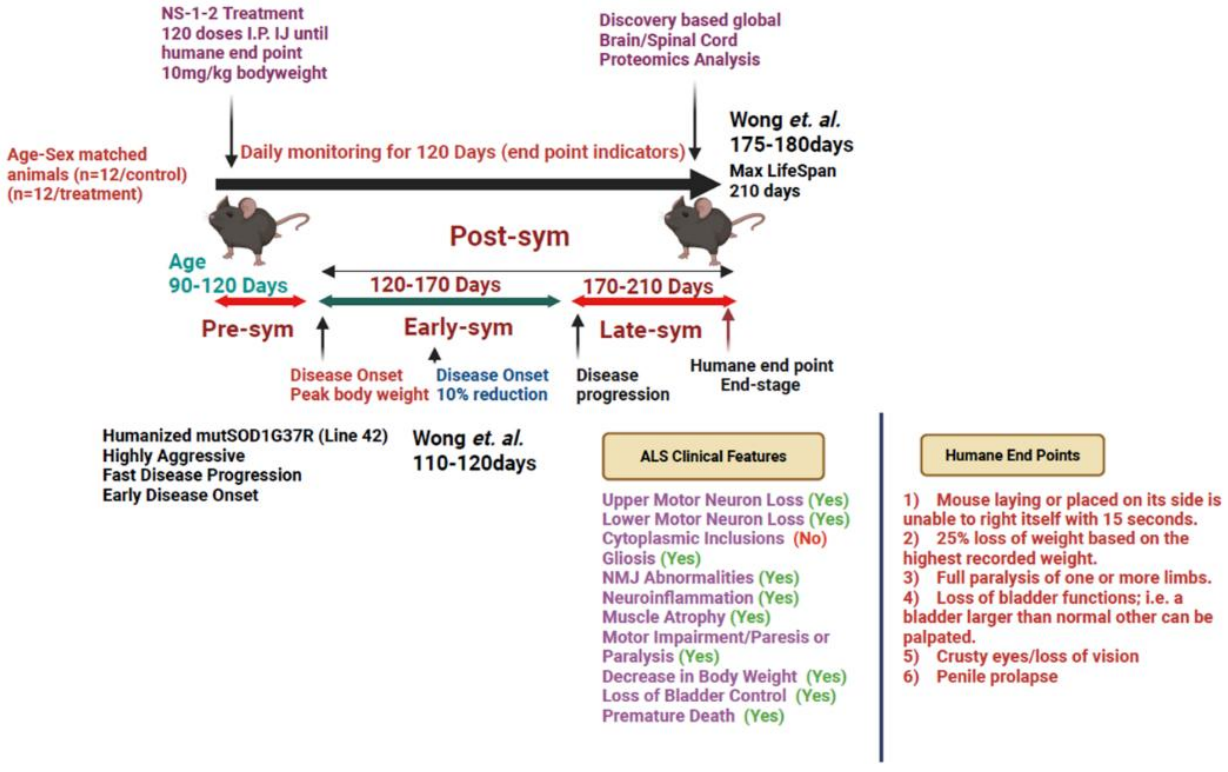

Figure 60. Schematic illustration of the experimental plan for the preclinical study in Humanized mutSOD1G37R(42) mice.

Also, shows different ALS clinical phenotypes or pathologies that mimic the clinical features of human ALS. In addition, it includes various defined humane endpoints for preclinical research.

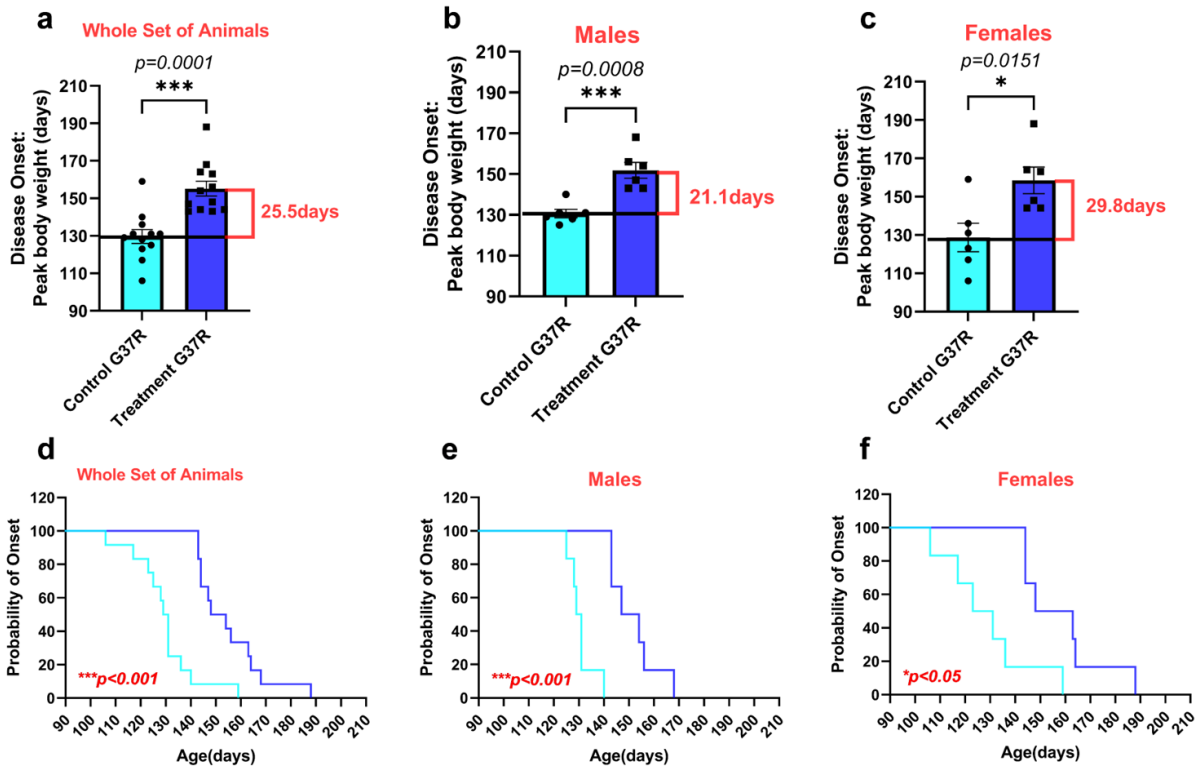

Figure 61. Edaravone prodrug NS-1-2 delays the disease onset (based on age to peak body weight before weight begins to decline).

a) Two-tailed (unpaired *t-test*) of the mean onset age showing that NS-1-2 delays the mean onset age from 129.7 days for G37R age-matched whole set of animals (control/n=12 mice; n=6 males and n=6 females) to 155.2 days (NS-1-2/n=12 mice; n=6 males and n=6 females); **b)** from 130.7 days for age-matched G37R males (control/n=6

mice), to 151.8 days for age-matched G37R males (NS-1-2/n=6 mice); **c)** from 128.7 days for age-matched G37R females (control/n=6 females), to 158.5 days for age-matched G37R females (NS-1-2/n=6 females). Data are presented as mean ± SEM (n=12) for the whole set of animals and n=6 for males and females. n= number of animals of the designated genotype. Data were analyzed using a two-tailed (unpaired *t-test*), with a significance set at *p<0.05*. Here, *p=0.0001, p=0.0008 and p=0.015,* with ****p<0.001, ***p<0.001 and *p<0.05* versus control G37R. **d)** Kaplan–Meier curves of the probability of disease onset showing that BSZ delays the median onset from 130 days for age-matched G37R whole set of animals (control/n=12 mice), including (n=6male and n=6 female) to 151 days (NS-1-2/n=12 mice), including (n=6male and n=6 female); **e)** from 130 days for age-matched G37R males (control/n=6 mice), to 150.5 days for age-matched G37R males (NS-1-2/n=6 males); **f)** from 127 days for age-matched G37R females (control/n=6 mice), to 155.5 days for age-matched G37R females (NS-1-2/n=6 females). Data are presented as mean ± SEM, n= number of animals of the designated genotype. Data were analyzed using a Kaplan-Meir Log-rank (Mantel-Cox) in SOD1-G37R ALS mice, with a significance set at *p<0.05*. Here, *p=0.0001, p=0.0006 and p=0.0107* with ****p<0.001, ***p<0.001 and *p<0.05* versus control G37R.

4.17 Edaravone prodrug NS-1-2 delayed the progression of symptom onset, defined as age to reach 10% weight loss, with muscle weakness, in the SOD1-G37R mouse model of ALS

Symptom onset or early symptomatic stage was also assessed in treated and control mice by measuring the age to reach a 10% loss of body weight based on the highest recorded weight (with muscle weakness). As shown in **(figure 62)**, daily intraperitoneal injection (IP, IJ) with NS-1-2 starting pre-symptomatically from the age of 90 days until the

humane endpoint (end-stage) delayed the progression of early symptom onset to a statistically significant degree ($p<0.05$) in the age-matched whole set of animals and in both the sexes (male/female) of SOD1-G37R ALS mice. For the whole set of animals, n=12/group including (6 male and 6 female) both in the vehicle-treated (control) and NS-1-2 treated group. The mean symptom onset age (loss of 10% body weight) differed significantly between the vehicle-treated (160.4 days) and NS-1-2 treated group (185.3 days). Further, the progression of early symptom onset was significantly delayed by around 24.9 days in the NS-1-2 treatment group compared to the control group. On sexual segregation, we found that NS-1-2 treated age-matched males (n=6), and age-matched females (n=6) displayed a delay of early-symptom onset (23.3 days) and (26.4 days) compared to the control group respectively, with a larger effect size in males ($p=0.0030$) compared to females (0.0622). Sex segregation demonstrated a pronounced therapeutic effect of BSZ in males compared to females, suggesting a sex-specific efficacy of NS-1-2. Alternately, there is a greater sex-specific variability in the female control animals, compared to make control animals, or both. However, based on probability of symptom onset analysis using a Kaplan-Meier Log-rank (Mantel-Cox), both sexes were found to be statistically significant ($p=0.0033$ males, $p=0.0195$ females). The symptom onset data is also in tabulated form **(Table 5)** below.

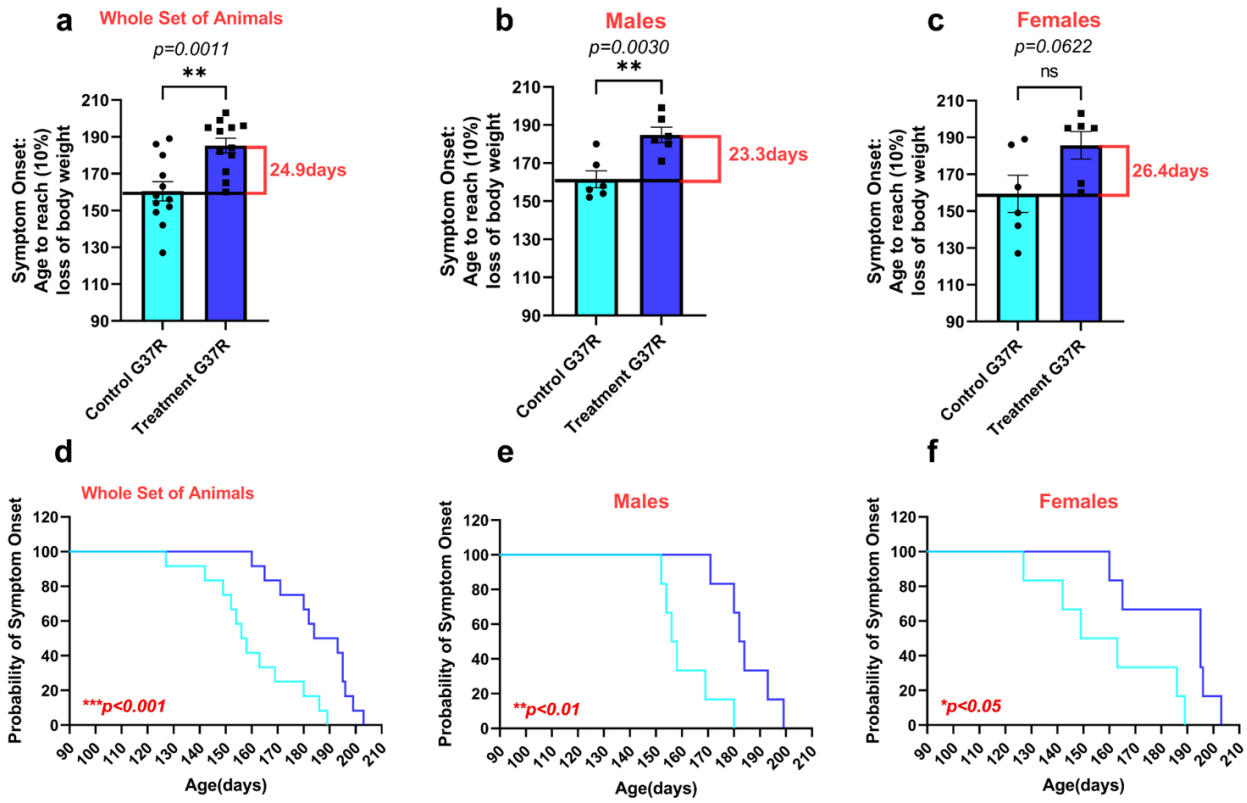

Figure 62. Edaravone prodrug NS-1-2 delays the symptom onset or early symptom progression (age to reach 10% weight loss, with muscle weakness).

a) Two-tailed (unpaired *t-test*) of the mean onset age showing that Ns-1-2 delays the mean symptom onset age from 160.4 days for G37R age-matched whole set of animals (control/n=12 mice; n=6 males and n=6 females) to 185.3 days (NS-1-2/n=12 mice; n=6males and n=6 females); **b)** from 161.5 days for age-matched G37R males (control/n=6 mice), to 184.8 days for age-matched G37R males (NS-1-2/n=6 mice); **c)** from 159.3 days for age-matched G37R females (control/n=6 females), to 185.7 days for age-matched G37R females (Ns-1-2/n=6 females). Data are presented as mean ± SEM (n=12), for the whole set of animals and (n=6) for males and females. n= number of animals of the designated genotype. Data were analyzed using a two-tailed (unpaired *t*-

test), with a significance set at *p<0.05*. Here, *p=0.001, p=0.0030 and p=0.0622,* with ***p<0.01, **p<0.01 and ns=non significant* versus control G37R. **d)** Kaplan–Meier curves of the probability of symptom onset showing that NS-1-2 delays the median symptom onset from 157 days for age-matched G37R whole set of animals (control/n=12 mice), including (n=6male and n=6 female) to 188.5 days (NS-1-2/n=12 mice), including (n=6males and n=6 females); **e)** from 157 days for age-matched G37R males (control/n=6 mice), to 183 days for age-matched G37R males (Ns-1-2/n=6 males); **f)** from 156 days for age-matched G37R females (control/n=6 mice), to 195 days for age-matched G37R females (NS-1-2/n=6 females). Data are presented as mean ± SEM. n= number of animals of the designated genotype. Data were analyzed using a Kaplan-Meier Log-rank (Mantel-Cox) in SOD1-G37R ALS mice, with a significance set at *p<0.05*. Here, *p=0.0009, p=0.0033 and p=0.0195* with ****p<0.001, **p<0.01 and *p<0.05* versus control G37R.

4.18 Edaravone prodrug NS-1-2 prolongs the life span and increases survival in the SOD1-G37R mouse model of ALS

As part of our current preclinical studies, we initiated the treatment of EDR prodrug NS-1-2 pre-symptomatically at the age of 90 days until the age of 210 days, and monitored daily longitudinally for several significant humane endpoint indicators throughout ALS disease progression including: a) Mouse unable to right itself in 15 seconds; b) 25% loss of weight on the highest recorded weight; c) Full paralysis of one or more hind limbs; d) Loss of bladder functions; e) Crusty eyes/loss of vision; and f) Penile prolapse. Further, the minimum primary humane endpoint of survival/lifespan/end stage of the mice was defined as the point when the mice were unable to right themselves in 15 seconds and

lost 25% of weight, which may also be accompanied by several other humane endpoint indicators of disease progression, as listed above.

As shown in **(figure 63)** daily intraperitoneal injection (IP, IJ) with NS-1-2 starting pre-symptomatically from the age of 90 days until the humane endpoint (end-stage) significantly prolongs the life span ($p<0.05$) in the age-matched whole set of animals and in SOD1-G37R ALS male mice, demonstrating the sex-specific differences following treatment with NS-1-2 in extending the life span of mice. For the whole set of animals, n=12/group including (6 male and 6 female) both in the vehicle-treated (control) and NS-1-2-treated group, the mean age of survival differed significantly between the vehicle-treated (177.9 days) and the NS-1-2-treated group (193 days). Further, the age of survival was significantly prolonged by around 15.1 days in the NS-1-2 treatment group compared to the control group. On sexual segregation, we found that NS-1-2-treated age-matched males (n=6), and age-matched females (n=6) displayed an extension of life span (16.5 days) and (13.7 days) compared to the control group, respectively, with a larger effect size in males ($p=0.0192$) compared to females ($p=0.2972$). Sex segregation demonstrated a pronounced therapeutic effect of NS-1-2 in males compared to females, suggesting a sex-specific efficacy of NS-1-2. Alternately, there is a greater sex-specific variability in the female control animals, compared to make control animals, or both. Upon closer inspection of the female cohort, the lack of statistical significance was largely due to the variance in the life span of female controls, ranging from 139 to 201 days (62-day span), as compared to male controls (162 to 195 days, 33-day span). The survival age data is also in tabulated form **(Table 5)** below.

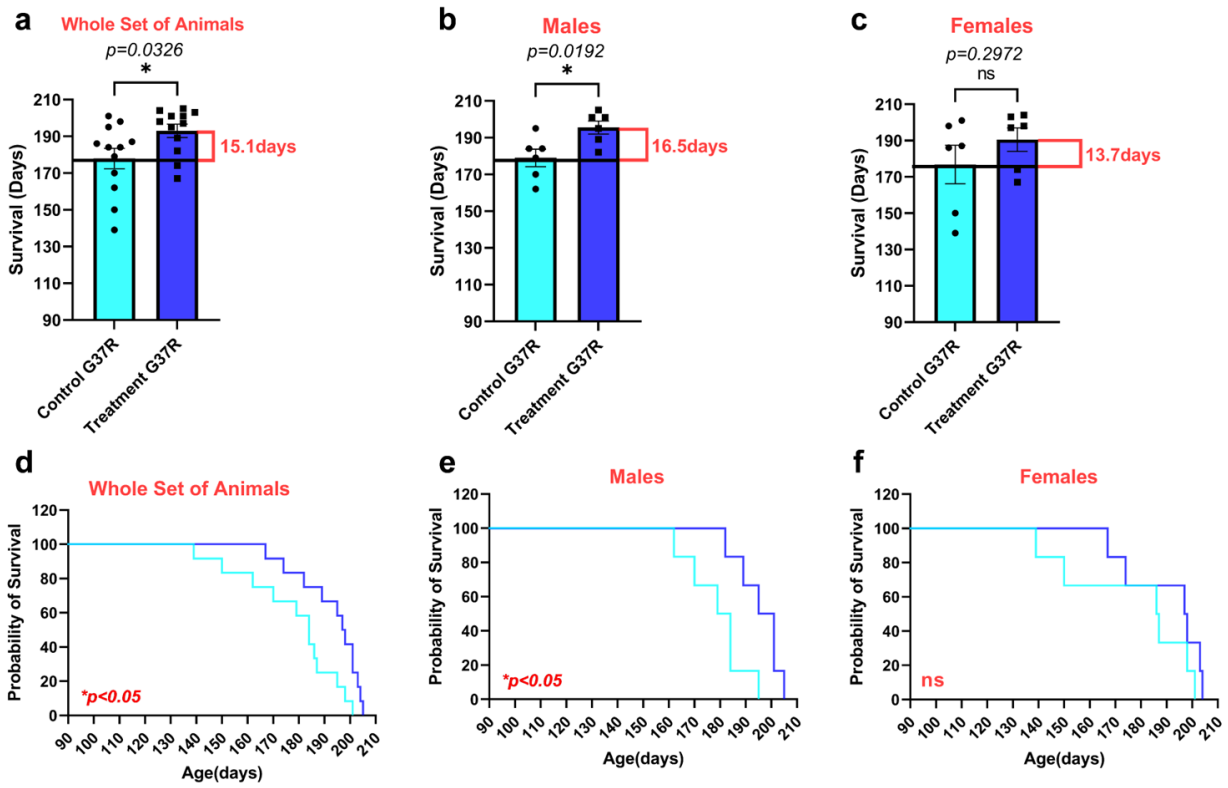

Figure 63. Edaravone prodrug NS-1-2 extends the lifespan in SOD1-G37R ALS mice.

a) Two-tailed (unpaired *t-test*) of the mean onset age showing that Ns-1-2 delays the mean symptom onset age from 177.9 days for G37R age-matched whole set of animals (control/n=12 mice; n=6 males and n=6 females) to 193 days (NS-1-2/n=12 mice; n=6males and n=6 females); **b)** from 179 days for age-matched G37R males (control/n=6 mice), to 195.5 days for age-matched G37R males (NS-1-2/n=6 mice); **c)** from 176.8 days for age-matched G37R females (control/n=6 females), to 190.5 days for age-matched G37R females (NS-1-2/n=6 females). Data are presented as mean ± SEM (n=12), for the whole set of animals and (n=6) for males and females. n= number of animals of the designated genotype. Data were analyzed using a two-tailed (unpaired *t-test*), with a significance set at *p<0.05*. Here, *p=0.0326 (whole set), p=0.0192 (male) and p=0.2972*

(female), with **p<0.05 and ns=non significant* versus control G37R. **d)** Kaplan–Meier curves of the probability of symptom onset showing that NS-1-2 prolongs the median the median survival from 184 days for age-matched G37R whole set of animals (control/n=12 mice), including (n=6male and n=6 female) to 197.5 days (NS-1-2/n=12 mice), including (n=6male and n=6 female); **e)** from 181.5 days for age-matched G37R males (control/n=6 mice), to 198 days for age-matched G37R males (NS-1-2/n=6 males); **f)** from 186.5 days for age-matched G37R females (control/n=6 mice), to 197.5 days for age-matched G37R females (NS-1-2/n=6 females). Data are presented as mean ± SEM. n= number of animals of the designated genotype. Data were analyzed using a Kaplan-Meir Log-rank (Mantel-cox) in SOD1G37R ALS mice, with a significance set at *p<0.05*. Here, *p=0.0174 (whole set), p=0.0232 (male) and p=0.2322 (female)* with **p<0.05 and ns* versus control G37R.

4.19 Edaravone prodrug NS-1-2 prevents ALS-induced weight loss or cachexia in the SOD1-linked model of ALS

Additionally, initiating the treatment of EDR prodrug NS-1-2 pre-symptomatically at the age of 90 days until the age of 210 days modified the clinical disease phenotypes of ALS-induced cachexia. Weight loss is regarded as the clinical prognostic marker for ALS disease progression due to muscle loss, fat loss, decreased caloric intake, and larger metabolic demand [359]. During the clinical progression of the disease after disease onset, the loss of motor neurons causes denervation which leads to loss of muscle fibers resulting in a decrease in muscle mass. Rapid denervation-induced weight loss has been recognized as an indicator of faster progression and shorter survival[359]. As part of our current animal studies, we evaluated weight loss from highest recorded weight to weight at humane endpoint/end stage for control versus treated. Body weight was monitored

daily longitudinally starting from age 90 days until the age 210 days for a total of four months.

As shown in **(figure 64)**, daily intraperitoneal injection (IP, IJ) with NS-1-2 starting pre-symptomatically from the age of 90 days until the humane endpoint (end-stage) significantly prevented the weight loss in the age-matched whole set of animals and both the sexes (male/female) of SOD1G37R ALS mice. For the whole set of animals, n=12/group including (6 male and 6 female) in both the vehicle-treated (control) and NS-1-2 treated group. The mean percentage loss of weight differed significantly between the vehicle-treated (27.13%) and NS-1-2 treated group (18.29%), representing a reduction in the overall percent weight loss in the NS-1-2 treatment group compared to the control of 8.838%. On segregation of sex, we found that NS-1-2 treated age-matched males (n=6), and age-matched females (n=6) demonstrated significant prevention of percentage weight loss (8.574%) and (9.103%) compared to the control group, respectively, with a larger effect size in males (p=0.0004) compared to females (p=0.0071). Sex segregation demonstrated a notable therapeutic effect of NS-1-2 in males compared to females, suggesting a stronger sex-specific efficacy of NS-1-2, yet the reduction in weight loss was significant in both sexes. The survival age data is also in tabulated form **(Table 5)** below.

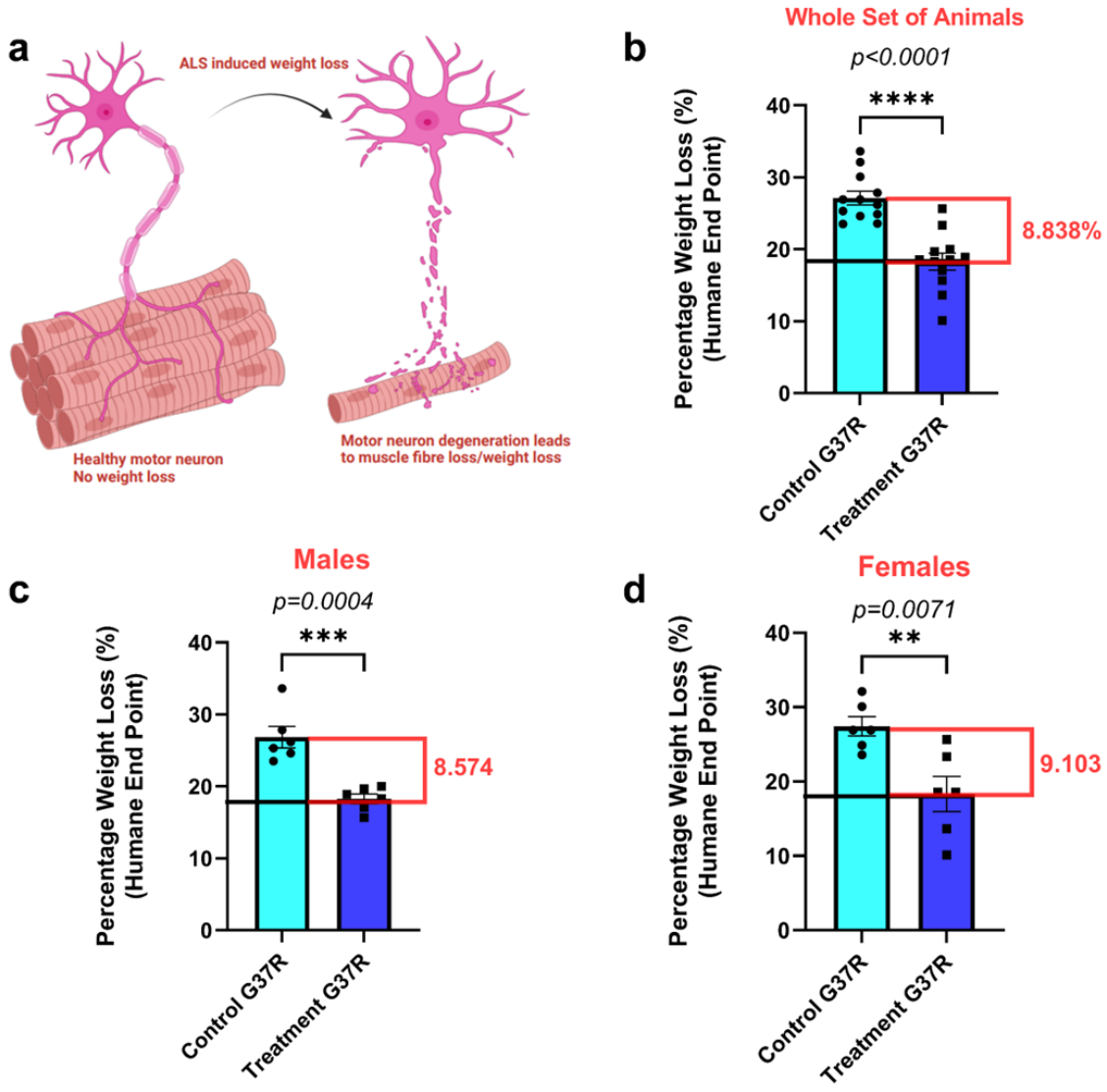

Figure 64. Edaravone prodrug NS-1-2 rescued weight loss in SOD1-G37R ALS mice.

a) Photograph showing progressive loss of motor neurons leads to loss in muscle fiber and hence, weight loss in ALS; **b)** Two-tailed (unpaired *t-test*) of the mean percentage loss of body weight at the humane endpoint showing that NS-1-2 prevented the weight loss from 27.41% days for G37R age-matched whole set of animals (control/n=12 mice; n=6 males and n=6 females) to 18.31% (NS-1-2/n=12 mice; n=6 males and n=6 females);

c) from 26.84% for age-matched G37R males (control/n=6 mice), to 18.27% for age-matched G37R males (NS-1-2/n=6 mice); **d)** from 27.41% for age-matched G37R females (control/n=6 females), to 18.31% for age-matched G37R females (NS-1-2/n=6 females). Data are presented as mean ± SEM (n=12), for the whole set of animals and (n=6) for males and females. n= number of animals of the designated genotype. Data were analyzed using a two-tailed (unpaired *t-test*), with a significance set at $p<0.05$. Here, $p=0.0001$, $p=0.0004$ *and* $p=0.0071$ with $***p<0.001$, $**p<0.001$ *and* $*p<0.05$ versus control G37R.

4.20 Edaravone prodrug NS-1-2, with longitudinal monitoring, improves several motor clinical phenotypes in the SOD1-G37R mouse model of ALS

Presymptomatic treatment with BSZ starting at the age of 90 days until the age of 210 days with daily monitoring for four months for several humane endpoint indicators ameliorated various clinical motor decline phenotypes in ALS mice, compared to vehicle-treated mice. NS-1-2, improved several observed markers for motor neurodegeneration during disease progression in SOD1-G37R ALS mice in terms of hindlimb clasping behavior, abnormal hindlimb flexion, and abnormal splay of the toe fingers **(figure 65)**.

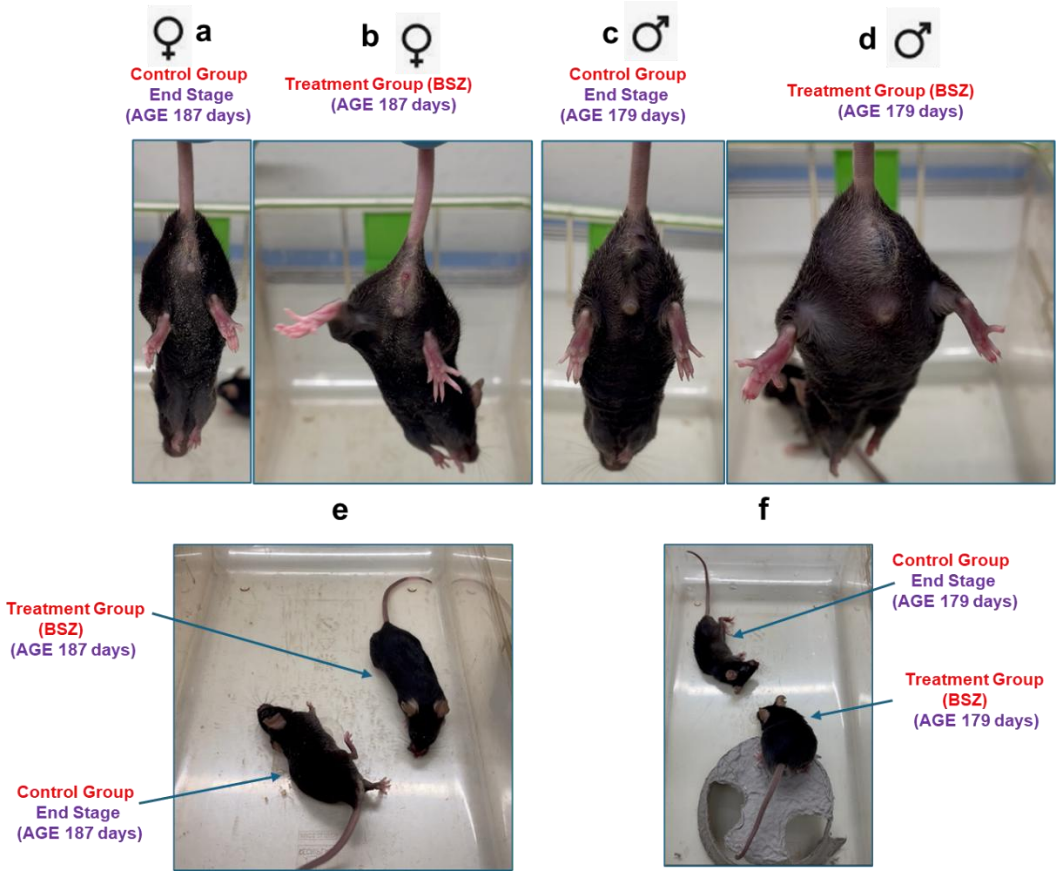
♀ a
Control Group
End Stage
(AGE 187 days)
b ♀
Treatment Group (BSZ)
(AGE 187 days)
c ♂
Control Group
End Stage
(AGE 179 days)
d ♂
Treatment Group (BSZ)
(AGE 179 days)
e
f
Treatment Group
(BSZ)
(AGE 187 days)
Control Group
End Stage
(AGE 187 days)
Control Group
End Stage
(AGE 179 days)
Treatment Group
(BSZ)
(AGE 179 days)

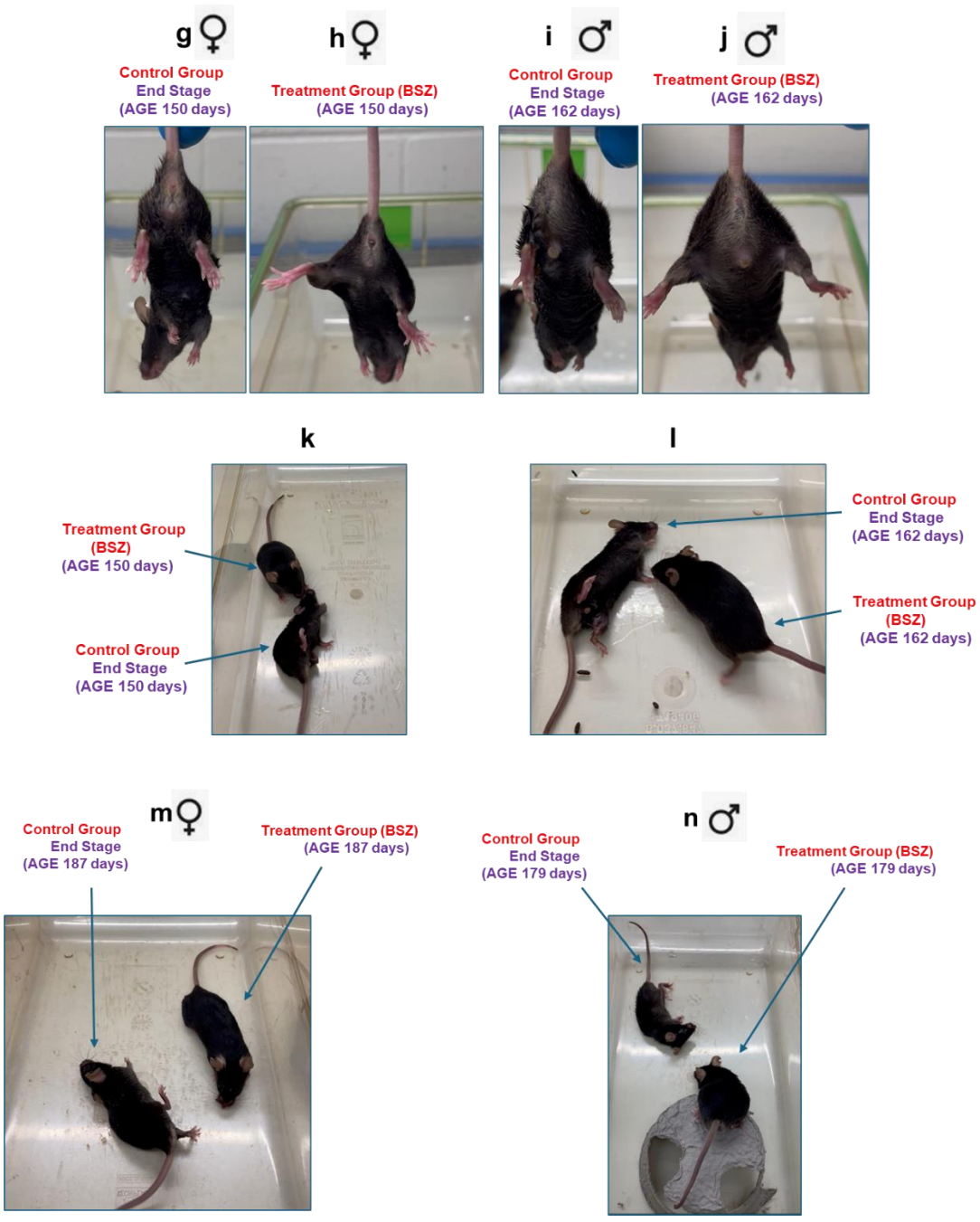
g ♀
Control Group
End Stage
(AGE 150 days)
h ♀
Treatment Group (BSZ)
(AGE 150 days)
i ♂
Control Group
End Stage
(AGE 162 days)
j ♂
Treatment Group (BSZ)
(AGE 162 days)
k
Treatment Group
(BSZ)
(AGE 150 days)
Control Group
End Stage
(AGE 150 days)
l
Control Group
End Stage
(AGE 162 days)
Treatment Group
(BSZ)
(AGE 162 days)
m ♀
Control Group
End Stage
(AGE 187 days)
Treatment Group (BSZ)
(AGE 187 days)
n ♂
Control Group
End Stage
(AGE 179 days)
Treatment Group (BSZ)
(AGE 179 days)

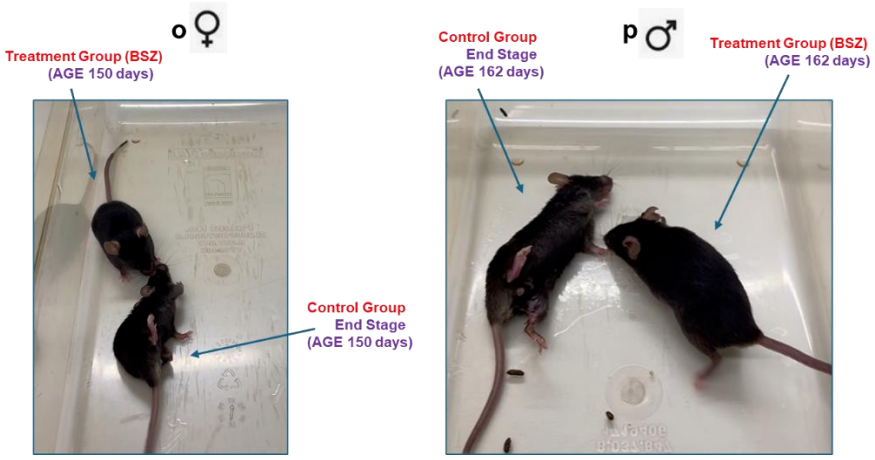

Figure 65. Representative pictures showing the longitudinal assessment of various gross motor clinical phenotypes and the effects of treatment BSZ in modifying the motor disease clinical phenotypes in G37R ALS mice.

Age-matched littermates (control vs treatment (NS-1-2)) showing various ALS clinical phenotypes/ALS Motor functions phenotypes/disease progression. When the female and male mice were suspended by their tail at the age of (187 and 179 days), respectively, the vehicle-treated control groups **a**, and **c**, showed immobile hindlimbs (no limb flexion) and hindlimbs falling towards midline of the abdomen (abnormal splay), whereas NS-1-2 treatment groups **b** and **d** showed mobile hindlimbs (limbs flexion), with hindlimbs splayed outwards away from the abdomen. Both the male and female vehicle-treated/control groups were unable to right themselves in 15 seconds compared to the NS-1-2 treated group, at the age of 187 days (**e**), and at the age of 179 days (**f**).

Table 5. Total number of age and sex-matched SOD1-G37R (42) mouse model used to evaluate the efficacy of the Edaravone prodrug NS-1-2 (BSZ).

The total number of age and sex-matched animals with segregation of sex in different cohorts (control and treatment) used in the study, including assessment of various

parameters (life span, disease onset, symptom onset, weight loss (%), with the total number of intraperitoneal injections (IP, IJ) was given to both cohorts. **Note: NS-1-2 refers to BSZ in figure 14 (a, b, c). NS-1-2 was initially developed in the lab and later trademarked as Borsantrazole (BSZ).**

To study the therapeutic effects of Borsantrazole (BSZ) in the SOD1-G37R mouse model of amyotrophic lateral sclerosis Protocol# 21-014, AC11693													
Control Treatment (N=12) including age-matched (6 males and 6 females)							BSZ Treatment (N=12) including age-matched (6 males and 6 females)						
Animal ID	Sex	Life span/Age of survival (days)	Total number of IP,IJ	Age to reach disease onset (days)	Age to reach symptom onset (days)	Weight Loss (%) at humane end point	Animal ID	Sex	Life span/Age of survival (days)	Total number of IP,IJ	Age to reach disease onset (days)	Age to reach symptom onset (days)	Weight loss (%) at humane end point
R651RR	Male	195	106	131	180	Weight Loss>25% Weight Loss (%): 25.324	R627R	Male	201	112	143	199	Weight Loss<25% Weight Loss (%): 17.056
R644LL	Male	184	95	129	169	Weight Loss<25% Weight Loss (%): 23.52	R711R	Male	201	112	143	171	Weight Loss<25% Weight Loss (%): 18.91
R624R	Male	179	90	140	156	Weight Loss>25% Weight Loss (%): 33.6	R715LR	Male	205	116	156	184	Weight Loss<25% Weight Loss (%): 19.67
R712LL	Male	170	81	131	158	Weight Loss<25% Weight Loss (%): 24.60	R736L	Male	189	100	147	180	Weight Loss<25% Weight Loss (%): 20
R751L	Male	184	95	128	152	Weight Loss>25% Weight Loss (%): 26.17	R739RR	Male	195	106	154	193	Weight Loss<25% Weight Loss (%): 15.68
R738LL	Male	162	73	125	154	Weight Loss>25% Weight Loss (%): 27.85	R635L	Male	182	93	168	182	Weight Loss<25% Weight Loss (%): 18.306
R647LLR	Female	186	97	136	149	Weight Loss>25% Weight Loss (%): 32.107	R638L	Female	198	109	164	195	Weight Loss<25% Weight Loss (%): 18.543
R697LL	Female	187	98	106	163	Weight Loss>25% Weight Loss (%): 26.923	R639R	Female	203	114	163	203	Weight Loss<25% Weight Loss (%): 10.122
R699R	Female	198	109	131	186	Weight Loss<25% Weight Loss (%): 23.58	R605L	Female	197	108	188	196	Weight Loss<25% Weight Loss (%): 13.66
R705LR	Female	150	61	123	142	Weight Loss>25% Weight Loss (%): 26.90	R700LR	Female	204	115	148	195	Weight Loss<25% Weight Loss (%): 18.548
R703LL	Female	201	112	159	189	Weight Loss<25% Weight Loss (%): 24.88	R701L	Female	174	85	144	165	Weight Loss<25% Weight Loss (%): 23.34
R634LL	Female	139	50	117	127	Weight Loss>25% Weight Loss (%): 30.081	R640LL	Female	167	78	144	160	Weight Loss>25% Weight Loss (%): 25.64

4.21 Proteomic and phosphoproteomic analyses reveal differentially regulated proteins in lumbar spinal cord samples from the SOD1-G37R mouse model of ALS, correlating with the efficacy of Edaravone prodrug NS-1-2

ALS is a highly complex and heterogeneous motor neurodegenerative disease resulting from multiple wide interacting pathophysiological mechanisms, culminating in the disruption of global proteome and phosphoproteome interacting networks in the brain, spinal cord, and muscle/neuromuscular junctions[360-362]. To gain insights into the multi-system changes in the proteomics and phosphoproteomics of the central nervous system

(CNS), the scientific community has recently utilized highly sensitive, reliable, precise, deep-coverage, and reproducible mass-spectrometry-based proteomics and phosphoproteomics approaches [363-365]. Further, proteomics studies have been identified as a reliable tool in detecting and developing novel biomarkers[366], that could help correlate the severity of ALS symptoms and the rate of disease progression longitudinally [365, 367-370]. Moreover, the global proteomics biomarker approach promotes a better understanding of meaningful drug target mechanisms and achieves positive clinical outcomes[371-375]. In an attempt to explore the therapeutic efficacy of novel boron-based EDR prodrug (NS-1-2), and to further move in our drug development process, we utilized a discovery-based LC-MS detection technique to profile the global changes in the proteome and phosphoproteome of mutant human G37R SOD1 mice spinal cord samples **(n=4)** from both control and treatment groups.

In an attempt to explore and rationalize the therapeutic efficacy of the novel boron-based EDR prodrug NS-1-2, and to further move forward in our drug development process, we utilized a discovery-based LC-MS detection technique to profile the global changes in the proteome and phosphoproteome of mutant human SOD1-G37R mice spinal cord samples (*n=4*) from both control and treated groups. Considering the significant efficacy results in the male cohort, we assessed the proteomic signatures of late-stage ALS male mice, which is one of the limitations of our study (male sex specificity). A total of 6,270 proteins were quantified in all replicates of either sham (vehicle-treated) or NS-1-2-treated samples. Differential analysis was performed using a moderated *t-test* (LIMMA)[376]. Intensities were log2-transformed, followed by K-nearest neighbor (KNN) imputation for Missing at Random (MAR) values. A total of 51 proteins with adjusted p-values <0.05

were statistically significantly differential between treated and sham. (see Supplementary Data for full proteomics data).

The three known ALS-relevant proteins ***Cplx2, Lrp4, and Sqstm1/p62*** were significantly increased in NS-1-2 treated group, while ***Ca3*** showed a significant decrease (see **Table 6**). These proteins are found to have a pathological link with the progression of ALS, and these differential expressions of proteins represent a positive correlation with the efficacy of the EDR prodrug NS-1-2 in terms of extension of survival, delay in onset, delay in symptom onset, and rescuing weight loss. We further discovered increased expressions of two proteins **(*Gan/KLHL16, Snx13*)** in the treatment (NS-1-2) group compared to the control group. These two proteins are not specific to ALS; however, their increased expression is implicated in the pathophysiology of neurodegenerative disease and in maintaining neuronal health **Table 6.**

Figure 66 illustrates an overview of the sample processing workflow for LC/MS-based global proteomics and phosphoproteomics from the lumbar spinal cord samples of G37R male mice. Also, volcano plots showing the differential regulation of proteins expressed in the lumbar spinal cord of hmutSOD1 G37R male mice. In addition, a Heat map showing unsupervised hierarchical clustering of z-scored log2 intensities of the 51 significantly regulated proteins for the BSZ and sham (control) group **(see the list of all the 51 proteins in Table 7).**

Table 6. Selected known and novel proteins with significantly differential abundance (adj $p<0.05$; $n=4$) in the lumbar spinal cord of human mutantSOD1 G37R male mice treated with NS-1-2 and sham (vehicle) based on quantitative proteomics.

UniProt Accession Number (Protein ID)	Abbreviated (Gene Symbol)	Protein Description	adj. p-value	ratio (BSZ/Sham)	Pathological Association to ALS Known/Novel
P16015	***Ca3***	Carbonic anhydrase 3	0.0279	0.3	Known
Q8CA72	***Gan/KLHL16***	Gigaxonin	0.0219	2.7	Novel
P84086	***Cplx2***	Complexin-2	0.00565	1.9	Known
Q6PHS6	***Snx13***	Sorting nexin-13	0.00144	2.5	Novel
Q8VI56	***Lrp4***	Low-density lipoprotein receptor-related protein 4	0.01020	3.6	Known
Q64337	***Sqstm1/p62***	Sequestosome-1	0.01140	3.0	Known

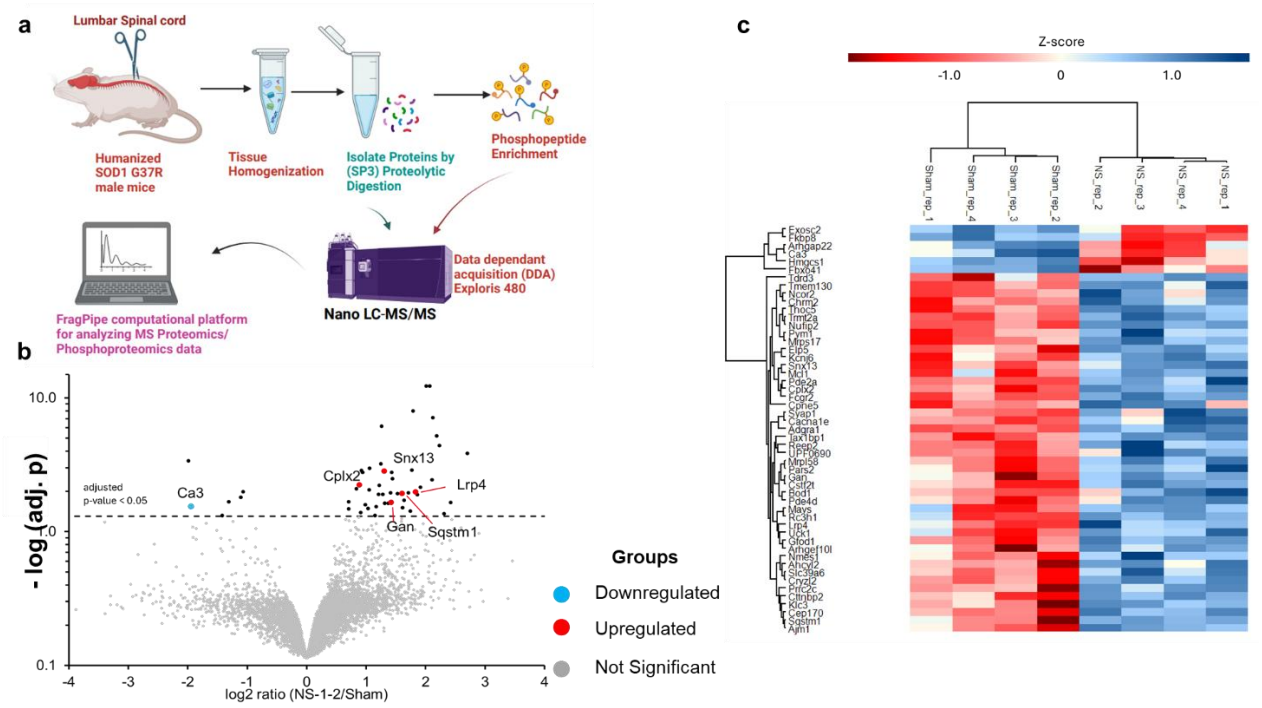

Figure 66 (a,b,c). Differential analysis of global proteome changes in hmutSOD1-G37R ALS mice.

a) Overview of the sample processing workflow for LC/MS-based global proteomics and phosphoproteomics from the lumbar spinal cord samples of G37R male mice. **b)** Volcano plots showing the differential regulation of proteins expressed in the lumbar spinal cord of hmutSOD1 G37R male mice. Based on log2-transformed intensities, 51 out of 6,270

proteins were significantly differential (adj. *p<0.05*; *n=4*). Selected proteins that are either up (red) or down (blue) regulated compared to controls are highlighted. **c)** Heat map showing unsupervised hierarchical clustering of z-scored log2 intensities of the 51 significantly regulated proteins for NS-1-2 and sham (control) group. Heatmap generated with Perseus 2.0.1.

Note: NS-1-2 refers to BSZ in figure 14 (a, b, c). NS-1-2 was initially developed in the lab and later trademarked as Borsantrazole (BSZ).

Table 7. List of 51 proteins with significantly differential abundance (adj p<0.05; n=4) in the lumbar spinal cord of human mutantSOD1 G37R male mice treated with BSZ, and sham (vehicle), discovery-based, unbiased global quantitative proteomics.

UniProt Accesion Number Protein ID	Gene Symbol	Protein Description	log2 "fold-change" (BSZ-Sham)	ratio (BSZ/Sham)	adj. p-value
Q5F2E7	***Nufip2***	FMR1-interacting protein NUFIP2	2.07	4.20	0.00000
Q8C4G9	***Adgra1***	Adhesion G protein-coupled receptor A1	2.01	4.03	0.00000
Q8BNV1	***Trmt2a***	tRNA (uracil-5-)-methyltransferase homolog A	1.79	3.46	0.00000
Q3UHD2	***Gfod1***	Glucose-fructose oxidoreductase domain-containing protein 1	2.12	4.35	0.00000
P08101	***Fcgr2***	Low affinity immunoglobulin gamma Fc region receptor II	1.26	2.39	0.00000
Q9CQE3	***Mrps17***	28S ribosomal protein S17, mitochondrial	2.19	4.56	0.00001
Q6NXM3	***Tmem130***	Transmembrane protein 130	2.23	4.69	0.00004
Q9ERZ4	***Chrm2***	Muscarinic acetylcholine receptor M2	2.70	6.50	0.00014
Q8VBV3	***Exosc2***	Exosome complex component RRP4	-1.99	0.25	0.00041
Q8R035	***Mrpl58***	Peptidyl-tRNA hydrolase ICT1, mitochondrial	1.25	2.38	0.00061
Q922S4	***Pde2a***	cGMP-dependent 3',5'-cyclic phosphodiesterase	1.06	2.08	0.00104
B9EJA2	***Cttnbp2***	Cortactin-binding protein 2	1.77	3.41	0.00129
Q3UKC1	***Tax1bp1***	Tax1-binding protein 1 homolog	0.92	1.90	0.00137
Q6PHS6	***Snx13***	Sorting nexin-13	1.30	2.46	0.00144
A2AJA9	***Ajm1***	Apical junction component 1 homolog	1.43	2.69	0.00166
Q8BKT7	***Thoc5***	THO complex subunit 5 homolog	0.94	1.92	0.00168
Q99L85	***Elp5***	Elongator complex protein 5	1.44	2.71	0.00329
Q61290	***Cacna1e***	Voltage-dependent R-type calcium channel subunit alpha-1E	2.11	4.32	0.00355
P84086	***Cplx2***	Complexin-2	0.89	1.85	0.00565
P48542	***Kcnj6***	G protein-activated inward rectifier potassium channel 2	1.22	2.33	0.00607
Q9CWU4		UPF0690 protein C1orf52 homolog	1.91	3.76	0.00714
Q6A065	***Cep170***	Centrosomal protein of 170 kDa	0.84	1.78	0.00805
Q8C7E9	***Cstf2t***	Cleavage stimulation factor subunit 2 tau variant	1.05	2.07	0.00871
Q8JZK9	***Hmgcs1***	Hydroxymethylglutaryl-CoA synthase, cytoplasmic	-1.07	0.48	0.01020
Q8VI56	***Lrp4***	Low-density lipoprotein receptor-related protein 4	1.83	3.56	0.01020
Q8CFI5	***Pars2***	Probable proline--tRNA ligase, mitochondrial	1.71	3.27	0.01110
Q9WU42	***Ncor2***	Nuclear receptor corepressor 2	1.41	2.66	0.01120
Q64337	***Sqstm1***	Sequestosome-1	1.60	3.03	0.01140
Q91W40	***Klc3***	Kinesin light chain 3	1.53	2.89	0.01200
Q4VGL6	***Rc3h1***	Roquin-1	1.21	2.31	0.01240
Q91W18	***Tdrd3***	Tudor domain-containing protein 3	1.28	2.43	0.01240
P97287	***Mcl1***	Induced myeloid leukemia cell differentiation protein Mcl-1 homolog	1.86	3.63	0.01270
Q6NS60	***Fbxo41***	F-box only protein 41	-1.11	0.46	0.01570
Q5SQY2	***Bod1***	Biorientation of chromosomes in cell division protein 1	1.64	3.12	0.01910
Q3UNZ8	***Cryzl2***	Quinone oxidoreductase-like protein 2	0.70	1.63	0.02100
O35465	***Fkbp8***	Peptidyl-prolyl cis-trans isomerase FKBP8	-1.31	0.40	0.02120
Q8CA72	***Gan***	Gigaxonin	1.42	2.68	0.02190
Q8JZW4	***Cpne5***	Copine-5	2.42	5.35	0.02210
Q01063	***Pde4d***	cAMP-specific 3',5'-cyclic phosphodiesterase 4D	1.37	2.58	0.02310
Q8CHP5	***Pym1***	Partner of Y14 and mago	1.31	2.48	0.02310
Q3TLH4	***Prrc2c***	Protein PRRC2C	0.99	1.98	0.02590
P16015	***Ca3***	Carbonic anhydrase 3	-1.95	0.26	0.02790
Q810Q5	***Nmes1***	Normal mucosa of esophagus-specific gene 1 protein	1.17	2.25	0.02890
Q68FL4	***Ahcyl2***	Putative adenosylhomocysteinase 3	1.61	3.05	0.03080
Q9D5V6	***Syap1***	Synapse-associated protein 1	1.03	2.04	0.03200
Q8VCD6	***Reep2***	Receptor expression-enhancing protein 2	0.71	1.63	0.03320
A2AWP8	***Arhgef10l***	Rho guanine nucleotide exchange factor 10-like protein	1.74	3.34	0.03710
Q8C145	***Slc39a6***	Zinc transporter ZIP6	0.91	1.88	0.04110
Q8VCF0	***Mavs***	Mitochondrial antiviral-signaling protein	2.31	4.96	0.04370
Q8BL80	***Arhgap22***	Rho GTPase-activating protein 22	-1.42	0.37	0.04770
P52623	***Uck1***	Uridine-cytidine kinase 1	1.15	2.22	0.04810

A total of 9541 phosphorylation sites were quantified and further filtered to retain high-quality data. Only phosphopeptides that were quantified in all 4 replicates of either treated or sham were kept, resulting in a total of 3945 high-quality phosphopeptides. Differential analysis was performed using a moderated *t-test* (LIMMA)[376]. Intensities were log2-transformed, followed by K-nearest neighbor (KNN) imputation for Missing at Random (MAR) values. A total of 29 phosphorylation sites with adjusted p-values <0.05 were considered statistically significantly differential between treated (BSZ) and sham groups **Table 8**.

Table 8. List of 29 phosphoproteins with significantly differential abundance (adj p<0.05; n=4) in the lumbar spinal cord of human mutantSOD1 G37R male mice treated with BSZ, and sham (vehicle), discovery-based, unbiased global quantitative phosphoproteomics.

UniProt Accesion Number Protein ID	Gene Symbol	Protein Description	Phospho Site	adj. p-value	log2 "fold-change" (BSZ-Sham)	ratio (BSZ/Sham)
P53668	***Limk1***	LIM domain kinase 1	T301	5.91E-13	4.50	22.63
Q9QYX7	***Pclo***	Protein piccolo	S3545	2.42E-08	2.65	6.28
Q61194	***Pik3c2a***	Phosphatidylinositol 4-phosphate 3-kinase C2 domain-containing subunit alpha	S261	1.27E-07	1.83	3.56
P35564	***Canx***	Calnexin	S563	2.33E-06	1.79	3.46
P05213	***Tuba1b***	Tubulin alpha-1B chain	S340	4.21E-05	-1.96	0.26
Q9R078	***Prkab1***	5'-AMP-activated protein kinase subunit beta-1	S108	5.59E-05	-1.95	0.26
Q99KK9	***Hars2***	Histidine--tRNA ligase, mitochondrial	S66	6.74E-05	1.38	2.60
Q9QYX7	***Pclo***	Protein piccolo	S4598	1.67E-04	1.95	3.86
P39053	***Dnm1***	Dynamin-1	S774	8.36E-04	-2.69	0.15
P09411	***Pgk1***	Phosphoglycerate kinase 1	S203	2.23E-03	-1.43	0.37
P70392	***Rasqrf2***	Ras-specific guanine nucleotide-releasing factor 2	S717	2.32E-03	1.41	2.66
P83093	***Stim2***	Stromal interaction molecule 2	S612	3.46E-03	2.14	4.41
A2AAY5	***Sh3pxd2b***	SH3 and PX domain-containing protein 2B	S768	5.51E-03	1.86	3.63
Q924H7	***Wac***	WW domain-containing adapter protein with coiled-coil	S511	5.80E-03	1.89	3.71
P00441	***SOD1***	Superoxide dismutase [Cu-Zn]	S135	7.28E-03	2.48	5.58
P19246	***Nefh***	Neurofilament heavy polypeptide	T72	7.73E-03	-5.76	0.02
P16330	***Cnp***	2',3'-cyclic-nucleotide 3'-phosphodiesterase	S169	9.06E-03	-1.77	0.29
Q9ESK9	***Rb1cc1***	RB1-inducible coiled-coil protein 1	S243	1.05E-02	1.16	2.23
P60904	***Dnajc5***	DnaJ homolog subfamily C member 5	S10	1.34E-02	-1.80	0.29
P60904	***Dnajc5***	DnaJ homolog subfamily C member 5	S12	1.58E-02	-1.41	0.38
E9Q3C1	***C2cd2***	C2 domain-containing protein 2	S436	1.60E-02	-2.96	0.13
Q8CGA2	***Tbc1d14***	TBC1 domain family member 14	S296	2.00E-02	2.08	4.23
Q8C052	***Map1s***	Microtubule-associated protein 1S	S660	2.10E-02	-1.93	0.26
E9Q5K9	***Ythdc1***	YTH domain-containing protein 1	S425	3.19E-02	-1.56	0.34
Q50H33	***Kctd8***	BTB/POZ domain-containing protein KCTD8	S331	3.55E-02	0.88	1.84
P47809	***Map2k4***	Dual specificity mitogen-activated protein kinase kinase 4	S88	3.86E-02	-1.63	0.32
P54227	***Stmn1***	Stathmin	S16	3.86E-02	-1.57	0.34
Q8R554	***Otud7a***	OTU domain-containing protein 7A	T804	4.57E-02	1.64	3.12
P08551	***Nefl***	Neurofilament light polypeptide	T317	4.72E-02	-1.60	0.33

Our phosphoproteomics data unraveled new phosphorylation sites in known protein biomarkers of ALS progression, ***Nefl*** and ***Nefh***. We found that 58 and 8 phosphorylated serine/threonine (S/T) sites are downregulated in the ***Nefh*** and ***Nefl*** region, respectively, following treatment with NS-1-2, reflecting a combination of a general slight reduction in protein expression also detected in our proteomics data and a decrease in phosphorylation. Overall, this observable trend in downregulation of neurofilament light and heavy chains correlates with the efficacy observed in our SOD1-G37R mouse model, among treated animals, and is representative of the benefits of BSZ treatment using a key marker of ALS disease progression (***Nefh*** and ***Nefl***). Importantly, phosphorylation of **T72** in Nefh and **T317** in Nefl was significantly reduced in the NS-1-2-treated group, such as **S203 in** Pgk1 (**Table 9**).

Table 9. Summary of known and novel proteins with significantly differential phosphorylation (adj. $p<0.05$; $n=4$) in the lumbar spinal cord of mutant SOD1 G37R male mice treated with BSZ and sham (vehicle), based on quantitative phosphoproteomics. For a full summary of the phosphoproteomics data for NS-1-2 and Sham (vehicle) samples, see **Table 8**.

UniProt Accession Number (Protein ID)	Abbreviated (Gene Symbol)	Protein Description	Phosphorylation Site	adj. p-value	ratio (BSZ/Sham)
P19246	***Nefh***	Neurofilament heavy polypeptide	**T72**	7.73E-03	<0.1
P09411	***Pgk1***	Phosphoglycerate kinase 1	**S203**	2.23E-03	0.4
P08551	***Nefl***	Neurofilament light polypeptide	**T317**	4.72E-02	0.3

4.22 Proteomic and phosphoproteomic analyses reveal differentially regulated proteins in the brain samples from the SOD1-G37R mouse model of ALS, correlating with the efficacy of Edaravone prodrug NS-1-2

Further, in an attempt to explore and rationalize the therapeutic efficacy of novel boron-based EDR prodrug (NS-1-2), and to further move in our drug development process, we utilized a discovery-based LC-MS detection technique to profile the global changes in the proteome and phosphoproteome of mutant human G37R SOD1 mice brain samples **(n=4)** from both control and treatment groups.

Considering the significant efficacy results in the male cohort, we assessed the proteomic signatures of late-stage ALS male mice, which is one of the limitations of our study (male sex specificity). A total of 8429 protein groups were quantified and further filtered to retain high-quality data. Only protein groups that had been quantified with at least 2 peptides in at least 3 out of 4 replicates of either sham or treated samples were retained.

Differential analysis was performed using a moderated t-test (LIMMA). Intensities were log2-transformed, followed by K-nearest neighbor (KNN) imputation for Missing at

Random (MAR) values. A total of 44 proteins with adjusted p-values <0.05 were statistically significantly differential between treated and sham.

Table 10. List of 44 proteins with significantly differential abundance (adj p<0.05; n=4) in the brain of human mutantSOD1 G37R male mice treated with BSZ, and sham (vehicle), discovery-based, unbiased global quantitative proteomics.

UniProt Accesion Number Protein ID	*Gene Symbol*	Protein Description	log2 "fold-change" (BSZ-Sham)	ratio (BSZ/Sham)	adj. p-value
Q6NV72	***Wdcp***	WD repeat and coiled-coil-containing protein	0.689	1.61	0.0000
Q711T7	***Nadsyn1***	Glutamine-dependent NAD(+) synthetase	-0.897	0.54	0.0000
Q9JJY3	***Smpd3***	Sphingomyelin phosphodiesterase 3	0.396	1.32	0.0003
Q8BML1;Q8CJ19	***Mical2;Mical3***	[F-actin]-monooxygenase MICAL2	0.571	1.49	0.0004
Q8K2Y9	***Ccm2***	Cerebral cavernous malformations protein 2 homolog	0.341	1.27	0.0068
Q8BFW6	***Entpd3***	Ectonucleoside triphosphate diphosphohydrolase 3	0.367	1.29	0.0088
Q7TNT2	***Far2***	Fatty acyl-CoA reductase 2	0.628	1.55	0.0096
Q7TT15	***Galnt17***	Polypeptide N-acetylgalactosaminyltransferase 17	-0.436	0.74	0.0106
Q3UM18	***Lsg1***	Large subunit GTPase 1 homolog	0.755	1.69	0.0108
Q8K354	***Cbr3***	Carbonyl reductase [NADPH] 3	0.421	1.34	0.0114
Q8JZW4;Q1RLL3;Q9DC53	***Cpne5;Cpne8;Cpne9***	Copine-9	0.573	1.49	0.0122
Q9ERL9	***Gucy1a1***	Guanylate cyclase soluble subunit alpha-1	0.31	1.24	0.0123
P08556;Q61411	***Hras;Nras***	GTPase NRas	0.243	1.18	0.0125
Q8C1B7;Q8CHH9	***Septin11;Septin8***	Septin-11	0.24	1.18	0.0156
Q61263	***Soat1***	Sterol O-acyltransferase 1	-0.456	0.73	0.0167
Q3UEZ8	***Slc10a4***	Sodium/bile acid cotransporter 4	1.16	2.23	0.0169
Q61503	***Nt5e***	5'-nucleotidase	0.478	1.39	0.0184
Q8BRU6	***Slc18a2***	Synaptic vesicular amine transporter	1.34	2.53	0.0201
Q9DCI9	***Mrpl32***	Large ribosomal subunit protein bL32m	-0.265	0.83	0.0228
P16045	***Lgals1***	Galectin-1	-0.299	0.81	0.0231
Q8CGQ8	***Slc24a4***	Sodium/potassium/calcium exchanger 4	0.302	1.23	0.0248
Q8CJ40	***Crocc***	Rootletin	0.246	1.19	0.0250
Q6PFX8	***Rimkla***	N-acetylaspartylglutamate synthase A	-1.07	0.48	0.0252
Q8VEL9	***Rem2***	GTP-binding protein REM 2	0.726	1.65	0.0281
Q8C4U2	***Tmem145***	Transmembrane protein 145	-0.761	0.59	0.0294
Q61879;Q6URW6	***Myh10;Myh14***	Myosin-10	0.197	1.15	0.0295
P52432	***Polr1c***	DNA-directed RNA polymerases I and III subunit RPAC1	-0.315	0.80	0.0323
P15626	***Gstm2***	Glutathione S-transferase Mu 2	-0.261	0.83	0.0331
Q8R361	***Rab11fip5***	Rab11 family-interacting protein 5	-0.173	0.89	0.0338
Q0GNC1	***Inf2***	Inverted formin-2	0.5	1.41	0.0340
P27671	***Rasgrf1***	Ras-specific guanine nucleotide-releasing factor 1	-0.232	0.85	0.0341
Q69Z89	***Radil***	Ras-associating and dilute domain-containing protein	0.558	1.47	0.0343
Q8JZW4	***Cpne5***	Copine-5	0.648	1.57	0.0348
Q80WM4	***Hapln4***	Hyaluronan and proteoglycan link protein 4	-0.346	0.79	0.0351
Q8JZW4;Q9DC53	***Cpne5;Cpne8***	Copine-5	0.568	1.48	0.0356
Q91YY4	***Atpaf2***	ATP synthase mitochondrial F1 complex assembly factor 2	-0.31	0.81	0.0359
Q9CR29	***Ccdc43***	Coiled-coil domain-containing protein 43	-0.253	0.84	0.0368
Q8C3X8	***Lmf2***	Lipase maturation factor 2	-0.299	0.81	0.0371
Q8R3H9	***Ttc4***	Tetratricopeptide repeat protein 4	-0.306	0.81	0.0377
P54227	***Stmn1***	Stathmin	0.205	1.15	0.0389
P99024	***Tubb5***	Tubulin beta-5 chain	0.231	1.17	0.0391
Q03249	***Galt***	Galactose-1-phosphate uridylyltransferase	0.306	1.24	0.0393
P63143	***Kcnab1***	Voltage-gated potassium channel subunit beta-1	0.239	1.18	0.0394
Q7TSK2	***Sez6***	Seizure protein 6	0.317	1.25	0.0450

The two known ALS-relevant proteins ***Soat1/ACAT1, Lgals1*** were significantly decreased in the BSZ-treated group **(**see **Table 8)**. These proteins are found to have a pathological link with the progression of ALS, and these differential expressions of proteins represent a positive correlation with the efficacy of the EDR prodrug BSZ in terms of extension of survival, delay in onset, delay in symptom onset, and rescuing weight loss. We further discovered increased expressions of three proteins **(*Ccm2, Smpd3,Entpd3/NTPDase3*)** in the treatment (NS-1-2) group compared to the control group. These two proteins are not specific to ALS; however, their increased expression is implicated in the pathophysiology of neurodegenerative disease and in maintaining neuronal health **(Table 11).**

Table 11. Selected known and novel proteins with significantly differential abundance (adj $p<0.05$; n=4) in the brain of human mutantSOD1 G37R male mice treated with NS-1-2 and sham (vehicle) discovery-based, unbiased global quantitative proteomics.

UniProt Accession Number (Protein ID)	Abbreviated(Gene Symbol)	Protein Description	adj. p-value	ratio (BSZ/Sham)	Pathological Association to ALS Known/Novel
Q61263	***Soat1/ACAT1***	Sterol O-acyltransferase 1	0.0167	0.7	Known
P16045	***Lgals1***	Galectin-1	0.0231	0.8	Known
Q8K2Y9	***Ccm2***	Cerebral cavernous malformations protein 2 homolog	0.00684	1.26	Novel
Q9JJY3	***Smpd3***	Sphingomyelin phosphodiesterase 3	0.00029	1.32	Novel
Q8BFW6	***Entpd3/NTPDase3***	Ectonucleoside triphosphate diphosphohydrolase 3	0.00880	1.29	Novel

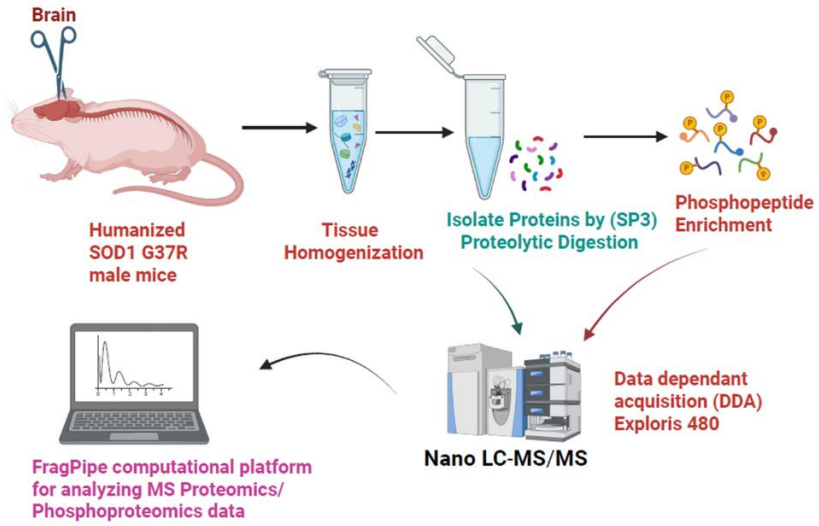

Figure 67. Overview of the sample processing workflow for LC/MS-based global proteomics and phosphoproteomics from the brain samples of G37R male mice.

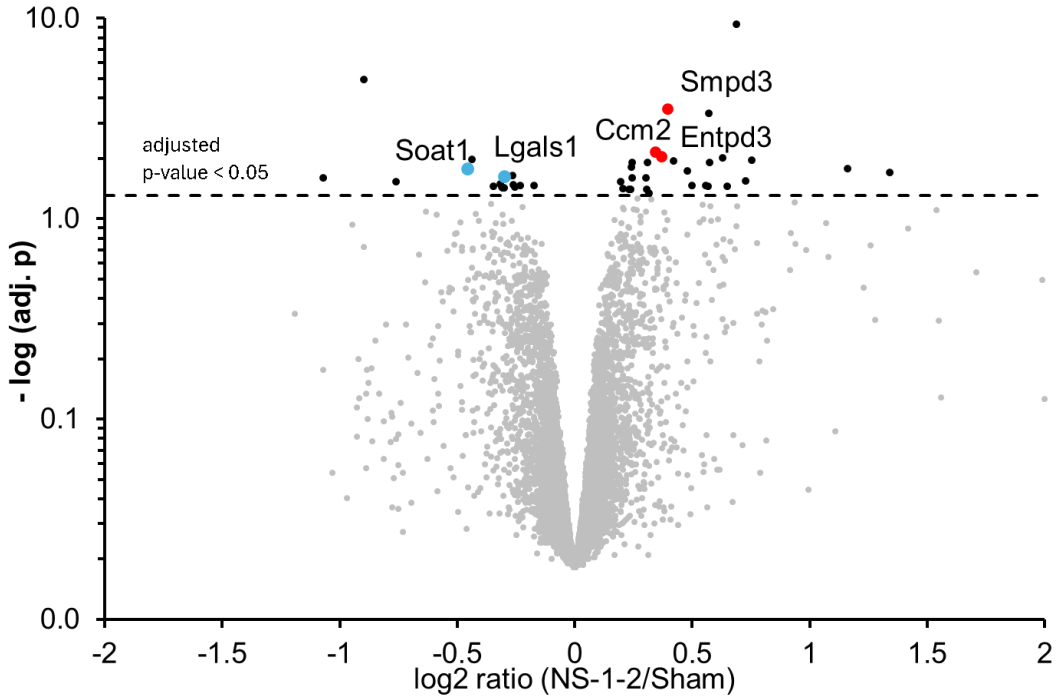

Figure 68. Differential analysis of global proteome changes in hmutSOD1-G37R ALS mice.

Volcano plots showing the differential regulation of proteins expressed in the brain of hmutSOD1 G37R male mice. Based on log2-transformed intensities, 44 out of 8429 proteins were significantly differential (adj. $p<0.05$; $n=4$). Selected proteins that are either up (red) or down (blue) regulated compared to controls are highlighted.

Note: NS-1-2 refers to BSZ in figure 68. NS-1-2 was initially developed in the lab and later trademarked as Borsantrazole (BSZ).

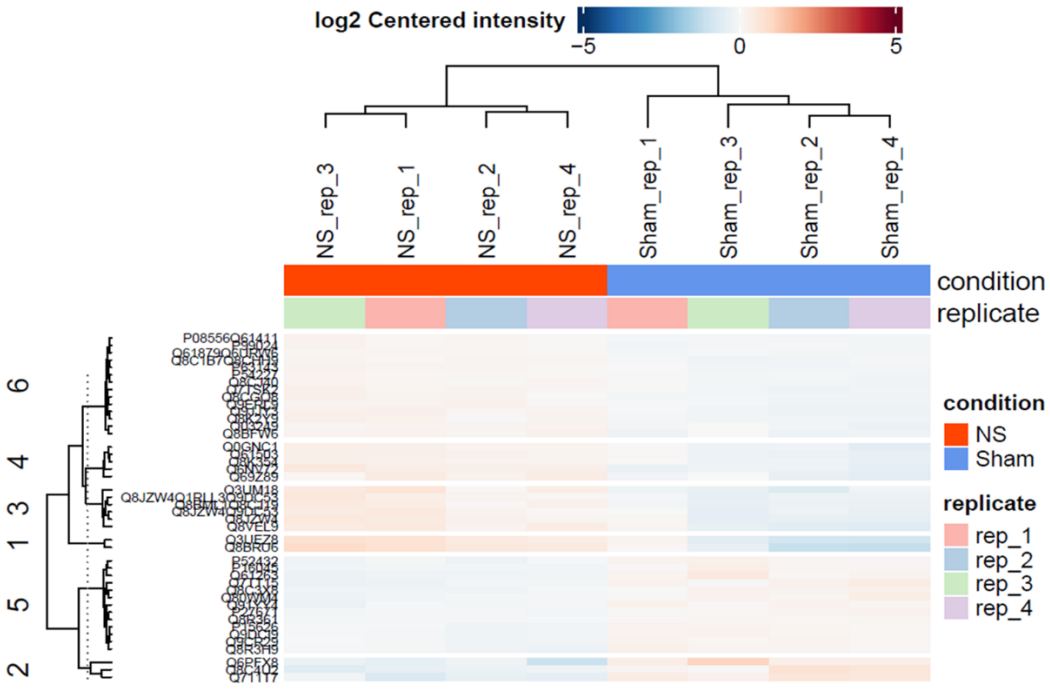

Figure 69. Differential analysis of global proteome changes in hmutSOD1-G37R ALS mice.

Heat map showing unsupervised hierarchical clustering of z-scored log2 intensities for the 44 significantly regulated proteins in the NS-1-2 and sham (control) groups. Heatmap generated with Perseus 2.0.1.

Note: NS-1-2 refers to BSZ in figure 69. NS-1-2 was initially developed in the lab and later trademarked as Borsantrazole (BSZ).

Table 12. Summary of known and novel proteins with significantly differential phosphorylation (adj. $p<0.05$; $n=4$) in the lumbar spinal cord and brain of mutant SOD1 G37R male mice treated with NS-1-2 and sham (vehicle), based on quantitative phosphoproteomics and their pathological association and role with various neurological diseases.

Changes in Phosphoproteome/Proteome biomarkers in the brain of mutSOD1G37R mice under treatments (Sham Vs NS-1-2) Phosphoproteome/Proteome biomarker changes (Sham Vs NS-1-2 treatment) in the MutantSOD1G37R mice mimicking clinical phenotypes of familial mutant SOD1 human ALS				
Proteome expressions are differentially increased/decreased in the brain/spinalcord (mutant SOD1 G37R ALS mice) of the treatment group (NS-1-2, n=4) as compared to that of the control (1:20; DMSO: PBS, n=4) group	**Abbreviated (Gene Symbol)**	**Protein Description**	**Pathological Association with other diseases**	**Role of Protein in Disease Pathologies**
Proteome/Brain Decreased	***Soat1/ACAT1***	Sterol O-acyltransferase 1	**Alzeimer's disease Parkinson disease**	**Increased expression of Sterol O-acyltransferase 1 causes Cholesterol dyshomeostasis, Mitochondrial, and ER stress, Amyloidosis**
Proteome/Brain Decreased	***Lgals1***	Galectin-1	**Alzeimer's disease Parkinson disease Aging**	**Increased expression of Galectin-1 causes Axonopathy and Aging**
Proteome/Brain Increased	***Ccm2***	Cerebral cavernous malformations protein 2 homolog	**Stroke Neurological defects Seizures**	**Decreased expression of CCM2 (also known as OSM and malcavernin) causes cerebral cavernous malformations (CCMs). These abnormalities are characterized by dilated leaky blood vessels, especially in the neurovasculature, that result in an increased risk of stroke, focal neurological defects, and seizures.**
Proteome/Brain Increased	***Smpd3***	Sphingomyelin phosphodiesterase 3	**Alzheimer's disease Duchenne muscular dystrophy**	**Decreased expression of Sphingomyelin phosphodiesterase 3 causes Amyloidosis, Taupathy, Cognitive impairment, Defective proteostasis**
Proteome/Brain Increased	***Entpd3/NTPDase3***	Ectonucleoside triphosphate diphosphohydrolase 3	**Alzheimer's disease**	**Decreased expression causes a decrease in mitochondrial ATP production. Play a role in the hypothalamic regulation of homeostatic systems, including feeding, sleep-wake behavior, and reproduction**
Proteome/Spinal Cord Decreased	***Ca3***	Carbonic anhydrase 3	**Aging**	**Increased Expression of Carbonic anhydrase 3 causes skeletal muscle damage in Neuromuscular disorders**
Proteome/Spinal Cord Increased	***Gan/KLHL16***	Gigaxonin	**Giant axonal neuropathy**	**Decreased expression of Gigaxonin causes impaired autophagy, Neurofilament aggregation/disorganization, Axonopathy**
Proteome/Spinal Cord Increased	***Cplx2***	Complexin-2	**Alzheimers disease Schizophrenia**	**Decreased expression of Complexin-2 causes Cognitive dysfunction**
Proteome/Spinal Cord Increased	***Snx13***	Sorting nexin-13	**Development protein/Cardiac performance**	**Decreased expression of Sorting nexin-13 causes growth retardation and heart failure.**
Proteome/Spinal Cord Increased	***Lrp4***	Low-density lipoprotein receptor-related protein 4	**Alzeimer's disease**	**Decreased expression of Low-density lipoprotein receptor-related protein 4 causes amyloid aggregation and cognitive impairment. It is required for neuromuscular junction formation. Studies have shown the presence of anti-LRP4 antibodies and defective neuromuscular transmission in ALS.**
Proteome/Spinal Cord Increased	***Sqstm1/p62***	Sequestosome-1	**Alzeimer's disease Parkinson disease Aging**	**Decreased expression of Sqstm1/p62 causes aggregation of various neuropathological proteins via negative regulation of autophagy leading to neurodegeneration and aging.**

Objective 8: To apply global mass spectrometry-based proteomic approaches to discover and identify biomarkers from samples collected at symptom onset, clinical end of study, and humane endpoint within treated SOD1-G37R mice, B5-EDR prodrug NS-1-2 versus sham controls.

4.23 Edaravone prodrug NS-1-2 ameliorated symptom onset (symptom onset, defined as age to reach 10% weight loss, with muscle weakness) in SOD1-G37R mouse model of ALS

Our findings from the untargeted, unbiased, unsupervised quantitative proteomics and phosphoproteomic biomarker analysis of male mouse samples, which reached a humane endpoint, opened avenues for further studies considering different clinical stages of ALS progression with longitudinal monitoring. To further advance our drug development process, we employed a discovery-based LC-MS detection technique to profile the global changes in the proteome and phosphoproteome of brain and spinal cord samples from mutant human SOD1-G37R mice (n=6) in both control and treated groups at different stages of G37R ALS clinical progression. Firstly, we designed a symptom onset biomarker study, where the mice were treated presymptomatically with both (vehicle/and NS-1-2) daily until they reached symptom onset. For this study, we first defined the clinical end of study humane endpoint as Symptom onset.

Symptom onset or early symptomatic stage was also assessed in treated and control mice by measuring the age to reach a 10% loss of body weight based on the highest recorded weight (with muscle weakness), with the end of study endpoint. The end of study endpoint was defined as follows: If any one mouse from either the Sham/Treatment group reaches the symptom onset of a 10% loss of body weight with muscle weakness, both

the control and treatment groups will be euthanized at the same time point to isolate different tissues for discovery-based proteomics and phosphoproteomics experiments. Secondly, both males and females were included in this study. However, first, depending on the availability of animals, we started with age-matched females (n = 3) in each group.

According to the experimental plan as shown in **(figure 70),** we performed the experiments for the symptom onset biomarker study for the first time in G37R(42) mice model. As demonstrated in **(figure 71)**, daily intraperitoneal injection (IP, IJ) with NS-1-2 started pre-symptomatically from the age of 90 days until the end of the study, ameliorated the weight loss in age-matched females of SOD1G37R ALS mice. We found that NS-1-2-treated age-matched females (n = 3) demonstrated a prevention of percentage weight loss (4.9%) at the study endpoint compared to the control group (n = 3). Furthermore, the vehicle-treated females (n=3) lost more than 10% of their body weight according to the study endpoint criteria. However, all the NS-1-2-treated females (n=3) lost less than 10%, demonstrating that NS-1-2 prevented weight loss compared to the vehicle-treated group. Additionally, all the control females (n=3) reached the study endpoint of symptom onset at an average of 166.3 days, with a loss of more than 10% of body weight, indicating clinical symptom onset. Moreover, this also shows less variation in the age at which the control groups reached symptom onset. This evidence will aid in designing future experiments. Both males and females were included in the study examining symptom onset biomarkers with longitudinal weight monitoring. However, first, depending on the availability of animals, we started with age-matched females (n = 3) in each group.

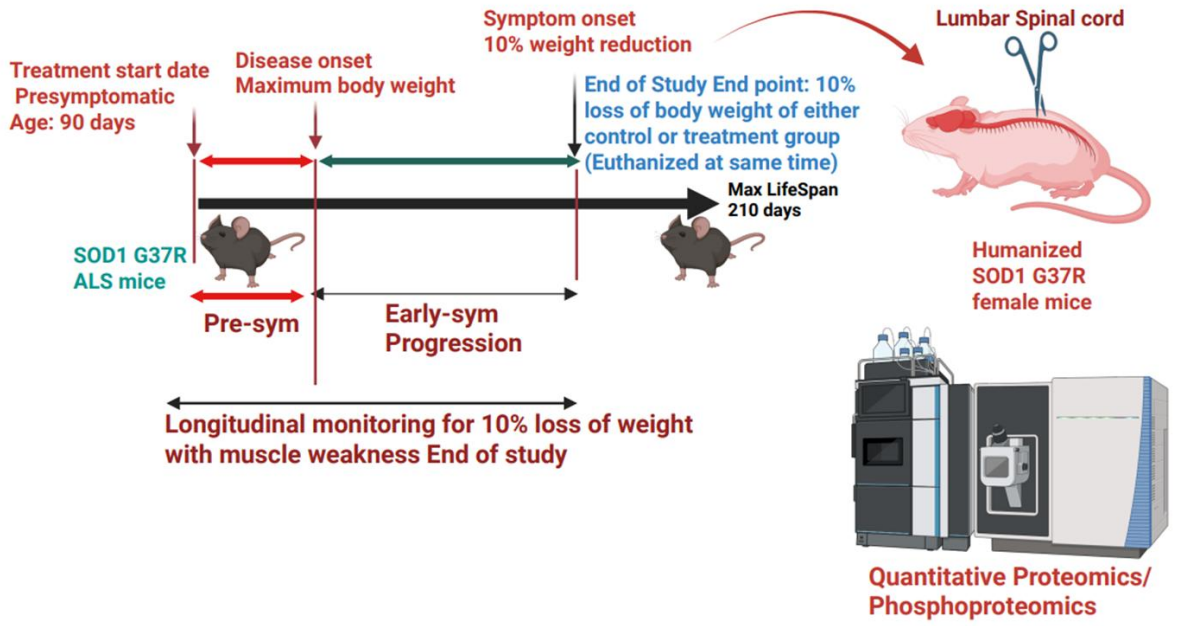

Figure 70. Diagram outlining the experimental plan for symptom onset biomarker study with end-of-study clinical humane endpoint in SOD1-G37R ALS mouse model of ALS.

The study design included dosing of vehicle and treatment presymptomatically at 90 days of age in SOD1-G37R ALS female mice until the mice reached symptom onset, end of study humane endpoint received a single intraperitoneal (IP) injection of BSZ at a dose of 10 mg/kg bodyweight. The mice were longitudinally observed and monitored for until the mice reached symptom onset. At the experimental end of the study endpoint, animals were euthanized, and lumbar spinal cord tissues were collected for discovery-based quantitative proteomics and phosphoproteomics.

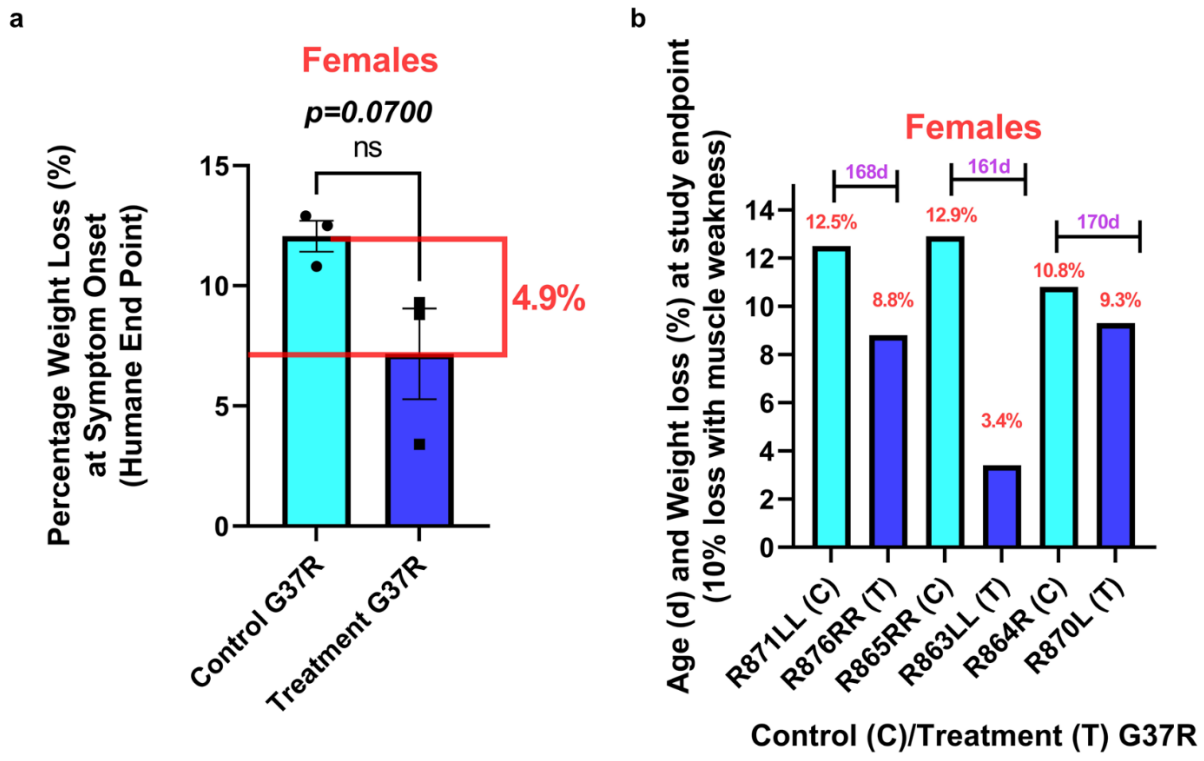

Figure 71. Edaravone prodrug NS-1-2 rescued ALS-induced weight loss at clinical symptom onset.

Symptom onset or early symptomatic stage was also assessed in treated and control mice by measuring the age to reach a 10% loss of body weight based on the highest recorded weight (with muscle weakness), with the end of study endpoint. The end of study endpoint was defined as follows: If any one mouse from either the Sham/Treatment group reaches the symptom onset of a 10% loss of body weight with muscle weakness, both the control and treatment groups will be euthanized at the same time point. **a)** Two-tailed (unpaired *t-test*) of the mean percentage loss of body weight at the end of study humane endpoint showing that BSZ prevented the weight loss from 12.1% for G37R age-matched females (control/n=3 mice), to 7.2% (NS-1-2/n=3 mice); **b)** Pairwise comparisons of age-

matched females from control and BSZ group. Vehicle-treated control (C) mice R71LL, R865RR and R864R lost 12.5%, 12.9% and 10.8% weight, respectively, which is more than 10% loss of body weight and more than end the study humane endpoint criteria. In comparison to NS-1-2-treated (T) mice R76RR, R63LL, and R870L lost 8.8%, 3.4% and 9.3% respectively which is less than 10% loss of body weight and more than end of study humane endpoint criteria. Data are presented as mean ± SEM (n=6), for the whole set of females. n= number of animals of the designated genotype. Data were analyzed using a two-tailed (unpaired *t-test*), with a significance set at $p<0.05$. Here, *p=0.0700, ns=non significant versus control G37R.*

4.24 Longitudinal symptom onset biomarker study: Proteomic analyses reveal differentially regulated proteins in lumbar spinal cord samples from the SOD1-G37R mouse model of ALS, correlating with the efficacy of Edaravone prodrug NS-1-2

Our findings from the symptom onset biomarker study with longitudinal monitoring, which defined the study endpoint as a 10% loss of body weight, demonstrated that NS-1-2 prevented weight loss compared to the vehicle-treated mice. These results supported our hypothesis that NS-1-2 improves weight loss, a marker of neurodegeneration, and correlates positively with clinical survival. However, to correlate these results of NS-1-2 preventing weight loss, we conducted global proteomic profiling of the lumbar spinal cord isolated from G37R female mice at the study endpoint.

A total of 8263 protein groups were quantified at 1% false discovery rate (FDR) and further filtered to retain high-quality data. Only protein groups that (i) had been quantified with at least 2 peptides in all 3 replicates of either sham or treated samples were retained and (ii) had maximum relative standard deviation of 30% in both groups, were considered.

The resulting list of 4975 proteins with high confidence quantitative data was further analyzed using Perseus, including log2-transformation of intensities, imputation of missing values, determination of ratios and p-values, as well as multiple testing correction to report significantly differential proteins at an FDR of 5%. In addition, 2 proteins (***Ncf4, Raver1***) that did not pass the significance threshold but were quantified with 2 peptides in all three sham samples but not detected in all treated samples, were considered as differentially regulated.

Table 13. List of 7 proteins with significantly differential abundance (adj p<0.05; n=3) in the lumbar spinal cord of human mutantSOD1 G37R male mice treated with BSZ, and sham (vehicle), discovery-based, unbiased global quantitative proteomics.

UniProt Accesion Number Protein ID	Gene Symbol	Protein Description	log2 "fold-change" (BSZ-Sham)	ratio (BSZ/Sham)	adj. p-value
Q9WUE4	***Nprl2***	GATOR complex protein NPRL2	0.68	1.60	3.24
Q9R257	***Hebp1***	Heme-binding protein 1	-0.86	0.55	3.00
Q8R4C2	***Rufy2***	RUN and FYVE domain-containing protein 2	-0.98	0.51	2.83
Q8BQQ1	***Zdhhc14***	Palmitoyltransferase ZDHHC14	-1.05	0.48	3.66
P36423	***Tbxas1***	Thromboxane-A synthase	-1.06	0.48	2.37
P17918	***Pcna***	Proliferating cell nuclear antigen	-1.21	0.43	2.20
Q9Z1B5	***Mad2l1***	Mitotic spindle assembly checkpoint protein MAD2A	-1.56	0.34	2.07

We discovered decreased differential expressions of three proteins **(*Hebp1, Tbxas1 and Pcna*)** and an increased differential expression of one protein **(*Nprl2/ GATOR1 complex subunit)*** in the treatment (BSZ) group compared to the control group. These four proteins are not specific to ALS; however, their increased expression is implicated in the pathophysiology of neurodegenerative disease and in maintaining neuronal health, **Table 14.**

Table 14. Selected known and novel proteins with significantly differential abundance (adj p<0.05; n=3) in the lumbar spinal cord of human mutantSOD1 G37R male mice treated with BSZ, and sham (vehicle) based on quantitative proteomics.

UniProt Accession Number (Protein ID)	Abbreviated (Gene Symbol)	Protein Description	ratio (BSZ/Sham)	Pathological Association to ALS Known/Novel	Known Pathological Association with Disease
Q9WUE4	***Nprl2***	GATOR 1 complex protein NPRL2	1.6	Novel	Seizures
Q9R257	***Hebp1***	Heme-binding protein 1	0.6	Novel	Alzheimer's disease
P36423	***Tbxas1***	Thromboxane-A synthase	0.5	Novel	Alzheimer's disease/Stroke
P17918	***Pcna***	Proliferating cell nuclear antigen	0.4	Novel	Alzheimer's disease

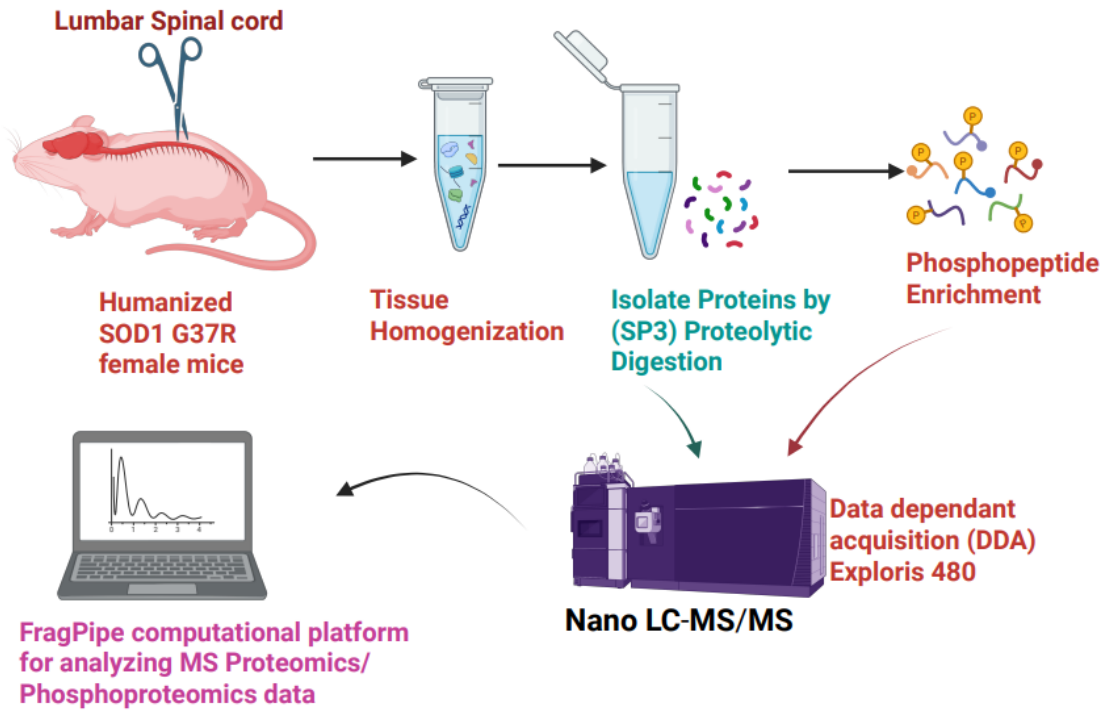

Figure 72. Overview of the sample processing workflow for LC/MS-based global proteomics and phosphoproteomics from the lumbar spinal cord samples of G37R female mice.

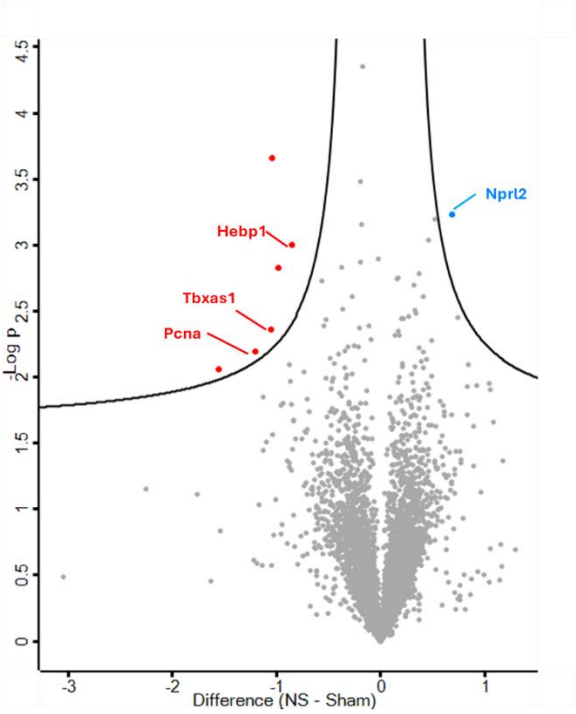

Figure 73. Differential analysis of symptom onset global proteome changes in hmutSOD1-G37R ALS mice.

Volcano plots showing the differential regulation of proteins expressed in the lumbar spinal cord of hmutSOD1 G37R male mice. Based on log2-transformed intensities, 7 out of 4975 proteins were significantly differential (adj. $p<0.05$; $n=3$). Selected proteins that are either up (red) or down (blue) regulated compared to controls are highlighted.

Note: NS-1-2 (NS), which refers to BSZ in figure 73. NS-1-2 was initially developed in the lab and later trademarked as Borsantrazole (BSZ).

5 Discussions

A large number of investigations, both in SOD1 ALS mouse models and in sALS and fALS ALS patients, have demonstrated the potential role of oxidative stress in the pathophysiology of ALS[377-379]. A recent study identified distinct molecular subtypes of ALS from postmortem cortex samples of ALS patients. Out of 148 ALS postmortem cortex samples collected from the NYGC ALS Consortium, most patients exhibited features of sALS. The largest subgroup (61%) showed evidence of oxidative and proteotoxic stress[380]. Furthermore, recent studies in 2025 from The NYGC ALS Consortium, which included transcriptomes for 664 ALS and control spinal cord samples from 406 donors: 331 ALS and 75 non-ALS, showed that despite this heterogeneity, the transcriptional patterns in ALS spinal cords were mainly driven by OS pathways. This emphasizes that OS is a key contributor to disease pathology in ALS[381].

Therefore, alleviating or attenuating oxidative stress is an attractive therapeutic target and offers an opportunity for protecting motor neurons both in the brain and spinal cord from cellular redox damage[378]. Consequently, it is reasonable to develop small-molecule antioxidants that represent a viable strategy for slowing down the death of motor neurons during ALS progression and as a means to discover novel ALS therapeutics[377, 382]. To date, several antioxidant compounds have been tested in human ALS clinical trials, but none of the compounds have succeeded in meeting the primary endpoint of extending survival[383]. Based on results from a pivotal phase 3 clinical trial in Japan, EDR is the only small molecule antioxidant that demonstrated improvement in the physical functional decline of ALS patients, as measured by the ALSFRS-R score and improved quality of life as measured by the ALS 40-item assessment questionnaire[384]. However, EDR has

failed to show a significant extension in the life span of ALS mice [305] and ALS patients[385], although, EDR was successful in translating slower disease progression between SOD1 ALS mice models to ALS patients. Regardless of its ineffectiveness in extending survival in both preclinical animal models and ALS patients, EDR offers hope to slow down the progression of ALS. Being a potent free radical scavenger, there are several limitations of EDR, which we believe can be overcome by applying our novel multifunctional boron-based prodrug approach.

In the present study, we tailored the EDR molecule through a novel synthetic methodology to introduce a boron scaffold as a means to develop a trifunctional boron-containing pyrazole ALS therapeutic. We first synthesized the boron prodrug of EDR by introducing a boron functional group in the 5^{th} position of a pyrazole ring to produce the pre-clinical drug candidate BSZ. Although EDR is considered a potent antioxidant, we recognized several limitations of this approved drug, starting from its synthesis to its development as a therapeutic agent for ALS patients. Firstly, the use of genotoxic, hemotoxic, tumorigenic, air-sensitive, and temperature-sensitive phenyl hydrazine as a starting material for the synthesis of EDR utilizing the Knorr pyrazole synthesis procedure[162, 386, 387]. Secondly, the presence of oxidizing chemicals in the reaction mixture using the conventional **Knorr pyrazole** procedure leads to EDR decomposition during its synthesis and hence, low yield. Thirdly, EDR is highly unstable in aerobic intravenous aqueous solutions with pH>7 due to the presence of EDR anion, which undergoes decomposition in the presence of aerobic conditions and leads to the formation of oxidatively stable products like 2-oxo-3-(phenylhydrazono)butanoic acid (OPB) and an inactive stable yellow-colored precipitate of EDR trimer and toxic phenylhydrazine[147, 158]. Fourthly,

the use of sodium bisulfite ($NaHSO_3$) as a stabilizer to prevent the oxidation of EDR[157], causes severe allergic reactions, and the use is cautioned by the FDA[158]. Lastly, poor patient compliance, due to daily, long-term intravenous infusions of 60mg EDR over 60 minutes once daily for an initial 14-days, followed by a 14-day drug–free period, for several treatment cycles, with no defined limit of treatment cycles of EDR by the FDA for achieving therapeutic benefit to slow down the progression of neurodegeneration[385]. Oral formulations of EDR do exist; however, the efficacy of oral EDR formulations has not been independently evaluated. In the present work, we have recognized the potential of EDR in reducing the etiology of global oxidative stress in ALS and overcome some of the limitations of EDR by tailoring/modifying the privileged pyrazole core nucleus of EDR using boron as a key strategy. Herein, we utilized a unique prodrug approach to introduce a boron scaffold (boronates) in the **C-5** position of a pyrazole ring to synthesize an oxidatively activated boron prodrug of EDR. Derivatization of the C-5 (keto-enol) group of EDR by a versatile, nature-abundant, non-toxic, free radical-loving, biocompatible, boron functional group[388] that is believed to be activated under pathological cellular oxidative stress ROS (e.g. H_2O_2)[389-391] conditions to release EDR *in vivo*, gave access to a viable ALS therapeutic.

In our laboratory, for the first time, we have developed an alternate, greener, and environmentally sustainable route for the synthesis of EDR. Until now, all reported procedures for the synthesis of EDR utilize a Knorr pyrazole synthesis, using PHZ, a hazardous chemical, as a starting material. Our current synthetic procedure has many advantages over the conventional route. Firstly, the use of greener reagents, which are biocompatible, such as boronic acid (isopropoxyboronic acid pinacol ester), lactic acid,

and H_2O_2. The second is energy use minimization, as the reaction was carried out for 10 min at 50°C in a microwave synthesizer, in comparison to the prolonged heating at reflux, found in the classical process for 2-4h, which causes degradation of EDR. Overall, using the above procedure, the typical yield for the synthesis of EDR, following recrystallization, is 85+%.

Overall, our current novel approach and strategy allows NS-1-2 to exert a triple mode of therapeutic action with the added advantage of targeted drug delivery, **(figure 74)**. Firstly, NS-1-2 is chemoselectively oxidized by high or pathological concentrations of H_2O_2, and proportionately, reducing H_2O_2-mediated neurotoxicity, and associated neurodegeneration. Secondly, H_2O_2-mediated boronate oxidation results in the generation of potent FDA-approved antioxidant EDR, which confers its antioxidant activities and therapeutic nature to the neurons undergoing oxidative stress. Thirdly, the by-product of this biotransformation is boric acid, which, according to emerging reports, acts as an antioxidant to reduce cellular oxidative damage[392]. Recent reports have shown that boric acid is known to activate ***Nrf2***, an antioxidant response element[393]. Further, boric acid reduces oxidative stress by increasing the levels of thiol-containing antioxidant glutathione[394]. In addition to the triple-role antioxidant effects, NS-1-2 will also act as a targeted therapy for quenching excessive H_2O_2, as its biotransformation would preferentially take place within regions of high oxidative stress, a known cause of neurodegeneration. This gives the additional advantage of targeting regions of both upper and lower motor neurodegeneration where oxidative stress is implicated as a primary culprit. Additionally, other free radicals are implicated in the pathology of ALS, and we propose that these free radicals (such as hydroxyl radicals (HO•), lipid peroxides, or

superoxide) also produce EDR through a redox reaction between the reactive oxygen species (ROS) and boron. Appropriately, we propose that H_2O_2 should serve as the main *in vivo* ROS that transforms NS-1-2 into EDR (prodrug action) as H_2O_2 has a long half-life and is more stable than other ROS oxidants, whilst also being the product of superoxide dismutase (SOD1) and mutant SOD1, whose toxic gain-of-function is a predominant cause of fALS. Additionally, we would like to emphasize that BSZ should be especially effective at targeting regions of high H_2O_2 production and/or high SOD1 activity, such as in patients with mutant SOD1 fALS/sALS. The targeted nature of NS-1-2 provides some notable advantages over EDR, such as tissue specificity (brain/spinal cord, where H_2O_2 is known to be highly active) and stimulus sensitivity (target regions of high oxidative stress), which should enhance the efficacy of the drug, with a decrease in side effects. H_2O_2 tends to accumulate in cells in high concentrations that are experiencing oxidative stress, resulting in a redox imbalance, and hence, causing impaired redox signaling cascades vital for maintaining healthy cells, and often resulting in neurodegeneration. For these reasons, the pathological concentration of H_2O_2 is a valid and attractive target for neurodegenerative diseases like ALS (and other redox-sensitive diseases). NS-1-2, being a H_2O_2 reactive prodrug, will be activated specifically in regions undergoing overproduction of cellular H_2O_2, as demonstrated during the pathophysiology of ALS[326, 395], and should provide added therapeutic benefits compared to non-targeting EDR.

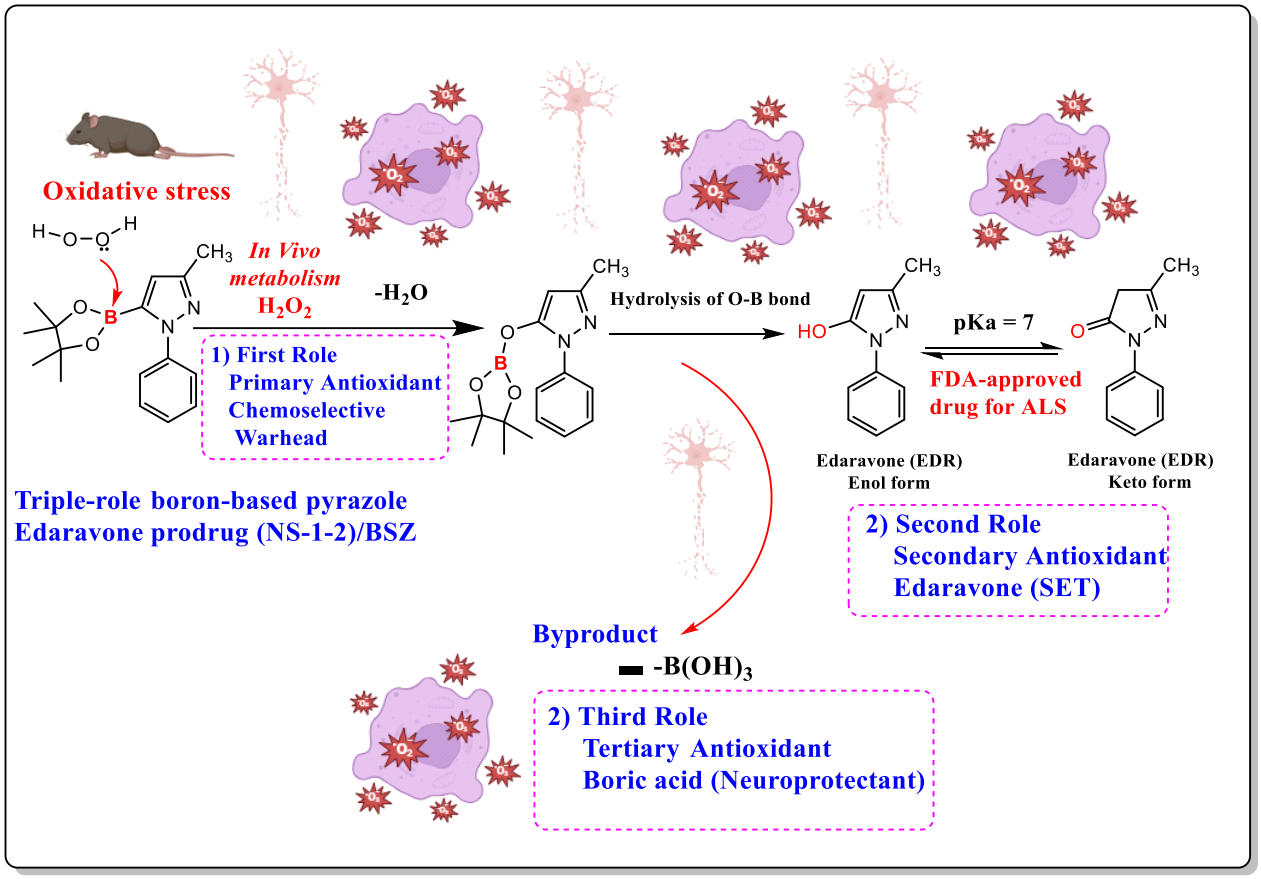

Figure 74. Schematic illustration of the targeted delivery of a triple-role boron-based pyrazole BSZ as an ALS therapeutic.

NS-1-2, (a boron-based prodrug of EDR) initially serves as an antioxidant by chemoselective *in vivo* reaction with reactive oxygen species, such as H_2O_2, which results in the generation of EDR (secondary role). Advantageously, the oxidative reaction also results in the production of byproduct boric acid, a known neuroprotectant, as a tertiary role.

In the current study, we have synthesized a ROS-responsive prodrug [252] of EDR by taking advantage of boron as the key mediator for targeting neurodegeneration. Our initial conjecture was that NS-1-2 would chemoselectively target the pathological concentration

of neurotoxic free radical H_2O_2 [391] known to cause oxidative stress and misfolding of SOD1 during the progression of ALS[133, 141, 324].

Figure 36

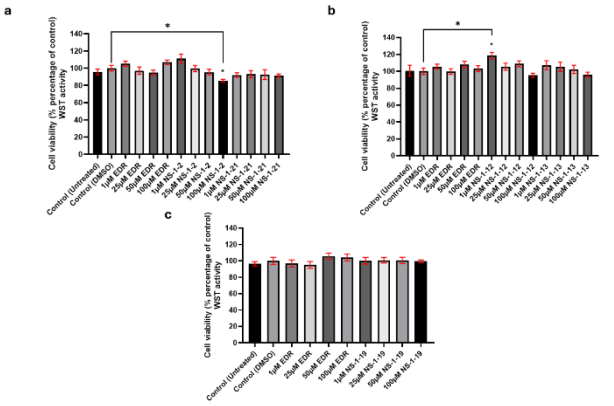

Initially, our first step was to evaluate the safety profile of EDR, EDR prodrug (NS-1-2 and NS-1-21), and EDR analogues (NS-1-12, NS-1-13, and NS-1-19) in NSC-34 cells **(figure 36)** and PCNC cells **(figure 37)**.In the present study, we first asked the question of whether the newly synthesized novel prodrugs of EDR, analogues of EDR, and EDR are safe in motor neuron-like systems *in vitro* and induce no neurotoxicity. To test the effects on the cell viability of EDR prodrug (NS-1-2 and NS-1-21), EDR analogues (NS-1-12, NS-1-13, and NS-1-19), and EDR, using the WST-8 metabolism endpoint, we used neuroblastoma spinal cord hybrid cell line (NSC-34), which is a model for spinal cord motor neuron study and is accepted for studying cellular-level ALS pathology[396]. We found that EDR and its prodrug (NS-1-2 and NS-1-21) and analogues (NS-1-2, NS-1-13, and NS-1-19) demonstrated excellent cell viability at around 90-100% in the NSC-34 cells with no neurotoxicity. Furthermore, to make this analysis more reliable and to support the observed safety profile of newly synthesized small molecules EDR prodrugs and EDR analogues in NSC-34 cells, we used primary cortical neurons (PCNC) prepared from embryonic day 17-18 (E17-E18) mouse brain; equivalent to the third trimester of a human pregnancy and exhibited various unique features that cannot be adequately mimicked by cell lines. We found that lower concentrations (10μM and 1μM) of EDR prodrugs and EDR analogues have shown good cell viability of around (90-100%) on

PCNC, and is similar to that of EDR; however, higher concentrations of 25µM of EDR and its prodrug (NS-1-2, NS-121) and its analogues (NS-1-2, NS-1-13, and NS-1-19) showed around (70 ± 10%) cell viability on PCNC.

Figure 37

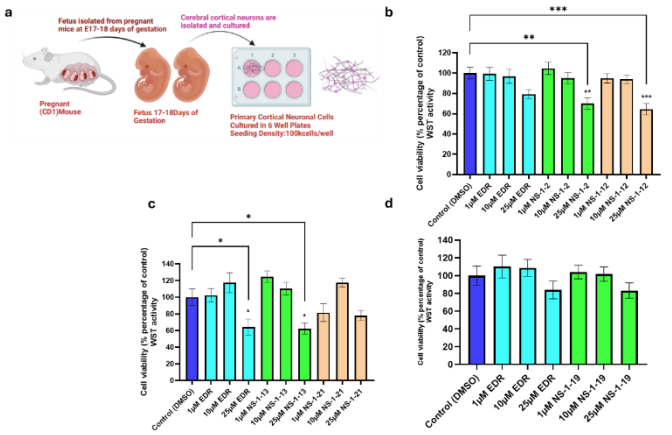

The initial safety screening of BSZ in *in vitro* models validated the safety of our novel small organic molecules and gave us confidence to proceed further to ALS mouse models.

In addition, we also analyzed the neuroprotective role of EDR, EDR prodrug (NS-1-2 and NS-1-21), and EDR analogues (NS-1-12, NS-1-13, and NS-1-19) in NSC-34 cells against neurotoxic H_2O_2 challenge **(figure 39)**. The major ROS involved in the pathophysiology of ALS is H_2O_2[141]. The pathological concentration of H_2O_2 is known to cause damage to neurons and further creates an oxidizing cellular environment by initiating Fenton's reaction and Heber-Weiss reaction, leading to the generation of the highly reactive oxidant, hydroxyl radical (HO•), regarded as the most reactive free radical, subsequently causing neuronal damage and death[325]. Therefore, H_2O_2 has been used by a large number of groups to induce neuronal injury and explore the neuroprotective potential of new small organic molecules therapeutics[397-402]. In the present study, we also used H_2O_2 neurotoxin to generate an *in vitro* model of oxidative stress. The positive results from the *in vitro* safety profile studies allowed us to ask further questions, such as, whether the newly synthesized drug, like EDR prodrugs and EDR analogues could confer neuroprotective activity against neurotoxic free radical H_2O_2 in spinal cord motor neuron-like cell lines (NSC-34). The

prophylactic treatment of EDR prodrug (NS-1-2 and NS-1-21), EDR analogues (NS-1-12, NS-1-13, and NS-1-19), and EDR significantly attenuated H_2O_2-induced neurotoxic insults, maintaining neuronal viability. The EDR prodrug (NS-1-2 and NS-1-21) and EDR analogues (NS-1-12, NS-1-13, and NS-1-19), demonstrated higher neuronal viability at lower doses of (1μM and 25μM), showing that the novel EDR prodrugs and EDR analogues are more potent than EDR; on the other hand, EDR prodrug (NS-1-2 and NS-1-21), EDR analogues (NS-1-12, NS-1-13, and NS-1-19), provided equal neuroprotection at higher concentrations of (50μM and 100 μM).

Figure 39

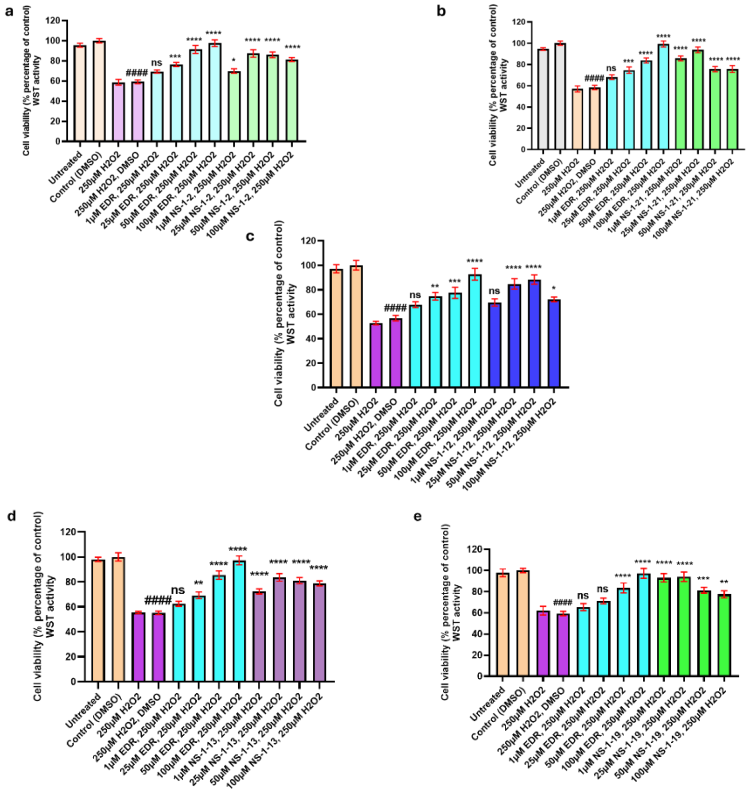

Overall, we discovered that the EDR prodrug (NS-1-2 and NS-1-21), EDR analogues (NS-1-12, NS-1-13, and NS-1-19), have an excellent safety profile both in NSC-34 and PCNC cells and exerted an excellent neuroprotective profile against H_2O_2-induced neurotoxicity in NSC-34 cells.

Furthermore, advancing our early-phase drug discovery with the goal of moving toward preclinical studies in humanized ALS mouse models and then in humans. All the novel EDR prodrugs (NS-1-2 and NS-1-21) and EDR analogues (NS-1-12, NS-1-19, and NS-1-13) demonstrated excellent safety and efficacy in preliminary *in vitro* experiments using neuronal-like cell

lines. However, we selected NS-1-2, a closely related structural analogue and prodrug of EDR, to progress in the preclinical humanized SOD1 ALS models. This decision was based on several reasons. First, the synthesis of NS-1-2 was easier and more optimized compared to other prodrugs and analogues, with no complicated purification steps. Second, the yield of NS-1-2 was high, around 95%+, providing a basis for scalable synthesis in grams for preclinical studies. Third, since NS-1-2 is the closest structural analogue with a highly lipophilic boronate group at the 5th position of pyrazole, we believed it would exhibit better pharmacokinetic properties than EDR and thus be a more suitable candidate for animal studies. Therefore, we moved forward with the EDR prodrug NS-1-2 for additional biochemical and *in vitro* studies to increase our confidence before initiating *in vivo* preclinical trials.

We first evaluated the effect of NS-1-2 on mitochondrial potential **(ΔΨM)** of NSC-34 cells using the JC-10 mitochondrial potential probe. Mitochondrial dysfunction is one of the earliest pathological events in the clinical progression of both forms of ALS. Mutant SOD1 proteins tend to aggregate and accumulate in healthy mitochondria, leading to toxicity and mitochondrial damage. This is primarily due to an increase in calcium ions, defects in the electron transport chain, enhanced apoptotic signaling, and a pathological rise in free radicals, such as H_2O_2[403]. Several reports have shown that pathological oxidative stress causes depolarization and initiates cascades of pathological defects, causing neurodegeneration [404, 405]. Therefore, we investigated the effects of EDR and its prodrug, NS-1-2, on the mitochondrial membrane potential **(ΔΨM)** of NSC-34 cells using the JC-10 Assay and staurosporin as a positive control for apoptosis. Our findings (**figure 43)** indicated that both EDR and EDR prodrug NS-1-2, do not induce depolarization of

the mitochondrial membrane of NSC-34 cells and therefore have a safe profile towards mitochondria. However, the lower dose of 1 µM of NS-1-2 is found to induce mitochondrial polarization compared to the control.

Figure 43

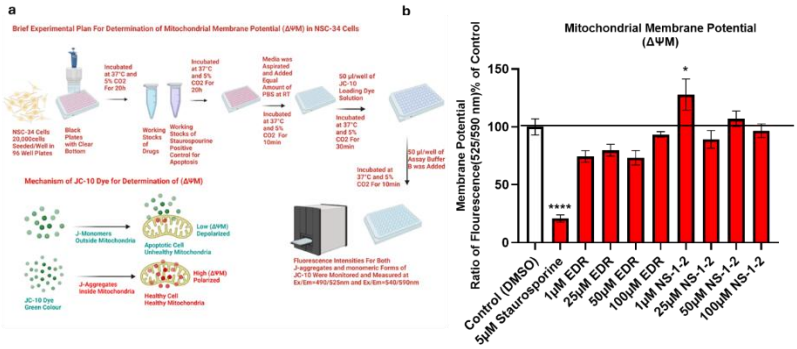

Moreover, NS-1-2 also showed better polarization of mitochondria compared to EDR. Therefore, it is expected that NS-1-2 will confer better protection of the mitochondria from oxidative damage caused by free radicals and restore their function, including normalizing mitochondrial potential. The **(ΔΨM)** is crucial for the mitochondrial energy (ATP). Compounds that stabilize **(ΔΨM)** can restore cellular energy levels and overall mitochondrial function. Reduced neuronal **(ΔΨM),** also known as mitochondrial depolarization, leads to increased oxidative stress, resulting in pathological concentrations of free radicals, such as H_2O_2, which cause defects in the electron transport chain (ETC). This is implicated in the pathophysiology of both forms of ALS, i.e., fALS and sALS[406]. Furthermore, we used staurosporine, a well-studied, cell-permeable, and validated inducer of neuronal apoptosis (programmed cell death). It works by inhibiting protein kinase. Additionally, staurosporine is known to increase oxidative stress and deplete glutathione, a mechanism that induces apoptosis in both neuronal and non-neuronal cells[407]. Our experiments using staurosporine as a positive control for mitochondrial depolarization demonstrated that both EDR and NS-1-2 are non-toxic to NSC-34 cells through mechanisms that do not involve apoptosis or oxidative stress. However, further studies using our compounds to determine if they can

protect neuronal cells from staurosporine-induced apoptosis are necessary, and this will be our focus in the future plan. Thus, this initial evidence of maintaining the mitochondrial potential in NSC-34 neuronal-like cells by NS-1-2 encouraged us to move towards *in vivo* experiments in ALS animal models as a means to slow down the progression of ALS.

Secondly, we investigated the ability of EDR prodrug NS-1-2 to scavenge H_2O_2 using the Amplex Red assay **(figure 45)**.

Figure 45

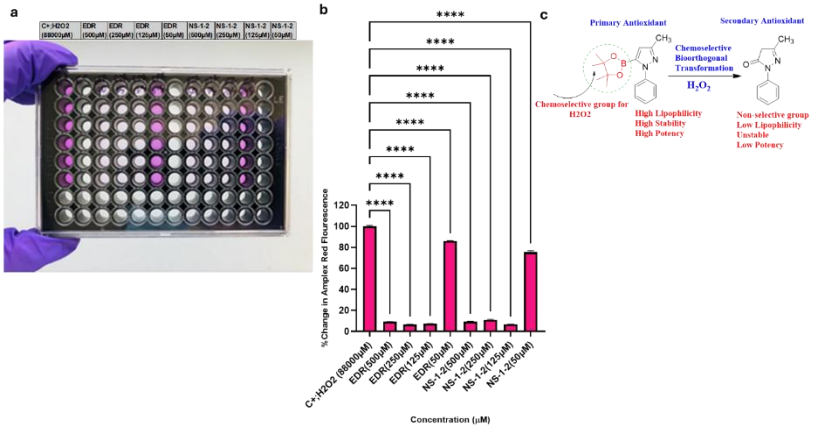

The addition of EDR and NS-1-2 at the concentration of (500-120μM) resulted in a significant reduction in the concentration of neurotoxic H_2O_2, supporting our belief that NS-1-2 readily reacts following biorthogonal chemistry with H_2O_2 to render efficient removal of H_2O_2 in the biochemical assays. Thus, this initial evidence of the efficient H_2O_2 scavenging ability of NS-1-2 gave us an encouragement to move towards *in vivo* experiments in ALS animal models as a means to slow down the progression of ALS via removing pathological H_2O_2, while simultaneously holding a promising approach to increase the selectivity/targeting and efficacy of an existing ALS therapeutic (EDR).

Further, for the first time, we have investigated the ability of EDR and EDR prodrug NS-1-2 to inhibit the amyloid aggregation of SOD1 monomer protein in the presence of preformed fibril. Both forms of SOD1, i.e., mutant SOD1 (mSOD1) and wildtype SOD1 (wSOD1), acquire a toxic gain of function, leading to a change in its structure and hence misfolding to neurotoxic aggregates. Several reports have suggested that wSOD1

proteins become neurotoxic under aberrant post-translational modifications, mimicking fALS-linked SOD1 mutants[25]. Several studies have shown the presence of Human wild-type SOD1 (HuwtSOD1) protein in both forms of ALS[138, 408, 409], i.e., sALS and fALS. This toxic gain-of-function of both forms of SOD1 is due to oxidative stress. Modification of the Cys111 residue with increased free radicals, such as H_2O_2, leads to a conformational change and enhances the propensity for misfolding and aggregation under oxidative conditions. Misfolded forms of human wildtype SOD1 (HuwtSOD1) proteins in the absence of SOD1 mutations suggest that non-native conformers of SOD1 may play a key pathological role in all forms of ALS[324]. Further supporting the fact that, regardless of the SOD1 genetic mutations, misfolding of wSOD1 and its biophysical change with aberrant conformation under an oxidative environment is a common pathological mechanism in both forms of ALS. Multiple studies indicate that apo-SOD1, the monomeric form lacking metal cofactors (Cu and Zn), is more susceptible to oxidation under oxidative stress, leading to misfolded SOD1 aggregates. In contrast, the native, matured, or dimeric holo-SOD1, which contains these cofactors, is more stable. The absence of metal cofactors and disulfide bonds makes monomeric forms less stable in oxidative environments. These aggregates form toxic beta fibrils and are considered a hallmark of ALS pathology. Consequently, reduced apo-SOD1 is the least stable and most prone to misfolding[410-413]. Research by Furukawa and colleagues[414] shows that apoSOD1, a reduced form lacking a disulfide bond between Cys57 and Cys146 but containing thiol (-SH) groups, is especially prone to forming amyloid-like fibrillar aggregates. This evidence was further supported by studies [415, 416] that demonstrate the detection of only monomeric or misfolded SOD1 by specific antibodies that do not

bind to the natively folded protein in spinal cord motor neurons of ALS patients with SOD1 mutations. In addition, various studies have investigated how SOD1 fibrils function as seeds to trigger the aggregation of endogenously expressed SOD1, leading to the propagation of pathology and further aggregation of SOD1 in ALS[417].

Considering that human wtSOD1 and the monomeric reduced form of SOD1 are implicated in the pathophysiology of ALS, and SOD1 fibrils induce the aggregation of SOD1, we conducted an experiment to assess whether EDR and NS-1-2 can inhibit the fibrillization of human monomeric SOD1 in the presence of preformed fibrils. As demonstrated in (**figure 48),** EDR prodrug NS-1-2 significantly inhibits the fibrillization of monomeric SOD1, as shown by the decrease in the ThT fluorescence.

Figure 48

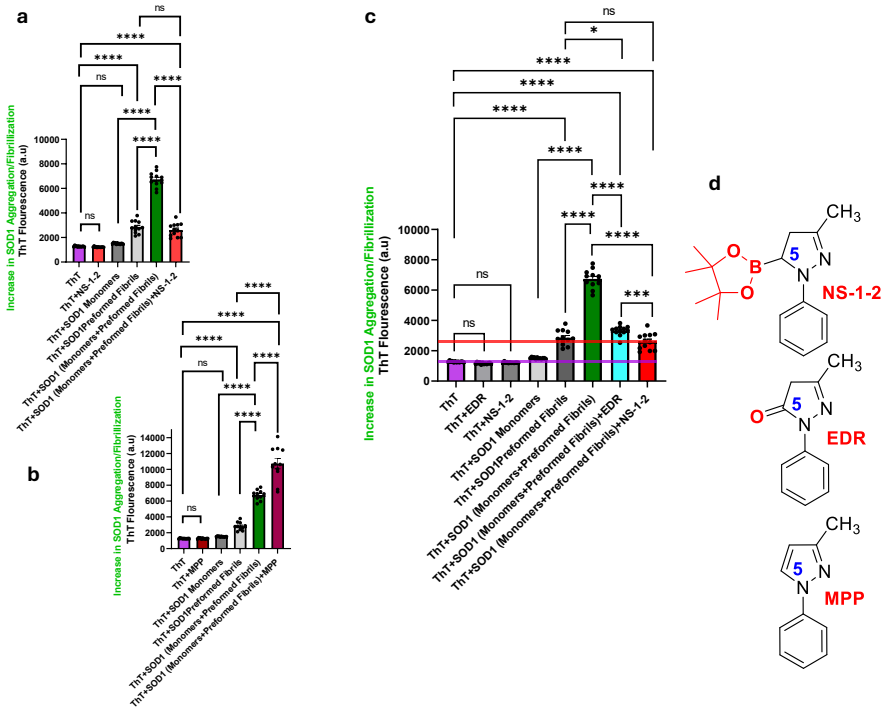

In contrast to EDR and NS-1-2, MMP significantly enhanced the fibrillization of SOD1, as evidenced by an increase in ThT fluorescence.

Figure 49

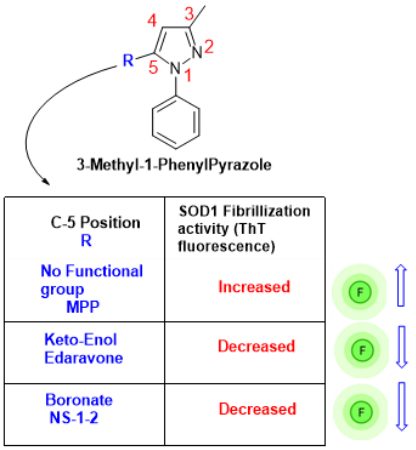

These observations reveal the structure-activity relationship **(SAR)** between EDR, NS-1-2, and MMP, highlighting the significance of the functional group at the **C-5** position in EDR, which contains a keto-enol group, and in NS-1-2, which has a boronate **(Figure 49),** in reducing SOD1 fibrillization. In contrast, MMP lacks a functional group at **C-5** and shows increased fibrillization of SOD1. Our study for the first time highlighted the importance of the **C-5** position in the 3-methyl-1-phenyl pyrazole core. Taken together, for the first time, boronate compounds have been investigated for their anti-SOD1 fibrillization activity. Furthermore, our findings suggest that NS-1-2 could be used as a potential compound in the search for anti-SOD1 amyloid drugs to slow down the progression of amyloid propagation in neurodegeneration. Additionally, exploration of this mechanism is necessary.

These supplemental *in vitro* experiments, which demonstrated excellent safety and efficacy, supported our decision to proceed with further testing of the **EDR prodrug NS-1-2, now trademarked as Borsantrazole (BSZ).**

We evaluated the safety profile of the prodrug of EDR, NS-1-2 (BSZ), in wild-type animals. We determined the safety of NS-1-2 with a single dose of 10mg/kgbodyweight (acute toxicity, **figure 54a, b)** and 120 daily doses (chronic toxicity, 10mg/kgbodyweight/day, **figure 54c, d)** with longitudinal monitoring.

Figure 54

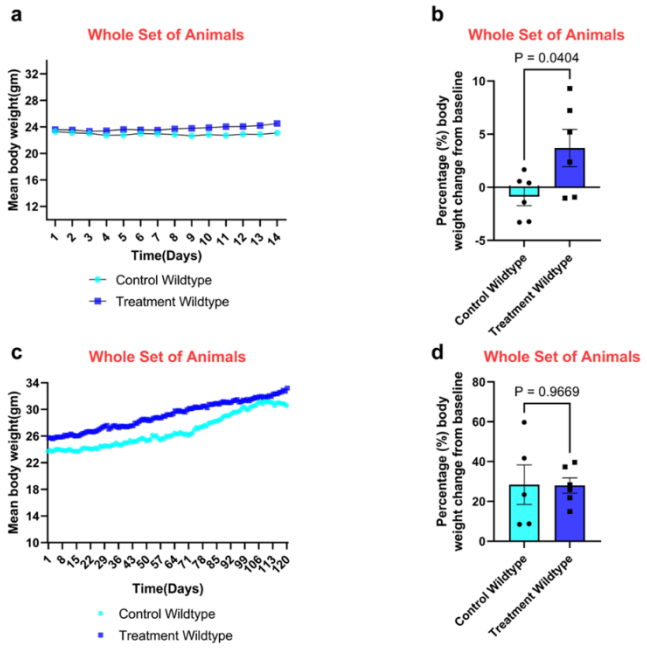

According to regulatory authorities, a decrease in body weight acts as a reliable, sensitive, and robust indicator for determining chemical toxicity; therefore, we analyzed the treatment-associated change in body weight after treatment for 14 days in case of acute toxicity following a single dose and for 120 daily doses in case of chronic toxicity. Further, we also monitored any symptoms associated with the treatment. Additionally, we considered to deduce the sex-specific differences in toxicity in both male and female mice. Both the acute and chronic safety evaluation with NS-1-2 demonstrated no symptoms of acute treatment-associated toxicity in both the sexes. Secondly, no treatment-associated decrease in body weight changes in the whole set of animals, and lastly, no signs of treatment-associated hematological toxicity (acute toxicity **figure 55,56**) and (chronic toxicity **figure 57, 58**) among the sexes were observed.

It is noteworthy to highlight that the results obtained from both the acute and chronic toxicity studies demonstrate that the average percentage weight change from baseline

indicates that the NS-1-2 group, in both acute and chronic toxicity evaluations, did not demonstrate a reduction in body weight compared to the control group. This observation suggests that there are no indications of toxicity associated with NS-1-2 at the end of the study in either group (acute toxicity **figure 55,56**) and (chronic toxicity **figure 57, 58**).

Figure 55

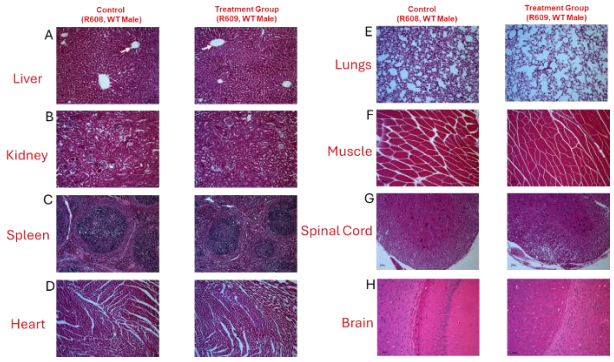

Figure 56

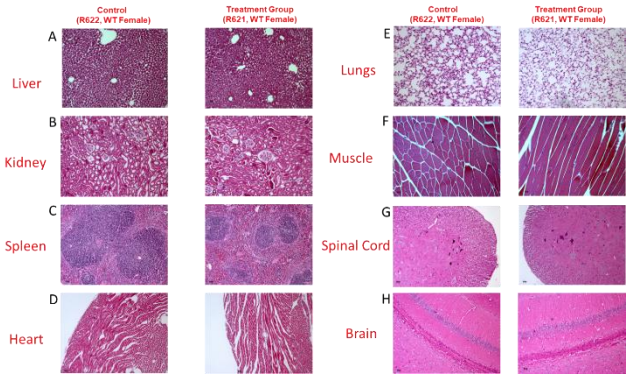

Figure 57

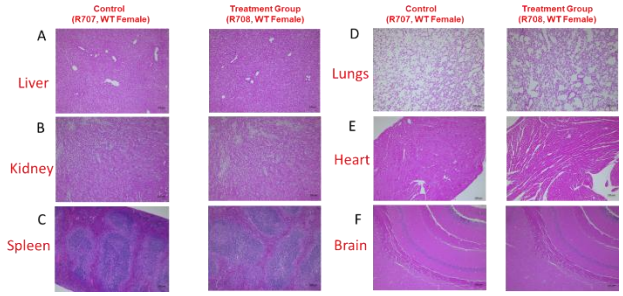

Figure 58

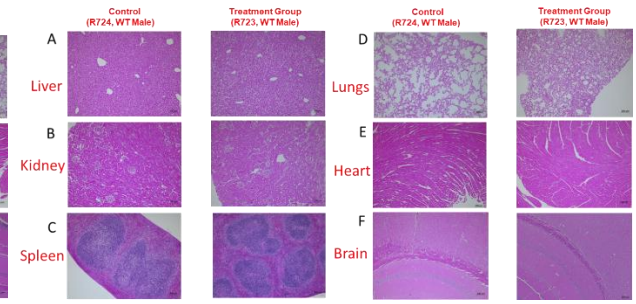

We also propose that during the *in vivo* metabolic biotransformation of NS-1-2 to EDR, the major by-products of the biotransformation are boric acid and pinacol. The LD_{50} of pinacol in mice is 3,380 mg/kg oral dose[353], and the LD_{50} of boric acid in rats is 2660 mg/kg[353]. In addition, the daily acceptable intake of boron recommended by the WHO for adults is 1–13 mg/d. This clinical data suggests that side effects due to the boronate scaffold in NS-1-2 should be minimal or non-existent[418]. The excellent preliminary

safety profile of NS-1-2 gives us confidence to move further ahead with our efficacy study in ALS mouse models.

Moreover, in the present preclinical study, we evaluated the disease-modifying effects of an EDR prodrug NS-1-2 in the humanized SOD1-G37R mice model of ALS. Considering the neuroprotective role of NS-1-2 in *in vitro* assays and its satisfactory safety profile in both *in vitro* and *in vivo* models, gave an impetus to test the efficacy of BSZ in the SOD1-G37R ALS mice model. As part of this early phase drug discovery process, we utilized a pragmatic randomization of animals with a longitudinal monitoring approach, which we hope to translate into human trials. We analyzed the disease-modifying effects of a newly synthesized prodrug of EDR called NS-1-2 in high copy number, early onset, and fast progressor hmutantSOD1-G37R familial mice model of ALS. The ALS clinical features/clinical phenotypes/progression of disease in these humanized mice models of ALS mimics clinical deterioration seen in human ALS. Long-term treatment with longitudinal monitoring of NS-1-2 significantly delays the disease onset and symptom onset in both sexes (male/female) of ALS mice. However, the delay in disease onset and symptom onset is diminished in females compared to males (disease onset **figure 61**), and (symptom onset **figure 62**).

Figure 61

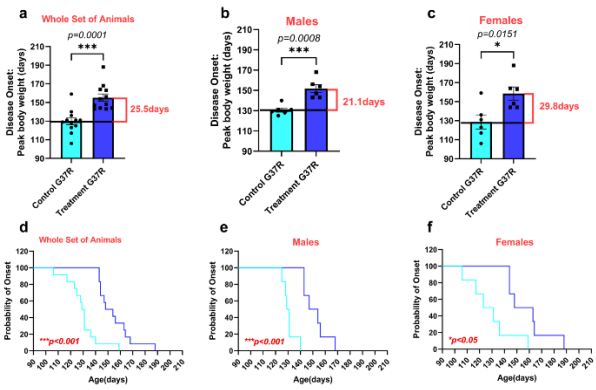

Figure 62

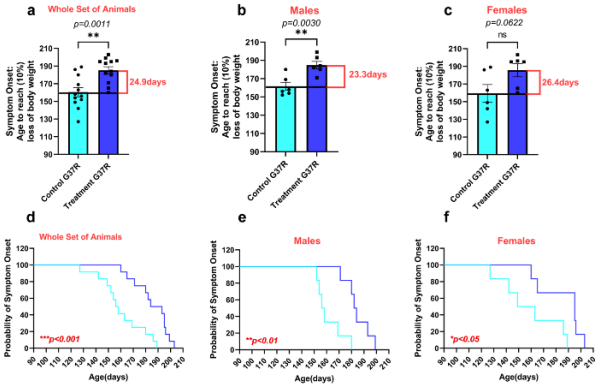

Further, long-term treatment of a novel molecule (NS-1-2) significantly rescued ALS-induced weight loss (cachexia) in both sexes (male/female) **(figure 64)**.

Figure 64

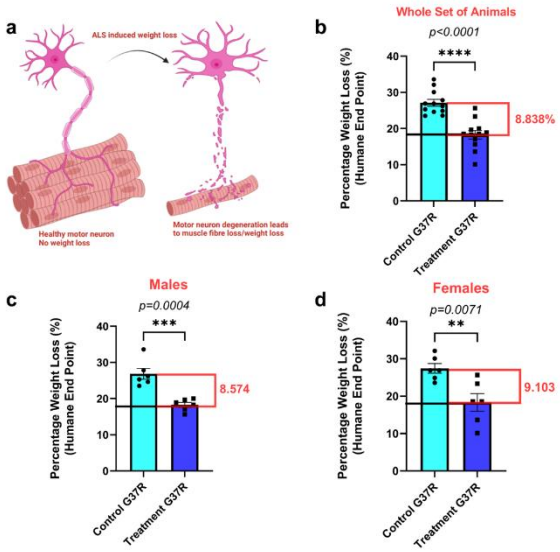

However, the observed weight loss (male, *p=0.0004* vs female, *p=0.0071*) demonstrates a larger clinical effect size in males compared to females. In addition, long-term treatment of NS-1-2 demonstrated an extension in survival in both sexes. NS-1-2 treatment significantly prolongs the life span of male ALS mice and the whole set of animals overall **(figure 63)**.

The efficacy observed in terms of disease onset, symptom onset, life span, and weight loss demonstrated the sex-specific differences of a newly synthesized prodrug of EDR, NS-1-2, with males benefiting to a greater degree.

We have also recognized limitations in earlier preclinical studies of EDR. Ito and his group investigated the efficacy of EDR and started treatment after symptom onset in a female SOD1-G93A ALS mouse model. The G93A mice model of ALS is an early-onset and fast-progressing model, and considering the early onset nature of the disease in these genetic (fALS) animal models, starting treatment at symptom onset is not a pragmatic approach to see the efficacy of the drug in modifying disease pathology. Secondly, the investigators used only female mice and did not account for the effect of EDR in demonstrating sex-specific differences. Mounting evidence from previously published studies shows sex differences in response to drug treatment; therefore, it is important to include sex-specific analysis in preclinical trials as a means to better translate animal models to human clinical trials[419]. In the present study, we have overcome these limitations to improve the preclinical translational capability of EDR by choosing presymptomatic treatment and included both sexes (male and female) in our treatment and control groups. Moreover, in previous studies, EDR did not demonstrate statistically significant differences in the mean extension of survival in female mice compared to the control female mice. The increase was only 1.5 days and 2.2 days in 5-mg/kg and 15-mg/kg EDR groups, respectively. Compared to these unsatisfactory survival results, NS-1-2 or Borsantrazole (BSZ) in the present efficacy study has demonstrated an increase in survival in both males (16.5 days) and females (13.7 days) with a significant extension

Figure 63

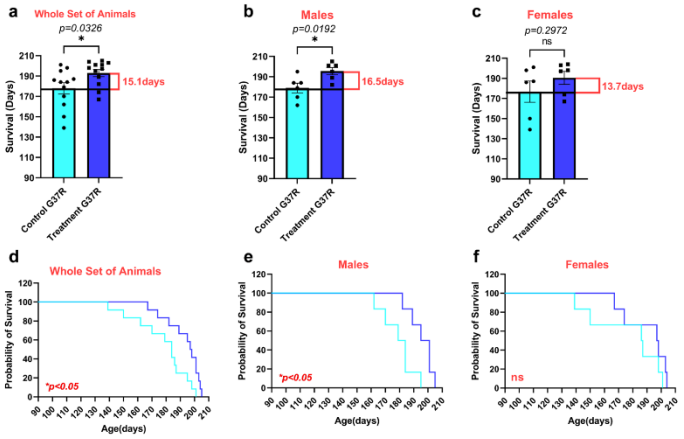

of survival in males compared to females, and a significant extension in survival when analysing the whole set of animals (i.e. males and females). It is noteworthy to mention that we used 10mg/kgbodyweight of NS-1-2 compared to a higher dose of 15mg/kgbody weight of EDR used in the previous *Ito et al.* studies. The potent efficacy of lower dose NS-1-2 compared to EDR is supported by the *in vitro* low-dose neuroprotective role of NS-1-2 in NSC-34 cells. One possible reason for increasing the life span of both sexes in our study is the reduction of weight loss reported during the progression of ALS. Ito and the group did not account for the effect of EDR treatment on weight loss due to ALS progression. Potentially, the effect of EDR treatment on weight improvement was found to be negligible, which is well evident with the negligible effect on the survival of female mice. However, we have recognized weight loss as a clinical prognostic marker for ALS progression[359] and included it in our analysis to see the effect of NS-1-2 in ameliorating disease phenotype by preventing weight loss (ALS-induced cachexia). The prolonged life span of both sexes following NS-1-2 treatment may be due to the reduction of weight loss observed, resulting in a delay in disease progression in these familial mice models of ALS. Further, NS-1-2 has shown a profound effect in ameliorating the disease phenotypes in terms of delaying the disease onset and symptom onset while accounting for the sex-specific differences.

Further, the only FDA and EMA-approved ALS drug known to prolong survival in ALS patients is Riluzole, by only 2-3 months. However, despite the modest positive clinical trial results in ALS patients, Riluzole has never been shown to extend the life span to a statistically significant degree in familial mouse models of ALS[298]. Riluzole only marginally improves median survival by 3.3% ($p=0.0525$), when used in the SOD1-G37R

mice model, however, the major limitations of the study were firstly, the study did not mention the line of G37R mice they used. Secondly, the study did not account for the treatment response with sex differences, although they did mention the distribution and randomization of the groups with equal genders[420]. In comparison to the efficacy of Riluzole, the newly synthesized NS-1-2 demonstrated significant disease-modifying effects in the highly aggressive line-42 SOD1-G37R mice model while also demonstrating sex differences in response to treatment. NS-1-2 significantly prolonged the probability of survival in the whole set of animals with p=0.0174. Further, treatment using NS-1-2 increased the probability of survival in both males and females, although only significantly improved the probability of survival in males (*p=0.0232)* compared to females *(p=0.2322).* Using clinically relevant and comprehensive treatment paradigms in the preclinical model, the prodrug of EDR, NS-1-2, was found to be effective in modifying the disease phenotypes in line 42 SOD1-G37R mice model, an early onset and highly aggressive SOD1 familial ALS preclinical model.

Recently, in 2023, pridopidine, an oral small molecule designed to selectively bind to and activate the sigma-1 receptor (S1R), a protein that is vital for the function and survival of nerve cells, failed to meet its primary endpoints of survival in the phase 2 HEALEY human platform clinical trial. We believe this failure of improving survival was observed previously in animal models, as pridopidine treatment failed to prolong survival in the familial SOD1-G93A mice model of ALS; however, pridopidine did prevent ALS-induced weight loss/cachexia[421]. These reports from human clinical studies do not support the data published in previous pre-clinical animal studies, according to which ALS-induced weight loss is recognized as an independent predictor of a shorter life span in ALS[422]. Further,

according to the ENMC report, weight is regarded as a preferable secondary endpoint to be considered in preclinical studies[423]. Reassuringly, in the present preclinical study, NS-1-2 was found to prevent ALS-induced cachexia in the high copy number G37R mice model, which is a recognized marker of survival, which we hope to translate in future human clinical trials.

Apart from reducing oxidative stress in familial SOD1 mice, we plan to also explore the therapeutic avenues that are possible in targeting oxidative stress in TDP-43 mouse models. Emerging new studies have shown that oxidative stress is also involved in the abnormal misfolding of RNA processing protein (TDP-43), a major pathological hallmark in all forms of ALS. TDP-43 gains cytotoxicity due to aggregation in the cytoplasm and accounts for 90 to 95% of sALS cases[424, 425], and the majority of fALS cases[426]. The initial trigger for the abnormal aggregation of TDP-43 is due to pathological oxidative stress[427, 428] caused by a global imbalance in the bioenergetics of mitochondria[429-431], which increases the propensity of TDP-43 aggregations and hence the gain of neurotoxic function, leading to the death of motor neurons[427]. Consequently, oxidative boron targeting could be a novel avenue to slow down the progression in patients suffering from TDP-43 pathology. In the future, we will be planning to utilize the triple role benefit of NS-1-2 by targeting oxidative stress in the TDP-43 animal models of ALS.

Furthermore, to correlate the efficacy of NS-1-2 in the SOD1 G37R mice model of ALS, we performed untargeted, unbiased discovery-based global proteomics and phosphoproteomics of lumbar spinal cord samples from end-stage male mice. ALS is a complex, heterogeneous, and incurable motor neurodegenerative disorder. It has been nearly 150 years since French neurologist Dr. Jean-Martin Charcot first described ALS,

and over 30 years since Gurney's 1994 discovery of the SOD1 preclinical mouse model that mimics the clinical pathology and motor symptoms seen in humans. Despite this progress, only a few drugs offer modest survival benefits. One major obstacle in ALS clinical trials is the disease's heterogeneity and the involvement of multiple etiological factors in its progression. Recent breakthroughs in quantitative, unbiased, global proteomics could help address these challenges by revealing comprehensive changes at each disease stage in mouse models, surpassing the limitations of traditional Western blotting. Additionally, tracking proteomic changes over time in SOD1 mice could provide valuable translational insights, supporting the development and validation of biomarkers from preclinical SOD1 mouse models to human ALS cases.

Based on recent advancements in the field of discovery-based proteomics and phosphoproteomics, we believe that a proteomics tool could overcome the challenge of biomarker discovery, which could aid in diagnosing and monitoring longitudinal disease progression in ALS clinical trials. Furthermore, proteomic studies have been identified as a reliable tool for detecting and developing novel biomarkers[366] that could help correlate the severity of ALS symptoms with the rate of disease progression[365, 367-370] Moreover, a global proteomics biomarker approach promotes a better understanding of meaningful drug target mechanisms and achieves positive clinical outcomes[371-373, 375].

Recently, the scientific community has been debating whether proteomics represents a paradigm shift in the fields of cellular biology and biomedicine. The debate primarily centers on two key questions. Firstly, can proteomics outperform traditional Western blotting (WB) methods? Secondly, is there a need to cross-validate the results of

proteomics with WB? Explanations have been provided by various experts in the field, based on several convincing rationales[363, 432, 433] Firstly, the use of antibodies, through which scientists determine a specific signal of the protein in a biased and targeted manner, allows for unexpected changes in the cellular components to go unnoticed, and researchers run after the same signal again and again rather than identifying alterations in the signal from the whole cellular system. Hence, the WB is a semiquantitative method with a problem of poor specificity. Whereas proteomics is a purely quantitative method of analysis (typically several independent peptide fragments of the same protein are targeted to quantify a protein) of whole cellular changes, through which the researchers make sure that the investigated change is the major one out of all changes[364, 434]. Secondly, with WB, there is a lack of specificity concerning antibodies; several antibodies are absent or may never have existed due to the large number of proteins that have not been studied until now. However, all these proteins with broader coverage can be detected by quantitative mass spectrometry (MS)[363]. Thirdly, in the case of WB, the antibody cannot detect the cellular signal at lower sample numbers (below nanogram levels). In contrast, the latest advancements in MS can detect as low as pico- and femtogram levels with high specificity[435]. Lastly, researchers use polyclonal antibodies, which provide broader specificity, leading to a high probability of false-positive signals. In Contrast, MS analysis offers a large number of peptide identifications with high statistical confidence. Recently, vendors started selling MS-validated antibodies following published guidance from the International Working Group for Antibody Validation (IWGAV)[436, 437]. The more significant advantage of exploring distinct cellular events with a single experiment using a lower sample amount is that it offers the opportunity to quantify global

proteome changes in cases of rare diseases like ALS, due to the lack of readily detectable and reliable blood and urine biomarkers[438].

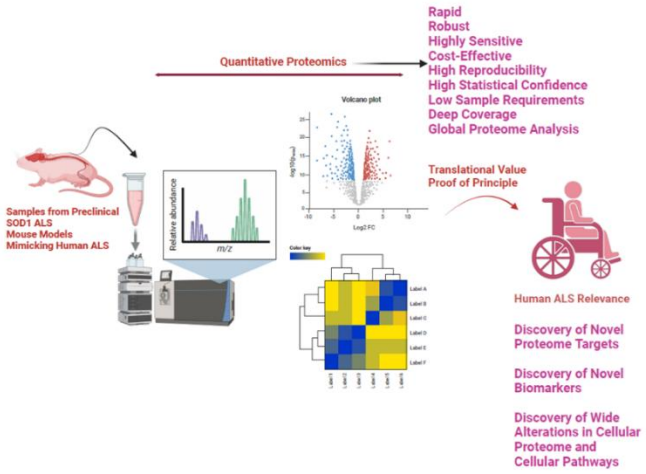

Figure 75. Schematic picture illustrating several advantages of proteomics, demonstrating proof of principle and translational value from ALS mouse models to human ALS cases.

The figure is adapted from our latest publication. Sanghai N, Tranmer GK. Use of Proteomics to Explore Biomarkers of Amyotrophic Lateral Sclerosis (ALS): Proof of Principle from Humanized SOD1 Mouse to Human ALS. ***ACS Pharmacology & Translational Science. 2025 Jul 28.***

Therefore, to gain insights into the multi-system changes in the proteomics of the central nervous system (CNS) of G37R ALS mice, we utilized highly sensitive, reliable, precise, deep-coverage, and reproducible mass-spectrometry-based proteomics approaches. Considering the reliability and the numerous advantages of proteomics and phosphoproteomics, which are well-validated by the global scientific community, we decided to conduct global untargeted, unbiased, and unsupervised discovery-based proteomics and phosphoproteomics in collaboration with the **Manitoba Centre for Proteomics and Systems Biology**. One of the limitations of this analysis was the use of lumbar spinal cord samples from male mice that had reached a humane endpoint. According to our animal protocol approval, we have collected samples of the lumbar spinal cord from both the male and female cohorts reaching the humane endpoint.

However, based on the significant extension of survival from the male cohort compared to the female cohort, we initially thought of investigating the global changes of proteome and phosphoproteome in the male cohort. The primary objective of our *in vivo* animal efficacy protocol was to evaluate the therapeutic potential of NS-1-2 in delaying disease onset and extension of survival in an ALS mouse model with longitudinal monitoring for weight loss starting from age 90 days until endpoint. In 2020, when we started our preclinical studies, we chose “Survival” as the principal primary endpoint of preclinical studies for several reasons. Firstly, according to the guidelines on using preclinical SOD1 ALS models for *in vivo* evaluation of pharmacological interventions by the 142nd European Neuromuscular Centre (ENMC) international meeting held in Holland, "Survival is considered the principal primary endpoint of preclinical studies”[423]. Secondly, according to the ENMC report, weight is considered the preferable secondary endpoint because weight loss is considered an independent strong predictor of decline in survival in ALS mice and patients[439]. We know that most of the molecular pathways get dysregulated and compromised due to the fast disease progression in ALS mice. However, based on our intriguing data that demonstrated the efficacy of NS-1-2, and findings of a significant extension of survival in male cohorts, we thought of taking a chance to profile the discovery-based global proteomics and phosphoproteomics of spinal cord samples from male cohorts reaching the humane endpoint. Surprisingly, we discovered differential regulation of known and unknown global proteins and phosphoproteins in the end-stage samples. Further investigations based on published works of the literature identified several dysregulated crucial pathways relevant to ALS and other overlapping neurodegenerative diseases. Despite the limitations of our study, we aimed to provide

valuable insights into the molecular pathways altered in ALS mouse models following treatment with NS-1-2. Analyzing (*n=4*) samples helped identify differentially regulated proteins, with hopes of revealing a biochemical basis for the observed efficacy. Prospectively, a large sample size with defined cohorts directed toward protein profiling could have provided a large number of altered proteins across the groups. Nevertheless, analyzing the lumbar spinal cord tissues from the end stage of the ALS progression provided evidence that NS-1-2 (BSZ) is an ideal candidate to move forward as disease-modifying therapeutics in ALS.

Global proteomics and phosphoproteomics analysis have identified several known and unknown pathways relevant to ALS represented with a discovery-based untargeted unbuffered proteomics and phosphoproteomics workflow, volcanoplots, and heat maps showing the differential regulation of proteins in the NS-1-2 group compared to the vehicle-treated group (**Figure 66)**.

Figure 68

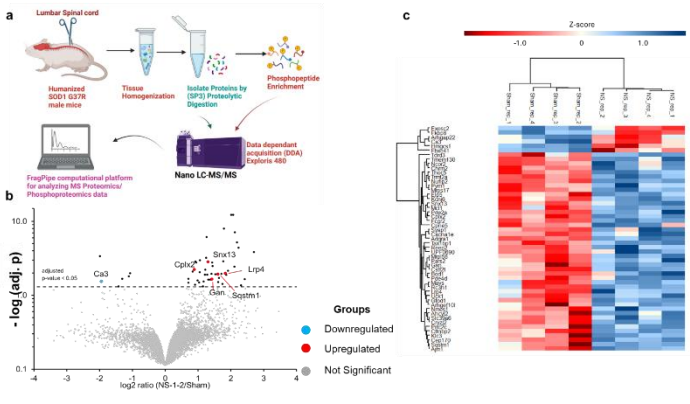

The differential expression levels of the proteins and phosphoproteins detected from the end-stage mice demonstrated different pathological links with neurodegeneration and ALS, as detailed in **Tables 6 and 9**, respectively. The increased expression (3-fold upregulation) of ***Sqstm1/p62*** in the treatment group correlates with observed efficacy as ***Sqstm1/p62*** is known to bind with the activator of autophagy marker protein ***LC3***[440] (essential to autophagosome formation) to facilitate the degradation and removal of ubiquitinated toxic misfolded SOD1

aggregates by autophagy[441, 442]. The decreased expression of ***Sqstm1/p62*** reduces mitophagy in ALS mice[443], leading to a disease phenotype. Furthermore, decreased ***Sqstm1/p62*** expression leads to the accumulation of various neuropathological proteins via negative regulation of autophagy implicated in the huntingtin aggregates[444], Alzheimer's disease[445, 446], Parkinson disease[447], spinal and bulbar muscular atrophy[448] and aging[449]. In addition, ***Sqstm1/p62*** controls various cellular activities and the decreased expression of ***Sqstm1/p62*** protein leads to mitochondrial dysfunction[450], cellular oxidative stress[451, 452], and defective protein homeostasis[453]. Thus, the ***Sqstm1/p62*** protein acts as a signaling protein for regulating multiple cellular pathways and is a vital protein for removing unwanted toxic proteins in ALS and other neurodegenerative diseases. Reassuringly, the decrease in expression of ***Sqstm1/p62*** observed in the untreated control samples can provide a biochemical rationale as to the decrease in survival and advancement of an ALS disease phenotype observed in the control animals. Another protein, ***Lrp4***, was found to be differentially upregulated in the NS-1-2-treated groups. Expression of ***Lrp4*** is associated with the formation of neuromuscular junction[454], modulation of neuronal excitability[455], and astrocytic amyloid beta clearance[456]. Recent studies have detected ***Lrp4*** antibodies in the serum and CSF of ALS patients. However, the link of ***Lrp4*** to ALS pathology is not fully understood[457]. Furthermore, we also detected the increased expression of ***Cplx2***, which is important for neurotransmitter release, in the NS-1-2 treated group. Decreased expression of ***Cplx2*** protein is known to be associated with neurological deficits in various neurological disorders, including Alzheimer’s disease[458], Parkinson’s disease[459], Schizophrenia[460, 461], and Huntington’s disease[462]. In addition, recent

transcriptome sequencing revealed the downregulation of ***Cplx2*** in ALS patients and mouse models[463, 464]. We also discovered the downregulation of ***Ca3*** in the NS-1-2 treated group, which a sensitive marker of muscle damage in neurological disorders[465] and aging[466]. Recently, the ***Ca3*** protein was found to be significantly upregulated in the CSF of ALS patients compared to controls in a large discovery cohort, identifying ***Ca3*** as a novel candidate biomarker[467], where increased ***Ca3*** is associated with ALS. In 2025, Alam and his team completed a milestone project analyzing the plasma proteome, identifying disease-specific protein variations associated with the severity of neurodegeneration. This dataset from the Global Neurodegeneration Proteomics Consortium (GNPC) is among the world's largest, with about 250 million protein measurements from over 35,000 biofluid samples collected from 23 partners. It includes clinical data on AD, PD, FTD, and ALS. This landmark study found that the circulating blood proteome from a large group of ALS patients exhibited significantly increased levels of ***CA3*** in ALS patients compared to controls, which is related to skeletal muscle structure and function[468].

As a result, a decrease in ***Ca3*** found in the treated group can infer decreased neuromuscular degeneration, in comparison to control animal samples. Furthermore, recent emerging evidence of increased expression of ***CA3*** in large cohorts of ALS patients validates the proof of principle for investigating biomarkers in the humanized SOD1 G37R mouse model and its relevance to human ALS. In addition to the known (ALS-associated) proteomics signatures described above, we unraveled novel increased expression of ***Gan/KLHL16****, and* ***Snx13*** in the NS-1-2 treated group, which are known to be related to neurodegeneration, but unreported in ALS models (to the best of our knowledge). Subtle

evidence, from various emerging reports, has shown that the decreased expression of ***Gan***, a cytoskeletal protein that causes impaired autophagy by reducing ubiquitination and hence the formation of ***ATG16L1*** aggregates[469, 470], is related to, or causes, neurodegeneration. This dysregulation of ***ATG16L1*** causes the deactivation of ***LC3-II*** lipidation, an autophagic protein biomarker, and dysregulation of ***P62,*** the main autophagic receptor[470]. Therefore, *Gan* has recently been considered a novel regulator and thus governs the autophagic machinery. In addition, the downregulation of ***Gan*** activates the disorganization of intermediate filament (IFs) proteins, instigating the accumulation and aggregation of neurofilament (NFs) in the axons of neurons, thus causing axonopathy[471-474]. Elevation of neurofilaments is the most investigated and promising biomarker that can be correlated with the progression of neurodegenerative diseases, including presymptomatic and phenoconversion of ALS. This mounting evidence suggests that ***Gan*** is a novel and unique protein regulating the key pathways known in the progression of ALS, thus representing a novel pharmacodynamic target for slowing the progression of ALS[475, 476]. Nevertheless, the potential role of ***Gan*** in ALS pathogenesis should be investigated in the future. Moreover, following proteomic profiling, we unveiled the novel increased expression of the ***Snx13*** protein, which maintains cellular cholesterol homeostasis by an endolysosomal cholesterol export mechanism[477]. Other reports have shown the pathological link between lipid dysregulation and various neurodegenerative diseases [478], thus, upregulation of ***Snx13*** protein could help alleviate the pathology of neurodegeneration. **Figure 76** shows the proposed mechanism of NS-1-2 based on the differential expression of proteins identified through an unbiased, global proteomics discovery approach.

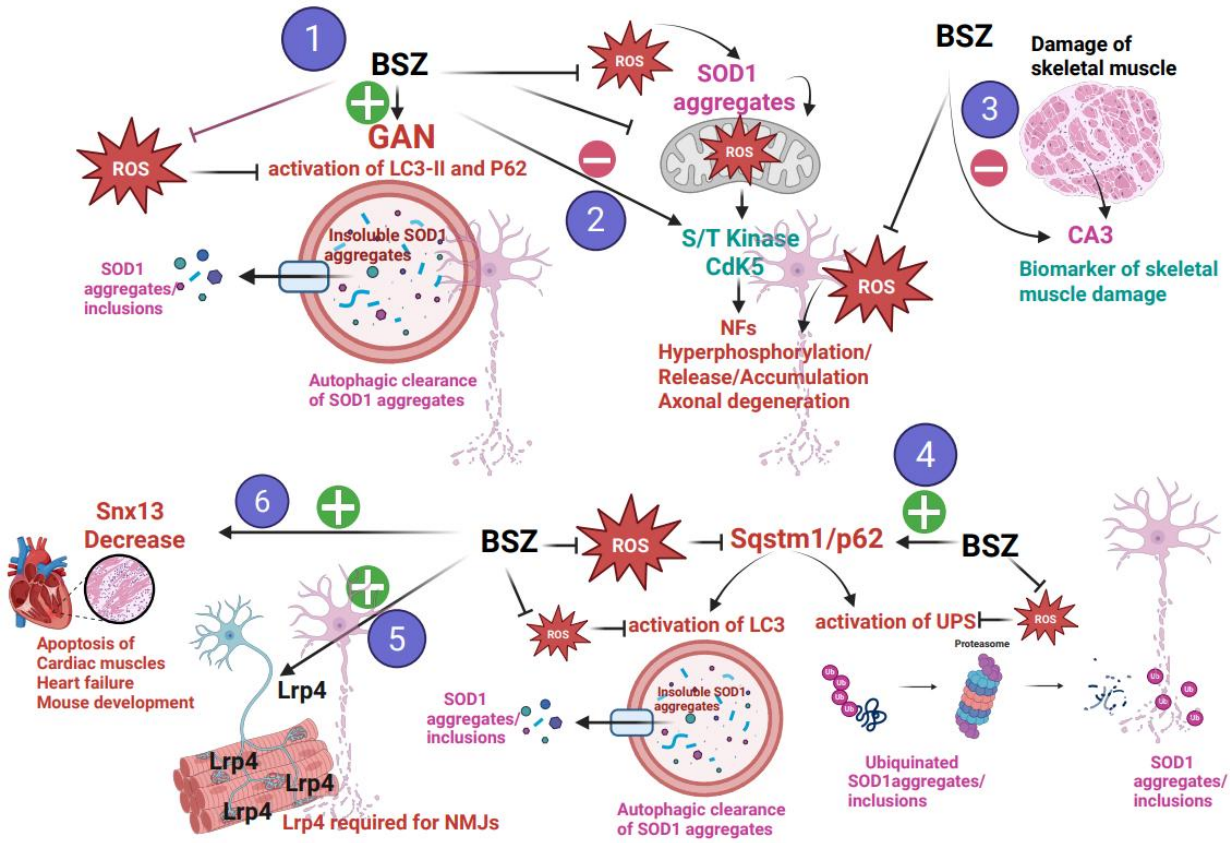

Figure 76. Schematic illustration of the putative mechanism of NS-1-2 based on the differential expression of proteins in an unbiased, untargeted discovery-based global proteomics approach.

Schematic illustration of the putative mechanism of NS-1-2 based on the differential expression of proteins in an unbiased, untargeted discovery-based global proteomics approach. BSZ increases the expression of proteins in pathways **1, 4, and 5,** compared to the vehicle-treated group, modulating different pathways involved in the pathophysiology of neurodegeneration. In contrast, increased expression of proteins in pathway **6** in BSZ compared to the vehicle-treated group is related to heart and mouse development. Pathways **2 and 3** show decreased expression in the BSZ group compared to the vehicle-treated group. Both these pathways are known to be implicated in the

pathology of neurodegeneration. **Note: NS-1-2 was developed in the lab and later trademarked as Borsantrazole (BSZ).**

In our discovery-based untargeted phosphoproteome analysis of spinal cord samples, **Table 7**, we interestingly found that recently reported ***Pgk1*** serine 203 (S203) phosphorylation levels were downregulated in the NS-1-2 treated group compared to the vehicle-treated group. The latest studies from Xu and his colleagues delineated the role of S203 phosphorylation in mitigating the oxidative stress in spinal cord neurons caused by spinal cord ischemia-reperfusion (IR) injury (SCIRI). Biochemically, they demonstrated that G-protein-coupled receptor (GPCR) kinase 2-interacting protein-1 (Git1) is a GTPase-activating protein, interacts with ***Pgk1*** protein, thereby reducing the S203 site phosphorylation level, hence leading to accumulation of metabolites generated during glycolysis in neurons. Further, these metabolites result in the dimerization of Keap1, thereby, resulting in reducing the degradation of an antioxidant response protein called ***Nrf2***[479]. The increased expression of ***Nrf2*** maintains the redox homeostasis of the neurons by conferring antioxidant defense to the cells[480]. Thus, mechanistically, decreased expression of ***S203 Pgk1*** phosphorylation is associated with neuroprotective mechanisms via decreased S203 phosphorylation. A large body of evidence has shown the potential role of the antioxidant KEAP1-NRF2 system as a therapeutic avenue to slow down the progression of ALS via combating oxidative stress[481], however, none of the reports have reported the activation of the ***KEAP1-NRF2*** system via downregulating S203 phosphorylation of ***Pgk1***. Therefore, NS-1-2 could be a compelling therapeutic agent for slowing down the progression of ALS by modulating the antioxidant KEAP1-NRF2 pathways.

Furthermore, as presented in (**table 9),** we also identified novel and known phosphosites of both neurofilament light chain (***Nefl***) and neurofilament heavy chain (***Nefh***) proteins in the spinal cord of hSOD1 mice. Neurofilaments are cytoskeleton proteins of long myelinated motor neuron axons. Increased levels of CSF ***Nefl*** and CSF phosphorylated (pNefh)[482] and serum NFL levels due to progressive neurodegeneration have been reported to slower axonal transport, leading to axonopathy and neuromuscular decline in both SOD1 ALS patients and hSOD1 mouse models[483]. These findings suggest the role of abnormal hyperphosphorylation in SOD1 ALS pathogenesis[483]. In mature myelinated axons, the major sites of phosphorylation in ***Nefh*** are **Lys-Ser-Pro** (KSP) repeats in the carboxy-terminal tail domain, which is essential for maintaining axon caliber, stability, growth, protecting ***Nefh*** from proteolysis and calcium buffering. Additionally, threonine phosphosites in both the mammal and human samples of neurofilaments are reported [484-486]. Recently, neurofilaments (NFs) have been regarded as the most reliable biomarkers dictating ALS stages, acting both as a valuable tool for prognosis and diagnosis in longitudinal studies during the pathogenesis of ALS[487, 488]. Due to their reliability and translational value, NFs are used as a biomarker for the development of ALS therapeutics, with one such example being the discovery and development of tofersen[489, 490]. With the evolution of NFs as a benchmark universal biomarker in several neurological diseases, it is important to account for emerging techniques to determine multiple sites of phosphorylation of NFs. This will advance our knowledge without bias to see the changes in the global phosphosites in relation to the disease progression in the case of ALS. Several reports have investigated the increase in the ***Nefh*** and ***Nefl*** serine phosphosites in ALS, but threonine phosphosites have never

been investigated in Nefh and Nefl. Herein, utilizing an untargeted, unbiased MS discovery-based phosphoproteomics approach, we have studied and uncovered both serine and threonine phosphosites in the spinal cord of SOD1-G37R mice. We found that 58 serine/threonine (S/T) sites are downregulated for ***Nefh*** and 8 S/T sites are downregulated for ***Nefl***, following treatment with NS-1-2. Overall, quantification of the S/T phosphorylation sites provides for a general trend of reduction in phosphorylation of ***Nefh*** and ***Nefl***, in the NS-1-2 treated group, which also correlates to the general trend of decreased protein expression also detected in our proteomics data for ***Nefh*** and ***Nefl***. Overall, this observable trend in downregulation of neurofilaments in NS-1-2 treated mice correlates with increased survival, as in general, increases in Nefh/Nefl are seen as being indicative of elevated neurodegeneration. Importantly, phosphorylation of **T72** in ***Nefh*** and **T317** in ***Nefl*** was significantly reduced in the NS-1-2-treated group. To the best of our knowledge, both the T72 and T317 phosphosites have not been reported in the literature. Due to the significance of our proteomic and phosphoproteomic analyses, as it relates to the therapeutic effects of BSZ, we are planning a more complete description of our ALS biomarker with a longitudinal approach in the near future. Overall, applying an untargeted, unbiased discovery-based proteomics and phosphoproteomics approach, we were able to identify known pathological pathways that are perturbed in ALS and discovered unknown pathological pathways that present interest for further investigation.

Further, for the first time, we moved one step ahead to profile the brain of G37R SOD1 mice brain samples (n=4) from both sham and treatment (NS-1-2) groups. We utilized an untargeted/unbiased proteomics approach for the investigations/and discovery of known/novel biomarkers correlating with the efficacy of NS-1-2. Intriguingly, as shown in **(figure 68) and table 11**, we discovered both known and novel differential expressions of proteins in brain samples treated with NS-1-2 compared to the control group.

Figure 68

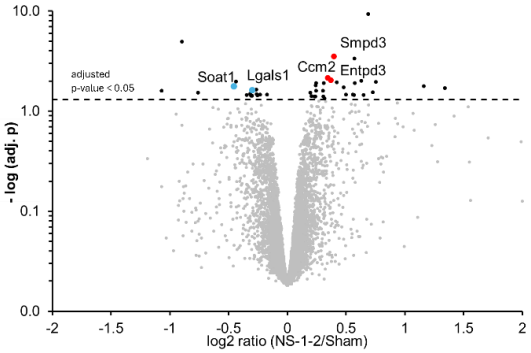

Our findings indicated that two proteins, both known to be pathologically associated with ALS progression—Sterol O-acyltransferase 1 ***(Soat1/ACAT1)*** and Galectin-1 ***(Lgals1)*** are notably downregulated in the NS-1-2-treated brain samples relative to the vehicle-treated ones. In addition, ***LGals1*** is also found to have a pathological association with aging. Recent findings from Cai and colleagues[491] revealed a significant increase in the mRNA expression of ***Lgals1*** in patients with ALS. Additionally, they discovered elevated levels of ***Lgals1*** in the serum samples from ALS patients. This study highlighted the profound association of aberrantly elevated expressions of ***Lgals1*** during the progression of ALS. Another study found the abnormal increase resulting in the accumulation of ***Lgals1*** in the neurofilamentous lesions of spinal cords of both sALS and fALS patients. Further, these findings were supported by Kobayakawa and his group[492] in SOD1 G93A preclinical models of ALS. Very importantly, they found that ***Lgals1*** deficiency improves degeneration due to axonal swelling of motor neurons in presymptomatic stage SOD1G93A mice. Furthermore, recent studies have highlighted ***Lgals1*** as a marker of

non-neuronal immune cells, specifically microglia, in the aging brain. The increased expression of ***Lgals1*** activates microglial cells, thereby contributing to neuroinflammation in the aging brain. Another protein, ***Soat1/ACAT1***, associated with lipid metabolism and cholesterol homeostasis, catalyses the esterification reaction of free cholesterol to cholesteryl ester in nerve cells, and its activity is indicated by the cholesterol-to-sterol ester ratio (CHO/SE). Increased expression of ***ACAT1*** was observed in ALS motor neurons, attributed to an increase in SE levels[493]. Murphy et al[494]. have shown that blocking the ACAT1/SOAT1 expression in the brain decreases the levels of amyloid Aβ1–42 in the 3XTg-AD mice. Further, blocking ACAT1 reduces amyloid plaques, tau tangles, and stimulates autophagy to clear misfolded proteins in preclinical AD models[495, 496]. Together, increased expression of both ***Lgals1 and ACAT1*** *is known to be involved in the progression of neurodegeneration, including ALS.* Therefore, the decreased expression of ***Lgals1 and ACAT1*** in the NS-1-2-treated group, which showed improved motor phenotypes compared to the control group, demonstrated the correlation of its efficacy.

In addition, we also found increased expressions of three proteins: cerebral cavernous malformation protein 2 homolog (***Ccm2***), sphingomyelin phosphodiesterase 3 (***Smpd3***), and Ectonucleoside triphosphate diphosphohydrolase 3 (***Entpd3/NTPDase3***), which have unknown associations with ALS. However, these proteins are involved in the process of neurodegeneration. Decreased expression of ***CCM2*** (also known as OSM and malcavernin) causes cerebral cavernous malformations (CCMs). These abnormalities are characterized by dilated, leaky blood vessels, especially in the neurovasculature, that result in an increased risk of stroke, focal neurological defects, and seizures[497]. Whereas, decreased expression of ***Smpd3*** amyloidosis, taupathy, cognitive impairment

and defective proteostasis[498]. Furthermore, the downregulation of neuronal Ectonucleoside triphosphate diphosphohydrolase 3 (***Entpd3/NTPDase3***) is linked to decreased mitochondrial ATP production. Additionally, it also plays a role in regulating ATP for excitatory neurotransmission across the synapse[499]. The presence of ***NTPDase3*** in the hypothalamus suggests its role in the modulation of neuronal communication and energy balance. A study by Belen and his group[500], identified decreased mRNA expression levels of total purine metabolism enzymes, including ***Entpd3***, in the brain of AD cases. While decreased expression of ***Ccm2, Smpd3,*** *and* ***Entpd3/NTPDase3*** is not directly linked to the cause of ALS, these proteins are expressed in neurons, and their downregulation has been associated with neurological conditions. Our discovery-based approach revealed increased expression of these proteins in the NS-1-2-treated group, correlating with the efficacy of NS-1-2. It is essential to acknowledge that, to the best of our knowledge, our methodology of profiling the global proteome in G37R mice utilizing the boronate compound (NS-1-2) is novel and has identified significant pathways involved in neurological conditions, which could potentially be modulated by NS-1-2.

One of the limitations of our global proteomics and phosphoproteomics data was using samples (spinal cord and brain) from mice that reached a humane endpoint in both cohorts (NS-1-2 treated vs. control). Although both groups reached end stage, we were able to observe significant differential regulation of known and unknown proteins involved in the etiopathological process of neurological conditions in both cohorts. We attempted to address this limitation by designing the experiment to profile the global proteome and phosphoproteome over time during various clinical stages of disease progression,

including presymptomatic, disease onset, symptom onset, and death. Furthermore, clinical phenoconversion refers to the transition from a presymptomatic clinical stage with no symptoms to a clinical symptom stage or symptom onset of the disease. All these stages should be considered and stratified for proteomic profiling. Each stage of profiling will provide insight into biomarker-driven drug development and solve the puzzle of complexity in ALS[501]. Therefore, to explore further the effects of EDR prodrug NS-1-2, we designed a biomarker symptom onset study where we pretreated the mice with NS-1-2 and vehicle until they reached symptom onset with weakness and 10% loss of body weight. Depending upon the availability of animals, we used age and sex-matched females (n=3) in both the cohorts. As shown in **figure 71,** the symptom onset biomarker study demonstrated that NS-1-2 prevented the weight loss at the end of the study, humane endpoint by 4.9% compared to the vehicle-treated group, where the weight loss of all the mice in the cohort was found to be more than 10%.

Figure 71

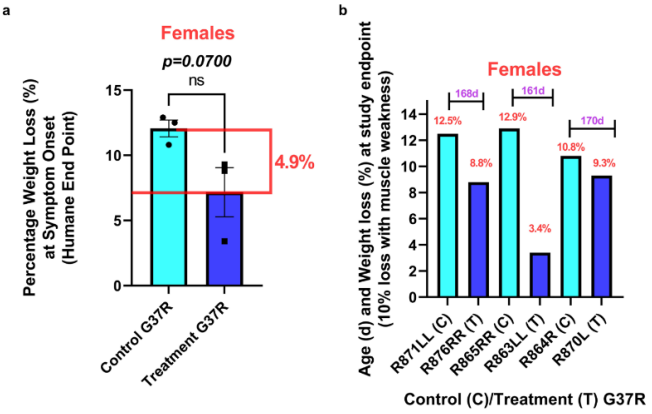

Notably, our study revealed that all the mice (n = 6) in both cohorts reached symptom onset at approximately 165 days of age. The data from this study (age of symptom onset) will help us to design future experiments, where we can manipulate the treatment start date before the symptom onset date; however, a larger number of animals are needed to validate this data.

Later, as shown in **table 14** and **figure 73,** the comprehensive, unbiased analysis of spinal cord samples from both groups (NS-1-2 and control) at the study's end identified four new proteins with different expression levels.

These proteins are not directly linked to ALS but are known to play roles in neurological diseases such as seizures, AD, and stroke. Out of the four proteins we investigated, three (***Hebp1, Tbxas1,*** and ***Pcna***) were found to be decreased in the NS-1-2-treated group, whereas ***NPRL2*** was found to be increased in the NS-1-2-treated group compared to the vehicle-treated group.

Figure 73

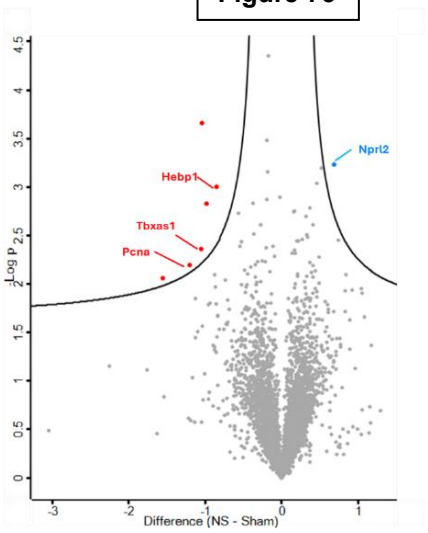

NPRL2 (nitrogen permease regulator-like 2) is a requisite component of the GATOR1(GAP activity towards rags complex 1) proteins, which are inhibitors of the amino acid-sensing branch of the mTORC1 pathway. ***NPRL2*** functions as a negative regulator of the mammalian target of rapamycin complex 1 (mTORC1) kinase under conditions of low intracellular amino acid concentrations. A recent study investigated the loss of function of NPRL2, which is related to the pathogenesis of epilepsy[502]. Furthermore, a significant study by Hui and his colleagues found that the loss of ***NPRL2*** expression in excitatory glutamatergic neurons of the mouse leads to the development of epilepsy. Additionally, the decrease in ***NPRL2*** expression in the brain leads to an increase in mTORC1 activity, thereby disrupting the brain's amino acid homeostasis. Moreover, they demonstrated that the loss of ***NPRL2*** decreases dendritic branching in neurons and increases the expression of epilepsy linked sodium channels[503]. Furthermore, ***NPRL2***

is an essential protein subunit component of GATOR1, acting as a negative regulator of mTORC1. While ***NPRL2*** is not directly involved in ALS pathophysiology, the mTORC1 pathway, regulated by ***GATOR1***, plays a role[504]. Evidence suggests that inhibiting mTORC1 benefits ALS models by promoting autophagy, which facilitates the clearance of misfolded SOD1 proteins that cause aggregation and toxicity in motor neurons. This is supported by a study in which rapamycin, an mTORC1 inhibitor, activates autophagy and extends the lifespan of ALS mice[505]. Consequently, NS-1-2, which increases ***NPRL2*** expression—a ***GATOR1*** component, could potentially modulate mTORC1 negatively, thereby activating a neuroprotective pathway called autophagy.

Proliferating cell nuclear antigen (***PCNA***) is a protein essential for DNA replication and repair, as well as for various other cellular processes[506]. It is observed in both glial cells and neurons, with increased expression often linked to the progression of AD. Higher expression of PCNA has recently been identified as a marker of neurodegeneration in AD[507]. Heme-binding protein 1 (***Hebp1***) is an intracellular protein mainly in neurons, interacting with the multi-subunit complex present in the inner mitochondrial membrane (MICOS) complex at mitochondria. It regulates, synthesizes, and transports heme and mediates heme-induced cytotoxicity via apoptosis. ***Hebp1*** is linked to AD, possibly contributing to neuronal loss. Numerous studies have demonstrated the pathological role of higher ***Hebp1*** expression in both preclinical AD mouse models and humans. Higher elevation of ***Hebp1*** is reported in the hippocampus of young AppNL-F [508] and in the brains 3×Tg-AD transgenic mice models of AD[509]. Interestingly, higher expression of Hebp1 was found in the brains of patients with rapidly progressing forms of AD[509]. In addition, thromboxane-A synthase (***Tbxas1***) protein is a molecule involved in blood

clotting and inflammation[510]. Higher levels of ***Tbxas1*** production are observed in AD, potentially contributing to the disease's progression[511]. Additionally, increased expression of ***Tbxas1*** has been reported in stroke patients[512]. Collectively, these findings from the proteome profile at symptom onset in the G37R mice model have identified new druggable targets associated with neurogenerative disease. Furthermore, this new symptom-onset biomarker study found links between ALS and other neurodegenerative diseases like AD.

6 Significance of the study

We have been continuously making efforts since 2019 toward early-phase drug discovery to bring "Hope" to the lives of patients suffering from incurable and highly complex orphan disease ALS. With this important work, our goal is to bring hope and improve the quality of life. Since 2019, we have been leveraging the concepts of both medicinal chemistry and neuroscience to develop novel organic chemical molecules that can slow down the progression of incurable ALS. This marks the first time our lab has ventured into the field of neurodegeneration, utilizing a novel medicinal chemistry approach to target ALS. We have developed a new, improved version of a United States Food and Drug Administration (FDA) approved Edaravone (EDR), overcoming its limitations. The new molecule NS-1-2 is a boron warhead, chemoselective redox regulator with a triple role benefit over EDR and has shown excellent *in vivo* proof of concept **(POC)** in terms of delaying disease onset, symptom onset, extending lifespan, and preventing weight loss. Further, we have initiated pharmacokinetic studies to advance the development of the patented NS-1-2 molecule. Additionally, for the first time, we performed discovery-based, global, untargeted, and unbiased proteomics and phosphoproteomics studies to correlate the efficacy of NS-1-2 *in vivo* and to identify potential biomarkers.

Since 2019, we have achieved several milestones in our project, including filing a patent application and converting a patent to national phase applications in different jurisdictions. Currently, the best-in-class lead small molecule NS-1-2, developed in our lab, is trademarked as Borsantrazole (BSZ), which is registered by Innovation, Science and Economic Development Canada and is protected under patent **PCT/CA2023/051352 (WO 2024/103151)**. The project received a strong endorsement through an international

search report (ISR) statement of assessment from the World Intellectual Property Organization (WIPO), which confirms that it meets the criteria of novelty, inventive step, industrial utility, and applicability. Furthermore, our project**, "Development of a biomarker-driven 'best-in-class' treatment for amyotrophic lateral sclerosis: Discovery and proof-of-concept,"** ranked near the top in a CIHR project grant competition and received a CIHR grant. CIHR (Canadian Institutes of Health Research) awards are highly prestigious within the Canadian health research community and beyond. They are recognized for supporting and celebrating Canada's top health researchers and their transformative contributions to the field of health research.

Since 2019, the preliminary findings from early phases of drug discovery have opened numerous avenues. This year, we initiated a collaboration with Devi Atukorallaya (Associate Professor, Department of Oral Biology, Dr. Gerald Niznick College of Dentistry, Rady Faculty of Health Sciences, the University of Manitoba) to assess the effects of BSZ on neurodegeneration in cavefish, as well as in Mexican and zebrafish models. Additionally, we have been collaborating with Dr. Paul C. Marcogliese (Assistant Professor in the Department of Medical and Human Genetics, the University of Manitoba) to investigate the therapeutic implications of BSZ in a SOD1- and TDP-43-induced fruit fly model, with the aim of mitigating neurodegenerative progression. We are collaborating with Dr. Rene Zahedi (Manitoba Centre for Proteomics, the University of Manitoba) and Dr. Amir Ravandi (St. Boniface Hospital Research Centre) to study the differential expression of proteins, phosphoproteins, and lipids in a preclinical ALS mouse model treated with BSZ. Our research further extends to exploring the therapeutic potential of BSZ using the induced pluripotent stem cell (iPSC) model in collaboration with Dr. Erik P.

Pioro, Chair of the ALS Society of BC and Professor of ALS Research at UBC. Additionally, we plan to evaluate the application of BSZ in a preclinical Alzheimer's model in collaboration with Dr. Jillian Stobart, an Associate Professor in the College of Pharmacy at the University of Manitoba. Furthermore, we are working with Dr. Abdelilah Soussi Gounni, a Professor in the Department of Immunology at the University of Manitoba, to study the effects of BSZ in asthma mouse models. We have also been assessing how BSZ might reduce the risk of diabetes in animal models, in collaboration with Dr. Lucy Marzban, an Associate Professor at the University of Manitoba's College of Pharmacy. With every step, we aim to advance from the lab to clinical applications for ALS patients and to explore the therapeutic effects of BSZ across different disease pathologies in a diverse and collaborative environment.

To date, we have obtained significant preliminary results that demonstrate the significance of our project in the development of a novel small molecule aimed at slowing the progression of an incurable condition ALS: i) support the validation of our prodrug ‘proof-of-concept'; ii) establish the neuroprotective ability and limited neurotoxicity of our compounds; iii) demonstrate that a B5-EDR compound is not acutely or chronically toxic; and most importantly, iv) show statistically significant *in vivo* results such as increased survival (days), delayed disease onset, decreased cachexia, and improved ALS biomarkers in the SOD1-G37R line 42 mouse model (control vs. a B5-EDR analog), v) we filed a patent application (No. PCT/CA2023/051352) and received a positive WIPO ISR, validating our patent as novel and original, containing an inventive step, and demonstrating utility and industrial application. Additionally, these milestones and

preliminary findings have opened up several new scientific avenues for collaboration with various scientists to explore the role of BSZ across multiple disease pathologies.

Overall, our goal is to develop biomarker-driven dual-role B5-EDR analogs as effective candidate ALS therapeutic(s), in terms of improved ALS biomarkers compared to EDR, while simultaneously understanding the biomarker signature of the FDA/Health Canada-approved drug EDR. Above all, our study provides new experimental bases for considering the use of the boron class of compounds as a pharmacological treatment for ALS.

Our project highlights several other impactful results that should attract significant interest and hold scientific significance for future studies and collaborations, summarized below:

- To the best of our knowledge, this is the first time we have tailored the existing FDA-approved EDR molecule to include a biologically compatible boron element in the scaffold. The newly developed small organic molecule Borsantrazole is a trifunctional boron-based pyrazole, with three proposed modes of action that position our drug to become a ‘best-in-class’ ALS therapeutic. Our strategy, which leverages the principles of both medicinal chemistry and neuroscience, is highly innovative. We aim to utilize boron functional groups as key mediators of therapeutic action in ALS, a strategy that is currently underdeveloped and rare in the vast scientific literature.
- To the best of our knowledge, this is the first time we have utilized green chemistry approaches to synthesize EDR. Synthesis of EDR involves chemoselective *ipso* hydroxylation of boron-based prodrug (NS-1-2) under microwave conditions. Bio-based green reagents, which are biocompatible and non-toxic, like boronic acid

ester, trifloroborates, lactic acid, and hydrogen peroxide, were utilized for the synthesis of EDR. The present innovation passed the litmus test from WIPO with the assessment for novelty, inventive step, and industrial applicability.

- To the best of our knowledge, this is the first time we've used the Amplex Red assay to evaluate the H_2O_2 scavenging ability of our novel NS-1-2 containing boronated scaffold. The innovative approach of boronates in scavenging free radicals can be adopted by other scientists to develop boronates as free radical scavengers for the treatment of neurodegeneration.
- To our knowledge, this is the first development of an SOD1 fibrillization assay to examine the anti-fibrillization activity of SOD1 with NS-1-2. This innovative approach, demonstrating boronates' capacity to inhibit SOD1 fibrillization, can be adopted by other researchers to develop boronates as potential anti-SOD1 fibrillization agents for neurodegenerative diseases.
- To the best of our knowledge, this is the first time we have conducted discovery-based, global, untargeted, and unbiased proteomic and phosphoproteomic analyses that link our observed efficacy with known and unknown ALS-related protein and phosphoprotein expression levels. Our proteomic and phosphoproteomic findings are likely to have a significant impact on the field, as we demonstrate changes in ALS-associated biomarkers in response to drug treatment. Overall, we identified 51 proteins and 29 phosphorylation sites with statistically significant expression changes. These findings include notable alterations in the levels of both known and unknown neurodegenerative biomarkers. This innovative approach, which demonstrates boronates' ability to

differentially regulate known and unknown proteins and phosphoproteins in preclinical SOD1 models of ALS, can be adopted by other researchers to develop boronates as potential agents to slow the progression of ALS and other neurodegenerative diseases, including aging.

- To the best of our knowledge, for the first time, we have discovered statistically significant changes in the phosphorylation of neurofilament light and heavy chain, which is correlated with drug treatment (downregulation) at threonine sites. Hyperphosphorylation of neurofilaments negatively correlates with the survival of preclinical ALS mouse models and in clinical human ALS cases. Further, neurofilaments are regarded as a pharmacodynamic marker and a biomarker for the diagnosis and prognosis of ALS. To the best of our knowledge, there are no reports in the literature of phosphorylation of threonine sites associated with ALS, T72 for Nefh and T317 Nefl, reported herein. Additionally, there are very few reports that can correlate the therapeutic effects observed in animal models with differential protein and phosphoprotein expression following discovery-based global, untargeted, and unbiased proteomic and phosphoproteomic analysis. These results have the potential to serve as a notable example of the correlation between observed therapeutic effects and biomarkers. Furthermore, these results will be crucial in demonstrating the proof-of-concept pharmacodynamic properties of our drug, NS-1-2, thereby showcasing the translational value from bench to bedside.
- To the best of our knowledge, for the first time, we have done a symptom onset biomarker study to see the effects of NS-1-2 versus controls during symptom onset

on differential regulations of cellular proteins. The findings from the proteome profile at symptom onset in the G37R mice model have identified new druggable targets associated with neurogenerative disease. Furthermore, this new symptom-onset biomarker study found links between ALS and other neurodegenerative diseases like AD.

7 Limitations of the study

The current early-phase drug discovery offers a unique approach to synthesize, characterize, and develop compounds that could slow the progression of highly complex and incurable ALS. This preclinical study encompasses various aspects of drug discovery, including a medicinal chemistry approach to rationalize the synthesis of improved versions of FDA-approved EDR, the synthesis of EDR prodrugs and analogues, and the characterization of these compounds. *In vitro* screening of compounds (analogues and NS-1-2) for safety and efficacy, *in vivo* screening of NS-1-2 in a humanized preclinical SOD1 model of ALS, and global proteomics and phosphoproteomics to identify new druggable targets for the synthesized molecule NS-1-2. While the current study provides valuable insight into various phases of early phase drug discovery, it is crucial to acknowledge various limitations that require careful consideration when interpreting the findings.

- Our findings in the PCNC experiments demonstrated the safety profile of EDR analogues and EDR prodrugs. However, due to time constraints and our primary focus on developing the compounds in preclinical models, we were unable to perform free radical challenge assays (in the presence of H_2O_2) with our compounds. Therefore, further studies are needed to investigate the free radical scavenging ability of our compounds in PCNC cells.
- Furthermore, to advance our primary goal of conducting *in vivo* experiments with only the EDR prodrug NS-1-2, we performed most of the *in vitro* and biochemical assays for NS-1-2. This was to support our hypothesis that NS-1-2, a direct prodrug of EDR, could be a promising candidate for further *in vivo* preclinical

studies. This is why; after analyzing the *in vitro* profiling of all synthesized compounds (EDR analogues and EDR prodrugs) in NSC-34 cells, we further evaluated their safety in a more biologically relevant PCNC to better support and confirm our safety hypothesis. Therefore, following the NSC-34 and PCNC experiments, we performed additional tests using only NS-1-2, including JC-10 mitochondrial potential, Amplex Red, and SOD1 fibrillization assays.

- A single concentration of 25 μM for all compounds was used to examine the influence of molecules on the modulation of SOD1 monomer fibrillization. Future studies are needed to explore the effects of these molecules on SOD1 monomer fibrillization under varying conditions, including the use of different concentrations of molecules, extended incubation periods, temperature changes, and increased plate agitations.
- In our *in vivo* efficacy studies, EDR was not employed as a comparison group to evaluate the *in vivo* efficacy of NS-1-2 relative to EDR. This decision was primarily due to resource limitations and time constraints. However, we have included the EDR group in the approved animal protocol. Future investigations comparing NS-1-2 with EDR are necessary in G37R preclinical models.
- In the initial phase of our *in vivo* global untargeted, unbiased proteomics and phosphoproteomics study, only male mice were utilized to assess the differential regulation or alterations of proteins and phosphoproteomics between the NS-1-2-treated group and the vehicle-treated group. This decision was based on the observation that male mice exhibited higher survival rates compared to the female group, with statistically significant differences (***p=0.0192*** versus ***p=0.2972*** for

females). However, further studies are needed to determine the global proteomics and phosphoproteomics of female mice.

- Further, for a global, untargeted, unbiased proteomics and phosphoproteomics study, we utilized samples from the humane endpoint or the end stage of male mice from both the NS-1-2 and control-treated groups. Future global profiling of proteomics and phosphoproteomics is necessary during each clinical stage of progression in mice, encompassing the presymptomatic stage (where disease is active, but no symptoms are present), the onset of disease, symptom onset, humane endpoint, and end-stage disease.
- In our symptom onset biomarker study, we used only female mice (n=3) to profile the global, untargeted, and unbiased proteomics, depending on the availability of animals. However, we have included the males in the approved animal protocol. Further studies are needed to profile the males and consider sex-specific differences.

8 Future directions of the study

The present early-phase drug discovery study provides medicinal chemistry approaches and strategies for synthesizing, characterizing, and developing compounds that could slow the progression of highly complex and incurable ALS. Furthermore, this study has opened several avenues that require direction in the future to significantly advance current research from the bench to the bedside.

- In the present study, we have used NSC-34 cell lines (to evaluate safety and efficacy against free radical challenge) and PCNC (only for safety evaluation) for the *in vitro* evaluation of our compounds. However, future experiments are needed to investigate the effects of our compounds (EDR analogues and EDR prodrugs) in biologically relevant PCNC cells. Using PCNC culture to screen the efficacy of drugs is challenging compared to cell line culture, which will be overcome by training from experts and collaboration efforts.
- Repeated experiments will be conducted to assess the ability of our compound to inhibit SOD1 fibrilization activity. In the current study, we have used only NS-1-2 to evaluate the SOD1 fibrilization activity with different controls. Furthermore, we used a concentration of only 25μM in these experiments. Intrigued by these results, further experiments will be conducted with other molecules under varying experimental conditions.
- Further, ALS is a highly complex and multifactorial disease. Applying cell lines and animal models cannot accurately reflect the pathological characteristics of ALS. Therefore, induced pluripotent stem cells (iPSCs) -derived motor neurons are crucial for understanding the complex mechanisms of motor neuron dysfunction

and death both in spinal cord and brain of ALS patients. iPSCs are highly relevant for ALS research because they allow scientists to reprogramme the skin or blood cells from someone living with the disease and turn them into motor neurons and other relevant cells specific to ALS pathology. Further, iPSCs can be derived from somatic cells of both forms of ALS, i.e., fALS and sALS, possessing the ability to self-renew and differentiate into a variety of motor neuronal and non-neuronal glial cells. Moreover, patient-derived iPSCs are generated from the patient's own somatic cells, mitigating ethical concerns and reducing the risk of immune rejection. These patient-specific iPSCs offer a valuable opportunity to screen potential lead compounds, study ALS-specific motor neuron disease mechanisms, and develop personalized treatment strategies[513-516]. Therefore, our future plan is to collaborate with experts to evaluate the toxicity and efficacy of our drug, as well as its pharmacodynamic mechanisms in iPSC-derived motor neuronal cells relevant to human ALS. This approach will enable us to screen multiple drugs efficiently using high-throughput methods and ultimately select a lead clinical candidate to transition from basic research to the bedside of ALS patients[517].

- Preclinical *in vivo* CNS studies often do not report PK results. For successful translation from preclinical to clinical research, it is crucial to consider the various ADME profiles of the drug. Recent studies also demonstrate that tolerable and pharmacologically active dose ranges in human clinical trials can be predicted accurately from preclinical data. Therefore, it is essential to investigate the different dose effects in animals with the investigational drug before submitting the Investigational New Drug (IND) document to initiate the regulatory approval

process for human clinical trials. In the current study, we used 10mg/kg body weight of NS-1-2 in the *in vivo* studies; however, our future plan is to test different doses of our lead molecule, NS-1-2, to determine the no observed adverse effect level (NOAEL): The maximum dose in animal species that does not produce a significant increase in adverse events when compared to those in the control group and the pharmacologically active dose (PAD): The lowest dose tested in animal species with intended pharmacological activity[518]. This will prepare us to move forward with preparing the IB with preclinical data, paving the way for human clinical trials.

- **Copy number determination:** Assessing the mutant SOD1 copy number is a crucial part of ALS research. The variability of transgene levels within treatment groups can influence disease symptoms and pathology and also impact the reproducibility of drug effects. In this study, we conducted validated and reproducible genotyping to determine the SOD1 transgene presence before using the animals and creating the cohorts[519]. Additionally, we made efforts to randomly assign littermates with matched age and sex to different groups. However, for better clinical translation from preclinical to human applications, we plan to determine the copy number of each mouse before randomly assigning them to different groups. This approach will help reduce variability and improve the reliability of preclinical findings.
- **Presymptomatic treatment:** In the current project, we have determined the efficacy of NS-1-2 in humanized mutant SOD1 G37R line 42 mice, which is an early-onset and highly aggressive preclinical model for ALS. It recapitulates the

clinical motor phenotypes and pathophysiology of ALS in humans. Also, the model is clinically relevant. Previous studies in patients carrying different SOD1 mutations indicate that mutations with SOD1 gene mutations often experience early onset, highly aggressive disease course, and shorter survival compared to other forms of ALS[19]. The age of onset and disease duration are key indicators of disease severity among SOD1-related ALS patients, with the majority of patients suffering from early onset disease at the age of less than 50 years[520]. Therefore, we have stated the treatment pre-symptomatically in our *in vivo* efficacy studies to delay the onset and different motor disease phenotypes of ALS models. In-addition, we started treatment presymptomatically, to delay the phenoconversion of disease, which is again clinically relevant to the patient suffering from SOD1 mutations[501]. However, a significant delay in diagnosis is common for patients with SOD1 mutations. This delay happens because SOD1-related ALS can look like other neurological conditions, and SOD1 mutations are not always easy to detect. Therefore, our approach is patient-first and patient-centric. We want to cover all patients irrespective of whether they are presymptomatic or at different clinical stages of the disease. Therefore, in the future, we are planning to investigate our treatment at different stages of disease progression in the G37R mouse model.

- **TDP-43 drug discovery:** Oxidative stress due to free radicals mainly H_2O_2 is implicated in the pathophysiology of all forms of ALS (sALS and fALS)[378]. Proteinopathy due to oxidative stress is reported in the postmortem tissues of patients suffering from both forms of ALS[521]. A large number of studies have established that more than 90% of ALS cases exhibit TDP-43 proteinopathy[522].

Furthermore, previous studies have reported that the TDP-43 proteinopathy is caused by the free radical-induced oxidative stress[427, 523]. Our study has demonstrated that NS-1-2 works as a redox regulator by reducing the oxidative stress implicated in the pathophysiology of ALS. Therefore, in the future, our goal is to target TDP-43 proteinopathy first in TDP-43 animal models to establish the safety and efficacy profile of NS-1-2 during different stages of disease progression in these models.

- Consideration of sex and gender effects, which merit consideration to remove bias and generalizability: There is accumulating evidence that ALS affects males more than females, and gender plays an important role in the clinical progression of the disease. However, variations in clinical presentations like progression of disease, onset of disease, symptom onset of disease, survival, motor phenotypes, weight loss, spinal onset, and bulbar onset are not fully understood[524, 525]. Health research becomes more reliable when both sexes are well represented, from preclinical studies to clinical trials. Additionally, it helps prevent the assumption that findings in one sex of animals can be applied to both males and females. In addition, Increasing the number of animals, matched for age and sex with their littermates in a study, generally enhances the statistical power of the analysis, making it more likely to detect a significant effect. Currently, we have results from a whole set of animals with a sample size of N = 12 per group. We have considered sex-specific differences in N=12/group; however, it is essential to consider sex-specific differences in larger cohorts, which increases the power and reliability of the study. In our early-phase drug discovery project, we will take every

responsibility to evaluate the sex-specific differences of our best-in-class molecule NS-1-2 (Borsantrazole). The following will be considered to assess sex-specific/gender-specific differences once the clinical effect size of N=24/group is reached. We will then reanalyze once the sample size reaches a larger clinical effect size of N=24/group: Treatment-associated decrease in body weight in both sexes; Treatment-associated hematological toxicity in tissues of both sexes; Treatment-associated change in clinical motor phenotypes in both sexes; Treatment-associated change in clinical progression of disease in terms of onset of disease, symptom onset, survival, and weight loss; and Treatment-associated change in global proteome and target engagement in both sexes. We believe that the above evaluations will highlight the importance of considering sex-specific factors in understanding the complex ALS pathophysiology and provide insight into how our new molecule affects clinical phenotypes or progression in males and females. Further, this will help design tailored therapeutic strategies in the future[525].

- **Targeted proteomics and phosphoproteomics:** Targeted quantitative proteomics and phosphoproteomics play a vital role in linking biomarker discovery with clinical application. It allows for precise, quantitative analysis of specific proteins, offering high sensitivity, reproducibility, and throughput, essential qualities for creating reliable clinical assays. This approach is particularly utilized for validating potential biomarkers identified through global discovery proteomics, thereby aiding in their development into diagnostic and prognostic tools[526]. Initially, in this early phase of the drug discovery approach, we have been doing

profiling of global unsupervised proteomics and phosphoproteomics to correlate the efficacy of the newly synthesized EDR prodrug NS-1-2. This approach is used because we do not yet know the specific targets or cellular proteomic pathways affected by NS-1-2 compared to the control. Once we identify both the known and unknown proteomic pathways involved in the neurodegeneration of G37R mice, we will use targeted proteomics to validate the targets and assess the druggability of NS-1-2. Applying both global and targeted proteomics will help us understand the mechanism, ultimately enabling us to translate the drug from the lab to clinical use with a validated pharmacodynamic profile.

- **Global lipidomics:** ALS affects motor neurons in both the brain and spinal cord. The entire brain, including myelin and other cell structures, contains about 50-60% lipids of its dry weight[527]. Evidence from a large number of studies has demonstrated that perturbations in lipid metabolism profiles and changes in their biophysical properties are present in ALS. These changes involve modifications in cholesterol, triglycerides, sphingolipids, and phospholipids, which are associated with different clinical stages of disease progression[528]. Moreover, multiple pathways are disrupted during the pathophysiology of ALS[493]. Furthermore, the changes that occur during the clinical progression of the disease can be used for prognosis and diagnosis of ALS[529]. Therefore, our future goal is to profile changes in lipids during different clinical stages of ALS progression while conducting efficacy studies with NS-1-2 versus control in G37R mouse models. Our approach will be to perform longitudinal, global, untargeted, and unbiased lipidomic analysis of the lumbar spinal cord and brain from the G37R ALS mouse

model, which will provide us with new insights into the multiple lipid pathways of lipid dysregulation in ALS.

- **Aging drug discovery:** Ageing population is a risk factor for ALS[530]. Multiple studies have identified shared cellular and molecular features between ageing and ALS. The main common drivers include genomic instability, telomere shortening, epigenetic changes, proteostasis failure, autophagy dysregulation, and mitochondrial issues[531]. Nevertheless, both ageing and ALS are complex conditions involving multiple systems, and their precise causes remain unclear. Additionally, understanding the biochemical pathways involved in ageing could help us decode the risk factors for ALS, which tend to rise with age. The current body of evidence suggests that oxidative modifications of the central dogma, including DNA, RNA, and proteins, are implicated in the pathophysiology of both aging and ALS. Moreover, proteinopathy due to oxidative stress is known for both ageing and ALS[532, 533]. In this project, we demonstrated that NS-1-2 functions as an antioxidant redox regulator. Additionally, proof-of-concept studies using humanized SOD1 G37R mice showed that NS-1-2 can extend lifespan and modify motor disease phenotypes. Our comprehensive proteomics and phosphoproteomics analyses identified shared and converging biomarkers of aging and ALS. This research opens up the possibility of using NS-1-2 to slow the aging process in the future.
- **Platform drug discovery:** In this project, we have synthesized six novel molecules as EDR analogues and prodrugs. All the six molecules have shown an excellent safety profile in *in vitro* cell lines and PCNC cells. Also, all the molecules

have shown the potential of reducing free radicals (H_2O_2) in an *in vitro* system. Due to limited budget and resources, we were unable to test all the molecules for proof-of-concept in *in vivo* animal models. Therefore, we advanced only one molecule, NS-1-2, to *in vivo* studies. NS-1-2 has demonstrated an excellent safety profile and *in vivo* proof of concept in the preclinical G37R ALS model, we believe other molecules also have the potential to be advanced in earlier clinical stages. However, conducting preclinical studies in a mouse model are resource-intensive and costly. Additionally, it is crucial to employ a de-risking drug discovery approach to enhance the chances of success and maximize the return on investment[534]. Therefore, our future goal is to establish a de-risking platform for drug discovery with increased collaboration efforts, where we will use Drosophila (fruit flies), cave fish, Mexican fish, and zebrafish for screening new molecules. These models are generally more cost-effective than traditional mouse models due to their smaller size, shorter breeding cycles, ease of maintenance, and genetic tractability. These features will enable high-throughput screening, which will reduce both the time and costs associated with drug discovery.

- **International Collaborations: Professor Dame Pamela Shaw, professor of Neurology and director of the Sheffield Institute for "Translational Neuroscience (SiTraN)**, is like a mentor to me. During my visit to present my PhD work on the discovery of BSZ at the ALS MND symposium in Montreal and the Gordon Research Conference in Maine, USA, she showed interest in my work. Currently, she is establishing a drug discovery platform in the UK with the goal of testing small molecules in different iPSC models derived from heterogeneous ALS

patients. During our discussion, she expressed interest in using our molecule alongside others in her platform trials. I will leverage my expertise in coordinating the project from the University of Manitoba, including scientific meetings, discussions, ensuring scientific rigor, and communication about our molecule. This collaboration will help us advance our novel molecule, BSZ, from bench side to clinical trials, creating hope for ALS patients. **Professor Elizabeth Fisher, University College, London.** During my visit to present my PhD work on the discovery of BSZ at the Gordon Research Conference in Maine, USA, she showed interest in my work. Currently, she is establishing TDP-43 animal models in her lab with the goal of testing small molecules in these models. TDP-43 proteinopathy is known to be present in 90% of ALS patients, and there are no established models or drugs to treat the TDP-43-induced pathophysiology of ALS. During our discussion, she expressed interest in using our molecule and wants to collaborate with us to test it in TDP-43 models. I will leverage my expertise in coordinating the project from the University of Manitoba, including organizing scientific meetings, discussions, ensuring scientific rigor, and facilitating communication about our molecule. This collaboration will help us advance our novel molecule, BSZ, from the bench to clinical trials, offering hope to ALS patients.

9 Conclusions

Amyotrophic lateral sclerosis (ALS) is a highly complex, heterogeneous, idiopathic, and multifactorial disease. The endpoint of ALS is always death. However, mutations in the SOD1 gene result in a toxic gain-of-function in SOD1 proteins. These toxic proteins are thought to mediate many biochemical pathological pathways in the brain and spinal cord and cause the degeneration and death of motor neurons. Preclinical transgenic mouse models of ALS and clinical studies from postmortem tissues of human ALS patients demonstrate that the oxidatively modified misfolding of human wSOD1 and mutSOD1 shares a common pathogenic pathway leading to the progressive death of motor neurons. Therefore, oxidatively modified SOD1 due to pathological cellular oxidative stress acts as a common neurotoxic determinant in both forms of ALS, i.e., fALS and sALS. This accumulating evidence from different studies is further supported by the presence of oxidative stress biomarkers during the disease progression of ALS, both in transgenic murine models of ALS and in human ALS patients. Additionally, there is no definitive biomarker that can track disease progression over time or demonstrate target engagement of drugs. Recently, Tofersen received accelerated approval from the FDA based on its ability to reduce neurofilament light chain (NefL), a biomarker of neuroaxonal damage in (SOD1)-ALS patients. However, it is still regarded as a nonspecific biomarker for the diagnosis and treatment of neurodegenerative diseases. Moreover, it raises questions about differentiating different forms of ALS from other neurodegenerative conditions. Furthermore, the potential of neurofilament heavy chain (Nefh) is underestimated due to limitations in assay sensitivity.

Currently, more than 200,000 people around the world live with ALS, and the number is expected to increase by more than 350,000 cases by 2040, yet there is no cure available. Since the discovery of ALS in 1869, only two fully FDA-approved drugs are available: Edaravone (EDR), an antioxidant, and Riluzole (RZ), an anti-glutamatergic agent. Riluzole modestly extends survival in ALS patients by only 2-3 months but fails to demonstrate survival efficacy in the familial mice model of ALS. Furthermore, EDR effectiveness is limited to short-term improvements in physical functional outcomes, with no observed survival benefits in ALS patients. It was repurposed for ALS after being developed as a free radical scavenger and was originally created to treat acute stroke in Japan. However, EDR was approved based on its efficacy in improving the physical functional decline as measured by the ALSFRS-R score and improved quality of life as measured by the ALS 40-item assessment questionnaire.

Regardless of its ineffectiveness in extending survival in both preclinical and ALS patients, EDR offers hope to slow down the progression of ALS. Moreover, the recent clinical pipeline results are unfortunate and disappointing, as drugs fail to meet their primary and secondary endpoints. As a result, there is a large unmet need to find new treatment options for ALS. As part of our current early-phase drug discovery project, we tried to explore and extend the potential of EDR by adding the advantage of a boron scaffold and developing a triple-role antioxidant molecule that can combat the pathological neurotoxic free radical H_2O_2. H_2O_2, a neurotoxin, is implicated in the pathophysiology of ALS in both familial SOD1 ALS mice and human ALS patients.

In our pursuit of finding new avenues to modify the severe disease phenotypes in the familial SOD1 mouse model of ALS, we have developed a ROS-responsive and H_2O_2-

activatable chemoselective boron prodrug of EDR called NS-1-2, which has shown its therapeutic potential in the SOD1-G37R line (42) ALS mouse model (early onset and highly aggressive high copy number) via a proposed triple-role antioxidant effect. The novel bio-based prodrug NS-1-2 demonstrated an excellent safety profile both *in vitro* and *in vivo*. Furthermore, the findings from our early phase drug discovery efforts in a validated familial SOD1-G37R (42) mice model, indicate that the EDR prodrug, NS-1-2, was able to significantly modify motor disease phenotypes in terms of delaying the onset of disease, delaying the symptom onset of disease, extending the life span of SOD1-G37R (42) mice and reducing the ALS induced weight loss/cachexia. Considering that sex is an independent risk factor in the progression of ALS, we have accounted for and further evaluated the treatment response of NS-1-2 in both sexes (age- and sex-matched, males and females) and found that NS-1-2 has profound effects on modifying motor disease phenotypes in the G37R (42) mouse model.

Our approach, which explored the discovery-based, untargeted, and unsupervised differential cellular protein expressions in the lumbar spinal cord and brain of G37R ALS (42) mice, unveiled both known and unknown proteins and phosphoproteins involved in the pathophysiology of ALS. However, we acknowledge that a major limitation of our study was the analysis of samples from male mice (treated vs. untreated) that reached the humane endpoint in our efficacy studies, as well as samples from female mice (treated vs. untreated) in the symptom biomarker study. Intriguingly, the unbiased and untargeted results of differential regulation of cellular proteins correlated with the efficacy of NS-1-2 and indicated that known biomarkers for proteins and phosphoproteins are differentially regulated in the treatment group compared to the control group, which motivated us to

investigate more in defining new preclinical ALS mice cohorts where we could do a longitudinal analysis considering different stages of ALS progression until a humane endpoint validating our current results. Further, the newly discovered unknown proteins and phosphoproteome biomarkers in the ALS mouse models will help us understand the overlapping pathophysiological mechanisms across various neurodegenerative diseases. These observations, for the first time, act as a stepping stone for our novel NS-1-2 redox regulator, which has opened the door to further research into the role of novel molecule EDR prodrug NS-1-2 in treating ALS and linking these biomarkers to the common pathogenic mechanism of other neurodegenerative diseases. We believe that these exciting findings will provide a foundation for developing small molecules incorporating boron and investigating their efficacy in slowing the progression of ALS and other neurodegenerative diseases, such as AD and PD, as well as aging. Further, this novel prodrug strategy should minimize side effects while selectively targeting the CNS, which is vulnerable to pathological H_2O_2 and other neurotoxic free radicals. We anticipate that NS-1-2 could be a novel and effective therapeutic option for targeting the oxidative stress-associated pathology of neurodegeneration and will foster further research into the potential of boron in neurodegenerative diseases, such as ALS. The efficacy results of NS-1-2 support our belief that the prodrug of EDR could fill the gap of lacking translation of FDA-approved drugs from preclinical to clinical studies. In the current invention, we have identified the limitations of our study, including the need for pharmacokinetic studies, to define further better cohorts and endpoints for investigating longitudinal changes in proteomics and phosphoproteomics in response to treatments. Additionally, we recognize the importance of comparing the efficacy of the EDR prodrug to EDR in the G37R (42)

model. We acknowledged these limitations in the present study, and we have started moving forward in these areas to address these limitations. However, we believe that these initial drug discovery innovations in developing EDR prodrugs incorporating boron, with excellent safety, significant efficacy, and discovery-based differential profiling of the global proteome and phosphoproteome at end-stage and symptom onset, will open new avenues for contemplating the role of boron in neurodegeneration therapeutics.

Our idea focused on innovative methods to advance the small organic compound NS-1-2 from a preclinical to a clinical candidate. This effort aimed to protect the intellectual property related to NS-1-2, which is planned for future human trials. After filing a PCT patent application, WIPO provided a strong international search report, confirming that our novel approach to target neurodegeneration in ALS involves an inventive step, has novelty, and possesses industrial utility and applicability. Furthermore, NS-1-2 was developed in our lab and successfully trademarked as Borsantrazole (BSZ) by Innovation, Science, and Economic Development Canada. These milestones reinforce our confidence that NS-1-2 could expand the limited treatment options for ALS. Our early drug discovery results, along with the WIPO ISR report, suggest that NS-1-2 might offer a treatment for all ALS types, regardless of disease cause. Nonetheless, further research into BSZ's pharmacokinetics and biomarker investigations is essential.

10 Total number of compounds synthesized

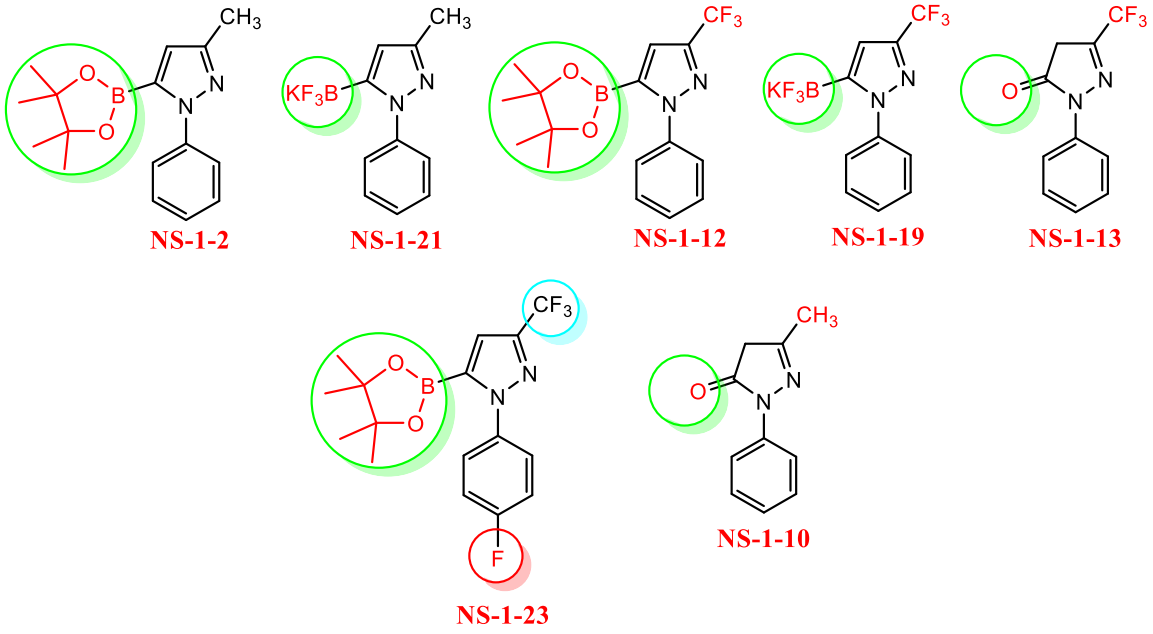

11 Materials, methods, and characterization of organic molecules

11.1 Experimental

General considerations: ^{1}H and ^{13}C nuclear magnetic resonance (NMR) spectra were recorded on a Bruker 500 MHz spectrometer, Billerica, MA, USA, using DMSO-d_6 **(CAS-2206-27-1)**, as a solvent with tetramethylsilane (TMS) as an internal standard. *J* values are given in Hz. Mass spectra were recorded Bruker Daltonik GmbH, LCMS–100-600 (esi.m), Orbitrap Exploris 480, 60K Resolution, ESI Thermofisher (for HRMS) mass spectrometers. Microwave reactions were carried out in the CEM explorer hybrid-12 microwave reactor. n-Butyllithium, 2.5M solution in hexanes, Acros organics **(CAS-109-72-8)** product of Germany; 2-Isopropoxy-4,4,5,5-tetramethyl-1,3,2-dioxaborolane **(CAS-61676-62-8)** purchased from Sigma-Aldrich, St. Louis, MO, USA; 3-Methyl-1-phenyl-1H-

pyrazole (**Number: AK139802**) was purchased from Ark Pharm, Inc., Arlington Heights, IL, USA. Hydrogen peroxide (H_2O_2) **(CAS-7722-84-1)** was purchased from Sigma-Aldrich, St. Louis, MO, USA. Lactic acid **(CAS-7732-18-5)** was purchased from Acros Organics. Potassium hydrogen fluoride (KHF_2), 3-triflоromethyl-1-phenyl-1H-pyrazole, 3-triflоromethyl-1H-Pyrazole, 4-fluorophenylboronic acid, Copper(I) oxide. The reactions were monitored by TLC (Sigma, Silica gel 60 F_{254}). The crude reaction mixture was purified with silica gel column chromatography on a CombiFlash® Rf 200 purification system, Teledyne Isco, USA. Organic solvents were ordered from BDH, VWR Analytical, unless specified otherwise. All chemicals were used without further purification unless stated otherwise.

11.2 Representative experimental procedure for synthesis of *N*-arylated pyrazole boronic acid pinacol ester was carried out according to the below reported procedure with slight modifications, as shown in the Scheme I

Synthesis of Edaravone prodrug (NS-1-2) was carried out according to the reported procedure[535] with slight modifications, scheme I, (**figure 24)**. n-Butyllithium (2.5 M in hexane, 1.5 mL, 3.793 mmol) was added dropwise to a solution of *N*-arylated substituted pyrazole (500mg, 0.471mL, 3.161mmol) in anhydrous THF (22 mL) at -78 °C under argon. The reaction mixture was stirred for 45 minutes at -78°C. 2-Isopropoxy-4,4,5,5-tetramethyl1,3,2-dioxaborolane (646.93mg, 709.5µl, 3.477 mmol) was added dropwise to the reaction mixture at -78°C, and the mixture was stirred for 1.5h. The mixture warmed to room temperature over 1h and glacial acetic acid (208.79mg, 199 µl, 3.477 mmol) was added. The mixture was filtered through a celite pad, which was washed with EtOAc (100 mL). The organic solvent was removed in vacuo to afford a crude product. TLC confirmed

the expected product (20% EtOAc/Hex). The crude product was then purified with silica gel column chromatography on a CombiFlash® Rf 200 purification system, Teledyne Isco, USA, with ethyl acetate and hexane from 0% to 10%. Residual solvent was evaporated under vacuum to a final light brown crystalline solid product (815mg, 90%). Compound (NS-1-2) was synthesized by following this reaction procedure. The structure was characterized by 1H, 13C NMR, ESI, and HRMS.

11.2.1 Characterization

3-methyl-5-(4,4,5,5-tetramethyl-1,3,2-dioxaborolan-2-yl)-1-phenyl1H-pyrazole (NS-1-2): Prodrug of Edaravone, figure 77.

Crystalline solid (815mg, 90%); 1H NMR (500 MHz, DMSO-d6). δH(500 MHz; DMSO-d6; Me4Si) 3.63 (6 H, s), δ 7.50-7.48 (2H, m, *J* = 10Hz), δ 7.47-7.44 (2H, m, *J* = 15 Hz),7.39-7.36 (1H, m, *J* = 15Hz), δ 6.64(1H, S), δ 2.32(3H, S) δ 1.25(12H, S); 13C NMR (500MHz, DMSO-d6) δ 149.2, 141.2, 128.9, 127.5, 117.8, 84.5, 82.7, 24.7, 13.2 (C ipso to B not observed). 11B NMR (500MHz, DMSO-d6) δ 27.8. 1.8. HRMS (ESI) Calcd. for C16H21B1N2O2 [M + H]$^+$ 285.17686., found *m/z* 285.176. For details of ^{1}HNMR, ^{13}CNMR, and HRMS (see appendix 1-6)

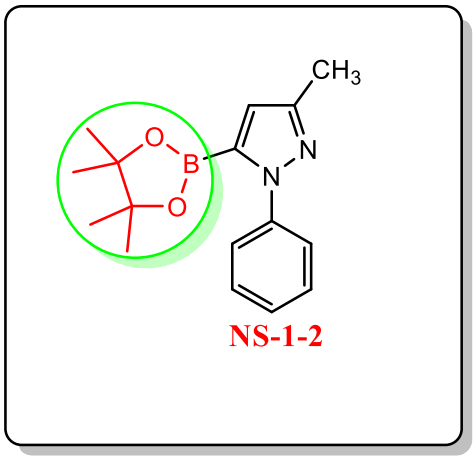

Figure 77. Prodrug of Edaravone (NS-1-2).

11.3 Representative procedure for synthesis of *N*-arylated pyrazole potassium trifluoroborates from *N*-arylated substituted pyrazole boronic acid pinacol ester was carried out according to the below-reported procedure with slight modifications

Synthesis of Edaravone prodrug was carried out according to the reported procedure[344] with slight modifications, scheme II, **(figure 25)**. To a stirred solution of boronic ester (0.5 mmol) in methanol (3 mL) was added potassium hydrogen fluoride (KHF_2) (0.5 mL of 4.5M saturated aqueous solution, 0.5 mmol, 2.25 equiv., 1.125-fold excess) was added dropwise. The resulting mixture was stirred at room temperature, and the progress of the reaction was monitored by TLC after every 15 minutes. The reaction was completed with a new spot in the TLC after 1hrfor and 2.5hr for. The resulting crude reaction mixture was filtered using 11cm Whatman's filter paper and the filter paper was washed thoroughly with hot acetone to filter all the product from the crude reaction mixture. The residue left in the filter paper is a white amorphous solid, which was dissolved in ethyl acetate and TLC was observed under UV. There was no spot corresponding to the product. The filtrate was concentrated in vacuo to remove all the volatile material. The resulting waxy syrup was re-dissolved in 50% aq. MeOH (4 mL) and all volatile materials were evaporated again on a rotary evaporator (5-1 mbar/45–50 C; undesirable bumping of the mixture can be significantly minimized by adjusting the rotation speed). This Evaporation–dissolution cycles were repeated until 1H NMR analysis of an aliquot of the reaction mixture showed less than 1 mol% of pinacol. The evaporation–dissolution cycles were optimized for the synthesis of prodrugs. The optimized cycled were 10 for synthesis of prodrug. The final concentrated residue obtained as an amorphous solid, which was finally dried over a

desiccator overnight to give the product as a white amorphous solid (815mg, 90%). Some minor loss of product is mainly associated with evaporation/drying/substance transfer manipulations. Compound (NS-1-21) was synthesized by following this reaction procedure. The structure was characterized by 1H, 13C NMR, and Mass confirmed by HRMS (ESI).

11.3.1 Characterization

Potassium trifluoro(3-methyl-1phenyl-1H-pyrazol-5-yl) borate (NS-1-21): Prodrug of Edaravone, figure 78.

Amorphous solid (125.2mg, 94.8%); 1H NMR (400 MHz, acetone-d6) δ 7.27-7.20 (2H, m, J = 16 Hz), δ 6.54-6.50 (2H, m, J = 16 Hz),6.36-6.31(1H, m, J = 20Hz), δ 5.35(1H, S), δ 1.42(3H, S); 13C NMR (300MHz, MeOD-d6) δ 127.8, 125.7, 123.9, 111.3, 74.4, 23.6, 11.5 (C ipso to B not observed). For details of ^{1}HNMR, ^{13}CNMR, and HRMS (see appendix 7-9)

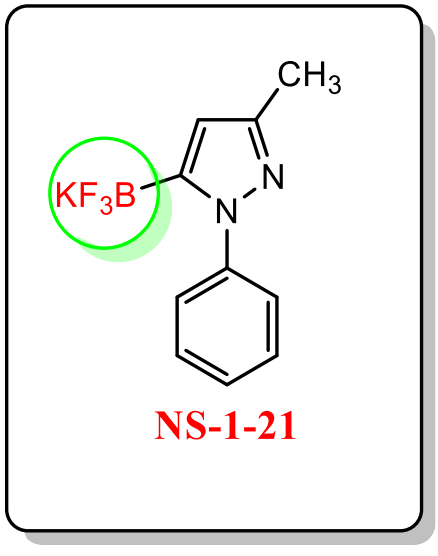

Figure 78. Prodrug of Edaravone (NS-1-21).

11.4 Microwave synthesis of Edaravone from its prodrug (NS-1-2) 3-methyl-5-(4,4,5,5-tetramethyl-1,3,2-dioxaborolan-2-yl)-1-phenyl1H-pyrazole. Utilizing scheme III (a)

The synthesis of Edaravone from its prodrug BSZ is influenced by the bio-inspired catalyst-free reported procedure[536]. Reactions carried out in microwave irradiations **(300Psi, premixed 15sec, 200watt)** were performed on a **0.5**mmol scale. *N*-phenyl-3-methylpyrazole boronic ester **(1.0 equiv.)** and diethyl ether **(3.5mL in excess)** were added to a 10mL microwave vial equipped with a stir bar, followed by the addition of lactic acid **(10 equiv.)** and hydrogen peroxide **(30%w/w, 1.1 equiv.).** The mixture was then capped and placed in the microwave reactor and heated to **50 ^{0}C** for **10** min. After completion of the reaction, the reaction was allowed to cool at RT. The vial was removed from the microwave, and a small aliquot was taken for TLC analysis. A single new spot corresponding to Edaravone was observed under UV in TLC. The reaction mixture was diluted with water (5 mL) and extracted with **(10 mL ethyl acetate and 2 mL hexane).** The organic extract was dried in vacuo and subjected to flash chromatography (EtOAc/hexanes) to afford the desired product. The purified solution obtained after flash chromatography was dried in vacuo to obtain edaravone in the form of a clear oil.

Recrystallization: The clear oily oil was cooled in the ice bath, and a small amount of diethyl ether was added dropwise (0.5-1mL). The resulting oily solution was stirred vigorously in a water bath sonicator for 5 minutes. The white crystalline solid reappeared during sonication. The resulting white crystalline solid was dried completely under vacuum to obtain pure Edaravone. The purified product was sealed with paraffin in the glass vial and stored under 4^{0}C. Compound NS-1-10 (120mg, 84.50%, product

chromatogram NS-1-10 purified) was prepared by this method and imparted 1-d-proton NMR data similar to those reported in the literature for Edaravone.

TLC Observations:

TLC observation of Crude reaction mixture. The TLC was carried out in the solvent system of 50% ethyl acetate and hexane. Rf observed for Edaravone, crude reaction mixture, and the isolated product was found to be equal i.e. 0.55. Edaravone (NS-1-10) was synthesized by following this reaction procedure. The structure was characterized by 1H, 13C NMR, and Mass confirmed by HRMS (ESI).

11.4.1 Characterization

3-methyl-1-phenyl-2-pyrazolin-5-one (NS-1-10): Edaravone, figure 79.

Crystalline solid (120mg, 84.50%); 1H NMR (500 MHz, DMSO-d6). δH(500 MHz; DMSO-d6; Me4Si) 11.42 (OH, s), δ 7.70-7.69 (2H, d, J = 5Hz), δ 7.42-7.39 (2H, t, J = 15 Hz),7.21-7.18 (1H, t, J = 15Hz), δ 5.37(1H, S), δ 2.11-2.10(3H, d); 13C NMR (500MHz, DMSO-d6) δ 171.7, 158.9, 153.5, 139.4, 138.6, 129.2, 125.4, 124.8, 121.0, 118.4, 88.0, 43.4, 17.1, 14.7.HRMS (ESI) Calcd. for C10H10N2O [M + H]+ 175.087753., found *m/z* 175.086. For details of ^{1}HNMR, ^{13}CNMR, and HRMS (see appendix 10-13)

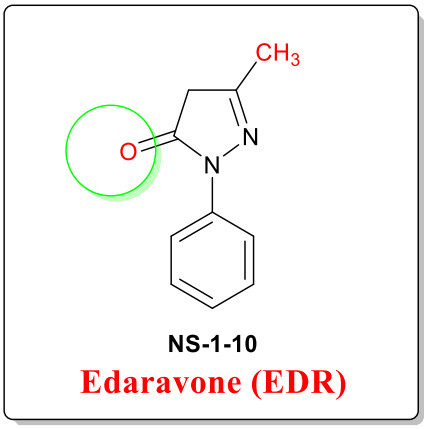

Figure 79. Edaravone (NS-1-10).

11.5 Scheme IV for the synthesis of Boron-based Edaravone analogue (*N*-arylated pyrazole boronic acid pinacol ester) via a two-step synthetic procedure in situ

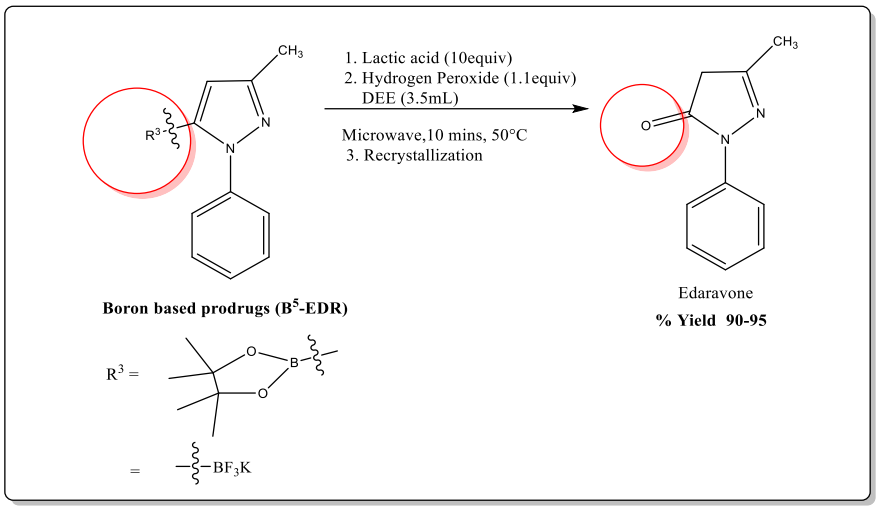

Figure 80. Scheme IV synthesis of EDR analogues.

11.5.1 Characterization

3-triflouromethyl-5-(4,4,5,5-tetramethyl-1,3,2-dioxaborolan-2-yl)-1-phenyl1H-pyrazole (NS-1-12), figure 81.

Crystalline solid (902mg, 91.9%); 1H NMR (400 MHz, CDCL3-d6) δ 7.55-7.52 (2H, m, J = 12Hz), δ 7.45-7.41 (3H, m, J = 16 Hz),7.11(1H, S), δ 1.26(12H, S); 13C NMR (300MHz, DMSO-d6) δ 142.6, 142.1, 140.4, 129.3, 129.2, 125.3, 115.2, 85.1, 24.7 (C ipso to B not observed). For details of ^{1}HNMR, ^{13}CNMR, and HRMS (see appendix 14-16)

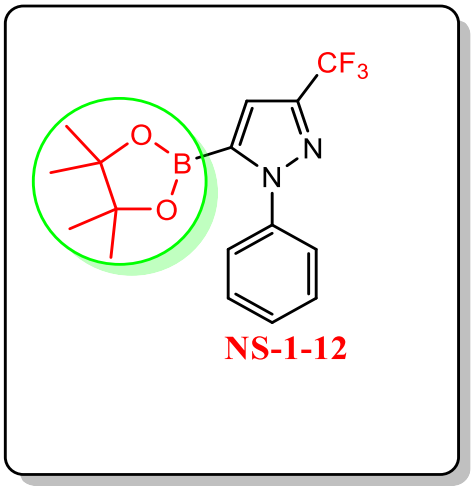

Figure 81. Boron Edaravone (B5-EDR) analogue (NS-1-12).

Potassium trifluoro(3-triflouromethyl-1phenyl-1H-pyrazol-5-yl)borate (NS-1-19), figure 82.

Amorphous solid (143.5mg, 90.2%); 1H NMR (400 MHz, acetone-d6) δ 7.27-7.20 (2H, m, J = 28 Hz), δ 6.67-6.63 (2H, m, J = 16 Hz),6.56-6.52 (1H, m, J =16Hz), δ 5.86(1H, S); 13C NMR (300MHz, acetone-d6) δ129.6, 127.9, 127.6, 126.1, 123.5, 119.4, 28.9 (C ipso to B not observed). For details of ^{1}HNMR, ^{13}CNMR, and HRMS (see appendix 17-19)

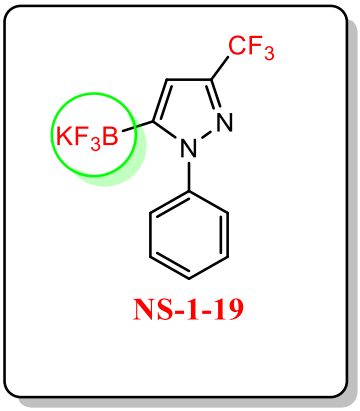

Figure 82. Boron Edaravone (B5-EDR) analogue (NS-1-12).

11.6 Representative experimental procedure for synthesis of 3-trifluoro-methyl-5-(4,4,5,5-tetramethyl-1,3,2-dioxaborolan-2-yl)-4-Fluoro-1-phenyl1H-pyrazole was carried out according to the below-reported procedure with slight modifications

The first step involves *N*-Arylation of pyrazoles with Arylboronic Acid at ambient conditions. 1mol% Cu_2O (10mmol, 1.02eq.) was added to a mixture of pyrazole (10mmol, 1equiv) and arylboronic acid (10mmol, 1.2eqiv) in MeOH (3ml/mol) at r.t., and the mixture was stirred for 5h under an atmosphere of air. The progress of the reaction was monitored by TLC and on completion of the reaction, the crude reaction mixture was concentrated under reduced pressure to give the crude product. The crude product was then purified with silica gel column chromatography on a CombiFlash® Rf 200 purification system, Teledyne Isco, USA, with ethyl acetate and hexane from 0%-2%. Residual solvent was evaporated under vacuum to give the light green waxy syrup, which, when kept in an ice bath for 20 minutes, appeared as green crystals to give the product as a light green crystalline form (2096mg, 90.8%). Compound (NS-1-22) is synthesized by following this reaction procedure. Their structures were characterized by 1H and 13C NMR.

In the second step n-Butyllithium (2.5 M in hexane, 1.4 cm^3, 3.5mmol, 1equiv.) was added dropwise to a solution of *N*-arylated substituted pyrazole (667mg, 2.9mmol, 1equiv.) in anhydrous THF (20 cm^3) at -78 ◦C under argon. The reaction mixture was stirred for 45 min at -78°C. 2-Isopropoxy-4,4,5,5-tetramethyl1,3,2-dioxaborolane (620µl, 3.1mmol, 1equiv.) was added dropwise to the reaction mixture at -78 ◦C and the mixture was stirred for 1.5 h. The mixture was warmed to room temperature over 1 h and glacial acetic acid (180µl, 3.2mmol) was added. The mixture was filtered through a celite pad, which was washed with EtOAc (100 cm3). The organic solvent was removed in vacuo to afford a

crude product. The expected product confirmation was done by TLC (20% EtOAc/Hex). The crude product was then purified with silica gel column chromatography on a CombiFlash® Rf 200 purification system, Teledyne Isco, USA, with ethyl acetate and hexane from 0% to 5%. Residual solvent was evaporated under vacuum to give the crude product in the form of a waxy syrup. The syrup was dissolved in pure hexane and kept in -80 °C overnight. After 12h hexane was removed by rotavapor, and the product was isolated as crystals (556mg, 53.8%), under room temperature. Compound **(NS-1-23)** is synthesized by following this reaction procedure. Their structures were characterized by 1H and 13C NMR.

11.6.1 Characterization

3-triflouromethyl-5-(4,4,5,5-tetramethyl-1,3,2-dioxaborolan-2-yl)-4-flouro-1 phenyl1H-pyrazole (NS-1-23), figure 83.

Crystalline solid (556mg, 53.8%); 1H NMR (300 MHz, DMSO-d6) δ 7.66-7.61 (2H, m, J = 15Hz), δ 7.36-7.22 (2H, m, J = 42Hz),7.22(1H, S), δ 1.20(12H, S); 13C NMR (300MHz, DMSO-d6) δ 142.6, 136.9, 127.8, 127.7, 116.1, 115.8, 115.2, 85.0, 24.8 (C ipso to B not observed); F19 NMR (300MHz, DMSO-d6) δ -60.32. For details of ^{1}HNMR, ^{13}CNMR, and HRMS (see appendix 20-23).

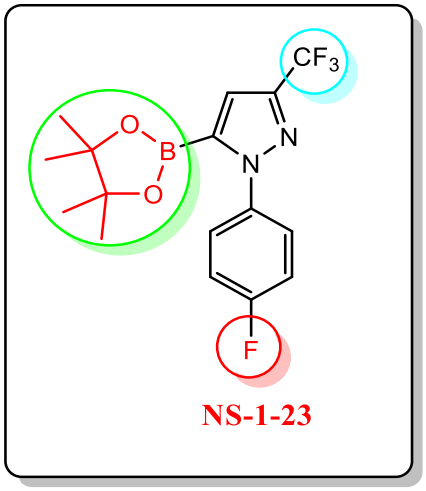

Figure 83. Boron Edaravone (B5-EDR) analogue (NS-1-23).

11.7 Representative experimental procedure for NMR kinetics

NS-1-2 and EDR were added to D_2O containing H_2O_2, and the changes in the proton chemical shift signal were monitored over time. Stock solutions of 40 mM of NS-1-2 and EDR were prepared in dDMSO in a 1.5 ml tube and vortexed. Stocks of 400 mM of H2O2 were prepared from 8.8 M (30% w/w) stock solutions. First, 6 M H_2O_2 was prepared by diluting 8.8 M H_2O_2 with deuterated water (dH_2O). Finally, 400 mM of H_2O_2 was added to the 40 mM NS-1-2 and EDR stocks at room temperature. The resulting mixture of NS-1-2 and EDR in H_2O_2 was transferred to NMR capillary tubes for analysis using a Bruker Avance III 500 MHz NMR.

11.8 Methodology for neurotoxicity/cell viability analysis of EDR prodrug NS-1-2 in primary cortical neuronal cells (PCNC)

Briefly, the cerebral cortex was isolated from the fetus of the mouse at about 17-18 days gestation. After meninges and blood vessels were removed, the tissue was digested with trypsin for about 15 min at about 37°C, then incubated with DNase for about another

15 min at about 37°C and terminated with DMEM plus about 10% fetal bovine serum. After the supernatant was removed, the tissue was added with about 5-ml neurobasal medium (Life Technologies Inc) and triturated by gently pipetting. Neuronal cells contained in the supernatant were transferred to poly-D-lysine-coated plastic culture plates, adjusted to approximately 106 cells/ml, and cultured in neurobasal medium with GS21 supplements (Sigma–Aldrich Canada), 1X GlutaMax (Life Technologies Inc,) and about 1% penicillin–streptomycin at about 37°C under about 5% CO2. About 100k cells/100µl/well were seeded in 96 well plates for 2Div. At 2Div, the neurons were treated with different concentrations of EDR (1, 10, and 25 µM) and EDR analogues NS-1-2, (1, 10, and 25 µM) and incubated until 8Div. On the 8th Div of neurons, about 10 µl of WST reagent was added to each well and incubated for about 2h. After about 2h of incubation, the absorbance of soluble coloured formazan dye was measured calorimetrically at about 450nM using a microplate reader (Biotek instruments) with the background control as a blank. The cell viability was determined by comparing the absorbance of compounds treated cells to that of control cells. Data are representative of two independent experiments, with each measurement or dose tested six times.

11.9 Methodology for neurotoxicity/cell viability analysis of EDR prodrug NS-1-2 in neuroblastoma-spinal cord hybrid (NSC-34) cells

Briefly, NSC-34 cells with about 20k cells per well in 96 well plates were cultured in a complete medium consisting of high glucose Dulbecco's modified eagle medium (DMEM) (Thermo Fisher Scientific) supplemented with about 10% US-origin fetal bovine serum (Thermo Fisher Scientific), GlutaMAX-1, about 200 mM (100X) (Thermo Fisher Scientific), about 1% 100 mM Sodium pyruvate and about 1% 10,000 U/mL penicillin-streptomycin

solution (Thermo Fisher Scientific) for about 20h to reach confluency of about 70% - 80%%. All the cells were cultured in an incubator with about 5% of CO_2 at about 37°C. About 20k cells/100µl/well were seeded in 96 well plates for about 20h in triplicates. Cells were treated with different concentrations of NS-1-2 (and incubated for about 20h. About 10 µl of WST reagent was added to each well and incubated for about 2.5h. After about 2.5h of incubation, the absorbance of soluble coloured formazan dye was measured calorimetrically at about 450nM using a microplate reader (Biotek instruments) with the background control as a blank. The cell viability was determined by comparing the absorbance of compounds treated cells to that of control cells. All the experiments were repeated at least three times and measurements were run in triplicates.

11.10 Methodology for neuroprotective effect/cell viability analysis of EDR prodrug NS-1-2 in neuroblastoma-spinal cord hybrid (NSC-34) cells

Briefly, NSC-34 cells with about 20k cells per well in 96 well plates were cultured in a complete medium consisting of high glucose Dulbecco's modified eagle medium (DMEM) (Thermo Fisher Scientific) supplemented with about 10% US-origin fetal bovine serum (Thermo Fisher Scientific), GlutaMAX-1, about 200 mM (100X) (Thermo Fisher Scientific), about 1% 100 mM Sodium pyruvate and about 1% 10,000 U/mL penicillin-streptomycin solution (Thermo Fisher Scientific) for about 20h to reach confluency of about 70% - about 75%. All the cells were cultured in an incubator with about 5% of CO2 at about 37°C. About 20k cells/100µl/well were seeded in 96-well plates for about 20h in triplicate. After about 20h, the media was changed, and the cells were pre-treated or prophylactically treated with different doses of EDR analogue (NS-1-2) and EDR for about 1h. After about

1h, the cells were treated with 250 µM of H_2O_2 for about 2h. After a total period of about 3h, about 10µl of WST-8 reagent was added to each well, and the absorbance readings were recorded after about 2.5h at about 450nm. All the experiments were repeated at least three times, and measurements were run in triplicate.

11.11 Methodology for assessment of mitochondrial membrane potential (ΔΨM) as an indicator of neurotoxicity in NSC-34 cells using JC-10 probe

Mitochondrial membrane potential was measured according to the manufacturer's protocol (Sigma-Aldrich) with some modifications. 20k NSC-34 cells/100µl/well were seeded in 96-well plates for 20h in triplicates. After 20h, the cells were treated with different concentrations of Edaravone analogues, Edaravone, and staurosporine as a negative control for 20h. After 20h, the media was aspirated carefully, and an equal amount of PBS was added at RT and incubated for 10 minutes. 50 µl/well of JC-10 loading dye solution was added after 10 minutes, and the cells were incubated for 30 minutes. After 30 minutes, 50 µL/well of assay buffer B was added and incubated for 10 minutes. The fluorescence intensities for both J-aggregates and monomeric forms of JC-10 were monitored and measured at Ex/Em=490/525nm and Ex/Em=540/590nm with (BioTek, Gen5 Microplate Reader).

11.12 Methodology for amplex red assay to determine the hydrogen peroxide (H_2O_2)-scavenging ability of EDR and NS-1-2

The assay was performed using Amplex™ Red Hydrogen Peroxide/Peroxidase Assay Kit, Catalog number: A22188, Invitrogen™. H_2O_2 solution (88 mM) was mixed with different working solutions of Edaravone or NS-1-2 and incubated at RT for 30 min. After

30 minutes, the reaction was initiated by adding Amplex Red (100 µM) to a final reaction volume of 100 µl and incubating at room temperature (RT) for 30 minutes. The final concentration of Amplex Red reagent was (50µM) in the HRP working solutions. Note that the reaction was carried out in the absence of light. The H_2O_2 scavenging ability of the compounds was measured by fluorometric assay at (em/ex=590nm/530nm). In the presence of Horseradish peroxidase (HRP), an Iron (Fe)-metalloenzyme, the Amplex Red reagent reacts with H_2O_2 in a 1:1 stoichiometric ratio to produce the red fluorescent oxidation product, resorufin.

11.13 Methodology for SOD1 monomer fibrillization assay using thioflavin T fluorescence

All solutions were filtered through a 0.22-µm syringe filter before use. Briefly, a 1 mM thioflavin stock was prepared in cold PBS (pH 7.4). Then, 25 µM of ThT was prepared by diluting 1.25 mL of a 1 mM ThT stock solution in 50 mL of cold PBS and kept at room temperature (RT). Preparation of SOD1 monomers: Human recombinant superoxide dismutase protein monomer (expressed in E. coli) was purchased from Stress Marq Biosciences INC. **(Catalog No. SPR-435), Lot No. MH588110**. SOD1 monomers stored at -80°C were thawed on ice (4°C) for 1.5 hours. Preparation of SOD1 fibrils: Human recombinant superoxide dismutase protein preformed fibrils (expressed in E. coli) were purchased from Stress Marq Biosciences INC. **(Catalog No. SPR-470), Lot No. PH788120**. SOD1 preformed fibrils stored at -80°C were thawed at room temperature (RT) and sonicated for 1.5 hours. After 1.5 hours of sonication, the solution was pipetted up and down to mix, preventing sedimentation of the preformed fibrils. Following this, 1 mL of 25 µM ThT was added to a 1.5 mL tube at room temperature (RT) and mixed with

the first 5 µL of SOD1 monomer from stock solutions (2 mg/mL) to yield a total of 10 µg of SOD1 monomer in solution. The mixture was then vortexed for 10 seconds. 1 µL from 25 mM stocks of both Edaravone (EDR) and NS-1-2 was added to the (ThT + SOD1 monomer) solution to get a final of 25 µM of both EDR and NS-1-2. The solution was vortexed for 5 seconds. The final solution of (ThT + SOD1 monomers + EDR/NS-1-2) was supplemented with 0.5 µL of SOD1 preformed fibrils from stocks of (2 mg/mL) to give a total of 1 µg of SOD1 preformed fibrils in solution and vortexed for 10 seconds. Finally, 100 µL/well of the final solution containing **(ThT + SOD1 monomers + EDR/NS-1-2+SOD1 preformed fibrils)** was taken in 96-well plates (black plate with clear bottom). The plate was wrapped with aluminum foil and placed in the incubator at 37°C for 30 minutes. The plate was shaken at 250 RPM. After 30 minutes of incubation, the fluorescence signal was measured at excitation and emission wavelengths of 450 and 485 nm, respectively, using a **BioTek, Gen5** Microplate Reader (bottom read mode). An ultrasonic cleaner from VWR International, LLC (model number 97043-964, 117V-60Hz) was used for sonication of preformed fibrils. An incubating orbital shaker from VWR was used.

11.14 Animal models

To study the safety profile of small organic molecule NS-1-2, both in terms of evaluation of acute toxicity (single dose) and chronic toxicity (120 doses), we used naïve wild-type SOD1 mice (non-transgenics) according to the principles of preclinical toxicity determination of molecule by most of the studies. We used the commonly used C57BL/6J strain of mice to study the toxicity effects of NS-1-2 both acutely and chronically. Many SOD1 mouse models have been created, out of which the most studied and commonly

used SOD1 mouse models to study ALS are SOD1G93A and SOD1G37R. These humanized SOD1 mice develop the clinical genotype, phenotype, and pathology of ALS as observed in humans[537].

We have used a human (h) SOD1-G37R line 42 mouse to evaluate the efficacy of EDR prodrug NS-1-2. The hSOD1-G37R line 42 transgenic strain was designed with a mutant human SOD1 gene (harboring a single amino acid substitution of glycine to arginine at codon 37) driven by its endogenous human promoter. Wong et al. assessed the survival of the line (42) strain on mixed genetic background and noted that death occurred around 3.5-4 months of age. However, the original allele has been backcrossed to C57BL/6J and made fully congenic, with increased survival of line-42 strain to (6-7 months or 180-210 days). The line (42) expresses 14.5-fold elevated levels of total SOD1 activity relative to control in the spinal cord. This SOD1-G37R line 42 is most similar to the G93A-high copy (HC) line with respect to disease onset age (~3.5-4 months or 105-120 days) and survival (6-7 months). With G93A-HC, the disease onset age (4 months) and survival age (~6 months). The other G37R mouse line 29 has an increased survival age (~17 months) with prolonged disease onset age (~10 months)[519]. The clinical phenotypes that resemble the clinical phenotypes of humans include fine axial tremors, asymmetric weakness of limbs, poor grooming, rough coat, muscle wasting around the flanks, kyphosis, hind limb paralysis, and abnormal splay of toes[538]. The SOD1-G37R line 42 used in this study is highly aggressive and demonstrates fast disease progression with an early disease onset and symptoms with muscle weakness according to the original investigator and most of the studies[538].

11.15 Mice and tissue preparation

Transgenic mice carrying human G37R mutant SOD1 (B6. Cg Tg (SOD1*G37R) 42Dpr/J) were obtained from the Jackson Laboratory (Bar Harbor, ME, USA). These mice were crossed with female mice with a C57BL/6 background for at least four generations. Colonies are maintained in the Central Animal Care Services (CACS), University of Manitoba, in an environment free of pathogens. The mice were used in accordance with the Guide of Care and Use of Experimental Animals of the Canadian Council on Animal Care. Transgenic offspring were genotyped by PCR of DNA obtained from ear biopsies, see below, using a protocol provided by the Jackson Laboratory. All animal experiments for this study followed protocol 21-014(AC11693), approved by CACS at the University of Manitoba.

11.16 DNA isolation and genotyping

A total volume of 300 μl of TNES buffer (1 M Tris, pH 8.5, 0.5 M EDTA, about 10% SDS, 5 M NaCl, and distilled water) supplemented with 20 mg/ml of Proteinase K (25530049, Fisher), was used to lyse ear samples overnight at 55 °C. After complete lysis, the mixture was combined with an equal volume of phenol and chloroform (1:1) and mixed well. After centrifugation at 14,500 rpm for 15 min, the samples were cleared of debris, and the DNA-rich supernatant was collected. The DNA was then precipitated by adding 200 µL of supernatant with 200 µL of 95 % ethanol (stored at -20 °C). The mixture was kept at 4 °C for 30 min. The DNA was then pelleted by centrifuging at 14,500 rpm at 4 °C for 10 min. The pellet was then rinsed with 70 % ethanol and centrifuged at 14,500 rpm for 10 min, 4 °C to remove residual solvent. Any remaining ethanol was evaporated in the ventilated hood over an hour. After the tubes were dried completely, 30 µL of nuclease-free water,

not DEPC-Treated (Fisher, AM9939) was added to the DNA, and the mixture was heated for 55°C for 10min. The genotype determination was applied via the Polymerase Chain Reaction (PCR) with a. PCR reactions mixture for genotyping (23 µL/ well) was prepared over ice by mixing Phusion High-Fidelity PCR kit (M0530S, New England Biolabs Inc.). The PCR reaction mixture was made by adding 14.75 μl of nuclease-free water, 5 μl 5x Phusion HF reaction buffer from the PCR kit, about 0.5 μl of about 10 mM dNTPs (New England Biolabs, N0447S), 1.25 μl of about 10 μM forward primer (5'-CATCAGCCCTAATCCATCTGA-3') (Fisher, 10336022), about 1.25 μl of about 10 μM reverse primer (5'-CGCGACTAACAATCAAAGTGA-3') (Fisher, 10336022), and finally about 0.25 μl of Phusion HF DNA polymerase (added near the freezer) kept at -20°C from the PCR kit, lastly, 2 μl of DNA extracted sample was added into each well. PCR program for the above PCR reaction includes initial denaturation at 98 °C for 30s, followed by 30 cycles of 10s at 98 °C, then 30s at 54 °C, and 30 s at 72 °C. A final step at 72 °C for 7 min terminated the amplification. The resulting PCR products were stained with GelRed Prestatin (Cedarlane, 41011, BT) and separated on a 1 % agarose gel. The gel was visualized using GeneSys imager software on a G: BOX imager (Syngene, UK).

11.17 Group assignment, drug formulation, storage, and administration of compound group assignment for determination of acute toxicity in wild-type SOD1mice

The Wild-type SOD1 mice were randomly assigned to 2 groups: For the acute toxicity experiments, a total of 6 animals per group (3 male and 3 female) were used in the study. **Group 1:** Sham treatment 1 (1:20 DMSO/PBS) and **Group 2:** NS-1-2 (10mg/kg body weight). According to an acute toxicity study requirement, 6-10 animals should be used to evaluate the effect of a substance. However, as the new analogues are structurally

similar to Edaravone, having a single-dose safety profile of 450mg/kg, the mortality of the Edaravone analogues at a dose of 10mg/kg body weight/day was not expected. Considering the above literature evidence, for the present acute study, the minimum number of animals was 6 per group. Morphological alterations, histological changes, and mean body weight assessments for the whole set of animals, for both the Wild-type SOD1 control groups (N=6; 1:20, DMSO: PBS) and Wild-type SOD1 treated groups (N=6; BSZ; 10mg/kg body weight) were assessed during the longitudinal 14-day acute toxicity assessment, by giving a single IP injection to the mouse starting at 2 months of age (see further detail in (1.8) below). Thus, a total of 12 Wild-type SOD1 mice were used.

11.18 Group assignment, drug formulation, storage, and administration of compound for determination of chronic toxicity in wild-type SOD1 mice

The Wild-type SOD1 mice were randomly assigned to 2 groups: For the chronic toxicity experiments, a total of 6 animals per group (3 male and 3 female) were used in the study. **Group 1:** Sham treatment 1 (1:20 DMSO/PBS) and **Group 2:** NS-1-2 (10mg/kg body weight). Morphological alterations, histological changes, and mean body weight assessments for the whole set of animals, for both the Wild-type SOD1 mice control groups (N=5; 1:20, DMSO: PBS) and Wild-type SOD1 mice treated groups (N=6; BSZ; 10mg/kg body weight) were assessed during the 120-day chronic toxicity assessment, by giving daily of 120 IP injection to the mouse starting at 3 months of age. Thus, a total of 11 Wild-type SOD1 mice were used. Only one male mouse from group 1 (control) was terminated unexpectedly, which was likely due to an accidental error in injection (discussed with Central Animal Care Services, veterinarians, and staff). IP injections may be difficult because of the aggressiveness of mice (particularly the male mice, during

physical restraint). In total, 1320 (11 X 120) daily IP injections were proposed for the chronic toxicity assessment (see further detail in (1.8) below).

11.19 Drug formulation, storage, and route of administration determination for the acute and chronic toxicity evaluation in the wild-type SOD1 mice

For intraperitoneal administration, about 1:20 of DMSO/PBS, at a pH of about 7.4 was used for the suspension of NS-1-2 test substance. A volume of about 400 µl from the final reconstituted solution was aliquoted and stored at about -80 °C until further use. For acute toxicity experiments, a single dose of about 10 mg/kg body weight of BSZ was intraperitoneally injected into group 2, wild-type mice model at the age of 2 months. The wild-type mice in group 1 received an injection of an equal volume of (about 1:20; DMSO: PBS) instead. For chronic toxicity experiments, 120 daily doses of about 10 mg/kg bodyweight of NS-1-2 was intraperitoneally injected into the group 2, WG37R mice model at the age of 3 months for 120 days, until the age of 7 months. The wild-type mice in group 2 received an injection of an equal volume of (about 1:20; DMSO: PBS) instead.

11.20 Hematoxylin and eosin (H&E) staining and microscopy

Wild-type (WT) G37R mice received a single dose (about 0.2 ml) IP injection of Sham suspended in (about 1:20; DMSO: PBS) and a single dose of about 10 mg/kg body weight (about 0.2 ml) IP injection of NS-1-2 suspended in about 1:20; DMSO: PBS at the age of 2 months. The mice were observed longitudinally for 2 weeks. At the experimental endpoint, the mice were first deeply anesthetized with a mixture of about 20% v/v isoflurane/propylene glycol (about 1 ml of the mixture per about 500ml of bell jar space, University of Manitoba animal care SOP A003) and than exsanguination was done by cutting the animal's right atrium followed by an intracardiac perfusion with about 0.9%

NaCl. During perfusion, a syringe barrel nosecone was used for prolonged anesthesia. Cardiac perfusion was followed by perfusion with about 4% paraformaldehyde for histology (H&E staining) analysis. Mouse tissues (brain, heart, spinal cord, kidney, liver, muscle, lung, and spleen) were fixed for about 48h in about 4% buffered formalin at about 4°C. Only the spinal cord was processed after about 24hr to remove the spine and again fixed for about another 24hr. Samples were processed and embedded into paraffin blocks at the Histomorphology and Ultrastructural Imaging platform, Dept. of Human Anatomy and Cell Science, University of Manitoba. Briefly, the embedded tissues were cut into about 5µm thickness, mounted on super frost plus slides, and dried overnight at about 37°C. Slides were deparaffinized in about 2 changes of xylene and rehydrated in descending alcohols (about 2 changes of about 100% Ethanol and about 2 changes of about 95% Ethanol) and tap water. Slides were stained with Harris Haematoxylin followed by differentiation with acid alcohol. After rinsing in tap water, saturated lithium carbonate was used for Blueing the nucleus. After that, the slides were rinsed in tap water and counter-stained with eosin. Following eosin staining, the slides were dehydrated using ascending alcohols, cleared with xylenes, and mounted coverslips on sections with paramount. The mounted slides were then visualized, and the images were taken using a Zeiss Imager M2 microscope using ZEN 3 Pro software with camera AxioCam HRc – colour. Similar to the acute toxicity experiments, hematoxylin and eosin (H&E) staining and microscopy experiments were done for the animals assigned to the chronic toxicity group.

11.21 Group assignment for evaluation of therapeutic efficacy in terms of delaying the disease onset, symptom onset, extending survival, and decreasing weight loss (cachexia) of EDR prodrug BSZ, in direct comparison to the control/sham group in the human SOD1-G37R mouse model of ALS

For these efficacy experiments, a set of experiments was carried out having two groups of mice: **Group 1:** Sham treatment (1:20 DMSO/PBS); and **Group 2:** NS-1-2 treatment (1:20 DMSO/PBS) (10mg/kg body weight/day). For these experiments, age-matched Het human SOD1-G37R (Line 42) mice were administered vehicle (1:20, DMSO: PBS) or treatment (BSZ; 10mg/kg body weight), daily, starting pre-symptomatically at the age of 90 days until the age of 210 days, and monitored longitudinally for several significant humane point indicators/end stage including, a) Mouse unable to right itself in 15 sec b) 25% loss of weight on the highest recorded weight c) Full paralysis of one or more hind limbs d) Loss of bladder functions e) Crusty eyes/loss of vision and/or f) Penile prolapse. Weight loss or ALS-induced cachexia due to disease progression is an independent predictor of survival and disease progression. We have evaluated the weight loss based on the highest recorded weight at the (humane endpoint/end stage)[359].

11.22 Definitions and criteria for determining disease onset and symptom onset

The disease onset and symptom onset in SOD1-G37R ALS mice were evaluated in the current study based on the following mentioned criteria, which are being used by numerous studies conducted in the ALS mice models. The definitions of disease course and progression analysis are illustrated in **(figure 84)**.

11.22.1 Criteria for disease onset

Disease onset is retrospectively defined as the age at which the mouse reaches peak weight, well before the denervation-induced muscle atrophy and weight loss[539].

11.22.2 Criteria for symptom onset

Symptom onset or early symptomatic progression stage is defined as the age to reach 10% body weight loss based on the highest or peak recorded weight with muscle weakness. The loss of 10% of body weight is often accompanied by the appearance of symptoms of muscle weakness[540]. Symptom onset is the early symptomatic disease progression stage called early symptomatic stage (Early-sym).

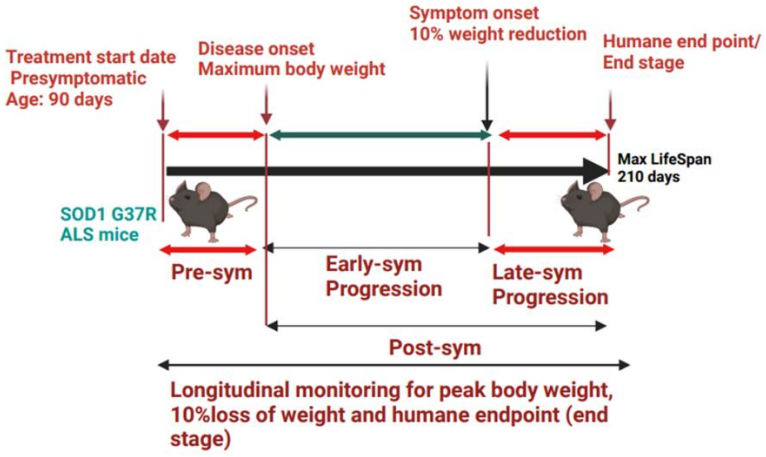

Figure 84. Diagram outlining the definition of pathological stages of the SOD1-G37R ALS mice mouse model of ALS.

11.23 Injection sites and determination of sample size for efficacy studies of BSZ

Also, injection sites were alternated between the right and left sides of the mice to reduce pain/inflammation. To see the effect of treatment in these experiments, a sample size of 12 per group was used. The mean deviation of oxidative SOD1 level is 20%. At least 30%

reduction of oxidative SOD1 with the treatments, with an S/N ratio of 1.5, a power of 0.9, and a significance level of 0.05, the required sample size is 12. If any less is used, the data would not be statistically significant. In this efficacy study of EDR prodrug BSZ, a total of 12 animals per group (6 male and 6 female) have been used. Thus, a total of 24 SOD1-G37R mice were used.

11.24 The rationale for the presymptomatic treatment start date

The treatment of EDR prodrug BSZ in the efficacy studies was initiated well before the disease onset i.e., started pre-symptomatically. According to the original investigator Wong et al., highly expressed SOD1-G37R line 42 mice, a familial model of ALS, demonstrate the onset of motor neurodegeneration at the age of (3.5 to 4 months or 105-120 days). At the earliest age of (15 weeks or 105 days), progressive neuropathological abnormalities associated with loss of motor neurons in the spinal cord and brain stem was observed, which is associated with ventral root exit swelling and vacuolization. According to several studies, it is well known that both the forms of ALS i.e., sALS and fALS are clinically and pathologically indistinguishable, further studies have shown the shared genetics risk in both forms of ALS. Further, evidence from the studies in ALS mice models and human forms of ALS demonstrates that the neurodegenerative process in ALS starts before the manifestations of ALS clinical symptoms or disease onset, culminating into a complex process and further leading to an aggressive and fatal form of disease progression. Therefore, better outcomes of therapeutic intervention in all forms of ALS could be achieved if we initiate a treatment presymptomatically to slow the fundamental root cause of neurodegeneration in the disease course. In addition, presymptomatic treatment gives an opportunity to delay the phenoconversion in ALS (i.e.,

the transition between pre-symptomatic and clinical symptomatic phases of the disease). There are several advantages of using early intervention to slow down the progression of highly complex ALS. Firstly, highly aggressive forms of neurodegeneration later, after the onset of the disease could mitigate the therapeutic potential of the drug therefore, initiating the intervention presymptomatically in early-phase drug discovery could be advantageous, secondly, rescuing the postmitotic neurons is more pragmatic than the regeneration of dead or diseased neurons, thirdly, it is preferred to start early intervention to slow the disease progression, when the disability is minimal and lastly, high levels of phosphorylated neurofilaments (pNefl) levels in the serum of presymptomatic ALS patients and ALS mice models demonstrates that the neurodegenerative process is active at the clinically presymptomatic stage[476]. This cumulating evidence endorses and supports the initiation of the BSZ presymptomatically in the current SOD1-G37R mice model to successfully translate the results from preclinical to human studies in the future.

Overall, a total of 47 mice participated in this early drug discovery phase, based on approved #protocol 21-014(AC11693) CACS, University of Manitoba. To evaluate the safety of BSZ (in terms of both acute and chronic) and efficacy of BSZ (in terms of delaying disease onset, extending life span, and reducing weight loss). A total of (12 wildtype SOD1 mice) were a part of acute toxicity studies, a total of (11 wild-type SOD1 mice) were a part of chronic toxicity experiments, and a total of (24 human SOD1 G37R mice) were a part of efficacy studies.

11.25 Discovery-based untargeted and unbiased proteomics on human mutant G37R mouse lumbar spinal cord and brain tissue samples

11.25.1 Tissue sample preparation

For homogenization, a lysis buffer comprised of 4% SDS and 1x Halt™ Phosphatase Inhibitor Cocktail (Thermo Scientific, cat no. 78426) in 100 mM TRIS (pH 8.5) was added to each sample and a probe sonicator was used. Protein concentrations of the lysates were determined using the Thermo Scientific PierceTM Detergent Compatible Bradford Assay Kit (product number. 23246) as per the manufacturer protocol. Per sample, 300-ug aliquots were further processed and volumes were adjusted to 30 µL using lysis buffer.

11.25.2 Proteolytic digestion

Lysates were reduced with 10 mM dithiothreitol (DTT) for 30 min at 57˚C followed by alkylation using 50 mM iodoacetamide (IAA) for 45 min in the dark at room temperature. Samples were processed using single-pot solid-phase-enhanced sample preparation (SP3)[541]. Thus, two types of carboxylate-modified SeraMag Speed beads (GE Life Sciences) were combined 1:1 (v/v), rinsed, and reconstituted in water at a concentration of 20 µg/µL. Next, 30 µL of the bead mix was added to each lysate, and the samples were adjusted to pH 7.0 using TRIS buffer. To promote protein binding, acetonitrile (ACN) was added to a final concentration of 70% (v/v), and samples were incubated at room temperature on a tube rotator for 18 min. Subsequently, beads were immobilized on a magnetic rack for 1 min. The supernatant was discarded, and the pellet was rinsed twice with 200 µL of 70% ethanol and once with 180 µL of 100% ACM while on the magnetic rack. Rinsed beads were resuspended in digestion buffer, 120 µL of 50 mM TRIS buffer (pH 8.5) supplemented with trypsin (sequencing grade, Promega) at an enzyme-to-

protein ratio of 1:25 (w/w). Samples were incubated for 16 hours at 37˚C. Supernatants were collected in clean tubes. To increase recovery, the beads were removed from the rack and sonicated in a bath sonicator with 50 µL of digestion buffer without trypsin. Supernatants were added to their respective tubes from the previous step. Next, 170 µL of 1% trifluoracetic acid (TFA) was added to samples and the generated peptides were desalted on Waters C18 100mg Cartridges (Sep-pac, part no. WAT023590). The desalted samples were dried in a speed vac and resuspended in 0.1% formic acid (FA).

11.25.3 Phosphopeptide enrichment

Immobilized metal ion affinity chromatography (IMAC)-based phosphopeptide enrichment was performed with aliquots of 145 µg and 105 µg of peptide for brain and spinal cord samples, respectively, using the High Select™ Phosphopeptide Enrichment Kit (Thermo Scientific, cat no. A32992) kit as per manufacturer protocols. Phosphopeptide eluates were dried in a speedvac and resuspended in 15 µL of 0.2% FA.

11.25.4 LC-MS/MS analysis of the spinal cord proteome

Per sample, an equivalent of 1.25 µg of peptide was analyzed by nanoflow LC-MS/MS using an Easy-nLC 1200 system coupled to an Orbitrap Exploris 480 with FAIMS (both Thermo Fisher Scientific). Samples were separated on a self-packed C18 analytical column (Luna C18(2), 3 µm particle, 100 µm ID x 30 cm, Phenomenex, Torrance, CA) using water with 0.1% FA (mobile phase A) and 80% ACN with 0.1% FA (mobile phase B) using a binary gradient starting with 5% B for 3 min, 5 – 7 % B over 2 min, 7-25% B over 87 min, 25 – 60 % B over 15 min, 60 – 95% B over 1 min, with final elution of 95% B for 15 min at a flow rate of 300 nL/min. A standard nitrogen flow of 4.1L/min is used for all experiments with user gas kept at 0 L/min. MS acquisition was conducted in data-

dependent acquisition mode (DDA) with a cycle time of 1.5 s for both CV -50 and -70. Full MS scans were acquired at a resolution of 120,000 from 380 – 1500 m/z (AGC 300%, 50 ms max injection time). Precursor ions with charge states between +2 and +5 were isolated with a m/z 1.6 window and fragmented with a normalized collision energy of 30%. MS/MS spectra were acquired at a resolution of 15,000 (AGC 100%, automated max injection time). Dynamic exclusion was set to 25 s.

11.25.5 LC-MS/MS analysis of the spinal cord phosphoproteome

Per sample, 50% of the enriched phosphopeptides were analyzed by nanoflow LC-MS/MS using an Easy-nLC 1200 system coupled to an Orbitrap Exploris 480 (both Thermo Fisher Scientific). Samples were separated on a C18 analytical column (Luna C18(2), 3 µm particle, 100 µm ID x 30 cm, Phenomenex, Torrance, CA) using water with 0.1% FA (mobile phase A) and 80% ACN with 0.1% FA (mobile phase B) using a binary gradient ranging from 2-6% B in 5 min, 6-30% B in 62 min, 30-45% B in 7 min, 45-90% B in 1 min, and with final elution of 90% B for 15 min at a flow rate of 300 nL/min. MS acquisition was conducted in data-dependent acquisition mode (DDA) with a cycle time of 1.0 s. Full MS scans were acquired at a resolution of 60,000 from 380 – 1500 m/z (AGC 300%, 50 ms max injection time). Precursor ions with charge states between +2 and +6 were isolated with a m/z 1.6 window and fragmented with a normalized collision energy of 30%. MS/MS spectra were acquired at a resolution of 30,000 (AGC 100%, automated max injection time). Dynamic exclusion was set to 15 s.

11.25.6 Data analysis of the spinal cord proteome

Raw data was analyzed using FragPipe 21.1 with MSFragger[542] 4.0, IonQuant 1.10.12, and Philosopher 5.1.0. Data was searched against a mouse SwissProt database

(downloaded from uniprot.org on October 23, 2022, with 17,197 target proteins) complemented with decoys and common contaminants. Trypsin was selected as an enzyme with a maximum of 1 missed cleavage, and mass tolerances for recalibration were set to 10 ppm for both MS and MS/MS spectra. Peptide length was restricted to 7-35 amino acids, carbamidomethylation of Cys (+57.02146 Da) was selected as fixed, and oxidation of Met (+15.9949 Da), pyro-Glu formation from *N*-terminal Gln (-17.0265 Da) and *N*-terminal Glu (-18.0106 Da) were selected as variable modifications, with a maximum of 3 allowed variable modifications per peptide. MS Booster, Percolator, and Philosopher were used for validation. Label-free quantitation (LFQ) was performed using IonQuant, enabling matching between runs with an ion false discovery rate of 1% and only using unique peptides for quantitation. The minimum number of scans was set to 5, all other parameters were kept to default settings. Data was filtered to a 1% false discovery rate on peptide and protein levels. A total of 8832 proteins were quantified and further filtered to retain high-quality data. Thus, all proteins quantified with less than 2 peptides and in less than 3 of 4 replicates of either treated or sham were removed, resulting in a total of 6761 proteins. Differential analysis was performed using moderated t-test (LIMMA)[376] and considering only 6270 proteins that were quantified in all replicates of either sham or treated samples. Intensities were log2-transformed, followed by K-nearest neighbor (KNN) imputation for Missing at Random (MAR) values. A total of 51 proteins with adjusted p-values <0.05 were considered statistically significantly differential between treated and sham. In addition, 23 proteins that were quantified in 3 replicates of one condition but in no replicate of the other condition were labeled as

potentially differential, as well as 2 proteins quantified in 3 replicates of the treated replicates but in only 1 one control replicate with >4 and >10 times lower intensity.

11.25.7 Data analysis of the spinal cord phosphoproteome

Raw data was analyzed using FragPipe 21.1 with MSFragger 4.0, IonQuant 1.10.12, and Philosopher 5.1.0. Data was searched against a mouse swissprot database (downloaded from uniprot.org on January 25, 2024, with 17,197 target proteins) complemented with decoys and common contaminants. Trypsin was selected as an enzyme with a maximum of 2 missed cleavages, and mass tolerances for recalibration were set to 20 ppm for both MS and MS/MS spectra. Peptide length was restricted to 7-35 amino acids, carbamidomethylation of Cys (+57.02146 Da) was selected as fixed, and oxidation of Met (+15.9949 Da), phosphorylation of Ser/Thr/Tyr (+79.96633 Da) and deamidation of Asn, Gln (+0.984016 Da) were selected as variable modifications, with a maximum of 4 allowed variable modifications per peptide. MS Booster, Percolator, and Philosopher were used for validation, and PTM Prophet was used to determine site localization probabilities of all variable post-translational modifications. Label-free quantitation (LFQ) was performed using IonQuant, enabling matching between runs with an ion false discovery rate of 1% and only using unique peptides for quantitation. The minimum number of scans was set to 5, all other parameters were kept to default settings, with a minimum site localization probability of 75%. Data was filtered to a 1% false discovery rate on peptide and protein levels. A total of 9541 phosphorylation sites were quantified and further filtered to retain high-quality data. Only phosphopeptides that were quantified in all 4 replicates of either treated or sham were kept, resulting in a total of 3945 high-quality phosphopeptides. Differential analysis was performed using a moderated *t-test* (LIMMA)[376]. Intensities

were log2-transformed, followed by K-nearest neighbor (KNN) imputation for Missing at Random (MAR) values. A total of 29 phosphorylation sites with adjusted p-values <0.05 were considered statistically significantly differential between treated and sham.

11.25.8 LC-MS/MS analysis of the brain proteome

Per sample, an equivalent of 200 ng of peptide was analyzed by nanoflow LC-MS/MS using an EvoSep One coupled to a TimsTOF Pro2 operating in DIA-PASEF (data independent acquisition-parallel accumulation-serial fragmentation) mode. An EvoSep EV1137 column was used to separate peptides (1.5 µm particle, 150 µm ID x 15 cm, EvoSep) with 0.1% formic acid in water (mobile phase A) and 0.1% formic acid in acetonitrile (mobile phase B) using the preset 30 samples-per-day gradient and flowrate. Inverse reduced ion mobility (1/K0) values and the TIMS funnel voltages were calibrated linearly through three selected ions (m/z 622, 922, 1222) using the Agilent ESI-L Tuning Mix (Agilent, Santa Clara, CA, US). The source parameters were set as follows: 1700 V for emitter voltage, 3.0 L/min for dry gas and 200 ℃ for dry temperature. The DIA-PASEF method was optimized using py_diAID17 over an m/z range from 350.2 to 1493.2. Each DIA-PASEF scan used variable isolation window widths that were split along two ion mobility ranges adjusted based on precursor intensity. One DIA-PASEF cycle consisted of 17 scans and the cycle time was 1.91 s. The ion mobility was scanned from 0.7-1.5 Vs/cm2 at a ramp time of 100 ms while ramp and accumulation times were locked to 100% duty cycle. The collision energy was ramped linearly as a function of the mobility from 59 eV at 1/K0 = 1. 6 Vs cm-2 to 20 eV at 1/K0 = 0.6 Vs cm-2.

11.25.9 Data analysis of the brain proteome

Raw data was analyzed using DIA-NN 1.8.2, using an in-silico generated spectral library based on a mouse swissprot database (downloaded from uniprot.org on January 25, 2024, with 17,197 target proteins). In-silico library generation settings were: trypsin as enzyme with a maximum of 1 missed cleavage site, peptide length of 7-35 amino acids, precursor m/z range from m/z 300-1800 with charge states 1-4. Carbamidomethylation of Cys (+57.02146 Da) was used as fixed modification. Peptides were deemed proteotypic based on FASTA database protein entries. Samples were analyzed in double-pass mode using RT-dependent normalization and smart profiling. A total of 8429 proteins groups were quantified and further filtered to retain high quality data. Only protein groups that had been quantified with at least 2 peptides in at least 3 out of 4 replicates of either sham or treated samples were retained. Differential analysis was performed using a moderated t-test (LIMMA). Intensities were log2-transformed, followed by K-nearest neighbor (KNN) imputation for Missing at Random (MAR) values. Proteins with adjusted p-values <0.05 were considered statistically significantly differential between treated and sham.

11.26 Discovery-based untargeted and unbiased LC-MS/MS analysis of symptom onset biomarker proteome of human mutant G37R ALS mice model

Per sample, an equivalent of 200 ng of peptide was analyzed by nanoflow LC-MS/MS using an EvoSep One coupled to a TimsTOF Pro2 operating in DIA-PASEF (data independent acquisition-parallel accumulation-serial fragmentation) mode. An EvoSep EV1137 column was used to separate peptides (1.5 µm particle, 150 µm ID x 15 cm, EvoSep) with 0.1% formic acid in water (mobile phase A) and 0.1% formic acid in acetonitrile (mobile phase B) using the preset 30 samples-per-day gradient and flow rate.

Inverse reduced ion mobility (1/K0) values and the TIMS funnel voltages were calibrated linearly through three selected ions (m/z 622, 922, 1222) using the Agilent ESI-L Tuning Mix (Agilent, Santa Clara, CA, US). The source parameters were set as follows: 1700 V for emitter voltage, 3.0 L/min for dry gas and 200 ℃ for dry temperature. The DIA-PASEF method was optimized using py_diAID17 over an m/z range from 350.2 to 1493.2. Each DIA-PASEF scan used variable isolation window widths that were split along two ion mobility ranges adjusted based on precursor intensity. One DIA-PASEF cycle consisted of 17 scans and the cycle time was 1.91 s. The ion mobility was scanned from 0.7-1.5 Vs/cm2 at a ramp time of 100 ms while ramp and accumulation times were locked to 100% duty cycle. The collision energy was ramped linearly as a function of the mobility from 59 eV at 1/K0 = 1. 6 Vs cm-2 to 20 eV at 1/K0 = 0.6 Vs cm-2.

11.26.1 Data analysis symptom onset proteome

Raw data was analyzed using DIA-NN 1.9, using an in-silico generated spectral library based on a mouse swissprot database (downloaded from uniprot.org on January 25, 2024, with 17,197 target proteins). In-silico library generation settings were: trypsin as enzyme with a maximum of 1 missed cleavage site, peptide length of 7-35 amino acids, precursor m/z range from m/z 300-1800 with charge states 1-4. Carbamidomethylation of Cys (+57.02146 Da) was used as fixed modification. Peptides were deemed proteotypic based on FASTA database protein entries. Samples were analyzed in double-pass mode using RT-dependent normalization and smart profiling.

A total of 8263 proteins groups were quantified at 1% false discovery rate (FDR) and further filtered to retain high quality data. Only protein groups that (i) had been quantified with at least 2 peptides in all 3 replicates of either sham or treated samples were retained

and (ii) had maximum relative standard deviation of 30% in both groups, were considered. The resulting list of 4975 proteins with high confidence quantitative data was further analyzed using Perseus, including log2-transformation of intensities, imputation of missing values, determination of ratios and p-values, as well as multiple testing correction to report significantly differential proteins at an FDR of 5%. In addition, 2 proteins (Ncf4, Raver1) that did not pass the significance threshold but were quantified with 2 peptides in all three sham samples but not detected in all treated samples, were considered as differentially regulated.

11.27 Statistical analysis

All statistical analyses were performed using GraphPad Prism software version 9 (GraphPad Software Inc.). Data represent the mean and standard error of the mean (SEM). An unpaired two-tailed Student's *t-test* was used for the comparison of two means. One-way ANOVA followed by Dunnett's multiple comparisons test was used for the multiple-group analysis. The Kaplan-Meier method with the Log-rank test was used for disease onset and survival analysis. The significance level for the two-sided analyses was set at $P < 0.05$.

12 References

1. Przedborski S, Vila M, Jackson-Lewis V. Neurodegeneration: what is it and where are we? J Clin Invest. 2003;111(1):3-10.
2. Sweeney P, Park H, Baumann M, Dunlop J, Frydman J, Kopito R, et al. Protein misfolding in neurodegenerative diseases: implications and strategies. Transl Neurodegener. 2017;6:6.
3. Imam F, Saloner R, Vogel JW, Krish V, Abdel-Azim G, Ali M, et al. The Global Neurodegeneration Proteomics Consortium: biomarker and drug target discovery for common neurodegenerative diseases and aging. Nat Med. 2025.
4. Brown RH, Al-Chalabi A. Amyotrophic Lateral Sclerosis. N Engl J Med. 2017;377(2):162-72.
5. Zarei S, Carr K, Reiley L, Diaz K, Guerra O, Altamirano PF, et al. A comprehensive review of amyotrophic lateral sclerosis. Surg Neurol Int. 2015;6:171.
6. Wolf J, Safer A, Wöhrle JC, Palm F, Nix WA, Maschke M, et al. Factors predicting one-year mortality in amyotrophic lateral sclerosis patients--data from a population-based registry. BMC Neurol. 2014;14:197.
7. Román GC. Neuroepidemiology of amyotrophic lateral sclerosis: clues to aetiology and pathogenesis. J Neurol Neurosurg Psychiatry. 1996;61(2):131-7.
8. Longinetti E, Regodón Wallin A, Samuelsson K, Press R, Zachau A, Ronnevi LO, et al. The Swedish motor neuron disease quality registry. Amyotroph Lateral Scler Frontotemporal Degener. 2018;19(7-8):528-37.
9. Palese F, Sartori A, Verriello L, Ros S, Passadore P, Manganotti P, et al. Epidemiology of amyotrophic lateral sclerosis in Friuli-Venezia Giulia, North-Eastern Italy, 2002-2014: a retrospective population-based study. Amyotroph Lateral Scler Frontotemporal Degener. 2019;20(1-2):90-9.
10. Rose L, McKim D, Leasa D, Nonoyama M, Tandon A, Bai YQ, et al. Trends in incidence, prevalence, and mortality of neuromuscular disease in Ontario, Canada: A population-based retrospective cohort study (2003-2014). PLoS One. 2019;14(3):e0210574.
11. Zhou S, Zhou Y, Qian S, Chang W, Wang L, Fan D. Amyotrophic lateral sclerosis in Beijing: Epidemiologic features and prognosis from 2010 to 2015. Brain Behav. 2018;8(11):e01131.
12. Nelson LM, Topol B, Kaye W, Williamson D, Horton DK, Mehta P, et al. Estimation of the Prevalence of Amyotrophic Lateral Sclerosis in the United States Using National Administrative Healthcare Data from 2002 to 2004 and Capture-Recapture Methodology. Neuroepidemiology. 2018;51(3-4):149-57.
13. Nakken O, Lindstrøm JC, Tysnes OB, Holmøy T. Assessing amyotrophic lateral sclerosis prevalence in Norway from 2009 to 2015 from compulsory nationwide health registers. Amyotroph Lateral Scler Frontotemporal Degener. 2018;19(3-4):303-10.
14. Mehta P, Kaye W, Raymond J, Punjani R, Larson T, Cohen J, et al. Prevalence of Amyotrophic Lateral Sclerosis - United States, 2015. MMWR Morb Mortal Wkly Rep. 2018;67(46):1285-9.
15. Longinetti E, Fang F. Epidemiology of amyotrophic lateral sclerosis: an update of recent literature. Curr Opin Neurol. 2019;32(5):771-6.
16. Mejzini R, Flynn LL, Pitout IL, Fletcher S, Wilton SD, Akkari PA. ALS Genetics, Mechanisms, and Therapeutics: Where Are We Now? Front Neurosci. 2019;13:1310.
17. Rosen DR, Siddique T, Patterson D, Figlewicz DA, Sapp P, Hentati A, et al. Mutations in Cu/Zn superoxide dismutase gene are associated with familial amyotrophic lateral sclerosis. Nature. 1993;362(6415):59-62.
18. Mathis S, Goizet C, Soulages A, Vallat JM, Masson GL. Genetics of amyotrophic lateral sclerosis: A review. J Neurol Sci. 2019;399:217-26.

19. Berdyński M, Miszta P, Safranow K, Andersen PM, Morita M, Filipek S, et al. SOD1 mutations associated with amyotrophic lateral sclerosis analysis of variant severity. Sci Rep. 2022;12(1):103.
20. Chen LX, Xu HF, Lin HX, Yang XX, Li HF, Wu ZY. Pathogenicity classification of SOD1 variants of uncertain significance by in vitro aggregation propensity. Neurobiol Aging. 2023;123:182-90.
21. Kabashi E, Valdmanis PN, Dion P, Rouleau GA. Oxidized/misfolded superoxide dismutase-1: the cause of all amyotrophic lateral sclerosis? Ann Neurol. 2007;62(6):553-9.
22. Bosco DA, Landers JE. Genetic determinants of amyotrophic lateral sclerosis as therapeutic targets. CNS Neurol Disord Drug Targets. 2010;9(6):779-90.
23. Orrell RW. Amyotrophic lateral sclerosis: copper/zinc superoxide dismutase (SOD1) gene mutations. Neuromuscul Disord. 2000;10(1):63-8.
24. Andersen PM. Amyotrophic lateral sclerosis associated with mutations in the CuZn superoxide dismutase gene. Curr Neurol Neurosci Rep. 2006;6(1):37-46.
25. Rotunno MS, Bosco DA. An emerging role for misfolded wild-type SOD1 in sporadic ALS pathogenesis. Front Cell Neurosci. 2013;7:253.
26. Balendra R, Isaacs AM. C9orf72-mediated ALS and FTD: multiple pathways to disease. Nat Rev Neurol. 2018;14(9):544-58.
27. Birsa N, Bentham MP, Fratta P. Cytoplasmic functions of TDP-43 and FUS and their role in ALS. Semin Cell Dev Biol. 2020;99:193-201.
28. Prasad A, Bharathi V, Sivalingam V, Girdhar A, Patel BK. Molecular Mechanisms of TDP-43 Misfolding and Pathology in Amyotrophic Lateral Sclerosis. Front Mol Neurosci. 2019;12:25.
29. Rakhit R, Chakrabartty A. Structure, folding, and misfolding of Cu,Zn superoxide dismutase in amyotrophic lateral sclerosis. Biochim Biophys Acta. 2006;1762(11-12):1025-37.
30. Ezzi SA, Urushitani M, Julien JP. Wild-type superoxide dismutase acquires binding and toxic properties of ALS-linked mutant forms through oxidation. J Neurochem. 2007;102(1):170-8.
31. Forsberg K, Andersen PM, Marklund SL, Brännström T. Glial nuclear aggregates of superoxide dismutase-1 are regularly present in patients with amyotrophic lateral sclerosis. Acta Neuropathol. 2011;121(5):623-34.
32. Gurney ME, Pu H, Chiu AY, Dal Canto MC, Polchow CY, Alexander DD, et al. Motor neuron degeneration in mice that express a human Cu,Zn superoxide dismutase mutation. Science. 1994;264(5166):1772-5.
33. Wong PC, Pardo CA, Borchelt DR, Lee MK, Copeland NG, Jenkins NA, et al. An adverse property of a familial ALS-linked SOD1 mutation causes motor neuron disease characterized by vacuolar degeneration of mitochondria. Neuron. 1995;14(6):1105-16.
34. Bruijn LI, Becher MW, Lee MK, Anderson KL, Jenkins NA, Copeland NG, et al. ALS-linked SOD1 mutant G85R mediates damage to astrocytes and promotes rapidly progressive disease with SOD1-containing inclusions. Neuron. 1997;18(2):327-38.
35. Wiedau-Pazos M, Goto JJ, Rabizadeh S, Gralla EB, Roe JA, Lee MK, et al. Altered reactivity of superoxide dismutase in familial amyotrophic lateral sclerosis. Science. 1996;271(5248):515-8.
36. Wang J, Xu G, Li H, Gonzales V, Fromholt D, Karch C, et al. Somatodendritic accumulation of misfolded SOD1-L126Z in motor neurons mediates degeneration: alphaB-crystallin modulates aggregation. Hum Mol Genet. 2005;14(16):2335-47.
37. Jonsson PA, Graffmo KS, Andersen PM, Brännström T, Lindberg M, Oliveberg M, et al. Disulphide-reduced superoxide dismutase-1 in CNS of transgenic amyotrophic lateral sclerosis models. Brain. 2006;129(Pt 2):451-64.
38. Julien JP, Kriz J. Transgenic mouse models of amyotrophic lateral sclerosis. Biochim Biophys Acta. 2006;1762(11-12):1013-24.

39. De Giorgio F, Maduro C, Fisher EMC, Acevedo-Arozena A. Transgenic and physiological mouse models give insights into different aspects of amyotrophic lateral sclerosis. Dis Model Mech. 2019;12(1).
40. Ingre C, Roos PM, Piehl F, Kamel F, Fang F. Risk factors for amyotrophic lateral sclerosis. Clin Epidemiol. 2015;7:181-93.
41. Logroscino G, Traynor BJ, Hardiman O, Chiò A, Mitchell D, Swingler RJ, et al. Incidence of amyotrophic lateral sclerosis in Europe. J Neurol Neurosurg Psychiatry. 2010;81(4):385-90.
42. Oskarsson B, Gendron TF, Staff NP. Amyotrophic Lateral Sclerosis: An Update for 2018. Mayo Clin Proc. 2018;93(11):1617-28.
43. Shoesmith C, Abrahao A, Benstead T, Chum M, Dupre N, Izenberg A, et al. Canadian best practice recommendations for the management of amyotrophic lateral sclerosis. Cmaj. 2020;192(46):E1453-E68.
44. Arthur KC, Calvo A, Price TR, Geiger JT, Chiò A, Traynor BJ. Projected increase in amyotrophic lateral sclerosis from 2015 to 2040. Nat Commun. 2016;7:12408.
45. Pasinelli P, Brown RH. Molecular biology of amyotrophic lateral sclerosis: insights from genetics. Nature Reviews Neuroscience. 2006;7(9):710-23.
46. Chiò A, Benzi G, Dossena M, Mutani R, Mora G. Severely increased risk of amyotrophic lateral sclerosis among Italian professional football players. Brain. 2005;128(Pt 3):472-6.
47. Chapman L, Cooper-Knock J, Shaw PJ. Physical activity as an exogenous risk factor for amyotrophic lateral sclerosis: a review of the evidence. Brain. 2023;146(5):1745-57.
48. Julian TH, Glascow N, Barry ADF, Moll T, Harvey C, Klimentidis YC, et al. Physical exercise is a risk factor for amyotrophic lateral sclerosis: Convergent evidence from Mendelian randomisation, transcriptomics and risk genotypes. EBioMedicine. 2021;68:103397.
49. Gallo V, Bueno-De-Mesquita HB, Vermeulen R, Andersen PM, Kyrozis A, Linseisen J, et al. Smoking and risk for amyotrophic lateral sclerosis: analysis of the EPIC cohort. Ann Neurol. 2009;65(4):378-85.
50. Wang H, O'Reilly É J, Weisskopf MG, Logroscino G, McCullough ML, Thun MJ, et al. Smoking and risk of amyotrophic lateral sclerosis: a pooled analysis of 5 prospective cohorts. Arch Neurol. 2011;68(2):207-13.
51. Santos AE, Duarte CB, Iizuka M, Barsoumian EL, Ham J, Lopes MC, et al. Excitotoxicity mediated by Ca2+-permeable GluR4-containing AMPA receptors involves the AP-1 transcription factor. Cell Death Differ. 2006;13(4):652-60.
52. Shaw PJ, Ince PG. Glutamate, excitotoxicity and amyotrophic lateral sclerosis. J Neurol. 1997;244 Suppl 2:S3-14.
53. Armada-Moreira A, Gomes JI, Pina CC, Savchak OK, Gonçalves-Ribeiro J, Rei N, et al. Going the Extra (Synaptic) Mile: Excitotoxicity as the Road Toward Neurodegenerative Diseases. Front Cell Neurosci. 2020;14:90.
54. Connolly NM, Prehn JH. The metabolic response to excitotoxicity - lessons from single-cell imaging. J Bioenerg Biomembr. 2015;47(1-2):75-88.
55. Foran E, Trotti D. Glutamate transporters and the excitotoxic path to motor neuron degeneration in amyotrophic lateral sclerosis. Antioxid Redox Signal. 2009;11(7):1587-602.
56. Pehar M, Harlan BA, Killoy KM, Vargas MR. Role and therapeutic potential of astrocytes in amyotrophic lateral sclerosis. Current pharmaceutical design. 2017;23(33):5010-21.
57. Wang R, Reddy PH. Role of glutamate and NMDA receptors in Alzheimer's disease. Journal of Alzheimer's Disease. 2017;57(4):1041-8.
58. Iovino L, Tremblay ME, Civiero L. Glutamate-induced excitotoxicity in Parkinson's disease: The role of glial cells. J Pharmacol Sci. 2020;144(3):151-64.

59. Granzotto A, Canzoniero LMT, Sensi SL. A Neurotoxic Ménage-à-trois: Glutamate, Calcium, and Zinc in the Excitotoxic Cascade. Front Mol Neurosci. 2020;13:600089.
60. Gleitze S, Paula-Lima A, Núñez MT, Hidalgo C. The calcium-iron connection in ferroptosis-mediated neuronal death. Free Radic Biol Med. 2021;175:28-41.
61. Doble A. The role of excitotoxicity in neurodegenerative disease: implications for therapy. Pharmacology & therapeutics. 1999;81(3):163-221.
62. Sanghai N, Tranmer GK. Biochemical and molecular pathways in neurodegenerative diseases: an integrated view. Cells. 2023;12(18):2318.
63. Cobley JN, Fiorello ML, Bailey DM. 13 reasons why the brain is susceptible to oxidative stress. Redox biology. 2018;15:490-503.
64. Barnham KJ, Masters CL, Bush AI. Neurodegenerative diseases and oxidative stress. Nature reviews Drug discovery. 2004;3(3):205-14.
65. Petillon C, Hergesheimer R, Puy H, Corcia P, Vourc'h P, Andres C, et al. The Relevancy of Data Regarding the Metabolism of Iron to Our Understanding of Deregulated Mechanisms in ALS; Hypotheses and Pitfalls. Front Neurosci. 2018;12:1031.
66. Trist BG, Genoud S, Roudeau S, Rookyard A, Abdeen A, Cottam V, et al. Altered SOD1 maturation and post-translational modification in amyotrophic lateral sclerosis spinal cord. Brain. 2022;145(9):3108-30.
67. Min JH, Sarlus H, Harris RA. Copper toxicity and deficiency: the vicious cycle at the core of protein aggregation in ALS. Front Mol Neurosci. 2024;17:1408159.
68. Chen L, Shen Q, Liu Y, Zhang Y, Sun L, Ma X, et al. Homeostasis and metabolism of iron and other metal ions in neurodegenerative diseases. Signal Transduct Target Ther. 2025;10(1):31.
69. Wang L, Yin YL, Liu XZ, Shen P, Zheng YG, Lan XR, et al. Current understanding of metal ions in the pathogenesis of Alzheimer's disease. Transl Neurodegener. 2020;9:10.
70. Sies H. Role of metabolic H2O2 generation: redox signaling and oxidative stress. J Biol Chem. 2014;289(13):8735-41.
71. Krols M, Bultynck G, Janssens S. ER-Mitochondria contact sites: A new regulator of cellular calcium flux comes into play. J Cell Biol. 2016;214(4):367-70.
72. Marino SM, Gladyshev VN. Cysteine function governs its conservation and degeneration and restricts its utilization on protein surfaces. J Mol Biol. 2010;404(5):902-16.
73. Sies H. Hydrogen peroxide as a central redox signaling molecule in physiological oxidative stress: Oxidative eustress. Redox Biol. 2017;11:613-9.
74. Gülden M, Jess A, Kammann J, Maser E, Seibert H. Cytotoxic potency of H2O2 in cell cultures: impact of cell concentration and exposure time. Free Radic Biol Med. 2010;49(8):1298-305.
75. Juarez JC, Manuia M, Burnett ME, Betancourt O, Boivin B, Shaw DE, et al. Superoxide dismutase 1 (SOD1) is essential for H2O2-mediated oxidation and inactivation of phosphatases in growth factor signaling. Proc Natl Acad Sci U S A. 2008;105(20):7147-52.
76. Clément MV, Ponton A, Pervaiz S. Apoptosis induced by hydrogen peroxide is mediated by decreased superoxide anion concentration and reduction of intracellular milieu. FEBS Lett. 1998;440(1-2):13-8.
77. Gutiérrez-Venegas G, Guadarrama-Solís A, Muñoz-Seca C, Arreguín-Cano JA. Hydrogen peroxide-induced apoptosis in human gingival fibroblasts. Int J Clin Exp Pathol. 2015;8(12):15563-72.
78. Zhao L, Lin H, Chen S, Chen S, Cui M, Shi D, et al. Hydrogen peroxide induces programmed necrosis in rat nucleus pulposus cells through the RIP1/RIP3-PARP-AIF pathway. J Orthop Res. 2018;36(4):1269-82.

79. Halliwell B, Gutteridge JM. Free radicals in biology and medicine: Oxford university press, USA; 2015.
80. Saito Y, Nishio K, Ogawa Y, Kimata J, Kinumi T, Yoshida Y, et al. Turning point in apoptosis/necrosis induced by hydrogen peroxide. Free Radic Res. 2006;40(6):619-30.
81. Teramoto S, Tomita T, Matsui H, Ohga E, Matsuse T, Ouchi Y. Hydrogen peroxide-induced apoptosis and necrosis in human lung fibroblasts: protective roles of glutathione. Jpn J Pharmacol. 1999;79(1):33-40.
82. Troyano A, Sancho P, Fernández C, de Blas E, Bernardi P, Aller P. The selection between apoptosis and necrosis is differentially regulated in hydrogen peroxide-treated and glutathione-depleted human promonocytic cells. Cell Death Differ. 2003;10(8):889-98.
83. Cookson MR, Ince PG, Shaw PJ. Peroxynitrite and hydrogen peroxide induced cell death in the NSC34 neuroblastoma x spinal cord cell line: role of poly (ADP-ribose) polymerase. J Neurochem. 1998;70(2):501-8.
84. Zhao ZY, Luan P, Huang SX, Xiao SH, Zhao J, Zhang B, et al. Edaravone protects HT22 neurons from H2O2-induced apoptosis by inhibiting the MAPK signaling pathway. CNS Neurosci Ther. 2013;19(3):163-9.
85. Bian YY, Guo J, Majeed H, Zhu KX, Guo XN, Peng W, et al. Ferulic acid renders protection to HEK293 cells against oxidative damage and apoptosis induced by hydrogen peroxide. In Vitro Cell Dev Biol Anim. 2015;51(7):722-9.
86. Xiang J, Wan C, Guo R, Guo D. Is Hydrogen Peroxide a Suitable Apoptosis Inducer for All Cell Types? Biomed Res Int. 2016;2016:7343965.
87. Ali MA, Kandasamy AD, Fan X, Schulz R. Hydrogen peroxide-induced necrotic cell death in cardiomyocytes is independent of matrix metalloproteinase-2. Toxicol In Vitro. 2013;27(6):1686-92.
88. Ohguro N, Fukuda M, Sasabe T, Tano Y. Concentration dependent effects of hydrogen peroxide on lens epithelial cells. Br J Ophthalmol. 1999;83(9):1064-8.
89. Okuda S, Nishiyama N, Saito H, Katsuki H. Hydrogen peroxide-mediated neuronal cell death induced by an endogenous neurotoxin, 3-hydroxykynurenine. Proc Natl Acad Sci U S A. 1996;93(22):12553-8.
90. Huang BK, Sikes HD. Quantifying intracellular hydrogen peroxide perturbations in terms of concentration. Redox Biol. 2014;2:955-62.
91. Sanghai N, Tranmer GK. Hydrogen Peroxide and Amyotrophic Lateral Sclerosis: From Biochemistry to Pathophysiology. Antioxidants (Basel). 2021;11(1).
92. Zelko IN, Mariani TJ, Folz RJ. Superoxide dismutase multigene family: a comparison of the CuZn-SOD (SOD1), Mn-SOD (SOD2), and EC-SOD (SOD3) gene structures, evolution, and expression. Free Radic Biol Med. 2002;33(3):337-49.
93. Fukai T, Ushio-Fukai M. Superoxide dismutases: role in redox signaling, vascular function, and diseases. Antioxid Redox Signal. 2011;15(6):1583-606.
94. Pardo CA, Xu Z, Borchelt DR, Price DL, Sisodia SS, Cleveland DW. Superoxide dismutase is an abundant component in cell bodies, dendrites, and axons of motor neurons and in a subset of other neurons. Proc Natl Acad Sci U S A. 1995;92(4):954-8.
95. Furukawa Y, Torres AS, O'Halloran TV. Oxygen-induced maturation of SOD1: a key role for disulfide formation by the copper chaperone CCS. Embo j. 2004;23(14):2872-81.
96. Lepock JR, Arnold LD, Torrie BH, Andrews B, Kruuv J. Structural analyses of various Cu2+, Zn2+-superoxide dismutases by differential scanning calorimetry and Raman spectroscopy. Arch Biochem Biophys. 1985;241(1):243-51.
97. Tainer JA, Getzoff ED, Richardson JS, Richardson DC. Structure and mechanism of copper, zinc superoxide dismutase. Nature. 1983;306(5940):284-7.

98. Tainer JA, Getzoff ED, Beem KM, Richardson JS, Richardson DC. Determination and analysis of the 2 A-structure of copper, zinc superoxide dismutase. J Mol Biol. 1982;160(2):181-217.
99. Kayatekin C, Zitzewitz JA, Matthews CR. Zinc binding modulates the entire folding free energy surface of human Cu,Zn superoxide dismutase. J Mol Biol. 2008;384(2):540-55.
100. Rakhit R, Cunningham P, Furtos-Matei A, Dahan S, Qi XF, Crow JP, et al. Oxidation-induced misfolding and aggregation of superoxide dismutase and its implications for amyotrophic lateral sclerosis. J Biol Chem. 2002;277(49):47551-6.
101. Dafforn TR, Smith CJ. Natively unfolded domains in endocytosis: hooks, lines and linkers. EMBO Rep. 2004;5(11):1046-52.
102. Anzai I, Tokuda E, Handa S, Misawa H, Akiyama S, Furukawa Y. Oxidative misfolding of Cu/Zn-superoxide dismutase triggered by non-canonical intramolecular disulfide formation. Free Radic Biol Med. 2020;147:187-99.
103. Cleveland DW, Liu J. Oxidation versus aggregation - how do SOD1 mutants cause ALS? Nat Med. 2000;6(12):1320-1.
104. Liu D, Wen J, Liu J, Li L. The roles of free radicals in amyotrophic lateral sclerosis: reactive oxygen species and elevated oxidation of protein, DNA, and membrane phospholipids. Faseb j. 1999;13(15):2318-28.
105. Yim MB, Chock PB, Stadtman ER. Copper, zinc superoxide dismutase catalyzes hydroxyl radical production from hydrogen peroxide. Proc Natl Acad Sci U S A. 1990;87(13):5006-10.
106. Jewett SL, Rocklin AM, Ghanevati M, Abel JM, Marach JA. A new look at a time-worn system: oxidation of CuZn-SOD by H2O2. Free Radic Biol Med. 1999;26(7-8):905-18.
107. Sampson JB, Beckman JS. Hydrogen peroxide damages the zinc-binding site of zinc-deficient Cu,Zn superoxide dismutase. Arch Biochem Biophys. 2001;392(1):8-13.
108. Seetharaman SV, Winkler DD, Taylor AB, Cao X, Whitson LJ, Doucette PA, et al. Disrupted zinc-binding sites in structures of pathogenic SOD1 variants D124V and H80R. Biochemistry. 2010;49(27):5714-25.
109. Li HT, Jiao M, Chen J, Liang Y. Roles of zinc and copper in modulating the oxidative refolding of bovine copper, zinc superoxide dismutase. Acta Biochim Biophys Sin (Shanghai). 2010;42(3):183-94.
110. Boyd SD, Ullrich MS, Calvo JS, Behnia F, Meloni G, Winkler DD. Mutations in Superoxide Dismutase 1 (Sod1) Linked to Familial Amyotrophic Lateral Sclerosis Can Disrupt High-Affinity Zinc-Binding Promoted by the Copper Chaperone for Sod1 (Ccs). Molecules. 2020;25(5).
111. Mendonça DM, Chimelli L, Martinez AM. Quantitative evidence for neurofilament heavy subunit aggregation in motor neurons of spinal cords of patients with amyotrophic lateral sclerosis. Braz J Med Biol Res. 2005;38(6):925-33.
112. Zucchi E, Bonetto V, Sorarù G, Martinelli I, Parchi P, Liguori R, et al. Neurofilaments in motor neuron disorders: towards promising diagnostic and prognostic biomarkers. Mol Neurodegener. 2020;15(1):58.
113. Falzone YM, Russo T, Domi T, Pozzi L, Quattrini A, Filippi M, et al. Current application of neurofilaments in amyotrophic lateral sclerosis and future perspectives. Neural Regen Res. 2021;16(10):1985-91.
114. Pierson KB, Evenson MA. 200 Kd neurofilament protein binds Al, Cu and Zn. Biochem Biophys Res Commun. 1988;152(2):598-604.
115. Crow JP, Sampson JB, Zhuang Y, Thompson JA, Beckman JS. Decreased zinc affinity of amyotrophic lateral sclerosis-associated superoxide dismutase mutants leads to enhanced catalysis of tyrosine nitration by peroxynitrite. J Neurochem. 1997;69(5):1936-44.

116. Crow JP, Ye YZ, Strong M, Kirk M, Barnes S, Beckman JS. Superoxide dismutase catalyzes nitration of tyrosines by peroxynitrite in the rod and head domains of neurofilament-L. J Neurochem. 1997;69(5):1945-53.
117. Gaggelli E, Kozlowski H, Valensin D, Valensin G. Copper homeostasis and neurodegenerative disorders (Alzheimer's, prion, and Parkinson's diseases and amyotrophic lateral sclerosis). Chem Rev. 2006;106(6):1995-2044.
118. Bourassa MW, Brown HH, Borchelt DR, Vogt S, Miller LM. Metal-deficient aggregates and diminished copper found in cells expressing SOD1 mutations that cause ALS. Front Aging Neurosci. 2014;6:110.
119. Roberts BR, Lim NK, McAllum EJ, Donnelly PS, Hare DJ, Doble PA, et al. Oral treatment with Cu(II)(atsm) increases mutant SOD1 in vivo but protects motor neurons and improves the phenotype of a transgenic mouse model of amyotrophic lateral sclerosis. J Neurosci. 2014;34(23):8021-31.
120. Nikseresht S, Hilton JBW, Kysenius K, Liddell JR, Crouch PJ. Copper-ATSM as a Treatment for ALS: Support from Mutant SOD1 Models and Beyond. Life (Basel). 2020;10(11).
121. Kurahashi T, Miyazaki A, Suwan S, Isobe M. Extensive investigations on oxidized amino acid residues in H(2)O(2)-treated Cu,Zn-SOd protein with LC-ESI-Q-TOF-MS, MS/MS for the determination of the copper-binding site. J Am Chem Soc. 2001;123(38):9268-78.
122. Hodgson EK, Fridovich I. The interaction of bovine erythrocyte superoxide dismutase with hydrogen peroxide: inactivation of the enzyme. Biochemistry. 1975;14(24):5294-9.
123. Hough MA, Grossmann JG, Antonyuk SV, Strange RW, Doucette PA, Rodriguez JA, et al. Dimer destabilization in superoxide dismutase may result in disease-causing properties: structures of motor neuron disease mutants. Proc Natl Acad Sci U S A. 2004;101(16):5976-81.
124. Arnesano F, Banci L, Bertini I, Martinelli M, Furukawa Y, O'Halloran TV. The unusually stable quaternary structure of human Cu,Zn-superoxide dismutase 1 is controlled by both metal occupancy and disulfide status. J Biol Chem. 2004;279(46):47998-8003.
125. Lynch SM, Boswell SA, Colón W. Kinetic stability of Cu/Zn superoxide dismutase is dependent on its metal ligands: implications for ALS. Biochemistry. 2004;43(51):16525-31.
126. Julien JP. Amyotrophic lateral sclerosis. unfolding the toxicity of the misfolded. Cell. 2001;104(4):581-91.
127. Coelho FR, Iqbal A, Linares E, Silva DF, Lima FS, Cuccovia IM, et al. Oxidation of the tryptophan 32 residue of human superoxide dismutase 1 caused by its bicarbonate-dependent peroxidase activity triggers the non-amyloid aggregation of the enzyme. J Biol Chem. 2014;289(44):30690-701.
128. Graffmo KS, Forsberg K, Bergh J, Birve A, Zetterström P, Andersen PM, et al. Expression of wild-type human superoxide dismutase-1 in mice causes amyotrophic lateral sclerosis. Hum Mol Genet. 2013;22(1):51-60.
129. Guareschi S, Cova E, Cereda C, Ceroni M, Donetti E, Bosco DA, et al. An over-oxidized form of superoxide dismutase found in sporadic amyotrophic lateral sclerosis with bulbar onset shares a toxic mechanism with mutant SOD1. Proc Natl Acad Sci U S A. 2012;109(13):5074-9.
130. Bakavayev S, Chetrit N, Zvagelsky T, Mansour R, Vyazmensky M, Barak Z, et al. Cu/Zn-superoxide dismutase and wild-type like fALS SOD1 mutants produce cytotoxic quantities of H(2)O(2) via cysteine-dependent redox short-circuit. Sci Rep. 2019;9(1):10826.
131. Fujiwara N, Nakano M, Kato S, Yoshihara D, Ookawara T, Eguchi H, et al. Oxidative modification to cysteine sulfonic acid of Cys111 in human copper-zinc superoxide dismutase. J Biol Chem. 2007;282(49):35933-44.
132. de Beus MD, Chung J, Colón W. Modification of cysteine 111 in Cu/Zn superoxide dismutase results in altered spectroscopic and biophysical properties. Protein Sci. 2004;13(5):1347-55.

133. Chen X, Shang H, Qiu X, Fujiwara N, Cui L, Li XM, et al. Oxidative modification of cysteine 111 promotes disulfide bond-independent aggregation of SOD1. Neurochem Res. 2012;37(4):835-45.
134. Shafiq K, Sanghai N, Guo Y, Kong J. Implication of post-translationally modified SOD1 in pathological aging. Geroscience. 2021;43(2):507-15.
135. Bosco DA, Morfini G, Karabacak NM, Song Y, Gros-Louis F, Pasinelli P, et al. Wild-type and mutant SOD1 share an aberrant conformation and a common pathogenic pathway in ALS. Nat Neurosci. 2010;13(11):1396-403.
136. Strange RW, Antonyuk SV, Hough MA, Doucette PA, Valentine JS, Hasnain SS. Variable metallation of human superoxide dismutase: atomic resolution crystal structures of Cu-Zn, Zn-Zn and as-isolated wild-type enzymes. J Mol Biol. 2006;356(5):1152-62.
137. Cohen TJ, Hwang AW, Unger T, Trojanowski JQ, Lee VM. Redox signalling directly regulates TDP-43 via cysteine oxidation and disulphide cross-linking. Embo j. 2012;31(5):1241-52.
138. Pokrishevsky E, Grad LI, Yousefi M, Wang J, Mackenzie IR, Cashman NR. Aberrant localization of FUS and TDP43 is associated with misfolding of SOD1 in amyotrophic lateral sclerosis. PLoS One. 2012;7(4):e35050.
139. Jiang LL, Che MX, Zhao J, Zhou CJ, Xie MY, Li HY, et al. Structural transformation of the amyloidogenic core region of TDP-43 protein initiates its aggregation and cytoplasmic inclusion. J Biol Chem. 2013;288(27):19614-24.
140. Robinson JL, Geser F, Stieber A, Umoh M, Kwong LK, Van Deerlin VM, et al. TDP-43 skeins show properties of amyloid in a subset of ALS cases. Acta Neuropathol. 2013;125(1):121-31.
141. Xu WC, Liang JZ, Li C, He ZX, Yuan HY, Huang BY, et al. Pathological hydrogen peroxide triggers the fibrillization of wild-type SOD1 via sulfenic acid modification of Cys-111. Cell Death Dis. 2018;9(2):67.
142. Chang CK, Chiang MH, Toh EK, Chang CF, Huang TH. Molecular mechanism of oxidation-induced TDP-43 RRM1 aggregation and loss of function. FEBS Lett. 2013;587(6):575-82.
143. Lin Y, Zhou X, Kato M, Liu D, Ghaemmaghami S, Tu BP, et al. Redox-mediated regulation of an evolutionarily conserved cross-β structure formed by the TDP43 low complexity domain. Proc Natl Acad Sci U S A. 2020;117(46):28727-34.
144. Wood A, Gurfinkel Y, Polain N, Lamont W, Lyn Rea S. Molecular Mechanisms Underlying TDP-43 Pathology in Cellular and Animal Models of ALS and FTLD. Int J Mol Sci. 2021;22(9).
145. Hinchcliffe M, Smith A. Riluzole: real-world evidence supports significant extension of median survival times in patients with amyotrophic lateral sclerosis. Degener Neurol Neuromuscul Dis. 2017;7:61-70.
146. Jaiswal MK. Riluzole and edaravone: A tale of two amyotrophic lateral sclerosis drugs. Med Res Rev. 2019;39(2):733-48.
147. Watanabe K, Tanaka M, Yuki S, Hirai M, Yamamoto Y. How is edaravone effective against acute ischemic stroke and amyotrophic lateral sclerosis? J Clin Biochem Nutr. 2018;62(1):20-38.
148. Kikuchi K, Takeshige N, Miura N, Morimoto Y, Ito T, Tancharoen S, et al. Beyond free radical scavenging: Beneficial effects of edaravone (Radicut) in various diseases (Review). Exp Ther Med. 2012;3(1):3-8.
149. Kikuchi K, Uchikado H, Miyagi N, Morimoto Y, Ito T, Tancharoen S, et al. Beyond neurological disease: new targets for edaravone (Review). Int J Mol Med. 2011;28(6):899-906.
150. Lapchak PA. A critical assessment of edaravone acute ischemic stroke efficacy trials: is edaravone an effective neuroprotective therapy? Expert Opin Pharmacother. 2010;11(10):1753-63.
151. Breiner A, Zinman L, Bourque PR. Edaravone for amyotrophic lateral sclerosis: barriers to access and lifeboat ethics. Cmaj. 2020;192(12):E319-e20.

152. Sinha M, Anuradha H, Juyal R, Shukla R, Garg R, Kar A. Edaravone in acute ischemic stroke, An Indian experience. Neurology asia. 2009;14(1).
153. Cruz MP. Edaravone (Radicava): A Novel Neuroprotective Agent for the Treatment of Amyotrophic Lateral Sclerosis. P t. 2018;43(1):25-8.
154. Bala V, Rao S, Bateman E, Keefe D, Wang S, Prestidge CA. Enabling oral SN38-based chemotherapy with a combined lipophilic prodrug and self-microemulsifying drug delivery system. Molecular pharmaceutics. 2016;13(10):3518-25.
155. Rong WT, Lu YP, Tao Q, Guo M, Lu Y, Ren Y, et al. Hydroxypropyl-sulfobutyl-β-cyclodextrin improves the oral bioavailability of edaravone by modulating drug efflux pump of enterocytes. J Pharm Sci. 2014;103(2):730-42.
156. Ma L, Sun J, Peng Y, Zhang R, Shao F, Hu X, et al. Glucuronidation of edaravone by human liver and kidney microsomes: biphasic kinetics and identification of UGT1A9 as the major UDP-glucuronosyltransferase isoform. Drug Metab Dispos. 2012;40(4):734-41.
157. Tanaka M, Sugimura N, Fujisawa A, Yamamoto Y. Stabilizers of edaravone aqueous solution and their action mechanisms. 1. Sodium bisulfite. J Clin Biochem Nutr. 2017;61(3):159-63.
158. Tanaka M, Motomiya S, Fujisawa A, Yamamoto Y. Stabilizers of edaravone aqueous solution and their action mechanisms. 2. Glutathione. J Clin Biochem Nutr. 2017;61(3):164-8.
159. Amekura S, Nakajima M, Watanabe M, Saitoh M, Iida S, Yamamoto Y, et al. 4-Cl-edaravone and (E)-2-chloro-3-[(E)-phenyldiazenyl]-2-butenoic acid are the specific reaction products of edaravone with hypochlorite. J Clin Biochem Nutr. 2020;67(2):159-66.
160. Parikh A, Kathawala K, Tan CC, Garg S, Zhou XF. Self-nanomicellizing solid dispersion of edaravone: part I - oral bioavailability improvement. Drug Des Devel Ther. 2018;12:2051-69.
161. Watanabe T, Tahara M, Todo S. The novel antioxidant edaravone: from bench to bedside. Cardiovasc Ther. 2008;26(2):101-14.
162. Francisco AP, Ressurreição AS, de Jesus Perry M, Lopes F. 4.2. 3.1. Knorr Pyrazole Synthesis of Edaravone. 2016.
163. Pandey K, Meena AK, Jain A, Singh R. Molecular mechanism of phenylhydrazine induced haematotoxicity: a review. Ame J Phytomed Clin Therapeut. 2014;2(3):390-4.
164. Berger J. Phenylhydrazine haematotoxicity. J Appl Biomed. 2007;5(3):125-30.
165. Reddy MV, Shyamala P, Sharma AK, Sahu PN, Subramaniyam K, Harihar S, et al. Synthesis and evaluation of edaravone-1, 3, 4-oxadiazole derivatives as potential anti-cancer inhibitors. New Journal of Chemistry. 2025;49(27):11870-84.
166. Colombo E, Olla S, Minnelli C, Formato A, Veroni C, Corbisiero S, et al. Synthesis and Characterization of Edaravone Analogues as Remyelinating Agents and Putative Mechanistic Probes. Molecules. 2023;28(19):6928.
167. Antre RV, Cendilkumar A, Goli D, Andhale GS, Oswal RJ. Microwave assisted synthesis of novel pyrazolone derivatives attached to a pyrimidine moiety and evaluation of their anti-inflammatory, analgesic and antipyretic activities. Saudi pharmaceutical journal. 2011;19(4):233-43.
168. Zhou S, Hong Q, Mei W, He Y, Wu C, Sun T. Scale-up of a continuous manufacturing process of edaravone. Organic Process Research & Development. 2021;25(9):2146-53.
169. Abd EL-Rahman NM, Saleh TS, Mady MF. Ultrasound assisted synthesis of some new 1, 3, 4-thiadiazole and bi (1, 3, 4-thiadiazole) derivatives incorporating pyrazolone moiety. Ultrasonics sonochemistry. 2009;16(1):70-4.
170. Touaibia M, Levesque NA. Synthesis, Copper Chelation, and Free Radical Scavenging Ability of Edaravone: An Undergraduate Medicinal Chemistry Laboratory Experiment. Journal of Chemical Education. 2024;101(11):4924-30.

171. Watanabe K, Morinaka Y, Iseki K, Watanabe T, Yuki S, Nishi H. Structure–activity relationship of 3-methyl-1-phenyl-2-pyrazolin-5-one (edaravone). Redox report. 2003;8(3):151-5.
172. Gay-Lussac JL, Thénard LJ. Sur la décomposition et la recomposition de l'acide boracique. Ann Chim Phys. 1808;68:169-74.
173. Brown HC, Malhotra SV, Ramachandran PV. Organoboranes for synthesis 17. Generality of hydroboration-amination for the conversion of terpenes into enantiomerically pure terpenylamines. Their utility for gas chromatographic analysis of chiral carboxylic acids. Tetrahedron: Asymmetry. 1996;7(12):3527-34.
174. Yang W, Gao X, Wang B. Boronic acid compounds as potential pharmaceutical agents. Medicinal research reviews. 2003;23(3):346-68.
175. DeFrancesco H, Dudley J, Coca A. Boron chemistry: an overview. Boron reagents in synthesis. 2016:1-25.
176. Martin R, Buchwald SL. Palladium-catalyzed Suzuki– Miyaura cross-coupling reactions employing dialkylbiaryl phosphine ligands. Accounts of chemical research. 2008;41(11):1461-73.
177. Buskes MJ, Blanco M-J. Impact of cross-coupling reactions in drug discovery and development. Molecules. 2020;25(15):3493.
178. Diaz DB, Yudin AK. The versatility of boron in biological target engagement. Nature Chemistry. 2017;9(8):731-42.
179. Fernandes GFS, Denny WA, Dos Santos JL. Boron in drug design: Recent advances in the development of new therapeutic agents. European Journal of Medicinal Chemistry. 2019;179:791-804.
180. Lorand JP, EDWARDS JO. Polyol complexes and structure of the benzeneboronate ion. The Journal of Organic Chemistry. 1959;24(6):769-74.
181. Springsteen G, Ballard CE, Gao S, Wang W, Wang B. The development of photometric sensors for boronic acids. Bioorganic chemistry. 2001;29(5):259-70.
182. Cammidge AN, Crépy KV. Synthesis of chiral binaphthalenes using the asymmetric Suzuki reaction. Tetrahedron. 2004;60(20):4377-86.
183. Lamandé L, Boyer D, Munoz A. Structure et acidite de composes a atome de bore et de phosphore hypercoordonnes. Journal of organometallic chemistry. 1980;329(1):1-29.
184. Stowell SR, Ju T, Cummings RD. Protein glycosylation in cancer. Annual Review of Pathology: Mechanisms of Disease. 2015;10:473-510.
185. Jin S, Cheng Y, Reid S, Li M, Wang B. Carbohydrate recognition by boronolectins, small molecules, and lectins. Medicinal research reviews. 2010;30(2):171-257.
186. Yang W, Fan H, Gao X, Gao S, Karnati VVR, Ni W, et al. The first fluorescent diboronic acid sensor specific for hepatocellular carcinoma cells expressing sialyl Lewis X. Chemistry & biology. 2004;11(4):439-48.
187. Yang W, Gao S, Gao X, Karnati VVR, Ni W, Wang B, et al. Diboronic acids as fluorescent probes for cells expressing sialyl Lewis X. Bioorganic & Medicinal Chemistry Letters. 2002;12(16):2175-7.
188. Wang Z, Zhang D, Zhu D. A new saccharide sensor based on a tetrathiafulvalene–anthracene dyad with a boronic acid group. The Journal of Organic Chemistry. 2005;70(14):5729-32.
189. Manimala JC, Wiskur SL, Ellington AD, Anslyn EV. Tuning the specificity of a synthetic receptor using a selected nucleic acid receptor. Journal of the American Chemical Society. 2004;126(50):16515-9.
190. Baker SJ, Zhang Y-K, Akama T, Lau A, Zhou H, Hernandez V, et al. Discovery of a new boron-containing antifungal agent, 5-fluoro-1, 3-dihydro-1-hydroxy-2, 1-benzoxaborole (AN2690), for the potential treatment of onychomycosis. Journal of medicinal chemistry. 2006;49(15):4447-50.

191. Windsor IW, Palte MJ, Lukesh III JC, Gold B, Forest KT, Raines RT. Sub-picomolar inhibition of HIV-1 protease with a boronic acid. Journal of the American Chemical Society. 2018;140(43):14015-8.
192. Chong PY, Shotwell JB, Miller J, Price DJ, Maynard A, Voitenleitner C, et al. Design of N-benzoxaborole benzofuran GSK8175—optimization of human pharmacokinetics inspired by metabolites of a failed clinical HCV inhibitor. Journal of Medicinal Chemistry. 2019;62(7):3254-67.
193. Malouff TD, Seneviratne DS, Ebner DK, Stross WC, Waddle MR, Trifiletti DM, et al. Boron neutron capture therapy: a review of clinical applications. Frontiers in oncology. 2021;11:351.
194. Génin E, Reboud-Ravaux M, Vidal J. Proteasome inhibitors: recent advances and new perspectives in medicinal chemistry. Current topics in medicinal chemistry. 2010;10(3):232-56.
195. Gupta AK, Versteeg SG. Tavaborole–a treatment for onychomycosis of the toenails. Expert Review of Clinical Pharmacology. 2016;9(9):1145-52.
196. Richardson PG, Zweegman S, O'Donnell EK, Laubach JP, Raje N, Voorhees P, et al. Ixazomib for the treatment of multiple myeloma. Expert Opin Pharmacother. 2018;19(17):1949-68.
197. Jarnagin K, Chanda S, Coronado D, Ciaravino V, Zane LT, Guttman-Yassky E, et al. Crisaborole Topical Ointment, 2%: A Nonsteroidal, Topical, Anti-Inflammatory Phosphodiesterase 4 Inhibitor in Clinical Development for the Treatment of Atopic Dermatitis. J Drugs Dermatol. 2016;15(4):390-6.
198. Burgos RM, Biagi MJ, Rodvold KA, Danziger LH. Pharmacokinetic evaluation of meropenem and vaborbactam for the treatment of urinary tract infection. Expert Opin Drug Metab Toxicol. 2018;14(10):1007-21.
199. Fazal T, Ali F, Hosmane NS, Zhu Y. Boron compounds for catalytic applications. Advances in Catalysis. 71: Elsevier; 2022. p. 169-99.
200. Lopalco A, Lopedota AA, Laquintana V, Denora N, Stella VJ. Boric acid, a Lewis acid with unique and unusual properties: formulation implications. Journal of Pharmaceutical Sciences. 2020;109(8):2375-86.
201. Korich AL, Iovine PM. Boroxine chemistry and applications: A perspective. Dalton Transactions. 2010;39(6):1423-31.
202. Zumreoglu-Karan B, Kose DA. Boric acid: a simple molecule of physiologic, therapeutic and prebiotic significance. Pure and Applied Chemistry. 2015;87(2):155-62.
203. Brooks WLA, Deng CC, Sumerlin BS. Structure-Reactivity Relationships in Boronic Acid-Diol Complexation. ACS Omega. 2018;3(12):17863-70.
204. Miwa K, Takano J, Omori H, Seki M, Shinozaki K, Fujiwara T. Plants tolerant of high boron levels. Science. 2007;318(5855):1417-.
205. Park M, Li Q, Shcheynikov N, Zeng W, Muallem S. NaBC1 is a ubiquitous electrogenic Na+-coupled borate transporter essential for cellular boron homeostasis and cell growth and proliferation. Molecular cell. 2004;16(3):331-41.
206. Scorei IR. Calcium fructoborate: plant-based dietary boron as potential medicine for cancer therapy. Frontiers in Bioscience-Scholar. 2011;3(1):205-15.
207. Calvo MB, Figueroa A, Pulido EG, Campelo RG, Aparicio LA. Potential role of sugar transporters in cancer and their relationship with anticancer therapy. International journal of endocrinology. 2010;2010.
208. Murray FJ. A comparative review of the pharmacokinetics of boric acid in rodents and humans. Biological trace element research. 1998;66:331-41.
209. Moseman RF. Chemical disposition of boron in animals and humans. Environmental health perspectives. 1994;102(suppl 7):113-7.
210. Jansen JA, Andersen J, Schou JS. Boric acid single dose pharmacokinetics after intravenous administration to man. Archives of toxicology. 1984;55:64-7.

211. Wiley H. Results of experiments on the effect of borax administered with food. Analyst. 1904;29(December):357-70.
212. PFEIFFER CC, Hallman LF, GERSH I. Boric acid ointment: a study of possible intoxication in the treatment of burns. Journal of the American Medical Association. 1945;128(4):266-74.
213. Murray FJ, Schlekat CE. Comparison of risk assessments of boron: alternate approaches to chemical-specific adjustment factors. Human and Ecological Risk Assessment. 2004;10(1):57-68.
214. Locksley HB, Sweet WH. Tissue distribution of boron compounds in relation to neutron-capture therapy of cancer. Proceedings of the Society for Experimental Biology and Medicine. 1954;86(1):56-63.
215. Weir Jr RJ, Fisher RS. Toxicologic studies on borax and boric acid. Toxicology and Applied Pharmacology. 1972;23(3):351-64.
216. Williams M, Mumtaz M, Fay M, Scinicariello F, Jenkins K, Lumpkin M. Draft toxicological profile for boron. 2007.
217. Trace elements in human nutrition and health. World Health Organization. 1996.
218. Zhong Q, Zhang C, Zhang Q, Miele L, Zheng S, Wang G. Boronic prodrug of 4-hydroxytamoxifen is more efficacious than tamoxifen with enhanced bioavailability independent of CYP2D6 status. BMC cancer. 2015;15(1):1-9.
219. Trippier PC, McGuigan C. Boronic acids in medicinal chemistry: anticancer, antibacterial and antiviral applications. MedChemComm. 2010;1(3):183-98.
220. Baker SJ, Ding CZ, Akama T, Zhang Y-K, Hernandez V, Xia Y. Therapeutic potential of boron-containing compounds. Future medicinal chemistry. 2009;1(7):1275-88.
221. Soriano-Ursúa MA, Farfán-García ED, Geninatti-Crich S. Turning fear of boron toxicity into boron-containing drug design. Current medicinal chemistry. 2019;26(26):5005-18.
222. Lu CJ, Hu J, Wang Z, Xie S, Pan T, Huang L, et al. Discovery of boron-containing compounds as Aβ aggregation inhibitors and antioxidants for the treatment of Alzheimer's disease. Medchemcomm. 2018;9(11):1862-70.
223. Ozansoy M, AltintaŞ M, Ozansoy MB, GÜnay N, KiliÇ E, KiliÇ Ü. Two boron-containing compounds affect the cellular viability of SH-SY5Y cells in an in vitro amyloid-beta toxicity model. Turk J Biol. 2020;44(4):208-14.
224. Ciofani G, Danti S, D'Alessandro D, Ricotti L, Moscato S, Bertoni G, et al. Enhancement of neurite outgrowth in neuronal-like cells following boron nitride nanotube-mediated stimulation. ACS Nano. 2010;4(10):6267-77.
225. Cacciatore I, Turkez H, Di Rienzo A, Ciulla M, Mardinoglu A, Di Stefano A. Boron-based hybrids as novel scaffolds for the development of drugs with neuroprotective properties. RSC Med Chem. 2021;12(11):1944-9.
226. Maiti P, Manna J, Burch ZN, Flaherty DB, Larkin JD, Dunbar GL. Ameliorative Properties of Boronic Compounds in In Vitro and In Vivo Models of Alzheimer's Disease. International Journal of Molecular Sciences. 2020;21(18):6664.
227. Routray I, Ali S. Boron inhibits apoptosis in hyperapoptosis condition: Acts by stabilizing the mitochondrial membrane and inhibiting matrix remodeling. Biochimica et Biophysica Acta (BBA)-General Subjects. 2019;1863(1):144-52.
228. Ly JD, Grubb DR, Lawen A. The mitochondrial membrane potential (Δψ m) in apoptosis; an update. Apoptosis. 2003;8:115-28.
229. Baldwin AG, Rivers-Auty J, Daniels MJ, White CS, Schwalbe CH, Schilling T, et al. Boron-based inhibitors of the NLRP3 inflammasome. Cell chemical biology. 2017;24(11):1321-35. e5.
230. McGettrick A, O'Neill L. NLRP3 and IL-1 β in macrophages as critical regulators of metabolic diseases. Diabetes, Obesity and Metabolism. 2013;15(s3):19-25.

231. Heneka MT, Golenbock DT, Latz E. Innate immunity in Alzheimer's disease. Nature immunology. 2015;16(3):229-36.
232. Penland JG. The importance of boron nutrition for brain and psychological function. Biol Trace Elem Res. 1998;66(1-3):299-317.
233. Ercal N, Gurer-Orhan H, Aykin-Burns N. Toxic metals and oxidative stress part I: mechanisms involved in metal-induced oxidative damage. Current topics in medicinal chemistry. 2001;1(6):529-39.
234. Birla H, Minocha T, Kumar G, Misra A, Singh SK. Role of oxidative stress and metal toxicity in the progression of Alzheimer's disease. Current Neuropharmacology. 2020;18(7):552-62.
235. Vasudevaraju P, Govindaraju M, Palanisamy A, Sambamurti K, Rao K. Molecular toxicity of aluminium in relation to neurodegeneration. Indian Journal of Medical Research. 2008;128(4):545-56.
236. Kumar V, Gill KD. Oxidative stress and mitochondrial dysfunction in aluminium neurotoxicity and its amelioration: a review. Neurotoxicology. 2014;41:154-66.
237. Özdemir Ç, Arslan M, Küçük A, Yığman Z, Dursun AD. Therapeutic Efficacy of Boric Acid Treatment on Brain Tissue and Cognitive Functions in Rats with Experimental Alzheimer's Disease. Drug Design, Development and Therapy. 2023:1453-62.
238. Penland JG. Dietary boron, brain function, and cognitive performance. Environmental health perspectives. 1994;102(suppl 7):65-72.
239. Yildirim C, Cevik S, Yamaner H, Orkmez M, Eronat O, Bozdayı MA, et al. Boric acid improves the behavioral, electrophysiological and histological parameters of cisplatin-induced peripheral neuropathy in rats. Journal of Trace Elements in Medicine and Biology. 2022;70:126917.
240. Kızılay Z, Erken HA, Çetin NK, Aktaş S, Abas Bİ, Yılmaz A. Boric acid reduces axonal and myelin damage in experimental sciatic nerve injury. Neural regeneration research. 2016;11(10):1660.
241. Hacioglu C, Kar F, Kar E, Kara Y, Kanbak G. Effects of curcumin and boric acid against neurodegenerative damage induced by amyloid beta (1-42). Biological Trace Element Research. 2021;199:3793-800.
242. Kuivila HG. Electrophilic displacement reactions. III. Kinetics of the reaction between hydrogen peroxide and benzeneboronic Acid1. Journal of the American Chemical Society. 1954;76(3):870-4.
243. Kuivila HG, Armour AG. Electrophilic displacement reactions. IX. Effects of substituents on rates of reactions between hydrogen peroxide and benzeneboronic acid1-3. Journal of the American Chemical Society. 1957;79(21):5659-62.
244. Sikora A, Zielonka J, Lopez M, Joseph J, Kalyanaraman B. Direct oxidation of boronates by peroxynitrite: mechanism and implications in fluorescence imaging of peroxynitrite. Free Radical Biology and Medicine. 2009;47(10):1401-7.
245. Zielonka J, Sikora A, Joseph J, Kalyanaraman B. Peroxynitrite Is the Major Species Formed from Different Flux Ratios of Co-generated Nitric Oxide and Superoxide: DIRECT REACTION WITH BORONATE-BASED FLUORESCENT PROBE*♦. Journal of Biological Chemistry. 2010;285(19):14210-6.
246. Zielonka J, Sikora A, Hardy M, Joseph J, Dranka BP, Kalyanaraman B. Boronate probes as diagnostic tools for real time monitoring of peroxynitrite and hydroperoxides. Chemical research in toxicology. 2012;25(9):1793-9.
247. Bhalani DV, Nutan B, Kumar A, Singh Chandel AK. Bioavailability Enhancement Techniques for Poorly Aqueous Soluble Drugs and Therapeutics. Biomedicines. 2022;10(9).
248. Rocha B, de Morais LA, Viana MC, Carneiro G. Promising strategies for improving oral bioavailability of poor water-soluble drugs. Expert Opin Drug Discov. 2023;18(6):615-27.

249. Huitema AD, Spaander M, Mathĵt RA, Tibben MM, Holtkamp MJ, Beijnen JH, et al. Relationship between exposure and toxicity in high-dose chemotherapy with cyclophosphamide, thiotepa and carboplatin. Ann Oncol. 2002;13(3):374-84.
250. Fischer MA, Jan A. Medication-Overuse Headache. StatPearls. Treasure Island (FL) ineligible companies. Disclosure: Arif Jan declares no relevant financial relationships with ineligible companies.: StatPearls Publishing

251. Turnheim K. When drug therapy gets old: pharmacokinetics and pharmacodynamics in the elderly. Exp Gerontol. 2003;38(8):843-53.
252. Peiró Cadahía J, Previtali V, Troelsen NS, Clausen MH. Prodrug strategies for targeted therapy triggered by reactive oxygen species. Medchemcomm. 2019;10(9):1531-49.
253. Hatanaka H. A revised boron-neutron capture therapy for malignant brain tumors. II. Interim clinical result with the patients excluding previous treatments. J Neurol. 1975;209(2):81-94.
254. Mishima Y, Ichihashi M, Hatta S, Honda C, Yamamura K, Nakagawa T. New thermal neutron capture therapy for malignant melanoma: melanogenesis-seeking 10B molecule-melanoma cell interaction from in vitro to first clinical trial. Pigment Cell Res. 1989;2(4):226-34.
255. Kabalka GW, Yao ML. The synthesis and use of boronated amino acids for boron neutron capture therapy. Anticancer Agents Med Chem. 2006;6(2):111-25.
256. Wittig A, Sauerwein WA, Coderre JA. Mechanisms of transport of p-borono-phenylalanine through the cell membrane in vitro. Radiat Res. 2000;153(2):173-80.
257. Koc ER, Gökce EC, Sönmez MA, Namuslu M, Gökce A, Bodur AS. Borax partially prevents neurologic disability and oxidative stress in experimental spinal cord ischemia/reperfusion injury. J Stroke Cerebrovasc Dis. 2015;24(1):83-90.
258. Moseman RF. Chemical disposition of boron in animals and humans. Environ Health Perspect. 1994;102 Suppl 7(Suppl 7):113-7.
259. Coban FK, Ince S, Kucukkurt I, Demirel HH, Hazman O. Boron attenuates malathion-induced oxidative stress and acetylcholinesterase inhibition in rats. Drug Chem Toxicol. 2015;38(4):391-9.
260. Klimenko LL, Skalny AV, Turna AA, Tinkov AA, Budanova MN, Baskakov IS, et al. Serum Trace Element Profiles, Prolactin, and Cortisol in Transient Ischemic Attack Patients. Biol Trace Elem Res. 2016;172(1):93-100.
261. Ciofani G. Potential applications of boron nitride nanotubes as drug delivery systems. Expert opinion on drug delivery. 2010;7(8):889-93.
262. Levêque D, Carvalho MC, Maloisel F. Review. Clinical pharmacokinetics of bortezomib. In Vivo. 2007;21(2):273-8.
263. Zhong Q, Zhang C, Zhang Q, Miele L, Zheng S, Wang G. Boronic prodrug of 4-hydroxytamoxifen is more efficacious than tamoxifen with enhanced bioavailability independent of CYP2D6 status. BMC Cancer. 2015;15:625.
264. Park H, McEachon JD, 2nd, Pollock JA. Synthesis and characterization of hydrogen peroxide activated estrogen receptor beta ligands. Bioorg Med Chem. 2019;27(10):2075-82.
265. Charkoudian LK, Pham DM, Franz KJ. A pro-chelator triggered by hydrogen peroxide inhibits iron-promoted hydroxyl radical formation. J Am Chem Soc. 2006;128(38):12424-5.
266. Franks AT, Franz KJ. A prochelator with a modular masking group featuring hydrogen peroxide activation with concurrent fluorescent reporting. Chem Commun (Camb). 2014;50(77):11317-20.
267. Domingo JL. Developmental toxicity of metal chelating agents. Reprod Toxicol. 1998;12(5):499-510.

268. Lin VS, Dickinson BC, Chang CJ. Boronate-based fluorescent probes: imaging hydrogen peroxide in living systems. Methods Enzymol. 2013;526:19-43.
269. Hampton MB, Orrenius S. Dual regulation of caspase activity by hydrogen peroxide: implications for apoptosis. FEBS Lett. 1997;414(3):552-6.
270. Peiró Cadahía J, Bondebjerg J, Hansen CA, Previtali V, Hansen AE, Andresen TL, et al. Synthesis and Evaluation of Hydrogen Peroxide Sensitive Prodrugs of Methotrexate and Aminopterin for the Treatment of Rheumatoid Arthritis. J Med Chem. 2018;61(8):3503-15.
271. Hoang TT, Smith TP, Raines RT. A Boronic Acid Conjugate of Angiogenin that Shows ROS-Responsive Neuroprotective Activity. Angewandte Chemie. 2017;129(10):2663-6.
272. Greenway MJ, Andersen PM, Russ C, Ennis S, Cashman S, Donaghy C, et al. ANG mutations segregate with familial and'sporadic'amyotrophic lateral sclerosis. Nature genetics. 2006;38(4):411-3.
273. Van Es MA, Schelhaas HJ, Van Vught PW, Ticozzi N, Andersen PM, Groen EJ, et al. Angiogenin variants in Parkinson disease and amyotrophic lateral sclerosis. Annals of neurology. 2011;70(6):964-73.
274. Chen Y, Qin C, Huang J, Tang X, Liu C, Huang K, et al. The role of astrocytes in oxidative stress of central nervous system: A mixed blessing. Cell proliferation. 2020;53(3):e12781.
275. Barber SC, Mead RJ, Shaw PJ. Oxidative stress in ALS: a mechanism of neurodegeneration and a therapeutic target. Biochimica et Biophysica Acta (BBA)-Molecular Basis of Disease. 2006;1762(11-12):1051-67.
276. Bozzo F, Mirra A, Carrì M. Oxidative stress and mitochondrial damage in the pathogenesis of ALS: New perspectives. Neuroscience letters. 2017;636:3-8.
277. Robberecht W. Oxidative stress in amyotrophic lateral sclerosis. Journal of neurology. 2000;247:I1-I6.
278. D'Amico E, Factor-Litvak P, Santella RM, Mitsumoto H. Clinical perspective on oxidative stress in sporadic amyotrophic lateral sclerosis. Free radical biology and medicine. 2013;65:509-27.
279. Shaw PJ, Ince PG, Falkous G, Mantle D. Oxidative damage to protein in sporadic motor neuron disease spinal cord. Annals of Neurology: Official Journal of the American Neurological Association and the Child Neurology Society. 1995;38(4):691-5.
280. Ferrante RJ, Browne SE, Shinobu LA, Bowling AC, Baik MJ, MacGarvey U, et al. Evidence of increased oxidative damage in both sporadic and familial amyotrophic lateral sclerosis. Journal of neurochemistry. 1997;69(5):2064-74.
281. Beal MF, Ferrante RJ, Browne SE, Matthews RT, Kowall NW, Brown Jr RH. Increased 3-nitrotyrosine in both sporadic and familial amyotrophic lateral sclerosis. Annals of Neurology: Official Journal of the American Neurological Association and the Child Neurology Society. 1997;42(4):644-54.
282. Shibata N, Nagai R, Uchida K, Horiuchi S, Yamada S, Hirano A, et al. Morphological evidence for lipid peroxidation and protein glycoxidation in spinal cords from sporadic amyotrophic lateral sclerosis patients. Brain research. 2001;917(1):97-104.
283. Bogdanov M, Brown Jr RH, Matson W, Smart R, Hayden D, O'Donnell H, et al. Increased oxidative damage to DNA in ALS patients. Free Radical Biology and Medicine. 2000;29(7):652-8.
284. Smith RG, Henry YK, Mattson MP, Appel SH. Presence of 4-hydroxynonenal in cerebrospinal fluid of patients with sporadic amyotrophic lateral sclerosis. Annals of Neurology: Official Journal of the American Neurological Association and the Child Neurology Society. 1998;44(4):696-9.
285. Andrus PK, Fleck TJ, Gurney ME, Hall ED. Protein oxidative damage in a transgenic mouse model of familial amyotrophic lateral sclerosis. Journal of neurochemistry. 1998;71(5):2041-8.

286. Liu R, Althaus JS, Ellerbrock BR, Becker DA, Gurney ME. Enhanced oxygen radical production in a transgenic mouse model of familial amyotrophic lateral sclerosis. Annals of neurology. 1998;44(5):763-70.
287. Bu X-L, Xiang Y, Guo Y. The role of iron in amyotrophic lateral sclerosis. Brain Iron Metabolism and CNS Diseases. 2019:145-52.
288. Sheykhansari S, Kozielski K, Bill J, Sitti M, Gemmati D, Zamboni P, et al. Redox metals homeostasis in multiple sclerosis and amyotrophic lateral sclerosis: a review. Cell death & disease. 2018;9(3):348.
289. Zheng Y, Gao L, Wang D, Zang D. Elevated levels of ferritin in the cerebrospinal fluid of amyotrophic lateral sclerosis patients. Acta Neurologica Scandinavica. 2017;136(2):145-50.
290. Winterbourn CC. Toxicity of iron and hydrogen peroxide: the Fenton reaction. Toxicology letters. 1995;82:969-74.
291. Guo H, Aleyasin H, Dickinson BC, Haskew-Layton RE, Ratan RR. Recent advances in hydrogen peroxide imaging for biological applications. Cell & bioscience. 2014;4:1-10.
292. Wang Q, Franz KJ. Stimulus-responsive prochelators for manipulating cellular metals. Accounts of chemical research. 2016;49(11):2468-77.
293. Lippert AR, Van de Bittner GC, Chang CJ. Boronate oxidation as a bioorthogonal reaction approach for studying the chemistry of hydrogen peroxide in living systems. Accounts of chemical research. 2011;44(9):793-804.
294. Cadahía JP, Previtali V, Troelsen NS, Clausen MH. Prodrug strategies for targeted therapy triggered by reactive oxygen species. MedChemComm. 2019;10(9):1531-49.
295. Peng X, Gandhi V. ROS-activated anticancer prodrugs: a new strategy for tumor-specific damage. Therapeutic delivery. 2012;3(7):823-33.
296. Pan Q, Zhang B, Peng X, Wan S, Luo K, Gao W, et al. A dithiocarbamate-based H 2 O 2-responsive prodrug for combinational chemotherapy and oxidative stress amplification therapy. Chemical Communications. 2019;55(92):13896-9.
297. Bao X-Z, Wang Q, Ren X-R, Dai F, Zhou B. A hydrogen peroxide-activated Cu (II) pro-ionophore strategy for modifying naphthazarin as a promising anticancer agent with high selectivity for generating ROS in HepG2 cells over in L02 cells. Free Radical Biology and Medicine. 2020;152:597-608.
298. Hogg MC, Halang L, Woods I, Coughlan KS, Prehn JHM. Riluzole does not improve lifespan or motor function in three ALS mouse models. Amyotroph Lateral Scler Frontotemporal Degener. 2018;19(5-6):438-45.
299. Li J, Sung M, Rutkove SB. Electrophysiologic biomarkers for assessing disease progression and the effect of riluzole in SOD1 G93A ALS mice. PLoS One. 2013;8(6):e65976.
300. Perrin S. Preclinical research: Make mouse studies work. Nature. 2014;507(7493):423-5.
301. Chiarotto GB, Cartarozzi LP, Perez M, Biscola NP, Spejo AB, Gubert F, et al. Tempol improves neuroinflammation and delays motor dysfunction in a mouse model (SOD1(G93A)) of ALS. J Neuroinflammation. 2019;16(1):218.
302. Jablonski MR, Markandaiah SS, Jacob D, Meng NJ, Li K, Gennaro V, et al. Inhibiting drug efflux transporters improves efficacy of ALS therapeutics. Ann Clin Transl Neurol. 2014;1(12):996-1005.
303. Scott S, Kranz JE, Cole J, Lincecum JM, Thompson K, Kelly N, et al. Design, power, and interpretation of studies in the standard murine model of ALS. Amyotroph Lateral Scler. 2008;9(1):4-15.
304. Rothstein JD. Edaravone: A new drug approved for ALS. Cell. 2017;171(4):725.

305. Ikeda K, Iwasaki Y. Edaravone, a Free Radical Scavenger, Delayed Symptomatic and Pathological Progression of Motor Neuron Disease in the Wobbler Mouse. PLoS One. 2015;10(10):e0140316.
306. Ohta Y, Nomura E, Shang J, Feng T, Huang Y, Liu X, et al. Enhanced oxidative stress and the treatment by edaravone in mice model of amyotrophic lateral sclerosis. J Neurosci Res. 2019;97(5):607-19.
307. Blasco H, Garcon G, Patin F, Veyrat-Durebex C, Boyer J, Devos D, et al. Panel of Oxidative Stress and Inflammatory Biomarkers in ALS: A Pilot Study. Can J Neurol Sci. 2017;44(1):90-5.
308. Dobrowolny G, Aucello M, Rizzuto E, Beccafico S, Mammucari C, Boncompagni S, et al. Skeletal muscle is a primary target of SOD1G93A-mediated toxicity. Cell Metab. 2008;8(5):425-36.
309. Tokuda E, Ono S, Ishige K, Naganuma A, Ito Y, Suzuki T. Metallothionein proteins expression, copper and zinc concentrations, and lipid peroxidation level in a rodent model for amyotrophic lateral sclerosis. Toxicology. 2007;229(1-2):33-41.
310. Liu R, Li B, Flanagan SW, Oberley LW, Gozal D, Qiu M. Increased mitochondrial antioxidative activity or decreased oxygen free radical propagation prevent mutant SOD1-mediated motor neuron cell death and increase amyotrophic lateral sclerosis-like transgenic mouse survival. Journal of neurochemistry. 2002;80(3):488-500.
311. Bruijn L, Beal M, Becher M, Schulz J, Wong P, Price DL, et al. Elevated free nitrotyrosine levels, but not protein-bound nitrotyrosine or hydroxyl radicals, throughout amyotrophic lateral sclerosis (ALS)-like disease implicate tyrosine nitration as an aberrant in vivo property of one familial ALS-linked superoxide dismutase 1 mutant. Proceedings of the National Academy of Sciences. 1997;94(14):7606-11.
312. Miana-Mena FJ, González-Mingot C, Larrodé P, Muñoz MJ, Oliván S, Fuentes-Broto L, et al. Monitoring systemic oxidative stress in an animal model of amyotrophic lateral sclerosis. Journal of neurology. 2011;258:762-9.
313. Iłzecka J. Total antioxidant status is increased in the serum of amyotrophic lateral sclerosis patients. Scand J Clin Lab Invest. 2003;63(4):297-302.
314. Ferrante RJ, Browne SE, Shinobu LA, Bowling AC, Baik MJ, MacGarvey U, et al. Evidence of increased oxidative damage in both sporadic and familial amyotrophic lateral sclerosis. J Neurochem. 1997;69(5):2064-74.
315. Beal MF, Ferrante RJ, Browne SE, Matthews RT, Kowall NW, Brown RH, Jr. Increased 3-nitrotyrosine in both sporadic and familial amyotrophic lateral sclerosis. Ann Neurol. 1997;42(4):644-54.
316. Abe K, Pan LH, Watanabe M, Kato T, Itoyama Y. Induction of nitrotyrosine-like immunoreactivity in the lower motor neuron of amyotrophic lateral sclerosis. Neurosci Lett. 1995;199(2):152-4.
317. Simpson EP, Henry YK, Henkel JS, Smith RG, Appel SH. Increased lipid peroxidation in sera of ALS patients: a potential biomarker of disease burden. Neurology. 2004;62(10):1758-65.
318. Smith RG, Henry YK, Mattson MP, Appel SH. Presence of 4-hydroxynonenal in cerebrospinal fluid of patients with sporadic amyotrophic lateral sclerosis. Ann Neurol. 1998;44(4):696-9.
319. Przedborski S, Donaldson D, Jakowec M, Kish SJ, Guttman M, Rosoklija G, et al. Brain superoxide dismutase, catalase, and glutathione peroxidase activities in amyotrophic lateral sclerosis. Annals of neurology. 1996;39(2):158-65.
320. Shefner JM, Cudkowicz ME. Failures to Replicate: What Recent Negative Phase 3 Trials Have Taught Us about Amyotrophic Lateral Sclerosis Clinical Research. Ann Neurol. 2024;96(2):211-5.
321. Turner MR, Thompson AG, Teunissen CE. Blood level of neurofilament light chain as a biomarker for neurological disorders. BMJ Med. 2025;4(1):e000958.

322. De Schaepdryver M, Goossens J, De Meyer S, Jeromin A, Masrori P, Brix B, et al. Serum neurofilament heavy chains as early marker of motor neuron degeneration. Ann Clin Transl Neurol. 2019;6(10):1971-9.
323. Lovett A, Chary S, Babu S, Bruneteau G, Glass JD, Karlsborg M, et al. Serious Neurologic Adverse Events in Tofersen Clinical Trials for Amyotrophic Lateral Sclerosis. Muscle Nerve. 2025;71(6):1006-15.
324. Bosco DA, Morfini G, Karabacak NM, Song Y, Gros-Louis F, Pasinelli P, et al. Wild-type and mutant SOD1 share an aberrant conformation and a common pathogenic pathway in ALS. Nature neuroscience. 2010;13(11):1396-403.
325. Liu D, Wen J, Liu J, Li L. The roles of free radicals in amyotrophic lateral sclerosis: reactive oxygen species and elevated oxidation of protein, DNA, and membrane phospholipids. The FASEB Journal. 1999;13(15):2318-28.
326. Yim M, Chock P, Stadtman E. Copper, zinc superoxide dismutase catalyzes hydroxyl radical production from hydrogen peroxide. Proceedings of the National Academy of Sciences. 1990;87(13):5006-10.
327. Jewett SL, Rocklin AM, Ghanevati M, Abel JM, Marach JA. A new look at a time-worn system: oxidation of CuZn-SOD by H2O2. Free Radical Biology and Medicine. 1999;26(7-8):905-18.
328. Sampson JB, Beckman JS. Hydrogen peroxide damages the zinc-binding site of zinc-deficient Cu, Zn superoxide dismutase. Archives of Biochemistry and Biophysics. 2001;392(1):8-13.
329. Rakhit R, Cunningham P, Furtos-Matei A, Dahan S, Qi X-F, Crow JP, et al. Oxidation-induced misfolding and aggregation of superoxide dismutase and its implications for amyotrophic lateral sclerosis. Journal of Biological Chemistry. 2002;277(49):47551-6.
330. Anzai I, Tokuda E, Handa S, Misawa H, Akiyama S, Furukawa Y. Oxidative misfolding of Cu/Zn-superoxide dismutase triggered by non-canonical intramolecular disulfide formation. Free Radical Biology and Medicine. 2020;147:187-99.
331. Yim MB, Kang JH, Yim HS, Kwak HS, Chock PB, Stadtman ER. A gain-of-function of an amyotrophic lateral sclerosis-associated Cu,Zn-superoxide dismutase mutant: An enhancement of free radical formation due to a decrease in Km for hydrogen peroxide. Proc Natl Acad Sci U S A. 1996;93(12):5709-14.
332. de Beus MD, Chung J, Colón W. Modification of cysteine 111 in Cu/Zn superoxide dismutase results in altered spectroscopic and biophysical properties. Protein Science. 2004;13(5):1347-55.
333. Valle C, Carrì MT. Cysteine Modifications in the Pathogenesis of ALS. Front Mol Neurosci. 2017;10:5.
334. Álvarez-Zaldiernas C, Lu J, Zheng Y, Yang H, Blasi J, Solsona C, et al. Cellular Redox Systems Impact the Aggregation of Cu,Zn Superoxide Dismutase Linked to Familial Amyotrophic Lateral Sclerosis. J Biol Chem. 2016;291(33):17197-208.
335. Karch CM, Borchelt DR. A limited role for disulfide cross-linking in the aggregation of mutant SOD1 linked to familial amyotrophic lateral sclerosis. J Biol Chem. 2008;283(20):13528-37.
336. Li C, Xu WC, Xie ZS, Pan K, Hu J, Chen J, et al. Cupric ions induce the oxidation and trigger the aggregation of human superoxide dismutase 1. PLoS One. 2013;8(6):e65287.
337. Ilieva H, Polymenidou M, Cleveland DW. Non–cell autonomous toxicity in neurodegenerative disorders: ALS and beyond. Journal of Cell Biology. 2009;187(6):761-72.
338. Carvalho ES, Santa-Brígida SA, Queiroz AN, Silva JR, Silva OP, Barros CA, et al. Edaravone toxicity can be related to redox properties of their oxidized derivatives. Chemical Data Collections. 2017;7:51-7.
339. Meanwell NA. Fluorine and fluorinated motifs in the design and application of bioisosteres for drug design. Journal of medicinal chemistry. 2018;61(14):5822-80.

340. Pérez-González A, Galano A. OH radical scavenging activity of Edaravone: mechanism and kinetics. J Phys Chem B. 2011;115(5):1306-14.
341. Pérez-González A, Galano A. On the outstanding antioxidant capacity of edaravone derivatives through single electron transfer reactions. J Phys Chem B. 2012;116(3):1180-8.
342. Wang L, Xie S, Ma L, Chen Y, Lu W. 10-Boronic acid substituted camptothecin as prodrug of SN-38. Eur J Med Chem. 2016;116:84-9.
343. Peng X, Gandhi V. ROS-activated anticancer prodrugs: a new strategy for tumor-specific damage. Ther Deliv. 2012;3(7):823-33.
344. Yuen AK, Hutton CA. Deprotection of pinacolyl boronate esters via hydrolysis of intermediate potassium trifluoroborates. Tetrahedron letters. 2005;46(46):7899-903.
345. Sreedhar B, Venkanna GT, Kumar KBS, Balasubrahmanyam V. Copper (I) oxide catalyzed N-arylation of azoles and amines with arylboronic acid at room temperature under base-free conditions. Synthesis. 2008;2008(05):795-9.
346. Tovar-y-Romo LB, Santa-Cruz LD, Tapia R. Experimental models for the study of neurodegeneration in amyotrophic lateral sclerosis. Molecular neurodegeneration. 2009;4(1):31.
347. Hemendinger RA, Armstrong III EJ, Radio N, Brooks BR. Neurotoxic injury pathways in differentiated mouse motor neuron–neuroblastoma hybrid (NSC-34D) cells in vitro—Limited effect of riluzole on thapsigargin, but not staurosporine, hydrogen peroxide and homocysteine neurotoxicity. Toxicology and applied pharmacology. 2012;258(2):208-15.
348. Barber SC, Higginbottom A, Mead RJ, Barber S, Shaw PJ. An in vitro screening cascade to identify neuroprotective antioxidants in ALS. Free Radical Biology and Medicine. 2009;46(8):1127-38.
349. Sahu MP, Nikkilä O, Lågas S, Kolehmainen S, Castrén E. Culturing primary neurons from rat hippocampus and cortex. Neuronal Signal. 2019;3(2):Ns20180207.
350. Chamchoy K, Pakotiprapha D, Pumirat P, Leartsakulpanich U, Boonyuen U. Application of WST-8 based colorimetric NAD(P)H detection for quantitative dehydrogenase assays. BMC Biochem. 2019;20(1):4.
351. Corpas FJ, Barroso JB. NADPH-generating dehydrogenases: their role in the mechanism of protection against nitro-oxidative stress induced by adverse environmental conditions. Frontiers in Environmental Science. 2014;2:55.
352. Chamchoy K, Pakotiprapha D, Pumirat P, Leartsakulpanich U, Boonyuen U. Application of WST-8 based colorimetric NAD (P) H detection for quantitative dehydrogenase assays. BMC biochemistry. 2019;20(1):4.
353. Zhong Q, Zhang C, Zhang Q, Miele L, Zheng S, Wang G. Boronic prodrug of 4-hydroxytamoxifen is more efficacious than tamoxifen with enhanced bioavailability independent of CYP2D6 status. BMC cancer. 2015;15:1-9.
354. Yılmaz Sarıaltın S, Üstündağ A, Mhlanga Chinheya R, İpek S, Duydu Y. Cytotoxicity, genotoxicity, oxidative stress, apoptosis, and cell cycle arrest in human Sertoli cells exposed to boric acid. J Trace Elem Med Biol. 2022;70:126913.
355. Younes N, Alsahan BS, Al-Mesaifri AJ, Da'as SI, Pintus G, Majdalawieh AF, et al. JC-10 probe as a novel method for analyzing the mitochondrial membrane potential and cell stress in whole zebrafish embryos. Toxicol Res (Camb). 2022;11(1):77-87.
356. Zorova LD, Popkov VA, Plotnikov EY, Silachev DN, Pevzner IB, Jankauskas SS, et al. Mitochondrial membrane potential. Anal Biochem. 2018;552:50-9.
357. Antonsson A, Persson JL. Induction of apoptosis by staurosporine involves the inhibition of expression of the major cell cycle proteins at the G2/M checkpoint accompanied by alterations in Erk and Akt kinase activities. Anticancer research. 2009;29(8):2893-8.

358. Chae H-J, Kang J-S, Byun J-O, Han K-S, Kim D-U, Oh S-M, et al. Molecular mechanism of staurosporine-induced apoptosis in osteoblasts. Pharmacological research. 2000;42(4):373-81.
359. Moglia C, Calvo A, Grassano M, Canosa A, Manera U, D'Ovidio F, et al. Early weight loss in amyotrophic lateral sclerosis: outcome relevance and clinical correlates in a population-based cohort. Journal of Neurology, Neurosurgery & Psychiatry. 2019;90(6):666-73.
360. Mead RJ, Shan N, Reiser HJ, Marshall F, Shaw PJ. Amyotrophic lateral sclerosis: a neurodegenerative disorder poised for successful therapeutic translation. Nat Rev Drug Discov. 2023;22(3):185-212.
361. Grossman M. Amyotrophic lateral sclerosis - a multisystem neurodegenerative disorder. Nat Rev Neurol. 2019;15(1):5-6.
362. Feldman EL, Goutman SA, Petri S, Mazzini L, Savelieff MG, Shaw PJ, et al. Amyotrophic lateral sclerosis. Lancet. 2022;400(10360):1363-80.
363. Mehta D, Ahkami AH, Walley J, Xu SL, Uhrig RG. The incongruity of validating quantitative proteomics using western blots. Nat Plants. 2022;8(12):1320-1.
364. Collins BC, Hunter CL, Liu Y, Schilling B, Rosenberger G, Bader SL, et al. Multi-laboratory assessment of reproducibility, qualitative and quantitative performance of SWATH-mass spectrometry. Nat Commun. 2017;8(1):291.
365. Thompson AG, Oeckl P, Feneberg E, Bowser R, Otto M, Fischer R, et al. Advancing mechanistic understanding and biomarker development in amyotrophic lateral sclerosis. Expert Rev Proteomics. 2021;18(11):977-94.
366. Lewczuk P, Riederer P, O'Bryant SE, Verbeek MM, Dubois B, Visser PJ, et al. Cerebrospinal fluid and blood biomarkers for neurodegenerative dementias: An update of the Consensus of the Task Force on Biological Markers in Psychiatry of the World Federation of Societies of Biological Psychiatry. World J Biol Psychiatry. 2018;19(4):244-328.
367. Raghunathan R, Turajane K, Wong LC. Biomarkers in Neurodegenerative Diseases: Proteomics Spotlight on ALS and Parkinson's Disease. Int J Mol Sci. 2022;23(16).
368. Oh S, Jang Y, Na CH. Discovery of Biomarkers for Amyotrophic Lateral Sclerosis from Human Cerebrospinal Fluid Using Mass-Spectrometry-Based Proteomics. Biomedicines. 2023;11(5).
369. Hedl TJ, San Gil R, Cheng F, Rayner SL, Davidson JM, De Luca A, et al. Proteomics Approaches for Biomarker and Drug Target Discovery in ALS and FTD. Front Neurosci. 2019;13:548.
370. Leoni E, Bremang M, Mitra V, Zubiri I, Jung S, Lu CH, et al. Combined Tissue-Fluid Proteomics to Unravel Phenotypic Variability in Amyotrophic Lateral Sclerosis. Sci Rep. 2019;9(1):4478.
371. Kraus VB. Biomarkers as drug development tools: discovery, validation, qualification and use. Nat Rev Rheumatol. 2018;14(6):354-62.
372. Gromova M, Vaggelas A, Dallmann G, Seimetz D. Biomarkers: Opportunities and Challenges for Drug Development in the Current Regulatory Landscape. Biomark Insights. 2020;15:1177271920974652.
373. van der Burgt YEM. Protein biomarker discovery is still relevant and has entered a new phase. EBioMedicine. 2019;43:15.
374. Domon B, Broder S. Implications of new proteomics strategies for biology and medicine. J Proteome Res. 2004;3(2):253-60.
375. Belbin O, Lehmann S, Sabidó E, Hirtz C. Editorial: Proteomics as a Tool for Biomarker and Drug Target Discovery: Improving the Diagnosis and Treatment of Neurodegenerative Diseases. Front Aging Neurosci. 2020;12:232.

376. Schwämmle V, León IR, Jensen ON. Assessment and improvement of statistical tools for comparative proteomics analysis of sparse data sets with few experimental replicates. J Proteome Res. 2013;12(9):3874-83.
377. Barber SC, Shaw PJ. Oxidative stress in ALS: key role in motor neuron injury and therapeutic target. Free Radical Biology and Medicine. 2010;48(5):629-41.
378. Cunha-Oliveira T, Montezinho L, Mendes C, Firuzi O, Saso L, Oliveira PJ, et al. Oxidative Stress in Amyotrophic Lateral Sclerosis: Pathophysiology and Opportunities for Pharmacological Intervention. Oxid Med Cell Longev. 2020;2020:5021694.
379. Carrí MT, Ferri A, Cozzolino M, Calabrese L, Rotilio G. Neurodegeneration in amyotrophic lateral sclerosis: the role of oxidative stress and altered homeostasis of metals. Brain Res Bull. 2003;61(4):365-74.
380. Tam OH, Rozhkov NV, Shaw R, Kim D, Hubbard I, Fennessey S, et al. Postmortem Cortex Samples Identify Distinct Molecular Subtypes of ALS: Retrotransposon Activation, Oxidative Stress, and Activated Glia. Cell Rep. 2019;29(5):1164-77.e5.
381. O'Neill K, Shaw R, Bolger I, Tam OH, Phatnani H, Gale Hammell M. ALS molecular subtypes are a combination of cellular and pathological features learned by deep multiomics classifiers. Cell Rep. 2025;44(3):115402.
382. Forman HJ, Zhang H. Targeting oxidative stress in disease: promise and limitations of antioxidant therapy. Nat Rev Drug Discov. 2021;20(9):689-709.
383. Petrov D, Mansfield C, Moussy A, Hermine O. ALS Clinical Trials Review: 20 Years of Failure. Are We Any Closer to Registering a New Treatment? Front Aging Neurosci. 2017;9:68.
384. Safety and efficacy of edaravone in well defined patients with amyotrophic lateral sclerosis: a randomised, double-blind, placebo-controlled trial. Lancet Neurol. 2017;16(7):505-12.
385. Witzel S, Maier A, Steinbach R, Grosskreutz J, Koch JC, Sarikidi A, et al. Safety and Effectiveness of Long-term Intravenous Administration of Edaravone for Treatment of Patients With Amyotrophic Lateral Sclerosis. JAMA Neurol. 2022;79(2):121-30.
386. Shukla P, Yadav NK, Singh P, Bansode F, Singh R. Phenylhydrazine induced toxicity: a review on its haematotoxicity. Int J Basic Appl Med Sci. 2012;2(2):86-91.
387. Rajagopal RE, Balasubramanian M, Kalyanaraman S. Phenylhydrazine hydrochloride induced dosedependent embryo cytotoxicity in zebrafish. Bioinformation. 2019;15(4):255.
388. Diaz DB, Yudin AK. The versatility of boron in biological target engagement. Nat Chem. 2017;9(8):731-42.
389. Maslah H, Skarbek C, Pethe S, Labruère R. Anticancer boron-containing prodrugs responsive to oxidative stress from the tumor microenvironment. Eur J Med Chem. 2020;207:112670.
390. Song S, Gao P, Sun L, Kang D, Kongsted J, Poongavanam V, et al. Recent developments in the medicinal chemistry of single boron atom-containing compounds. Acta Pharm Sin B. 2021;11(10):3035-59.
391. Chen JW, Wu TC, Liang W, Ciou JJ, Lai CH. Boronates as hydrogen peroxide-reactive warheads in the design of detection probes, prodrugs, and nanomedicines used in tumors and other diseases. Drug Deliv Transl Res. 2023;13(5):1305-21.
392. Ince S, Kucukkurt I, Cigerci IH, Fatih Fidan A, Eryavuz A. The effects of dietary boric acid and borax supplementation on lipid peroxidation, antioxidant activity, and DNA damage in rats. J Trace Elem Med Biol. 2010;24(3):161-4.
393. Yamada KE, Eckhert CD. Boric Acid Activation of eIF2α and Nrf2 Is PERK Dependent: a Mechanism that Explains How Boron Prevents DNA Damage and Enhances Antioxidant Status. Biol Trace Elem Res. 2019;188(1):2-10.

394. Cao J, Jiang L, Zhang X, Yao X, Geng C, Xue X, et al. Boric acid inhibits LPS-induced TNF-alpha formation through a thiol-dependent mechanism in THP-1 cells. J Trace Elem Med Biol. 2008;22(3):189-95.
395. Goto JJ, Gralla EB, Valentine JS, Cabelli DE. Reactions of hydrogen peroxide with familial amyotrophic lateral sclerosis mutant human copper-zinc superoxide dismutases studied by pulse radiolysis. J Biol Chem. 1998;273(46):30104-9.
396. Maier O, Böhm J, Dahm M, Brück S, Beyer C, Johann S. Differentiated NSC-34 motoneuron-like cells as experimental model for cholinergic neurodegeneration. Neurochem Int. 2013;62(8):1029-38.
397. Carrera-Juliá S, Moreno ML, Barrios C, de la Rubia Ortí JE, Drehmer E. Antioxidant alternatives in the treatment of amyotrophic lateral sclerosis: a comprehensive review. Frontiers in physiology. 2020;11:63.
398. Wu HT, Yu Y, Li XX, Lang XY, Gu RZ, Fan SR, et al. Edaravone attenuates H(2)O(2) or glutamate-induced toxicity in hippocampal neurons and improves AlCl(3)/D-galactose induced cognitive impairment in mice. Neurotoxicology. 2021;85:68-78.
399. Doi K, Suzuki Y, Nakao A, Fujita T, Noiri E. Radical scavenger edaravone developed for clinical use ameliorates ischemia/reperfusion injury in rat kidney. Kidney international. 2004;65(5):1714-23.
400. Desagher S, Glowinski J, Prémont J. Pyruvate protects neurons against hydrogen peroxide-induced toxicity. J Neurosci. 1997;17(23):9060-7.
401. Khin Aung ZM, Jantaratnotai N, Piyachaturawat P, Sanvarinda P. A pure compound from Curcuma comosa Roxb. protects neurons against hydrogen peroxide-induced neurotoxicity via the activation of Nrf-2. Heliyon. 2022;8(11):e11228.
402. Drummond NJ, Davies NO, Lovett JE, Miller MR, Cook G, Becker T, et al. A synthetic cell permeable antioxidant protects neurons against acute oxidative stress. Scientific Reports. 2017;7(1):11857.
403. Smith EF, Shaw PJ, De Vos KJ. The role of mitochondria in amyotrophic lateral sclerosis. Neurosci Lett. 2019;710:132933.
404. Guo C, Sun L, Chen X, Zhang D. Oxidative stress, mitochondrial damage and neurodegenerative diseases. Neural Regen Res. 2013;8(21):2003-14.
405. Zong Y, Li H, Liao P, Chen L, Pan Y, Zheng Y, et al. Mitochondrial dysfunction: mechanisms and advances in therapy. Signal Transduct Target Ther. 2024;9(1):124.
406. Singh T, Jiao Y, Ferrando LM, Yablonska S, Li F, Horoszko EC, et al. Neuronal mitochondrial dysfunction in sporadic amyotrophic lateral sclerosis is developmentally regulated. Sci Rep. 2021;11(1):18916.
407. Pong K, Doctrow SR, Huffman K, Adinolfi CA, Baudry M. Attenuation of staurosporine-induced apoptosis, oxidative stress, and mitochondrial dysfunction by synthetic superoxide dismutase and catalase mimetics, in cultured cortical neurons. Exp Neurol. 2001;171(1):84-97.
408. Tokuda E, Takei YI, Ohara S, Fujiwara N, Hozumi I, Furukawa Y. Wild-type Cu/Zn-superoxide dismutase is misfolded in cerebrospinal fluid of sporadic amyotrophic lateral sclerosis. Mol Neurodegener. 2019;14(1):42.
409. Forsberg K, Jonsson PA, Andersen PM, Bergemalm D, Graffmo KS, Hultdin M, et al. Novel antibodies reveal inclusions containing non-native SOD1 in sporadic ALS patients. PLoS One. 2010;5(7):e11552.
410. Lang L, Kurnik M, Danielsson J, Oliveberg M. Fibrillation precursor of superoxide dismutase 1 revealed by gradual tuning of the protein-folding equilibrium. Proc Natl Acad Sci U S A. 2012;109(44):17868-73.

411. Teilum K, Smith MH, Schulz E, Christensen LC, Solomentsev G, Oliveberg M, et al. Transient structural distortion of metal-free Cu/Zn superoxide dismutase triggers aberrant oligomerization. Proc Natl Acad Sci U S A. 2009;106(43):18273-8.
412. Nordlund A, Oliveberg M. Folding of Cu/Zn superoxide dismutase suggests structural hotspots for gain of neurotoxic function in ALS: parallels to precursors in amyloid disease. Proc Natl Acad Sci U S A. 2006;103(27):10218-23.
413. Sen Mojumdar S, Z NS, Dee DR, Rouleau L, Anand U, Garen C, et al. Partially native intermediates mediate misfolding of SOD1 in single-molecule folding trajectories. Nat Commun. 2017;8(1):1881.
414. Furukawa Y, Kaneko K, Yamanaka K, O'Halloran TV, Nukina N. Complete loss of post-translational modifications triggers fibrillar aggregation of SOD1 in the familial form of amyotrophic lateral sclerosis. J Biol Chem. 2008;283(35):24167-76.
415. Da Cruz S, Bui A, Saberi S, Lee SK, Stauffer J, McAlonis-Downes M, et al. Misfolded SOD1 is not a primary component of sporadic ALS. Acta Neuropathol. 2017;134(1):97-111.
416. Rakhit R, Robertson J, Vande Velde C, Horne P, Ruth DM, Griffin J, et al. An immunological epitope selective for pathological monomer-misfolded SOD1 in ALS. Nat Med. 2007;13(6):754-9.
417. Furukawa Y, Kaneko K, Watanabe S, Yamanaka K, Nukina N. Intracellular seeded aggregation of mutant Cu,Zn-superoxide dismutase associated with amyotrophic lateral sclerosis. FEBS Lett. 2013;587(16):2500-5.
418. Nielsen FH, Meacham SL. Growing evidence for human health benefits of boron. Journal of Evidence-Based Complementary & Alternative Medicine. 2011;16(3):169-80.
419. Zamani A, Thomas E, Wright DK. Sex biology in amyotrophic lateral sclerosis. Ageing Res Rev. 2024;95:102228.
420. McAllum EJ, Lim NK, Hickey JL, Paterson BM, Donnelly PS, Li QX, et al. Therapeutic effects of CuII(atsm) in the SOD1-G37R mouse model of amyotrophic lateral sclerosis. Amyotroph Lateral Scler Frontotemporal Degener. 2013;14(7-8):586-90.
421. Estévez-Silva HM, Mediavilla T, Giacobbo BL, Liu X, Sultan FR, Marcellino DJ. Pridopidine modifies disease phenotype in a SOD1 mouse model of amyotrophic lateral sclerosis. Eur J Neurosci. 2022;55(5):1356-72.
422. Nakayama Y, Shimizu T, Matsuda C, Haraguchi M, Hayashi K, Bokuda K, et al. Body weight variation predicts disease progression after invasive ventilation in amyotrophic lateral sclerosis. Sci Rep. 2019;9(1):12262.
423. Ludolph AC, Bendotti C, Blaugrund E, Hengerer B, Löffler JP, Martin J, et al. Guidelines for the preclinical in vivo evaluation of pharmacological active drugs for ALS/MND: report on the 142nd ENMC international workshop. Amyotroph Lateral Scler. 2007;8(4):217-23.
424. Tziortzouda P, Van Den Bosch L, Hirth F. Triad of TDP43 control in neurodegeneration: autoregulation, localization and aggregation. Nature Reviews Neuroscience. 2021;22(4):197-208.
425. Kim G, Gautier O, Tassoni-Tsuchida E, Ma XR, Gitler AD. ALS genetics: gains, losses, and implications for future therapies. Neuron. 2020;108(5):822-42.
426. Sreedharan J, Blair IP, Tripathi VB, Hu X, Vance C, Rogelj B, et al. TDP-43 mutations in familial and sporadic amyotrophic lateral sclerosis. Science. 2008;319(5870):1668-72.
427. Zuo X, Zhou J, Li Y, Wu K, Chen Z, Luo Z, et al. TDP-43 aggregation induced by oxidative stress causes global mitochondrial imbalance in ALS. Nature structural & molecular biology. 2021;28(2):132-42.
428. Colombrita C, Zennaro E, Fallini C, Weber M, Sommacal A, Buratti E, et al. TDP-43 is recruited to stress granules in conditions of oxidative insult. J Neurochem. 2009;111(4):1051-61.

429. Lei Y, Zhang Z-F, Lei R-X, Wang S, Zhuang Y, Liu A-C, et al. DJ-1 suppresses cytoplasmic TDP-43 aggregation in oxidative stress-induced cell injury. Journal of Alzheimer's Disease. 2018;66(3):1001-14.
430. Gao J, Wang L, Yan T, Perry G, Wang X. TDP-43 proteinopathy and mitochondrial abnormalities in neurodegeneration. Mol Cell Neurosci. 2019;100:103396.
431. Streit L, Kuhn T, Vomhof T, Bopp V, Ludolph AC, Weishaupt JH, et al. Stress induced TDP-43 mobility loss independent of stress granules. Nature Communications. 2022;13(1):5480.
432. Aebersold R, Burlingame AL, Bradshaw RA. Western blots versus selected reaction monitoring assays: time to turn the tables? Mol Cell Proteomics. 2013;12(9):2381-2.
433. Mann M. Can proteomics retire the western blot? J Proteome Res. 2008;7(8):3065.
434. Selevsek N, Chang CY, Gillet LC, Navarro P, Bernhardt OM, Reiter L, et al. Reproducible and consistent quantification of the Saccharomyces cerevisiae proteome by SWATH-mass spectrometry. Mol Cell Proteomics. 2015;14(3):739-49.
435. Brunner AD, Thielert M, Vasilopoulou C, Ammar C, Coscia F, Mund A, et al. Ultra-high sensitivity mass spectrometry quantifies single-cell proteome changes upon perturbation. Mol Syst Biol. 2022;18(3):e10798.
436. Uhlen M, Bandrowski A, Carr S, Edwards A, Ellenberg J, Lundberg E, et al. A proposal for validation of antibodies. Nat Methods. 2016;13(10):823-7.
437. Edfors F, Hober A, Linderbäck K, Maddalo G, Azimi A, Sivertsson Å, et al. Enhanced validation of antibodies for research applications. Nat Commun. 2018;9(1):4130.
438. Sanghai N, Tranmer GK. Use of Proteomics to Explore Biomarkers of Amyotrophic Lateral Sclerosis (ALS): Proof of Principle from Humanized SOD1 Mouse to Human ALS. ACS Pharmacology & Translational Science. 2025.
439. Li JY, Sun XH, Cai ZY, Shen DC, Yang XZ, Liu MS, et al. Correlation of weight and body composition with disease progression rate in patients with amyotrophic lateral sclerosis. Sci Rep. 2022;12(1):13292.
440. Lamark T, Johansen T. Autophagy: links with the proteasome. Curr Opin Cell Biol. 2010;22(2):192-8.
441. Gal J, Ström AL, Kwinter DM, Kilty R, Zhang J, Shi P, et al. Sequestosome 1/p62 links familial ALS mutant SOD1 to LC3 via an ubiquitin-independent mechanism. J Neurochem. 2009;111(4):1062-73.
442. Mitsui S, Otomo A, Sato K, Ishiyama M, Shimakura K, Okada-Yamaguchi C, et al. SQSTM1, a protective factor of SOD1-linked motor neuron disease, regulates the accumulation and distribution of ubiquitinated protein aggregates in neuron. Neurochem Int. 2022;158:105364.
443. Rogers RS, Tungtur S, Tanaka T, Nadeau LL, Badawi Y, Wang H, et al. Impaired Mitophagy Plays a Role in Denervation of Neuromuscular Junctions in ALS Mice. Front Neurosci. 2017;11:473.
444. Bjørkøy G, Lamark T, Brech A, Outzen H, Perander M, Overvatn A, et al. p62/SQSTM1 forms protein aggregates degraded by autophagy and has a protective effect on huntingtin-induced cell death. J Cell Biol. 2005;171(4):603-14.
445. Zhang D, Zhang Y, Pan J, Cao J, Sun X, Li X, et al. Degradation of NLRP3 by p62-dependent-autophagy improves cognitive function in Alzheimer's disease by maintaining the phagocytic function of microglia. CNS Neurosci Ther. 2023;29(10):2826-42.
446. Ono M, Komatsu M, Ji B, Takado Y, Shimojo M, Minamihisamatsu T, et al. Central role for p62/SQSTM1 in the elimination of toxic tau species in a mouse model of tauopathy. Aging Cell. 2022;21(7):e13615.
447. Tanji K, Odagiri S, Miki Y, Maruyama A, Nikaido Y, Mimura J, et al. p62 Deficiency Enhances α-Synuclein Pathology in Mice. Brain Pathol. 2015;25(5):552-64.

448. Doi H, Adachi H, Katsuno M, Minamiyama M, Matsumoto S, Kondo N, et al. p62/SQSTM1 differentially removes the toxic mutant androgen receptor via autophagy and inclusion formation in a spinal and bulbar muscular atrophy mouse model. J Neurosci. 2013;33(18):7710-27.
449. Kwon J, Han E, Bui CB, Shin W, Lee J, Lee S, et al. Assurance of mitochondrial integrity and mammalian longevity by the p62-Keap1-Nrf2-Nqo1 cascade. EMBO Rep. 2012;13(2):150-6.
450. Bartolome F, Esteras N, Martin-Requero A, Boutoleau-Bretonniere C, Vercelletto M, Gabelle A, et al. Author Correction: Pathogenic p62/SQSTM1 mutations impair energy metabolism through limitation of mitochondrial substrates. Sci Rep. 2018;8(1):4064.
451. Du Y, Wooten MC, Wooten MW. Oxidative damage to the promoter region of SQSTM1/p62 is common to neurodegenerative disease. Neurobiol Dis. 2009;35(2):302-10.
452. Filomeni G, De Zio D, Cecconi F. Oxidative stress and autophagy: the clash between damage and metabolic needs. Cell Death Differ. 2015;22(3):377-88.
453. Carroll B, Otten EG, Manni D, Stefanatos R, Menzies FM, Smith GR, et al. Oxidation of SQSTM1/p62 mediates the link between redox state and protein homeostasis. Nat Commun. 2018;9(1):256.
454. Weatherbee SD, Anderson KV, Niswander LA. LDL-receptor-related protein 4 is crucial for formation of the neuromuscular junction. Development. 2006;133(24):4993-5000.
455. Faissner A. Low-density lipoprotein receptor-related protein-1 (LRP1) in the glial lineage modulates neuronal excitability. Front Netw Physiol. 2023;3:1190240.
456. Zhang H, Chen W, Tan Z, Zhang L, Dong Z, Cui W, et al. A Role of Low-Density Lipoprotein Receptor-Related Protein 4 (LRP4) in Astrocytic Aβ Clearance. J Neurosci. 2020;40(28):5347-61.
457. Lei L, Shen XM, Wang SY, Lu Y, Wang SB, Chen H, et al. Presence of antibodies against low-density lipoprotein receptor-related protein 4 and impairment of neuromuscular junction in a Chinese cohort of amyotrophic lateral sclerosis. Chin Med J (Engl). 2019;132(12):1487-9.
458. Tannenberg RK, Scott HL, Tannenberg AE, Dodd PR. Selective loss of synaptic proteins in Alzheimer's disease: evidence for an increased severity with APOE varepsilon4. Neurochem Int. 2006;49(7):631-9.
459. Basso M, Giraudo S, Corpillo D, Bergamasco B, Lopiano L, Fasano M. Proteome analysis of human substantia nigra in Parkinson's disease. Proteomics. 2004;4(12):3943-52.
460. Eastwood SL, Harrison PJ. Hippocampal synaptic pathology in schizophrenia, bipolar disorder and major depression: a study of complexin mRNAs. Mol Psychiatry. 2000;5(4):425-32.
461. Sawada K, Young CE, Barr AM, Longworth K, Takahashi S, Arango V, et al. Altered immunoreactivity of complexin protein in prefrontal cortex in severe mental illness. Mol Psychiatry. 2002;7(5):484-92.
462. Morton AJ, Faull RL, Edwardson JM. Abnormalities in the synaptic vesicle fusion machinery in Huntington's disease. Brain Res Bull. 2001;56(2):111-7.
463. D'Erchia AM, Gallo A, Manzari C, Raho S, Horner DS, Chiara M, et al. Massive transcriptome sequencing of human spinal cord tissues provides new insights into motor neuron degeneration in ALS. Sci Rep. 2017;7(1):10046.
464. Ziff OJ, Clarke BE, Taha DM, Crerar H, Luscombe NM, Patani R. Meta-analysis of human and mouse ALS astrocytes reveals multi-omic signatures of inflammatory reactive states. Genome Res. 2022;32(1):71-84.
465. Väänänen HK, Takala TE, Tolonen U, Vuori J, Myllylä VV. Muscle-specific carbonic anhydrase III is a more sensitive marker of muscle damage than creatine kinase in neuromuscular disorders. Arch Neurol. 1988;45(11):1254-6.
466. Dowling P, Gargan S, Zweyer M, Sabir H, Swandulla D, Ohlendieck K. Proteomic profiling of carbonic anhydrase CA3 in skeletal muscle. Expert Rev Proteomics. 2021;18(12):1073-86.

467. Dergai O, Wuu J, Koziczak-Holbro M, Malaspina A, Granit V, Hernandez JP, et al. Skeletal muscle biomarkers of amyotrophic lateral sclerosis: a large-scale, multi-cohort proteomic study. medRxiv. 2025:2025.04. 23.25326161.
468. Imam F, Saloner R, Vogel JW, Krish V, Abdel-Azim G, Ali M, et al. The Global Neurodegeneration Proteomics Consortium: biomarker and drug target discovery for common neurodegenerative diseases and aging. Nature Medicine. 2025:1-11.
469. Scrivo A, Codogno P, Bomont P. Gigaxonin E3 ligase governs ATG16L1 turnover to control autophagosome production. Nat Commun. 2019;10(1):780.
470. Bomont P. GAN (gigaxonin) E3 ligase and ATG16L1: master and commander of autophagosome production. Autophagy. 2019;15(9):1650-2.
471. Renganathan B, Zewe JP, Cheng Y, Paumier JM, Kittisopikul M, Ridge KM, et al. Gigaxonin is required for intermediate filament transport. Faseb j. 2023;37(5):e22886.
472. Mahammad S, Murthy SN, Didonna A, Grin B, Israeli E, Perrot R, et al. Giant axonal neuropathy-associated gigaxonin mutations impair intermediate filament protein degradation. J Clin Invest. 2013;123(5):1964-75.
473. Nath B, Phaneuf D, Julien JP. Axonal Transport Defect in Gigaxonin Deficiency Rescued by Tubastatin A. Neurotherapeutics. 2023;20(4):1215-28.
474. Ganay T, Boizot A, Burrer R, Chauvin JP, Bomont P. Sensory-motor deficits and neurofilament disorganization in gigaxonin-null mice. Mol Neurodegener. 2011;6:25.
475. Benatar M, Zhang L, Wang L, Granit V, Statland J, Barohn R, et al. Validation of serum neurofilaments as prognostic and potential pharmacodynamic biomarkers for ALS. Neurology. 2020;95(1):e59-e69.
476. Benatar M, Wuu J, Andersen PM, Lombardi V, Malaspina A. Neurofilament light: A candidate biomarker of presymptomatic amyotrophic lateral sclerosis and phenoconversion. Ann Neurol. 2018;84(1):130-9.
477. Lu A, Hsieh F, Sharma BR, Vaughn SR, Enrich C, Pfeffer SR. CRISPR screens for lipid regulators reveal a role for ER-bound SNX13 in lysosomal cholesterol export. J Cell Biol. 2022;221(2).
478. Lan ZQ, Ge ZY, Lv SK, Zhao B, Li CX. The regulatory role of lipophagy in central nervous system diseases. Cell Death Discov. 2023;9(1):229.
479. Xu T, Gao P, Huang Y, Wu M, Yi J, Zhou Z, et al. Git1-PGK1 interaction achieves self-protection against spinal cord ischemia-reperfusion injury by modulating Keap1/Nrf2 signaling. Redox Biol. 2023;62:102682.
480. Benarroch EE. Nrf2, cellular redox regulation, and neurologic implications. Neurology. 2017;88(20):1942-50.
481. Bono S, Feligioni M, Corbo M. Impaired antioxidant KEAP1-NRF2 system in amyotrophic lateral sclerosis: NRF2 activation as a potential therapeutic strategy. Mol Neurodegener. 2021;16(1):71.
482. Ackerley S, Thornhill P, Grierson AJ, Brownlees J, Anderton BH, Leigh PN, et al. Neurofilament heavy chain side arm phosphorylation regulates axonal transport of neurofilaments. J Cell Biol. 2003;161(3):489-95.
483. Rouleau GA, Clark AW, Rooke K, Pramatarova A, Krizus A, Suchowersky O, et al. SOD1 mutation is associated with accumulation of neurofilaments in amyotrophic lateral sclerosis. Ann Neurol. 1996;39(1):128-31.
484. Jaffe H, Veeranna, Shetty KT, Pant HC. Characterization of the phosphorylation sites of human high molecular weight neurofilament protein by electrospray ionization tandem mass spectrometry and database searching. Biochemistry. 1998;37(11):3931-40.

485. Julien JP, Mushynski WE. Multiple phosphorylation sites in mammalian neurofilament polypeptides. J Biol Chem. 1982;257(17):10467-70.
486. Huttlin EL, Jedrychowski MP, Elias JE, Goswami T, Rad R, Beausoleil SA, et al. A tissue-specific atlas of mouse protein phosphorylation and expression. Cell. 2010;143(7):1174-89.
487. Gaiani A, Martinelli I, Bello L, Querin G, Puthenparampil M, Ruggero S, et al. Diagnostic and Prognostic Biomarkers in Amyotrophic Lateral Sclerosis: Neurofilament Light Chain Levels in Definite Subtypes of Disease. JAMA Neurol. 2017;74(5):525-32.
488. Behzadi A, Pujol-Calderón F, Tjust AE, Wuolikainen A, Höglund K, Forsberg K, et al. Neurofilaments can differentiate ALS subgroups and ALS from common diagnostic mimics. Sci Rep. 2021;11(1):22128.
489. Benatar M, Wuu J, Turner MR. Neurofilament light chain in drug development for amyotrophic lateral sclerosis: a critical appraisal. Brain. 2023;146(7):2711-6.
490. Meyer T, Schumann P, Weydt P, Petri S, Koc Y, Spittel S, et al. Neurofilament light-chain response during therapy with antisense oligonucleotide tofersen in SOD1-related ALS: Treatment experience in clinical practice. Muscle Nerve. 2023;67(6):515-21.
491. Cai Z, Yin K, Liu Q, Liu M, Yang X, Cui L. Association between abnormal expression and methylation of LGALS1 in amyotrophic lateral sclerosis. Brain Res. 2022;1792:148022.
492. Kobayakawa Y, Sakumi K, Kajitani K, Kadoya T, Horie H, Kira J, et al. Galectin-1 deficiency improves axonal swelling of motor neurones in SOD1(G93A) transgenic mice. Neuropathol Appl Neurobiol. 2015;41(2):227-44.
493. Díaz M, Fabelo N, Martín MV, Santos G, Ferrer I. Evidence for alterations in lipid profiles and biophysical properties of lipid rafts from spinal cord in sporadic amyotrophic lateral sclerosis. J Mol Med (Berl). 2024;102(3):391-402.
494. Murphy SR, Chang CC, Dogbevia G, Bryleva EY, Bowen Z, Hasan MT, et al. Acat1 knockdown gene therapy decreases amyloid-β in a mouse model of Alzheimer's disease. Mol Ther. 2013;21(8):1497-506.
495. Shibuya Y, Chang CC, Chang TY. ACAT1/SOAT1 as a therapeutic target for Alzheimer's disease. Future Med Chem. 2015;7(18):2451-67.
496. Shibuya Y, Chang CC, Huang LH, Bryleva EY, Chang TY. Inhibiting ACAT1/SOAT1 in microglia stimulates autophagy-mediated lysosomal proteolysis and increases Aβ1-42 clearance. J Neurosci. 2014;34(43):14484-501.
497. Fischer A, Zalvide J, Faurobert E, Albiges-Rizo C, Tournier-Lasserve E. Cerebral cavernous malformations: from CCM genes to endothelial cell homeostasis. Trends Mol Med. 2013;19(5):302-8.
498. Stoffel W, Jenke B, Schmidt-Soltau I, Binczek E, Brodesser S, Hammels I. SMPD3 deficiency perturbs neuronal proteostasis and causes progressive cognitive impairment. Cell Death Dis. 2018;9(5):507.
499. Kiss DS, Zsarnovszky A, Horvath K, Gyorffy A, Bartha T, Hazai D, et al. Ecto-nucleoside triphosphate diphosphohydrolase 3 in the ventral and lateral hypothalamic area of female rats: morphological characterization and functional implications. Reprod Biol Endocrinol. 2009;7:31.
500. Ansoleaga B, Jové M, Schlüter A, Garcia-Esparcia P, Moreno J, Pujol A, et al. Deregulation of purine metabolism in Alzheimer's disease. Neurobiol Aging. 2015;36(1):68-80.
501. Benatar M, Wuu J, Huey ED, McMillan CT, Petersen RC, Postuma R, et al. The Miami Framework for ALS and related neurodegenerative disorders: an integrated view of phenotype and biology. Nat Rev Neurol. 2024;20(6):364-76.
502. Zhang J, Shen Y, Yang Z, Yang F, Li Y, Yu B, et al. A splicing variation in NPRL2 causing familial focal epilepsy with variable foci: additional cases and literature review. J Hum Genet. 2022;67(2):79-85.

503. Hui JB, Silva JCH, Pelaez MC, Sévigny M, Venkatasubramani JP, Plumereau Q, et al. NPRL2 Inhibition of mTORC1 Controls Sodium Channel Expression and Brain Amino Acid Homeostasis. eNeuro. 2022;9(2).
504. Nogueira-Machado JA, Rocha-Silva F, Gomes NA. The Role of mTOR in Amyotrophic Lateral Sclerosis. Biomedicines. 2025;13(4).
505. Staats KA, Hernandez S, Schönefeldt S, Bento-Abreu A, Dooley J, Van Damme P, et al. Rapamycin increases survival in ALS mice lacking mature lymphocytes. Mol Neurodegener. 2013;8:31.
506. Paunesku T, Mittal S, Protić M, Oryhon J, Korolev S, Joachimiak A, et al. Proliferating cell nuclear antigen (PCNA): ringmaster of the genome. International journal of radiation biology. 2001;77(10):1007-21.
507. Wharton SB, Williams GH, Stoeber K, Gelsthorpe CH, Baxter L, Johnson AL, et al. Expression of Ki67, PCNA and the chromosome replication licensing protein Mcm2 in glial cells of the ageing human hippocampus increases with the burden of Alzheimer-type pathology. Neurosci Lett. 2005;383(1-2):33-8.
508. Aladeokin AC, Akiyama T, Kimura A, Kimura Y, Takahashi-Jitsuki A, Nakamura H, et al. Network-guided analysis of hippocampal proteome identifies novel proteins that colocalize with Aβ in a mice model of early-stage Alzheimer's disease. Neurobiol Dis. 2019;132:104603.
509. Yagensky O, Kohansal-Nodehi M, Gunaseelan S, Rabe T, Zafar S, Zerr I, et al. Increased expression of heme-binding protein 1 early in Alzheimer's disease is linked to neurotoxicity. Elife. 2019;8.
510. Nakahata N. Thromboxane A2: physiology/pathophysiology, cellular signal transduction and pharmacology. Pharmacol Ther. 2008;118(1):18-35.
511. Ciabattoni G, Porreca E, Di Febbo C, Di Iorio A, Paganelli R, Bucciarelli T, et al. Determinants of platelet activation in Alzheimer's disease. Neurobiol Aging. 2007;28(3):336-42.
512. Szczuko M, Kozioł I, Kotlęga D, Brodowski J, Drozd A. The Role of Thromboxane in the Course and Treatment of Ischemic Stroke: Review. Int J Mol Sci. 2021;22(21).
513. Du H, Huo Z, Chen Y, Zhao Z, Meng F, Wang X, et al. Induced Pluripotent Stem Cells and Their Applications in Amyotrophic Lateral Sclerosis. Cells. 2023;12(6).
514. Mazzini L, De Marchi F. iPSC-based research in ALS precision medicine. Cell Stem Cell. 2023;30(6):748-9.
515. Cerneckis J, Cai H, Shi Y. Induced pluripotent stem cells (iPSCs): molecular mechanisms of induction and applications. Signal Transduct Target Ther. 2024;9(1):112.
516. Workman MJ, Lim RG, Wu J, Frank A, Ornelas L, Panther L, et al. Large-scale differentiation of iPSC-derived motor neurons from ALS and control subjects. Neuron. 2023;111(8):1191-204.e5.
517. Sayed N, Liu C, Wu JC. Translation of Human-Induced Pluripotent Stem Cells: From Clinical Trial in a Dish to Precision Medicine. J Am Coll Cardiol. 2016;67(18):2161-76.
518. Ferreira GS, Dijkstra FM, Veening-Griffioen DH, Boon WPC, Schellekens H, Moors EHM, et al. Translatability of preclinical to early clinical tolerable and pharmacologically active dose ranges for central nervous system active drugs. Transl Psychiatry. 2023;13(1):74.
519. Zwiegers P, Lee G, Shaw CA. Reduction in hSOD1 copy number significantly impacts ALS phenotype presentation in G37R (line 29) mice: implications for the assessment of putative therapeutic agents. J Negat Results Biomed. 2014;13:14.
520. Huang M, Liu YU, Yao X, Qin D, Su H. Variability in SOD1-associated amyotrophic lateral sclerosis: geographic patterns, clinical heterogeneity, molecular alterations, and therapeutic implications. Transl Neurodegener. 2024;13(1):28.
521. D'Amico E, Factor-Litvak P, Santella RM, Mitsumoto H. Clinical perspective on oxidative stress in sporadic amyotrophic lateral sclerosis. Free Radic Biol Med. 2013;65:509-27.

522. Scotter EL, Chen HJ, Shaw CE. TDP-43 Proteinopathy and ALS: Insights into Disease Mechanisms and Therapeutic Targets. Neurotherapeutics. 2015;12(2):352-63.
523. Feneberg E, Gordon D, Thompson AG, Finelli MJ, Dafinca R, Candalija A, et al. An ALS-linked mutation in TDP-43 disrupts normal protein interactions in the motor neuron response to oxidative stress. Neurobiology of disease. 2020;144:105050.
524. Grassano M, Moglia C, Palumbo F, Koumantakis E, Cugnasco P, Callegaro S, et al. Sex Differences in Amyotrophic Lateral Sclerosis Survival and Progression: A Multidimensional Analysis. Ann Neurol. 2024;96(1):159-69.
525. McCombe PA, Henderson RD. Effects of gender in amyotrophic lateral sclerosis. Gend Med. 2010;7(6):557-70.
526. Harlan R, Zhang H. Targeted proteomics: a bridge between discovery and validation. Expert Rev Proteomics. 2014;11(6):657-61.
527. Hussain G, Wang J, Rasul A, Anwar H, Imran A, Qasim M, et al. Role of cholesterol and sphingolipids in brain development and neurological diseases. Lipids Health Dis. 2019;18(1):26.
528. Phan K, He Y, Bhatia S, Pickford R, McDonald G, Mazumder S, et al. Multiple pathways of lipid dysregulation in amyotrophic lateral sclerosis. Brain Commun. 2023;5(1):fcac340.
529. Ingre C, Chen L, Zhan Y, Termorshuizen J, Yin L, Fang F. Lipids, apolipoproteins, and prognosis of amyotrophic lateral sclerosis. Neurology. 2020;94(17):e1835-e44.
530. Pandya VA, Patani R. Decoding the relationship between ageing and amyotrophic lateral sclerosis: a cellular perspective. Brain. 2020;143(4):1057-72.
531. Jagaraj CJ, Shadfar S, Kashani SA, Saravanabavan S, Farzana F, Atkin JD. Molecular hallmarks of ageing in amyotrophic lateral sclerosis. Cell Mol Life Sci. 2024;81(1):111.
532. Barja G. Free radicals and aging. Trends Neurosci. 2004;27(10):595-600.
533. Wickens AP. Ageing and the free radical theory. Respir Physiol. 2001;128(3):379-91.
534. Etkin A, Powell J, Savitz AJ. Opportunities for use of neuroimaging in de-risking drug development and improving clinical outcomes in psychiatry: an industry perspective. Neuropsychopharmacology. 2024;50(1):258-68.
535. Clapham KM, Batsanov AS, Bryce MR, Tarbit B. Trifluoromethyl-substituted pyridyl-and pyrazolylboronic acids and esters: synthesis and Suzuki–Miyaura cross-coupling reactions. Organic & biomolecular chemistry. 2009;7(10):2155-61.
536. Gupta S, Chaudhary P, Seva L, Sabiah S, Kandasamy J. Bio-based green solvent for the catalyst free oxidation of arylboronic acids into phenols. RSC Advances. 2015;5(108):89133-8.
537. Todd TW, Petrucelli L. Modelling amyotrophic lateral sclerosis in rodents. Nat Rev Neurosci. 2022;23(4):231-51.
538. Wong PC, Pardo CA, Borchelt DR, Lee MK, Copeland NG, Jenkins NA, et al. An adverse property of a familial ALS-linked SOD1 mutation causes motor neuron disease characterized by vacuolar degeneration of mitochondria. Neuron. 1995;14(6):1105-16.
539. Boillée S, Yamanaka K, Lobsiger CS, Copeland NG, Jenkins NA, Kassiotis G, et al. Onset and progression in inherited ALS determined by motor neurons and microglia. Science. 2006;312(5778):1389-92.
540. Tan H, Chen M, Pang D, Xia X, Du C, Yang W, et al. LanCL1 promotes motor neuron survival and extends the lifespan of amyotrophic lateral sclerosis mice. Cell Death Differ. 2020;27(4):1369-82.
541. Yokosawa N, Kurokawa Y, Tsuzuki K, Syuto B, Fujii N, Kimura K, et al. Binding of Clostridium botulinum type C neurotoxin to different neuroblastoma cell lines. Infect Immun. 1989;57(1):272-7.
542. Kong AT, Leprevost FV, Avtonomov DM, Mellacheruvu D, Nesvizhskii AI. MSFragger: ultrafast and comprehensive peptide identification in mass spectrometry-based proteomics. Nat Methods. 2017;14(5):513-20.

13 Appendices

13.1 Appendix Figure 1: Chromatogram of NS-1-2 (BSZ)

Sample: NS-1-2 (BSZ) | Rf+ | Friday 30 May 2025 04:43PM

RediSep Column: Silica 12g
SN: E04150D568749C Lot: 301621207X
Flow Rate: 30 ml/min
Equilibration Volume: 100.8 ml
Initial Waste: 0.0 ml
Air Purge: 0.5 min
Solvent A: Hexane
Solvent B: Ethyl Acetate

Peak Tube Volume: Max.
Non-Peak Tube Volume: Max.
Loading Type: Solid (Pause)
Wavelength 1 (red): 254nm
Peak Width: 1 min
Threshold: 0.20 AU
Wavelength 2 (purple): 280nm

Run Notes:

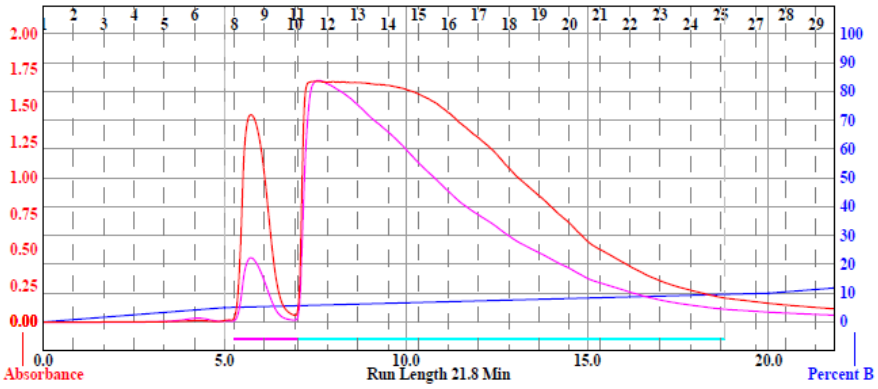

Rack A

18 mm x 150 mm Tubes

Peak #	Start Tube	End Tube
1	A:8	A:10
2	A:11	A:25

Duration	%B	Solvent A	Solvent B
0.0	0.0	Hexane	Ethyl Acetate
5.0	5.0	Hexane	Ethyl Acetate
15.0	10.0	Hexane	Ethyl Acetate
1.8	11.8	Hexane	Ethyl Acetate

Page 1 of 1

13.2 Appendix Figure 2: ^{1}HNMR of NS-1-2 (BSZ)

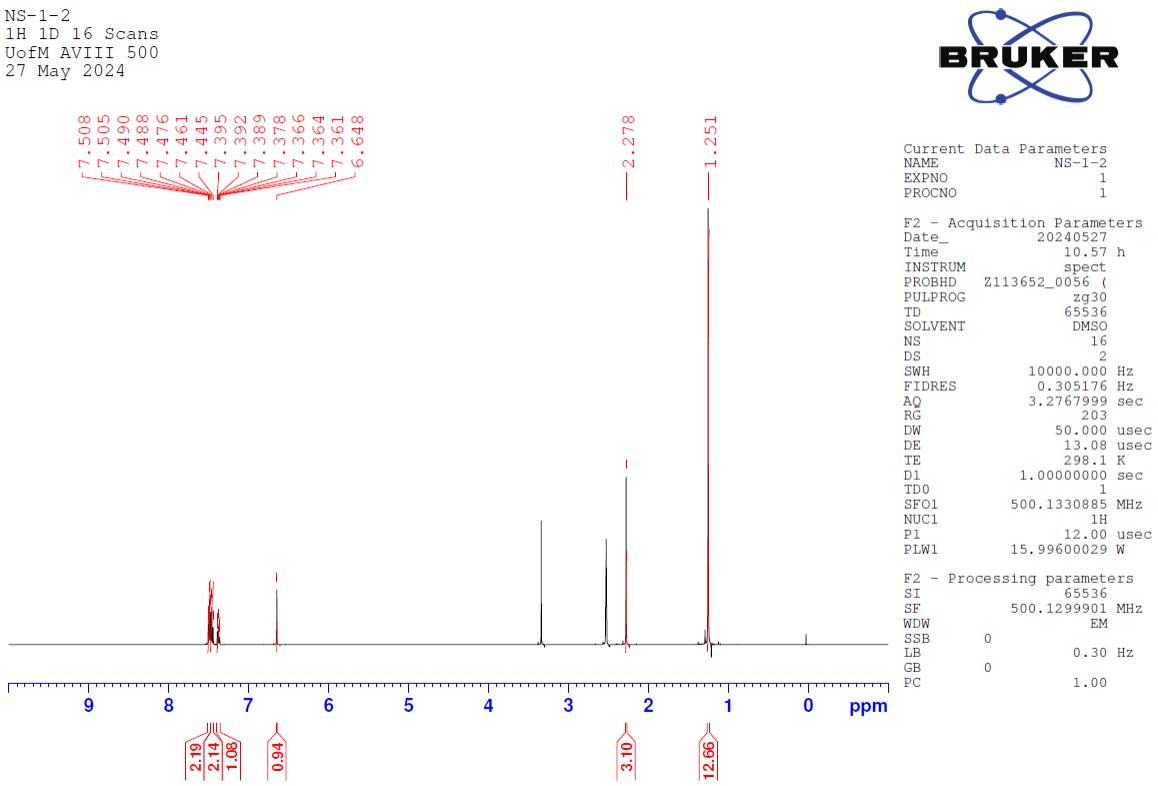

13.3 Appendix Figure 3: ^{13}CNMR of NS-1-2 (BSZ)

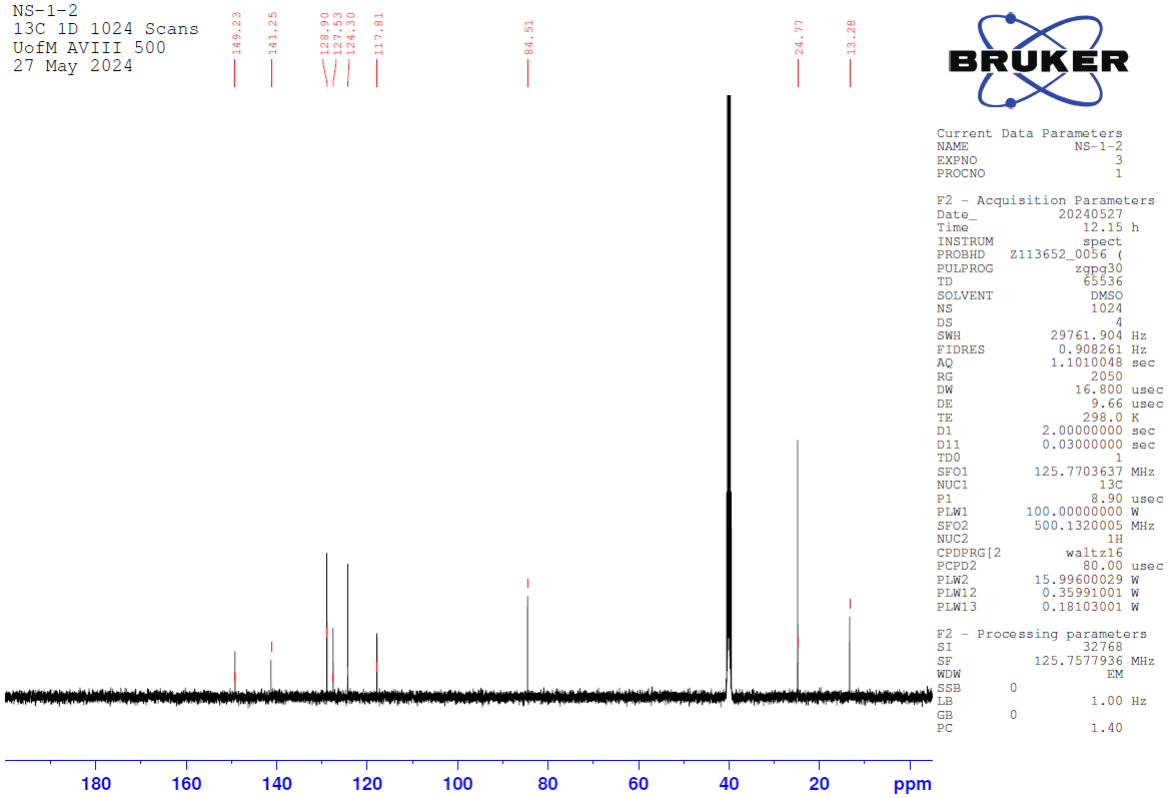

13.4 Appendix Figure 4: ^{11}BNMR of NS-1-2 (BSZ)

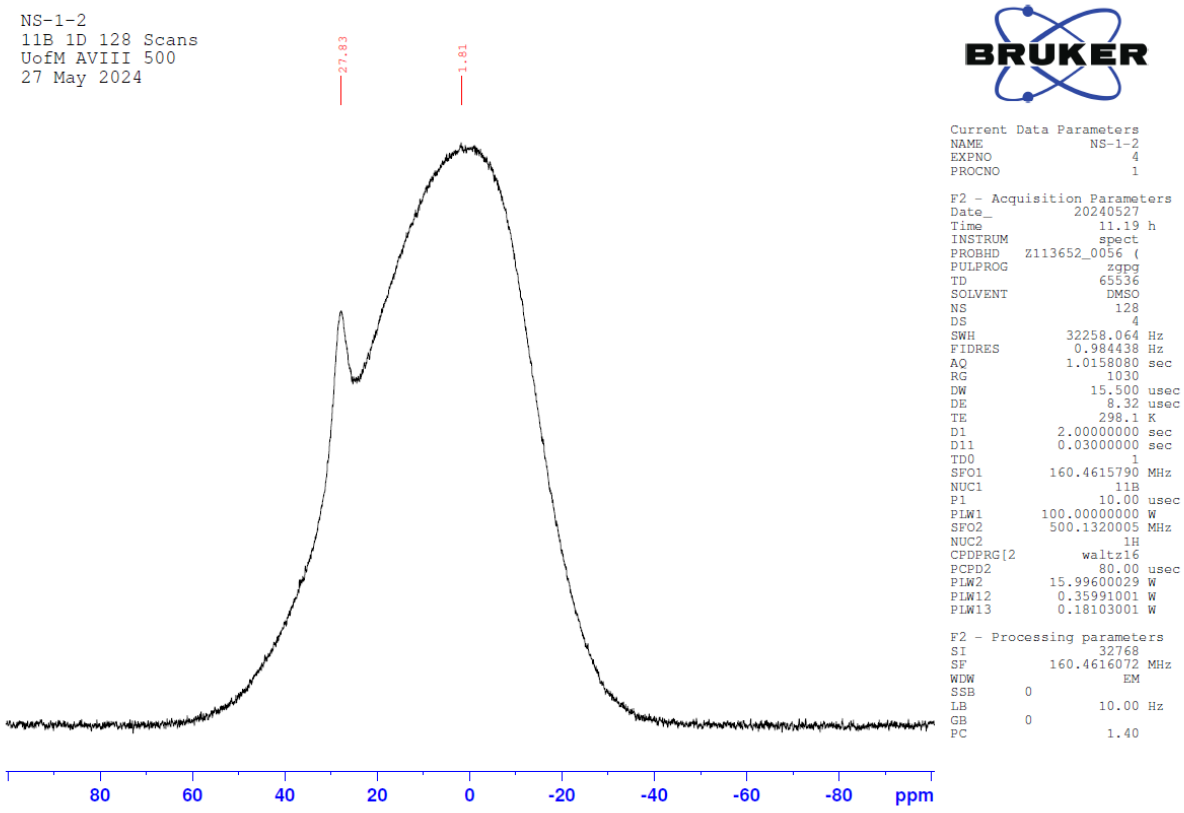


```
Current Data Parameters
NAME                  NS-1-2
EXPNO                      4
PROCNO                     1

F2 - Acquisition Parameters
Date_              20240527
Time                 11.19 h
INSTRUM               spect
PROBHD    Z113652_0056 (
PULPROG                zgpg
TD                    65536
SOLVENT                DMSO
NS                      128
DS                        4
SWH              32258.064 Hz
FIDRES            0.984438 Hz
AQ               1.0158080 sec
RG                     1030
DW                  15.500 usec
DE                   8.32 usec
TE                  298.1 K
D1               2.00000000 sec
D11              0.03000000 sec
TD0                       1
SFO1           160.4615790 MHz
NUC1                   11B
P1                   10.00 usec
PLW1          100.00000000 W
SFO2           500.1320005 MHz
NUC2                   1H
CPDPRG[2           waltz16
PCPD2                80.00 usec
PLW2          15.99600029 W
PLW12          0.35991001 W
PLW13          0.18103001 W

F2 - Processing parameters
SI                    32768
SF           160.4616072 MHz
WDW                      EM
SSB       0
LB                   10.00 Hz
GB        0
PC                    1.40
```

13.5 Appendix Figure 5: HRMS of NS-1-2 (BSZ)

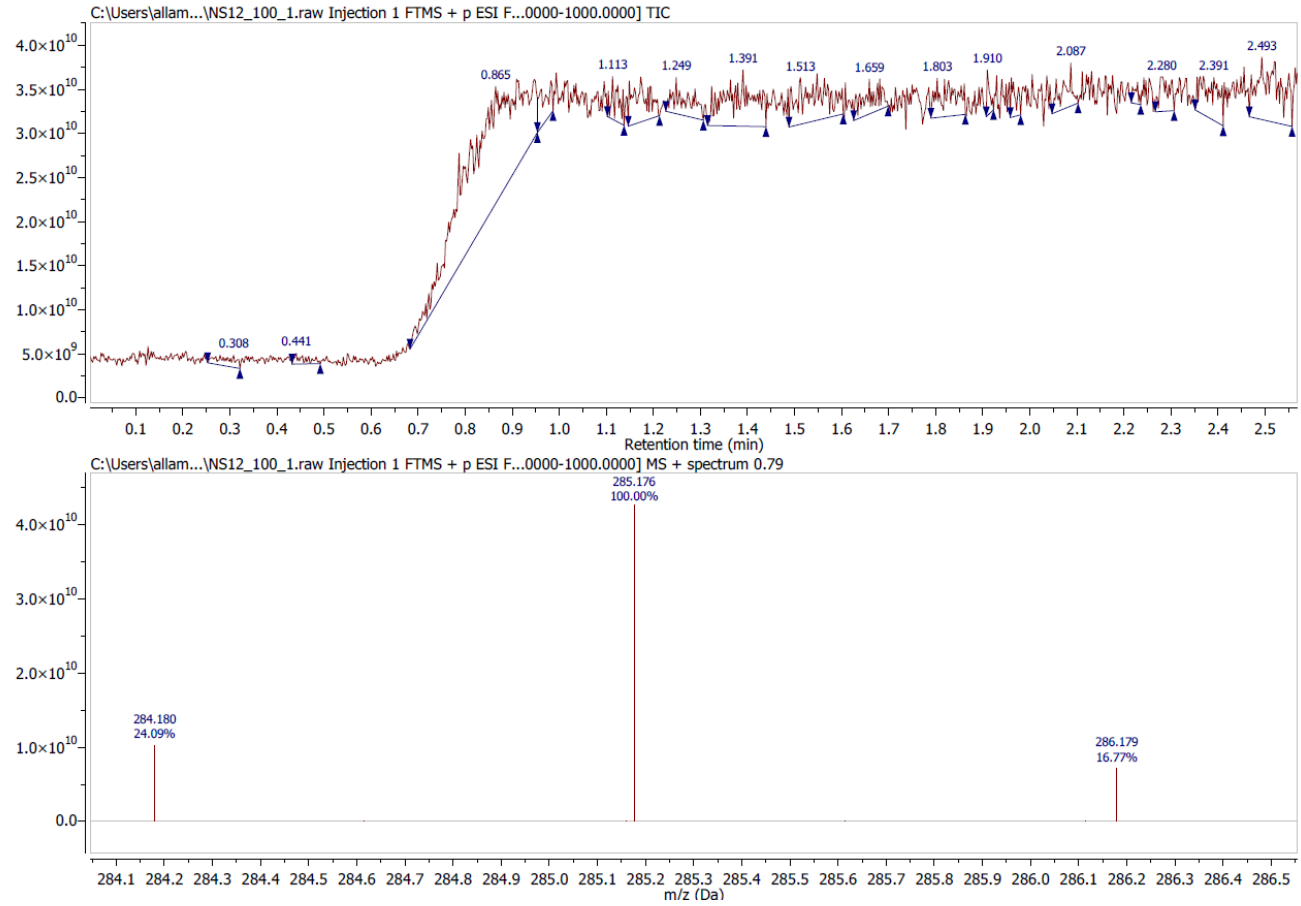

13.6 Appendix Figure 6: ESI of NS-1-2 (BSZ)

Compound Spectrum List Report

Analysis Info

Acquisition Date 5/17/2024 2:36:41 PM

Analysis Name C:\Users\Emy\OneDrive - University of Manitoba\Desktop\Ahmet\5-17-2024_NS-1-2 - C16H21B1N2O2_12915.d

Method lc 100-600 esi.m
Operator Demo User
Sample Name NS-1-2 - C16H21B1N2O2
Instrument compact 8255754.20171
Comment

Acquisition Parameter

Source Type	ESI	Ion Polarity	Positive	Set Nebulizer	0.4 Bar
Focus	Active	Set Capillary	4000 V	Set Dry Heater	200 °C
Scan Begin	50 m/z	Set End Plate Offset	-500 V	Set Dry Gas	4.0 l/min
Scan End	700 m/z	Set Charging Voltage	2000 V	Set Divert Valve	Source
		Set Corona	0 nA	Set APCI Heater	0 °C

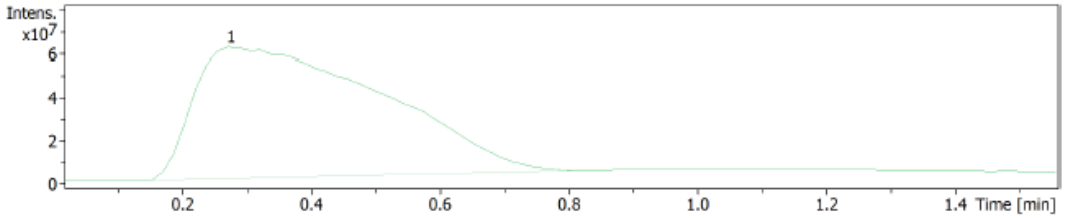

#	RT [min]	Area	Int. Type	I	S/N	Trace	Max. m/z	FWHM [min]
1	0.3	1222794496	Chromatogram	63135656	198.9	BPC +All MS	285.1744	0.4

Cmpd 1, 0.3 min

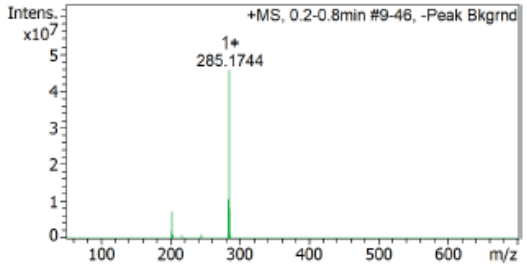

#	m/z	Res.	S/N	I	I %	FWHM
1	202.1002	15946	5141381.0	2106573	4.6	0.0127
2	203.0965	18170	17681340.0	7244558	15.9	0.0112
3	204.0998	13765	2610944.3	1069780	2.3	0.0148
4	217.1125	14556	2486841.5	1018931	2.2	0.0149
5	245.1438	15505	2722523.0	1115497	2.4	0.0158
6	284.1778	20979	25796214.0	10569457	23.1	0.0135
7	285.1744	21248	111457024.0	45667176	100.0	0.0134
8	285.4116	9373	2402938.8	984554	2.2	0.0304
9	286.1777	20306	19927086.0	8164705	17.9	0.0141
10	287.1809	14990	2605934.3	1067727	2.3	0.0192

13.7 Appendix Figure 7: ^{1}HNMR of NS-1-21

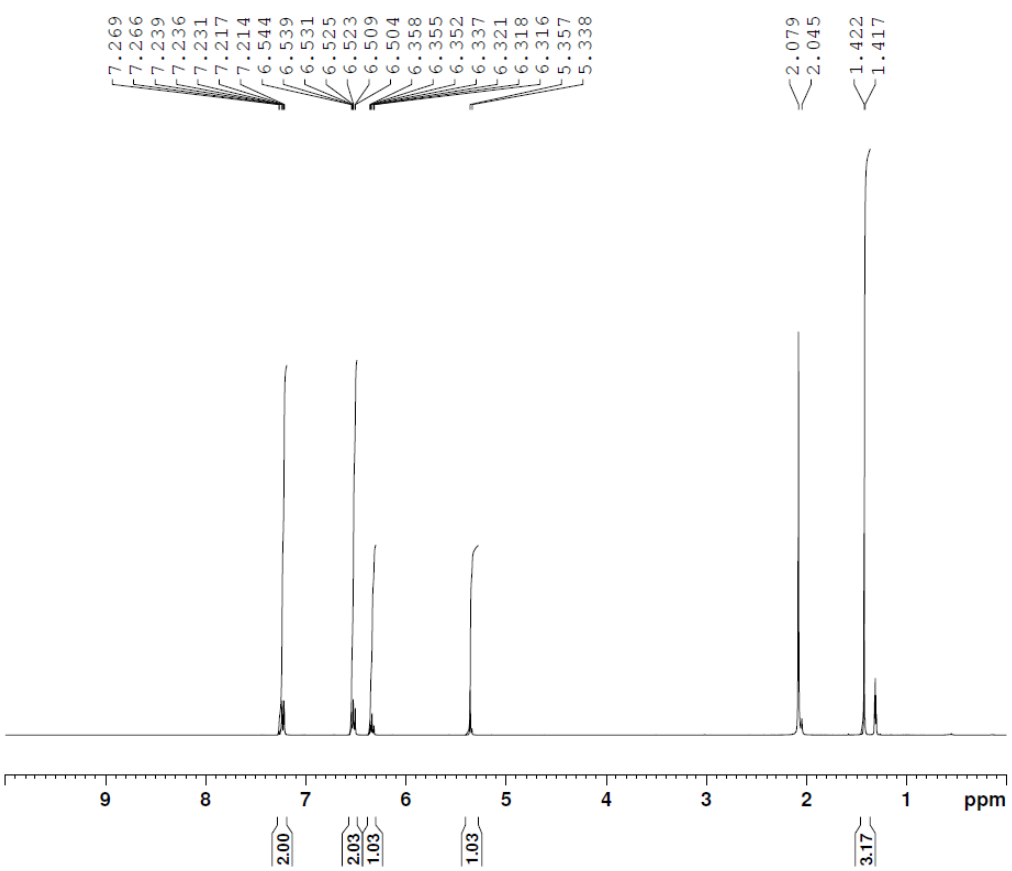

```
Current Data Parameters
NAME      NS-1-21-1_Final
EXPNO                   2
PROCNO                  1

F2 - Acquisition Parameters
Date_            20190708
Time                15.27
INSTRUM             spect
PROBHD    5 mm PABBO BB-
PULPROG              zg30
TD                  65536
SOLVENT           Acetone
NS                     16
DS                      2
SWH              8012.820 Hz
FIDRES           0.122266 Hz
AQ               4.0894465 sec
RG                    287
DW                 62.400 usec
DE                  6.50 usec
TE                 298.0 K
D1            1.00000000 sec
TD0                     1

======== CHANNEL f1 ========
SFO1          400.3324722 MHz
NUC1                    1H
P1                  14.00 usec
PLW1          14.22799969 W

F2 - Processing parameters
SI                    65536
SF            400.3303027 MHz
WDW                     EM
SSB       0
LB                  0.30 Hz
GB        0
PC                  1.00
```

13.8 Appendix Figure 8: ^{13}CNMR of NS-1-21

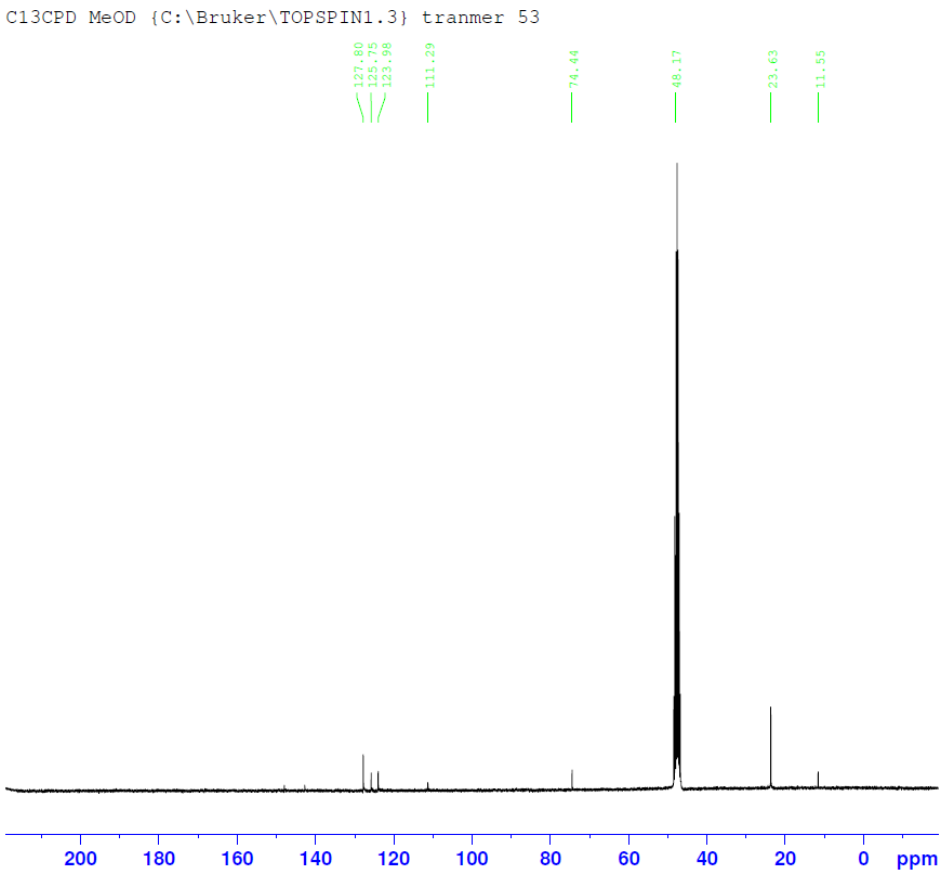

BRUKER

```
Current Data Parameters
NAME                  NS-1-21
EXPNO                       2
PROCNO                      1

F2 - Acquisition Parameters
Date_                20210423
Time                    21.23
INSTRUM                 spect
PROBHD    5 mm QNP  1H/1
PULPROG                zqpg30
TD                      65536
SOLVENT                  MeOD
NS                       1024
DS                          4
SWH                17985.611 Hz
FIDRES              0.274439 Hz
AQ                  1.8219008 sec
RG                       3251
DW                     27.800 usec
DE                      6.00 usec
TE                     298.2 K
D1                 2.00000000 sec
d11                0.03000000 sec
DELTA              1.89999998 sec
TD0                         1

======== CHANNEL f1 ========
NUC1                      13C
P1                       5.60 usec
PL1                     -6.00 dB
SFO1               75.4752953 MHz

======== CHANNEL f2 ========
CPDPRG[2               waltz16
NUC2                       1H
PCPD2                  80.00 usec
PL2          0 dB
PL12                    18.06 dB
PL13                    24.00 dB
SFO2              300.1312005 MHz

F2 - Processing parameters
SI                       32768
SF                 75.4677490 MHz
WDW                         EM
SSB          0
LB                       1.00 Hz
GB           0
PC                       1.40
```

13.9 Appendix Figure 9: HRMS of NS-1-21

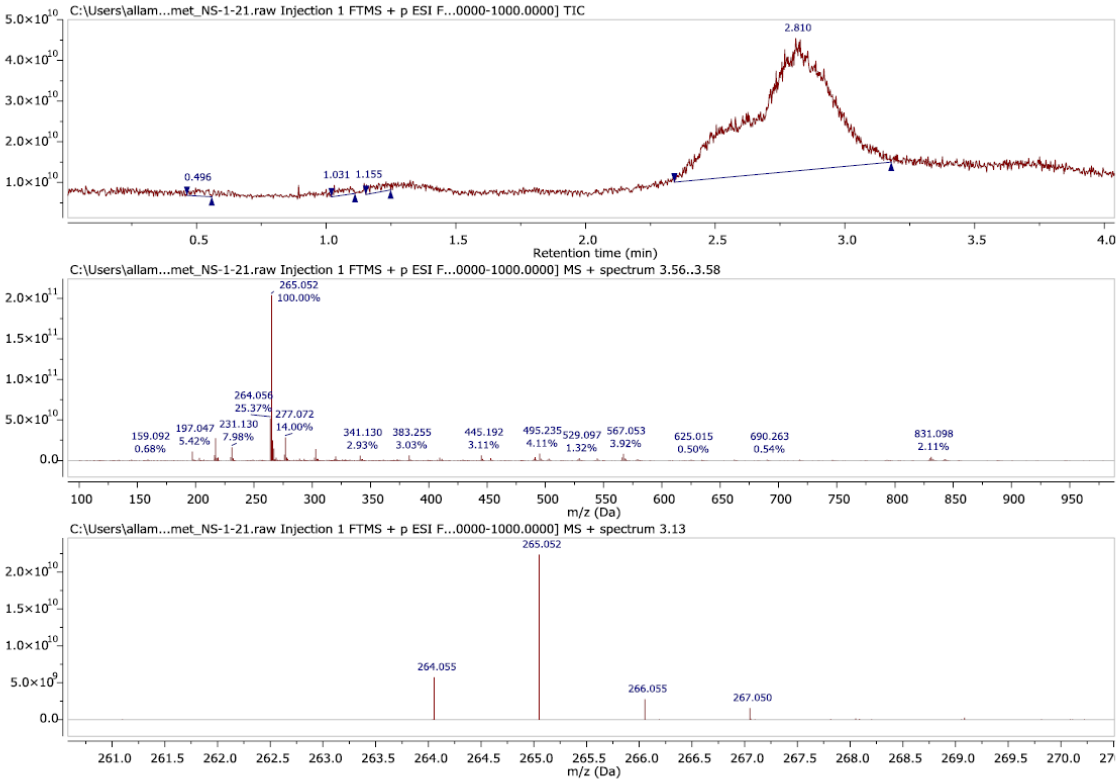

13.10 Appendix Figure 10: Chromatogram of NS-1-10(EDR)

Sample: EDR | Rf 200 | Friday 05 April 2019 04:00PM

RediSep Column: Silica 12g
SN: E041503AE4B628 Lot: 2616305030W
Flow Rate: 30 ml/min
Equilibration Volume: 100.8 ml
Initial Waste: 0.0 ml
Air Purge: 0.5 min
Solvent A: hexane
Solvent B: ethyl acetate

Peak Tube Volume: Max.
Non-Peak Tube Volume: Max.
Loading Type: Solid
Wavelength 1 (red): 254nm
Peak Width: 1 min
Threshold: 0.20 AU
Wavelength 2 (purple): 280nm

Run Notes:

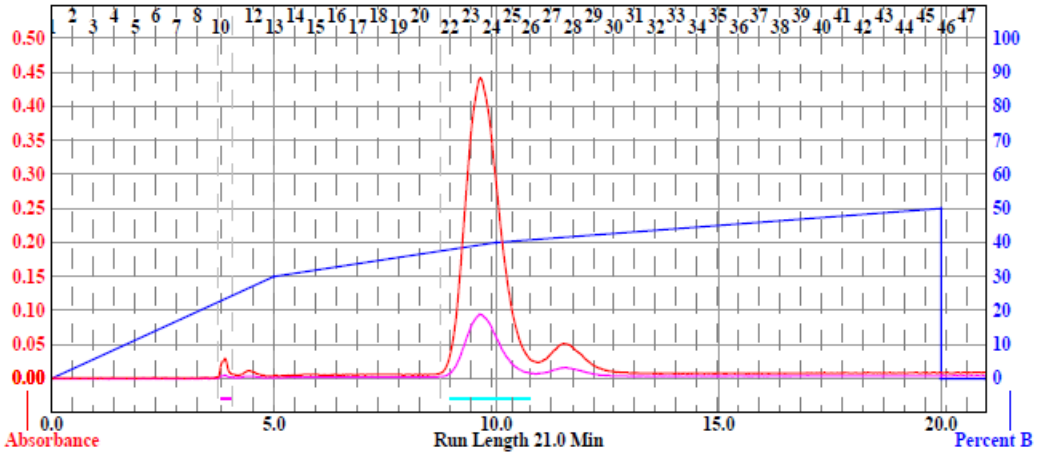

Rack A

16 mm x 125 mm Tubes

Peak #	Start Tube	End Tube
1	A:10	A:10
2	A:22	A:25

Duration	%B	Solvent A	Solvent B
0.0	0.0	hexane	ethyl acetate
5.0	30.0	hexane	ethyl acetate
5.0	40.0	hexane	ethyl acetate
10.0	50.0	hexane	ethyl acetate
0.0	0.0	hexane	ethyl acetate
1.0	0.0	hexane	ethyl acetate

Page 1 of 2

13.11 Appendix Figure 11: ^{1}HNMR of NS-1-10 (EDR)

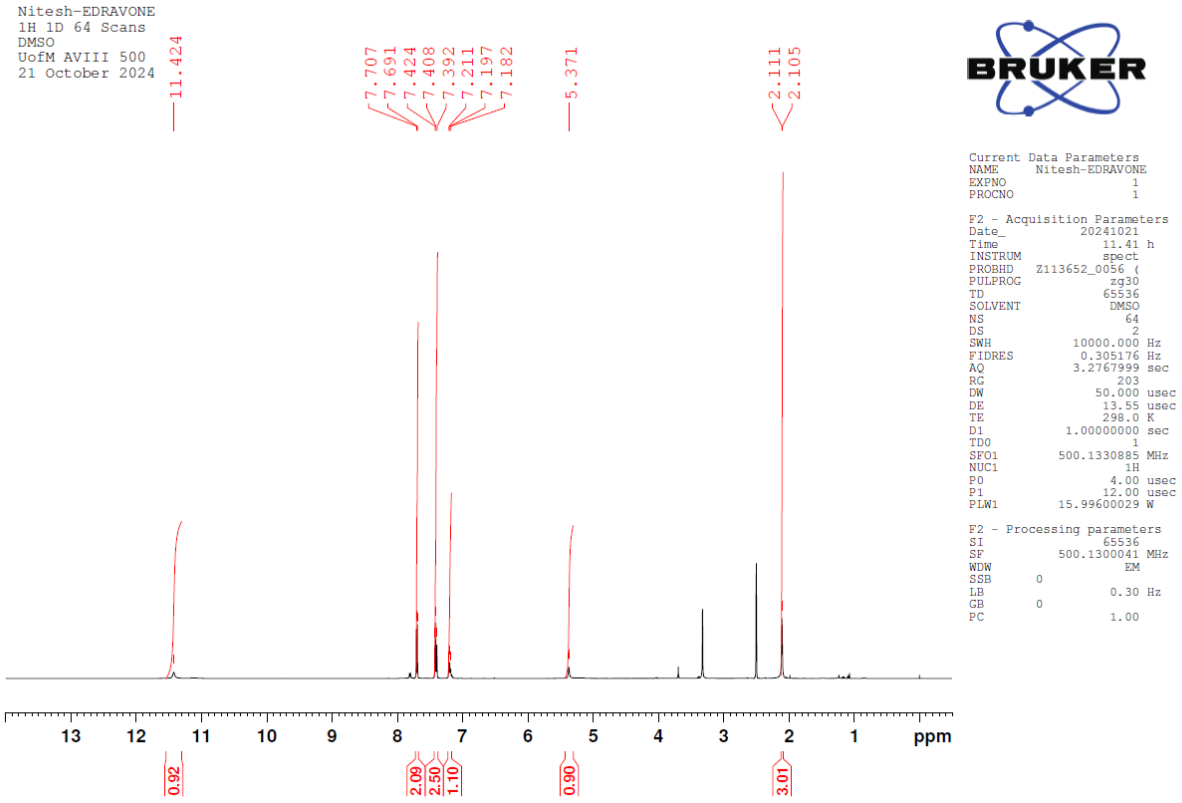

13.12 Appendix Figure 12: ^{13}CNMR of NS-1-10 (EDR)

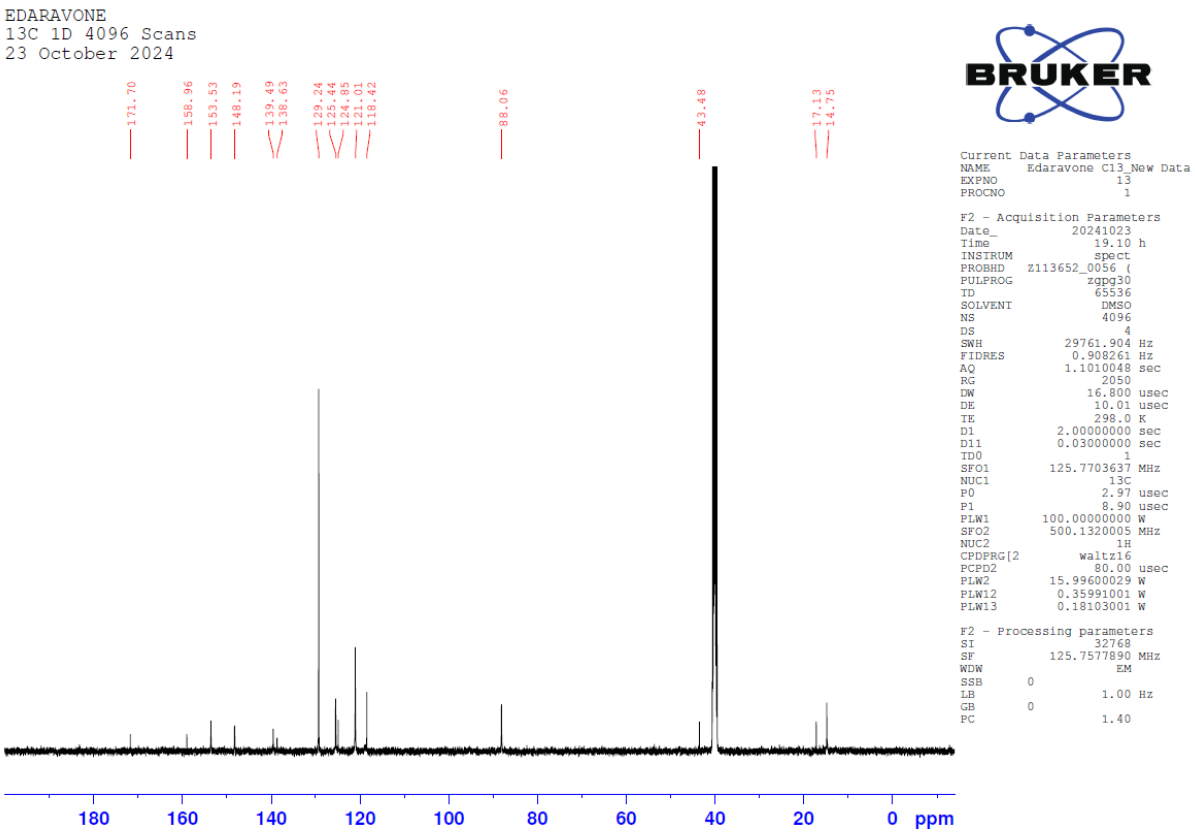

13.13 Appendix Figure 13: HRMS of NS-1-2 (EDR)

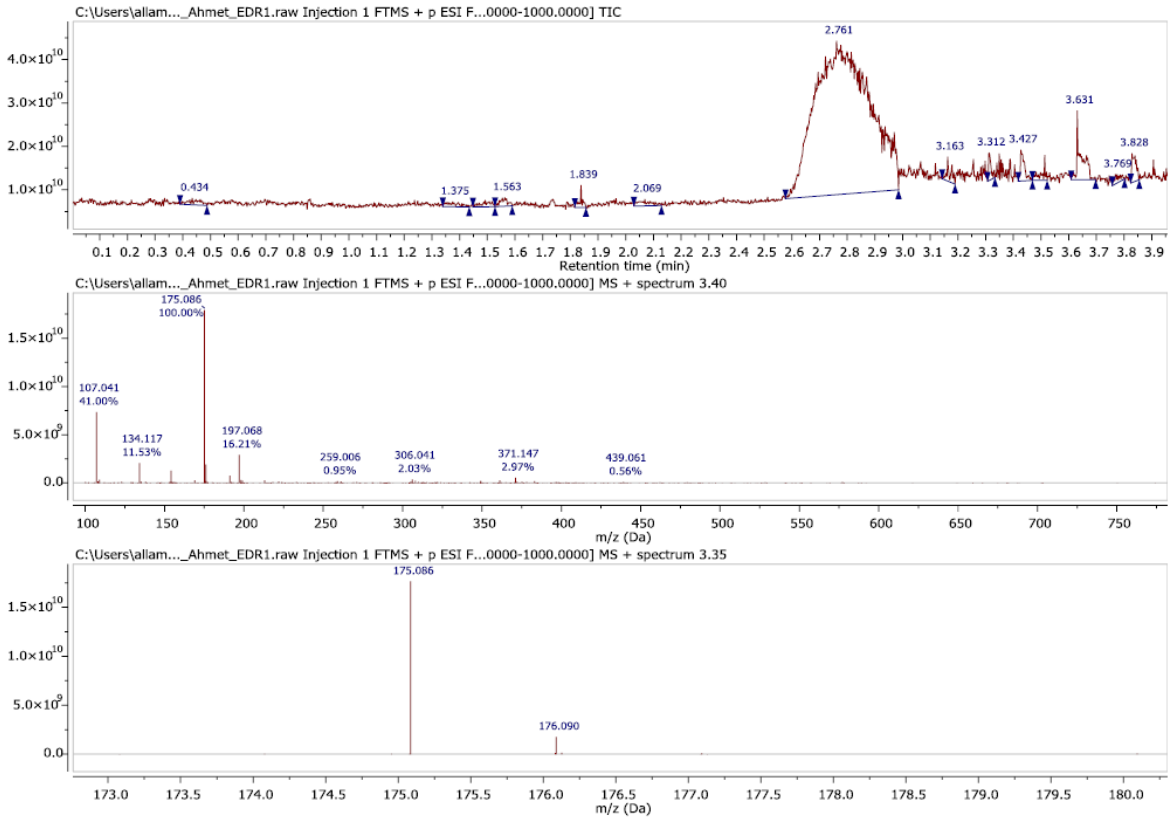

13.14 Appendix Figure 14: ^{1}HNMR of NS-1-12

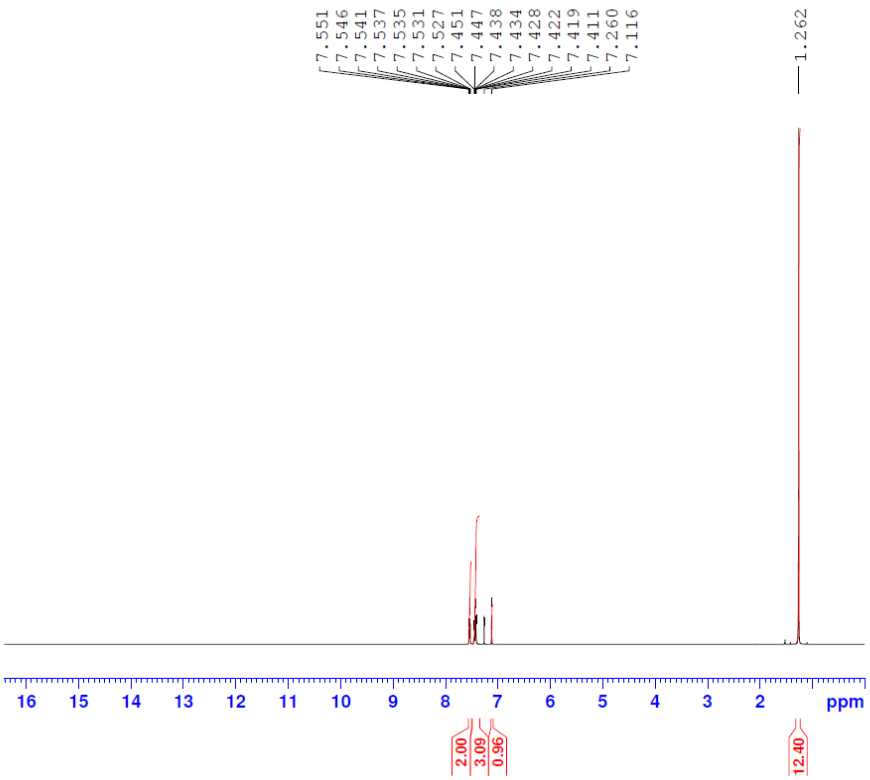


```
Current Data Parameters
NAME       NS-1-12_CDCL3
EXPNO                  5
PROCNO                 1

F2 - Acquisition Parameters
Date_           20190424
Time               17.49
INSTRUM            spect
PROBHD   5 mm PABBO BB-
PULPROG             zg30
TD                 65536
SOLVENT            CDC13
NS                    16
DS                     2
SWH             8223.685 Hz
FIDRES          0.125483 Hz
AQ              3.9845889 sec
RG                   287
DW                60.800 usec
DE                 6.50 usec
TE                298.2 K
D1           1.00000000 sec
TD0                    1

======== CHANNEL f1 ========
SFO1         400.3324722 MHz
NUC1                   1H
P1                 14.00 usec
PLW1        14.22799969 W

F2 - Processing parameters
SI                 32768
SF           400.3300089 MHz
WDW                   EM
SSB       0
LB                 0.30 Hz
GB        0
PC                 1.00
```

13.15 Appendix Figure 15: ^{13}CNMR of NS-1-12

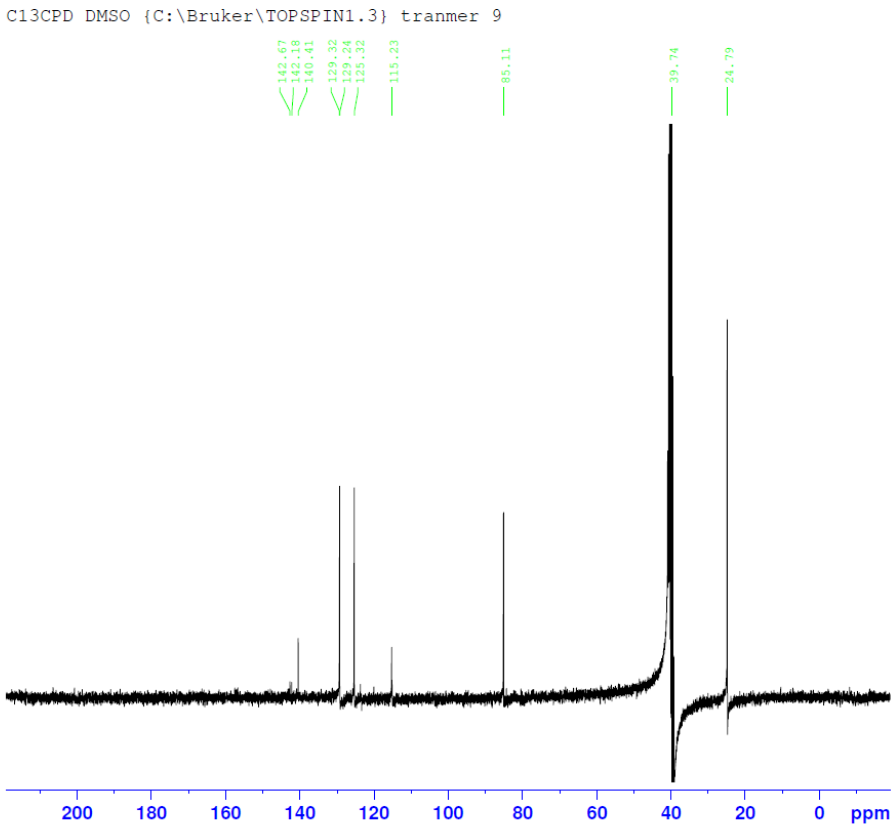

BRUKER

```
Current Data Parameters
NAME                  NS-1-12
EXPNO                       1
PROCNO                      1

F2 - Acquisition Parameters
Date_              20210316
Time                  23.43
INSTRUM               spect
PROBHD    5 mm QNP  1H/1
PULPROG               zgpg30
TD                     65536
SOLVENT                DMSO
NS                      1024
DS                         4
SWH               17985.611 Hz
FIDRES             0.274439 Hz
AQ                 1.8219008 sec
RG                     645.1
DW                    27.800 usec
DE                     6.00 usec
TE                    298.2 K
D1                 2.00000000 sec
d11                0.03000000 sec
DELTA              1.89999998 sec
TD0                         1

======== CHANNEL f1 ========
NUC1                      13C
P1                       5.60 usec
PL1                     -6.00 dB
SFO1              75.4752953 MHz

======== CHANNEL f2 ========
CPDPRG[2               waltz16
NUC2                       1H
PCPD2                  80.00 usec
PL2          0 dB
PL12                   18.06 dB
PL13                   24.00 dB
SFO2             300.1312005 MHz

F2 - Processing parameters
SI                        32768
SF                75.4677490 MHz
WDW                          EM
SSB          0
LB                      1.00 Hz
GB           0
PC                      1.40
```

13.16 Appendix Figure 16: HRMS of NS-1-12

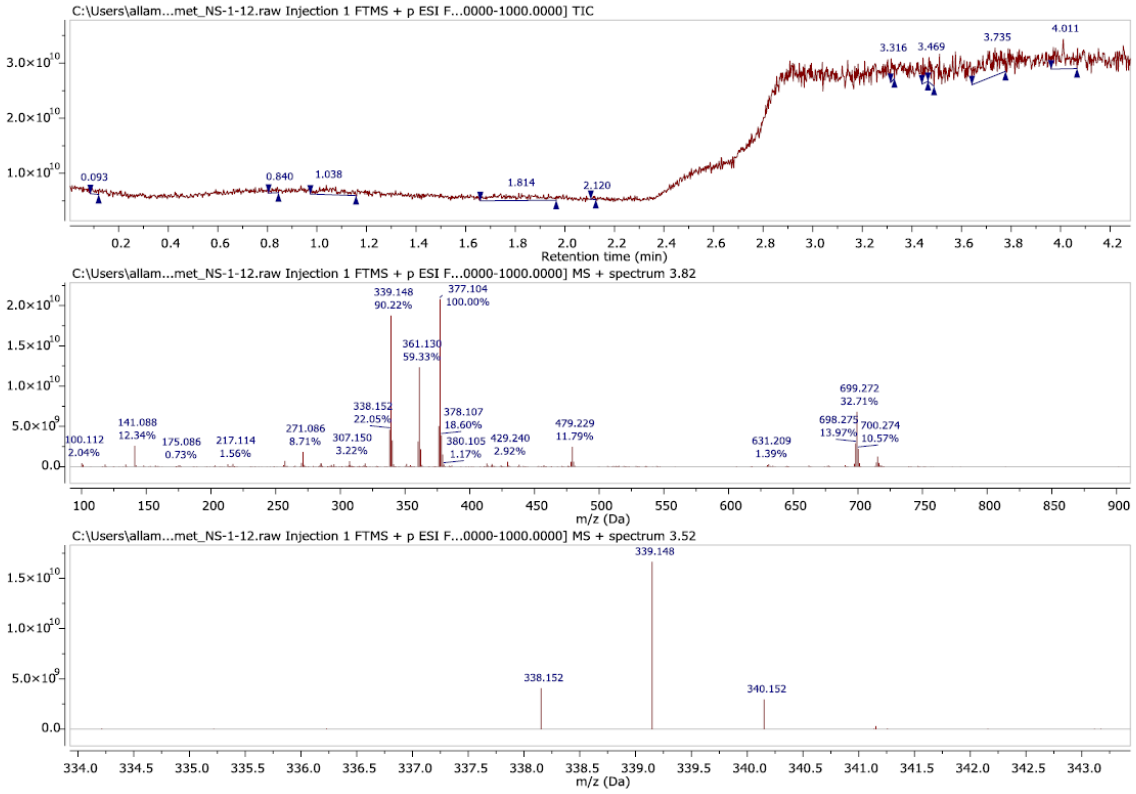

13.17 Appendix Figure 17: ^{1}HNMR of NS-1-19

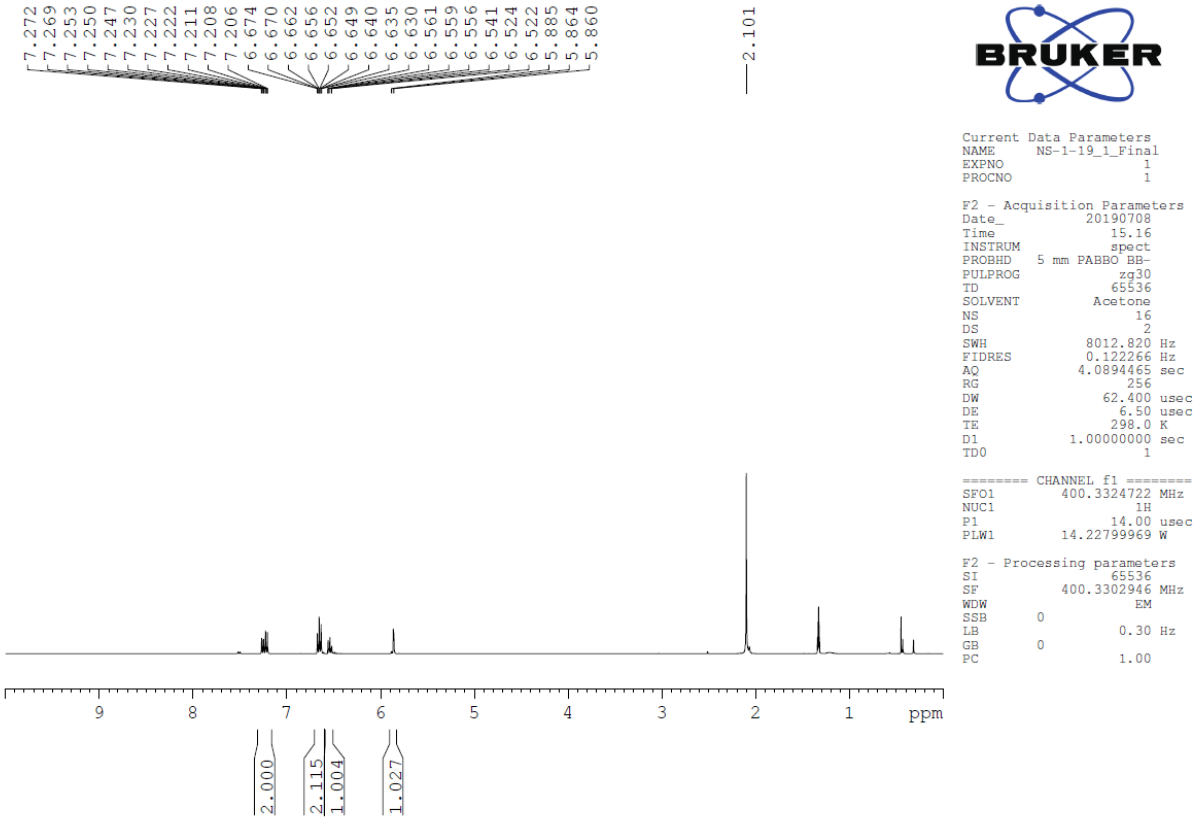


```
Current Data Parameters
NAME      NS-1-19_1_Final
EXPNO                   1
PROCNO                  1

F2 - Acquisition Parameters
Date_           20190708
Time               15.16
INSTRUM             spect
PROBHD   5 mm PABBO BB-
PULPROG             zg30
TD                 65536
SOLVENT          Acetone
NS                    16
DS                     2
SWH             8012.820 Hz
FIDRES          0.122266 Hz
AQ              4.0894465 sec
RG                   256
DW                62.400 usec
DE                 6.50 usec
TE                298.0 K
D1             1.00000000 sec
TD0                    1

======== CHANNEL f1 ========
SFO1         400.3324722 MHz
NUC1                   1H
P1                 14.00 usec
PLW1         14.22799969 W

F2 - Processing parameters
SI                 65536
SF           400.3302946 MHz
WDW                   EM
SSB       0
LB                 0.30 Hz
GB        0
PC                 1.00
```

13.18 Appendix Figure 18: ^{13}CNMR of NS-1-19

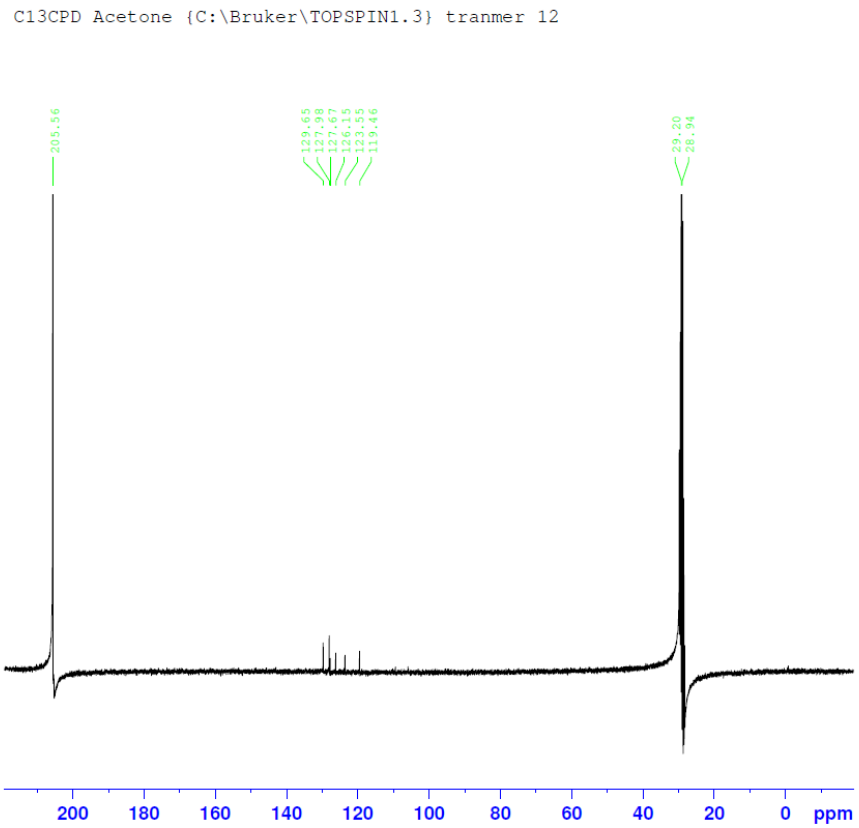

BRUKER

```
Current Data Parameters
NAME         C13_Acetone
EXPNO                  2
PROCNO                 1

F2 - Acquisition Parameters
Date_           20210407
Time               20.43
INSTRUM            spect
PROBHD   5 mm QNP  1H/1
PULPROG          zgpg30
TD                65536
SOLVENT         Acetone
NS                 1024
DS                    4
SWH           17985.611 Hz
FIDRES         0.274439 Hz
AQ            1.8219008 sec
RG               2896.3
DW               27.800 usec
DE                6.00 usec
TE               298.2 K
D1            2.00000000 sec
d11           0.03000000 sec
DELTA         1.89999998 sec
TD0                    1

======== CHANNEL f1 ========
NUC1                 13C
P1                  5.60 usec
PL1                -6.00 dB
SFO1          75.4752953 MHz

======== CHANNEL f2 ========
CPDPRG[2          waltz16
NUC2                 1H
PCPD2              80.00 usec
PL2       0 dB
PL12               18.06 dB
PL13               24.00 dB
SFO2         300.1312005 MHz

F2 - Processing parameters
SI                  32768
SF            75.4677490 MHz
WDW                    EM
SSB       0
LB                  1.00 Hz
GB        0
PC                  1.40
```

13.19 Appendix Figure 19: HRMS of NS-1-19

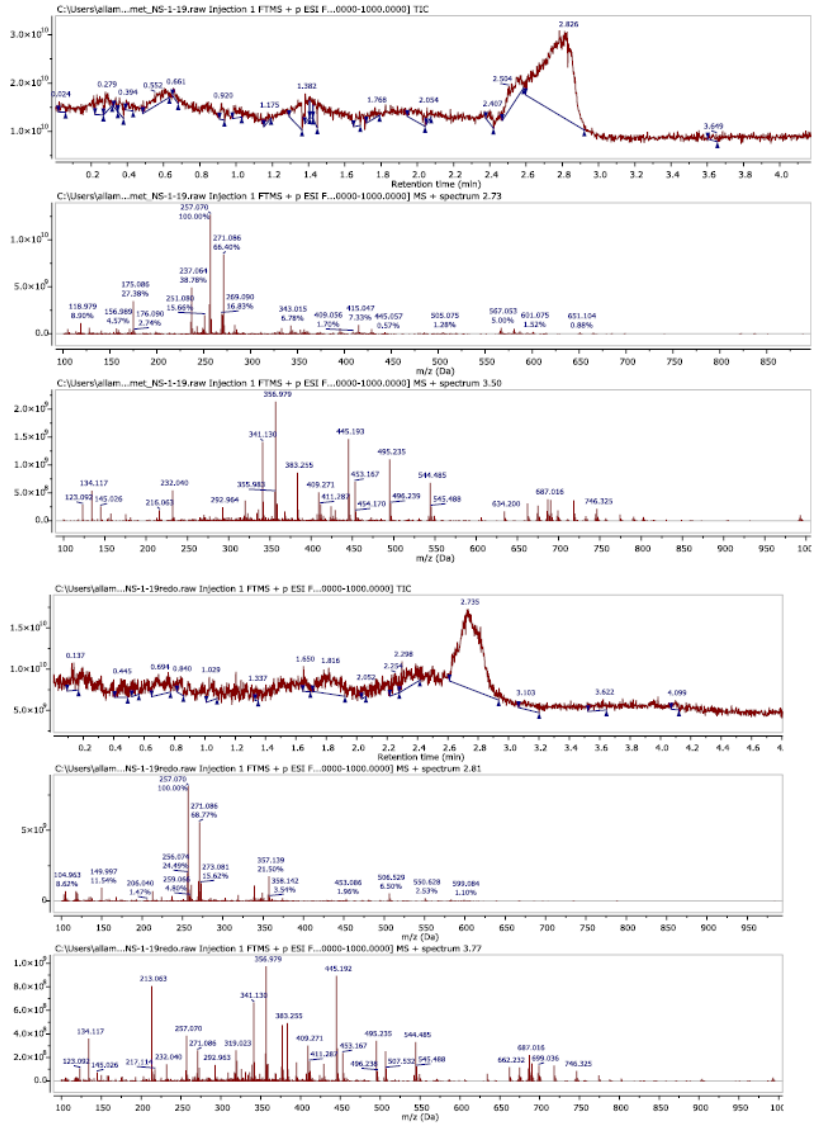

13.20 Appendix Figure 20: ^{1}HNMR of NS-1-23

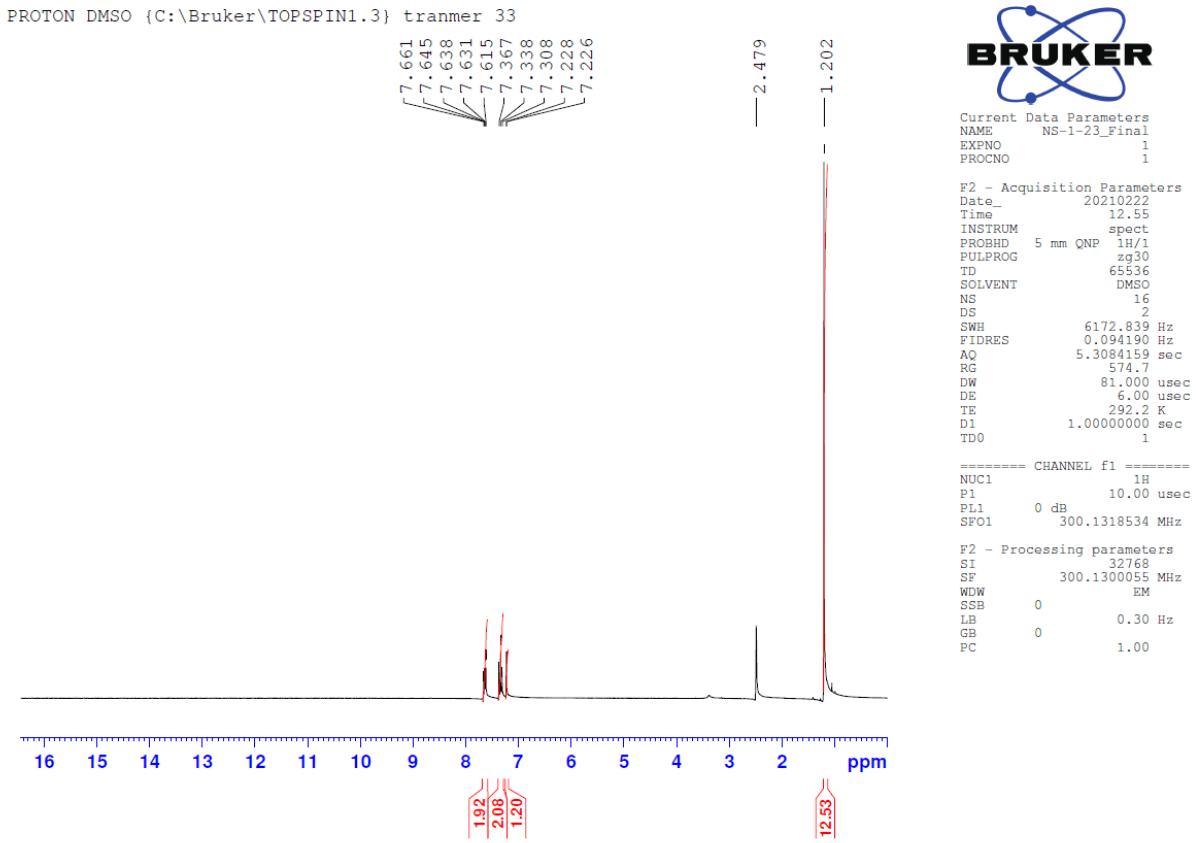

13.21 Appendix Figure 21: ^{13}CNMR of NS-1-23

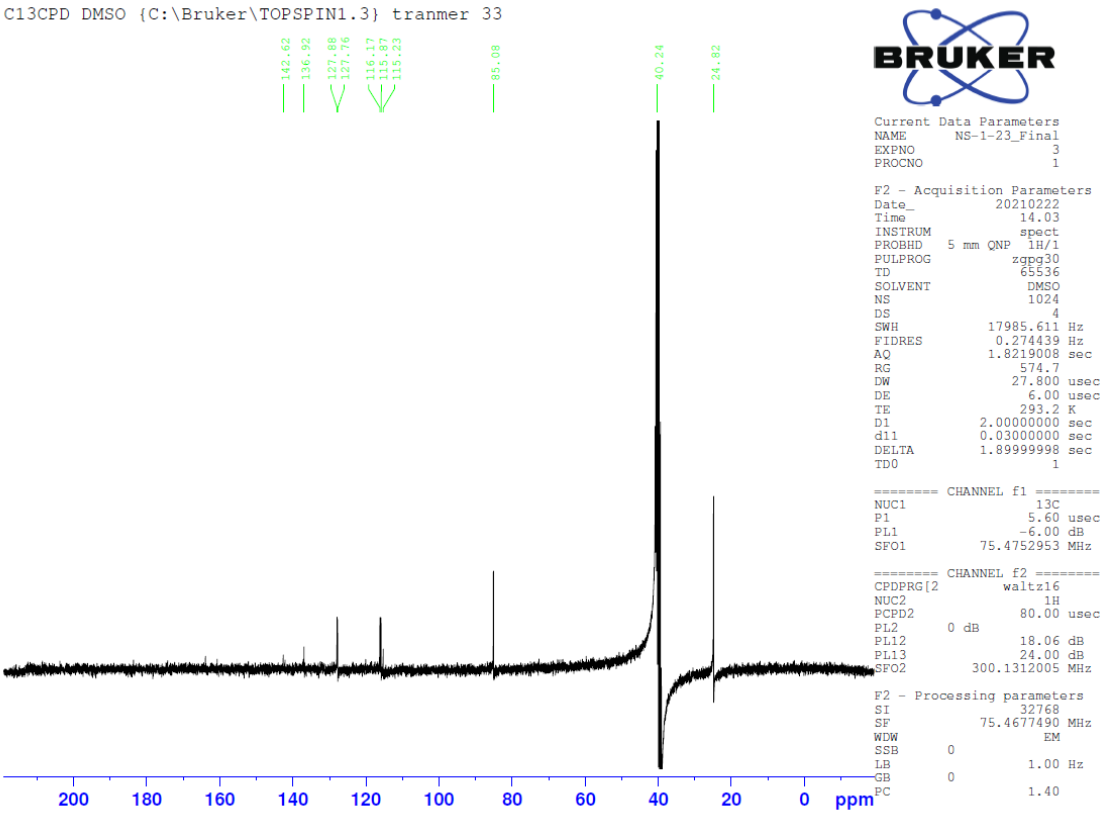

13.22 Appendix Figure 22: ^{19}FNMR of NS-1-23

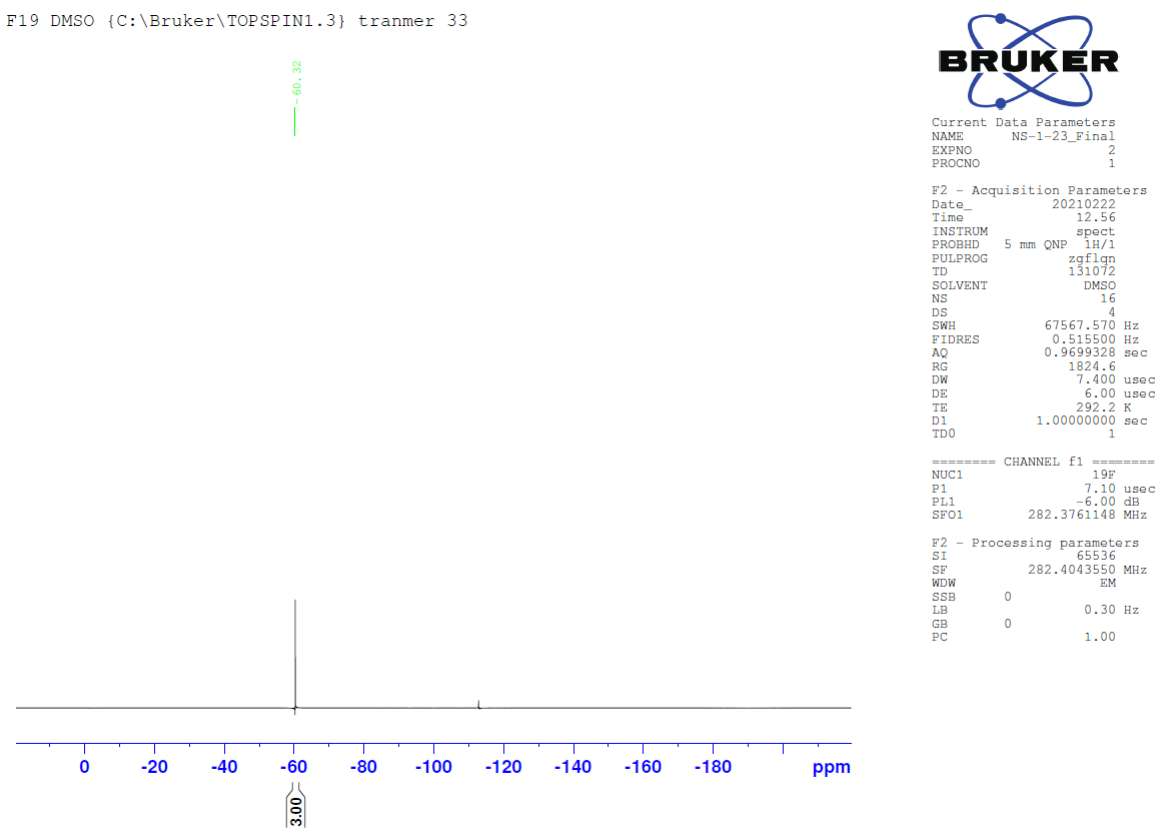

13.23 Appendix Figure 23: HRMS of NS-1-23